PHY

VOLUME II

THE PHYSICAL REVIEW

A journal of experimental and theoretical physics established by E. L. Nichols in 1893

Published by the American Institute of Physics
for the
AMERICAN PHYSICAL SOCIETY

Officers

President

C. C. Lauritsen
California Institute of Technology
Pasadena, California

Vice-President

J. H. Van Vleck
Harvard University
Cambridge, Massachusetts

Secretary

K. K. Darrow
Bell Telephone Laboratories
After
Columbia University
New York 27, New York

Treasurer

G. B. Pegram
Columbia University
New York 27, New York

Local Secretary
for the Pacific Coast

J. Kaplan
University of California at Los Angeles
Los Angeles, California

Managing Editor

S. A. Goudsmit
Brookhaven National Laboratory
Upton, Long Island, New York

BOARD OF EDITORS

Editor

S. A. Goudsmit

Assistant Editor

S. Frankel

Associate Editors

J. Barnes — Harvey Brooks — M. Goldhaber
C. Bonner — R. F. Christy — R. Hofstadter
R. G. Herb — C. L. Critchfield — A. W. Lawson
W. E. Lamb, Jr. — M. Deutsch — A. Pais
A. J. F. Siegert — T. H. Johnson — R. Serber
W. E. Stephens — Bruno Rossi — C. H. Townes

Manuscripts for publication should be submitted to S. A. Goudsmit, Brookhaven National Laboratory, Upton, Long Island, New York. The authors' institutions are requested to pay a publication charge of $9 per page which, if honored, entitles them to 100 free reprints. Instructions will be sent with galley proofs.

Proof and all correspondence concerning papers in the process of publication should be addressed to the Publication Manager, American Institute of Physics, 57 East 55 Street, New York 22, New York.

Subscription Price

United States and Canada $25.00
Elsewhere $27.00

Back Numbers[1]

Yearly back number rate when complete year is available:
Prior to 1949: $20.00
Thereafter: $27.00

Single copies: $2.00 each, prior to July, 1929;
$1.00 each, July, 1929–December, 1941;
$2.00 each, January, 1942–December, 1946;
$3.00 each, January, 1947–December, 1948;
$3.25 each, thereafter.

General index, 1893–1920: $4.00.

Subscriptions, renewals, and orders for back numbers should be addressed to the American Institute of Physics, 57 East 55 Street, New York 22, New York.

Changes of address in the case of members of the American Physical Society should be addressed to the Treasurer; in the case of other subscribers to the American Institute of Physics.

[1] Set Series I, Index of Physics Department, Cornell University, Ithaca, New York.

The Physical Review is published semi-monthly at Prince and Lemon Streets, Lancaster, Pennsylvania.
Entered as second-class matter January 6, 1947, at the Post Office at Lancaster, Pennsylvania, under the Act of March 3, 1879.
Acceptance for mailing at special rate of postage provided for in paragraph (d-2), section 34.40, P. L. & R. of 1948, authorized January 16, 1947.

THE
PHYSICAL REVIEW

A journal of experimental and theoretical physics established by E. L. Nichols in 1893

SECOND SERIES, VOL. 81, NO. 4 FEBRUARY 15, 1951

Stopping Power and Energy Loss for Ion Pair Production for 340-Mev Protons*

C. J. BAKKER† AND E. SEGRÈ
Department of Physics, Radiation Laboratory, University of California, Berkeley, California
(Received October 23, 1950)

The relative stopping powers for 300-Mev protons of H, Li, Be, C, Al, Fe, Cu, Ag, Sn, W, Pb, and U have been measured. The energy spent per ion-pair production in the gases H_2, He, N_2, O_2, Ne, A, and air at 340-Mev proton energy has also been measured. The results are given in Tables I and II.

I. INTRODUCTION

THE average rate of energy loss of fast particles due to ionization only is given by the well-known Bethe formula,[1]

$$-dE/dx=(4\pi e^4z^2/mv^2)NZ \times[\ln(2mv^2/I)-\ln(1-\beta^2)-\beta^2], \quad (1)$$

in which e and m are the electronic charge and mass, ez is the charge of the incident particle, NZ is the number of electrons per unit volume of stopping material of atomic number Z, $\beta=v/c$, and I is the mean excitation potential of the atoms in the stopping material.

The formula holds when $v\gg u_k$, where u_k is the velocity of the orbital electrons in the K-shell of the atoms in the stopping material. Effects such as radiation, nuclear interactions, and so on are not taken into account in formula (1); they may play an increasingly important part at higher energies.

Extensive tables based on formula (1) have been computed by Aron, Hoffman, and Williams[2] of the Radiation Laboratory of the University of California. In these tables the mean excitation potential, I, was chosen proportional to Z, in accordance with Bloch's theory[3] developed on the basis of the Thomas-Fermi model of the atom. The value of the Bloch constant I/Z was chosen to be 11.5 ev in accordance with measurements by Wilson.[4] In cases in which the condition $v\gg u_k$ was not fulfilled, correction terms were added to formula (1) given by Livingston and Bethe.[1]

II. EXPERIMENTAL

Since the 340-Mev protons of the Berkeley cyclotron afford a good opportunity for checking the semi-empirical part of the stopping power calculation and the result is of practical importance, we decided, using these particles, to measure the stopping power of various elements spread over the periodic system.

The high energy protons of the 184-in. cyclotron are stopped by 93.7 g/cm² of copper (ionization extrapolated range) as measured from the Bragg curve at the end of the range (Figs. 1, 2). In the experiments approximately 30 g/cm² of copper were replaced by the material to be investigated. By again measuring the Bragg curve at the end of the range the mass stopping

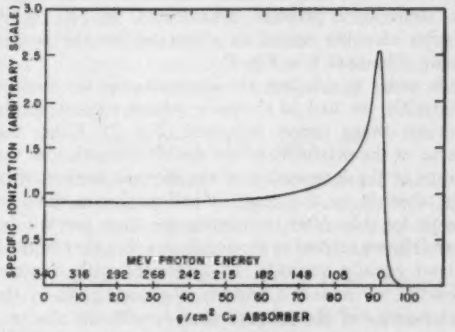

FIG. 1. The complete experimental Bragg curve for 340-Mev protons stopped by copper.

* This work was performed under the auspices of the AEC.
† Zeeman Laboratory, University of Amsterdam, The Netherlands.
[1] M. S. Livingston and H. A. Bethe, Revs. Modern Phys. 9, 285 (1937).
[2] Aron, Hoffman, and Williams, *Range-Energy Curves*, AECU-663 (UCRL-121), unpublished.
[3] F. Bloch, Z. Physik 81, 363 (1938).
[4] R. R. Wilson, Phys. Rev. 60, 749 (1941).

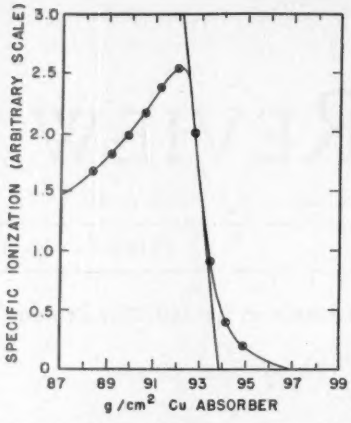

FIG. 2. The end section of the Bragg curve on an enlarged scale. The crosses and circles denote measurements at different times. The steepest tangent has been drawn in.

power of the various materials relative to copper could be determined. At the initial energy of the protons (measured as 340 Mev from the radius of the orbit and magnetic field in the cyclotron) the energy loss induced by 30 g/cm² of copper amounts to about 75 Mev. The mean energy of the protons in the absorbing material is therefore about 300 Mev. The experimental arrangement is shown schematically in Fig. 3. The fast protons emerged from the concrete wall surrounding the 184-in. cyclotron through a collimator of ½-inch inner diameter at the exit, passed successively through the material to be investigated, through 56.70 g/cm² of copper, and then, in order to measure the Bragg curve, through layers of copper which could be varied from 0 to 11 times 0.72 g/cm². The latter were mounted in 2-in. holes arranged near the circumference of a large wheel which could be rotated from a distance. The measurements of all 12 positions could be made in about 10 min. As a measuring instrument for the protons we used an ionization chamber filled with argon to atmospheric pressure (Chamber C in Fig. 3). A similar chamber served as a monitor for the proton beam (Chamber B in Fig. 3).

In order to compare the absorption in the various materials, we had to choose a reference point in the various Bragg curves measured (Fig. 2). Either the range at the maximum of the specific ionization, or the range at the intersection of the steepest tangent with the abscissa, or the range at half-maximum could be taken for this. After considering the three possibilities carefully we arrived at the conclusion that they were all about equally accurate. In agreement with common practice we chose as a reference the range given by the intersection of the steepest tangent with the abscissa, usually referred to as the ionization extrapolated range.

As the absorption in copper was used as a standard, in the course of the run of the measurements the Bragg curve of the copper absorber was remeasured intermittently. The result was always the same within the experimental errors, which indeed is an excellent proof of the constancy of the energy of the proton beam of the 184-in. cyclotron. This may be seen from Fig. 2, where the circles and crosses denote different measurements.

Actually, the ordinate show $(n/w)dE/dx$ *versus* range, where n is the number of protons crossing the ionization chamber per unit time and W is the energy spent per ion pair produced. The number n itself varies along the beam owing to nuclear scattering with an approximate law $n=n(0)e^{-\lambda x}$, where λ is the mean free path for nuclear scattering. For this reason the Bragg curve is not directly comparable with a dE/dx curve.

III. RESULTS

By dividing the number of g/cm² of copper by the equivalent number of g/cm² of the element under investigation one obtains the mass stopping power relative to copper. Table I, column 2, shows the results of the measurements. The mean experimental error of these numbers, except for hydrogen, should be about 1 percent. The value for hydrogen was obtained by subtraction of the carbon figure from the measurement on polyethylene, which consists of long chain molecules and has a chemical composition CH_2. The error in the hydrogen figure is about 5 percent. Moreover, it must be remembered that the chemical binding of the hydrogen in polyethylene may have considerable influence. (Experiments on the effect of chemical binding in stopping power will be carried out in the near future in this Laboratory.)

As it is common practice to tabulate the mass stopping power relative to aluminum, we also calculated this quantity from our measurements. The data are shown in column 3 of Table I.

It is of interest to determine from our data the stopping power per electron. According to formula (1) this

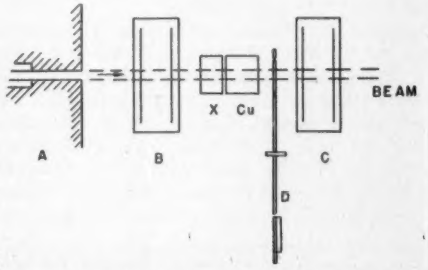

FIG. 3. The experimental arrangement. *A* is the concrete wall surrounding the 184-in. cyclotron. The 340-Mev protons pass through a collimator with ½-in. diameter exit hole. *B* and *C* are ionization chambers. *X* is the material under investigation, with stopping power equivalent to about 30 g/cm² of copper. Cu is 56.70 g/cm² of copper absorber. *D* is a wheel, by which different thicknesses of copper absorber could be inserted.

quantity is

$$-(dE/dx)/NZ=(4\pi^4z^2e^4/mv^2)\times[\ln(2mv^2/I)-\ln(1-\beta^2)-\beta^2]. \quad (2)$$

The stopping power per electron relative to aluminum is

$$q=\frac{-\ln(I)+[\ln(2mv^2)-\ln(1-\beta^2)-\beta^2]}{-\ln(I_{Al})+[\ln(2mv^2)-\ln(1-\beta^2)-\beta^2]} \quad (3)$$

which was calculated from our data by multiplying the figures of Table I, column 3 by $(A/A_{Al})\cdot(Z_{Al}/Z)$, in which A and Z are the atomic weight and the atomic number of the element under investigation, and $A_{Al}=26.97$, $Z_{Al}=13$, the corresponding numbers for aluminum. Column 4 of Table I shows the result.

Bethe has kindly pointed out to us that the most favorable method for the further analysis of our results is to use formula (3) to calculate the mean excitation potentials, I. The absolute value of I can be based on Wilson's determination of 150 ev as the mean excitation potential for aluminum, which is accurate to ±3 percent. Wilson's measurement, however, does not give a satisfactory value for the Bloch constant I/Z, as aluminum is too light an element for the Bloch theory to be valid.

Introducing in formula (3) $I_{Al}=150$ ev and $\beta=0.65$, so that

$$[\ln(2mv^2)-\ln(1-\beta^2)-\beta^2]=13.112,$$

it follows that

$$\ln(I)=13.112-8.096\cdot q. \quad (4)$$

The values of I and I/Z are tabulated in columns 5 and 6 of Table I, including a small correction due to multiple scattering.

It is seen from the last column that the Bloch "constant" is nearly constant for $Z>26$. The average value is 9.4 ev. This value is somewhat lower than the value Bethe derived in a similar way from Stephan and Thornton's[5] total range measurements of 194-Mev deuterons, namely, slightly over 10 ev. Our value should probably be considered as the more accurate one, although it is clear from Eq. (4) above that an error of q of 1 percent gives an error in I of 10 percent.

As also pointed out to us by Bethe, a satisfactory result confirming the analysis is the average potential for beryllium, which comes out to be 60.4 ev. Madsen and Venkateswarlu[6] have determined this value by a direct and absolute experiment and found it to be 64±5 ev. This result is not as accurate as Wilson's, but has the advantage of being a direct absolute determination, in which unlike Wilson, Madsen, and Venkateswarlu did not make use of the stopping power for air. The agreement within experimental errors serves to confirm Wilson's values for aluminum to some extent.

[5] W. Stephan and R. L. Thornton, unpublished.

[6] C. P. Madsen and P. Venkateswarlu, Phys. Rev. **74**, 648 (1948).

TABLE I. Mass stopping powers.

Element	Mass stopping power Cu=1	Mass stopping power Al=1	q=stopping power per electron Al=1	I_{ev}	I/Z (ev)
$_1H_2$ (in CH_2)	3.010	2.634	1.280	15.6	15.6
$_3$Li	1.214	1.062	1.184	34.0	11.3
$_4$Be	1.171	1.024	1.113	60.4	15.1
$_6$C	1.285	1.124	1.084	76.4	12.7
$_{13}$Al	1.143	1.000*	1.000*	150*	11.5*
$_{26}$Fe	1.036	0.906	0.941	243	9.3
$_{29}$Cu	1.000*	0.875	0.924	279	9.6
$_{47}$Ag	0.902	0.789	0.873	428	9.1
$_{50}$Sn	0.858	0.751	0.859	479	9.5
$_{74}$W	0.777	0.680	0.814	697	9.4
$_{82}$Pb	0.754	0.660	0.804	758	9.2
$_{92}$U	0.720	0.630	0.786	881	9.6

* In each column the reference value is marked by an asterisk.

IV. ANALYSIS OF STRAGGLING

Formula (1) gives the average energy loss suffered by a charged particle in traversing some stopping material. Actually, the number of collisions, which reduces the energy, is finite, and a statistical fluctuation in the amount of energy lost can be expected ("straggling").

Starting with particles of the same initial energy E_0, and R_0 being the average range, the probability for a particle to have a range R is given by the Gaussian

$$P(R)=[1/2\pi\langle(R-R_0)^2\rangle_{Av}]^{\frac{1}{2}}\times\exp[-(R-R_0)^2/2\langle(R-R_0)^2\rangle_{Av}].$$

It has been shown by Bohr[7] and by Livingston and Bethe[8] that for protons of high initial energy the mean square fluctuation in the range is

$$\langle(R-R_0)^2\rangle_{Av}=4\pi e^4NZ\int_0^{E_0}(dE/dx)^{-3}dE.$$

We have calculated $\langle(R-R_0)^2\rangle_{Av}$ for 340-Mev protons stopped in copper. The values of dE/dx as a function of E were taken from the tables of Aron, *et al.*[2] The result is

$$\langle(R-R_0)^2\rangle_{Av}=0.85(\text{g/cm}^2\text{ Cu})^2.$$

In order to compare this theoretical value of straggling in copper with the experimental Bragg curve we "folded" the one-particle ionization curve in argon[9] into a Gaussian form. It was found that reasonable agreement with the experimental Bragg curve was obtained if we chose

$$\langle(R-R_0)^2\rangle_{Av}=1.3(\text{g/cm}^2\text{ Cu})^2.$$

The difference between the experimental and the theoretical value of the straggling constant could be ascribed to inhomogeneities in the absorbing layer, which for copper are small, nuclear collisions and to the

[7] N. Bohr, Phil. Mag. **30**, 581 (1915); Kgl. Danske Videnskab., Selskab. Mat-fys. Medd. **18**, 8 (1948).

[8] M. S. Livingston and H. A. Bethe, Revs. Modern Phys. **9**, 245 (1937).

[9] Range-energy curves of Aron, *et al.* (reference 2), were used to determine this curve.

TABLE II. Values of $(-dE/dx)$ and w.

Gas	$-dE/dx$ (Mev/cm) 340-Mev p	w/w_A 340-Mev p	w(ev) 340-Mev p	w(ev) Po = α-particles
Hydrogen	5.84×10^{-4}	1.38	35.3	34.5; 36.1[a, b]
Helium	5.34×10^{-4}	1.17	29.9	30.6[a]
Nitrogen	3.49×10^{-3}	1.31	33.6	36.3; 37.2[b, c]
Oxygen	3.92×10^{-3}	1.23	31.5	32.4[d]
Neon	2.39×10^{-3}	1.12	28.6	27.2; 29.8[b, d]
Argon	4.02×10^{-3}	1.00	25.5	24.4; 28.4[b, d]
Air	3.58×10^{-3}	1.30	33.3	34.7; 35.7[b, c]

[a] L. H. Gray, Proc. Camb. Phil. Soc. **40**, 72 (1944).
[b] G. Stetter, Z. Physik **120**, 639 (1943).
[c] Alder, Huber, and Metzger, Helv. Phys. Acta **20**, 234 (1947).
[d] K. Schmieder, Ann. Physik **35**, 445 (1939), normalized in agreement with reference (c) above.

spread in energy of the initial protons. If we suppose the latter to be the main effect, it follows that the spread in initial energy of the 340-Mev proton beam gives rise to an additional straggling with $\langle(R-R_0)^2\rangle_{Av}=0.45$ (g/cm² Cu)², which denotes an average energy spread of the proton beam of about ½ percent. This value is in satisfactory agreement with what one expects from the geometrical arrangement of the collimators and the small magnet which bends the proton beam into the exit hole in the concrete wall surrounding the 184-in. cyclotron. Moreover, a similar result follows from the study of the threshold range of the reaction $C^{12}(p,pn)C^{11}$ by Peterson, Aamodt, and Phillips[10] of this Laboratory.

From our analysis we derive that the mean range R_0 of the protons is 92.4 g/cm² Cu, which according to the table of Aron, *et al.*, corresponds to 337.2-Mev initial proton energy. It should be remarked, however, that Aron, *et al.*, used for copper the value of $I=333.5$ ev, whereas according to the present paper $I_{Cu}=279$ ev.[11]

V. ENERGY FOR ION PAIR PRODUCTION

The energy for ion pair production by the 340-Mev protons of the 184-in. cyclotron was measured for the gases hydrogen, helium, nitrogen, oxygen, neon, argon, and air. The gases were tank gases, for which we have the following information on their purities (percent by volume). For hydrogen: H_2, 99.771; N_2, 0.03; O_2, 0.025; CH_4 and hydrocarbons, 0.01; trace of H_2O. For He: He≥99.95; traces of N_2 and O_2. For nitrogen: N_2, 99.99; impurities, O_2, H_2O. For oxygen: O_2>99.5; impurities, H_2, N_2, A; H_2O, 0.08 mg/liter. For Ne: spectroscopic grade. For argon: A≥99.9; impurities, N_2, O_2, H_2. The proton beam was allowed to cross two identical ionization chambers. One was filled with argon at atmospheric pressure and served as a monitor. The other was successively filled with the gases to be investigated. In order to compare the results, corrections were made for differences in temperature and filling pressure. Saturation of the ionization current was checked in every case by operating at vastly different beam intensity. The energy loss per ion produced, w, follows from

$$W=\text{energy loss/number of ion pairs produced.}$$

In this relation the numerator is the rate of energy loss $(-dE/dx)$, which for the various gases is to be found in the tables of Aron;[2] the denominator is proportional to the ionization measured in the ionization chamber.

The second column of Table II lists the values of $(-dE/dx)$ used to derive from our measurements the values of w relative to argon, which is shown in column 3. Note that the value of w for air agrees with the one obtainable by calculation[12] from the w values for N_2 and O_2.

Recently Chamberlain, Segrè, and Wiegand measured the number of ion pairs produced by one 340-Mev proton crossing 1 cm of argon at atmospheric pressure and 0°C; this number is 166 and was obtained by combining the ionization measurement with an absolute current measurement by means of a Faraday cup. It agrees with results independently obtained by Peterson. This result is of practical importance because it can be used to measure beam currents in a simple way, avoiding the somewhat tedious use of a Faraday cage.

Combining the last number with the theoretical value of $(-dE/dx)$ for argon we find $w_A=25.55$ ev/ion pair. This allows the determination of w for the other gases. The result is shown in column 4 of Table II. For comparing we added in column 5 of Table II the values of w measured at low energy (Po = α-particles) by various recent authors. Our values of w need still a small correction because we have neglected the fact that part of the ionization is due to stars (nuclear collisions). An estimate of this correction based on the data of Bernardini, *et al.*[13] indicates that the true values of w are a few percent larger than shown in the table.

We wish to thank Dr. Karl Strauch and Mr. T. Thompson for their help during the measurements.

[10] Peterson, Aamodt, and Phillips, to be published.
[11] An entirely independent measurement of the energy of the beam and corresponding ranges using the properties of the Čerenkov radiation is being performed by Mather and Segrè.
[12] Huber, Baldinger, and Häberli, Helv. Phys. Acta **23**, 85 (1950).
[13] Bernardini, Booth, and Lindenbaum, Phys. Rev. **80**, 905 (1950).

90-Mev Neutron-Proton Scattering at Large Proton Angles*

ROGER WALLACE
Radiation Laboratory, Department of Physics, University of California, Berkeley, California
(Received October 13, 1950)

Neutron-proton scattering with 90-Mev neutrons has been investigated by others, using a proportional counter technique and also using a cloud chamber, and the scattering cross section for neutrons for center-of-mass angles from 36° to 180° has been measured. The present experiment was an attempt to overlap the data of Hadley, *et al.*, from 74° to 36° and to extend the cross-section measurements to smaller angles. This experiment was performed with nuclear emulsions in order to permit the detection of protons down to about 1.5 Mev, and to avoid systematic errors which might be present in the case of other methods of detection. The results agree with those of Hadley, *et al.*, within the probable error, and the cross-section curve exhibits beyond 36° the same general trend as does their curve.

I. INTRODUCTION

NEUTRON–PROTON scattering cross sections have been measured by several different investigators, using the 90-Mev neutrons from the 184-in. Berkeley cyclotron. Hadley, *et al.*,[1] used two different arrangements of proportional counters. Their points do not lie on a curve that is symmetrical about 90°. The present experiment was performed to find whether the cross section rises in the small angle region. It has been felt by some that the cross-section curve was perhaps flat beyond 70° and did not rise. The results of this experiment serve to confirm the rising slope of the curve in the small angle range, in agreement with Hadley *et al.* Brueckner, *et al.*,[2] using a cloud-chamber technique, have observed an angular dependence of the n–p cross section similar to that observed by Hadley and his coworkers. The results of the present experiment also agree well with the cloud-chamber data.

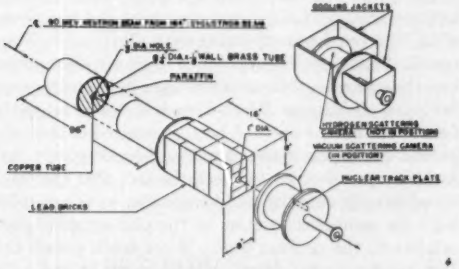

FIG. 1. Arrangement of the paraffin collimator and lead bricks in front of the scattering camera. The alternate cameras are shown. The vacuum camera is shown in bombardment position. The jacketed hydrogen chamber is shown at one side. The wood supports for the apparatus are not shown. Twelve nuclear track plates were arranged symmetrically around the beam at 30° intervals, of which one is indicated in the figure.

II. APPARATUS AND PROCEDURE

The main part of the apparatus consisted of a nuclear plate camera, similar in design to that used by Panofsky and Fillmore.[3] The camera and associated shielding (Fig. 1) were mounted on a support, aligned in the 90-Mev neutron beam of the 184-in. cyclotron, similar to the paraffin collimator mount used by Brueckner, *et al.*[2] The collimator was stopped down to a ½-in. diameter circle and additional lead bricks were added to reduce the background. The camera (Fig. 2) differed from that used by Panofsky and Fillmore[3] in that the plates were mounted farther from the beam and farther from each other. These dimensional changes were made since the neutron beam intensity of the cyclotron is much less than the proton beam intensity of the linear accelerator; thus it was necessary to include more beam area with a consequent relaxation of the geometrical precision of the experiment. At each end of the camera-scattering chamber there was a 0.005-in. duraluminum foil window. The cyclotron beam, collimated to ½ in. passed into and out of the camera through these foils. The exit foil was mounted on the end of a tube, as

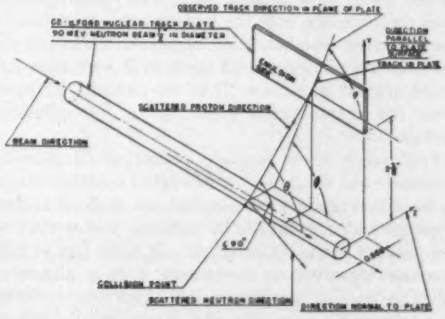

FIG. 2. Geometrical location of the nuclear track plates relative to the neutron beam. The variables used in the measurements and calculations are shown. All variables are in the laboratory system. The relations between the scattering angle θ and the observed angle ϕ are indicated.

* This paper is based on work performed under the auspices of the AEC.

[1] Hadley, Kelly, Leith, Segrè, Wiegand, and York, Phys. Rev. **75**, 351 (1949).

[2] Brueckner, Hartsough, Hayward, and Powell, Phys. Rev. **75**, 555 (1949).

[3] W. K. H. Panofsky and F. L. Fillmore, Phys. Rev. **79** 57 (1950).

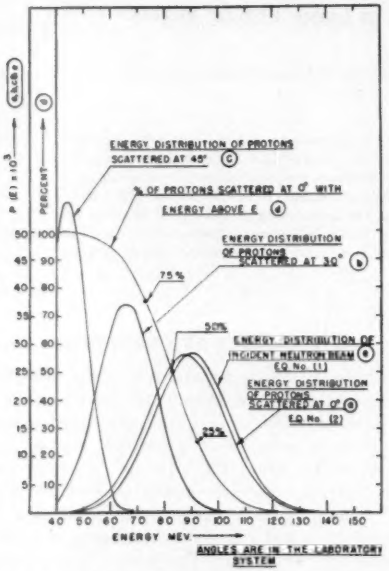
P (E) x 10³
PERCENT
ENERGY DISTRIBUTION OF PROTONS SCATTERED AT 45° (c)
% OF PROTONS SCATTERED AT 0° WITH ENERGY ABOVE E (d)
ENERGY DISTRIBUTION OF PROTONS SCATTERED AT 30° (b)
75%
50%
ENERGY DISTRIBUTION OF INCIDENT NEUTRON BEAM EQ No. (1) (e)
ENERGY DISTRIBUTION OF PROTONS SCATTERED AT 0° (a) EQ No. (2)
25%
ENERGY MEV
ANGLES ARE IN THE LABORATORY SYSTEM

FIG. 3. Functions dependent on the energy. Curves (*a*), (*b*), and (*c*) are the probability of a recoil proton being scattered at 0°, 30°, or 45° having a particular energy. It is seen that the absolute dispersion in energy decreases as the scattering angle increases. Curve (*d*) gives the percentage of the protons scattered at 0° with energy above a definite value *E*. This curve is secured directly from curve (*e*), the energy distribution of the "90-Mev" neutron beam from the 184-in. Berkeley cyclotron.

shown in Fig. 2, in order to reduce the background, on the plates, that might have come from particles scattered from the exit foil. Particles which might have been scattered from the entrance foil entered the plates at such an angle that tracks caused by them, when viewed under a microscope, were easily distinguished from those coming from the hydrogen gas contained in the scattering chamber, since the desired tracks and the foil scattered tracks entered the field of view from different angular directions. Thus the particles scattered from the entrance foil constitute a nonconfusable background.

Four point screw supports permitted the paraffin collimator and the camera to be aligned coaxially within $\frac{1}{16}$ in. The alignment was carried out with an optical telescope and was checked by exposing, during the first few minutes of the cyclotron run, an x-ray film located in a known position on the camera. A $\frac{1}{16}$-in. alignment tolerance does not introduce a first-order source of error since the plates were arranged symmetrically around the beam and the angular distribution data from all plates were combined. The plates were aligned in the camera by being held against a machined surface for which the geometric tolerance was less than 0.010 in.

Two identical cameras were constructed, one for hydrogen exposures, the other for vacuum-background exposures. The exposures from which the data were taken were made for 405 min at an average of 27½ R per hour for the hydrogen run, and 65 min at an average of 28 R per hour for the vacuum run. This made the hydrogen run 186 R and the neutron background run 30 R. This intensity (the R-unit is an arbitrary measure of intensity) corresponds to a neutron flux of approximately 10^6 neutrons/cm² sec.

The first few trial runs with hydrogen in the camera resulted in completely blackened plates. At first it was thought that the blackening was caused by impurities in the hydrogen gas, so the hydrogen was passed through a hot palladium leak, thus separating all other elements with the possible exception of a minute trace of helium. Since the blackening still occurred with this purified hydrogen it was concluded that the hydrogen itself must attack the emulsion. Webb[4] advised us later that it was possible that the photographic emulsions were fogged by pure hydrogen gas. The reason that Panofsky and Fillmore[3] did not experience this difficulty was that they used a lower hydrogen pressure than the two atmospheres used in this experiment, and somewhat shorter times during which the plates were exposed to the hydrogen. It was found that the blackening of the plates by the hydrogen was temperature sensitive, and that a reduction of temperature to −15° to −20°C would allow the plates to be only slightly fogged after 8 hours exposure. Consequently, a jacket filled with a eutectic mixture of rock salt and ice was installed, during the run, around the camera intended for hydrogen exposure. The plate temperature was thus maintained at about −15°C. Webb indicated that a reduction of the temperature to −15°C would probably not reduce the proton sensitivity of the plates.

The data were taken from the plates with a microscope, operating at 570×, scanning a swath 140 microns wide. The recoil proton tracks were identified by their specific ionization, their point of entrance dive angles into the emulsion, their azimuth angle in the microscope field, and their range. When a track seen to start in the field of the microscope had been recognized as that of a proton by its ionization density, the microscope was focused up and down to check the fact that the track dived into the emulsion at an angle that was compatible with the geometric location of the photographic plate relative to the neutron beam. If the track passed this test, the plate was moved until the point at which the track entered the emulsion was centered under the microscope reticule cross hairs. The cross hairs were then rotated until one was tangent to the track as near to the point of entry as possible. Panofsky and Fillmore[3] explain how this can be done with a minimum of setting error. The azimuth angle of the entry point was then measured with a goniometer attached to one of the microscope eyepieces. This azimuth angle was the only datum recorded for each track.

[4] J. Webb, Eastman Kodak Company, private communication.

The classical expression for the energy of the scattered protons varies as the cosine squared of the proton scattering angle. The incident neutron beam contains the distribution of energies given by Eq. (1), which will be discussed later. This distribution causes the protons that are scattered at any particular angle to also have an energy distribution. The energy distributions for proton recoil angles $\theta_L=0°$, 30°, and 45° in the laboratory system are shown in curves *a*, *b*, and *c* of Fig. 3. Curves of this general form give the emulsion range distributions and also the grain density distributions to be expected of the protons scattered at various angles.

Most spurious tracks were rejected on the basis of having the wrong ionization for their azimuth angle or because they were too short for their angle, although these rejection criteria did not need to be used on more than two percent of the otherwise acceptable tracks. Another reason for the rejection of tracks was that their dive angle into the emulsion was too steep for them to have been caused by protons coming from the beam cylinder. Tracks coming in the three other quadrants were easily eliminated, although their number was very limited. The scanning of vacuum background plates indicated that the confusable background was less than two percent.

Two observers examined 2734 tracks. Of these all proton recoils, 350 in number, observed in the 45° to 51° laboratory angle range were not included in the final results. These tracks were excluded since the specific ionization of tracks scattered at these angles, with energies of 35 to 50 Mev, is so low that an excessive number of tracks is missed by the observer. In addition, 157 tracks in the angular range of 79° to 85° in the laboratory system were not included in the final results since, as will be mentioned later, the correction factor for tracks that do not reach the plates is too large. The two observers read the same plate areas for 200 tracks and found that each missed above five percent of the tracks. The tracks missed were evenly distributed over all angles from 45° to 85° so this is a minor source of error.

The plates used were Ilford, type C-2, with 50-micron emulsions. They were developed for 30 min at 68°F in developer consisting of one part of D19 mixed with six parts of water.

III. TREATMENT OF DATA

The uncorrected data are shown in Fig. 4. The data are grouped into three-degree intervals in the laboratory system, so any corrections in the angular measurement that are small compared to three degrees will not be noticeable. The relativistic correction (Fig. 4, curve *a*) makes the observed laboratory scattering angle slightly smaller than the classical laboratory scattering angle.

The geometry of this experiment, although not nearly so precise as that of Panofsky and Fillmore,[3] did not make important corrections necessary. The tracks were observed in swaths 140 microns wide as the slides were moved under the microscope in a direction parallel to the x coordinate (Fig. 2). The swaths were all located, within ½ inch of the edges of the plates nearest the beam. The position of the particular swath, in which the microscope was working within the ½-in. wide band on the plates, was not recorded as part of the data. It must be pointed out that no attempt was made to determined from which part of the ½-in. diameter beam cylinder each individual track came, nor was any record kept of the point on the plates at which each particle struck the plates. Thus there is a rectangular distribution of the probability of a particle landing on a plate with a particular value of y. In addition the probability of a particle coming from a particular part of the cylindrical, uniform intensity beam is a sine distribution in z. These two distributions introduce a geometric uncertainty which must be included in a consideration of the precision of the results. The two probability distributions, one in y and one in z, must be combined by a folding process, which is really a

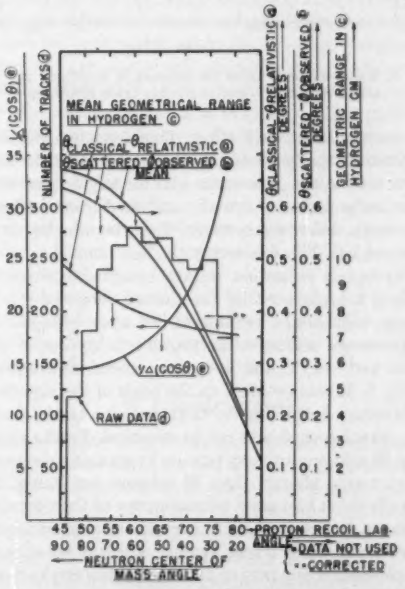
NUMBER OF TRACKS
MEAN GEOMETRICAL RANGE IN HYDROGEN
θ CLASSICAL
θ RELATIVISTIC
θ SCATTERED OBSERVED
MEAN
θ CLASSICAL - θ RELATIVISTIC DEGREES
θ SCATTERED - θ OBSERVED DEGREES
GEOMETRIC RANGE IN HYDROGEN CM
RAW DATA
45 50 55 60 65 70 75 80
90 80 70 60 50 40 30 20
PROTON RECOIL LAB. ANGLE
NEUTRON CENTER OF MASS ANGLE
DATA NOT USED
CORRECTED

FIG. 4. Functions depending on the laboratory angle at which the protons recoil. Curve (*a*) gives the difference between the classical recoil angle and the relativistic recoil angle. This correction is seen to be small. Curve (*b*) shows the mean correction made necessary by the geometry. Curve (*c*) gives the mean path distance through the hydrogen gas in the scattering chamber from the points of impact in the cylindrical beam region to the photographic plates. Curve (*d*) is a histogram of the raw data grouped in three-degree intervals. The data from 46° to 52° and from 79° to 82° were considered unreliable for reasons mentioned in the text. The data from 76° to 79° were corrected for limited proton range in the hydrogen and for small angle scattering in the gas and emulsion, as shown. Curve (*e*) is the multiplication factor for converting the laboratory coordinate data of curve (*d*) to the center of mass data of Fig. 8. The conversion factor is calculated for the same three-degree intervals into which the data are divided.

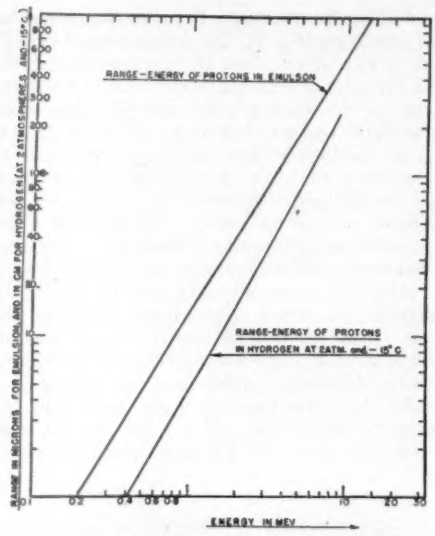
RANGE-ENERGY OF PROTONS IN EMULSION
RANGE-ENERGY OF PROTONS IN HYDROGEN AT 2 ATM. and -15° C
RANGE IN MICRONS FOR EMULSION AND IN CM FOR HYDROGEN (AT 2 ATMOSPHERES AND -15° C)
ENERGY IN MEV

FIG. 5. Range-energy curves for protons in hydrogen gas at 2 atmos and −15°C and in nuclear track emulsion.

two step random walk effect. Due consideration must be given to the geometrical relation between the angle ϕ observed in the microscope and the angle θ_L at which a particular proton is actually scattered from the beam. The mean difference between these two angles shown by curve *b* in Fig. 4 is seen to be less than $\frac{1}{2}°$.

The upper limitation on the observable scattering angle θ is introduced by the limited range of the low energy, high angle, protons in the hydrogen gas. The range-energy relations for protons in hydrogen at 2 atmos and −15°C and in nuclear emulsions are shown in Fig. 5. It was decided, on the basis of the experience of Panofsky and Fillmore,[5] that emulsion tracks shorter than 30 microns should not be recorded. Tracks shorter than 30 microns are easy to miss in scanning the plates. When tracks shorter than 30 microns are found, it is difficult to make a good measurement of their emulsion entrance angles, and there are also a large number of short background tracks against which it is tedious to discriminate if one tries to measure proton tracks shorter than 30 microns.

Since it was the purpose of this experiment to extend the cross section curve to smaller angles, it is important to investigate the limitations on the acceptability of the data in the range of small neutron scattering angles. There are four effects to be considered in deciding how far into the small angle region the data can be considered dependable. At about $\theta_L = 80°$ the energy of the scattered protons becomes so small that all of them do not have a long enough range in the hydrogen gas to allow them to strike the plates. Also, owing to their low energy, they experience appreciable amounts of small angle scattering in the hydrogen gas and in the photographic emulsions. This scattering introduces errors in the measurements of the scattering angles. Furthermore, in the region of 80°, as a result of the reduced proton energies as mentioned above, the ranges of the particles in the emulsions are in many cases too short to allow for accurate identification and measurement. The combined result of these four effects must be ascertained in order to evaluate the data properly.

The neutron beam produced by the bombardment of a $\frac{1}{2}$-in. beryllium target with 180-Mev deuterons is known to have a broad energy distribution. This distribution has been calculated by Serber,[6] and measured by Hadley, *et al.*[1] For energies above the maximum of the distribution curve the calculated and measured results agree, but the measured results are higher than the theoretical ones for energies below the maximum. For the purposes of this experiment it was assumed that the probability $P(E)$ of an incident neutron having the energy E in Mev has the form:

$$P(E) = K \exp\{-[(E-90)/20]^2\}. \qquad (1)$$

This relation, (Fig. 3, curve *e*), approximates the high energy distributions of both Serber[6] and Hadley, *et al.*, but only the measured values of Hadley, *et al.*, for energies less than 90 Mev. It was further assumed that the neutron-proton scattering cross section is inversely proportional to the energy in the energy range considered. Thus the neutron distribution that is effective in producing recoil protons is given by:

$$P'(E)_0 = K(1/E) \exp\{-[(E-90)/20]^2\} \qquad (2)$$

(Fig. 3, curve *a*). The integral of this curve gives the fraction of the recoil protons coming from that part of the beam for which the energy is below any given value,

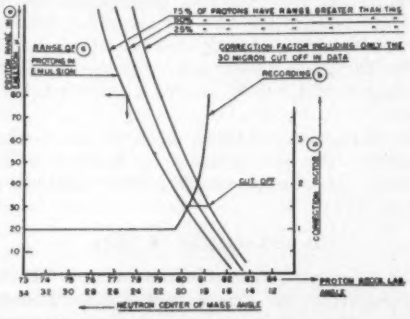
RANGE OF PROTONS IN EMULSION
CORRECTION FACTOR INCLUDING ONLY THE 30 MICRON CUT OFF IN DATA RECORDING
CUT OFF
CORRECTION FACTOR
PROTON RECOIL LAB. ANGLE
NEUTRON CENTER OF MASS ANGLE

FIG. 6. The experimental cutoff of tracks at the large proton angle limit is based on the three curves (*a*) of proton range in the emulsion for protons scattered at the angles shown, coming from the three positions on the beam energy distribution shown on curve (*d*), Fig. 3. The 30-micron cutoff shown above is explained in the text. Curve (*b*), the multiplicative correction factor that must be applied to the data as a result of the cutoff, is secured from the three curves (*a*) directly, and includes no correction for gas scattering.

[6] R. Serber, Phys. Rev. 72, 1007 (1947).

(Fig. 3, curve *d*). This relation will be used to calculate the fraction of the protons with energies too low to reach the plates at large scattering angles where the stopping power of the hydrogen is high. From the range-energy relations for protons, in hydrogen and emulsion (Fig. 5) the energy of the protons entering the emulsion coming from different energy regions of the beam can be calculated as a function of the laboratory proton scattering angle, θ_L. From these energies the ranges in the emulsion for the protons from different beam energy intervals can be plotted as a function of the angle (Fig. 6, curves *a*). Since no tracks shorter than 30 microns are to be considered, there will be a correction factor by which the track counts at various angles ϕ must be multiplied. The cutoff is shown crossing the three beam fraction curves. From the cut-off curve the initial correction curve is calculated (Fig. 6, curve *b*). This correction does not include the effects of gas and emulsion scattering.

In reality the correction factor has a very small influence on the final cross-section curve. The data that go into the single point for neutrons at 26° in the center-of-mass system are 71, 57, and 46 tracks at proton angles, $\theta_L = 76°$, 77°, and 78° respectively. When the correction factor is applied, the data are changed to 71, 62, and 62, respectively. This application of the cut-off correction factor raises the point at the center-of-mass angle of 26° by about 11 percent.

The corrected track counts, grouped in three-degree intervals, as a function of proton laboratory angle (Table I, column 4) were converted to numbers proportional to the n–p scattering cross section as a function of the neutron center-of-mass angles by the relation:

$$(d\sigma/d\omega)_{c.o.m} = \text{const.} N(\phi)_{\Delta\theta}[(z^2+y^2)/z](1/\Delta(\cos\theta_{c.o.m.})), \quad (3)$$

where $N(\phi)_{\Delta\theta}$ is the data divided by true scattering angles θ instead of observed angles ϕ. Actually the difference between these angles (Fig. 4, curve *b*) is such a slowly varying function of the angle that the correction for it was not applied. The geometrical factor $(z^2+y^2)/z$ is independent of the scattering angle. As a result of the geometrical parameters, when the two $\frac{1}{2}$-in. geometrical tolerances are combined properly, they produce a probable error of 1.54 in. in the geometrical factor, $(z^2+y^2)/z$, whose mean value is 13.12 in. This probable error only introduces a very small error into the relative cross section data which is combined with the statistical error and listed in Table I, column 7. The values of the $\Delta(\cos\theta)_{cm}$ factor of Eq. (3) for transformation from laboratory to center-of-mass angles are shown in Table I, column 5. The corrected data divided by these and multiplied by a factor to normalize the results to the absolute cross sections of Hadley *et al.*,[1] are given in Table I, column 6, and plotted with probable errors in Fig. 7, in combination with the points measured by Hadley, *et al.*

TABLE I. Data on the recoil proton tracks.

1 Proton laboratory angle range	2 No. of tracks observed	3 Mean neutron cm angle	4 No. of tracks corrected	5 $\Delta(\cos\theta)_{cm}$ transformation factor	6 $\left(\frac{d\sigma}{d\omega}\right)_{cm}$ in 10^{-27} cm^2	7 Combined probable error
46–48	114	86	114	0.06963		
49–51	181	80	181	0.06874		
52–54	241	74	241	0.06710	4.28	0.19
55–57	260	68	260	0.06472	4.80	0.20
58–60	280	62	280	0.06163	5.42	0.22
61–63	266	56	266	0.05787	5.48	0.22
64–66	270	50	270	0.05347	6.02	0.24
67–69	248	44	248	0.04848	6.11	0.26
70–72	240	38	240	0.04298	6.77	0.29
73–75	248	32	248	0.03699	8.01	0.34
76–78	174	26	195	0.03060	7.60	0.39
79–81	120	20				
82–84	32	14				

Total—2734 tracks observed

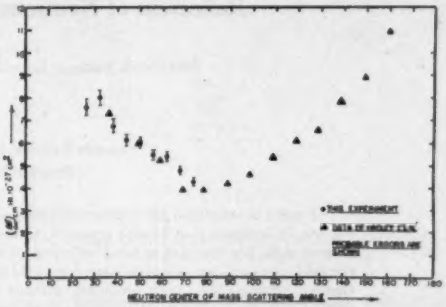

FIG. 7. The final corrected data are shown by the circles above. The results of Hadley, *et al.* (reference 1), are shown by the triangles. It is seen that the slopes of the results of the two experiments agree between 36° and 60°.

IV. CONCLUSIONS

The n–p scattering cross section can be measured with the nuclear emulsion method for 90-Mev neutrons between neutron angles in the center-of-mass system of approximately 26° to 80°. In general the results agree with those secured by Hadley, *et al.*, with counters. The slopes of the curves agree between 36° and 60°. The results of this experiment confirm the increasing slope of the cross-section curve in the small angle region; however, the asymmetry of the curve about 90° is based on the Hadley data since the curve from this experiment is normalized to the Hadley results.

The author wishes to express his appreciation to Keith Brueckner who aided in the design of the apparatus, to Jack Steller who helped with the runs and microscope reading, and to Professor W. K. H. Panofsky, under whose direction the work was carried out.

Reflection of Neutrons from Magnetized Mirrors*

D. J. HUGHES
Brookhaven National Laboratory, Upton, Long Island, New York

AND

M. T. BURGY
Argonne National Laboratory, Chicago, Illinois

(Received September 25, 1950)

The index of refraction for neutrons in ferromagnetic materials has been studied by total reflection from mirrors. It is shown that Bloch's constant, C, is unity; i.e., that the effective field for neutrons in a ferromagnet is **B**. For the case of total reflection, it is found that the magnetic part of the index is given by the field averaged over a region large compared to the size of the magnetic domains. Completely polarized thermal neutrons have been produced, without the necessity of monochromatization, by reflection from magnetized cobalt. Measurement of the polarization, performed by reflection at a second cobalt mirror, requires careful elimination of reorientation effects in the region between the mirrors.

I. INTRODUCTION

THE neutron reflection experiments reported here are an outgrowth of the study of magnetic refraction of neutrons at domain boundaries already described by Hughes, Burgy, Heller, and Wallace.[1] The small angle deviations observed by them when neutrons were transmitted through unmagnetized iron were explained in terms of the variation of the index of refraction from domain to domain, which variation is caused by changes in the direction of magnetization. It was felt that the multiple refraction of neutrons in iron could be exhibited in a much more striking way by utilizing critical reflection from mirrors, a technique already used by Fermi and Zinn,[2] and Fermi and Marshall.[3] For each index of refraction there should be a corresponding critical angle which could be measured rather accurately. Because of the variation of critical angle with neutron spin orientation, the neutrons reflected from a magnetized mirror should be partly polarized;[1,4,5] and an additional purpose of the mirror experiments was to investigate the feasibility of reflection as a means of production of polarized neutrons.

After the experiments were begun, several theoretical papers[6,7] appeared concerning reflection from magnetized mirrors, and it became clear that the experimental methods in use were valuable for elucidating some of the fundamental features of the neutron-electron magnetic interaction. Additional ramifications developed when the correctness of the fundamental equation then in use for the index of refraction was questioned by Ekstein.[8] As a result of the theoretical uncertainties, the experiments were extended in scope until all the doubtful points could be resolved experimentally. In the present report the theory will be outlined briefly and the experimental results presented in some detail.[8a]

II. NEUTRON REFLECTION THEORY

The index of refraction for neutrons, and hence the critical angle, depends only on the average potential which the neutron experiences in a medium and is independent of molecular and crystalline structure. For a mirror of a single element with small neutron absorption the index of refraction, n, and the critical glancing angle θ_c, are given by:

$$n^2 = 1 - \lambda^2 N a/\pi \tag{1}$$

$$\theta_c = \lambda(Na/\pi)^{\frac{1}{2}}. \tag{2}$$

Here λ is the neutron wavelength, N is the density of nuclei, and a is the average coherent scattering amplitude. The variation of scattering amplitude from nucleus to nucleus, which may be caused by the presence of isotopes of different scattering amplitude, or of spin-dependent scattering, will produce a slight diffuse scattering and will have essentially no effect on the critical angle. The sign convention is such that a positive value of a corresponds to a phase shift of 180°, an index less than unity, and the occurrence of total reflection. It is noteworthy that θ_c depends on the coherent amplitude in a very direct way, there being no corrections for form factors, temperature diffuse scattering or crystal effects. As pointed out by Hamermesh,[6,9] this simplicity, which follows from the fact that the scattering is essentially forward, implies that the measurement of critical angles is a method of obtaining accurate coherent amplitudes in such important cases as n-p scattering[10] and the neutron-electron spin-independent interaction.

* Research carried out under contract with AEC.

[1] Hughes, Burgy, Heller, and Wallace, Phys. Rev. **75**, 565 (1949).

[2] E. Fermi and W. Zinn, Phys. Rev. **70**, 103 (1946).

[3] E. Fermi and L. Marshall, Phys. Rev. **71**, 666 (1947).

[4] A. Achieser and J. Pomeranchuck, J. Exper. Theor. Phys. U.S.S.R. **18**, 475 (1948).

[5] O. Halpern, Phys. Rev. **75**, 343 (1949).

[6] M. Hamermesh, Argonne Laboratory Report ANL 4298 (May, 1949).

[7] O. Halpern, Phys. Rev. **76**, 1130 (1949).

[8] H. Ekstein, Phys. Rev. **76**, 1328 (1949); **78**, 731 (1950).

[8a] A preliminary account of some of the results has already been given in Phys. Rev. **76**, 1413 (1949).

[9] M. Hamermesh, Phys. Rev. **77**, 140 (1950).

[10] Hughes, Burgy, and Ringo, Phys. Rev. **77**, 291 (1950).

For the case of a material containing several elements the correct coherent amplitude is simply the average value, due account being taken of the algebraic sign of the individual coherent amplitudes. For a ferromagnetic material, the question of the correct coherent amplitude becomes very difficult to answer and has been the source of divergent opinions during the course of these experiments. The viewpoint adopted in the paper of Hughes, Burgy, Heller, and Wallace[1] was that the neutrons in a domain (in which the magnetic induction always has the saturated value, $\mathbf{B}_s$) experience a two-valued potential, $\pm\mu B_s$. It follows that there are just two distinct indices of refraction for neutrons in iron, whether the iron is magnetized or not in the macroscopic sense

$$n^2=1-\lambda^2 Na/\pi\pm\mu B/E, \qquad (3)$$

where E is the neutron energy.

The index of refraction as given in Eq. (3) had been obtained by Halpern, Hamermesh, and Johnson[11] for the special case of neutron propagation direction perpendicular to $\mathbf{B}_s$. Achieser and Pomeranchuck[4] derived the same formula, under the assumption that the neutron wavelength was greater than the lattice spacing (no Bragg reflections), but with no specific orientation of neutron direction relative to $\mathbf{B}_s$. Hamermesh[6] extended the treatment of Halpern, *et al.*[11] and found an index containing a term depending on the angle between the direction of neutron motion and $\mathbf{B}_s$. Ekstein[8] and Halpern,[7] however, concluded that there are only two indices as given in Eq. (3), regardless of the orientation of $\mathbf{B}$ and of wavelength. In view of these differences in results it was quite desirable to obtain experimental data on the index in magnetized iron as a function of magnetization direction.

In addition to the possible variation of index with magnetization direction, there was an uncertainty concerning the form of the neutron-electron magnetic interaction. The original form of the neutron-electron magnetic interaction used by Bloch[12] (dipole-dipole) in his discussion of magnetic scattering leads to a different angular distribution of scattered neutrons than the Dirac interaction used by Schwinger[13] and Halpern, *et al.*[11] Ekstein[8] showed that the different forms of interaction, when applied to the case of refraction, resulted in a simple interpretation: the Dirac interaction led to Eq. (3), whereas the Bloch interaction led to the same formula with $\mathbf{B}$ replaced by $\mathbf{H}$. An experimental verification of Eq. (3) by means of a measurement of the critical angle would thus demonstrate that the field affecting the neutron in its passage through iron is $\mathbf{B}$ rather than $\mathbf{H}$.

In order to produce polarized neutrons by reflection from magnetized iron, it would be necessary to use an angle of incidence which is greater than the critical angle for one spin state, for which the reflectivity is practically zero, and less than the critical angle for the other spin state. Because the critical angles depend on wavelength it would be necessary also to use monoenergetic neutrons to prevent overlapping of the critical angles. Hamermesh[9] suggested that all wavelengths might be used, however, if the mirror should be made of cobalt instead of iron. The magnetic term in Eq. (3) for cobalt is larger than the nuclear term so one index will be less than, and the other greater than, unity for all wavelengths. The neutrons for which the index is greater than unity will reflect to a negligible amount while the others will reflect totally and hence will be completely polarized.

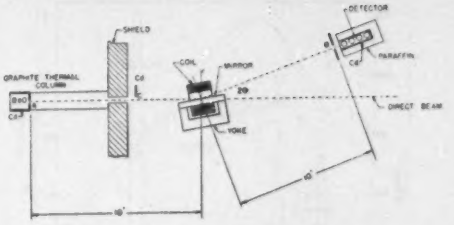

FIG. 1. Plan view of apparatus for reflection of neutrons from magnetized mirrors.

III. EXPERIMENTAL METHOD

Slow neutrons, from the thermal column of the Argonne deuterium-moderated pile, were used for the mirror experiments in the manner shown in Fig. 1. Because of the dependence of the critical angle on the wavelength as well as the amplitude a, the most direct method of measurement of a would consist of a determination of the critical angle for monochromatic neutrons. However, selection of monochromatic neutrons from the thermal column beam, as by Bragg reflection at a single crystal, involves a great loss in intensity. The BeO filter of Fig. 1 was chosen instead of a monochromator to obtain higher intensity. The scattering of polycrystalline BeO is exceedingly small for neutrons of wavelength greater than 4.4A (twice the largest lattice spacing in BeO) hence a block of BeO surrounded by Cd, as shown in Fig. 1, acts as a neutron filter. The neutrons of wavelength less than 4.4A are scattered in the block and captured by Cd while those of longer wavelength are transmitted almost completely. Although a monoenergetic beam is not obtained by this method, a distribution with high intensity and an exceedingly sharp cutoff on the short wavelength side results. The combination of sharp cut-off wavelength and high intensity is especially desirable for the determination of critical angles.

The filtered neutrons strike the mirror, usually 4 in. high by 10 in. in length, and are detected by a set of enriched BF_3 proportional counters connected in paral-

[11] Halpern, Hamermesh, and Johnson, Phys. Rev. **59**, 981 (1941).
[12] F. Bloch, Phys. Rev. **50**, 259 (1936); **51**, 994 (1937).
[13] J. Schwinger, Phys. Rev. **51**, 544 (1937).

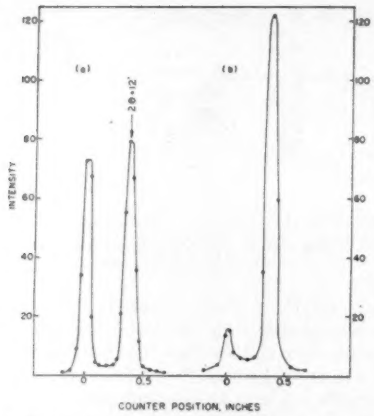

FIG. 2. Neutron beams observed with the apparatus of Fig. 1. The mirror intercepts about half the incident beam in (a) and almost the entire beam in (b). The direct beam is at the zero counter position while the reflected beam is at a position corresponding to a mirror angle, θ, of 6 minutes.

lel, which are placed in a shield of cadmium surrounded by paraffin (this shielding arrangement being effective for the fast neutron background). The collimating slits at A and B are 0.1 in. wide and 4 in. high while the width of the mirror normal to the beam is also 0.1 in. at an incident angle of 30 minutes. As 0.1 in. subtends an angle of 3 minutes as a distance of 10 ft there will be a spread in incident angles of about 3 minutes for a particular setting of the mirror. The result of the angular spread is that the sharp drop in intensity which would occur at the critical angle for monochromatic neutrons is smoothed out over a range of several minutes.

The incident angle, θ, is measured in terms of the angle, 2θ, between the reflected and the direct beam. The direct beam is located by moving the mirror sidewise slightly so that some of the incident neutrons miss the mirror and are detected by the counter with the counter in the position marked "direct beam" in Fig. 1. The counter and the slit B are mounted together on a platform, which is moved by a calibrated screw, and the distance between the direct and the reflected beam can be measured accurately enough so that θ can be determined to about 0.1 minute. Examples of the direct and reflected beams are shown in Fig. 2, for a case (a) in which the direct beam is about equal in intensity to the reflected beam and (b) in which the mirror is moved to reduce the direct beam and to increase the reflected beam. It was found to be simpler to line up the mirrors and counters and to measure the incident angles by use of the neutron beams than by use of auxiliary optical methods. The counting rates, shown on an arbitrary scale in Fig. 2, are actually of the order of several thousand counts per minute.

The intensity of the reflected beam is measured as θ is increased by moving the detector so as to keep it at an angle of 2θ to the direct beam. The intensity measured in this way will at first increase linearly with θ, because the mirror intercepts more of the incident beam as θ increases, and the reflectivity is complete provided θ is less than θ_c, the critical angle for 4.4A. After θ_c is passed the intensity will drop as neutrons of wavelength greater than 4.4A are successively eliminated from the reflected beam. The intensity will actually decrease as θ^{-3} because the wavelength distribution at low velocity, as seen by an opaque ("black") detector is proportional to λ^{-3}, its integral (the mirror reflects everything from λ_c to ∞) to λ^{-4}, or θ^{-4} [Eq. (1)], and the recorded intensity, finally, to θ^{-3}, as the factor, θ, for the increase in beam intercepted is included.

The intensity expected from the previous description is shown by the "ideal" solid line of Fig. 3, which is calculated for a Be mirror with θ_c taken to be 25.8 min. As already mentioned, the actual intensity curve will be rounded off because of the finite resolution in angle (about ± 1.5 minutes), and this effect can easily be calculated by graphical integration of a series of slightly displaced ideal intensity curves. Another refinement in the calculated curve is necessitated by the fact that the reflectivity[14] above the critical angle does not go to zero immediately but rather decreases as

$$R=\left[\frac{1-(1-\theta_c^2/\theta^2)^{\frac{1}{2}}}{1+(1-\theta_c^2/\theta^2)^{\frac{1}{2}}}\right]^2. \tag{4}$$

The dotted curve of Fig. 3 is the result of correction of the ideal curve for both the finite resolution and the finite reflectivity effects. It is seen that the sharp peak at the critical angle disappears but that it should nevertheless be a simple matter to correlate an observed intensity curve with the appropriate critical angle.

The experimental points of Fig. 3 are those obtained for a Be mirror during some exploratory runs. The

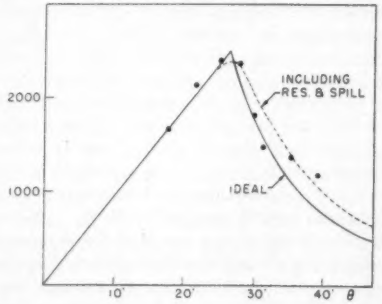

FIG. 3. Intensity of filtered neutrons reflected from a Be mirror as a function of incident angle, θ. The solid line is a theoretical curve for infinite resolution and zero reflectivity above the critical angle, while the dashed curve includes corrections for finite resolution and partial reflectivity above the critical angle ("spillover").

[14] M. L. Goldberger and F. Seitz, Phys. Rev. 71, 294 (1947).

mirror which was plane to better than half a fringe (NaD line) per inch when measured with an optical flat, was made in the machine and optical shops of the Argonne Laboratory. The dotted curve, with $\theta_c = 25.8$ min, was calculated for an amplitude of 2.42×10^{-13} cm to correspond with a scattering cross section ("free atom" value, measured at a neutron energy of several electron volts) for Be of 6.0 barns. In the calculation, the assumption was made that the 6.0 barn cross section was entirely coherent and hence that the coherent amplitude, a, could be obtained from the relation $\sigma_b = 4\pi a^2$ where σ_b is the bound atom cross section $[\sigma_b = 6 \times (10/9)^2 = 7.2$ barns$]$. The agreement between the calculated curve and the point supports the correctness of the calculated intensity curve and the supposition that the scattering in Be is largely coherent. Of course, only spin dependent scattering could invalidate this supposition, for Be has no isotopes (no isotope disorder scattering), and inelastic scattering does not affect mirror reflection (because of unit form factor as already discussed). The results for Be show that the method described is a reliable one for critical angle and coherent amplitude measurements. Because of the preliminary nature of the experiments at the time, no effort was made to obtain careful quantitative results for the Be mirror.

The absolute reflectivity for the Be mirror for angles less than critical was also measured by comparing the reflected beam intensity with that of the direct beam, using a collimating slit at C (Fig. 1) small enough so that the whole mirror was not illuminated with neutrons. The intensity of the reflected beam was found to be within three percent of the direct beam intensity, where the latter intensity was measured with the mirror moved out of the beam.

IV. CRITICAL ANGLE MEASUREMENTS WITH IRON AND COBALT MIRRORS

As the results with the beryllium mirror had shown that the method of critical angle measurements using BeO filtered neutrons was satisfactory, the more complicated case of neutron reflection from iron was next studied. Corresponding to the two indices of refraction of Eq. (3) for neutrons in iron there will be two critical angles,

$$\theta_c = \left[\frac{\lambda^2 \mathrm{Na}}{\pi} \pm \frac{\mu(H + 4\pi CI)}{E} f(\phi)\right]^{\frac{1}{2}}. \qquad (5)$$

Equation (5) is written in the most general way, to include all of the theoretical uncertainties already mentioned which were to be investigated experimentally. The constant C (called "Bloch's constant" by Ekstein[8]) would be zero for the dipole-dipole neutron-electron interaction first used by Bloch,[12] and unity for the Dirac formulation used by the later theorists.[11, 13] The function $f(\phi)$ is that of Hamermesh,[8] which function causes the critical angle to depend on the angle, ϕ,

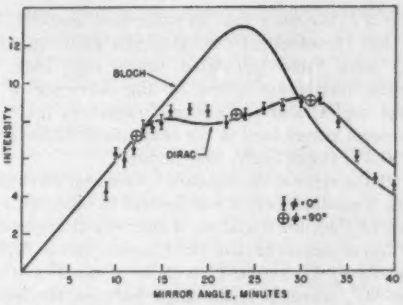

FIG. 4. Intensity of filtered neutrons reflected from a magnetized iron mirror. The theoretical curve labeled "Bloch" corresponds to Bloch's constant, C equal to zero, while "Dirac" corresponds to $C = 1$. Experimental points for two directions of magnetization, $\phi = 0°$ and 90°, are shown.

between the neutron propagation direction and the magnetic field, in a way which will not be described in detail. All of the theorists considered mainly the practical case in which the magnetization is in the plane of the mirror, with the somewhat artificial assumption that the field in the region outside the mirror is zero.

The first measurements with magnetized iron mirrors were designed to demonstrate the doubly refracting nature of iron and to determine Bloch's constant, C. The apparatus was as shown in Fig. 1 and as can be seen in that figure, the angle ϕ was essentially zero (to eliminate any effect of $f(\phi)$ which is unity for $\phi = 0$). Under these conditions it is seen that if $C = 0$ there will be no magnetic term, as **H** is continuous across the boundary, and only a single critical angle, corresponding to the nuclear scattering alone, should result. On the other hand, if $C = 1$ there should be two well separated values of θ_c, because the field discontinuity at the boundary is $4\pi I$ (or essentially **B**, because of the small value of **H**).

The results of the experimental determination of Bloch's constant are seen in Fig. 4. The solid lines are the intensity distributions expected for $C = 0$ (labeled "Bloch") and $C = 1$ ("Dirac"), assuming a nuclear amplitude based on a coherent scattering cross section[15] of 10.3 and a B of 22,500 gauss. The curves have been corrected for "spill-over" (finite reflectivity above the critical angle) and angular resolution. The $C = 1$ curve starts to drop as the lower critical angle is passed because neutrons of one spin orientation begin to disappear from the reflected beam, then rises as the mirror angle is increased and finally drops again after the mirror angle exceeds critical for the other spin orientation. The points agree quite well with the $C = 1$ curve, thus proving that the Dirac interaction is correct and that the effective field in the iron is **B** rather than **H**. The present results do not constitute a precise determi-

[15] C. Shull and E. Wollan, private communication.

nation of C but show that its value is at least 0.9. The fact that the observed critical angles agree quantitatively with those calculated shows that both the magnetic interaction (given by the difference of the critical angles) and the nuclear interaction (given by their mean value) used in the calculation, 22,500 gauss and 10.3 b, respectively, were correct.†

With the value of the constant C definitely established by the work described, it was decided to investigate the reality of $f(\phi)$, the variation of the critical angles with direction of magnetization. The function $f(\phi)$, as derived originally by Hamermesh,[6] is unity at $\phi=0°$ and zero at $\phi-90°$, where ϕ is the angle between the field $\mathbf{B}$ (assumed in the plane of the mirror) and the direction of motion of the neutrons. For $\phi=0°$ the expected intensity curve is the same as the one marked "Dirac" in Fig. 4 and hence $f(\phi)$ is in agreement with the experimental results for $\phi=0°$. For $\phi=90°$, however, the $f(\phi)$ function leads to a single critical angle, thus a curve identical with the one labeled "$C''=0''$ in Fig. 4, which is the curve expected for the nuclear scattering alone.

The study of the angular dependence was made essentially as shown in Fig. 1, with the mirror now 4×4 in. in size, and the coil moved back on the iron yoke so that the mirror and yoke could be rotated 90° about a horizontal line perpendicular to the neutron direction. With this arrangement, a few points were run with $\phi=0°$ to check the curve already obtained, then three points were run carefully with $\phi=90°$. The 90° results, shown on Fig. 4 fall exactly on the 0° line and thus indicate that there is no variation of the critical angle with ϕ. The finding that the critical angle, and hence the index of refraction, has only two constant values, is in agreement with the results of Ekstein.[8] Ekstein has recently shown (second paper of reference 8) that the $f(\phi)$ function arises from an ambiguity in the usual expression for the scattered wave function in the limit of forward scattering. The correct form of Eq. (5) is finally seen to be:

$$\theta_c=\left[\frac{\lambda^2 \mathrm{Na}}{\pi}\pm\frac{\mu B_s}{E}\right]^{\frac{1}{2}}. \tag{6}$$

Strictly speaking, $\mathbf{B}_s-\mathbf{H}$ should be used rather than $\mathbf{B}$ because of the continuity of $\mathbf{H}$ across the boundary (fields parallel to surface), but $\mathbf{H}$ is usually negligible compared to $\mathbf{B}_s$.

Before Eq. (6) was established some results had been obtained which seemed at the time to lend support to the idea that θ_c varied with direction of magnetization. The results concerned the reflected neutron intensity at a fixed incident angle as a function of current in the magnetizing coil. For these measurements the BeO filter was not used and the entire Maxwell velocity distribution was incident on the mirror. In general, without a filter, only those neutrons of wavelength greater than the limiting wavelength value given by Eq. (2) will reflect from a mirror. The particular value of θ used will of course determine two limiting wavelengths for a magnetized mirror, one for each neutron spin state, and these wavelengths will be given by Eq. (6) which can be rewritten as

$$\lambda=\theta_c\left[\frac{\mathrm{Na}}{\pi}\pm\frac{2m\mu B_s}{h^2}\right]^{\frac{1}{2}}. \tag{7}$$

Because of the larger range of reflected wavelengths, there will be more neutrons of the spin state corresponding to the shorter limiting wavelength than for the other spin state. If Eq. (6) is correct for an unmagnetized as well as for a magnetized mirror (the individual domains of both of course are magnetized to saturation) then one might expect the same two limiting wavelengths as for a magnetized mirror. It would then follow the reflected intensity would be independent of the state of magnetization of the mirror.

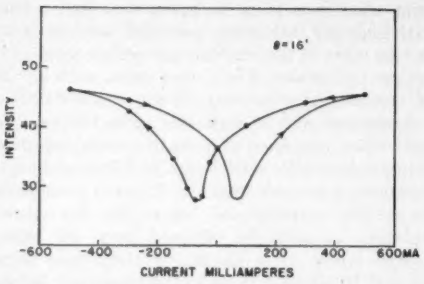

FIG. 5. Intensity of unfiltered neutrons reflected from a cobalt mirror as a function of magnetization.

Equation (6) was checked as a function of magnetization by measuring the intensity of unfiltered neutrons reflected from a cobalt mirror at a fixed incident angle while the mirror magnetization was carried through a complete cycle by varying the magnetizing current. Cobalt was used instead of iron because, as will be shown later, the ratio of magnetic to nuclear scattering is larger than for iron. The results for an incident angle of 16 min are given in Fig. 5. They show that the reflected intensity is certainly not constant, and instead is a function of magnetization as is evidenced by the hysteresis-like form of the curve. It is thus clear that the limiting wavelength (which determines the intensity) for a certain incident angle varies with magnetization. Such behavior was thought at the time to support the $f(\phi)$ function because the variation of ϕ with magnetization would cause a variation in the limiting wavelength. However, after the investigations for $\phi=0°$ and 90° had shown no change of critical angle

† *Note added in proof:* Hamermesh and Eisner, Phys. Rev. **79**, 888 (1950), have pointed out that the data of Fig. 4 also show directly that the neutron spin is 1/2. The results constitute the equivalent of a Stern-Gerlach experiment for the neutron as a spin of 3/2 would have resulted in four values of the index of refraction rather than the two observed.

with magnetization it was necessary to seek some other explanation of the intensity results of Fig. 5.

The measurements of Fig. 4 has shown that Eq. (6) was certainly correct for a mirror magnetized to saturation, and those of Fig. 5 just as certainly that the critical angle for an unsaturated mirror varied with magnetization. Snyder[16] suggested that if the neutron scattering is coherent over an appreciable number of domains (even though the domain size is approximately 10^{-3} cm and the neutron wavelength about 10^{-8} cm) then the field to be used in Eq. (6) is the average **B** which could be anything from zero to the saturated value. As the magnetic small angle scattering results of Hughes, Burgy, Heller, and Wallace[1] had shown that when neutrons are transmitted through unmagnetized iron each domain has its discrete index of refraction, it had been expected that individual domains on the mirror surface would have discrete critical angles, hence constant limiting wavelengths. The suggestion that the average field was effective in determining the critical

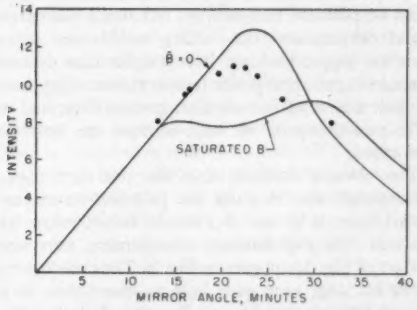

FIG. 6. Intensity of filtered neutrons reflected from an unmagnetized iron mirror as a function of incident angle, θ. The curves are the expected intensities for two values of the effective magnetic field in the iron.

angle furnished a qualitative explanation of the intensity changes of Fig. 5 which did not necessitate invoking $f(\phi)$, and hence was consistent with Eq. (6).

In order to check Snyder's suggestion, the effect of the average field on the critical angle was determined from an intensity curve of the type of Fig. 3, using the BeO filter for an unmagnetized iron mirror. The results, shown in Fig. 6 are distinctly different from those for the $\phi=0°$ and 90° magnetized cases and hence cannot be considered as a result of random values of ϕ. Comparing Fig. 6 with Fig. 4, one sees that the points have moved toward the curve expected for $\mathbf{B}=0$ but are in a position to indicate a finite value of **B**, less than the saturated value. It thus seems certain that the coherent averaging of scattering amplitude over domains takes place but that the averaging does not result in an exactly zero effective field. The failure to reach exact zero field may be caused by incomplete demagnetization, although the mirror was carefully demagnetized by reversing the current as its value decreased. It is also possible that the coherent averaging does not extend over a sufficient number of domains to produce a zero average.

Some complex intensity *vs* magnetizing current curves were obtained with the cobalt mirror at a small incident angle, results which were puzzling for a time. The curve shown in Fig. 7, for example, obtained with unfiltered neutrons incident at an angle of 6′, is very similar to that of Fig. 5 with the exception of the sudden rise in intensity where the field **B** is expected to be small. These intensity changes can be explained in terms of the averaging process, keeping in mind the fact that the magnetic scattering in cobalt is larger than the nuclear scattering. When the cobalt is saturated, only half the neutrons, those in one spin state, will reflect as the others have an index greater than unity. As the average **B** is reduced the limiting wavelength for the particular incident angle used will increase [Eq. (7) with the negative sign] and the intensity therefore will decrease. At a certain value of the average **B**, however, the previously nonreflecting neutrons [positive sign in Eq. (7)] will begin to reflect, the long wavelengths first, as their index drops below unity. As the field is reduced further the two limiting wavelengths will approach each other and the reflected intensity will change in a manner that depends on the shape of the neutron distribution in the neighborhood of the limiting wavelengths. If the shorter wavelength is initially at a part of the distribution where there are few neutrons (extremely short wavelength), then neutrons of the other spin state will increase rapidly in intensity as the corresponding limiting wavelength, initially very long, approaches the wavelength of maximum intensity in the neutron distribution. The two limiting wavelengths will coincide when the average **B** is zero, and the intensity changes will then repeat in reverse order as the mirror is magnetized in the reverse direction. This explanation of the complex intensity curve of Fig. 7 requires that the initial value of the limiting wavelength be quite small, which object is attained by use of the small incident angle of 6 min. The curve of Fig. 5 has a much simpler shape because of the

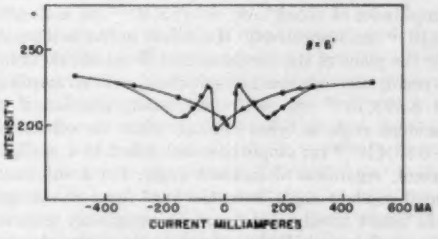

FIG. 7. Intensity curves similar to those of Fig. 5 but for a smaller value of θ.

[16] H. S. Snyder, private communication.

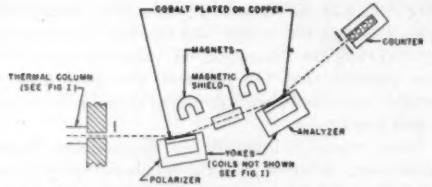

FIG. 8. Apparatus for the production of complete neutron polarization, and for measurement of polarization by the double reflection effect.

longer limiting wavelength, corresponding to the incident angle of 16 min which was used in that case.

All the measurements described thus far supported a simple interpretation of reflection of neutrons from magnetic mirrors.

(1) Equation (6) gives the correct values for the critical angles, in other words, Bloch's constant is unity and there is no angular dependence, $f(\phi)$.

(2) The value of **B** in Eq. (6) is the average over a region at least as large as several domains (domain size $\sim 10^{-3}$ cm). In addition, the results of Fig. 7 made it seem possible that mirror reflection from cobalt could be used to obtain completely polarized neutrons without monochromatization, as suggested by Hamermesh.[9] The neutrons reflected from an iron mirror without monochromatization are of course partially polarized because a larger range of wavelengths of one spin state are reflected than of the other. The polarization of the beam reflected from iron, for an incident Maxwell distribution, increases to an asymptotic value of about 90 percent as the incident angle is increased. On the other hand, the polarization would be 100 percent (neglecting spill-over) for monochromatic neutrons incident on an iron mirror at an angle between the two critical angles of Eq. (6). With saturated cobalt, of course, only one spin state reflects, regardless of wavelength (neglecting the small reflectivity for the index greater than unity), and the polarization should be complete without the loss of intensity involved in monochromatization.

V. NEUTRON POLARIZATION BY REFLECTION FROM COBALT

The nuclear and the saturated magnetic scattering amplitudes of cobalt[6] are $+3.78\times10^{-13}$ cm and $\pm4.61\times10^{-13}$ cm, respectively. If a cobalt mirror is saturated (in the plane of the mirror so that **B** outside the mirror is small) then one neutron spin state, with an amplitude of 8.39×10^{-13} cm, will show total reflection if the incident angle is below critical, while the other, with -0.83×10^{-13} cm amplitude, will reflect to a negligible extent, regardless of incident angle. For a sufficiently small incident angle, even the very short wavelengths will reflect totally and hence be completely polarized after reflection. If the mirror is unsaturated, as is quite likely because of the difficulty of saturating polycrystalline cobalt, then the average **B** will be effective, and the magnetic amplitude correspondingly reduced. The separation of the spin states will result only if the magnetic amplitude remains larger than the nuclear, that is if **B** is greater than 82 percent of saturation. For values of **B** between 82 and 100 percent of saturation, the polarization will be complete but the minimum wavelength reflected for a fixed incident angle will be less than for higher **B**.

Before the cobalt mirrors were used it was feared that complete polarization might be unattainable because of the difficulty of magnetizing cobalt[17] as well as the mechanical problem of producing a cobalt mirror surface. It was felt that, with the magnetic yoke and coils shown in Fig. 1, higher magnetization would result if a film of cobalt on a nonmagnetic backing were used, rather than a solid cobalt mirror. H. Ross of the Argonne machine shop succeeded, after considerable research, in producing a rugged 10-mil electroplated layer of cobalt on a copper plate. It was found that if the cobalt were annealed quickly after deposition it could be polished successfully, but if not then stresses would develop and the coating would soon separate from the copper backing. It is possible that deposition or annealing at appropriate temperatures might produce a cobalt mirror of increased magnetizability, and magnetic measurements of such mirrors are now being performed.

The obvious method, and the one first used, to demonstrate and measure the polarization of the reflected beam is by use of a second cobalt mirror as an analyzer. The experimental arrangement, very similar to that of Fig. 1, appears in Fig. 8. The cobalt mirrors, 4×10 in. long, were each held in iron yokes, in turn mounted on wooden frames. Because of the number of degrees of freedom involved in aligning the magnets, it proved simpler to adjust them by sliding and rotating the frames on the table top, than by use of adjustable mirror mounts. A mirror could be centered in the neutron beam and the incident angle determined by making a few counting rate measurements. The polarization of the beam leaving the first, or polarizer mirror, is detected and measured by noting the change in reflectivity of the analyzer mirror which results when the magnetization in the latter is reversed. If the analyzer is magnetized in the same direction as is the polarizer, it is expected that a completely polarized beam will reflect with no loss of intensity at the analyzer (provided of course that the incident angle at the analyzer is no larger than that at the polarizer). For antiparallel magnetization of the analyzer, however, zero reflected intensity is expected because the polarized neutrons would then have an index of refraction greater than unity in the analyzer mirror. Neutrons polarized by transmission through iron[18] have already been analyzed

[17] R. M. Bozorth, private communication.
[18] Burgy, Hughes, Wallace, Heller, and Woolf, Phys. Rev. **80**, 953 (1950).

by transmission through a second piece of iron (the "double transmission effect"). The mirror method would be completely analogous to the transmission method, and hence can be considered the "double reflection effect."

The use of the double reflection effect for measurement of polarization would be quite simple were it not for depolarization and reorientation of the neutron spins in the space between the mirrors. Experiments[18] on the double transmission effect had already demonstrated the great importance of stray fields on the spin orientation, and it was no surprise when the first measurements with the apparatus of Fig. 8 showed no intensity change with reversal of field in the analyzer mirror. The failure to observe an effect under these conditions is caused partly by the reorientation of the polarized beam and partly by its depolarization, both phenomena taking place in the stray fields between the mirrors. The field changes direction and magnitude slowly as the neutrons move between the mirrors of Fig. 8, hence they remain aligned with the field (magnetic moment parallel to **H**), rotating adiabatically with it. The neutrons will thus approach the second mirror aligned with the field (instead of antiparallel to it) and will exhibit total reflection. The field may actually reverse several times in the space between the mirrors but the neutrons will always reflect from the analyzer and no double reflection effect will be observed, although the neutrons may be completely polarized.

The reorientation of the spins, which destroys the double reflection effect, will always occur if the field changes slowly for the antiparallel magnetization. In order to maintain the neutron alignment in space while the field changes direction, it is necessary to produce a nonadiabatic transition of the neutron relative to the field; that is, the field must change direction in a time short compared with the Larmor precession time. If the field is made quite small at some point between the magnets and in addition is made to reverse in a few millimeters distance, then the neutrons will pass through the reversal region in a time shorter than the Larmor period and nonadiabatic transitions will result. The neutrons will then strike the second mirror antiparallel to the field and will not reflect, thus exhibiting the desired double reflection effect. If the stray fields are of a random nature some adiabatic changes (reorientation of the beam) will occur as well as nonadiabatic (neutron alignment remaining fixed in space). At some of the field irregularities the field reversal time might be of the same order of magnitude as the precession time and both types of transitions would result, causing partial depolarization of the beam. Thus depolarization (which actually is a partial reorientation of the spins) will cause a decrease in the double reflection effect for the same reason that complete reorientation removes it.

In the double transmission work[18] the nonadiabatic transition region was obtained by use of a magnetic shield to reduce the field and permanent magnets to attain a sharp reversal point. The same method of field adjustment was adapted to the reflection experiments after the first attempts had given a zero double reflection effect. The magnetic shield used was a set of concentric soft iron cylinders surrounding the neutron beam. Small Alnico magnets were placed near the ends of the cylinders and adjusted so that the field inside the central cylinder remained perpendicular to the neutron beam except for a region less than a millimeter in extent where the field reversed. The field was observed during the adjustment by means of a small compass needle which was moved along the neutron path. The field at the reversal point is made perpendicular to the beam because the sharpest reversal point may be obtained with this configuration. The neutrons are actually polarized parallel to the direction of motion at reflection but the stray field near the edge of the mirror magnet turns them through approximately 90° as they leave the mirror vicinity.

With the field adjusted in the manner just described, the double reflection effect was observed but was not as large as that expected from a completely polarized beam. The polarization, P, of the beam incident on the analyzer mirror is calculated from the ratio, R, of the intensity reflected from the analyzer in the parallel to that in the antiparallel case:

$$P=(R-1)/(R+1). \tag{8}$$

This equation is based on the assumption which was later shown to be correct, that only one spin state reflects from the analyzer mirror, and the assumption, which is probably incorrect, that the transitions at the cross-over point are completely nonadiabatic. If the transitions are partly adiabatic, Eq. (8) would require minor modification. The highest values of R obtained experimentally were about 3 (50 percent polarization) and very careful adjustment of the field at the transition point was necessary to attain these values. The two most likely reasons for the low R seemed to be: (a) the neutrons leaving the polarizer might be incompletely polarized, and (b) there might be some adiabatic reorientation of the polarized neutrons in spite of the careful field adjustment. It was impossible to decide from the measured intensities whether improvement was needed at the mirror, such as higher magnetization; or at the transition point, such as better field adjustment.

A method of polarization measurement was then devised which would not depend on sensitive field adjustment at the transition point. In the new method only parallel magnetization is used so that the field between the mirrors can be kept high and fixed in direction. Under such conditions it is easy to insure that no transitions take place in the region between the magnets. The polarization is measured by inserting a thin sheet (about 0.006 in.), of unmagnetized iron in the beam between the mirrors and recording the change in intensity reflected from the analyzer. As the beam is

completely depolarized in the iron sheet,[18] the polarized fraction of the beam, which before insertion of the iron sheet reflected completely at the analyzer, has a 50 percent reflectivity with the sheet in place. In other words, the sheet produces (for the polarized fraction of the neutrons) just half the effect that was produced in the old method by reversing the magnetization of the analyzer, but with no uncertainty concerning spin reorientation. The polarization is given directly in terms of the ratio, R_s, of the intensity before, to that after, insertion of the sheet (again with the assumption, later verified, that only one spin state reflects from the analyzer mirror):

$$P=R_s-1. \tag{9}$$

The sheet scatters some neutrons out of the beam but the reduction in intensity from this cause is easily determined.

Measurement of the polarization with the iron sheet method proved to be simple and it was found that the polarization was 50 percent, in agreement with the results of the double reflection method. It was then certain that the polarization was indeed low and that the first mirror was somehow at fault. The most likely explanations were: (1) the cobalt might be less than 82 percent saturated and as a result both spin states would reflect to some extent and (2) the reflected beam might depolarize in passing near the edge of the polarizer mirror where the field is very inhomogeneous. The variation of the polarization with neutron wavelength was then checked by varying the angles of incidence at the polarizer and analyzer (keeping the angle at the analyzer always slightly less than that at the polarizer). The 50 percent polarization had been obtained for an incident angle of 8 min, or a limiting wavelength (assuming magnetic saturation) of 1.5A. The polarization was then measured for a 4-min angle (0.7A) and it turned out to be extremely small, while a 11.5-min angle (2.1A) gave a polarization of 60 percent.

The finding that higher polarization was obtained for larger incident angles tended to confirm the suspicion that depolarization resulted when the neutrons passed through the strong field inhomogeneities at the edge of the mirror. Adiabatic rotation of the plane of polarization as the neutrons leave the mirror would have no effect on the iron sheet method of polarization measurement. However, nonadiabatic transitions of some of the neutrons would of course reduce the polarization. The transitions should be less likely at larger angles because the neutrons pass the mirror edge at a larger distance, and because they move more slowly through the changing field. The angle was finally increased to 20 min (3.7A limiting wavelength) and the value of R_s increased to 2.01, indicating a polarization of 100 percent within the statistical accuracy of about one percent. No careful attempt was made to demonstrate the complete polarization by means of the double reflection technique because the iron sheet depolarization method was much simpler. Time did not permit rebuilding the cobalt mirror mounting in such a manner as to obtain complete polarization at short wavelengths, but work in this direction is now proceeding. Although the cobalt mirror was certainly not saturated, the attainment of complete polarization demonstrates that the magnetization was certainly above the critical value of 82 percent of saturation.

It is quite certain that beams of completely polarized neutrons, which can now be produced with high intensity (of the order of 10^5 per minute), will be useful in the study of magnetic and nuclear properties. Such studies, which have already been started with incompletely polarized neutrons, will be continued with this new technique of polarization by reflection. We wish to express our thanks to Mr. H. Ross of the Argonne machine shop and Mr. Yoder of the optical shop who prepared the excellent mirrors for these experiments. Dr. M. Hamermesh and Dr. H. Ekstein have aided greatly through many discussions.

The Determination of Atomic Mass Doublets by Means of a Mass Spectrometer*

ALFRED O. NIER AND T. R. ROBERTS
Department of Physics, University of Minnesota, Minneapolis, Minnesota

(Received September 21, 1950)

A double-focusing mass spectrometer employing a 90° electrostatic analyzer followed by a 60° magnetic analyzer has been constructed having a resolution sufficiently great to permit mass difference measurements by the familiar doublet method. High stability is obtained by use of an auxiliary mass spectrometer tube which compensates for fluctuations in both the magnetic field and the source of potential for the deflecting and accelerating plates of the main spectrometer. Ion currents are measured electrically and data recorded automatically.

The doublets determined and their values in 10^{-4} amu are as follows: $D_2O^{16}-A^{36}/2$, 419.67±0.18; $D_2O^{16}-Ne^{20}$, 307.21±0.39; $Ne^{20}-A^{36}/2$, 112.80±0.18; $(C^{12})_2H_4-C^{12}O^{16}$, 364.43±0.22; $(N^{14})_2-C^{12}O^{16}$, 112.80±0.13; $(C^{12})_2H_8-(N^{14})_2O^{16}$, 617.6±0.9; $C^{12}H_4-O^{16}$, 364.78±0.22; $C^{12}H_3-N^{14}$, 125.86±0.13; $(C^{12})_2H_4-A^{40}$, 688.77±0.35; $(C^{12})_2H_4-Ca^{40}$, 685.39±0.46; $Ca^{40}-A^{40}$, 3.2±0.8; D_2-He^4, 256.12±0.09; $H_2O^{16}-A^{36}/2$, 267.02±0.40.

I. INTRODUCTION

THE generally accepted direct method of measuring atomic masses has been to use a double-focusing mass spectrograph.[1] Ney and Mann[2] have shown that, with a single-focusing mass spectrometer of the type now commonly used for measuring isotope abundances, remarkably accurate mass measurements are possible if one is content to work with molecular ions. Measurements on molecular ion fragments are not possible, since these fragments usually acquire initial kinetic energies in the dissociation process in which they are formed. They will then be focused in the instrument at lower energies than are the molecular ions, and a measurement of their relative positions in the mass spectrum will not be an accurate measure of the mass of the fragment. This limitation can be overcome only by using a double-focusing instrument, that is, one in which all ions of the same mass leaving an ion source and having a range of energies as well as a range of angles will be refocused at the same point.

A double-focusing mass spectrometer employing features of the usual single-focusing mass spectrometers has certain advantages over a conventional mass spectrograph. (1) The general procedure in making measurements differs sufficiently from that employed with mass spectrographs, so that the same systematic errors are not likely to appear in the two methods. (2) The mass doublet to be studied can be investigated carefully before actual measurements are taken. The intensities of the two peaks can be adjusted to be equal and measurement of resolution and other factors which might affect the mass measurement can be made. (3) Since focusing need be achieved at only one point, some of the compromises necessary in the design of the usual photographic plate instrument need not be made. (4) The ion currents are steady and hence may be measured conveniently with electrical instruments.

Among the disadvantages are: (1) some valuable mass doublets are not obtained, e.g., $D_3^+-(C^{12})^{++}$; (2) the photographic method, giving current integration, permits measurement of extremely small or unsteady ion currents; and (3) the doublet is scanned by changing the difference in potential across an electrostatic ana-

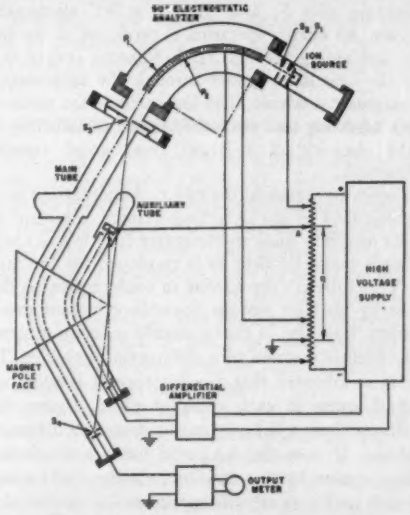

FIG. 1. Schematic drawing of mass spectrometer tubes showing action of regulation circuit. Mean radius of cylindrical electrostatic analyzer 18.87 cm. Separation of plates P_1 and P_2, 1 cm. Radius of magnetic analyzer in main and auxiliary tubes, 15.24 and 7.62 cm, respectively. Distances of S_3 and S_4 from effective pole faces are 34.77 and 20.73 cm, respectively. Asymmetrical construction reduces width of beam at S_4 owing to divergence of ion beam. S_1, S_2, S_3, and S_4 are 0.0025, 0.033, 0.25, 0.0025 cm, respectively, for most of data reported here. S_1 and S_2 are separated by 3.71 cm. Main and auxiliary tube ion accelerating potentials are approximately 4000 and 1000 v, respectively. Hence, gas used in auxiliary tube has approximately the same molecular weight as the doublet to be studied.

* This research was supported by the joint program of the ONR and AEC.

[1] For the different types of instruments used see F. W. Aston, *Mass Spectra and Isotopes* (Longmans, Green and Co., New York, 1942), second edition.

[2] E. P. Ney and A. K. Mann, Phys. Rev. 69, 239 (1946).

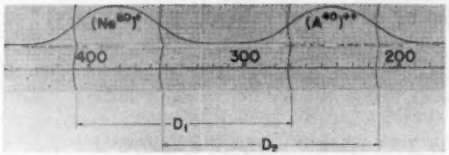

$$\frac{\text{Mass difference}}{\text{Mass number}} = \frac{1}{1776}$$

FIG. 2. Mass doublet $(Ne^{20})^+ - (A^{40})^{++}$. Mass difference is found by measuring distances on charts between corresponding half-heights of peaks. Distances are converted to mass units.

lyzer (and also changing the accelerating potential applied to the ions). Stray electric fields caused by charges on the analyzer plates could lead to errors. However, in practice this effect was shown to be negligible by comparing the mass difference of adjacent hydrocarbon ion peaks with the known mass of the hydrogen atom.

II. THE APPARATUS

Figure 1 shows a schematic view of the essential parts of the apparatus used in the present investigation.[3] Ions produced by electron impact or thermionic emission in the source of the main tube are sent through the collimating slits S_1 and S_2 into a 90° electrostatic analyzer. An energy spectrum is produced in the focal plane containing the slit S_3. Refocusing occurs at S_4 after the ions have passed through the asymmetrical 60° magnetic analyzer. The ion currents are measured with a vibrating reed electrometer and recorded by one of the channels of a Brush two-channel magnetic oscillograph.

In order to minimize the effect of fluctuations in the magnetic field or ion deflecting voltage, a second and smaller auxiliary mass spectrometer tube is mounted in the same magnetic field as is employed for the larger one. This tube is very similar in construction to those ordinarily used for isotope abundance measurements.[4] It differs, however, in that a double collector system is used which is coupled to a differential amplifier. This tube is so adjusted that the ion current is split, with one-half going to each collector plate. Under these conditions there will be no output from the differential amplifier. If now the magnetic field or accelerating voltage applied to the ions should change, the ion beam will shift and a signal will appear at the output of the differential amplifier. This signal is fed into the high voltage supply in a sense which tends to restore the ion beam to its original position. Since both spectrometer tubes obtain their ion accelerating and deflecting potentials from a common voltage divider, the action of the small tube corrects for fluctuations which would normally disturb the paths of ions in the main tube.

A mass spectrum in the main tube is obtained by varying resistance R, i.e., by moving the position of tap A. Since the auxiliary tube and the associated high voltage supply and divider constitute an inverse feed-back loop, it may be shown readily that the change in mass of the ions collected in the main tube is related to the change ΔR in R by the relation,

$$\Delta m/m = (\Delta R/R)[G/(G+1)],$$

where G is the open circuit gain of the feed-back loop.

III. RESULTS

Figure 2 shows a typical chart obtained for the doublet $(Ne^{20})^+ - (A^{40})^{++}$ when a mixture of neon and argon was placed in the main tube. Attached to the shaft of the 10-turn, 1000-ohm helical potentiometer used for scanning the mass spectrum is a 100-tooth gear on which ride Microswitches which open and close as the teeth go by. Signals from circuits attached to the switches are impressed on the second channel of the oscillograph and are printed simultaneously as indicated. Small lines indicate 1-ohm steps, large ones 10-ohm steps. Three large lines together indicate full turns (100 ohms) of the helical potentiometer. Since R is approximately 250,000 ohms, each small division represents a change of mass of 1/250,000. Inasmuch as the resistance R is in effect recorded simultaneously with the mass spectrum, errors associated with the running of the recorder are eliminated. The helical potentiometer is carefully calibrated along its entire length.

A run consisted of 10 consecutive spectra such as shown in Fig. 2, the potentiometer being driven alternately clockwise and counterclockwise. Distances D_1 and D_2 were projected on the reference scale as shown. From the calibration of the potentiometer the corresponding values ΔR_1 and ΔR_2 are determined. The average of the 20 resistance differences is then taken as ΔR for the run. G was determined before and after

TABLE I. Doublets at mass 20.

Row	Doublet	No. of runs	Av. in 10^{-4} amu	Previous work
1	$D_2O^{16} - A^{40}/2$	5	419.67±0.18 (0.08)	418.9 ±2.0[a]
2	$D_2O^{16} - Ne^{20}$	4	307.21±0.39	306.5 ±1.0[a] 308.3 ±4.0[b]
3	Row 1 − row 2		112.46±0.43	
4	$Ne^{20} - A^{40}/2$	2	112.65±0.40	113.0 ±2.0[a] 108.8 ±3.0[b] 111.42±0.38[c]
5	$(D_2O^{16} - A^{40}/2) - (D_2O^{16} - Ne^{20})$	2	112.84±0.21	

[a] E. B. Jordan and K. T. Bainbridge, Phys. Rev. 51, 385 (1937).
[b] F. W. Aston, Proc. Roy. Soc. (London) A163, 391 (1937).
[c] J. Mattauch, Physik. Z. 39, 892 (1938).

[3] A preliminary report on the apparatus and some results presented here have already been given: Nier, Roberts, and Franklin, Phys. Rev. 75, 346 (1949); T. R. Roberts and A. O. Nier, Phys. Rev. 77, 746 (1950).
[4] A. O. Nier, Rev. Sci. Instr. 18, 397 (1947).

TABLE II. Doublets containing combinations of C^{12}, H, N^{14}, and O^{16}.

Row	Doublet	No. of runs	Av. in 10^{-4} amu	Previous work
1	$(C^{12})_2H_4-C^{12}O^{16}$	3	364.43±0.22 (0.19)	
2	$(C^{12})_2H_4-(N^{14})_2$	12	251.70±0.25 (0.07)	
3	Row 1−row 2		112.73±0.33	
4	$(N^{14})_2-C^{12}O^{16}$	2	112.73±0.14	111.7 ±2.0[a] 112.22±0.40[b]
5	$[(C^{12})_2H_4-C^{12}O^{16}]-[(C^{12})_2H_4-(N^{14})_2]$	2	113.26±0.37	
6	$(C^{12})_3H_8-C^{12}(O^{16})_2$	8	729.68±0.44 (0.18)	
7	$(C^{12})_3H_8-(N^{14})_2O^{16}$	4	617.6 ±0.9	
8	Row 6−row 7		112.1 ±1.0	
9	$C^{12}H_4-O^{16}$ (Compare with row 1 and ½ row 6)	2	364.80±0.63	364.9 ±0.8[a] 360.1 ±1.6[c] 363.81±0.28[d] 364.2 ±0.9[e] 363.2 ±0.35[f]
10	$C^{12}H_2-N^{14}$ (Compare with ½ row 2)	6	125.97±0.21	127.4 ±0.8[a] 124.5 ±0.7[c] 125.78±0.21[d] 125.7 ±0.6[e] 125.60±0.15[f] 125.22±0.12[g]

[a] K. T. Bainbridge and E. B. Jordan. Data in article by M. S. Livingston and H. A. Bethe, Rev. Mod. Phys. 9, 370 (1937).
[b] J. Mattauch, Physik. Z. 39, 892 (1938).
[c] F. W. Aston, Proc. Roy. Soc. (London) A163, 391 (1937).
[d] J. Mattauch and A. Flammersfeld, *Isotopenbericht* (Verlag. Z. Natur., Tübingen, 1949).
[e] Asadz, Okuda, Ogata, and Yoshimoto, Proc. Phys. Math. Soc. Japan 22, 41 (1940).
[f] E. B. Jordan, Phys. Rev. 60, 710 (1941).
[g] H. Ewald, Z. Naturforsch. 1, 131 (1946).

each run. Its value lay between 60 and 100 for the data presented here and did not vary more than a few percent during a run.

IV. MASS 20 DOUBLETS

Table I gives the results for several doublets measured at the mass 20 position. Since readings taken at one time were very consistent, usually not more than one run on a given doublet was taken on a single day. The runs used in computing the averages in this and other tables of this paper were taken over a period of several months; the spectrometer ion source and electronic components frequently underwent revision between runs.

The probable errors given were computed by assuming the individual runs as independent when four or more runs were taken. The charts were read to the closest tenth of an ohm. Because of the finite size of wire on the helical potentiometer, a single reading could be determined only to 0.2 ohm. In many instances the agreement between runs was so good that the probable error was extremely small. In such cases the probable error given was taken arbitrarily as one-half the smallest difference which could be determined on the potentiometer due to the finite wire size. Where this was done, the actual computed probable error is given in parentheses under the assumed value.

Row 5 differs from row 3 in that the runs were taken in immediately consecutive pairs to determine the $Ne^{20}-A^{40}/2$ difference more accurately. Our final value for this difference is 112.80±0.18, a weighted average of rows 4 and 5. This result agrees best with that of Bainbridge and Jordan. The excellent agreement between rows 4 and 5 show that comparison with a third ion gives a reliable doublet measurement. This method can be employed for doublet separations which are too small to measure directly. As shown in Fig. 2, the lower limit of complete resolution at present is about 1 in 2000.

TABLE III. Doublets at mass 40.

Row	Doublet	No. of runs	Av. in 10^{-4} amu	Previous work
1	$(C^{12})_3H_4-A^{40}$	8	688.77±0.35	679 ±6[a] 679.3±0.7[b] 693.0±2.3[b]
2	$(C^{12})_3H_4-Ca^{40}$	5	685.39±0.46	
3	Row 1−row 2		3.38±0.58	
4	$Ca^{40}-A^{40}$	Too small for direct measurement		
5	$[(C^{12})_3H_4-A^{40}]-[(C^{12})_3H_4-Ca^{40}]$	5	3.2 ±0.8	

[a] F. W. Aston, Proc. Roy. Soc. (London) A163, 391 (1937).
[b] Okuda, Ogata, Aoki, and Sugawara, Phys. Rev. 58, 578 (1940).

V. DOUBLETS CONTAINING C^{12}, H, N^{14} AND O^{16}

Table II gives the results for various doublets containing combinations of C^{12}, H, N^{14}, and O^{16}. The ions used in the present work were molecular ions except O^{16} from carbon dioxide, N^{14} from nitrogen gas, and $C^{12}H_2$ from methane or ethylene. The first five rows in Table II correspond with those in Table I and, as before, the best value for $(N^{14})_2-C^{12}O^{16}$ is obtained from rows 4 and 5 as 112.80±0.13. Still another determination of this doublet is given in row 8 but was not included because with its higher probable error it would have little influence on the final value.

As shown in row 9, row 1 and one-half the value in row 6 also give the fundamental doublet, $C^{12}H_4-O^{16}$, which has been measured extensively by previous workers. If the probable error of ±0.18 derived directly from the data is used for row 6, the weighted average

TABLE IV. D_3-He^4 and $H_2O^{18}-A^{36}/2$ doublets.

Doublet	No. of runs	Av. in 10^{-4} amu	Previous work
D_3-He^4	2	256.12±0.09	256.1 ±0.4[a] 255.1 ±0.8[b] 256.04±0.08[c]
$H_2O^{18}-A^{36}/2$	5	267.02±0.40	271 ±3.6[b]

[a] K. T. Bainbridge and E. B. Jordan, Phys. Rev. 51, 384 (1937).
[b] F. W. Aston, Proc. Roy. Soc. (London) A163, 391 (1937).
[c] H. Ewald, Z. Naturforsch. 5a, 1 (1950).

of our three determinations is 364.78±0.22 (0.08). This measurement agrees best with that of Bainbridge and Jordan.

Combining our results in rows 2 and 10 we obtain a $C^{12}H_2-N^{14}$ value of 125.86±0.13 (0.04). This result is in substantial agreement with three of the four most recently published measurements.

VI. OTHER DOUBLETS

A preliminary report of the data in Table III has already been given.[5] In this case the $Ca^{40}-A^{40}$ separation was too small to measure directly so that the result given in row 5 is our best value.

Calcium ions were obtained by heating the metal in a furnace in the ion source. The $(C^{12})_3H_4$ ions were fragment ions obtained from cyclopropane. A correction amounting to 0.4 percent of the doublet width in rows 1 and 2 was made for the unresolved $(C^{12})_2C^{13}H_3$ peak on the low mass side of the $(C^{12})_3H_4$ peak. A correction of the same general type was made for C^{13} containing hydrocarbon ions in Table II. Failure to make such a correction probably accounts for the discrepancies in Okuda's two measurements listed in row 1. The abnormally high relative intensity of C_3H_3 ion fragments from hydrocarbons make this correction especially important for $(C^{12})_3H_4$ peaks. This isotopic correction has no effect on the result given in row 5.

Two other recent doublet measurements are listed in Table IV.

The above results indicate the practicability of using the mass spectrometer for precise mass difference measurements. A subsequent paper will discuss the determination of the isotopic weights of secondary mass standards.

The authors wish to acknowledge the very able assistance of R. B. Thorness and E. G. Franklin in designing and constructing the instrument, and the aid of W. H. Johnson and H. A. Lindgren in recording and computing the data. The construction of the apparatus was aided materially by grants from the Graduate School and the Minnesota Technical Research Fund subscribed to by General Mills, Inc., *Minneapolis Star and Tribune*, Minnesota Mining and Manufacturing Company, Northern States Power Company, and Minneapolis Honeywell Regulator Company.

[5] T. R. Roberts and A. O. Nier, Phys. Rev. **79**, 198 (1950).

PHYSICAL REVIEW VOLUME 81, NUMBER 4 FEBRUARY 15, 1951

Polonium Isotopes Produced with High Energy Particles*

D. G. KARRAKER AND D. H. TEMPLETON
Radiation Laboratory and Department of Chemistry, University of California, Berkeley, California

(Received October 27, 1950)

We have investigated four new isotopes of polonium produced from bismuth and lead by high energy spallation and have studied their decay products, which include three new lead and bismuth activities. The mass assignments are made by the identification of known activities as decay products. Some of the properties of these new isotopes are as follows:

Isotope	Half-life	Mode of decay	Energy in Mev: Alpha-particles	Energy in Mev: Gamma-rays
Po^{205}	1.5 hr	*EC*, α	5.22±0.10	
Po^{204}	3.8 hr	*EC*, α	5.37±0.02	
Po^{203}	47 min	*EC*		
Po^{202}	52 min	*EC*, α	5.59±0.03	
Bi^{204}	14.5 days	*EC*		0.431, 0.527 0.550, 0.746 1.84
Bi^{203}	95 min	*EC*		
Pb^{199}	25 min	*EC*		

I. INTRODUCTION

POLONIUM has eight isotopes, beta-stable or with neutron excess, which occur in the natural radioactive series or the artificial neptunium series. Cyclotron-induced transmutations now make possible the production of neutron-deficient polonium isotopes. Templeton, Howland, and Perlman[1] have produced by this means the three isotopes Po^{206}, Po^{207}, and Po^{208}, and Kelly and Segrè[2] have found Po^{209}. The present work was undertaken to extend our knowledge of polonium to the even lighter isotopes which can be made by the 184-inch Berkeley cyclotron. We have observed the radioactivities of the next four isotopes, Po^{205}, Po^{204}, Po^{203}, and Po^{202}. Experiments designed to establish the decay products and mass assignments of these radioactivities led to the discovery of two radioactive species of bismuth and one of lead. Our work was greatly aided by a parallel investigation of bismuth and lead isotopes carried out in this same laboratory by Neumann and Perlman, who have already reported their results.[3]

* This work was done under the auspices of the U. S. AEC.

[1] Templeton, Howland, and Perlman, Phys. Rev. **72**, 758 (1947).

[2] E. L. Kelly and E. Segrè, Phys. Rev. **75**, 999 (1949).

[3] H. M. Neumann and I. Perlman, Phys. Rev. **78**, 191 (1950).

II. EXPERIMENTAL METHODS

In most of the experiments a target of natural lead or bismuth was bombarded with particles accelerated in the 184-inch Berkeley cyclotron. Helium ions with lead or protons or deuterons with bismuth produced good yields of the polonium isotopes of interest, but also substantial amounts of other spallation and fission products. Particles of various energies were used to improve the relative yield of the isotope desired in a particular experiment. The target was made of metal in the form of strips 0.5 to 2 mm thick; or, when speed in chemical separation was required, bismuth oxide was used. This oxide can be dissolved in acids more rapidly than the metal.

All samples were separated chemically before measurements were made. Polonium was separated from other elements by a procedure using tellurium, with hold-back carriers added for thallium and lead. The tellurium was reduced to the element with stannous chloride, carrying with it the polonium and noble metals. The tellurium was dissolved and precipitated with sulfur dioxide, carrying again the noble metals, but leaving a carrier-free solution of polonium, with 85 to 95 percent yield. For further purification, polonium was extracted from 6*N* HCl into a mixture of 20 percent tributyl phosphate and 80 percent dibutyl ether. The extraction coefficient for polonium between the organic and acid layers is about 110. Lead and bismuth daughter activities were removed quantitatively by washing the organic layer with 6*N* HCl, and purified by precipitation—bismuth as BiOCl and lead as $PbSO_4$ or $PbCrO_4$.

Thallium activities were separated by oxidation of thallium to the thallic state with potassium permanganate, followed by the extraction of thallic chloride with diisopropyl ether saturated with HCl. Occasionally the thallium activities were further purified by evaporation of the ether, reduction of the thallium with hydrogen peroxide, and precipitation of the thallium as Tl_2PtCl_6 in the presence of lead and bismuth hold-back carriers.

Generally, the decay curve of the polonium Geiger activities is so complex that resolution is ambiguous. To avoid this difficulty, the half-lives were determined by separation of the daughter activities at a sequence of equal time intervals, the interval corresponding approximately to the half-life of the parent. The activity A_2 of the daughter at time t is given by:

$$A_2 = C_2[\lambda_2\lambda_1 N_0/(\lambda_2-\lambda_1)][\exp(-\lambda_1 t)-\exp(-\lambda_2 t)],$$

where C_2 is the counting efficiency of the daughter, including the geometry factor; λ_2 and λ_1 are the decay constants of daughter and parent, respectively; and N_0 is the number of atoms of parent at $t=0$. At the start of the time interval, the parent is purified chemically, so that the additional term in the general formula does not enter the expression. It will be observed that, if the time t is the same for all periods of growth of the daughter before separation from the parent, the exponential terms become a constant factor, and A_2 is proportional to the disintegration rate $(\lambda_1 N_0)$ of the parent at the beginning of the growth period. Thus, if one plots the logarithm of the initial activity of each daughter fraction against the time of separation, the slope of the line will correspond to the half-life of the parent.

In the identification of alpha-decay daughters, the thallium electron capture daughter of the lead alpha-decay daughter was usually separated for measurement, rather than the lead activity itself. This procedure was followed, since a greater degree of purity was attained in the thallium separations than in the lead separations; furthermore, the decay curve of the thallium activities is simpler than the decay curve of the lead activities, since no similar half-lives are found and no daughters are growing.

Isotopes of interest in this paper are shown in Table I, where isotopes enclosed in parentheses are isotopes identified by this work, and stable isotopes are indicated by the symbol ◈.

3.8-hr Po^{204}

The alpha-decay of polonium produced by high energy irradiation shows periods of about 45 min, 1.5 hr, and 4 hr, in addition to longer periods previously identified. To determine the mass assignments of these isotopes, their daughters were identified by the method sketched above. A pure sample of mixed polonium activities was separated from the bombarded target (elapsed time, 2 hr) and the daughter activities sep-

TABLE I. Table of isotopes studied.[a,b]

	198	199	200	201	202	203	204	205	206	207	208
Po					(52 min *EC*, α)	(47 min *EC*)	(3.8 hr *EC*, α)	(1.5 hr *EC*, α)	9 d *EC*, α	5.7 hr *EC*, α	3 yr α
Bi					(95 min *EC*)	12 hr *EC*	12 hr *EC*	(14.5 d *EC*)	6.4 d *EC*	long	
Pb	(25 min *EC*)	80 min *EC*	18 hr *EC*	8 hr *EC*	long	52 hr *EC*	68 min IT ◈	long ◈	◈	◈	◈
Tl	1.8 hr *EC*	7.3 hr *EC*	27 hr *EC*	72 hr *EC*	12 d *EC*	◈					
Hg	◈	◈	◈	◈	◈						

[a] G. T. Seaborg and I. Perlman, Revs. Modern Phys. 20, 585 (1948).
[b] See reference 3.

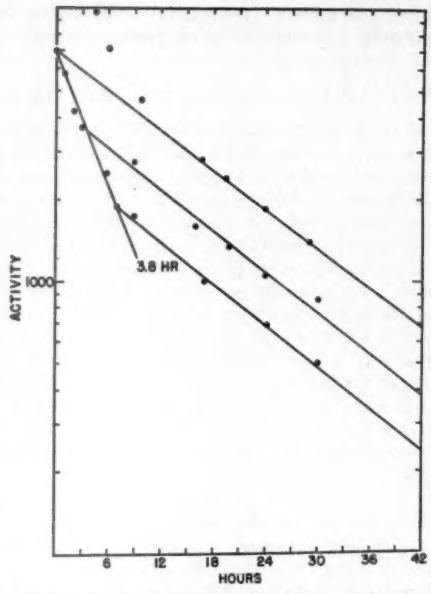

FIG. 1. Data showing the genetic relationship of 3.8-hr Po^{204} and 12-hr Bi^{204}.

arated at intervals of an hour. The decay of the purified bismuth fraction showed a 95-min period (which will be discussed later), a 12-hr period, and a longer period of 6 to 14 days, in low intensity. Figure 1 is a plot of the decay of the bismuth fractions for three of the separated samples where the 12-hr period has been extrapolated back to the time of separation. (Only three of the bismuth decay curves are shown, to avoid crowding. Extrapolated points from the decay curves of the other fractions are plotted at the time of separation.) It will be seen from Fig. 1 that the yields at the time of separation determine the half-life of the parent activity of the 12-hour bismuth as 3.8 hours, in agreement with the 3.8-hour value obtained from alpha-decay curves.

It will be seen from Table I that the establishment of a 12-hour bismuth activity as the daughter of the 3.8-hour polonium does not give an unambiguous mass number. A similar experiment was done to identify the alpha-decay daughter and fix the mass number. As before, a large sample of purified polonium activities was prepared, from which the bismuth and lead daughter activities were separated at 4-hour intervals. The bismuth activity could be ignored, as none of the bismuth daughters are alpha-emitters, and Po^{200} is presumed to be too short to produce any of the Tl^{200} through an electron capture chain. The lead alpha-daughter was allowed to grow its thallium daughter for about 18 hours; then the thallium was separated. Since the lead fraction had been separated at 4-hour intervals, the activity of the alpha-decay daughter of the 3.8-hour polonium would be decreased by approximately a factor of two between each of the fractions. The time allowed for the thallium to grow was the same for each fraction, so the activity of the lead alpha-daughter will be directly proportional to the activity of its thallium daughter. The principal, and virtually the only activity found was the 27-hr Tl^{200}. The results are shown in Table II.

TABLE II. Activities of 27-hr Tl fractions.

Fraction	27-hr Tl, counts/minute Observed	Calculated
1	3280	...
2	1740	1600
3	845	780

These experiments have fixed the 3.8-hour polonium at mass 204. Its alpha-decay daughter is the 18-hr Pb^{200}, which was shown by Neumann and Perlman[3] to be the parent of Tl^{200}. The electron capture daughter is Bi^{204}, which has been shown[4] to decay both to Pb^{204} and to Pb^{204m}. These decay relations are

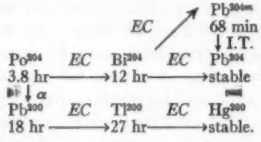

We have confirmed that Po^{204} gives rise to the 68-min Pb^{204m}, by an experiment which is described below.

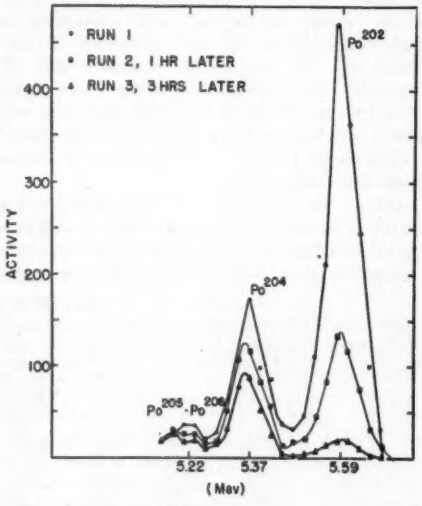

FIG. 2. Pulse analysis showing alpha-particle energies for polonium isotopes.

[4] Templeton, Howland, and Perlman, Phys. Rev. 72, 766 (1947).

Thus these assignments, which are based on the excitation curve for the formation of 27-hour thallium by alpha-irradiation of gold[5] are an independent check on the assignment[4] of Pb^{204m}. This isomer is of great interest because of its unique properties as a long-lived highly excited state of an even-even nucleus.

The energy of the alpha-particles from Po^{204} was determined as 5.37 ± 0.02 Mev by pulse analysis[6] (Fig. 2). The ratio of electron capture disintegrations to alpha-disintegrations has not been determined with accuracy. It is estimated as approximately 100 on the assumption that the cross section for the $(p,6n)$ reaction on bismuth is 0.1 barn at its maximum, which is at 70 to 80 Mev.

68-min Pb^{204m}

The discovery of two 12-hour bismuth isotopes forced a reconsideration of the mass assignment of Pb^{204m}, which was based in part on the observation that the 68-minute lead is a daughter of a 12-hour bismuth. The experiments[4] which showed that this is the case and that 52-hr Pb^{203} is not the daughter of the same 12-hour bismuth were done with bismuth from the alpha-irradiation of thallium at an energy which did not produce Bi^{208}. Had these experiments been done on the bismuth produced from lead, both daughters should have been found. The reasons cited[4] for the mass assignment are still valid, though some of them must now be stated in a more involved way to distinguish between the two 12-hour bismuth activities.

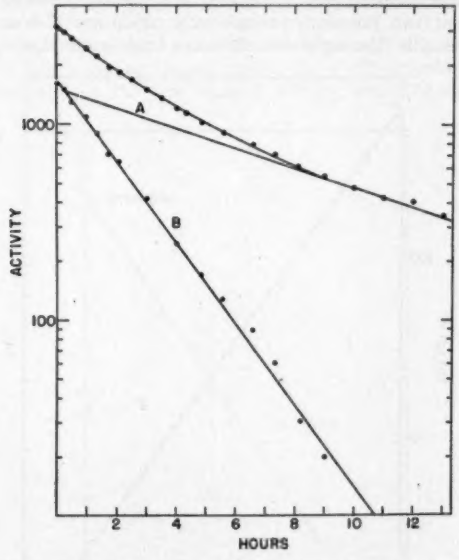

FIG. 3. Geiger decay curve of polonium from Pb^{204} with 37-Mev helium ions. A, 5.7-hr Po^{207}; B, 1.5-hr Po^{206}.

TABLE III. Activities of the 68-min Pb fractions.

Fraction	68-min Pb, counts/min Observed	Calculated
1	4900	...
2	2200	2350
3	1090	1120

To relate Pb^{204m} to Po^{204}, a large quantity of polonium was prepared and purified. Bismuth daughters were separated at 4-hour intervals. Each bismuth fraction was allowed to stand for 24 hours; then lead was separated from the bismuth. The yield of 68-minute activity in each sample is listed in Table III, which shows that the polonium ancestor has a 3.8-hour half-life.

1.5-hr Po^{205}

A 1.5-hour electron capture activity with associated alpha-particles was resolved from the decay curves of polonium produced by irradiation of lead enriched in mass 204 (27 percent)[7] with 37-Mev helium ions in the 60-inch Crocker Laboratory cyclotron (Fig. 3). The predominant product of 37-Mev helium ion bombardment of an element in this region is known to be the

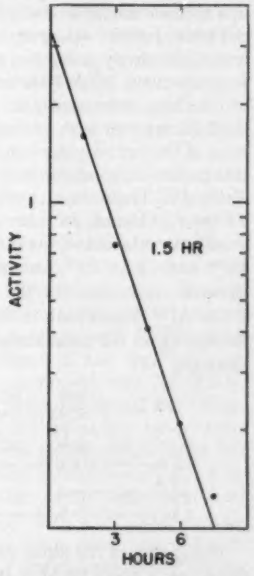

FIG. 4. Yield of 14.5-day bismuth activity plotted to give half-life of polonium parent.

[5] Orth, Marquez, Heiman, and Templeton, Phys. Rev. **75**, 1100 (1949).

[6] Ghiorso, Jaffey, Robinson, and Weissbourd, National Nuclear Energy Series, Plutonium Project Record, Vol. 14B, *The Transuranium Elements: Research Papers*, Paper No. 16.8 (McGraw-Hill Book Company, Inc., New York, 1949).

[7] This lead was enriched with a calutron in Berkeley. We are indebted to Dr. E. H. Huffman, Mr. R. C. Lilly, and Mrs. D. B. Stewart for its purification and to Mr. J. T. Vale for its mass analysis.

TABLE IV. Activities of the 72-hr Tl fractions.

Fraction	72-hr Tl, counts/min Observed	Calculated
1	650	...
2	300	325
3	160	163
4	85	81

$(\alpha,3n)$ product,[1,2] which in this case is Po^{205}. No lighter polonium should be produced in this irradiation; and since the heavier ones are already known, Po^{205} is the best assignment.

Periodic separations of the bismuth daughters from a large amount of mixed polonium activities at 1.5-hour intervals showed that the yield of longer bismuth periods (i.e., half-lives of the order of a week) indicated a parent with a half-life of 3 to 4 hours. Since the 9-day Po^{208} is known to grow the 6.4-day Bi^{206}, this clearly indicated a second polonium isotope of short half-life growing a longer bismuth. The decay of the bismuth activities showed that the first separation yielded principally a new activity of 14-day half-life, while the last fractions were almost pure 6.4-day Bi^{206}. After the decay of the Bi^{206}, the yield of the 14-day bismuth corresponded to a parent of 1.5 hours (Fig. 4). This is the half-life of Po^{205}, thus the new bismuth activity is also mass 205. Its radiation characteristics will be described presently.

The alpha-decay daughter of Po^{205} was identified in in a manner similar to that of Po^{204}. A large quantity of polonium activity was prepared and purified, and the lead alpha-decay daughter activity separated at 1.5-hour intervals. After 16 hours, the thallium daughters of the lead were separated from each sample. The thallium samples were exclusively the 72-hr Tl^{201}, since none of the lighter polonium isotopes were produced in this particular bombardment. The results are shown in Table IV. These data confirm the assignment of the 1.5-hour polonium to mass 205. Neumann and Perlman[3] have established the genetic relation between 8-hr Pb^{201} and 72-hr Tl^{201}. Barton, Ghiorso, and Perlman[8] showed, subsequent to the above experiments, that 5.5-hr At^{209} decays both to Bi^{205} and to Po^{209}, thus confirming again the mass assignments. These decay relations are

$$\begin{array}{ccccccc} & & At^{209} & EC & Po^{209} & ? & Bi^{209} \\ & & 5.5\text{ hr} & \longrightarrow & 200\text{ yr} & \longrightarrow & \text{stable} \\ & & \downarrow\alpha & & \downarrow\alpha & & \\ Po^{205} & EC & Bi^{205} & EC & Pb^{205} & ? & Tl^{205} \\ 1.5\text{ hr} & \longrightarrow & 14\text{ day} & \longrightarrow & \text{long} & \longrightarrow & \text{stable} \\ \downarrow\alpha & & & & & & \\ Pb^{201} & EC & Tl^{201} & EC & Hg^{201} & & \\ 8\text{ hr} & \longrightarrow & 72\text{ hr} & \longrightarrow & \text{stable}. & & \end{array}$$

The energy of the alpha-particles of Po^{205} was determined as 5.22 ± 0.10 Mev by following the decay of peaks obtained with the alpha-pulse analyzer. The peak corresponding to Po^{206} (5.22 Mev)[9] decayed about 20 percent in four hours. Neighboring peaks due to Po^{208} and Po^{210} prevented greater accuracy in the energy estimate.

The ratio of electron capture disintegrations to alpha-disintegrations is estimated as 400 by counting both the alpha-particles and the gross Geiger count, and making the crude assumption of one Geiger count (at 100 percent geometry) per electron capture event.

14.5-day Bi^{205}

The half-life of Bi^{205} produced by the decay of Po^{205} was found to be 14.5 days (Fig. 5). Aluminum absorption curves showed that about 15 percent of the Geiger counts of this isotope are due to electromagnetic radiation. Lead absorption measurements showed a gamma-ray of 1.7 Mev (half-thickness 14.5 g/cm²). With a beta-spectrometer we found conversion electrons corresponding to 1.84 Mev for this gamma-ray, as well as others for gamma-rays of 431, 527, 550, and 746 kev. The existing data are insufficient to establish the decay scheme.

47-min Po^{203}

Repetition of the experiment described above—separation of the 12-hour bismuth daughters from a large sample of polonium at regular intervals—indicated that two polonium parents were producing 12-hour bismuth. The significant difference from earlier experi-

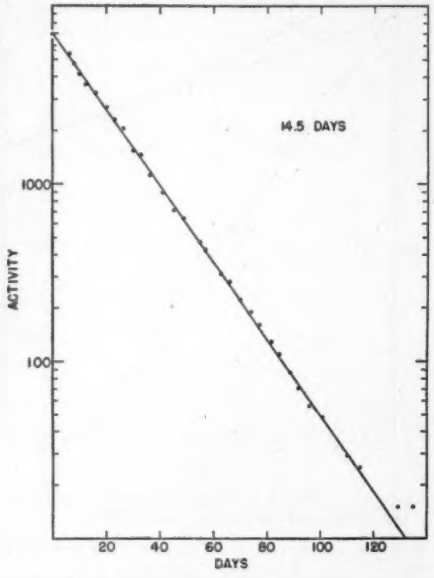

FIG. 5. Decay of 14.5-day Bi^{205}.

[8] Barton, Ghiorso, and Perlman, private communication.

[9] A. Ghiorso, private communication.

ments was that the polonium was purified fairly rapidly, so that the daughter separations were started within an hour of the end of the bombardment. The data indicated another polonium isotope of a shorter half-life than Po^{204}. It must be at mass 203, since 52-hr Pb^{203} appeared in the decay curves of the first bismuth fractions, but not in later ones.

The half-life of the Po^{203} was determined by preparing a large sample of polonium, purifying quickly after bombardment, and separating the bismuth daughters at 45-min intervals. The bismuth was allowed to decay for 24 hours, then the lead activity produced by bismuth decay was separated from the bismuth fraction. Since the lead daughters were allowed to grow into each bismuth fraction for the same period, the activity of 52-hr Pb^{203} grown in was directly proportional to the initial activity of Bi^{203} in each fraction. The data plotted in Fig. 6 determine the half-life as 47 ± 5 minutes.

52-min Po^{202} and 95-min Bi^{202}

In addition to the other bismuth activities mentioned above, we observed a 95-minute activity among the bismuth daughters (Fig. 7) of polonium produced in bombardments at fairly high energy (protons of more than 70 Mev on bismuth, or helium ions of more than 120 Mev on lead). The yield of this 95-minute activity as a function of separation time showed that its polonium parent has a half-life of 52 ± 5 minutes (Fig. 8). If this polonium parent were the Po^{203} described above, then the new bismuth activity would be an isomer of Bi^{203}. In all attempts to milk Pb^{203} from this bismuth the yield corresponded to a bismuth parent of 12-hour half-life. However, this result does not rule out isomerism; if the ratio of isomeric transition to electron capture for the upper state is equal to $(t_2-t_1)/t_1$, where t_1 and t_2 are the respective half-lives of the upper and lower states, the daughter is produced at a rate corresponding exactly to decay of a single parent of half-life t_2.

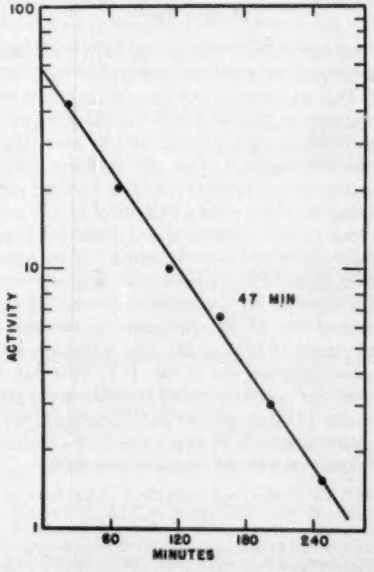

FIG. 6. Yield of 52-hr Pb^{202} showing a 47-minute polonium parent.

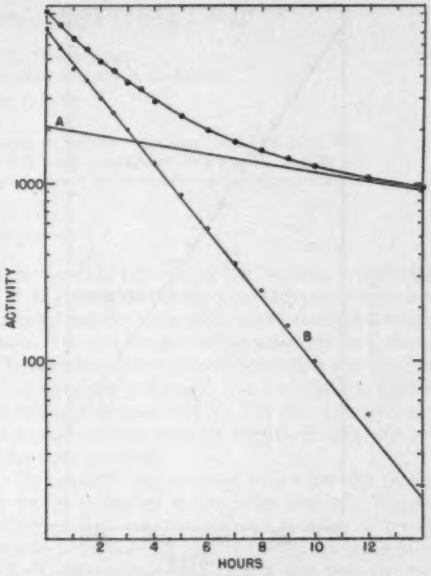

FIG. 7. Decay of bismuth daughter activities. A, 12-hr Bi^{203} and 12-hr Bi^{204}; B, 95-min Bi^{202}.

The 95-minute activity was not detected in bismuth formed by irradiation of lead, containing 27 percent Pb^{204}, with 18-Mev deuterons from the 60-inch cyclotron.[7] Since the $(d,3n)$ reaction is known to take place with high yield at this energy on bismuth,[2] it is expected to do the same on Pb^{204}. Bismuth of mass 203 was formed in this experiment, because lead separated from bismuth after a period of growth showed Pb^{203} in good yield. Therefore, it was presumed that the 95-minute activity is not Bi^{203}. If the assignment were 201 or 200, known lead and thallium activities should have been found as daughters. Thus, 202 is the best assignment.

Additional evidence for the assignment to mass 202 was obtained from an excitation experiment, which at the same time identified the alpha-particles of 5.59 $\pm$0.03-Mev energy (Fig. 2) with Po^{202}. The electrostatically deflected proton beam from the 184-inch cyclotron was directed on a target composed of copper absorbers with bismuth foils interposed. From each foil the polonium was separated and purified. Pulse analysis of an aliquot of the polonium gave the yield of the

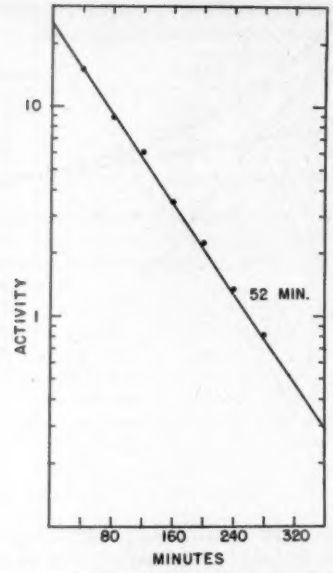

FIG. 8. Yield of 95-min Bi^{202} showing a 52-minute polonium parent.

48-minute alpha-activity. After a period of about two hours, the bismuth daughters were separated from the remainder of the polonium. Decay measurements on an aliquot of this bismuth gave the relative yield of Bi^{202} and thereby the yield of Po^{202}. The remainder of the bismuth was allowed to decay approximately a day, after which lead was separated and purified. The relative yield of Pb^{203}, and thereby of Po^{203}, was determined by following decay of this lead fraction. The resulting data are listed in Table V. From these data it is clear that the alpha-particles belong to the parent of the 95-minute bismuth and that the mass assignment is less than 203. The variation of the yields from one foil to another is not presented here because of uncertain chemical yields in the isolation of the polonium; however, these data are in agreement with a mass difference of one unit for the 95-minute bismuth and Pb^{203}.

No alpha-particles were observed which could be attributed to Po^{203}. However, if the electron capture to alpha-disintegration ratio were ten times larger than that of Po^{202}, it is doubtful if the alpha-particles could have been observed. From the energies of the alpha-particles of the other polonium isotopes, a reasonable prediction is that the alphas of Po^{203} have an energy of 5.4 ± 0.1 Mev.

No reliable data are available concerning the energies of the electrons and gamma-rays of Bi^{202}, since our samples were never pure. No positrons nor alpha-particles were found associated with it. If the alpha-decay to electron capture decay ratio is less than 10^{-5}, it is doubtful that alpha-decay would have been detected.

Identification of the lead alpha-decay products of Po^{202} and Po^{203}, or of the thallium daughters of these leads, failed for lack of sufficient radio-chemical purity of the daughter samples. The half-life of Pb^{198} was determined by an experiment described below. Thus the decay of Po^{202} is presumed to be:

$$\begin{array}{lllllllllll} Po^{202} & EC & Bi^{202} & EC & Pb^{202} & ? & Tl^{202} & EC & Hg^{202} \\ 52\text{ min} & \longrightarrow & 95\text{ min} & \longrightarrow & \text{long} & \longleftrightarrow & 12\text{ day} & \longrightarrow & \text{stable} \\ \downarrow\alpha & & & & \downarrow? & & & & \\ Pb^{198} & EC & Tl^{198} & EC & Hg^{198} & & & & \\ 25\text{ min} & \longrightarrow & 1.8\text{ hr} & \longrightarrow & \text{stable.} & & & & \end{array}$$

The long-lived Pb^{202} is still undetected.

TABLE V. Yields of 95-min, Bi and Pb^{203}.

Total absorber thickness (g/cm^2)	Proton energy[b] (Mev)	Relative yield[a] 95-min Bi	Pb^{203}
82.76	(90)	0.93	0.12
84.74	(80)	1.01	0.22
85.68	(75)	1.10	0.22
86.59	(70)	1.14	0.36
88.34	(60)	$\leqslant 1.3$[c]	4.5

[a] In arbitrary units, proportional to the yield of 48-minute alpha-activity in the same foil.
[b] Uncertain because the initial energy is not known exactly and because of straggling in the absorbers.
[c] Not detected.

25-min Pb^{198}

The half-life of Pb^{198} was estimated by establishing a genetic relation between the 1.8-hr Tl^{198} and its lead parent. This was done in the manner described before; a large sample of lead activities was prepared by bombarding thallium with protons of 120 Mev, the lead separated and purified, and the thallium daughters separated at 30-minute intervals. The resolved yields of the 1.8-hour thallium show a half-life of 25 ± 10 minutes for its lead parent. Neumann and Perlman[3] have observed directly a lead activity which had an apparent half-life of 25 minutes, in agreement with our value.

It is a pleasure for the authors to acknowledge the assistance of Dr. H. M. Neumann in the beta-spectrometric study of Bi^{205}, of Mr. Albert Ghiorso with the alpha-pulse analyzer, and of Mr. J. T. Vale, Mr. G. B. Rossi, and the cyclotron crews in making the irradiations on the 184-inch and 60-inch cyclotrons. We wish to thank Professors I. Perlman and G. T. Seaborg for helpful discussions in the course of this work.

Neutron Production by Cosmic Rays at Sea Level*

A. R. TOBEY† AND C. G. MONTGOMERY
Sloane Physics Laboratory, Yale University,‡ New Haven, Connecticut
(Received October 2, 1950)

Neutrons produced by the cosmic radiation at sea level in paraffin, aluminum, and lead have been measured in a boron-filled ionization chamber provided with boron guard rings. Proper application of the diffusion theory of slow neutrons was possible and absolute values of the rate of production of neutrons per gram per second were obtained.

I. INTRODUCTION

SEVERAL observers[1–4] have utilized the alpha-particles produced in the disintegration of B^{10} to estimate the number of slow neutrons that are the products of nuclear interactions of the cosmic radiation at sea level. In these experiments no account was taken of the effect of the detector on the neutron density in its neighborhood. In the measurements described here,[5] the geometrical conditions were such that the counting rate of the detector could be rigorously related to the rate of production of neutrons in the vicinity.

II. APPARATUS

The measurements were made in a large block of paraffin 65 cm wide, 65 cm high, and 93 cm long with the detector placed at the center of the block. The paraffin served a double role as neutron producer and moderator. Investigation of aluminum and lead was accomplished by placing sheets of these materials in a lattice structure in such a manner as to maintain a nearly homogeneous mixture with the paraffin throughout the block. The detector was a cylindrical ionization chamber filled with boron trifluoride of natural isotopic concentration. Guard cylinders also containing BF_3 were placed at each end of the chamber as indicated in Fig. 1. The amount of borax and the pressure of the gas in each chamber were adjusted so that the amount of boron per unit length of the assembly was constant. The chamber was constructed of copper and the dimensions are given in Table I. The chamber was filled to 1 atmosphere pressure at 0°C. The center conductor was supported at both ends by Stupakoff seals. No guard rings were provided.

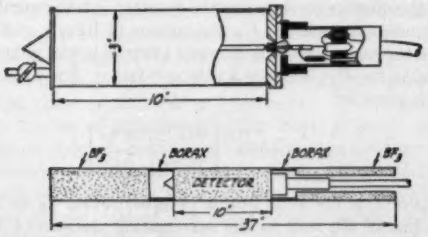

FIG. 1. Ionization chamber and arrangement of guard rings.

The chamber was operated with a positive potential of 450 volts applied to the outer electrode. The inner collecting electrode was within a fraction of a volt of ground potential and was connected to the grid of a VX-41 electrometer tube with a grid leak resistor of 10^{12} ohms. A switch was provided for grounding the grid. The electrometer tube was coupled directly to a balanced amplifier consisting of a pair of 6SH7 tubes. A 6-μf capacitor coupled the amplifier to a critically damped galvanometer with a free period of 1.1 sec and a sensitivity of 7.7×10^{-9} amp mm^{-1} at 1 meter. Light reflected from the galvanometer mirror fell on a slit behind which a strip of photographic paper (Eastman #797) moved at the rate of 40.8 in. hr^{-1}. An alpha-particle from a neutron capture produced a deflection of about 8 mm. By examining the record a pulse-height frequency distribution curve was obtained.

Some pulses observed corresponded to alpha-particles emitted from the chamber walls. Background measurements were taken with the chamber surrounded by a layer of borax at least 2 in. thick. Outside the borax, paraffin was placed in the same amount as was used for the neutron measurements. In some of the preliminary runs it was found that an appreciable number of neutrons were entering the detector from outside the paraffin block by traveling along the detector axis. These neutrons were eliminated by thick borax absorbers placed over the ends of the detector.

Observations were made with the large paraffin block of 770 lb and with the same amount of paraffin mixed

TABLE I. Dimensions of ionization chamber.

Inside diameter of cylinder	7.42 cm
Thickness of wall	0.10
Diameter of inner conductor	0.476
Inside length	25.40
Volume	1094. cm^3

* A portion of a thesis submitted by A. R. T. to the Graduate School of Yale University, May, 1948.
† Now at Armour Institute of Technology.
‡ Assisted by the Joint Program of the ONR and AEC.
[1] C. G. Montgomery and D. D. Montgomery, Phys. Rev. **56**, 10 (1939).
[2] S. A. Korff and E. T. Clarke, Phys. Rev. **61**, 422 (1942).
[3] M. Kupferberg and S. A. Korff, Phys. Rev. **65**, 253 (1944).
[4] B. Hamermesh and S. A. Korff, Phys. Rev. **70**, 429 (1946).
[5] A preliminary amount of these experiments has been published: Phys. Rev. **75**, 894 (1948). The results of subsequent experiments at mountain altitudes are given in Phys. Rev. **76**, 1478 (1949).

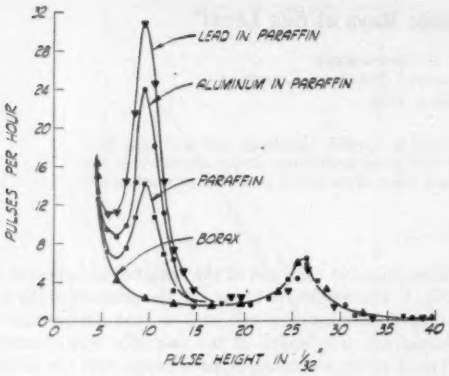

FIG. 2. Pulse-height distributions observed.

with 517 lb of lead and with 749 lb of aluminum. The lead was in the form of square sheets 5 in. on a side and 0.26 in. thick. Smaller pieces were cut and carefully arranged in the region near the detector so as to maintain a constant average density of lead and paraffin. The aluminum was in sheets 6.5 cm wide, 93 cm long, and 1.9 cm thick. Here also smaller pieces were used near the detector. Measurements were taken for each substance in several runs of five hours each to ensure constancy of operating conditions.

The apparatus was located in New Haven (60 meters elevation) on the second floor of a light wooden building in a room at an outside corner.

III. RESULTS

The principal observations resulted in the size distribution curves shown in Fig. 2. The peak caused by the neutrons is seen to be large compared with the background and well resolved. The total number of neutron pulses from paraffin, for example, is equal to the area between the background curve and paraffin curve. This area is best determined by counting the pulses greater than about $\frac{3}{16}$ in. For the smaller pulses some uncertainty exists because of confusion with the ion-chamber noise. The background was therefore subtracted from the number of pulses of each size and a symmetrical difference curve was plotted. An estimate of the area under the difference curve for sizes less than $\frac{3}{16}$ in. was taken to be the correct number of counts. Because of the finite resolving time two closely spaced pulses would be counted as one. The necessary correction was estimated using a resolving time of 0.5 sec. Each of these small corrections was less than the statistical uncertainty of the measurements. The peak at large pulse sizes was probably caused by radioactive contamination on the inner surface of the chamber.

TABLE II. Assumed values of nuclear cross sections in barns.

Substance	Total cross section	Capture cross section
H	41	0.29
B	830	830
C	4.6	0.0045
Al	1.6	0.23
Pb	11	0.17
Paraffin	86.4	0.59

TABLE III. Values of derived constants.

Substance	Diffusion length (cm)	Neutron mean life (sec)	Average density metal (g/cm³)	Average density paraffin (g/cm³)	$1/\phi$
BF_3 at 1 atmos	25.9	179	——	——	——
Paraffin	2.16	180	——	0.87	1.69
Pb par.	2.19	178	0.56	0.83	1.67
Al par.	2.57	197	0.64	0.66	2.03

TABLE IV. Rates of neutron production in units of 10^{-4} g^{-1} sec^{-1}.

Substance	Rate	Rate corrected for cosmic-ray absorption
Paraffin	1.98±0.07	2.6
C	2.31±0.08	3.0
Al	3.49±0.20	5.2
Pb	6.47±0.24	8.7

To calculate the rate of production of neutrons from the observed number of pulses, use was made of diffusion theory. The neutrons, produced at high energy, were rapidly slowed down to thermal energies in the paraffin and a continuous distribution of thermal neutron sources was effectively present. Since this work was done, diffusion calculations have been published by Draper.[6] His result can be written [see Eq. (14) of reference 6] as

$$\Sigma_i q_i \rho_i = n\tau_B / V_B \tau \phi, \tag{1}$$

where q_i and ρ_i are the rate of production of neutrons g^{-1} sec^{-1} and the average density of the ith component of the mixture surrounding the detector, n is the number of pulses per second, V_B the volume of BF_3, τ and τ_B are the mean lives of a thermal neutron in the mixture and in the BF_3 and ϕ is a diffusion factor. The value of ϕ is given by

$$\frac{1}{\phi} = \frac{1}{\rho} + \tfrac{1}{2}k^2 \frac{r\tau_B}{\tau_B L}\left[\frac{iH_0^{(1)}(ir_B/L)}{H_1^{(1)}(ir_B/L)}\right], \tag{2}$$

where k is the ratio of the detector radius r_B to the radius of the hole in the surrounding medium, L the diffusion length in the medium and $H_0^{(1)}$ and $H_1^{(1)}$ are the Hankel functions of the first kind. The quantity ρ is representative of the variation of neutron density over the volume of the counter. Its value is calculated also in reference 6. By some simplifying assumptions which are valid for the present experiment, it can be shown that

$$\rho = \frac{-2iJ_1(ir_B/L_B)}{(r_B/L_B)J_0(ir_B/L_B)}, \tag{3}$$

[6] J. E. Draper, Nucleonics 6, No. 3, 32 (1950).

where L_B is the diffusion length in the detector. In these experiments $\rho=0.996$. It can also be shown that a similar correction for the finite size of the paraffin is entirely negligible.

The nuclear cross sections used in the calculations are given in Table II. In Table III are the derived constants to be substituted in Eqs. (1–3). By combining the rates of production observed for paraffin and for the mixtures, the individual rates of production were obtained. There are given[7] in Table IV. The value for carbon was calculated from that found for paraffin assuming that the hydrogen did not contribute and that the composition was C_nH_{2n}.

Owing to the absorption of the radiation responsible for neutron production in the paraffin and in the metal some correction should be applied to the rates observed directly. With the paraffin alone present 29 g/cm² of paraffin was above the detector. The aluminum added an additional 28 g/cm² and the lead 19.5 g/cm². An approximate correction has been made as follows. The variation of the number of neutrons with elevation corresponds to a mean free path[8] in air of about 150 g/cm². It was assumed that this mean free path varies as the cube root of the mass number of the nucleus. Thus for lead, for example, the value of 366 g/cm² was calculated. The observed rates were then multiplied by the appropriate absorption correction factors and the results are given in the last column of Table IV. The corrected rates are, of course, uncertain not only because of inaccuracies in the assumed absorption coefficients but also from the neglect of possible transition effects.

[7] In the preliminary account of the exponents given in reference 5, the value for aluminum was in error because of a numerical mistake.

PHYSICAL REVIEW VOLUME 81, NUMBER 4 FEBRUARY 15, 1951

Alpha-Particle Groups from the $N^{14}(d, \alpha)C^{12}$ and $N^{15}(d, \alpha)C^{13}$ Reactions*

R. Malm† and W. W. Buechner
Physics Department and Laboratory for Nuclear Science and Engineering, Massachusetts Institute of Technology, Cambridge, Massachusetts

(Received October 26, 1950)

The alpha-particle groups from N^{14} and N^{15} targets bombarded with 1.4-Mev deuterons have been studied using a magnetic spectrometer. The Q-value for the $N^{14}(d, \alpha)C^{12}$ reaction is found to be 13.575 ±0.012 Mev, and the energies of the excited states observed in C^{12} are 4.438±0.014 and 9.620±0.013 Mev. For the $N^{15}(d, \alpha)C^{13}$ reaction, the Q-value is measured as 7.681±0.006 with excited states in C^{13} at 3.083 ±0.005 and 3.677±0.005 Mev.

I. INTRODUCTION

AMONG the various methods of exciting and studying the bound energy states of C^{12} and C^{13}, the $N^{14}(d, \alpha)C^{12}$ and $N^{15}(d, \alpha)C^{13}$ reactions have high Q-values, making them particularly suitable for investigating these nuclei over a wide range of excitation. The studies of the first reaction have shown[1,2] the presence of levels in C^{12} at 4.5 and 7.0 Mev, in general agreement with the results from other reactions. These results have recently been summarized by Hornyak, *et al.*[3] In the case of the $N^{15}(d, \alpha)C^{13}$ reaction, only the highest energy group of alpha-particles which is associated with the formation of C^{13} in the ground state has been observed.[1] With the objective of investigating these nuclei over a wider range of excitation, we have studied the alpha-particle groups emitted by thin targets containing N^{14} and N^{15} when bombarded with 1.4-Mev deuterons.

II. APPARATUS AND EXPERIMENTAL PROCEDURE

The experimental equipment has been described in previous papers.[4,5] Magnetic analysis was used both in the selection of the incident beam of deuterons of known energy and the investigation of the disintegration alpha-particles. The angle of observation was 90° with respect to the deuteron beam, and photographic detection was employed.

The energies of the observed alpha-particle groups were computed from measurements of the radii of curvature and the corresponding magnetic fields. The fields were measured with an analytical balance-type fluxmeter. The fluxmeter was calibrated on the basis of Brigg's value[6] for the Hr of RaC′ alpha-particles, from Lewis and Bowden's value[7] for the ratio of the

* This work has been assisted by the joint program of the ONR and AEC.
† AEC Predoctoral Fellow, now at Argonne Laboratories.
[1] M. G. Holloway and B. L. Moore, Phys. Rev. **58**, 847 (1940).
[2] Guggenheimer, Heitler, and Powell, Proc. Roy. Soc. (London) **A190**, 196 (1947).
[3] Hornyak, Lauritsen, Morrison, and Fowler, Revs. Modern Phys. **22**, 291 (1950).
[4] Buechner, Strait, Stergiopoulos, and Sperduto, Phys. Rev. **74**, 1569 (1948).
[5] R. Malm and W. W. Buechner, Phys. Rev. **80**, 771 (1950).
[6] G. H. Briggs, Proc. Roy. Soc. (London) **A157**, 183 (1936).
[7] W. B. Lewis and B. V. Bowden, Proc. Roy. Soc. (London) **A145**, 250 (1934).

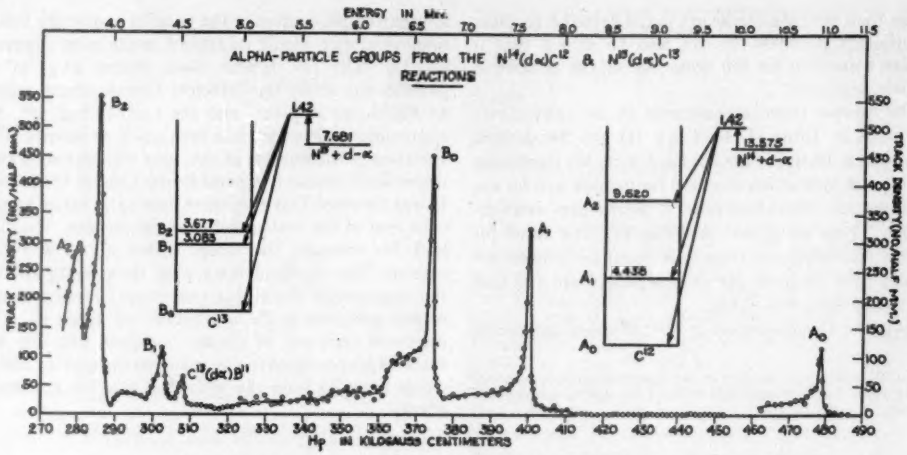

FIG. 1. Alpha-particle groups from tantalum-nitride target in which N^{14}:N^{15} ratio was 40:60. Energy of incident deuteron beam was 1.420 Mev.

velocities of these alpha-particles and polonium alpha-particles, and from measurements of the radius of curvature of polonium alpha-particles in the present analyzing magnet using a magnetic field of suitable strength. A value of 3.3159×10^5 gauss-cm for polonium alphas has been used in the calculations. In the conversion from the observed Hr values to the corresponding particle energies, a value[8] of 9652.2 emu/g has been used for the faraday. A similar fluxmeter has been used for the measurement of the fields of the magnet employed for deflecting the incident deuteron beam. This fluxmeter is calibrated from observations of the energy of the deflected deuterons after they have been scattered from thin foils.

Although we have often observed weak alpha-particle groups from the surface contamination of nitrogen on many targets, the low concentration of only 0.4 percent of N^{15} in normal nitrogen makes the use of such contamination layers impractical for studying the $N^{15}(d,\alpha)$ reaction. In the present work, the targets consisted of thin layers of tantalum nitride on tantalum, prepared as outlined in a previous paper.[5] For purposes of identifying the various groups observed, targets with both normal and enriched concentrations of N^{15} were used, together with observations on the changes in energy of the groups as the incident deuteron energy was varied. Surface contaminations on these targets were eliminated to a large extent by maintaining the targets at a dull red heat during bombardment. The thickness of those surface layers not removed in this way was determined from comparisons of the energy of one of the alpha-particle groups from the heated targets with that of the same group from a freshly prepared target consisting of a thin deposit of ammonium nitrate on platinum. Appropriate corrections for the effects of these surface layers were made in all of the measured particle energies. In no case was the correction more than 10 kev.

A disadvantage of the tantalum-nitride targets is that the nitrogen is not confined solely to a thin surface layer but appears to be present in small amounts to a considerable depth in the tantalum. Thus, there is associated with each group of alpha-particles a number of lower energy particles, which, together with those from $N^{14}(d,2\alpha)Be^8$, lead to a background between the observed peaks. A correction for the effects of this background was made when determining the radius of curvature of each group. An analytical correction to the measured radii of curvature was made for the small effects due to the finite acceptance angle of the nuclear-track plates and to the fact that the particles are emitted from a line rather than from a point source on the target.

III. RESULTS

In these experiments, each photographic plate was exposed at a fixed field strength and thus recorded an interval in the momentum spectrum of the charged particles emitted from the target. The alpha-particle groups shown in Fig. 1 were observed from an unheated tantalum-nitride target in which the N^{15} concentration was approximately 60 percent of the total nitrogen content. The results were obtained from a number of plates exposed at different magnetic fields so as to cover the range of alpha-particle energies from 3.5 to 11.5 Mev. The incident deuteron energy was 1.420 Mev, and the field strengths were so chosen that the regions covered by each plate overlapped slightly. Separate plates were taken on each of the observed groups using heated targets in order to minimize the effects of surface layers

[8] J. W. M. DuMond, Phys. Rev. 77, 411 (1950).

TABLE I. Data on $N^{14}(d, \alpha)C^{12}$.

Group	Q-value for $N^{14}(d, \alpha)C^{12}$ (in Mev)	Level in C^{12} (in Mev)
A_0	13.575±0.012	0
A_1	9.137±0.006	4.438±0.014
A_2	3.955±0.003	9.620±0.013

on the measured energies. The weak group at 308 kgauss-cm has been identified from other experiments as arising from carbon contamination and was not observed from the heated targets.

Three of the groups shown in Fig. 1 have been identified as arising from the $N^{14}(d, \alpha)C^{12}$ reaction. These are labeled A_0, A_1, and A_2. The Groups A_0 and A_1 have been observed previously[1,2] and correspond to transitions to the ground state and the first excited state of C^{12}. The A_2 group has not been reported by other observers, although the level in C^{12} at 9.7 Mev to which it corresponds is well known from studies of other reactions.[3] The measured Q-values for these groups are 13.622, 9.137, and 3.955 Mev.

We have considerable evidence that, at the high magnetic fields required for deflecting the A_0 group, the measured field strengths may be too high by approximately 0.1 percent. At these high fields, the iron of the magnet is close to saturation, and it appears that in this region the field at the position of the fluxmeter is not accurately proportional to that in which the particles are focused. This effect is probably associated with small irregularities in the magnet core. Consequently, we believe that a more precise value for the Q-value for the ground-state group A_0 is obtained by adding our measured Q-values for the $N^{14}(d, p)N^{15}$ and the $N^{15}(p, \alpha)C^{12}$ reactions. These are 8.615±0.009 and 4.960±0.007 Mev, respectively.[4,5] This cycle leads to a value of 13.575±0.012 Mev for the $N^{14}(d, \alpha)C^{12}$ reaction. The difference of 47 kev between this value and that directly measured is closely of the amount and in the direction to be expected from our measurements on the saturation effects in the magnet.

A similar value for the $N^{14}(d, \alpha)C^{12}$ reaction is obtained from the consideration of other cycles. Thus, using a value of 7.681±0.009 from the present paper for $N^{15}(d, \alpha)C^{13}$, 2.716±0.005 for $C^{12}(d, p)C^{13}$, and 8.615±0.009 Mev for $N^{14}(d, p)N^{15}$, we obtain 13.580 ±0.015 Mev. Additional confirmation of this value is obtained from the measured energy of the first excited state of C^{12} from the $N^{15}(p, \alpha)$ reaction. Schardt has measured the Q for the short-range alpha-particles from this reaction[5] as 0.529±0.008 Mev, while we find 4.960 ±0.007 for the ground-state group. These two values give 4.431±0.011 Mev for the first level in C^{12}, in agreement with measurements on the gamma-radiation from this level. This energy when added to the Q for the A_1 group which is associated with the same level leads to 13.568±0.012 Mev for $N^{14}(d, \alpha)C^{12}$.

[4] Strait, Van Patter, Buechner, and Sperduto (to be published).

The present results on this reaction are summarized in Table I.

Previous work on this and other reactions[3] indicates a level in C^{12} at approximately 7 Mev. Recently, from studies of the $Be^9(\alpha, n)$ reaction, Guier and Roberts[10] have also found groups which they attribute to this level and to one at 7.9 Mev. If these levels were excited in the present reaction, the corresponding alpha-particle groups would be observed in the region between 330 and 350 kgauss-cm. As can be seen in Fig. 1, there is no evidence for peaks in this region, although the alpha-particle background might obscure any weak groups if such were present. Since the reported groups corresponding to these levels have been of low intensity, it is probable that the levels would not be observed in the present work.‡

The alpha-particle groups arising from the $N^{15}(d, \alpha)C^{13}$ reaction are labeled B_0, B_1, and B_2 in Fig. 1. While only the B_0 group has been previously reported,[1] the excited states in C^{13} to which these groups correspond are well known from studies of other reactions. The Q-values for the groups measured in the present work are tabulated in Table II, together with the excited levels in C^{13} with which they are associated.

While these values for the levels in C^{13} are in general agreement with the results from other reactions,[3] the value for the first level observed in these experiments is somewhat lower than the value of 3.098±0.008 which we have reported[11] from the $C^{12}(d, p)C^{13}$ reaction. Recently we have remeasured this reaction in the light of improved values for certain geometrical and other factors. The more recent Q-value for this reaction is 2.716±0.005 Mev for the ground-state group. This leads to a value of 3.086±0.005 Mev for this level when measured from the $C^{12}(d, p)C^{13}$ reaction, in good agreement with that obtained in the present work.

It is interesting to note that, as in the previous work of Heydenburg, Inglis, Whitehead, and Hafner[12] and the work in this laboratory[11] on $C^{13}(d, p)C^{13}$, the data in Fig. 1 show no evidence for a group which would correspond to a level in C^{13} in the region from 0.8 to 1.0 Mev. Such a level has often been reported from the

TABLE II. Data on $N^{15}(d, \alpha)C^{13}$.

Group	Q-value (in Mev)	Level in C^{13} (in Mev)
B_0	7.681±0.006	0
B_1	4.598±0.004	3.083±0.005
B_2	4.004±0.003	3.677±0.005

[10] W. H. Guier and J. H. Roberts, Phys. Rev. 79, 719 (1950).

‡ *Note added in proof:* Recently, Terrell has studied the gamma-radiation from $Be^9(\alpha, n)C^{12*}$ using a pair spectrometer [Phys. Rev. 80, 1076 (1950)]. His work shows that, if a level in C^{13} at 7 Mev is excited in this reaction, the gamma-radiation associated with it has an intensity less than one-half percent that from the 4.44-Mev level in C^{12}.

[11] Buechner, Strait, Sperduto, and Malm, Phys. Rev. 76, 1543 (1949).

[12] Heydenburg, Inglis, Whitehead, and Hafner, Phys. Rev. 75, 1147 (1949).

$B^{10}(\alpha, p)C^{13}$ reaction; and, although the recent study of this reaction by Creagan[13] failed to show such a group, the result may not be definite, since this work also failed to show the well-known 3.1-Mev level. More recently, Berlman, using 10-Mev deuterons, has reported[14] a proton group from the $C^{12}(d, p)C^{13}$ reaction that leaves C^{13} in a 1.0-Mev excited state. If a level between 0.8 and 1.0 Mev were excited in the present reaction, the alpha-particle group would appear in the region between 355 and 360 kgauss-cm. While the background in this region would obscure weak groups, we conclude that, if such a level is excited, the intensity is less than 0.1 that of the ground-state transition.**

The measured half-widths of the alpha-particle groups in Fig. 1 have been compared with the half-widths that would be expected if the broadening of the lower energy peaks were due entirely to the effects of target thickness. The measured and computed half-widths are in reasonable agreement except for the $N^{14}(d, \alpha)C^{12}$ group labeled A_2. As can be seen from Fig. 1, the half-width of this group is nearly twice that of group B_2, which has nearly the same energy and which appeared on the same nuclear-track plate. Since there is no reason to expect a difference between the effective thicknesses of the TaN^{14} and TaN^{15} layers on the enriched target, it is believed that this increased width is not an instrumental effect. Although it is possible that the group A_2 actually consists of two closely spaced groups which were not resolved,§ it is to be noted that when C^{12} is in the 9.62-Mev excited state, a transition to Be^8 plus an alpha-particle is energetically possible. The possibility of this alternative mode of decay for this state may contribute to the width of the A_2 group.

In the recent work of Guier and Roberts[10] on the $Be^9(\alpha, n)C^{12}$ reaction, the neutron group associated with the 4.4-Mev level in C^{12} was found to have considerable breadth, and it was suggested that this level might not be single. The width of the peak A_1 in Fig. 1 suggests that such structure is not present in the level excited in the $N^{14}(d, \alpha)C^{12}$ reaction at the bombarding energies used in this work.

We are indebted to our colleagues in the High Voltage Laboratory for much helpful discussion and assistance. We are particularly grateful to Mrs. C. Bryant and Mr. W. A. Tripp for their careful measurements on the photographic plates.

[13] R. J. Creagan, Phys. Rev. **76**, 1769 (1949).
[14] I. B. Berlman, Phys. Rev. **79**, 411 (1950).

** Very recently, Blundell and Rotblat [Phys. Rev. **81**, 144 (1951)] have reported that their studies of the $C^{12}(d, p)C^{13}$ reaction using 8-Mev deuterons show no evidence of a level in C^{13} between the ground state and the 3.11-Mev state, and they suggest that the proton group reported as associated with a 1-Mev level in C^{13} may be due to oxygen contamination.

§ Since this manuscript was submitted for publication, we have learned from R. G. Thomas in a private communication that Rotblat has recently reported studies of $C^{12}(d, p)C^{13}$ which show a level in C^{13} at 3.9 Mev in addition to those at 3.1 and 3.7. In the present experiments, a level at 3.9 Mev would lead to an alpha-particle group at 280 kgauss-cm. From the variation of the yield of peak A_2 (Fig. 1) with the percentages of N^{14} and N^{15} in the targets, we conclude that no intense group corresponding to a 3.9-Mev level in C^{13} is present. However, the possibility of a weak group in this region from the $N^{15}(d, \alpha)C^{13}$ reaction cannot be excluded, and it is possible that the unexpected width of the A_2 peak arises from such a group. If this is the case, the Q-value reported here for the A_2 group and the corresponding level in C^{13} may be somewhat in error, the amount depending on the intensity and location of the other group.

Gamma-Radiation from Pb^{206}

D. E. Alburger and G. Friedlander
Brookhaven National Laboratory, Upton, New York*
(Received October 20, 1950)

Gamma-rays accompanying the electron capture decay of 6.4 day Bi^{206} and the alpha-decay of 138-day Po^{210} have been observed by measurement of internal conversion electrons and photo-electrons with a lens spectrometer. The bismuth activity showed resolved lines corresponding to gamma-rays of 182, 234, 260, 341, 396, 470, 505, 536, 590, 803, 880, 889, 1020, 1097, and 1720 kev. A thin Po^{210} source of 480-mc alpha-particle strength was found to emit gamma-rays of 800±6 kev energy which yielded K and L internal conversion lines in the ratio of 3.7±0.5 to 1. The 803-kev gamma-ray observed in both the Bi^{206} and Po^{210} activities is identified with a transition from the first excited state of Pb^{206} to the ground state.

I. INTRODUCTION

THE present investigation originated in connection with a study[1] of the 68-min isomer of Pb^{204} and its parent, 12-hr Bi^{204}. The bismuth was produced by cyclotron bombardment of lead according to the reaction $Pb^{204}(d,2n)Bi^{204}$. Studies of gamma-radiation from the Pb^{204} isomer, chemically separated from the Bi^{204} parent, were made with a lens spectrometer. Measurements were also attempted on sources of bismuth, chemically separated from targets of ordinary lead, in order to observe the spectrum of Bi^{204} in equilibrium with Pb^{204}. An intense and complex structure of lines was found, most of which decayed with a half-life of about 6 days. To clearly distinguish the 12-hour Bi^{204} lines from the other activity present, cyclotron targets enriched in Pb^{204} by a factor of 15 over normal lead were used. It was suspected that the background activity was that associated with the electron capture decay of 6.4-day Bi^{206} produced from the more abundant Pb^{206} isotope by the $Pb^{206}(d,2n)Bi^{206}$ reaction.[2]

Because of recent general interest in the isotopes of lead the 6-day activity has been investigated further with the aim of substantiating its assignment to Bi^{206} and studying transitions in the residual nucleus Pb^{206} both in this and related processes. No previous spectrometer measurements on Bi^{206} have been reported while absorption experiments have yielded a variety of results.[2]

Other processes known to lead to the same product nucleus are the β^- decay of 4.23-min Tl^{206} and the α-decay of 138-day Po^{210}. Facilities for investigating the former are not yet available here. However, the polonium problem seemed feasible and is of interest both on account of its relationship to Bi^{206} and because a well-defined spectrometer measurement had not been made. It was hoped that such a study might assist in the determination of the group structure of the Po^{210} alpha-particle spectrum.

The polonium spectrum has long been thought to consist of a single alpha-particle line at 5.3 Mev. Weak gamma-radiation was also known[3] to be associated with the decay of polonium to the extent of about 1 quantum per 10^5 alphas and having an energy of about 0.8 Mev as determined by absorption experiments. Bothe examined[4] the internal conversion lines from a 30-mc Po^{210} source by means of a semi-circular focusing spectrometer at 7 percent resolution. He reported gamma-ray energies of 202, (355), (433), 798, and 1068 kev, of which the 798 line was the most intense; those in parenthesis were considered doubtful. Later Siegbahn and Slätis measured[5] the photo-electrons from a lead converter in a lens spectrometer and found one gamma-ray having an energy of 0.773 Mev in approximate agreement with Bothe's most intense line. An 86-mc polonium source was used and the resolution was sufficient to show only the K-shell electron peak. In separate absorption experiments the energy was checked and no other components were detected. An absorption measurement by DeBenedetti and Kerner[6] gave a similar result, but Zajac, Broda, and Feather found[7] in addition to the 0.8-Mev component, soft gamma-ray lines of which the most intense was at 84 kev.

The presence of gamma-radiation in the decay of Po^{210} indicates weak branching to one or more excited states of Pb^{206} and suggests that alpha-particles of energy lower than the 5.3 Mev group should occur. Chang examined[8] this region with an alpha-particle spectrograph of high resolution and found 12 weak lines spaced about 100 kev apart. The existence of such lines with the observed intensities would have been difficult to explain theoretically. In an experimental check[9] Wadey failed to confirm this fine structure and attributed Chang's results to source backing effects. The most recent alpha-spectrograph study was made[10] by Wagner who discovered 30 groups of alpha-particles

* Under contract with the AEC.

[1] Sunyar, Alburger, Friedlander, Goldhaber, and Scharff-Goldhaber, Phys. Rev. **78**, 326A (1950); Phys. Rev. **79**, 181 (1950).

[2] G. T. Seaborg and I. Perlman, Revs. Modern Phys. **20**, 585 (1948).

[3] N. Feather, Phys. Rev. **70**, 88 (1946) gives a summary of experiments.

[4] W. Bothe, Z. Physik **96**, 607 (1935).

[5] K. Siegbahn and H. Slätis, Arkiv. Mat. Astron. Fys. **34A**, No. 15 (1947).

[6] S. DeBenedetti and E. H. Kerner, Phys. Rev. **71**, 122 (1947).

[7] Zajac, Broda, and Feather, Proc. Phys. Soc. London **60**, 501 (1948).

[8] W. Y. Chang, Phys. Rev. **69**, 60 (1946).

[9] W. G. Wadey, Phys. Rev. **74**, 1846 (1949).

[10] J. J. Wagner, Microfilm Abs. (Universal Microfilms, Ann Arbor, Michigan, 1950), Vol. X, No. 1, p. 122.

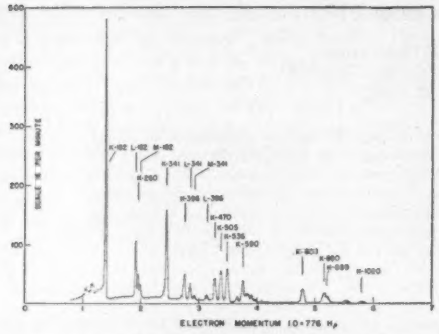

FIG. 1. Internal conversion spectrum of $Bi^{206}(K)Pb^{206}$ at 1.2 percent resolution.

from polonium samples. These were found to be independent of backing material and of intensity proportional to source thickness. It is stated, however, that the lines are probably not of nuclear origin, their explanation being unknown.

It appears, then, that a careful measurement of the polonium gamma-ray spectrum would serve as a guide to the location of the corresponding alpha-particle lines. In the present work this gamma-ray spectrum has been examined and compared with that of Bi^{206} decay.

II. EXPERIMENTAL

Gamma-ray measurements on bismuth and polonium activities were made with a lens spectrometer of conventional design. The instrument has a vacuum chamber 48 in. long and 10 in. i.d. and is equipped with a ring-focusing arrangement. With 5 mm diameter sources a resolution (full width at half maximum), of 1 percent can be attained. The coil current is regulated to about 0.1 percent by a circuit which compares the current shunt voltage with a potentiometer reference voltage. Calibration made with such standards as Cs^{137} or Co^{60} is generally reliable to about 0.5 percent.

Bi^{206} sources were prepared as follows: The deuteron-bombarded lead target was dissolved in hot 3 to 6N HNO_3, most of the lead removed as $PbCl_2$ by the addition of HCl, and the filtrate from the $PbCl_2$ made about 1N in HCl. This solution was then shaken for 20 to 30 minutes with a few hundred milligrams of nickel powder at 80 to 90°C in order to plate the carrier-free bismuth on the nickel. The nickel was centrifuged off, washed, and dissolved in hot 6N HNO_3, and 1 mg of iron as ferric salt was added to act as a carrier for the bismuth activity in the precipitation with excess ammonia which followed. To remove all the nickel, the ferric hydroxide (plus bismuth hydroxide) was washed, redissolved in acid, reprecipitated with ammonia, and washed again. It was then dissolved in 6N HCl, and the solution shaken with two successive portions of ethyl ether, previously equilibrated with 6N HCl. This removed the ferric ion almost quantitatively and left essentially carrier-free bismuth activity in the aqueous phase. The aqueous solution was heated to fuming with 1 ml of 6N H_2SO_4 to remove all chloride ions, and was then diluted to be about 2N in H_2SO_4. From this solution, the bismuth activity was deposited electrolytically. A small glass cell whose inside diameter at the bottom equalled the desired source diameter (usually 5 mm), was gasketed to a 0.001-in. thick copper foil which served as the cathode. A platinum stirrer was used as the anode and electrolysis was carried on for 30 to 90 minutes at a potential of about 3.5 volts. When no bismuth carrier was used the electrolysis yields were variable between 10 and 80 percent. Addition of 10 to 100 μg of bismuth carrier helped somewhat in assuring higher yields.

Observations were made on the 6-day bismuth spectrum after the 12-hour Bi^{206} lines had died out by measuring internal conversion lines in the lens spectrometer. Photo-electrons produced by Bi gamma-rays in a 21.5 mg/cm² lead converter were also examined. In this case a 2-mm thick brass plate separated the converter from the source in order to absorb the internal conversion electrons.

The Po^{210} source was specially prepared for this work by the AEC. It consisted of carrier-free polonium deposited on a nickel disk over an area 0.5 cm in diameter, and covered with 0.2 mil gold foil (~10 mg/cm²) for the purpose of reducing the spread of contamination. The foil had been clamped with a metal ring and sealed at the outer edges with a vacuum evaporated coating. At the time of frabrication the alpha-particle strength was 478 mc, and from this the thickness of the source is estimated to be ~0.5 mg/cm². Both the polonium internal conversion electrons and photo-electrons produced in a uranium converter by polonium gamma-rays were measured in the lens spectrometer.

III. EXPERIMENTAL RESULTS

Figure 1 shows the Bi^{206} internal conversion electron spectrum up to about 1.3 Mev taken at a resolution setting of 1.2 percent. Assignment of many of the resolved lines has been made as indicated in the figure. Not shown are weak K lines corresponding to 234- and 1097-kev gamma-rays. In addition, the internal conversion lines of a 1720 kev gamma-ray were observed after der Mateosian and Goldhaber[11] had shown that Bi^{206} produced photo-neutrons in beryllium but not in heavy water. The absence of background between the conversion lines in Fig. 1, other than that characteristic of scattering, indicates a K-capture process and no appreciable positron emission.

In the spectrum of photo-electrons due to Bi^{206} gamma-rays, many of the lines were not resolved because of the effects of converter thickness and the presence of a background of Compton electrons. However, the 1720-kev gamma-ray was again observed and

[11] E. der Mateosian and H. Goldhaber, Phys. Rev. **78**, 326(A) (1950).

a search made for other high energy lines which might have been missed in the internal conversion spectrum.

The half-life determined from measurements on the K-182 and K-341 lines over a period of 12 days was found to be 6.2±0.5 days in good agreement with the value 6.4 days assigned[12] to the K-capture decay of Bi^{206} by Templeton, Howland, and Perlman. All of the other prominent lines appeared to decay at this rate since their intensities relative to the K-182 line remained the same throughout the measurements. However the possibility that the weak 234- and 1097-kev lines decay at a somewhat different rate cannot be ruled out. The only other known activity of comparable half-life[13] which might be present is 14-day Bi^{205}.

Unresolved lines due to nuclear gamma-rays are still present in the internal conversion spectrum of Bi^{206} but intensities of sources were not sufficient to make the measurements at significantly better resolution (i.e. ~0.7 percent). The region between 50 and 80 kev shows a distribution which might well be Auger electrons due to x-rays following K-capture. This unresolved yield is indicated in Fig. 1 at a regulator dial setting in the vicinity of 1.2. Exposure of a Bi^{206} source in a 180° focusing spectrograph with a 100 gauss permanent magnet showed 6 resolved Auger lines between 55 and 73 kev. In addition, the K, L, M and N lines of the 182-kev gamma-ray and the K lines of 260- and 339-kev gamma-rays were observed in this instrument whose range is limited to below 300 kev.

Coincidence measurements carried out by A. W. Sunyar showed a rather large number of $\gamma\gamma$-coincidences from Bi^{206} sources, which is consistent with the very complex gamma-ray spectrum observed. But attempts to find delayed $\gamma\gamma$- or $X\gamma$-coincidences failed, which indicates that none of the excited states of Pb^{206} reached in the Bi^{206} decay has a half-life between 10^{-7} and 10^{-4} second. To establish whether any of these levels have life times above 1 second, rapid separations of lead from

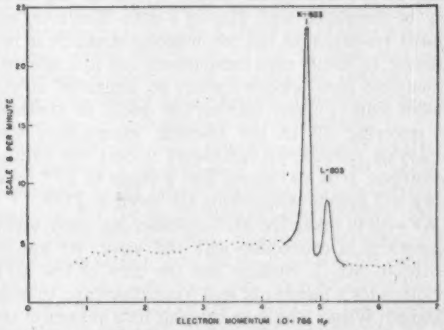

FIG. 2. Internal conversion electrons from a carrier-free Po^{210} source of 478 mc alpha-particle strength.

[12] Templeton, Howland, and Perlman, Phys. Rev. 72, 766 (1947).
[13] Way, Fano, Scott, and Thew, Nat. Bur. Standards, Circular 499.

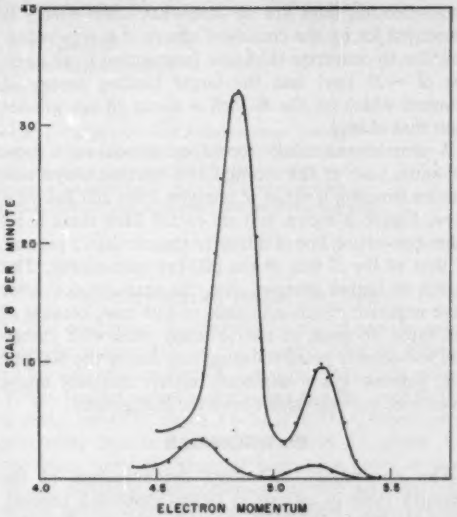

FIG. 3. A comparison of Po^{210} internal conversion electrons (upper curve) with photo-electrons from a 44 mg/cm² uranium converter (lower curve) both at 4.0 percent resolution.

Bi^{206} were carried out as follows. A small volume of hot 1N HCl solution of carrier-free Bi^{206} containing some Pb^{++} carrier was pulled through a bed of 200 mesh nickel powder placed on a sintered-glass funnel. Under the suction of flask receiving the filtrate was a G-M counter. The nickel removed 90 to 95 percent of the Bi, and the lead fraction could be counted within 1 to 2 seconds after separation. No active Pb^{206} of half-life greater than 1 second was found.

The Po^{210} internal conversion spectrum is given in Fig. 2 and shows that one gamma-ray is present yielding K and L-shell electrons in the ratio of 3.7±0.5 to 1. The gamma-ray energy is computed to be 800±6 kev, when a 10-kev correction has been made for energy loss in the gold foil protecting the source. The uncertainty of this correction is probably several kev because the foil thickness is not accurately known. The conversion lines here are somewhat asymmetrical due to scattering and absorption effects in both the source and protecting foil. This results in a line width of 2.5 percent although the spectrometer resolution in this case was 1.9 percent.

To study the Po^{210} gamma-ray spectrum further photo-electrons from uranium were examined at 4.0 percent resolution. The internally converted electrons were removed by a brass plate to which the uranium converter was attached and the arrangement was such that about 30 percent of all gamma-rays from the source were intercepted by the converter. The resulting photo-electron distribution is shown in the lower curve of Fig. 3 and may be compared with the internal conversion lines in the upper curve measured at the same spectrometer resolution setting. The fact that the

photo-electron lines are at somewhat lower energy is accounted for by the combined effects of energy reduction due to converter thickness (amounting to an average of ~23 kev) and the larger binding energy of uranium which for the K-shell is about 28 kev greater than that of lead.

A search was made for other gamma-rays from polonium both in the internal and external conversion studies covering a range of energies from 100 kev to 4 Mev. Figure 2 shows that up to 1.3 Mev there is no other conversion line of intensity greater than 5 percent of that of the K line of the 800-kev gamma-ray. The search at higher energies with the uranium converter gave negative results although, in this case, because of the rapid decrease of photoelectric yield with energy and the already small counting rate due to the 800-kev line, gamma-rays of moderate relative intensity might have been unobservable above the background.

IV. DISCUSSION

The uncertainty in energy determination of the bismuth lines is estimated to be about 0.5 percent. Since the 800-kev polonium gamma-ray is equal, within the probable error, to the 803-kev line is bismuth decay, it is reasonable to assume that both are, in fact, the result of the same nuclear transition. The bismuth value is considered to be the more accurate because of better resolution and the thinner sources used. The appearance of this gamma-ray in both spectra, taken together with the bismuth half-life measurement and lack of an electron continuum identifies the bismuth lines with the $Bi^{206}(K)Pb^{206}$ process.

Further evidence for the identity of the 803- and 800-kev gamma-rays might be obtained if a comparison of K/L ratios and internal conversion coefficients were possible. A measurement of the K/L ratio in the bismuth case could not be made because the L line is masked by the K lines of 880- and 889-kev gamma-rays. A determination of the internal conversion coefficient of the 803-kev bismuth line in the presence of so many other gamma-rays has not been feasible. In the polonium case an attempt to measure the conversion coefficient directly was made by W. Orr, but because of the very unfavorable source geometry, the results are at present inconclusive. However, with the following considerations a rough estimate of this coefficient may be obtained from the spectrometer curves of Fig. 3 in which the ratio of internal to external conversion is about 10. The yield of photo-electrons should be equal to the product of the gamma-ray strength, the efficiency of photoelectric conversion in the uranium converter including the solid angle it subtends at the source, a correction factor for the angular distribution of the photo-electrons, and the solid angle of the spectrometer. On the other hand, the internal conversion is isotropic so that in this case the yield is equal to the product of the gamma-ray strength, the conversion coefficient, and the spectrometer solid angle. In taking the ratio of these quantities the spectrometer solid angle and gamma-ray strength cancel giving the conversion coefficient in terms of the yield ratio and other factors which may be calculated. In this way, the conversion coefficient is found to lie between 0.01 and 0.05. This estimate has rather wide limits because the correction for the angular distribution of the photo-electrons is difficult to make under conditions in which the converter subtends a large solid angle at the source. Nothing definite can be said about the multipole order of the radiation since this range of values includes transitions from quadrupole to 2^4 pole according to the tables[14] of Rose, *et al.* Likewise, the measured K/L ratio cannot uniquely assign the multipole order since theoretical calculations at high Z have not as yet been made.

The absence of other lines from polonium suggests that the 803-kev gamma-ray is due to transition from the first excited state of Pb^{206} to the ground state. If lower excited states existed the barrier penetration probability for alpha-particle transitions to such states would be expected to be much greater than that for the transition to the 803-kev state because of the strong dependence of this probability on energy. Lower energy gamma-rays would therefore appear. States less than 100 kev above the ground state cannot be excluded since gamma-rays of such energy would not have been observable because of absorption of the conversion lines in the protective gold foil. The assignment of the 803-kev transition is in agreement with recent work by Harvey[15] in which the $Pb^{207}(d,t)Pb^{206}$ reaction was studied. Triton groups were observed corresponding to excited states in Pb^{206} at 0.86, 1.37, 1.71, 2.22, and 3.03 Mev. The curves[16] indicate a measuring accuracy of ~0.1 Mev; it is then possible that Harvey's first excited state corresponds to the 803-kev line found in the present work.

The remaining gamma-rays from Bi^{206} are presumably due to transitions from higher lying levels to the ground state, or between higher levels; several among these may be correlated with Harvey's data. However, the present resolution of the triton group structure is not sufficient to justify such comparisons and it is felt that a complete level scheme cannot be suggested at the present time. Further information would be obtained by resolving all of the bismuth gamma-rays and employing coincidence techniques to sort the various transitions. It is also hoped that a study of Tl^{206} beta-decay will help in establishing the levels in Pb^{206}.

We wish to thank Dr. M. Goldhaber for many useful suggestions in connection with this work. We are indebted to Mr. J. Bulkley and the crew of the MIT cyclotron for a number of lead irradiations and to Miss Elizabeth Wilson who gave valuable help in some of the source preparations and in the work with the 180° spectrograph.

[14] Rose, Goertzal, Spinrad, Harr, and Strong, private distribution.
[15] J. A. Harvey, MIT Prog. Report (April 1, 1950) (unpublished).
[16] J. A. Harvey (private communication to M. Goldhaber).

Coherent Scattering Amplitudes as Determined by Neutron Diffraction

C. G. SHULL AND E. O. WOLLAN
Oak Ridge National Laboratory, Oak Ridge, Tennessee
(Received October 6, 1950)

The coherent scattering properties of nearly 60 elements or nuclides for slow neutrons have been determined by neutron diffraction techniques and are summarized in the present paper. The phase of scattering and values for the coherent scattering amplitude and cross section and for the total scattering cross section are given. Pronounced differences in isotopic scattering properties have been found and many nuclides are shown to possess strong spin-dependent scattering properties. Illustrations of thermal diffuse scattering and nuclear spin incoherent scattering are given.

I. INTRODUCTION

CROSS sections for the interaction of fundamental particles with atomic nuclei are as yet essentially experimentally determined quantities. This will be the case until a much more detailed theory of nuclear structure than we now have is developed. The information furnished by a large variety of cross-section measurements will undoubtedly furnish much of the background for the development of nuclear theory.

It is with the measurement of scattering cross sections for neutrons of near thermal energy that this paper is concerned; more specifically, it will be concerned primarily with the measurement of coherent scattering cross sections.

For thermal neutrons the individual nuclear scattering processes will be elastic, since nuclear energy level spacings are large compared to kT. The existence of nuclear scattering resonances make neutron scattering cross sections vary widely with energy, but the cross sections for free nuclei will be essentially constant over the thermal region except in those cases where a resonance falls in this region. The actual value of the cross section in this region will depend, however, on the presence of resonance levels quite far removed from thermal energy, especially for light nuclei which have large neutron widths. Scattering cross sections may depend also on the spin of the scattering nucleus, there being two spin states ($i+\frac{1}{2}$ and $i-\frac{1}{2}$) of the compound nucleus, which may vary widely in their scattering properties. A combination of total and coherent scattering cross section measurements gives information on the amount of spin dependence in scattering.

Aside from the direct interest in neutron scattering cross sections, a knowledge of such cross sections is of importance in the interpretation of neutron diffraction patterns. For the application of neutron diffraction to crystallographic structure problems, accurate scattering cross section data fill the same role for neutrons as the structure amplitude data do in structure studies by x-ray diffraction. In the x-ray case, the necessary information has been determined theoretically by the Hartree method and the Thomas-Fermi model, which have been abundantly verified by experiment, whereas in the neutron case the corresponding data can, for the present at least, be determined only experimentally.

II. SCATTERING CROSS SECTIONS

The scattering of neutrons by nuclei can in many cases be represented as the scattering by an impenetrable sphere[1] of radius, R, equal to the nuclear radius. This is termed potential scattering and the cross section is given by $4\pi R^2$. Since $R \approx 1.5\times10^{-13}A^{\frac{1}{3}}$, this type of scattering cross section will increase as $A^{\frac{2}{3}}$, where A is the mass number. Thermal scattering cross sections should correspond approximately to this potential scattering when there are no resonances near thermal energy.

When resonance scattering effects make an important contribution to the cross section, large deviations from potential scattering may be observed.

When the scattering nucleus has a "spin" i, there will be two scattering amplitudes corresponding to the two spin states $i+\frac{1}{2}$ and $i-\frac{1}{2}$ of the compound nucleus. In the scattering of neutrons by free nuclei the cross sections for the two spin states cannot be observed separately, and the observed cross section is a weighted average for the two spin states. If we represent the amplitudes for scattering by a free nucleus by a, then the total cross section for scattering by a nucleus of spin i will be given by the weighted average

$$\sigma_s{}^f = 4\pi[(i+1/2i+1)a_{i+\frac{1}{2}}{}^2+(i/2i+1)a_{i-\frac{1}{2}}{}^2], \quad (1)$$

where the superscript f designates scattering by a free nucleus which one would have in a monatomic gas or in condensed systems when the incident neutron energy is large compared to the binding energies in the system. One method of observing free scattering cross sections is by transmission measurements, corrected for absorption effects, at energies greater than about 1 ev.

When cross section measurements are made on condensed systems with neutrons of near thermal energy, the effects of chemical binding and of interference between waves scattered by the various scattering entities making up the system must be understood and accounted for in deriving the true nuclear scattering effects.

Our measurements have been made on crystal powders with monochromatic neutrons of near thermal energy. In this case the scattered intensity shows the

[1] Feshbach, Peaslee, and Weisskopf, Phys. Rev. 71, 145 (1947).

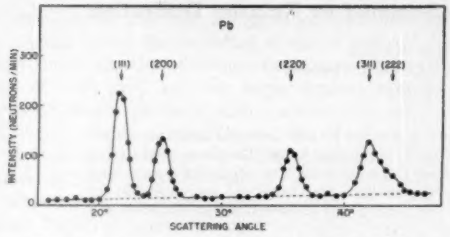

FIG. 1. Neutron diffraction pattern for powdered Pb.

usual Bragg interference lines, the intensities of which can be given in terms of the nuclear scattering amplitudes. These interference effects arise from the coherent scattering of neutrons from the regular array of atomic nuclei bound to discrete sites within a crystal. The amplitude of scattering by bound nuclei is related to the scattering amplitude for nuclei in the free state by

$$f=(A+1)a/A, \tag{2}$$

where f is the amplitude for bound, and a for free, nuclei. The total scattering cross sections for bound nuclei, σ_s^b, is obtained by substituting f for a in Eq. (1). In a crystal containing nuclei of one kind with spin i, the intensities in the interference peaks will result from a coherent cross section corresponding to the square of the sum of the bound spin amplitudes weighted for random distribution,

$$\sigma_{coh}=4\pi[(i+1/2i+1)f_{i+\frac{1}{2}}+(i/2i+1)f_{i-\frac{1}{2}}]^2, \tag{3}$$

and the effective coherent scattering amplitude will be $f_{coh}=\pm(\sigma_{coh}/4\pi)^{\frac{1}{2}}$.

When both the total and coherent scattering cross sections have been measured for a single nuclide with spin i, it is evident from Eqs. (1–3) that information concerning the individual spin amplitudes can be obtained. A large spin dependence corresponding to a large difference in $f_{i+\frac{1}{2}}$ and $f_{i-\frac{1}{2}}$ leads to a large difference in σ_s^b and σ_{coh}. This difference will show up as a spin diffuse scattering, which in most cases is approximated by $\sigma_s^b-\sigma_{coh}$, which equals

$$\sigma_{\text{spin diffuse}}=4\pi i(i+1)(f_{i+\frac{1}{2}}-f_{i-\frac{1}{2}})^2/(2i+1)^2. \tag{4}$$

When the weighted amplitudes are equal but opposite in sign, σ_{coh} goes to zero. When they are equal and of the same sign, as they will certainly be for zero-spin nuclei ($i=0$), $\sigma_s^b=\sigma_{coh}$.

Where a crystal contains an element having more than one isotope, each with spin i_n, the contribution of this element to the coherent scattering effects will be given by

$$\sigma_{coh}=4\pi\{\textstyle\sum_n p_n[(i_n+1/2i_n+1)f_{i_n+\frac{1}{2}}+(i_n/2i_n+1)f_{i_n-\frac{1}{2}}]\}^2, \tag{5}$$

where p_n is the fractional abundance of the nth isotope. The corresponding formula for the total bound scattering cross section involves the sum of the weighted individual amplitudes squared. It is evident that for an element containing several isotopes with different scattering amplitudes very little information about the individual amplitudes can be deduced from these two equations. If it is found experimentally that $\sigma_{coh}=\sigma_s^b$, it is evident that the individual amplitudes for the major isotopic constituents are very nearly equal, because only then are the coherent and total scattering cross sections equal.

III. POWDER DIFFRACTION TECHNIQUE

All of the data to be discussed have been obtained by the powder diffraction technique previously described for the case of neutrons.[2] At the present time two neutron diffraction spectrometers are in use at Oak Ridge. Both instruments are of the double-crystal type with monochromating crystals in the first position followed by the scattering sample (crystalline powder) at the second position. Most of the diffraction data have been collected with neutrons of wavelength 1.057A, although at some periods the spectrometers have been set for operation at 1.315A and also at intermediate wavelengths.

Both instruments are automatic in operation, being equipped with motor drives and recording counters. Small monitor counters are positioned in the monochromatic beams before the scattering sample and serve to monitor the number of neutrons incident upon the sample. Suitable recording of the primary intensity is done and this permits the diffracted intensities for a given pattern and for patterns from different samples to be adjusted to a common primary beam intensity. Figure 1 shows a typical powder pattern obtained with a sample of powdered Pb.

Single crystals of NaCl, Pb, Cu, Be, and Fe have been used as monochromators. In general the metallic crystals give more intense beams than does NaCl, since their mosaic spread more nearly matches the geometrical angular spread, about one degree, of the collimating system. This results in a more effective filling of the collimating system with radiation, although this is usually accomplished at some expense of wavelength resolution, so that the powder diffraction peaks are somewhat broadened particularly at the larger angles of scattering.

The powder samples to be studied are located on the center of the second spectrometer table. In the main two types of sample holders have been used. When sufficient material is available, a flat cell having an area of about 2 in.×2 in. and a thickness up to about $\frac{3}{4}$ in. is used. These cells are provided with thin windows of Al, glass, or quartz. The glass (~1 mm thick) windows attenuate the beam by about 4 percent and quartz (~0.5 mm thick) about 2 percent; but they give a good flat surface, so that the mass per unit area of the sample can be accurately determined; and they give rise to no sharp intensity peaks to contaminate the

[2] E. O. Wollan and C. G. Shull, Phys. Rev. 73, 822 (1948).

powder pattern. Thin Al windows give a negligible attenuation of the beam, and these can be used when the Al powder peaks do not coincide in angular position with peaks from the sample in question, In the study of diffuse scattering effects, the amorphous pattern produced by glass or vitreous quartz may be troublesome and it may be found desirable to use metallic foil windows.

When the available sample material is scarce, as in the case of separated isotope samples, a more efficient use of the sample may be effected by placing it within a thin-walled Al cylindrical tube. By having this tube diameter smaller than the beam width, all of the sample is bathed in neutron radiation and the absorption corrections are amenable to calculation, just as the extended flat specimens described above.

The powder pattern intensities give the coherent scattering cross sections or amplitudes of the elements making up the scattering sample. The power in a neutron beam coherently scattered from a flat plate of crystalline powder (oriented in the conventional method for scattering by transmission) is represented by the corresponding expression for x-ray diffraction except that in the neutron case the polarization factor is omitted

$$P_{hkl}=P_0\lambda^3 lh\rho' \exp(-\mu h \sec\theta) j_{hkl} N^2 F_{hkl}^2/4\pi r\rho \sin^2 2\theta, \quad (6)$$

where P_{hkl} is the total power in an (hkl) reflection as measured through a counter slit opening of height l at a distance r from the sample, P_0 the primary beam power, λ the neutron wavelength, ρ' the apparent density of the powder, ρ the density of the solid crystal, $e^{-\mu h}$ the transmission of the specimen of thickness h, θ the glancing or Bragg angle of reflection, j_{hkl} the multiplicity value, N the number of unit cells per cm^3 of crystal, and F_{hkl} the crystal structure scattering amplitude per unit cell at the crystal temperature at which the measurements are made,

$$F_{hkl}=\sum_{\substack{\text{atoms in}\\ \text{unit cell}}} \exp[2\pi i(hx_j+ky_j+lz_j)]\cdot f_j \cdot\exp[-W(T)\sin^2\theta_{hkl}/\lambda^2], \quad (7)$$

where f_j is the coherent scattering amplitude of the jth atom in the cell, and $\exp[-W(T)\sin^2\theta_{hkl}/\lambda^2]$, the Debye-Waller temperature factor for the hkl reflection in question.

The crystal structure scattering amplitude, F_{hkl}, as here used differs from common usage in x-ray terminology in that the dimensions of scattering amplitude are here retained in f_j. In any case, F_{hkl} is obtained by a suitable summation of scattering amplitudes over all of the uniquely-positioned atoms in the crystal, and hence it will depend upon the crystal structure of the sample. After such a summation is carried out, F_{hkl} will be represented as a simple function of the various atomic scattering amplitudes, and numerical evaluation of one or more F_{hkl} can be used to determine values for the individual atomic scattering amplitudes.

For the case of a cylindrical sample of volume V and cross-sectional area A completely bathed in primary radiation, the expression for the power in a diffracted beam becomes

$$P_{hkl}=P_0\lambda^3 lV\rho' N^2\cdot B j_{hkl}\cdot F_{hkl}^2/8\pi r A\rho \sin\theta \sin 2\theta, \quad (8)$$

with B being the absorption correction factor and all other terms similar to the above. The absorption correction factor B is a function of the scattering angle and linear absorption coefficient and has been calculated for the cylindrical sample case by Blake[3] and conveniently represented in several literature references.[4]

The scattering amplitude of an atom for neutrons arises primarily from nuclear scattering; but there may, in the special cases of ferromagnetic and antiferromagnetic materials, be a sizeable contribution to the coherent scattering owing to the magnetic interaction between the magnetic moment of the neutron and that of the ions in the crystals. Since this effect occurs to an appreciable extent only in very special cases, with which we shall not be concerned in this paper, the coherent scattering amplitude can be considered here as arising from nuclear scattering only. Some of the materials which have been included in the present study do show magnetic scattering effects, and for these it has been necessary to resolve the observed data into its nuclear and magnetic components.

When the diffraction pattern is measured for a crystalline compound, the coherent scattering amplitude for the individual elements involved can generally be determined as with x-rays by measuring several peaks for which the contributions to the crystal structure scattering amplitudes by the elements in question are different. In order, then, to determine the coherent nuclear scattering amplitude for the elements in a powdered crystal sample, one requires (a) the wavelength λ of the monochromatic neutron beam falling on the powdered sample to be known, (b) the attenuation $e^{-\mu h}$ of the neutron beam in passing through the sample when the plate is oriented perpendicular to the beam, (c) the integrated intensities P_{hkl} in a series of powder diffraction rings, (d) the power P_0 in the incident monochromatic beam, and (e) values for the temperature correction factors. The first two of these are directly measurable quantities. A determination of the diffracted and primary beam intensities on an absolute scale, however, offers considerable difficulty and is worthy of further discussion.

A. Calibration of Scattered Intensities

A direct measurement of the power P_0 in the monochromatic incident beam offers considerable difficulty because of its geometrical size (approximately 1 cm by 3 cm) and rather high intensity of about 200,000

[3] F. C. Blake, Revs. Modern Phys. 5, 169 (1933).

[4] Int. Crystal Structure Tables, Vol. II (Bornträger, Berlin, 1935) or C. S. Barrett, *Structure of Metals* (McGraw-Hill Book Company, Inc., New York, 1943).

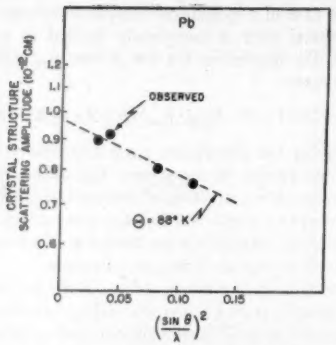

FIG. 2. Crystal structure scattering amplitudes for the Pb diffraction peaks of Fig. 1. The straight line shows the expected variation of the amplitudes for a Debye characteristic temperature of 88°K. The intercept of this line at zero scattering angle represents the coherent scattering amplitude for Pb.

neutrons/sec. It has been found more convenient and more accurate to compare the diffracted intensities of the sample with those produced by a substance of known coherent scattering cross section. In essence this means that P_0 is evaluated from the diffracted intensities of the calibrating substance, and then this value is used in other studies with the constancy of P_0 being established from the primary beam monitor response.

It has been mentioned earlier that for a monoisotopic element having zero nuclear spin that the coherent scattering cross section is identical with the total bound scattering cross section. Ideally, the above calibration should be performed with such an element, since its coherent cross section can be evaluated directly from a simple transmission experiment with due corrections applied for capture and crystal scattering effects. This has been done for a number of samples possessing the above characteristics as a test on the internal consistency of the method and these results have agreed well with each other.[5] Included in these calibrating substances have been ThO_2, C (diamond dust), $Ni^{58}O$, Ni^{58}, $Ca^{40}O$, and, less directly, other substances of established scattering cross-section value.

B. Determination of Nuclear Scattering Amplitudes

If the powder sample consists of only one element, the coherent nuclear scattering amplitude can be obtained directly from the crystal structure scattering amplitudes if the temperature correction factors are known. In many cases of present interest, data are available on the elastic constants or the Debye characteristic temperature of the substance to permit evaluation of the temperature correction factors. On the other hand, the diffraction data themselves can be used to determine these corrections if intensities are measured for a series of diffraction peaks. The Debye-Waller temperature factor for a given substance should vary exponentially with $\sin^2\theta$, attaining unit value at zero scattering angle. By studying the intensities of several reflections one can extrapolate the data to zero scattering angle, thereby obtaining directly the nuclear scattering amplitude. This is illustrated in Fig. 2, where the crystal structure scattering amplitudes are plotted semi-logarithmically *versus* $\sin^2\theta/\lambda^2$ for the case of the Pb diffraction pattern already given in Fig. 1. Extrapolation of the amplitudes to zero scattering angle gives 0.97×10^{-12} cm and 11.8 barns for the coherent nuclear scattering amplitude and cross section, respectively, for lead. The straight line drawn through the points of Fig. 2 represents the expected angular variation using 88°K as the Debye characteristic temperature for lead as obtained from specific heat measurements, and it is seen that the neutron scattering data agree satisfactorily with this.

While discussing the scattering pattern of Pb, it is worthwhile to point out the thermal diffuse scattering which is noticeable in the background of the pattern of Fig. 1. Since Pb has a low characteristic temperature of 88°K and a rather high scattering cross section, it would be expected that such an angularly dependent diffuse scattering would be observable. In treating the diffuse scattering quantitatively it is necessary to correct the data for multiple scattering and any isotopic or nuclear spin incoherent scattering which might be present. For lead, the coherent scattering cross section has been found to differ negligibly from the total scattering (see later section) and hence the isotope and spin incoherent effects can be ignored. The multiple scattering effects have been studied with samples for which all other diffuse scattering effects are negligible. Figure 3 shows the observed intensity of diffuse scattering expressed in absolute units as a differential scattering cross section for powdered Pb along with the experimentally determined multiple scattering and the calculated thermal diffuse scattering. The Debye expression $f^2(1-e^{-2W})$ has been used in calculating the thermal diffuse scattering. All of the data on Fig. 3 are on an absolute scale, and the agreement between observation and

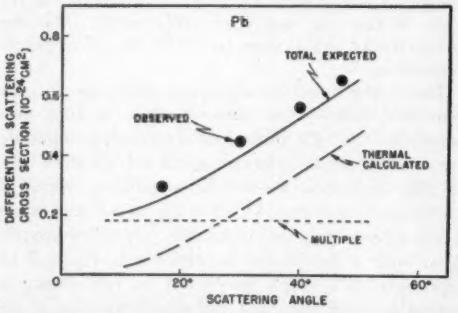

FIG. 3. Comparison between calculated and observed thermal diffuse scattering for powdered Pb. The multiple scattering was determined empirically.

[5] To be published.

experiment is good both in angular variation and in absolute value.

In addition to diffraction studies made on the chemical elements, many have been carried out on chemical compounds. The use of a chemical compound has the additional advantage that the relative phase of scattering for the elements in the compound can be determined as well as the scattering amplitudes. Figure 4 illustrates this in showing the crystal structure scattering amplitudes for a series of all-even and all-odd indexed reflections for NaF. In the case of crystals of this type, isomorphous with NaCl, the crystal structure scattering amplitudes per molecule become

$$F_{even}=f_R+f_x \quad \text{and} \quad F_{odd}=f_R-f_x.$$

Experimentally, it is found for NaF that F_{even} is larger than F_{odd}, and hence the nuclear scattering amplitudes for Na and F are of the same sign. Again by taking the the extrapolated values for the two experimental amplitude at zero scattering angle, thereby correcting the data for temperature effects, one can evaluate the individual nuclear coherent scattering amplitudes for Na and F. Just the opposite behavior is found in the case of LiF for which F_{odd} is larger than F_{even}, so that the signs of the two scattering amplitudes are opposite.

It is to be emphasized that the use of compounds gives only the *relative* phases of scattering and not their *absolute* phase. The absolute phase of scattering can be determined, however, by critical reflection of neutrons from mirrors, as Fermi and Marshall[6] have shown, or by reference to hydrogen, for which the phase has been interpreted from the relation of theory to scattering experiments. By intercomparison of the scattering phases of other elements with those which have been subjected to mirror experiments, or have been compared to hydrogen, it has been possible to assign an absolute phase of scattering to many elements or separated nuclei.

IV. EXPERIMENTAL RESULTS AND DISCUSSION

During the last three years, neutron powder diffraction patterns have been taken for well over a hundred elements or compounds, so that scattering cross section and scattering phase data are available for nearly sixty elements or separated nuclides. The chemical substances used for this purpose were of the highest purity commercially available or were of special preparation in this laboratory by Mr. D. Lavalle. In many cases the diffraction pattern itself served as an indication of the chemical or crystallographic purity of the substance, and in this we were greatly aided by having x-ray diffraction analysis by Dr. M. A. Bredig available as a further check. Some of the samples of the metallic elements, for instance, occasionally contained small quantities of oxide; and the presence of this could be detected by diffraction or chemical analysis and suitable corrections applied to the data allowing for this impurity.

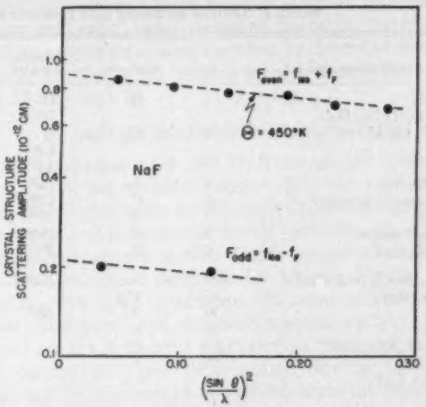

FIG. 4. Crystal structure scattering amplitudes for a series of even and odd indexed reflections of NaF. The intercepts at zero scattering angle can be used for evaluating the nuclear coherent scattering amplitudes of Na and F.

Most of the scattering data have been obtained for the same element contained in two or more compounds. This served to give several independent values for the scattering cross sections and provides a direct estimate of the consistency of the results. It is believed that in general the final cross-section values in this survey are accurate to within 6 or 8 percent, and thus the scattering amplitudes are accurate to 3 or 4 percent. For a few cases such as Li^6, Ca^{44}, and Cs the accuracy in the cross section values is not felt to be better than 10 to 15 percent because of limited sample availability or purity. For special problems this accuracy can be improved considerably, as, for instance, in a recent study of the scattering properties of the separated nickel isotopes,[7] where the scattering amplitudes have been determined to an accuracy of one percent. Special precautions as to sample purity and instrument performance must be taken in such cases, but it is well within the scope of the instrument operation to attain an accuracy of one percent.

The results of the measurements made to date are summarized in Table I. The first column gives a list of most of the crystalline elements or compounds which have been examined, the third column contains the elements for which the cross sections have been evaluated and the fourth column contains all cases for which a single nuclide is involved. This includes the cases for which measurements have been made on separated isotopes and all elements containing only a single isotope. For a few entries in this column the elements are so nearly monoisotopic that the measurements must

[6] E. Fermi and L. Marshall, Phys. Rev. **71**, 666 (1947).

[7] Koehler, Wollan, and Shull, Phys. Rev. **79**, 395 (1950).

TABLE I. Neutron scattering data as determined by neutron diffraction and transmission studies.

Samples examined	Z	Elements	Specific nuclides	Nuclear spin	f_{coh}[a] (10^{-12} cm)	σ_{coh} (barns)	σ_s[b] (barns)[b]	σ_{pot} (barns)
NaH	1	H	H^1	1/2	−0.40	2.0	80	
NaD, ThD_2, D_2O			H^2	1	0.64	5.2	7.4	
LiF, LiCl	3	Li			−0.18	0.4		
			Li^6	1	0.7[c]	~6		
			Li^7	3/2	−0.25	0.8	~2	
BeO, Be	4	Be	Be^9	3/2(?)	0.78	7.7	7.5	
Diamond, graphite	6	C	C^{12}[d]	0	0.64	5.2	5.2	
KN_3	7	N	N^{14}[d]	1	0.85	9.1	10	
many oxides	8	O	O^{16}[d]	0	0.58	4.2	4.2	
NaF, CaF_2	9	F	F^{19}	1/2	0.55	3.8	~3.5	
Na, NaCl, NaF, NaBr	11	Na	Na^{23}	3/2	0.35	1.5	3.5	
Mg, MgO	12	Mg			0.44	2.4	4.2	
Al	13	Al	Al^{27}	5/2	0.35	1.5	1.5	2.5
PbS	16	S			0.31	1.2	~1.2	
NaCl, KCl, CuCl	17	Cl			0.99	12.2	15	
KCl	19	K			0.35	1.5	~2	
CaO, CaF_2	20	Ca			0.49	3.0	3.5	
			Ca^{40}	0	0.49	3.0	3.2	
			Ca^{44}	0	0.18	0.4		
Ti, TiC	22	Ti			−0.38	1.8	~6	
V, VC	23	V	V^{51}	7/2	<0.09[e]	<0.1	5	3.7
Cr, FeCr	24	Cr			0.37	1.7	3.8	
MnO, Ni_3Mn	25	Mn	Mn^{55}	5/2	−0.33	1.35	2.2	3.8
Fe, FeO, Fe_2O_3	26	Fe			0.96	11.4	11.7	
			Fe^{54}	0	0.42	2.2	2.5	4.0
			Fe^{56}	0	1.00	12.6	13	
			Fe^{57}	(?)	0.23	0.64	2	
Co, CoO, FeCo	27	Co	Co^{59}	7/2	0.28	1.0	~5	4.2
Ni, NiO, Ni_3Mn	28	Ni			1.03	13.4	17.3	
			Ni^{58}	0	1.47	27.0	27.0	4.4
			Ni^{60}	0	0.28	0.97	1	
			Ni^{62}	0	−0.85	9.1	9	
Cu, Cu_2O, CuCl	29	Cu			0.76	7.3	7.8	
Zn, ZnO, CuZn	30	Zn			0.59	4.3	4.2	
Ge, GeO_2	32	Ge			0.84	8.8	8.5	
As, As_2O_3	33	As	As^{75}	3/2	0.63	5.0	~7	4.9
MnSe	34	Se			0.89	10.0	~10	
NaBr, KBr	35	Br			0.67	5.7	6.0	
RbCl	37	Rb			0.55	3.8	5.5	
SrO	38	Sr			0.57	4.1	9.5	
ZrC, ZrN	40	Zr			0.62	4.9	~7	
Cb	41	Cb	Cb^{93}	9/2	0.69[f]	6.0	6.2	5.9
Mo	42	Mo			0.64[f]	5.2	7.4	
Pd	46	Pd			0.63[f]	5.0	4.8	
Ag, AgCl	47	Ag			0.61	4.6	7	
			Ag^{107}	1/2	0.83	8.7	10	6.4
			Ag^{109}	1/2	0.43	2.3	6	6.4
Sn, SnO, SnO_2	50	Sn			0.61	4.6	4.9	
Sb, Sb_2O_3	51	Sb			0.54	3.7	4.2	
NaI, KI	53	I	I^{127}	5/2	0.52	3.4	3.8	6.9
CsCl	55	Cs	Cs^{133}	7/2	0.49	3.0	~7	7.1
Ta, TaC	73	Ta	Ta^{181}	7/2	0.70	6.1	7.0	9.0
W, WO_3	74	W			0.51	3.3	5.7	
Pt	78	Pt			0.95	11.2	11.2	
Au, Cu_3Au	79	Au	Au^{197}	3/2	0.77	7.5	~9	9.3
Pb, PbS	82	Pb			0.96	11.5	11.6	
Bi	83	Bi	Bi^{209}	9/2	0.89	10.1	10	10.0
Th, ThO_2	90	Th	Th^{232}	0	1.01	12.8	12.8	

[a] All signs of scattering amplitudes are positive except where specifically noted otherwise.
[b] The bound scattering cross-section values are obtained from total cross-section measurements by transmission. Transmission results are either from Oak Ridge data or from a composite of Oak Ridge data and literature values (see reference 8).
[c] By calculation from normal Li and LiF data.
[d] The scattering properties of C, N, and O are considered to be those of the major isotope since the element is so nearly monoisotopic.
[e] Phase of scattering unknown because of extremely small scattering cross section.
[f] Phase of scattering determined by R. J. Weiss from small angle scattering measurements (unpublished).

almost certainly represent within experimental error the contribution by the major isotopic constituent.

The fifth column gives the nuclear spin where this is known, all cases of even-even nuclei having been assumed to have zero spin. The sign of the scattering amplitude is positive (180° phase change on scattering) except where indicated to be negative or uncertain.

The coherent cross sections and the total cross sec-

tions obtained from our own transmission measurements or from the published literature[8] are listed in the eighth and ninth columns, respectively; and in the last column there is included for comparison the potential scattering cross sections of elements with $Z>13$. The total scattering cross sections σ_s[b] are for bound nuclei and differ from those for free nuclei by the reduced mass factor of Eq. (2).

One sees from this table that negative scattering amplitudes occur much less frequently than positive amplitudes, as is to be expected.[1] Wide variations in scattering cross sections from element to element are found, the smallest being less than 0.1 barn and the largest about 27 barns. In many cases pronounced differences between the total and coherent scattering data are to be noted, and this is a manifestation of the incoherent scattering processes discussed in an earlier section. It is obviously impracticable to discuss in detail the implications or peculiarities of the individual values so that the later discussion will center about some of the more interesting or illuminating features of the over-all data.

A. Sign of the Scattering Amplitude

Most of the scattering amplitudes which have been determined are seen to be of positive sign which for convenience has been taken to be characteristic of simple potential or geometrical scattering. Among the elements, H, Li, Ti, and Mn are seen to scatter neutrons with a negative amplitude; and among the separated nuclides, Li^7 and Ni^{62} also possess this property. Fermi and Marshall[6] have previously classified Li and possibly Mn in this category and Sidhu, Winsberg, and Meneghetti[9] have studied the Ti scattering properties. The appearance of a negative scattering amplitude is to be associated with the presence of a resonance scattering level at a neutron energy higher than that used in the observation. A negative amplitude can be described in terms of destructive interference between resonance scattering and potential scattering, so that low values of scattering cross section can be expected to be most probable under these conditions, and indeed this seems to be true. In the case of Mn, scattering resonances at 300 ev and at about[10] 2400 ev neutron energy are known to exist; and it appears that both of these resonances contribute to the negative scattering amplitude observed for Mn at thermal energies. Recent measurements of Adair[11] on Li have suggested a broad scattering resonance at about 1.1 Mev, and the magnitude and the negative scattering amplitude for Li can be accounted for on the basis of this resonance. The rather large negative amplitude for Ni^{62} suggests that resonance scattering has outweighed potential scattering and that the resonance energy must be closer to thermal energy relative to the resonance width than is the case for Mn, Li, and Ti.

B. Isotopic Incoherence in Scattering

As was mentioned in Sec. II, if the various isotopes making up an element possess different scattering properties, then there should result isotopic incoherent scattering and the coherent should be smaller than the total scattering cross section. This is indicated for many of the elements, in particular for Mg, Cl, Ti, Ni, Sr, and Ag. For those cases where the separated isotopes have also been studied, satisfactory agreement has been found for the incoherent scattering as calculated from the isotope data and as measured directly for the element. For elements of this classification the isotopic incoherent scattering should appear as a diffuse, isotropic scattering in the background of the neutron diffraction pattern. Since the intensity of scattering associated with the usual isotopic incoherence is quite small and generally a good deal smaller than the other diffusely scattered components such as thermal and multiple scattering, no serious attempt has been made to determine it quantitatively by direct experiment. Its presence has been noted qualitatively, however, in the various patterns.

Many elements possessing several isotopes seem to show little or no isotopic incoherence; and this indicates that the major isotopic constituents have similar scattering properties and the minor ones, if different, have little effect owing to their low abundance on the elemental properties. Cu, Zn, Ge, Pd, and Pb serve as examples for this.

C. Nuclear Spin Dependence of Scattering

If a specific nucleus possesses a resultant nuclear spin, a neutron can be scattered in either of two spin states with its spin parallel or antiparallel to that of the nucleus. There are thus two scattering amplitudes; and since nuclear forces are spin-dependent, the two amplitudes may be different. When this situation prevails, the coherent scattering for unaligned nuclei in a crystal will be smaller than the total scattering as has been discussed in Sec. II.

The effects of spin dependence on scattering can be most unambiguously observed for the single nuclides which are tabulated in the fourth column of Table I.

For the even charge—even mass nuclei of zero spin there will, of course, be no spin dependence of scattering; and in these cases the coherent and total scattering cross sections will be equal, and there will be no spin incoherent scattering. For many nuclei which possess a spin, a pronounced spin dependence of scattering is observed. A large spin dependence is evidenced by a large difference between coherent and total scattering cross sections, which corresponds also to a large

[8] See "Neutron cross sections of the elements" by Goldsmith, Ibser, and Feld, Revs. Modern Phys. 19, 259 (1947), and same title by Robert K. Adair, *ibid.* 22, 249 (1950), and individual papers by L. S. Rainwater and W. W. Havens and others, for which references are given in above review articles.

[9] Sidhu, Winsberg, and Meneghetti, Phys. Rev. 74, 222 (1948).

[10] Hibdon, Muehlhause, Selove, and Woolf, Phys. Rev. 77, 730 (1950).

[11] R. K. Adair, Phys. Rev. 79, 1018 (1950).

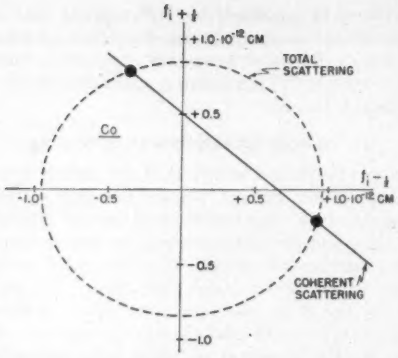

FIG. 5. Graphical evaluation of the two spin scattering amplitudes of Co. The intersection points between the two curves represent alternative values for the scattering amplitudes.

difference in the two spin amplitudes. A large spin dependence gives rise to a correspondingly large spin diffuse scattering. Hydrogen and vanadium are noteworthy examples of this, in which almost all of the scattering is incoherent. For such a situation to occur, the two spin scattering amplitudes must be of opposite sign and when multiplied by the spin weighting factors must be closely the same in numerical value. Equations (1) and (3) can be used to evaluate the individual spin amplitudes *within an algebraic sign ambiguity*. A graphical solution for the amplitudes is sometimes convenient and Fig. 5 illustrates this for the case of Co. The ellipse represents the range of possible combinations of the spin amplitudes as determined from the total scattering cross section, while the straight line corresponds to the possibilities allowed by the coherent scattering amplitude of *known sign*. In general, the two curves intersect at two points, and these are the alternative values for the amplitudes. This ambiguity is characteristic of the interpretation permitted by scattering measurements on systems of unaligned nuclei and can be resolved only by experimentation with nuclei whose spins are aligned with respect to the favored direction in a beam of polarized neutrons.[12] It is only in the case of the singlet and triplet scattering amplitudes for hydrogen that the ambiguity has been resolved and here because theoretical considerations on this simple system are able to eliminate one of the alternative sets of values.

The large amount of spin incoherent scattering for certain nuclei should be observable as a diffuse scattering in the neutron diffraction pattern. If the nucleus is heavy compared with the neutron or is bound tightly in the lattice (and hence is effectively heavy), the spin incoherent diffuse scattering should be isotropic. For hydrogen-containing materials there is always observed a very strong spin diffuse scattering which is not isotropic but rather shows a pronounced intensity fall-off with increasing angle of scattering. This is a consequence of the nonrigid binding of the protons in the lattice as referred to the neutron energy normally used in diffraction studies. For neutrons of sufficiently low energy the spin diffuse scattering for hydrogen would presumably become angularly independent in intensity.

Quantitative measurements of the spin diffuse scattering for vanadium have been made using the neutron diffraction pattern of pure VC. The observed diffuse scattering can contain three components arising from (1) thermal diffuse scattering by the lattice, (2) multiple scattering in the sample, and (3) spin incoherent scattering of vanadium. The first of these can be calculated using the Debye theory of thermal diffuse scattering and a characteristic temperature determined from the intensity variation with angle of the Bragg reflections, and multiple scattering effects can be evaluated empirically from a study of the diffuse scattering by substances known to possess no spin diffuse scattering. After correction of the observed diffuse scattering in VC for these extraneous effects, the resultant spin incoherent scattering per V atom expressed in absolute units of differential scattering cross section is shown in Fig. 6. It is to be seen that the spin incoherent scattering is essentially isotropic and is in excellent agreement with the differential scattering cross section value of 0.40 barn per steradian expected for the spin incoherent scattering in vanadium. The latter corresponds to the 5-barn difference between total scattering and the negligibly small coherent scattering of vanadium.

Some comment is warranted on the present status of the coherent scattering amplitude of hydrogen. These measurements are of particular importance in that they involve the interaction of two fundamental particles and are closely associated with the theoretical treatment of the range of forces in the n–p interaction. Several experimental determinations of the coherent scattering amplitudes for hydrogen have been made[13–15] by different experimental methods. The most recent measurements by Hughes, Burgy, and Ringo[15] by the method of total reflection from mirrors of hydrogen-containing liquids appears to give more accurate results than previous determinations. Since the time of our first report on hydrogen scattering by crystal diffraction, extensive additional measurements have been made on a purer and more completely analyzed sample of NaH. One of the uncertainties in the past was associated with the temperature vibration effects. However, studies which have now been made with both x-ray and neutron diffraction patterns for NaH permit of empirical correction for the temperature effects. The method of calibration of diffraction patterns in terms of absolute

[12] M. Hamermesh and J. Schwinger, Phys. Rev. **69**, 145 (1946). M. E. Rose, Phys. Rev. **75**, 213 (1949).

[13] Sutton, Hall, Anderson, Bridges, DeWire, Lavatelli, Long, Snydef, and Williams, Phys. Rev. **72**, 1147 (1947).

[14] Shull, Wollan, Morton, and Davidson, Phys. Rev. **73**, 842 (1948).

[15] Hughes, Burgy, and Ringo, Phys. Rev. **77**, 291 (1950).

cross sections has also been improved, as was discussed briefly in a previous section. As presently analyzed with these improvements our data give a value of $0.41\pm0.02 \times 10^{-12}$ cm for the hydrogen coherent amplitude. The difference between this value and that obtained by the mirror experiment is greater than we have been able to account for on the basis of known experimental errors. It is planned to give further consideration to these measurements and to report them more fully later.

We have previously reported the cross sections for deuterium as determined from measurements on NaD. Extensions of these measurements as well as measurements on other deuterium containing compounds make us confident that the results here reported are correct in their indication of a spin dependence for deuterium as evidenced by the difference in the coherent and total cross sections. Recent measurements by Hurst and Alcock[16] of scattering by D_2 gas seem to confirm these conclusions.

D. Nuclear Size Resonances

We have already mentioned features of the scattering data which bear on resonance effects. These effects show up as departures of the coherent scattering amplitudes from those calculated for potential scattering alone. Ford and Bohm[17] have made use of the coherent scattering data, prior to their publication here, in connection with a discussion on what they term "nuclear size resonances."

On their assumption of a free particle model with a constant well depth, resonances should appear at near thermal energy at definite values of the nuclear radius and hence at corresponding values of the mass number A. The region around $A=50$ to 60 (V to Ni) shows marked resonance effects in the coherent scattering amplitudes and on the basis of "nuclear size resonances" similar effects should show up in the region of $A\sim12$ and 150.

This picture of resonance behavior as a function of nuclear size can hardly be expected to give the details of variation over neighboring mass numbers, since for one thing no mention of the spin of the compound nucleus is made.

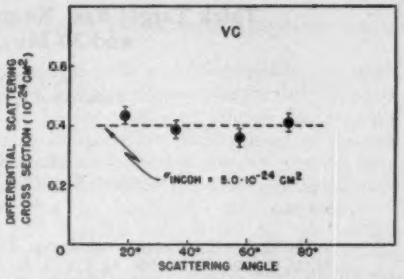

FIG. 6. Nuclear spin incoherent scattering for vanadium as determined from the diffraction pattern of vanadium carbide.

It would be expected that scattering amplitudes for zero-spin nuclei, where there is a single characteristic amplitude, would be most significant in showing nuclear size resonant effects. The experimental data for such cases are rather sparse but it is to be noted that the sequence Fe^{54}, Fe^{56}, Ni^{58}, Ni^{60}, and Ni^{62} shows an interesting variation in scattering amplitude. Undoubtedly, resonance conditions are being satisfied in this group. However, recent considerations by our colleague, Dr. L. C. Beidenharn, have shown the assumption of a constant well depth for these various nuclides to be inconsistent with the experimentally determined amplitudes. Thus, the scattering amplitude must depend upon a changing well depth as well as a changing radius and the picture becomes much more complicated. Further study with a more extensive series of zero spin nuclides is indicated before the resonance picture can be followed too closely.

We are indebted to Messrs. M. C. Marney, W. A. Strauser, and W. C. Koehler, who have at various periods assisted in the collection and analysis of the neutron scattering data. Also our appreciation should be expressed to Mr. D. Lavalle and Dr. M. A. Bredig for the careful preparation and chemical and x-ray diffraction analysis of many of the substances which have been examined.

[16] D. G. Hurst and N. Z. Alcock, Phys. Rev. **80**, 117 (1950).
[17] K. W. Ford and D. Bohm, Phys. Rev. **79**, 645 (1950).

Thick Target Fast Neutron Yield from 15-Mev Deuteron and 30-Mev Alpha-Bombardment*

A. J. ALLEN AND J. F. NECHAJ
University of Pittsburgh, Pittsburgh, Pennsylvania

AND

K.-H. SUN AND B. JENNINGS
Westinghouse Research Laboratories, East Pittsburgh, Pennsylvania

(Received May 25, 1950)

The total yield and angular distribution of fast neutrons from bombardment of thick targets of pure Be, Al, Ti, Cr, Mn, Co, Cb, Mo, Ag, Cd, Ta, Au, Pb, and Bi by 15-Mev deuterons and 30-Mev alpha-particles was measured. These studies were made using the reaction $S^{32}(n,p)P^{32}$ as a threshold detector and also with fission ionization chambers. The total neutron yield per second per μamp of the cyclotron beam, N, was observed to decrease with increase in nuclear charge, Z, of the target according to the approximate empirical equations, $\log N = 10.18 - 0.0234Z$ for deuteron bombardment and $\log N = 9.68 - 0.0234Z$ for alpha. In all cases studied, the angular distribution of fast neutrons from target bombarded by deuterons showed a pronounced peak in the yield in the forward direction.

I. INTRODUCTION

IT would be advantageous to know, for practical experimental purposes, the absolute high energy neutron yield from the cyclotron bombardment of various materials. This is important, not only in the use of the cyclotron and high energy electrostatic generator as a fast neutron source for experimental purposes, but also in the design of charged particle beam slits, beam tubes, etc., where a minimum neutron background is desirable owing to the impinging of the beam on these parts.

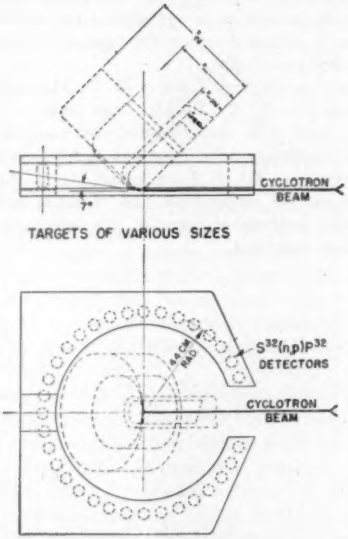

FIG. 1. Target and detector arrangement.

The present study[1] is concerned with the measurements of the angular distribution and total number of neutrons of over 1-Mev energy emitted from various thick targets, made of chemically pure but not necessarily single isotopes, when they are bombarded with 15-Mev deuterons or 30-Mev alphas from the University of Pittsburgh's 47-in. cyclotron. No attempt is made to distinguish neutrons from (d,n), $(d,2n)$, $(d,n\gamma)$, and other simultaneously occurring processes.

II. EXPERIMENTAL

The experiment was carried out using the internal beam of the cyclotron which was capable of producing 300 μamp of 7.5-Mev protons, 250 μamp of 15-Mev deuterons, and 15 μamp of 30-Mev alpha-particles. The

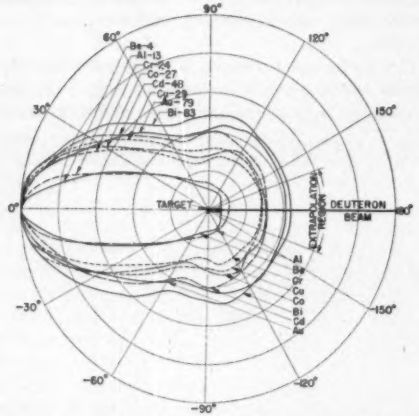

FIG. 2. Angular distribution of fast neutrons from 15-Mev deuteron bombardment of various thick targets.

* Assisted by the joint program of the ONR and AEC.

[1] Allen, Nechaj, Sun, and Jennings, Phys. Rev. 76, 188 and 463 (1949); 77, 752 (1950).

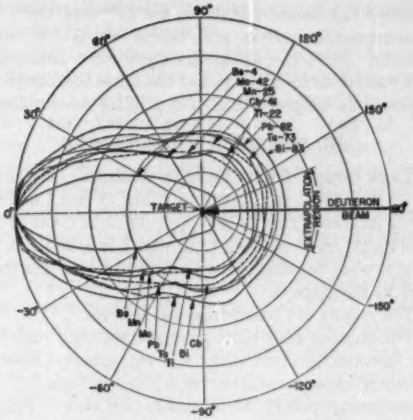

FIG. 3. Angular distribution of fast neutrons from 15-Mev deuteron bombardment of various thick targets.

voltages were estimated from the characteristics of the cyclotron and checked by measurements of the range in air of the external beam and were good to ±0.5 Mev. The beam current was measured both electrically and from the heat generated in the target.

The target, shown in Fig. 1, consists of a water-cooled cup at an angle of 45° with the cyclotron beam. During the early part of the work this cup was 2 in. in diameter, but in some of the targets used this dimension was reduced to ⅜ in. in order to achieve better geometry and performance. The targets were made, when possible, by machining or spinning the purest available elements into the form of the target cup. Low melting elements such as Pb, Sb, Bi, Sn, and Zn were "smeared" in a thick layer on a grooved Cu target, while elements

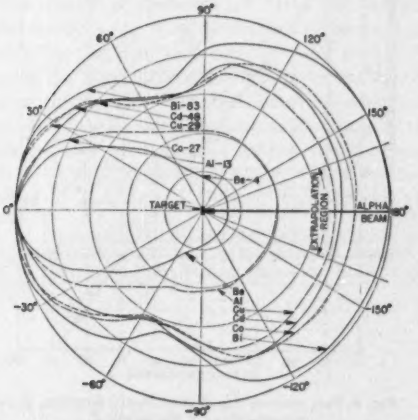

FIG. 4. Angular distribution of fast neutrons from 30-Mev alpha-bombardment of various thick targets.

such as Mn, Cr, and Au were electroplated on a copper target.

The neutron yield was determined by two methods; the measurement of the secondary activity induced in a detector by the integrated neutron flux through the detector, and the direct measurement of the neutron flux by a fission ionization chamber. For the majority of the measurements the activation method was adopted because of its simplicity and convenience. The $S^{32}(n,p)P^{32}$ reaction was chosen for the radioactive detector because the excitation function of this reaction is known,[2] and P^{32} has a convenient half-life (14.3 days) and emits only β-rays with fairly high energy (1.71 Mev max). The decay curve of this "sulfur" detector showed that one day after bombardment the activity was from P^{32} alone. The neutron cross section near the threshold of the reaction $S^{32}(n,p)P^{32}$ (0.97 Mev) is small, according to Klema and Hanson,[2] and rises rapidly as the energy

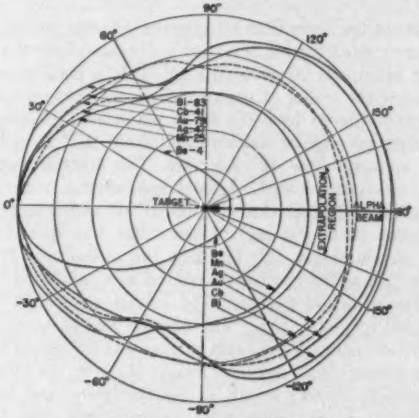

FIG. 5. Angular distribution of fast neutrons from 30-Mev alpha-bombardment of various thick targets.

increases and then levels off to a constant value (0.32 barn) from 4 Mev to about 6 Mev, where the measurement ends. There are indications that a majority of the neutrons involved in the present study will be in the neighborhood of a few Mev (say, 2 to 10 Mev) based on information from the neutron spectrum of deuteron bombardment on Be, Al, Co, and Cu by photographic techniques.[3] It was considered reasonable for the first approximation to adopt a constant value, namely, 0.32 barn for the $S^{32}(n,p)P^{32}$ cross section in all the measurements. Powdered sulfur (about 200 mg) was placed in small medical capsules and mounted around the target inside the cyclotron vacuum chamber as shown in Fig. 1. These detectors were placed approximately every 10° around the target on a 4.4-cm radius. In order to

[2] E. D. Klema and A. O. Hanson, Phys. Rev. 73, 106 (1948).
[3] B. L. Cohen and C. E. Falk, Carnegie Institute of Technology thesis, 1950, unpublished.

TABLE I. Fast neutron yield.

Target nuclei	φ, fast neutrons/sec/steradian/μamp in forward direction $\times 10^{-8}$		N, total fast neutrons/sec/μamp $\times 10^{-8}$		K, No. bombarding particles required to yield one fast neutron $\times 10^{-8}$	
	15-Mev deuterons	30-Mev alpha	15-Mev deuterons	30-Mev alpha	15-Mev deuterons	30-Mev alpha
$_4$Be	94	22	190	65	0.33	0.48
$_{13}$Al	30	3.1	64	18	0.98	1.6
$_{22}$Ti	.12		65		2.4	
$_{24}$Cr	7.2		29		1.8	
$_{25}$Mn	12	1.7	52	14	1.3	
$_{27}$Co	5.5	1.1	26	10	2.0	2.9
$_{29}$Cu	4.8	1.1	29	10	3.0	2.9
$_{41}$Cb	3.0		15		3.3	
$_{42}$Mo	3.1		15		4.0	
$_{47}$Ag	2.2	0.54	14	5.4	4.7	9.6
$_{48}$Cd	2.4	0.56	12	5.2	5.1	5.5
$_{73}$Ta	0.56		3.3		19	
$_{79}$Au	0.37	0.062	2.1	.65	27	48
$_{82}$Pb	0.36	0.18	2.1	1.6	30	19
$_{83}$Bi	0.23	0.044	1.3	.47	49	70

prevent the beam from striking the detector holder, the plane containing the detectors is displaced from that of the beam and target by 0.5 cm. This is equivalent to having the center of the capsule in the forward directions displaced from the beam plane by 7°, thus providing an angular measurement from $\pm 7°$ to $\pm 153°$ in approximately 10° intervals. The neutron flux at 0° was extrapolated. After bombardment with fast neutrons, the capsules were taken out and a weighted portion (5 to 100 mg) of the sulfur was spread out in an aluminum dish in ether, the radioactive P^{32} in the thin sulfur layer was counted in a calibrated end-window Geiger counter. The counts were then corrected for decay time. The neutron flux or neutrons/cm^2/sec/μamp of the beam current was calculated from the Geiger counts/sec/unit weight of sulfur, the counter geometry factor, length of bombardment and beam current. From the angular neutron flux, the total neutron flux was evaluated by graphical integration.

A similar detector using the reaction $P^{31}(n,p)Si^{31}$ was also used in some of the measurements. The cross section of this reaction as a function of neutron energy up to 4 Mev was measured by Taschek[4] and for this work a constant value of 0.08 barn was assumed. Since the half-life of Si^{31} formed is only 170 minutes, corrections were made for the decay of this nucleus during the bombardment time. The results were found to be consistent.

Fast neutron fission ionization counters with very thin uranium (Cd shielded) and thorium deposits were also used. An average fission cross section of 0.6 and 0.15 barn were assumed, respectively, based on the experimental data by Ladenburg, *et al.*[5] and Ageno, *et al.*[6] These detectors measure neutrons with energy above 1 Mev,[7] the fission thresholds for U^{238} and Th^{232}. The measurements agreed with those using the sulfur detector. Since the sulfur detectors were convenient, and yield data for all angles at the same bombardment, it then was adopted for all the angular measurements.

III. RESULTS AND DISCUSSION

Thick targets of pure Be (2 in. diameter), Mg (2 in.), Al (2 in.), Ti (2 in.), Cr (2 in.), Mn (1 in.) Co (2 in.), Cu ($\frac{3}{4}$ in.), Mo (2 in.), Cb (1 in.), Ag (2 in.), Cd (2 in.), Ta (1 in.), Au (1 in.), Pb (2 in. and $\frac{3}{4}$ in.), Bi (2 in. and $\frac{3}{4}$ in.), were bombarded with both 15-Mev deuterons and 30-Mev alphas.

The results are summarized as follows.

The angular distribution normalized with respect to the forward direction which was extrapolated from the corrected experimental curves is given in Figs. 2–5. The experimental points, 33 in number for each curve, fall closely on the curves and were omitted in the much condensed drawing to avoid confusion. The neutron flux at any angle for any target investigated can be obtained from these figures and the flux in the forward direction (see below). The angle at half-intensity for the case of

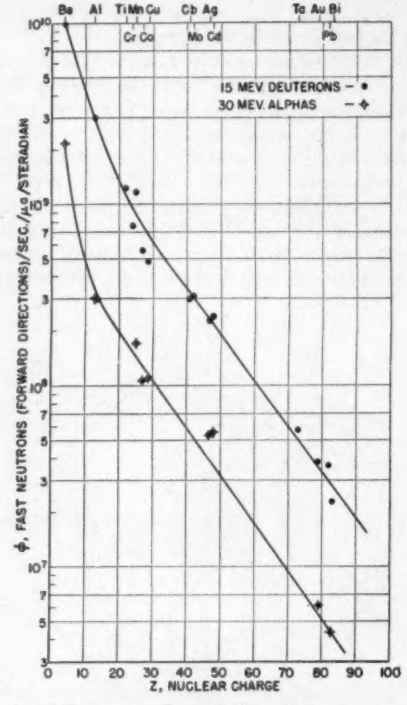
Be Al Ti Mn Cu Cb Ag Ta Au Bi
Cr Co Mo Cd Pb
15 MEV DEUTERONS – •
30 MEV ALPHAS – +
φ, FAST NEUTRONS (FORWARD DIRECTIONS)/SEC./μa/STERADIAN
Z, NUCLEAR CHARGE

FIG. 6. Fast neutron flux in the forward direction, φ, as nuclear charge of the target, Z.

[4] R. F. Taschek, MDDC 360, LADC 135, unpublished.

[5] Ladenburg, Kanner, Barschall, and Van Voorhis, Phys. Rev. 56, 168 (1939).

[6] Ageno, Amaldi, Borimarelli, Cacciapuoti, and Trabacchi, Phys. Rev. 60, 67 (1941).

[7] W. E. Shoupp and J. E. Hill, Phys. Rev. 75, 785 (1949).

deuteron bombardment increases with the increasing nuclear charge of the target.

The fast neutron flux, φ, in the forward direction (0°) expressed in number of fast neutrons per second per steradian per μamp of the beam current is given in Table I and plotted against nuclear charge of the targets, Z, as shown in Fig. 6. Figure 6 indicates that the neutron flux decreases with increase in the nuclear charge of target as would be expected. The number of fast neutrons in the forward direction per cm^2 per second per μamp at a distance r cm from the target may be obtained by dividing the value φ by r^2.

The total number of fast neutrons for various targets per second per μamp deuterons or alphas, N, is also given in Table I and plotted against nuclear charge of the target, Z, in Fig. 7. The total yield, N, can be calculated from the nuclear charge, Z, of the target by the following simple empirical relationship:

$$\log N = 10.18 - 0.0234Z \text{ for deuterom bombardment,}$$

and

$$\log N = 9.68 - 0.0234Z \text{ for alpha-bombardment.}$$

The values calculated from these equations might be somewhat low for those targets with a nuclear charge smaller than 10. Smith and Kruger[8] measured the total neutron yield (including slow neutrons) from various targets bombarded with 10-Mev deuterons. Their result also indicates a decrease in the yield with an increase in the nuclear charge of the targets. However, the total yield is higher than that found in the present investigations.

As shown in Figs. 2–5, the angular distribution for the production of fast neutrons by 15-Mev deuterons on a thick target has a very pronounced forward peak for all the targets studied (Z from 4 to 83). Conversion into the center-of-mass system using the limiting values for the energy of deuterons (2 Mev, the potential barrier for Be, to 15 Mev, the maximum energy of the bombarding particles) does not essentially change the shape of the angular distribution even for the lightest nucleus (Be) studied. For targets heavier than Be, the shapes and position of the angular distributions for the laboratory and center-of-mass systems would be very similar. Similar, though fragmentary, results were also observed by Roberts and Abelson,[9] Falk, Creutz, and Seitz,[3,10] and Ammiraju,[11] by using higher energy threshold detectors. Recently, Falk[3] found the similar forward peaks using a hydrogen recoil proportional counter telescope. As yet, no satisfactory theory has been developed to account for these results.

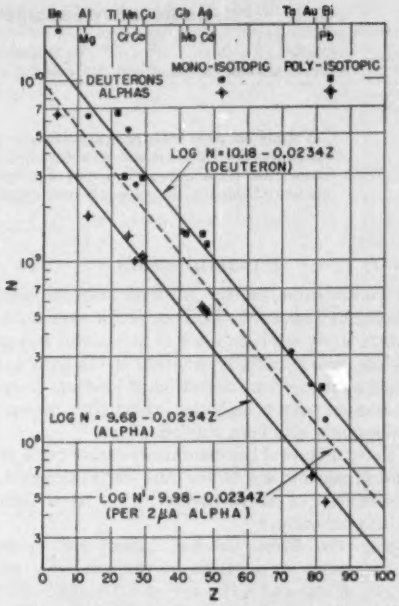
Be Al Ti Mn Cu Cb Ag Tg Au Bi
Mg Cr Co Mo Cd Pb
MONO-ISOTOPIC POLY-ISOTOPIC
DEUTERONS
ALPHAS
LOG N = 10.18 - 0.0234Z
(DEUTERON)
LOG N = 9.68 - 0.0234Z
(ALPHA)
LOG N = 9.98 - 0.0234Z
(PER 2μA ALPHA)
N
Z
0 10 20 30 40 50 60 70 80 90 100

FIG. 7. Total number of fast neutrons per second per μamp. 15-Mev deuterons and 30-Mev alphas, N, vs nuclear charge of the thick target, Z.

There were indications that the forward neutron yield may be resolved into two peaks. This was also found by Falk.[3]

The authors are greatly indebted to Miss F. A. Pecjak, Miss E. Waldron, and Mrs. D. Halliday for the assistance in many of these measurements and calculations. Thanks are due Dr. S. Barnartt and Dr. J. K. Stanley of the Westinghouse Research Laboratories for the valuable assistance in the securing or preparations of many targets, and Dr. W. E. Shoupp for encouragement throughout the work. The work would not have been completed without the support of the ONR and AEC.

[8] L. W. Smith and P. G. Kruger, Nuclear Science Series, Preliminary Report No. 4, NRC by A. O. Hanson and R. F. Taschek.
[9] R. B. Roberts and P. H. Abelson, Phys. Rev. 72, 76 (1947).
[10] Falk, Creutz, and Seitz, Phys. Rev. 76, 332 (1949).
[11] P. Ammiraju, Phys. Rev. 76, 1421 (1949).

Radioactive Isotopes of Lutetium and Hafnium*

G. WILKINSON† AND H. G. HICKS‡
Radiation Laboratory and Department of Chemistry, University of California, Berkeley, California
(Received October 26, 1950)

A study has been made of neutron-deficient radioactive isotopes of lutetium and hafnium produced by bombardments of thulium and ytterbium with alpha-particles of various energies; of ytterbium with 10-Mev protons, and of lutetium with protons of energies from 10 to 70 Mev. Seven radioactive isotopes of lutetium and four of hafnium, all previously unreported, are described.

I. INTRODUCTION

IN continuation of the investigations[1] on neutron-deficient radioactive isotopes of the rare earth elements, a study has been made of radioactive isotopes of lutetium. Since the interpretation of the data has depended upon the characterization of lutetium daughters of hafnium parent activities, radioactive isotopes of hafnium have also been studied.

The techniques of bombardments of rare earth oxides, chemical separations of the rare earth elements, the measurement of radioactivities, etc., have been described previously.[1a]

Using the 60-in. Crocker Laboratory cyclotron, bombardments were made of thulium with various energies of alpha-particles and of ytterbium with both alpha-particles and 10-Mev protons. Lutetium was bombarded with protons from 15- to 32-Mev energy using the linear accelerator and with protons of 40- to 75-Mev energy using the 184-in. cyclotron. Lutetium activities were also produced in spallation reactions of tantalum with 190-Mev deuterons.

After bombardment, the rare earth oxides were dissolved in hot perchloric acid, hafnium carrier was added, and the hafnium then precipitated from $3N$ acid solution as the phosphate. After metathesis to the hydroxide and solution in nitric acid, scavenging separations of rare earth fluorides were made and the hafnium was finally precipitated as barium hafnium fluoride. Hafnium was also separated by extraction with benzene solutions of thenoyltrifluoroacetone (TTA).

The rare earths were recovered after removal of hafnium by precipitation first of the hydroxide and subsequently of the fluoride and oxalate. The chemical identity of the rare earth activities was shown by separation using the ion-exchange resin column procedure. Chemical separation of lutetium daughter activities grown in hafnium samples was made by initial separation of the hafnium as phosphate, then repeated precipitation of the lutetium as fluoride and oxalate using lanthanum as a carrier.

The radiation characteristics of the radioactive isotopes were obtained from aluminum and lead absorption measurements; the contribution of soft quantum radiation was obtained by aluminum absorption after removal of electrons by beryllium foils of suitable thickness—a correction for absorption of the soft quantum radiation in this foil was made before resolution of the aluminum absorption curves. Electron radiations were also studied on a simple magnetic spectrometer. The approximate ratios of the various components of the complex radiations found in species studied decaying by orbital electron capture were obtained from the various measurements; activities were corrected for absorption of radiations in counter windows and air gap, fluorescence yields of L and K x-rays were taken as 0.5 and 0.8, respectively, and the counting efficiencies of L and K x-radiation of ytterbium and lutetium in the mica window argon-alcohol tubes used were taken as 4 percent and 0.5 percent, respectively. The decay of the lutetium and hafnium isotopes is accompanied by L and K x-radiation, the average half-thicknesses being 14 to 15 mg/cm² aluminum and 100 to 105 mg/cm² lead, respectively.

The data on lutetium and hafnium isotopes are summarized in Table I.

II. LUTETIUM ISOTOPES

Study of lutetium produced in the bombardment of thulium with alpha-particles of various energies from 15 to 38 Mev has led to the characterization of five radioactive isotopes of lutetium of half-lives 1.7-days, 8.5-days, ~600-days, 6.7-days and 4.0-hours; these have been allocated to masses 170, 171, 171, 172, and 172, respectively. From short bombardments at 38 Mev, the 1.7-day and 8.5-day activities were resolved; the disappearance of the 1.7-day activity below a bombarding energy of 30 Mev furnished identification of this activity as mass 170 produced by the $(\alpha, 3n)$ reaction. The 4.0-hour and 6.7-day activities were obtained at low energies by the (α, n) reaction and thus both have mass 172. At intermediate energies the decay and absorption curves were impossible to resolve by simple absorption methods in view of the similarities of the 6.7-day and 8.5-day activities. The ~600-day activity, considered to be Lu^{171}, was found at all bombarding energies.

* This work was carried out under the auspices of the AEC.
† Present address: Chemistry Department, Massachusetts Institute of Technology, Cambridge, Massachusetts.
‡ Present address: Chemistry Section, General Electric Company, Hanford Engineer Works, Richmond, Washington.
[1] G. Wilkinson and H. G. Hicks, (a) Phys. Rev. 75, 1370 (1949); (b) 75, 1687 (1949); (c) 79, 815 (1950).

In the bombardment of lutetium with 19-Mev deuterons, 10-Mev protons, and fast neutrons, a 165-day activity was produced; this can surely be allocated to mass 174 corresponding to $(d, p2n)$, (p, pn), and $(n, 2n)$ reactions.

The resolution of decay and absorption curves of lutetium activities produced in the proton and alpha-particle bombardments of ytterbium has proved difficult. The 4.0-hour Lu^{172} activity was recognized only through its positron emission, as the 3.7-hour Lu^{176} activity[2] is also formed in high yield, while the longer-lived activities form a very complex mixture.

A second very long-lived lutetium activity of half-life ~500 days was found in 30- to 50-Mev proton bombardments of lutetium, and was shown to be the daughter of the 23.6-hour Hf^{173} discussed below.

Lutetium isotopes have also been separated following growth from hafnium activities produced in alpha-particle bombardment of ytterbium and in proton bombardments of lutetium. The 1.7-day, 8.5-day, 6.7-day, and ~600-day activities have been resolved. The measurement of the radiation characteristics of these activities was more easily accomplished than was the resolution of decay and absorption data obtained from lutetium isotopes produced in Tm+α and Yb+p bombardments.

The 1.7-day, 8.5-day and long-lived (probably both the ~500 and ~600 day), lutetium isotopes have also been found in the ion-exchange column-separated lutetium fraction of rare earth activities produced in bombardment of tantalum with 190-Mev deuterons.

The existence of other, short-lived, activities of lutetium and also of hafnium is possible as species with a half-life less than about fifteen minutes, except for lutetium daughters of longer-lived hafnium parent activities, could not be studied in this work.

165±5-day Lu^{174}.—This activity was found in the lutetium fraction from bombardments of lutetium with fast neutrons, 10-Mev protons, and 19-Mev deuterons; it has also been found together with the well known[2] 6.7-day Lu^{177} in the bombardment of hafnium with 19-Mev deuterons. Allocation to mass 174 can be made with certainty on the basis of formation by $(n, 2n)$, (p, pn), and $(d, p2n)$ reactions in lutetium and the (d, α) reaction in hafnium. The value $\sim 5\times10^{-4}$ barns for the cross section for the $(d, p2n)$ reaction of the 19-Mev deuterons in lutetium was calculated from the ratios of the beta-particle activity of the 6.7-day Lu^{177} formed by Lu^{176}-d-p reaction and the activity of the 165-day Lu^{174}.[3] The decay of 165-day Lu^{174} has been followed through four half-lives. From the type of absorption curve obtained and from a study on a simple magnetic spectrometer, hard electrons observed in the radiations appear to be negative beta-particles. The x-radiation present is too abundant to be accounted for by isomeric transition. The isotope probably decays both by beta-emission and by orbital electron capture. The approximate ratios of the various radiations corrected for counting efficiencies are 0.16-Mev σ^-: 0.6-Mev β^-: L x-ray: K x-ray: γ-ray = ~0.7: ~0.2: ~1.5: 1: ~0.1. Allowing for L an K x-rays arising from conversion, the decay by beta-particle emission is about 20 percent of the total disintegrations.

~500-day Lu^{173}.—This activity has been found in bombardments of lutetium with 30- to 40-Mev protons, and has been separated at regular time intervals during the decay from the 23.6-hour hafnium activity formed in alpha-particle bombardments of ytterbium.

The quantity of residual lutetium activity formed in decay of a sample of pure 23.6-hour Hf^{173} made by the $(p, 3n)$ reaction in the bombardment of lutetium with 25-Mev protons in the linear accelerator, together with the estimated counting efficiencies, gives a half-life of 400 to 600 days for this isotope. The direct decay has been followed only through two years as yet, yielding a value ~500 days. The radiation characteristics are very similar to those of the ~600-day lutetium formed in alpha-particle bombardments of thulium, but the methods of production indicate the occurrence of two distinct species. The ratios of the various radiations obtained from samples of the activity produced by decay of the 23.6-hour Hf^{173} and directly in the proton bombardment of lutetium are 0.1-Mev σ^-: ~0.18-

TABLE I. Data on Lu and Hf isotopes.

Isotope	Type of radiation	Half-life	Energy of radiation in Mev: Particles	Energy of radiation in Mev: γ-rays	Produced by
Lu^{170}	K, σ^-, γ	1.7±0.1 days	0.1 •	~2.5	Tm-α-3n, Ta-d-3n12n, Hf^{170} K decay
Lu^{171m}	K, σ^-, γ	8.5±0.2 days	0.17, ~0.5 (weak)	~1.2	Yb-p-n Tm-α-2n Hf^{171} K decay Ta-d-3n12n
Lu^{171}	K, σ^-, γ	~600 days	~0.1	~1	Tm-α-2n
Lu^{172}	K, σ^-, γ	6.70±0.05 days	0.12, ~0.6 (weak)	1.2	Tm-α-n Hf^{172} K decay Yb-p-n
Lu^{172m}	β^+, K?	4.0±0.1 hours	1.2	—	Tm-α-n Yb-p-n Lu-p-p3n
Lu^{173}	K, σ^-, γ	~500 days	~0.1, ~0.18	~0.22 0.8	Lu-p-p2n Hf^{173} K decay Yb-p-n
Lu^{174}	K, σ^-, γ β^- (~20%)	165±5 days	0.16 σ^- 0.6 β^-	~1	Lu-n-2n Hf-d-α Lu-d-p2n Lu-p-pn
Hf^{170}	β^+, K?	112±2 minutes	2.6	—	Lu-p-6n
Hf^{171}	K, σ^-, γ	16.0±0.5 hours	0.15	1.4	Lu-p-5n Yb-α-3n
Hf^{172}	K, σ^-, γ	~5 years	0.23	~0.23 0.8	Lu-p-4n Yb-α-2n,3n Ta-d-3n11n
Hf^{173}	K, σ^-, γ	23.6±0.1 hours	~0.1, 0.22	~1	Lu-p-3n Yb-α-n,2n,3n

[2] A. Flammersfeld and J. Mattauch, Naturwiss. 31, 66 (1943). J. Mattauch and A. Flammersfeld, Isotopic Report, Z. Naturforsch., Tubingen (1949).

[3] From the measurement of the beta-particle activities of the 3.7-hour Lu^{176} and 6.7-day Lu^{177} activities, the isotopic cross sections for (d, p) reactions of 19-Mev deuterons in Lu^{175} and Lu^{176} were estimated to be $3.4\pm0.3\times10^{-2}$ and $5.9\pm0.4\times10^{-2}$ barns, respectively. The higher value for the cross section of Lu^{176} may be due to the neutron binding energy of about 1 Mev higher for the odd neutron nucleus over the even neutron nucleus.

Mev ϵ^-: L x-ray: K x-ray: ~0.22-Mev γ-ray: 0.8-Mev γ-ray = 0.3: ~0.01: ~0.8: 1: ~0.07: ~0.02.

4.0±0.1-hour Lu^{172}.—This activity was produced in all alpha-particle bombardments of thulium, but in highest yield at the lower bombarding energies indicating production of the (α, n) reaction. The hard particle radiation found in the aluminum absorption was shown to be a positron of maximum energy 1.2 Mev; sufficient activity was not available for good measurement of lead absorption, but the ratio of positrons to gamma-rays is about 1:2. The activity was also found in alpha-particle and proton bombardments of yttermium.

6.70±0.05 day Lu^{172}.—The decays of column-separated lutetium fractions from 10-Mev bombardments of ytterbium and low energy alpha-particle bombardments of thulium showed a half-life of about seven days, noticeably less than the half-life of the 8.5-day activity produced in 38-Mev alpha-particle bombardments of thulium. The hafnium activity of about five years half-life allocated to mass 172 has been found to have a lutetium daughter, the decay of which has been followed through over ten half-lives. The radiation characteristics agree well with those obtained for the activity produced in low energy alpha-particle bombardments of thulium, and it is fairly certain that the activities are due to the same isotope. The ratios of the various radiations of the 6.7-day activity are 0.13-Mev ϵ^-: ~0.6-Mev ϵ^-: L x-ray: K x-ray: 1.2-Mev γ-ray = ~0.2: ~0.01: ~0.5: 1: ~0.5.

8.5±0.2-day Lu^{171}.—In the 38-Mev alpha-particle bombardments this activity was observed through seven half-lives; in the lower energy bombardments, the half-life obtained was decidedly lower, undoubtedly due to the presence of the 6.7 day activity allocated to mass 173 and produced in the (α, n) reaction in thulium. While allocation to mass 171 is not certain only on the basis of yields in alpha-particle reactions in thulium, the isotope has been found to be produced by decay of a 16-hour Hf^{171} formed in proton bombardment of lutetium in highest yields at 50–60 Mev. Growth of the 1.7 day-Lu^{170} together with growth of the 8.5-day species was observed only in hafnium activities produced by 60 to 75-Mev protons on lutetium and hence, in view of the production of both isotopes in alpha-particle bombardments of thulium, allocation of the 8.5-day activity is made to mass 171. The aluminum absorptions of the radiations of the activities from Tm+α bombardments and from hafnium decays are identical. The ratios of the various radiations of the 8.5-day Lu^{171} are 0.17-Mev ϵ^-: ~0.5-Mev ϵ^-: L x-ray: K x-ray: 1.2-Mev γ-ray = ~0.05: ~0.005: ~0.5: 1: ~0.2.

~600-day Lu^{171}.—In all bombardments of thulium with alpha-particles, the column separated lutetium fractions contained a species decaying with a half-life of about 600 days. The decay has been followed as yet through only three years. The activities available, except those from a special long bombardment made to determine the radiation characteristics, were low, and the determination of yields was difficult. The yield of the 600-day activity in 38-Mev bombardments was about 0.2 that of the 8.5-day activity and appeared also to follow roughly the variation with bombarding energy to be expected for production by an $(\alpha, 2n)$ reaction. Provisional allocation is made to mass 171, making the 600-day activity isomeric with the 8.5-day Lu^{171}.

The radiation characteristics are very similar to those of the long-lived (~500-day) activity produced by decay of the 23.6-hour hafnium isotope which must be allocated to mass 173 from its method of production. The long-lived activity found in the lutetium fraction from spallation reactions in tantalum may be a mixture of long-lived isotopes (~500 day and ~600 day). The ratios of the various radiations of the ~600-day activity obtained from alpha-particle bombardments of thulium are ~0.1-Mev ϵ^-: L x-ray: K x-ray: ~1-Mev γ-ray = ~0.2: ~0.8: 1: ~0.01.

1.7±0.1-day Lu^{170}.—This activity was observed in bombardments of thulium with alpha-particles of energy greater than about 30 Mev. It was also found in the decay of a short-lived hafnium parent (112-min Hf^{170}). Allocation to mass 170 thus seems fairly certain. The approximate ratios of the various radiations are ~0.1-Mev ϵ^-: L x-ray: K x-ray: ~2.5-Mev γ-ray = ~0.3: ~0.5: 1: ~0.5. While the allocation of the 1.7-day activity to Lu^{170} is fairly certain, the yield of this isotope in the 38-Mev bombardment of thulium is only about 0.01 barn, a value much lower than that obtained for the $(\alpha, 3n)$ reaction in holmium.[1a] It is therefore possible that there exists a short-lived activity which is isomeric with the 1.7-day Lu^{170}.

III. HAFNIUM ISOTOPES

In addition to the 70 day Hf^{175} activity described previously,[4] the bombardments of ytterbium with 38- and 20-Mev alpha-particles and of lutetium with protons of 15- to 75-Mev energy have led to the recognition of four additional activities.

23.6±0.1 hour Hf^{170}.—In the bombardments of ytterbium with 20-Mev alpha-particles and of lutetium with 18- to 32-Mev protons from the linear accelerator, an activity of 23.6 hours half-life was obtained; the radiation characteristics were identical in both cases. In bombardments of ytterbium with 38-Mev alpha-particles the half-life obtained was somewhat shorter, which is undoubtedly due to the formation of the 16 hour Hf^{171} activity produced by $(\alpha, 3n)$ reactions in Yb^{170}; this shorter-lived activity would not be formed in the lower energy alpha-particle bombardments. The decay of 23.6 hour Hf^{170} has been followed through eight half-lives and the ratios of the radiations are: ~0.12 Mev ϵ^-: ~0.22 Mev ϵ^-: L x-ray: K x-ray: ~1 Mev γ-ray = ~0.3: ~0.02: ~0.3: 1: ~0.1. A search

[4] G. Wilkinson and H. G. Hicks, Phys. Rev. 75, 696 (1949).

for a short-lived lutetium daughter of this activity led to the conclusion that no Lu^{173} (isomeric with the ~500 day Lu^{173} produced in the decay), is found with half-life between 1 minute and the ~500 day Lu^{173}. Successive chemical separations of lutetium from hafnium activities produced in a long 30-Mev alpha-particle bombardment of ytterbium showed that the ~500 day lutetium activity was formed as the daughter of the 23.6 hour hafnium.

~5 year Hf^{171}.—This activity has been found in the hafnium fractions from bombardments of ytterbium with alpha-particles, of lutetium with protons, and of tantalum with 190-Mev deuterons, after decay of the 70-day Hf^{174}. The decay has been followed for over two years, and the half-life appears to be about five years. The activity is the parent of a 6.70-day lutetium daughter; both the decay of the separated daughter and its growth in purified hafnium have been studied. No other daughter activities with half-lives greater than one minute have been observed. The ~5-year activity decays predominantly by emission of x-radiation, only weak intensities of electrons and γ-rays being found; electron energies from a simple magnetic spectrometer correspond to the conversion of a 0.28-Mev γ-ray observed in lead absorption measurements. The ratios of the various radiations corrected for counting efficiencies, etc., are ~0.23-Mev ϵ^-: L x-ray: K x-ray: ~0.28-Mev γ-ray: 0.8-Mev γ-ray = ~0.05: ~1:1: ~0.06: ~0.06. The x-ray intensities of the ~5-year hafnium and the 6.70 day lutetium in secular equilibrium are in agreement with the assumption that the K x-radiation, corrected for contribution of x-rays arising from conversion, represents disintegration by orbital electron capture.

16.0±0.5-hour Hf^{171}.—In 38-Mev alpha-particle bombardments of ytterbium, a hafnium activity of ~22-hours half-life was obtained and ascribed to a mixture of the 16.0-hour Hf^{171} and the 23.6-hour Hf^{173}. The apparent half-life was observed to be greater at lower bombarding energies. In bombardments of lutetium with protons of energy 40- to 70-Mev, chemical separation showed that a 16.0±0.5 hour hafnium activity was produced in maximum yield at about 50 Mev. Successive chemical separations of lutetium showed that the decay of the 16-hour activity formed the 8.5-day Lu^{171}. No lutetium activities of half-lives greater than about one minute, other than the 8.5-day Lu^{171}, could be detected; the decay of the 8.5-day daughter activity was followed through over eight half-lives. The ratios of the radiations of the 16-hour activity obtained from absorption measurements on a sample from 50-Mev proton bombardment of lutetium are 0.15-Mev ϵ^-: L x-ray: K x-ray: 1.5-Mev γ-ray = ~0.2: ~1.5: 1: ~0.3. The radiations are different from the 23.6-hour hafnium, but some contamination due to the latter is probable. In tantalum the yield of the $(p, 3n)$ reaction at 50 to 60 Mev was less than 0.1, that of the $(p, 5n)$ reaction and the situation for lutetium is probably similar.

112±2-min Hf^{170}.—The 112-min activity was found in bombardments of lutetium with protons of energy greater than about 60 Mev. The activity decays with emission of positrons of maximum energy 2.4 Mev which were studied through six half-lives on a simple magnetic spectrometer. No appreciable amount of electromagnetic radiation, other than annihilation radiation, was observed to decay with this half-life. The isotope most likely decays by positron emission without appreciable electron capture. The 16-hour hafnium activity was also formed in the bombardments up to the maximum of 75 Mev studied, and the chemically separated lutetium daughter activities showed the presence of the 8.5-day Lu^{171}. However, the initial daughter separations showed that about 90 percent of the gross lutetium activity was caused by the 1.7-day Lu^{170} and that the yield of this activity fell roughly corresponding to the decay of the 112-min hafnium. In view of the comparatively weak activities available, the parent-daughter relationship of the 112-min hafnium and the 1.7-day lutetium activities was not studied in greater detail.

Thanks are due to T. M. Putnam, Jr., S. B. Rossi, J. T. Vale, R. D. Watt and the crews of the 60-in. and 184-in. cyclotrons and the linear accelerator for making bombardments possible. The advice and interest of Professor G. T. Seaborg and Professor I. Perlman is gratefully acknowledged. We are also indebted to Professor F. H. Spedding of Iowa State College for supplying part of the lutetium used in these studies.

On the Production of Mesons by Primary Cosmic Rays

H. D. RATHGEBER
Physics Department, University of Melbourne, Melbourne, Australia
(Received January 3, 1950)

The present ideas on the production of π-mesons by the primary cosmic rays and of their decay into μ-mesons lead to differences between the calculated and observed intensities, total energies of the components, and geomagnetic effects, which do not appear resolvable by any plausible adjustment. A consistent explanation of the several effects is found in the assumption of a further intermediate meson, which is identified with the τ-meson of about 900 electron masses. A model which agrees with the available data and is not contradicted by the facts of direct observation, such as in photographic emulsions, consists in the following assumptions:

(1) Production of τ-mesons and π-mesons in a ratio of 5 to 1 by the primary nucleons with a multiplicity $2.7\ P^{0.5}$ (P in Bev/c).
(2) Decay of the τ-mesons into π-mesons with a mean life of 10^{-10} sec.
(3) Decay of the π-mesons into μ-mesons.

I. INTRODUCTION

THE short range of nuclear forces led Yukawa to the assumption that the exchange forces were transmitted by a particle of several hundred electron masses. The identification of this particle with the penetrating component of cosmic rays opened up an avenue of research into nuclear forces at the highest energies.

Experimental investigations have shown that, on the one hand, the most abundant particle in the penetrating component of cosmic rays, the μ-meson, does not interact strongly with the nucleus[1] and on the other, that a particle occurring more rarely in the lower atmosphere, the π-meson, frequently produces nuclear disintegrations.[2] If it is not absorbed the π-meson is known to decay with a mean life[3] of 10^{-8} sec into a μ-meson. Hence it appears to be necessary to assume that the primary cosmic rays, on penetrating into our atmosphere, first produce π-mesons which then decay into μ-mesons. These deductions are based on the experimental study of the behavior of single particles.

In the present paper an attempt is made to apply these concepts to the explanation of observations which result from the superposition of the behavior of single particles. The approach is empirical. By a process of trial and error it is possible to arrive at definite conclusions concerning meson production. It is clear that by the introduction of parameters, such as the multiplicity of production, any single observational fact, such as the latitude effect, may be explained without having necessarily any significance. If the known facts, which previously could not be accounted for, are explained by the introduction of a new essential parameter, in the present case an additional decay, it must be concluded that it has some justification.

The experimental data used for comparison should fulfil two requirements. Firstly, the interpretation of the experimental results should be free from doubt. This is the case for measurements of the penetrating component in the lower part of the atmosphere where it is easily separated from the other cosmic-ray components. These measurements include the different aspects of the geomagnetic effects, the relationship between the momentum spectrum of the primaries and that of the mesons, the intensities at the limit of the atmosphere and at sea level, the total energy of cosmic rays impinging on the earth and of the several components, and, finally, the absorption of the meson component in the lower atmosphere. Secondly, if a model is rejected, the difference between the calculated results and the experimental data should exceed clearly the experimental errors as well as those introduced by approximations in the calculations.

II. THE MODELS WITH EQUIPARTITION OF THE ENERGY OF THE PRIMARY PARTICLE

The equal division of the energy of a primary particle among N μ-mesons is the simplest model. Certain further assumptions and data which we will not discuss further at this stage must be made for the comparison between the model and the observations:

(1) Intensity of primary cosmic rays[4] at the limit of the atmosphere (geomagnetic latitude $\lambda_m=41°$)

$$I_P=0.070 \text{ particles cm}^{-2} \text{ sec}^{-1} \text{ sterad}^{-1}.$$

(2) Differential momentum spectrum, subsequently abbreviated DMS, of the form $dp/p^{2.5}$ for $p>3$ Bev/c of the primary particles.[5]

(3) Deflection of all primary particles in the earth's magnetic field according to Stoermer's theory.[6]

(4) Production of all μ-mesons at an atmospheric depth of 100 mb.

(5) Mean life of 2.15×10^{-6} sec, mass of 216 electron masses, and energy loss independent of energy of 2 Bev for 1000 g cm^{-2} of air.

[1] Conversi, Pancini, and Piccioni, Phys. Rev. 71, 209 (1947).
[2] C. F. Powell, *Cosmic Radiation* (*Colston Papers*) (Butterworth, London, 1949), p. 83.
[3] P. R. Richardson, Phys. Rev. 74, 1720 (1948).
[4] J. A. Van Allen and J. F. Gangnes, Phys. Rev. 78, 50 (1950).
[5] L. Jánossy, *Cosmic Rays* (Oxford Press, Oxford, 1948), p. 300.
[6] M. S. Vallarta, Phys. Rev. 74, 1837 (1948).

TABLE I. Comparison of calculations and measurements at sea level.

Model	Multiplicity	Geomagnetic latitude of knee	Vertical latitude effect (percent)	Absolute intensity at sea level 10^{-3} part. cm^{-2} sec^{-1} $sterad^{-1}$	Energy of μ-mesons Bev cm^{-2} sec^{-1} $sterad^{-1}$	Exponent of differential momentum spectrum at production
Measured		40±2[a]	18±2[b]	7.7[c]	0.3[d]	3.0[e]
A	$N=1$	46	81	64	0.9	2.5
	$N=4$	34	30		0.9	2.5
	$N=5$	30	17		0.9	2.5
B	$N=3$	38	28	19	0.45	2.5
	$N=3.5$	36	19	17	0.45	2.5
	$N=4$	31	12	16	0.45	2.5

[a] P. S. Gill, Phys. Rev. **55**, 1151 (1939).
[b] See reference 17.
[c] See reference 11.
[d] See reference 13.
[e] J. G. Wilson, Nature **158**, 414 (1946).

(6) The energy of the produced mesons is equal to the energy in the primary beam.

The results obtained on this basis are summarized in Table I. Although the simple μ-meson model A gives a correct value of the latitude effect for a multiplicity $N=5$, it does not do so for the other effects. It has been shown[7] that the correct position of the knee may be obtained in this model by a multiplicity $N=k^2e^{-cb}$, which, however, does not bring the other quantities into agreement.

In model B it is further assumed that:

(7) Each primary produces only π-mesons.
(8) All π-mesons decay into μ-mesons.
(9) The probability of a μ-meson carrying off any momentum between 0 and p/N is constant.

Although this latter assumption is not correct, it is sufficiently accurate for the present purpose.

From Table I it is evident that the new model has decreased the differences between calculation and observation. We will therefore investigate whether further refinements will make the differences vanish.

III. THE MODEL WITH THE PSEUDOSCALAR π-MESON

For the analysis of this model we do not proceed as in the preceding section. Instead of calculating the different effects from the primary DMS we reconstitute the DMS of the π-mesons at production and compare it with that of the mesons produced by the primary nucleons according to the symmetrical pseudoscalar theory.[8] The results of the preceding section make us expect a gap between our results. To eliminate any possibility that this gap may be due to experimental errors we take for the primary DMS the lowest results compatible with the observational facts and for that of the μ-mesons the highest.

[7] L. Jánossy and P. Nicholson, Proc. Roy. Soc. (London) **A192**, 98 (1947).
[8] Lewis, Oppenheimer, and Wouthuysen, Phys. Rev. **73**, 127 (1948).

The μ-Meson Spectrum at Production

The DMS at production and at the knee of the geomagnetic effect(Fig. 1, curve 2) is calculated from that of particles penetrating 10 cm of lead at sea level and at a geomagnetic latitude $\lambda_m=46°$ (Fig. 1, curve 1)[9,10] after reducing to the known meson intensity[11] at sea level 0.0077 particles cm^{-2} sec^{-1} $sterad^{-1}$. The assumptions are that all observed particles are μ-mesons and that all μ-mesons are produced at the 100-mb level. The error in the μ-meson spectrum at production arising from the second assumption is small.[12]

This DMS, which stops at 2 Bev/c because of the energy loss of 1.8 Bev in 900 mb of the atmosphere and 0.2 Bev in 10 cm Pb, is extended towards lower values in the following way. The DMS, say, at 700 mb, is obtained from that at production by multiplication with the probabilities of arriving at that level. Integration gives the integral spectrum down to a momentum $2(1-0.7+0.1)=0.8$ Bev/c. As the total meson intensity at 700 mb is known[13] the integral spectrum is completed. From this further points on the DMS are obtained.

By repetition of this operation several times to a level of 300 mb the μ-meson DMS at production for momenta >0.4 Bev/c has been determined. This spectrum, which agrees with that found by more direct means,[14] was extended to 0.2 Bev/c with the help of the latter.

As this agreement gives confidence in our method, the μ-meson DMS at production at the equator was derived in the same way using the known values for the latitude effect[15,16] after correction to vertical incidence.[17]

The π-Meson Spectrum at Production

The energy and momentum conservation laws determine the probability $W(p_\mu, p_\pi)$ of production of a

[9] The momentum is measured in Bev/c at production.
[10] Caro, Parry, and Rathgeber, Nature **165**, 688 (1950).
[11] K. Greisen, Phys. Rev. **61**, 212 (1942).
[12] L. Jánossy and J. G. Wilson, Nature **158**, 450 (1946).
[13] B. Rossi, Revs. Modern Phys. **20**, 537 (1948).
[14] M. Sands, Phys. Rev. **77**, 180 (1950).
[15] W. C. Barber, Phys. Rev. **75**, 590 (1949).
[16] Biehl, Neher, and Roesch, Phys. Rev. **76**, 914 (1949).
[17] H. D. Rathgeber, Phys. Rev. **77**, 566 (1950).

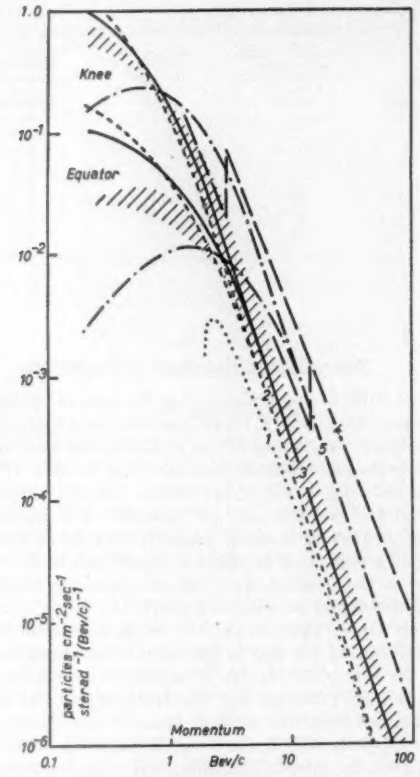

FIG. 1. Differential momentum spectra of: (1) μ-mesons at sea level and geomagnetic latitude 46°, (2) μ-mesons at production, (3) π-mesons at production, (4) primary nucleons, (5) mesons produced by primary nucleons with a multiplicity 1.2 $P^{0.5}$.

μ-meson of momentum p_μ by a π-meson of momentum p_π. Let us consider in the center-of-mass system the general case of the decay of a meson into another meson and a number n of other particles. Then the maximum kinetic energy of the decay meson is:

$$(E_2')_{K\,\max}=c^2([m_1-m_2]^2-n^2m_3^2)/2m_1,$$

in which m_1 is the rest mass of the decaying meson, m_2 that of the decay meson, and m_3 that of one of the other particles. It is found further that the maximum total energy of the decay meson is given by

$$(E_2')_{\max}=c^2(m_1^2+m_2^2-n^2m_3^2)/2m_1$$

and its maximum momentum by

$$(p_2')_{\max}=c\{[(m_1-m_2)^2-n^2m_3^2]\times[(m_1+m_2)^2-n^2m_3^2]\}^{\frac{1}{2}}/2m_1.$$

In the case of $\pi\rightarrow\mu$ decay, in which all μ-mesons emitted by a π-meson at rest have the same range,[18] the last two equations reduce to

$$E_\mu'=c^2(\pi^2+\mu^2)/2\pi, \tag{1}$$

$$p_\mu'=c(\pi^2-\mu^2)/2\pi, \tag{2}$$

in which π and μ are the rest masses of the π- and μ-mesons, respectively.

The transformation to the laboratory system

$$p=[\pm p'+\beta E'/c]/(1-\beta^2)^{\frac{1}{2}} \tag{3}$$

leads, for relativistic particles to

$$(p_\mu)_{\min}=(\mu/\pi)^2p_\pi=gp_\pi, \tag{4}$$

and

$$(p_\mu)_{\max}=p_\pi, \tag{5}$$

introducing the symbol g as a convenient abbreviation.

As the mesons are all emitted with the same momentum and with spherical angular symmetry in the CM-system, the probability $W(p_\mu, p_\pi)$ is constant in the interval from $(p_\mu)_{\min}$ to $(p_\mu)_{\max}$.[19] If $S_\pi(p_\pi)$ is the DMS of the π-mesons, that of the μ-mesons is

$$S_\mu(p_\mu)=\int_{p_\mu}^{p_\mu/g}\left[WS_\pi\Big/\int_{gp_\pi}^{p_\pi}Wdp_\mu\right]dp_\pi \tag{6}$$

for the case in which W is not normalized.

Applying this transformation to a $\pi-$DMS

$$S_\pi=A_\pi p_\pi^{-\gamma}$$

with $W=$constant, gives

$$S_\mu=A_\pi[(1-g^\gamma)\gamma^{-1}/(1-g)]p_\mu^{-\gamma}. \tag{7}$$

As part of the $\mu-$DMS is of the form $p^{-\gamma}$, the generating π-spectra over these ranges are found by multiplication of the μ-spectra by the factor

$$\gamma(1-g)/(1-g^\gamma)=1.57$$

with $\gamma=3.0$ and[20] $\pi/\mu=1.32$.

A correction must be applied to the resulting curve for the nuclear capture of part of the π-meson flux. Only a fraction[21] $R/(R+\rho L)$ of the π-mesons decay into μ-mesons, in which $R=20$ g/cm^2 is the range[21] of the π-mesons for nuclear capture, L is their mean decay path, and ρ is the air density at the 100-mb level. The range, which is smaller than that generally accepted, has been calculated from the density effect in the upper atmosphere[21] using 1×10^{-8} sec as the lifetime of the π-meson. The use of this small range is justified by the program followed in this paper; differences between quantities which are to be compared are made as small as is compatible with the measurements.

The straight part of the π-meson DMS at production has been obtained in this manner. The curved parts were found by assuming several π-meson DMS and

[18] G. P. S. Occhialini and C. F. Powell, Nature **162**, 168 (1948).

[19] See reference 5, p. 183.

[20] R. E. Marshak, Phys. Rev. **75**, 700 (1949).

[21] A. Duperier, Proc. Phys. Soc. (London) **A62**, 684 (1949).

calculating that of the μ-mesons by numerical methods until a fitting π-spectrum was found.

The Momentum Spectrum of the Primary Particles

The intensity of cosmic rays at the limit of the atmosphere has been measured with Geiger counter telescopes carried by rockets.[4] It was found to be 0.070 particles cm^{-2} sec^{-1} $sterad^{-1}$ at $\lambda_m=41°$ and 0.028 in the same units at the equator, which corresponds to a DMS of $p^{-1.9}$.

Measurements at $\lambda_m=52^\delta$ in balloon flights[22] with absorber thicknesses up to 6 cm Pb converge towards 0.17 particles cm^{-2} sec^{-1} $sterad^{-1}$. Correcting for the remaining latitude effect[23] and the absorption in the remaining layer of air this reduces to 0.11 for $\lambda_m=41°$. For the reasons already given we will take 0.070 at $\lambda_m=41°$, that is $p_{\min}=4.5$ Bev/c, as a basis for our calculations.

Assuming that the energy in the primary cosmic rays is proportional to the energy appearing as ionization in the atmosphere their DMS[5] is found to be of the shape $p^{-2.4}$. A DMS with exponent 1.9 extending to infinity would contain an infinite energy. A higher multiplicity of nuclear disintegrations at the equator in the rocket shell may increase the rate at the equator. As we consider the estimate based on the ionization measurements to be more reliable and as we want to take the lowest values we accept $\Gamma=2.5$ as the exponent of the DMS of the primary particles down to the geomagnetic cutoff of 3 Bev/c for $\lambda_m=46°$, the latitude at which we calculated the μ-meson spectrum. This decision is supported by the DMS of the heavy nuclei which follows the same exponent[24] and cannot have been influenced by multiple events.

Burst measurements in the stratosphere indicate that at most only a small proportion of the primaries can be electrons.[25] The east–west effect shows that the majority of the charged particles are positive. Photographic plate measurements[26] reveal that 25 percent of the primaries are stripped nuclei of $Z\geqslant 2$. Hence, we divide the primaries into 75 percent protons and 25 percent α-particles, neglecting the heavier nuclei. Supposing that the nucleons of an α-particle act independently, the number of meson producing nucleons in the α-particles is:

$$0.070\times 25 \text{ percent}\times 4=0.070 \text{ particles } cm^{-2}\ sec^{-1}\ sterad^{-1} \text{ at } \lambda_m=46°.$$

To obtain the energy spectrum of these it is necessary to find their cut-off momentum. They may be considered as packets of particles of two proton masses and unit charge. As the cut-off momentum is the same for all relativistic particles of unit charge each nucleon will carry a momentum of one-half of the cut-off value for a proton at the same latitude. The DMS of all primary nucleons are traced as curve 4 in Fig. 1 making allowance for the nonrelativistic velocity at the low momentum end.

The Momentum Spectrum of the Mesons Produced by the Primary Nucleons

The symmetrical pseudoscalar theory,[8] which appears to be the most probable from the observations of nuclear physics, gives the probability:

$$W(p, P)\sim N/P\exp\{-N[(p/P)+(1/2MP)]\} \quad (8)$$

of production of a meson of momentum p by a nucleon of momentum P if $N=KP^r$ is the multiplicity of production. We can estimate K and r from the disappearance of the latitude effect for different absorber thicknesses. Considering that the energy loss in the atmosphere is 2 Bev and that the knee of the latitude effect at sea level[27] occurs at $\lambda_m=40°$, corresponding to a cut-off momentum of 4.5 Bev/c, we conclude that the multiplicity for 4.5 Bev/c nucleons is $N=4.5/2=K(4.5)^r$. Furthermore, it has been observed[28] that the latitude effect disappears at a depth of water of 7 m, which is equivalent to a total energy loss of 3.4 Bev. Since the multiplicity in this case is $N=14/3.4=K(14)^r$, the constants are found to be $K=1.2$ and $r=0.5$.

An approximate transformation can be found by assuming that the probability of production of a meson is constant between the limits 0 and $2P/N$; this satisfies the condition that the energy of the N mesons is equal to that of the primary nucleon. By analogy with Eq. (6) the meson spectrum is then

$$S_p=\int_{2pN}^{\infty}\left[NS_P\Big/\int_0^{2P/N}dp\right]dP.$$

For a primary DMS given by $S_P=A_PP^{-\Gamma}$ this becomes

$$S_p=A_P[2^{\Gamma-2r-1}/(2r-\Gamma)]K^{(2-\Gamma)/(1-r)}p^{(2r-\Gamma)/(1-r)}$$
$$=A_PK^{-1}p^{-2}, \quad (9)$$

if $r=0.5$ and $\Gamma=2.5$, that is, the exponent of the meson DMS produced by the primaries is the same as that of the μ-meson DMS.

The DMS of the mesons below the cut-off momentum of the primaries, which is curved, and the intensity of its straight portion, which is sensitive to the shape of the probability function at high energies, were found by numerical and graphical methods. The proportionality constant in Eq. (8) was determined in the same manner, the condition being

$$\int_0^P W\,dp=KP^r.$$

The DMS of charged mesons at the knee and at the equator, multiplied by a factor 0.67 resulting from the

[22] M. A. Pomerantz, Phys. Rev. 75, 1721 (1949).
[23] M. A. Pomerantz, Phys. Rev. 77, 830 (1950).
[24] M. S. Vallarta, Phys. Rev. 77, 419 (1950).
[25] R. I. Hulsizer and B. Rossi, Phys. Rev. 73, 1402 (1948).
[26] H. L. Bradt and B. Peters, Phys. Rev. 77, 54 (1950).
[27] P. S. Gill, Phys. Rev. 55, 1151 (1939).
[28] J. Clay, Physica 2, 299 (1935).

assumed admixture of $\frac{1}{3}$ neutral mesons, are represented in curve 5, Fig. 1.

IV. INTRODUCTION OF A FURTHER DECAY

It is obvious that the DMS of the π-mesons (Fig. 1, curve 3) and that of the mesons produced by the primary nucleons (curve 5) do not agree. We now discuss several conceivable reasons for the difference of a factor 5.2 in the straight portion of the DMS.

(1) Errors in the π-Meson DMS

The experimental errors in this case are certainly below 10 percent for momenta greater than 1 Bev/c. It is known that, contrary to our assumptions, mesons are produced in the lower atmosphere. Their intensity however is much lower than has been estimated previously[29] from assumptions which are now known to be incorrect. The intensity of these mesons will not exceed 10 to 20 percent of the total intensity.

(2) Errors in the Primary DMS

Despite the deductions for showers, the intensity measured with Geiger counter telescopes may have been increased by multiplication processes in the matter surrounding them. This is not the case with heavy nuclei as observed in photographic plates. As any collision will destroy them, the observed rate of heavy nuclei is a minimum rate. The α-particles resulting from a disintegration of heavier nuclei will contribute only a negligible fraction. The consideration of collisions in interstellar space[26] shows that even if cosmic rays should consist exclusively of heavy nuclei at production, a considerable proportion would be separated into protons and neutrons, the latter decaying into protons and electrons. Furthermore, it would be strange if the mechanism which accelerates heavy nuclei did not accelerate protons also. We conclude thus that the proton intensity should be several times that of the heavy nuclei and that the intensity of the primary nucleons cannot be in error by more than 30 percent. Neither can the exponent of the primary DMS be too small. The value we choose is the highest of all the direct observations.

(3) Errors in the Production Process of Mesons

Direct observation of the production of mesons shows that the production process is multiple. The satisfactory agreement of the value for r obtained from the latitude effect and from the change in slope of the primary spectrum in transforming into a meson spectrum [meson decay does not alter the slope, see Eq. (7)] makes it evident that the values used are at least self-consistent. Variations of r within the limits imposed by experimental results will scarcely affect the meson intensity.

[29] H. D. Rathgeber, Phys. Rev. **61**, 207 (1942).

As the meson intensity at a momentum higher than the magnetic cutoff is inversely proportional to K [Eq. (7)], an error in K might cause the observed difference. However an increase in K by a factor 5.2 would bring the low momentum part to values exceeding the observed ones. Nevertheless, we shall not reject this explanation since the observed intensities at these momenta might have large errors.

We shall not take into consideration the possibility that the probability function used is altogether wrong. As the probability functions are determined mainly by the relativity transformation from the CM system to the laboratory system all plausible theories will give similar results.

(4) Suggestion of an Additional Intermediate Meson

The effect just discussed, which would be obtained by an increase in K, would also be produced by a decay of the directly produced mesons into π-mesons. As these assumed mesons would be heavier than the π-mesons, we identify them temporarily with the observed τ-mesons of about 900 electron masses, and discuss the effect of this assumption.

The π-mesons are nuclear force mesons, and probably have integral spin. The same considerations apply to the τ-meson. If we assume that in the $\tau \rightarrow \pi$ decay neutral particles are produced, the conservation of spin requires that the sum of their spins be integral. Since it will be shown later that a process which gives a maximum loss of detectable energy fits the experimental results best, we shall consider only the emission of a neutrino pair. In this case the π-meson is not emitted with a single momentum in the CM system, but with an unknown probability distribution between 0 and $(P')_{\max}=c(\tau^2-\pi^2)/2\tau$ [Eq. (2)]. However, it is possible to use the two limits for the calculation of two spectra which will bracket the true DMS whatever the probability distribution. For $p_\pi'=0$ the relativity transformation (3) yields for $\beta=1$

$$p_\pi=(E/\tau c^2)p_\tau=(\pi/\tau)p_\tau=hp_\tau.$$

A DMS of the producing mesons of the form $S_\tau=A_\tau(p_\tau)^{-\gamma}$ is transformed by the foregoing relation into

$$S_\pi=A_\tau h^{\gamma-1}(p_\pi)^{-\gamma}. \tag{10}$$

Using the maximum value for p_π' we find in analogy to Eq. (7)

$$S_\pi=A_\tau[(1-f^\gamma)/\gamma(1-f)](p_\pi)^{-\gamma} \tag{11}$$

in which $f=(\pi/\tau)^2$.

The domain between these limits is shown in Fig. 1 by the hatched areas. As the straight part of the π-meson spectrum falls within the limits, it is seen that this last explanation satisfies the conditions.

An alternative explanation is given by the direct decay of the heavy mesons into μ-mesons. With the

same reasoning as for the $\pi \rightarrow \mu$ decay [Eq. (7)] the μ-DMS for this case is found to be:

$$S_\mu = A_\tau [(1-j^\gamma)/\gamma(1-j)] p_\mu^{-\gamma}$$

in which $j=(\mu/\tau)^2$. This spectrum is higher by a factor 4 than the observed μ-meson spectrum and is therefore rejected.

V. THE TOTAL ENERGY IN THE PRIMARY COSMIC RAYS AND IN THE SEVERAL COMPONENTS

After the considerations in the preceding section we are left with the explanations that either the production of mesons occurs with a multiplicity 5 times higher than that assumed, or that another heavy meson occurs between the primaries and the π-mesons. The difference between the alternatives will lie in the intensity of the μ-mesons of momenta below 1.5 Bev/c. In the first, all of the energy which disappears in the range above 1.5 Bev/c will reappear as slow mesons; in the second, a major part will disappear completely as neutrinos and the intensity of the slow mesons will be diminished. As no measurements of the intensity of the very slow μ-mesons at their place of production exist we consider the next best quantity, which is the total energy in the μ-meson component. This choice has the further advantage that the analysis is simplified considerably.

The total energies in the μ-meson, the electron, and the nuclear component have been estimated[12] at 0.29, 0.20, and 0.12 Bev cm^{-2} sec^{-1} sterad^{-1}, respectively. Practically the whole of this energy is lost in the atmosphere as ionization. Ionization measurements at several latitudes[30] give the energy lost as ionization at $\lambda_m = 46°$ as 2.1 Bev cm^{-2} sec^{-1}. Taking into account that the cosmic rays are incident isotropically[31] on a plane layer we find:

$$2.1/\pi = 0.67 \text{ Bev cm}^{-2} \text{ sec}^{-1} \text{ sterad}^{-1},$$

which is 0.06 higher than the sum of the components in Rossi's estimate. Considering that we want to take the highest possible values, and that the electronic and nuclear components probably have been underestimated, we take 0.31, 0.22, and 0.14 as the respective values.

The total incident energy is found by integration of the spectra of the proton and α-particle components. The minimum incident energy is $0.95+0.28=1.23$ Bev cm^{-2} sec^{-1} sterad^{-1}. It is at once evident that this value is nearly twice the energy lost in ionization.

The energy of the μ-meson component can be calculated in the following manner. Deducting 0.14 Bev cm^{-2} sec^{-1} sterad^{-1}, the energy of the nuclear component, the energy available for meson production is found to be 1.09 Bev cm^{-2} sec^{-1} sterad^{-1}. Assuming again that $\frac{1}{3}$ of this is used in the production of neutral mesons, which decay into the electron component, 0.72 Bev cm^{-2} sec^{-1} sterad^{-1} is left as the energy of all of the charged mesons at production. From Eqs. (4) and (5) we derive that the average momentum of the μ-mesons is $(p_\mu)_{av} = [(\mu^2+\pi^2)/2\pi^2] p_\pi = 0.79 p_\pi$. For relativistic particles the same fraction of the energy will be transferred from the π-meson component to that of the μ-mesons, that is, 0.57 Bev cm^{-2} sec^{-1} sterad^{-1}. This is nearly twice the measured value. In this case we cannot have recourse, as in the intensity analysis, to a higher multiplicity of production for an explanation. The additional meson decay remains as the only proposition consistent with the observations.

The fraction of the energy of the τ-mesons going into the π-meson DMS is $(\pi^2+\tau^2)/2\tau^2 = 0.55$ for the case of maximum energy transfer. In the case of minimum transfer the fraction reduces to $\pi/\tau = 0.33$. According to theory[32] the probability function in the CM system for the type $m_1 \rightarrow m_2 + 2\nu$ of decay has a maximum in the upper half of the momentum range. Experiments[33] on the $\mu \rightarrow e$ decay have confirmed this. Therefore we will take the fraction as 0.45, which makes the energy in the μ-DMS 0.26 Bev cm^{-2} sec^{-1} sterad^{-1}.

Considering the several approximations involved the difference between the latter calculated value and the observed of 0.31 Bev cm^{-2} sec^{-1} sterad^{-1} does not appear significant by itself. It is known however that the π-mesons are nuclear force mesons.[34] We must therefore expect that some of the π-mesons are produced directly. Assuming that 5/6 of the mesons produced by the primary nucleons are τ-mesons and that the rest are π-mesons, the energy of the μ-component becomes:

$$(0.72\times0.17)+(0.72\times0.83\times0.45)\times0.79 = 0.31 \text{ Bev cm}^{-2} \text{ sec}^{-1} \text{ sterad}^{-1},$$

that is the measured value.

Let us consider the π-meson intensity $S_\pi dp_\pi$ for a momentum in the straight part of the DMS as split up into two parts of which the first is produced directly and the second by the intermediary of τ-mesons. If 0.30 is the weighted average of $h^{\gamma-1} = 0.11$ [Eq. (10)] and $(1-f^\gamma)\gamma^{-1}/(1-f) = 0.37$ obtained by the same reasoning as before, and $S_\tau dp_\tau$ is the intensity of the τ-mesons, $S_\tau dp_\tau = (0.17+0.83\times0.30) S_\tau dp_\tau = 0.42\, S_\tau dp_\tau$. The fraction of the π-component which is produced directly is then:

$$0.17/0.42 = 40 \text{ percent}.$$

The π-meson DMS found in this way is lower by a factor $5.2\times0.42=2.2$ than that derived from the primary nucleon DMS. This signifies that, according to Eq. (9), the constant K is too small by the same factor. Our first value for K was derived under the assumption that the energy of one primary particle was shared equally by all mesons. However, the probability distribution used in deriving Eq. (9) is a much better approximation. As the upper limit is $2\ P/N$ instead of

[30] Bowen, Millikan, and Neher, Phys. Rev. 53, 855 (1938).
[31] Stroud, Schenk, and Winckler Phys. Rev. 76, 1005 (1949).
[32] J. Tiomno and J. A. Wheeler, Phys. Rev. 21, 144 (1949).
[33] Leighton, Anderson, and Seriff, Phys. Rev. 75, 1432 (1948).
[34] W. Heitler, *Cosmic Radiation* (*Colston Papers*) (Butterworth, London, 1949), p. 119.

P/N, the constant K is increased by a factor 2. The theoretical distribution [Eq. (8)] having a finite value above $2\,P/N$ brings the factor to a somewhat higher value. For these reasons we use $K=1.2\times2.25=2.7$, for which value the τ-meson DMS has been recalculated (Fig. 2). The new value of K which has just been derived from considerations about the straight part of the DMS, also brings calculation and observation into satisfactory agreement for the curved parts of the DMS.

The multiplicity $N=KP^{\gamma}=2.7\times10^{0.5}=8.5$ for a momentum $P=10$ Bev/c, the average momentum of the primaries, agrees satisfactorily with the observed[35] multiplicity of between 6 and 7, assuming again that $\frac{1}{3}$ of the mesons are neutral.

VI. THE τ-MESON

Several particles with a mass between 700 and 1100 m_e have been reported in the literature.[36] Recently, observation of three more particles of 725 ± 40 m_e has been reported.[36] These are named τ-mesons.

Out of these three heavy mesons coming to rest in a photographic emulsion, one produces a star and two stop without producing tracks. In our model the τ-meson is supposed to decay into a π-meson and two neutrinos. Most frequently the π-meson will carry away more than $\frac{1}{3}$ of the mass difference, i.e., 75 Mev, as kinetic energy. As the maximum energy at which a π-meson is detectable in the Ilford C2 emulsion[37] used is 8.5 Mev practically all π-mesons would escape detection.

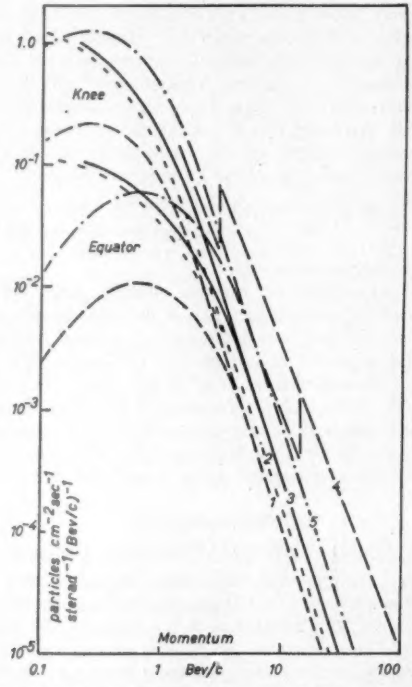

FIG. 2. Differential momentum spectra of: (1) π-mesons produced by primary nucleons, (2) π-mesons produced by τ-mesons, (3) π-mesons at production (observed), (4) primary nucleons, (5) τ-mesons produced by primary nucleons with a multiplicity $2.7\,P^{0.5}$.

Further, if the τ-meson is the main particle of the nuclear force field, it might be expected to occur in penetrating showers. In the region of minimum ionization their tracks would in general not be distinguishable from those of π- or μ-mesons. However, in the lower energy range the tracks of minimum ionization would show occasionally one sharp kink at the point of the $\tau\rightarrow\pi$ decay. In fact this has been observed under the expected conditions.[38] The fraction of the other observed cases of anomalous scattering of mesons due to this effect cannot be estimated at present.

Assuming that the τ-meson is produced in the wall of the cloud chamber or in the material surrounding it, a proper mean life of the τ-meson between 10^{-10} and 10^{-11} sec is derived. The decay of the neutral heavy meson observed in the same series leads to the same value. This latter observation, as well as other more recent ones[39] of pair production by non-ionizing agents support our assumption of the production of neutral mesons.[40]

These results have been confirmed by the most recent cloud-chamber observations.[41] In 11,000 tracks of penetrating showers 30 pairs produced by neutral particles were found. None of the charged particles showed the properties of electrons on traversing a lead plate. In the same experiment 4 more kinks were photographed. The failure to explain all of the observations by a heavy meson of a single mass is probably due to the production of neutral particles which may be neutrinos. The proper mean life of the neutral heavy meson has been estimated at 3×10^{-10} sec, that of the charged heavy meson is shorter.

The reported observation of the decay of a heavy meson[42] into 3π-mesons only, while supporting the idea of a $\tau\rightarrow\pi$ decay, would not give the loss of energy derived in this paper if it occurred in a high proportion of the $\tau\rightarrow\pi$ decays.

Further supporting evidence is found in the study of the π-meson. While there is no doubt that π-mesons interact strongly with nucleons, it appears that their coupling may be too small by a factor 10 or 10^2. In this

[35] Phyllis Freier and E. P. Ney, Phys. Rev. **77**, 337 (1950).
[36] N. Wagner and D. Cooper, Phys. Rev. **76**, 449 (1949).
[37] H. L. Bradt and B. Peters, *Cosmic Radiation* (*Colston Papers*) (Butterworth, London, 1949), p. 5.
[38] G. D. Rochester and C. C. Butler, Nature **160**, 855 (1947).
[39] Kaplon, Peters, and Bradt, Phys. Rev. **76**, 1735 (1949).
[40] R. E. Marshak, Phys. Rev. **76**, 1736 (1949).
[41] Seriff, Leighton, Hsiao, Cowan, and Anderson, Phys. Rev. **78**, 290 (1950).
[42] Brown, Camerini, Fowler, Muirhead, Powell, and Ritson, Nature **163**, 82 (1949).

case it would be necessary to assume the existence of another meson to account for the nuclear forces.[34]

The artificial production of τ-mesons by existing particle accelerators appears impossible as from 400 to 600 Mev will be required to achieve it.[43]

The frequency of observation of τ-mesons which is estimated as from 1 in 1000 π-mesons to 1 in 10,000, appears to contradict the important part attributed to the τ-meson in our model. However, closer analysis will show that this is not so. The ratio of the observations will be in the ratio of the total track length of the τ- and the π-mesons in the energy range in which they can be distinguished. Curves 2 and 3 in Fig. 2 show that τ-mesons occur only as frequently as π-mesons at these energies. As the ratio of their mean lives is of the order $10^{-8}/10^{-10}=10^2$ the ratio of the track lengths becomes about 10^2.

If, nevertheless, the frequency of observation of the τ-meson should turn out to be too small, there seems to be no objection to considering the τ-meson, like the meson in β-decay, as a virtual particle except where energy conditions are favorable.

In conclusion supporting evidence is found in the scarce direct observational material for the assumption of intermediate τ-mesons of some 900 electron masses with a lifetime of the order 10^{-10} sec.

VII. CONCLUSION

The degradation of energy and the disappearance of energy which have been shown to occur between the primary cosmic rays and the μ-meson component cannot be explained by the direct production of π-mesons alone. On the assumption that there are no fundamental errors in the measurement of the primary intensity we have come to the conclusion that a further meson decay takes place between the primary nucleons and the π-mesons. The particular model for this additional decay is not uniquely determined by the known facts; in fact, the observations quoted in the preceding section make it probable that a combination of several modes occurs.

We shall nevertheless give a general model of the three main cosmic-ray components (Fig. 3). The general genealogy of the μ-meson component has been discussed already. The electron component is presented as arising in the same process as the meson component. The constant relative density of mesons and electrons in extensive showers supports this point of view.[44,45] The electrons might be produced either by photons created in the nuclear collision[46] or by the decay of neutral mesons. The initiation of the electronic component by several of these particles originating in the same collision explains the rapid rise of the electron component in the first tenth of the atmosphere. The production by neutral mesons is made more probable by the observation[47] that the DMS of the particles producing the electron showers follows about the same exponential law as the meson DMS at production.

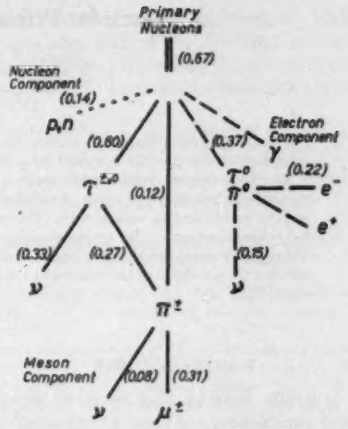

FIG. 3. Transformation model of primary cosmic rays into nucleon, electron, and meson components. The values in parentheses give the energy in Bev cm^{-2} sec^{-1} sterad^{-1}.

Finally, it is interesting to note that about half of the incident energy of cosmic rays disappears into undetectable radiation, according to our model, into neutrinos. It has been shown that the cross section of neutrinos[48] is smaller than 2.5×10^{-37} cm^2. Thus it appears that the entropy of the universe increases not only by the known processes at low energies but also by the production of neutrinos at high energies.

[43] W. H. Barkas, Phys. Rev. **75**, 1109 (1949).

[44] Cocconi, Cocconi-Tongiorgi, and Greisen, Phys. Rev. **76**, 1020 (1949).

[45] T. Ise and W. B. Fretter, Phys. Rev. **76**, 933 (1949).

[46] L. I. Schiff, Phys. Rev. **76**, 89 (1949).

[47] B. Rossi, Revs. Modern Phys. **21**, 104 (1949).

[48] D. Saxon, Phys. Rev. **76**, 986 (1949).

A Search for Primary Cosmic Gamma-Radiation. I

GILBERT J. PERLOW AND C. W. KISSINGER
U. S. Naval Research Laboratory, Washington, D. C.

(Received October 16, 1950)

A search has been made for primary cosmic gamma-radiation in the energy range 3.4 to 90 Mev. The apparatus was a counter telescope in which ionizing rays were excluded by anticoincidence and γ-rays detected by their conversion products in lead. The apparatus was carried above the atmosphere in a V-2 rocket launched at White Sands, New Mexico. The recorded γ-ray counting rate is reduced about a factor of 2 by corrections of various sorts. The variation of detection efficiency with energy permits the results to be stated in terms of the energy crossing unit horizontal area in unit time. The result is 1.4 Mev/cm²/sec. This is 1300 times less than the corresponding figure for the total cosmic-ray energy at this latitude. Considering the smallness of the result and the nature of the corrections, it is possible that the result is actually a null one.

I. INTRODUCTION

IT is generally believed that energetic gamma-rays cannot constitute more than a very small fraction of the primary cosmic radiation. Millikan and coworkers[1] have shown that sixty-five percent of the incoming energy is sensitive to the earth's magnetic field and hence is due to charged particles. Most of the remainder must be attributed to similar primaries of higher energy. A considerably lower limit to the gamma-ray intensity can be deduced from a recent cloud chamber measurement,[2] which demonstrates that at an atmospheric depth of 20 g/cm², the small number of electrons present with energies greater than 1 Bev sets an upper limit to the primary *electron* intensity of a few tenths percent of the total charged primary intensity. Since 20 g/cm² is an appreciable fraction ($\sim\frac{1}{2}$) of a radiation length, we may infer that primary photons of comparable energies are comparably rare.

No experiment reported to date however has established the absence of *low* energy primary gamma-rays. At balloon elevations, the soft-component produced in the remaining atmosphere makes any such measurement subject to difficulties of interpretation. We have therefore attempted to make a direct measurement by use of a rocket. Essentially three experiments were done. In the first we looked for gamma-rays in the energy interval 3.4 to 90 Mev, in the second for lower energies, down to 0.1 Mev, and in the third for a diurnal effect of the latter radiation. This paper reports on the first experiment. This was done in a V-2 at White Sands, New Mexico, on January 28, 1949.

II. THE EXPERIMENTAL METHOD

Figure 1 shows the apparatus schematically. Anticoincidences $AB-(C+D)$ were the primary data telemetered[3] from the rocket. Coincidences AB were telemetered for reference. The action of the counter trays and absorbers is as follows:

(1) A gamma-ray from above is distinguished from a similar ionizing ray by its failure to trip any counter in tray C.

(2) The gamma-ray produces electronic conversion products in the 6.3-mm lead annulus S_1, and these are detected by coincidence between the thin-walled counters A and B.

(3) A 1.9-mm Cu absorber S_2 between A and B insures that the recorded electron has energy >3.2 Mev and its parent γ-ray >3.4 Mev (if Compton effect is the conversion process).

(4) The electrons are absorbed in the 2.42-cm lead annulus S_3 whose existence is justified by its permitting the use of anticoincidence tray D. The latter rules out ionizing rays from below which might stop in S_1 and record as an apparent γ-ray from above. S_3 sets an upper limit on the energy. According to Snyder[4] a photon initiated cascade, developing through the combined thickness of S_1 and S_3, will degenerate to an average number of electrons $\bar{N}\leq 1$ emerging below if the photon energy was originally $\leq$90 Mev. It suffices in the present work to consider 90 Mev as the upper cutoff of the instrument.

The rocket was launched at 10:20 A.M., MST. For reasons not associated with the experiment the jet was turned off by radio signal before complete exhaustion of the fuel. The rocket rose to a peak altitude of 61 km above sea level corresponding to an atmospheric pressure of 0.16 mm Hg. This occurred 149 seconds after take-off. By this time the rocket zenith angle had advanced to about 20 degrees toward the north. The data taken between 90 and 167 seconds have been lumped together as being "above the atmosphere." The atmospheric pressure for this interval was less than 1.3 mm Hg and the zenith angle less than 45°.

Figure 2 shows the counting rates of coincidences and

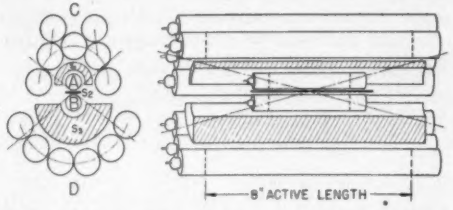

FIG. 1. Diagram of the apparatus. S_1 and S_3 are 6.3 mm and 2.42 cm of lead, respectively. S_2 is 1.9 mm of copper. Counters C and D have 0.8-mm copper walls. A and B have 0.15-mm aluminum walls.

[1] Bowen, Millikan, and Neher, Phys. Rev. **53**, 855 (1938). Millikan, Neher, and Pickering, Phys. Rev. **61**, 397 (1942). Millikan, Neher, and Pickering, Phys. Rev. **66**, 295 (1944).

[2] Critchfield, Ney, and Oleksa, Phys. Rev. **79**, 402 (1950).

[3] N. R. Best, *Electronics* August, **23**, 82 (1950).

[4] H. S. Snyder, Phys. Rev. **76**, 1563 (1949).

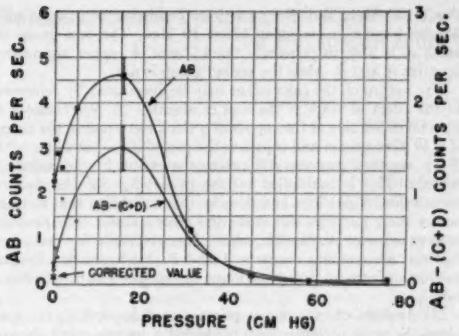

FIG. 2. Counting rates of coincidences and anticoincidences as a function of pressure altitude.

anticoincidences as a function of pressure altitude. Within the meager accuracy of this part of the data the gamma-radiation and the ionizing radiation peaks occur at the same altitude. The curves are uncorrected. The corrected value (discussed below) for the γ-ray point at "zero" pressure appears on the counting rate axis. The corrections are important only for this and neighboring points. The rate of coincidences AB corresponds to a particle intensity of 0.155 particle/cm²/sec/steradian. This is about a factor of two higher than what is believed on the basis of other measurements[5] to be the correct value; but it is not surprising when one considers the vulnerability of the AB rate to showers in the lead. The influence of this type of event on the anticoincidence rate is not large, and is considered in Appendix A.

Table I represents the data and corrections above the atmosphere. The uncorrected ratio $AB-(C+D)\div AB$ is 8.7 percent. Application of the corrections reduces this to 3.9 percent. Applying the telescope geometrical and efficiency factors (Appendix B) we arrive at an incoming γ-ray energy flow in this interval of 0.46 Mev/cm²/sec/steradian. If isotropy is assumed in the upper hemisphere, we have finally that the γ-ray energy flow across a horizontal surface in the energy range 3.4 to 90 Mev is 1.4 Mev/cm²/sec. The corresponding energy for the total radiation at this latitude as deduced from the ionization integrals[1] is 1.8×10^3 Mev/cm²/sec, or 1300 times greater. Considering the nature of the corrections discussed below and the smallness of the answer, there is a question as to whether our result is not actually a null one. In any case it is not far from being an upper limit.

Because of the recently renewed interest in the sun as a source of cosmic radiation, it is worth noting that there was no significant difference in counting rate during the interval in which the sun lay inside the solid angle of the telescope compared to that in which it lay outside. At the time of the launching on January 28 there was a large spot on the west limb of the sun. It had been active on January 24, 25, and 26 but was no longer so. Another smaller spot was also present and inactive.[6]

The writers wish to acknowledge the aid of their colleagues in the Rocket-Sonde Branch of the Naval Research Laboratory and also that of the personnel of the White Sands Proving Ground.

APPENDIX A. CORRECTIONS TO THE ANTICOINCIDENCE RATE

(1) Twofold accidentals of type AB. This is readily shown to be negligible with the coincidence resolving time of 5×10^{-6} second.

(2) Circuit and dead time of the anticoincidence trays. There was a dead time of 60 μsec associated with each C or D count. This was inherent in the electronic design. There was also a counter dead time of 200 μsec associated with each counter. There are many different ways in which these can conspire to make an AB event appear as $AB-(C+D)$, but the saving feature is that, since most of the rays above the atmosphere are penetrating,[7] if the C tray is dead, the D tray will generally suffice and *vice versa*. The result is that an inefficiency of 0.5 percent exists. This fraction applied to the AB counting rate gives the rate of spurious anticoincidences due to this cause.

(3) Lack of complete solid angle coverage of the telescope AB by the trays C and D. Presumably this is mainly so for rays of extreme obliquity. The effect has been estimated by plotting the anticoincidence rate on the ground as a function of the converter thickness and extrapolating to zero thickness. The converter is not entirely absent even when the lead S_1 is removed, since there

TABLE I. Experimental counting rates and corrected values.

Event	Counts/sec above atmosphere	Counts/sec sea level
AB	2.30±0.11	0.110 ±0.002
$AB-(C+D)$ (uncorrected)	0.20±0.04	0.0124±0.0005
Corrections to $AB-(C+D)$		
Accidentals	0.000	
Dead time	0.010	
Leakage	0.070	
Stars	0.025	
Showers	0.005	
Total	0.110	
$AB-(C+D)$ (corrected)	0.09±~0.05	
Geometrical* factor	14.8 counts = 1 count/cm²/ster	
Efficiency factor	1 count = 75 Mev (approx.)	
"Vertical" γ-ray energy flow		0.46 Mev/sec/cm²/ster
γ-ray energy flow across 1 horizontal cm² from upper hemisphere		1.4 Mev/cm²/sec
Total primary energy flow (Millikan, *et al.*)		1800 Mev/cm²/sec

* Computed from curves in H. E. Newell and E. Pressly, Rev. Sci. Instr. 20, 568 (1949).

[5] J. A. Van Allen and S. F. Singer, Phys. Rev. 78, 819 (1950). Winkler, Stix, Dwight, and Sabin, Phys. Rev. 79, 656 (1950).

[6] We are indebted to A. Shapley of the National Bureau of Standards for this information.

[7] G. J. Perlow and J. D. Shipman, Jr., Phys. Rev. 71, 325 (1947).

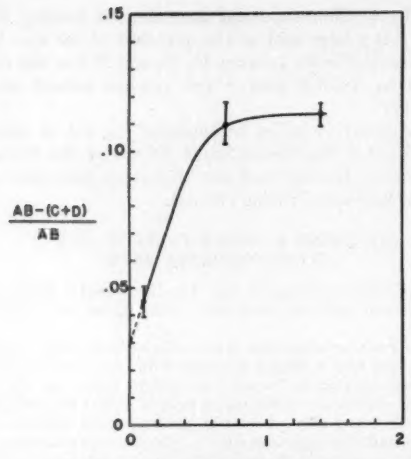

FIG. 3. Effect of varying converter thickness at sea level. The anticoincidence rate is expressed as a fraction of the coincidence rate obtained with full converter thickness.

remain still the counter walls and 3 mm of aluminum structure. In Fig. 3 this is taken into account by using as abscissa the thickness in radiation units of the total material lying between the active volumes of counters C and counter A. The curve rises steeply with thickness reaching a plateau in the neighborhood of 1 radiation unit. The extrapolation to zero thickness gives a leakage effect of about 3 percent of the AB counts. The number should possibly be increased when applied to the flight data, because the radiation is then more nearly isotropic. Counterbalancing this, however, is the circumstance that a considerable fraction of the AB rate is due to locally generated multiples. Thus, use of the observed AB rate over-emphasizes the intensity of the radiation available for the "leakage" effect. The difficulty in making a more precise correction for this effect causes the largest uncertainty in our final result.

(4) The anticoincidence rate is sensitive to stars produced in the region adjacent to counters A and B. The star production rate in a rocket has been determined by the plate measurements of Yagoda and co-workers[8] made in a V-2. Although the rate is dependent on the disposition of neighboring materials, we shall assume their figure of 5000/day/cm³ of emulsion. This figure is quite high, so that we are not likely to be underestimating the influence of stars.

Examination shows that the stars observed by Yagoda, *et al.*, have about the same distribution in regard to number of prongs as those observed by the Bristol group[9] at 11,000 ft, thus establishing their origin as secondaries for the most part. We have therefore used the latter data to obtain the distribution of the number and energy of particles in the stars. The class of star we must consider (0_s in the Bristol notation) is produced by neutral radiation and contains a variable number N of heavily ionizing particles. We may disregard those produced by a charged primary as well as those emitting fast "shower" particles, since these will almost always trip trays C or D. On the basis of the data of reference 9, it is convenient to divide the N particles in a star into two groups, g particles consisting mainly of protons averaging about 100 Mev, and $N-g$ particles consisting of protons and heavier fragments averaging about 10 Mev. The first group of particles is able to penetrate the 1.9 mm of copper separating counters A and B, while the second group is not.

The nature of the calculation may be illustrated by reference to the effect of stars in the copper absorber S_2. We consider a strip on either side of the copper of a thickness equal to the range of a 10-Mev proton and calculate the probability that a star with $N-g$ assumed protons will produce a count in the adjacent counter. This is multiplied by the probability for the star to contain just N particles and then by the probability that at least one of the g particles will strike the other counter. The product is summed over N. Similar calculations are made for the other material surrounding counters A and B. Multiplication by the production rate in the strips gives the required anticoincidence rate.

(5) Another effect is due to primary particles striking the lead pieces S_1 or S_3 obliquely and producing a narrow angle shower which trips A and B without C or D. Assuming a particle intensity of 0.07 particle/sec/cm²/steradian and a mean free path for interaction in lead of 160 gms/cm², one may make an estimate by considering the distribution in shower types as given by the high altitude Bristol data.[10] The correction is not to be trusted within perhaps a factor of three, but it is so small that it does not influence the results.

APPENDIX B. EFFICIENCY

The detection efficiency for γ-rays can be estimated fairly simply because of the circumstance that the converter S_1 is only slightly more than a radiation unit in thickness. It is therefore adequate to consider only the electrons of the initial conversion and not the further generations they would produce in greater thicknesses. Compton effect is not important except for the very bottom of the energy range and is therefore neglected.

A photon of energy W penetrates to a depth l (radiation units) and produces a pair in dl with probability $P(l, W)dl=\delta e^{-\delta l}dl$, $\delta=7/9$. For some energy $E<W$ the probability that at least one electron of the pair will have energy $>E$ can be shown to be

$$H(E,W)=\begin{cases}2(1-E/W), & \text{for } E\geq W/2\\ 1 & \text{for } E\leq W/2.\end{cases}$$

This assumes equal probability for any division of energy between the particles and $W\gg 2mc^2$. If we now take E as the energy necessary for an electron originating at l just to get through the remaining thickness l_0-l and after emerging to have enough energy left (3.2 Mev) to penetrate the copper absorber S_2, then the quantity,

$$\eta(W)=\int_{l=0}^{l_0}P(l,W)H(l_0-l,W)dl,$$

is the probability of a count and therefore the efficiency. The mean range of an electron in lead including radiation loss is obtained as a function of E from Heitler's tabulation.[11] We assume all electrons to have the mean range and neglect scattering and obliquity of path. $\eta(W)$ has been evaluated numerically. It is approximately proportional to W up to $W=35$ Mev and thereafter is constant at 70 percent. For photons of a given energy, W/η is the average energy corresponding to each count. If the ratio were a constant over the energy range of the instrument, the intensity of "counts" could be multiplied by W/η to give energy intensity. The ratio has the nearly constant value 50 Mev/count up to $W=35$ Mev. It then increases linearly to 125 Mev/count at $W=90$ Mev. A suitable average is 75 Mev/count, and this is the value used in calculating the incoming gamma-ray energy.

[8] Yagoda, de Carvalho, and Kaplan, Phys. Rev. **78**, 765 (1950).
[9] Brown, Camerini, Fowler, Heitler, King, and Powell, Phil. Mag. **40**, 862 (1949).
[10] Camerini, Coor, Davies, Fowler, Lock, Muirhead, and Tobin, Phil. Mag. **40**, 1073 (1949).
[11] W. Heitler, *The Quantum Theory of Radiation* (Oxford University Press, London, 1944), second edition, p. 223.

Barometric and Temperature Coefficients of Frequency of Small Cosmic-Ray Bursts and of Burst-Corrected Cosmic-Ray Ionization*

JAMES W. BROXON
Department of Physics, University of Colorado, Boulder, Colorado
(Received September 19, 1950)

Barometric and (surface) temperature coefficients are determined for a class of cosmic-ray bursts consisting of 1.2 to 1.9×10^6 ion pairs in argon at 20 atmospheres in a heavily shielded chamber, as well as for the burst-corrected ionization.

For the bursts the coefficients (particularly the temperature coefficient) are found to depend upon whether the multiple regression coefficient and partial correlation coefficient are computed from daily averages for individual months or for all 581 days, the latter yielding a positive temperature coefficient of 0.24 percent/°C, in which confidence is somewhat lacking because it depended upon four readers. For the bursts, the averages of the coefficients for 19 individual months are −1.54 percent/mm Hg and −0.98 percent/°C, while the averages for those months with significance ratios above the 2 percent level are −2.44 percent/mm Hg and −1.66 percent/°C.

For the burst-corrected CR ionization, the averages of the coefficients for 19 individual months are −0.154 percent/mm Hg and −0.038 percent/°C, while the values computed for 581 days are −0.174 percent/mm Hg and −0.056 percent/°C. Little differences from the latter values are found with computations based on monthly means.

Comparisons are made with earlier observations with the same chamber containing air at 160 atmos and with the observations of other experimenters and the relations of these to the explanation of the temperature dependence in terms of meson decay developed by Blackett and Duperier are discussed. Values for the mean free paths of the radiations producing the small bursts and the burst-corrected ionization are deduced on the basis of their respective barometric coefficients.

I. INTRODUCTION

IN a recent paper[1] the writer reported an investigation of the relation of the frequency of occurrence of a class of small cosmic-ray bursts to areas of sunspots and certain other variables. The data employed were obtained at Boulder, altitude 1646 m, geomagnetic latitude 49° N, by V. A. Long and R. M. Whaley during a period of 18 months in 1938–1939. There was found to be a lack of close correlation between the frequency of the small bursts and the cosmic-ray (CR) ionization after correction for bursts, and certain differences among the relations of these two variables to others. In the discussion it was pointed out that (as observed by others[2,3]) the small-burst frequency displayed much larger barometric coefficients for most of the months for which they were computed than was displayed by the burst-corrected CR ionization. These facts appeared to provide evidence that the small bursts were produced by a different type of radiation from that responsible for the major portion of the ionization after correction for bursts, although the heavy shielding permitted only quite penetrating radiations to enter the ionization chamber.

An opportunity arose to obtain a second series of continuous CR ionization records during a little more than 19 months from October 21, 1947, to June 1, 1949, inclusive. In addition to computing the barometric coefficients for the remaining months of the first series, barometric and also outdoor (surface) temperature coefficients have been computed for the new series.

II. APPARATUS

Considerable information regarding the high pressure-ionization-chamber, recording equipment has been given elsewhere.[4–8] For the 1938–1939 series, air at 160 atmos was employed, while for the 1947–1949 series, argon at 20.2 atmos was used. Further details are given in Appendix I.

The outdoor temperature and relative humidity were obtained from good recording instruments mounted about 5 ft above the ground in a well-ventilated shelter. Barometric pressure was recorded on a good microbarograph. Magnetic data were supplied from the Tucson (Arizona) Magnetic Observatory of the U. S. Coast and Geodetic Survey.

III. EXPERIMENTAL PROCEDURE

Apart from the employment of more convenient switching arrangements and more accurate meters for calibration, etc., the experimental procedure during the recent series of measurements which is described here did not differ much from that of the earlier series. The central system was grounded to its guard for one minute of each hour by means of an electric clock. By application of definite potentials to the central system for short intervals, the sensitivity of the electrometer was recorded on the photographic record each day just at the beginning and end of the daily record. In order to facilitate the reading and classification of bursts, the sensitivity was maintained very nearly constant with the exception of a period of three months, July 28 to October 27, inclusive, 1948, during which the records were not read promptly and a decrease of 10 percent in

* Presented at the meeting of the American Physical Society at Mexico City, Mexico, June 21–23, 1950.
[1] J. W. Broxon, Phys. Rev. **72**, 1187 (1947).
[2] Steinke, Gastell, and Nie, Naturwissenschaften **21**, 898 (1933).
[3] C. G. Montgomery and D. D. Montgomery, Phys. Rev. **47**, 429 (1935).
[4] J. W. Broxon, Phys. Rev. **37**, 1320 (1931).
[5] J. W. Broxon, Phys. Rev. **42**, 321 (1932).
[6] R. M. Whaley, thesis, University of Colorado (1940).
[7] J. W. Broxon, Phys. Rev. **38**, 1704 (1931).
[8] V. A. Long, thesis, University of Colorado (1940).

the sensitivity went unnoticed. This variation was corrected by Dr. Long (most experienced of the readers; reader A of the first series and 1 of the second) in the detailed reading of the records for this period. The vane potential and the applied ion-collecting potential were also read daily and maintained very nearly constant; the ion-collecting potential was given by a good microammeter in series with the high resistances of the capacitance-resistance bridge arrangement and was maintained extremely nearly constant. P_2O_5 was usually renewed twice a week in both the insulating box and the guard system, although occasionally the latter was renewed only once a week. The argon pressure was observed daily. Since the chamber had contained air at 2400 lb/in.^{2} for some years, no leak was anticipated or observed.

Calibrations of the CR apparatus were carried out carefully during the 1938–1939 measurements,[6,8] electrostatic induction coefficients being determined by employment of a Harms air condenser calibrated by the National Bureau of Standards. These were employed for the recent series after correction for the small changes resulting from the modifications described in Appendix I.

IV. READING OF RECORDS

In reading records from the microbarograph, thermograph, etc., an estimate was made visually of the average value for each hour as indicated by the graph. These values were recorded, and the average of the 24 hourly values for a G.M.T. day was taken as the average for that day.

The CR ionization records were read through a reading glass by means of a transparent millimeter scale maintained perpendicular to the time axis. In addition to the displacements at the initiation and termination of each 59-min collecting period, all bursts producing a sudden deflection of 1 mm or more were read, all readings being estimated to 0.1 mm.

Before beginning to read the CR records for the 1938–1939 series, Long[4] gave particular attention to the problem of distinguishing between bursts and statistical fluctuations, considering particularly the work of Evans and Neher,[9] and Bennett, Brown, and Rahmel.[10] He computed the maximum time for collection of all the ions of a burst in the air at 160 atmos as used for the earlier observations to be 28 sec, and by running the drum holding the photographic paper at 12 times its normal speed he found the maximum time experimentally to be 25 sec. Considering the normal rate of advance of the photographic record, he found that a burst producing a deflection of 1 mm (the smallest read) should cause the photographic record to deviate not more than 8° from the normal to the time axis, while deflections for larger bursts should deviate correspondingly less. All bursts of that series were selected on this basis.

Following Bennett, Brown, and Rahmel,[10] Long computed the probability that one of the apparent 1-mm bursts of the earlier series might actually have been the result of statistical fluctuation of the radiation responsible for the burst-corrected ionization. He found the probability to be only 0.1 percent for 1-mm bursts and less for larger ones, of course.

For the 1947–1949 series, the maximum time for the collection of all of the ions of a burst in the radial field employed was computed, assuming a mobility of 1.37 cm/sec per v/cm for the slowest ions in argon at atmospheric pressure, to be 3.4 sec. With the photographic paper advancing at the rate of 20 in. in 25 hr along the time axis, a 1-mm burst should correspond to a deflection in the record deviating just 1° from the normal to the time axis, while larger bursts should deviate less. Actually, all bursts down to 1 mm seemed to be practically perpendicular to the time axis, and appeared as quite clear breaks in the photographic record. The much shorter interval for collection of the ions in the later series would appear to make it less likely than in the earlier series that a supposed burst of 1 mm should actually represent a statistical fluctuation, in spite of the increase in the sensitivity of the electrometer.

Doubtless the most convincing criterion for the reality of the bursts is the fact that they are always in the sense indicating a sudden increase rather than a decrease in the ionization in the high-pressure chamber. This condition was almost wholly fulfilled. On about a dozen occasions there appeared to be "negative" bursts. It was thought at first that these might represent rare events in the compensating condenser. It was later found, however, that such deflections could be produced by a conductor which inadvertently had been left so that it could occasionally make contact with one terminal of the high potential system and thereby affect the potential of the central system. It was concluded that only one or possibly two of the supposed "negative" bursts could not be explained entirely satisfactorily on this basis. The many thousands of bursts recorded (there were an average of about 10 per hour in the 1- to 1.5-mm class during the 582 days for which records were obtained) were otherwise all in the positive sense.

Usually 10 to 20 min of one hour of each day were required for calibration, checking potentials, inserting dryer, changing the record, etc. For such hours the number of 1-mm bursts and the burst-corrected ionization current were corrected for the time lost on the assumption that they would have continued at the same rate for the normal collection period of 59 min., the latter not being adjusted to the 60 min/hr. On other occasions records for one or more hours of a day were lost because of adjustment of apparatus, poor photographic conditions, etc. These were similarly corrected to correspond to a full 24-hr day. In no event

[9] R. D. Evans and H. V. Neher, Phys. Rev. 45, 144 (1934).
[10] Bennett, Brown, and Rahmel, Phys. Rev. 47, 437 (1935).

was the record for an hour retained and adjusted unless there was an actual record for at least half of the hour, nor for a day unless there were records for at least half of the hours of the day. There were very few hours and very few days for which this lower limit was approached, only one of the 582 days' records being based on 12 hr, 4 on 15 hr, 2 on 16 hr, 1 on 17 hr, 6 on 18 hr, 3 on 19 hr, 6 on 20 hr, 8 on 21 hr, 14 on 22 hr, and 44 on 23 hr. As is shown in the tables, records for a few days were rejected entirely. Burst totals for the day and daily average values for all the other variables were used in determining the coefficients listed in the tables.

It had become apparent from the reading of the first series of records that in spite of consultation and training, and serious efforts to apply the same criteria, two readers, although they could reproduce their own readings fairly well, were inclined to disagree noticeably in the reading and classification of bursts according to size. An attempt was made, therefore, to have all bursts of the recent series read by a single reader. This was found to be impossible, however, and instead, four readers had to be employed. Dr. Long, who was reader A of the first series and read the records for two-thirds of that series, was reader No. 1 of the later series and the instructor for reader No. 2. Numbers (in the tables) were assigned to the readers in the order in which each received instruction from the next preceding. The first three readers were physicists with considerable experience beyond the Ph.D. degree. Reader No. 4 was a young lady with no training in physics or other science. Unexpectedly great differences in reading the small bursts were found by having the records for a few of the months read by more than one reader. This situation is shown graphically by Fig. 1 which gives the average frequency of bursts in the 1.0 to 1.5 mm range during each month (or portion thereof for October, 1947, and March, 1948) as determined by the reader whose number is designated. Because the breaks representing bursts were so sharp and were practically perpendicular to the time axis, it is presumed that the difficulty must have been one of deciding just where the photographic trace ended and began on either side of the burst. The magnification was perhaps inadequate, also. In order to minimize effects of fatigue, the readers generally did not continue reading for more than two hours at a time.

V. DETERMINATION OF COEFFICIENTS

Assuming linear relations, simple barometric coefficients were determined for each month for the 1-mm bursts of the 1938–1939 series, and partial barometric and (surface) temperature coefficients for the 1-mm bursts and for the CR ionization after correction for all bursts ≥ 1 mm, for the 1947–1949 series, by the method of least squares. For the first series, 1-mm bursts were defined to be those producing deflections of 1 to 1.2 mm of the photographic record, and represented the production of (2.9 to 3.6)$\times 10^8$ ion pairs, while the 1-mm bursts of the second series were defined to be those producing 1.0- to 1.5-mm deflection and represented the production of (1.2 to 1.9)$\times 10^8$ ion pairs. Taking the average length of path of the burst-producing particles to be 19.1 cm in the chamber, and supposing these to produce 100 ion pairs per cm per atmosphere in the argon, the 1-mm bursts of the second series appear to correspond to the passage of about 31 to 50 particles through the chamber, or to an average flux density of 0.045 to 0.072 particles/cm^2. Details of the statistical procedure are given in Appendix II.

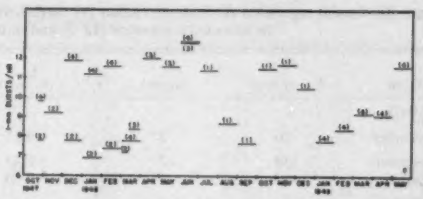

FIG. 1. Monthly average values of frequency of 1-mm bursts. Readers are designated by numbers in parentheses.

VI. DATA AND DISCUSSION

The values of the coefficients obtained in this manner are shown in the tables. Table I shows the simple barometric coefficients, b_{12}, in percent/mm Hg for the 1-mm bursts of the first series for each month, together with the corresponding correlation coefficients and their significance ratios. For one month no correlation was obtained, while positive coefficients were obtained for

TABLE I. Simple regression (b) and correlation (r) coefficients and significance ratios (t) for frequency of 1-mm bursts with respect to barometric pressure for the 1938–1939 series. [The 1-mm bursts of this table represent (2.9 to 3.6)$\times 10^8$ ion pairs, while the 1-mm bursts of the 1947–1949 series represent (1.2 to 1.9) $\times 10^8$ ion pairs.]

Month	Reader	b_{12} (%/mm)	r_{12}	t_{12}
(1938)				
June	A	−3.2	−0.25	−1.35
July	A	−2.0	−0.18	−0.94
Aug.	A	2.4	0.18	0.94
Sept.	A	0.0	0.00	0.00
Oct.	A	−4.0	−0.48	−2.63
Nov.	A	−1.1	−0.30	−1.62
Dec.	A	−1.2	−0.21	−1.15
(1939)				
Jan.	A	−2.3	−0.42	−2.22
Feb.	A	−2.4	−0.57	−2.91
Mar.	A	−3.5	−0.60	−3.29
Apr.	A	−1.6	−0.23	−1.24
May	A	−3.5	−0.47	−2.49
June	B	−2.7	−0.28	−1.51
July	B	−2.0	−0.24	−1.31
Aug.	B	−2.1	−0.18	−0.97
Sept.	B	1.5	0.22	1.18
Oct.	B	−1.7	−0.38	−2.08
Nov.	B	−4.2	−0.42	−2.26

Average of 18 monthly values of $b_{12} = -1.87$ percent/mm.
Average of 4 values of b_{12} above 2 percent level $= -3.35$ percent/mm.

TABLE II. Partial regression (b) and correlation (r) coefficients and significance ratios (t) for frequency of 1-mm bursts with respect to barometric pressure (12·3) and outdoor temperature (13·2) for individual months.

Month	No. of days	Reader	$b_{12\cdot3}$ (%/mm)	$r_{12\cdot3}$	$t_{12\cdot3}$	$b_{12\cdot3}$ (%/°C)	$r_{12\cdot3}$	$t_{12\cdot3}$
(1947)								
November	26	2	−3.11	−0.552	−2.71	−0.98	−0.226	−1.11
December	30	2	−0.43	−0.103	−0.55	−0.34	−0.100	−0.53
December	30	4*	−0.20	−0.077	−0.41	−1.13	−0.450	−2.38
(1948)								
January	31	2	−2.00	−0.478	−2.57	−1.48	−0.649	−3.50
January	31	4*	−4.39	−0.639	−3.44	−2.76	−0.743	−4.00
February	28	2	−1.47	−0.353	−1.80	−0.69	−0.315	−1.61
February	29	4*	−1.32	−0.515	−2.67	−0.13	−0.110	−0.57
March	31	(2 and 3)	0.83	0.105	0.57	1.49	0.326	1.76
March	31	4*	−1.36	−0.517	−2.78	−0.77	−0.524	−2.82
April	30	3	−1.86	−0.590	−3.12	−0.36	−0.155	−0.82
May	31	3	−1.46	−0.526	−2.83	−1.05	−0.533	−2.87
June	30	3*	−1.03	−0.199	−1.05	−2.53	−0.543	−2.88
June	30	4	−0.26	−0.068	−0.36	−0.14	−0.306	−1.62
July	31	1	−5.79	−0.441	−2.37	−4.37	−0.351	−1.89
August	31	1	1.01	0.120	0.64	−2.93	−0.457	−2.46
September	27	1	−1.53	−0.314	−1.57	0.50	0.116	0.58
October	31	1	−0.35	−0.058	−0.31	−1.73	−0.297	−1.60
November	30	1	−0.44	−0.095	−0.50	0.53	0.172	0.91
December	31	1	−3.27	−0.516	−2.78	−1.49	−0.300	−1.61
(1949)								
January	31	4	−1.03	−0.250	−1.35	−0.51	−0.188	−1.01
February	28	4	−0.80	−0.461	−2.35	−0.05	−0.062	−0.32
March	31	4	−0.97	−0.416	−2.24	0.18	0.107	0.58
April	30	4	−0.99	−0.568	−3.01	−0.48	−0.526	−2.78
May	31	4	−0.39	−0.079	−0.42	1.49	0.355	1.91

* Choosing reader designated by asterisk for months with 2 readers:
average of 19 monthly values of $b_{12\cdot3} = -1.54$ percent/mm;
average of 19 monthly values of $b_{13\cdot2} = -0.98$ percent/°C.
(Average of 19 monthly values of $b_{13} = -1.28$ percent/mm;
average of 19 monthly values of $b_{13} = -0.78$ percent/°C.)
Average of 10 monthly values of $b_{12\cdot3}$ with $t_{12\cdot3}$ above 2 percent level = −2.44 percent/mm;
average of 7 monthly values of $b_{13\cdot2}$ with $t_{13\cdot2}$ above 2 percent level = −1.66 percent/°C.
(Average of 8 monthly values of b_{13} with t_{13} above 2 percent level = −1.58 percent/mm;
average of 5 monthly values of b_{13} with t_{13} above 2 percent level = −1.97 percent/°C.)
The magnitude of the normal t employed = 2.33 at the 2 percent level.

two. For them, low significance ratios were obtained. The remaining 15 months provided negative coefficients. The average of all 18 monthly (simple) barometric coefficients is −1.87 percent/mm Hg. Only four of these have significance ratios above the 2 percent level, and these all have quite large negative regression coefficients. The average of these four is −3.35 percent/mm Hg. The earlier report[1] on the barometric coefficient for some of these months includes a discussion of conditions, shows the results of certain manipulations of the data for a couple of the months, and points out the (fair) agreement in magnitude with values obtained by other observers.[2,3] Messerschmidt[11] also found a coefficient of −1 to −2 percent/mm Hg, the latter being emphasized. Hogg[12] found a barometric coefficient of −0.75 percent/mm Hg for a class of bursts with an average frequency of 0.88 per hour.

[11] W. Messerschmidt, Z. Physik **103**, 27 (1936).
[12] A. R. Hogg, Nature **138**, 77 (1936).

Table II shows barometric coefficients (partial regression coefficients $b_{12\cdot3}$) and outdoor temperature coefficients (partial regression coefficients $b_{13\cdot2}$) in columns 4 and 7, followed by the corresponding correlation coefficients and their significance ratios, for the frequency of the 1-mm bursts for each of the individual 19 full months of the 1947–1949 series. Column 3 designates the number of the reader, and column 2 gives the number of days for which records were retained by that reader for the month designated in column 1.

It will be noted that there was only one month, August, 1948, for which only a positive barometric coefficient was obtained, and that the correlation coefficient for this month was small with a small significance ratio. Table I shows that August, 1938, also had a positive barometric coefficient with poor correlation, while August, 1939, had a negative barometric coefficient, but with poor correlation. September, 1948, differs from September of 1938 and 1939 in displaying

TABLE III. Partial regression and correlation coefficients and significance ratios as in Table II, but for the longer intervals specified below.

Time interval	$b_{12\cdot3}$ (%/mm)	$r_{12\cdot3}$	$t_{12\cdot3}$	$b_{12\cdot3}$ (%/°C)	$r_{12\cdot3}$	$t_{12\cdot3}$
6 mo.; Nov. '47–Apr. '48	−0.55	−0.299	−3.96	−0.35	−0.143	−1.89
6 mo.; May '48–Oct. '48	−1.54	−0.192	−2.57	−1.32	−0.307	−4.10
6 mo.; Nov. '48–Apr. '49	−0.96	−0.201	−2.69	0.43	0.178	2.38
Average of 6-mo. values	−1.02			−0.41		
18 mo.; Nov. '47–Apr. '49	−0.60	−0.105	−2.43	0.18	0.079	1.84
581 days during 21 Oct. '47 to 31 May '49	−0.64	−0.113	−2.72	0.24	0.105	2.52

a negative barometric coefficient, but the correlation is not very high. While the correlation coefficients and their significance ratios, as well as the regression coefficients, are seen to vary a good deal from month to month, and the disagreement among the readers is apparent, there are 10 months for which significance ratios above the 2 percent level were obtained. To form an average of the monthly values, it seemed proper to choose the values obtained by one or the other of the readers for those months read by two readers. For determining such averages, then, as well as for determining the values listed in Table III, the readings obtained by the reader whose number is marked with an asterisk in column 3 were arbitrarily employed. On this basis, the average of the 19 monthly barometric coefficients is $b_{12\cdot3}=-1.54$ percent/mm Hg, while the average of the 10 monthly coefficients with $t_{12\cdot3}$ above the 2 percent level is $b_{12\cdot3}=-2.44$ percent/mm Hg. At the bottom of the table the corresponding average values of the simple barometric coefficients, b_{12}, are also listed. These averages are seen to be quite comparable to those obtained from the earlier observations, though they are a little smaller.

The temperature coefficients of the burst frequencies listed in column 7 of Table II are also seen to be predominantly negative, although for these there are 4 months for which only positive values were obtained. All these display quite low correlation coefficients and significance ratios except May, 1949, which is near the 5 percent level. In fact, only 7 of the months have significance ratios above the 2 percent level, and these are all negative. Selecting readers as before, the average of the 19 monthly temperature coefficients is $b_{13\cdot2}=-0.98$ percent/°C; and the average of the 7 monthly values with $t_{13\cdot2}$ above the 2 percent level is $b_{13\cdot2}=-1.66$ percent/°C. The corresponding average values of the simple temperature coefficients are also given at the bottom of the table.

Table III shows coefficients corresponding to those in Table II, computed by grouping together all the daily values in each of the successive 6-month intervals designated in the first three rows; those for all 18 of these months for the fourth row; and for the fifth row, all for the 19 months of Table II plus those for the last 11 days of October, 1947. For all these cases negative barometric coefficients are displayed, with all significance ratios above the 2 percent level. The negative barometric coefficients are generally smaller, however, than the averages obtained from the monthly values. The temperature coefficients are rather strikingly different from those of Table II. While negative coefficients are obtained for the first two 6-month intervals, all the other groupings produce positive temperature coefficients. In particular, the third 6-month interval and the entire period of 581 days show positive temperature correlation with significance ratios above the 2 percent level. In contemplating this situation, it should be borne in mind that all the readers were involved in the last case, while the individual monthly values were generally dependent upon a single reader. Also, although the partial correlation procedure is supposed to remove the effect of barometric variations, it seems to the reader that the large corresponding seasonal variations in temperature and barometric pressure may have produced some effect. These variations are shown in Fig. 2, where monthly average values of barometric pressure and temperature are represented. According to information supplied by a geographer, the positive correlation between seasonal variations in barometric pressure and temperature displayed here are quite unusual for an inland station; but a similar relation was observed during the 1938–1939 observations. Perhaps an explanation of the differences between the temperature coefficients of Tables II and III might be found in terms of the differences between variations in the atmospheric temperature at the surface of the earth and at higher levels. Duperier[13] has found a positive meson temperature coefficient of 0.12 percent/°C with respect to temperature of the air layer between 200 and 100 mb (a layer of 4.2 km average depth and 14 km mean height), which he explains in terms of π-meson decay.

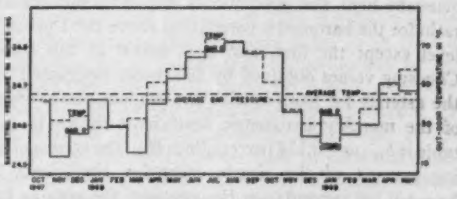

FIG. 2. Monthly average values of barometric pressure and outdoor temperature.

[13] A. Duperier, Proc. Phys. Soc. (London) **A62**, 684 (1949).

TABLE IV. Partial regression and correlation coefficients and significance ratios as in Table II, for the cosmic-ray ionization after correction for all bursts producing deflections of 1 mm or more on the photographic record.

Month	No. of days	Reader	$b_{12\cdot3}$ (%/mm)	$r_{12\cdot3}$	$t_{12\cdot3}$	$b_{12\cdot3}$ (%/°C)	$r_{12\cdot3}$	$t_{12\cdot3}$
(1947)								
November	26	2	−0.065	−0.518	−2.54	−0.070	−0.588	−2.88
December	30	2*[b]	−0.141	−0.882	−4.67	−0.014	−0.222	−1.18
December	30	4	−0.143	−0.823	−4.35	−0.009	−0.115	−0.61
(1948)								
January	31	2*	−0.151	−0.768	−4.14	−0.052	−0.661	−3.56
January	31	4	−0.127	−0.675	−3.64	−0.038	−0.498	−2.68
February	28	2	−0.137	−0.823	−4.20	−0.023	−0.416	−2.12
February	29	4*	−0.139	−0.805	−4.18	−0.028	−0.461	−2.39
March	31	(2 and 3)*	−0.144	−0.778	−4.19	−0.051	−0.628	−3.38
March	31	4	−0.127	−0.622	−3.35	−0.029	−0.317	−1.71
April	30	3	−0.144	−0.939	−4.97	−0.044	−0.675	−3.57
May	31	3	−0.202	−0.707	−3.81	−0.037	−0.249	−1.34
June	30	3	−0.172	−0.850	−4.50	0.008	0.128	0.68
June	30	4*	−0.174	−0.900	−4.76	−0.015	−0.225	−1.19
July	31	(1 and 3)*	−0.144	−0.687	−3.70	−0.067	−0.410	−2.21
July	31	1	−0.084	−0.279	−1.50	0.011	0.037	0.20
August	31	1	−0.175	−0.697	−3.75	−0.017	−0.137	−0.74
September	27	1	−0.132	−0.742	−3.71	−0.062	−0.492	−2.46
October	31	1	−0.220	−0.916	−4.93	−0.045	−0.451	−2.43
November	30	1	−0.123	−0.894	−4.73	−0.047	−0.757	−4.01
December	31	1	−0.178	−0.778	−4.19	−0.032	−0.263	−1.42
(1949)								
January[a]	29	4	−0.159	−0.883	−4.58	−0.039	−0.560	−2.91
February	28	4	−0.179	−0.909	−4.63	−0.039	−0.713	−3.64
March	31	4	−0.184	−0.953	−5.13	−0.016	−0.335	−1.80
April	30	4	−0.136	−0.601	−3.18	−0.027	−0.265	−1.40
May	31	4	−0.140	−0.667	−3.59	−0.027	−0.210	−1.13
All	581		−0.174	−0.751	−18.06	−0.056	−0.673	−16.19
Average of 19 monthly[b] values			−0.154			−0.038		
Average of 10 monthly[b] $b_{12\cdot3}$ with $t_{12\cdot3}$ above 2 percent level						−0.048		

[a] Two days of high magnetic disturbance omitted in Jan., 1949.
[b] When 2 readers for same month, values by starred reader chosen.

Table IV contains coefficients for the CR ionization currents of the 1947–1949 series after correction for all bursts $\geqslant 1$ mm, corresponding to the coefficients for the 1-mm bursts given in Table II. In this, all the barometric coefficients given in column 4 are seen to be negative, and there is much better agreement among the different readers. The correlation coefficients are generally high, and every month displays a significance ratio for the barometric correlation above the 1 percent level except the first, and it is nearly at this level. Choosing values obtained by the reader designated by the asterisk for months with two readers, the average of the monthly barometric coefficients shown in the table is $b_{12\cdot3}=-0.154$ percent/mm Hg. The corresponding average of the simple regression coefficients is $b_{12}=-0.145$ percent/mm Hg, precisely the same as for the 18 months of the 1938–1939 series. Grouping together the data for the last 11 days of October, 1947, as well as for those of all the months shown in the table, the barometric coefficient computed for the 581 days is $b_{12\cdot3}=-0.174$ percent/mm Hg with the correlation coefficient $r_{12\cdot3}=-0.75$ and the large significance ratio $t_{12\cdot3}=-18.06$.

The temperature coefficients in column 7 are seen to be more consistently negative than in the case of the 1-mm bursts, each month displaying a negative coefficient according to at least one reader. The average of the monthly temperature coefficients (using values of the reader indicated by an asterisk in the case of two readers) is $b_{13\cdot2}=-0.038$ percent/°C, while the average of the 10 monthly values with $t_{13\cdot2}$ above the 2 percent level is $b_{13\cdot2}=-0.048$ percent/°C. The temperature coefficient obtained by grouping together the data for all the 581 days specified above is $b_{13\cdot2}=-0.056$ percent/°C with the correlation coefficient $r_{13\cdot2}=-0.67$ and the large significance ratio $t_{13\cdot2}=-16.19$. This is a far different situation from that found for the 1-mm bursts.

VII. COMPARISON WITH OTHERS AND FURTHER DISCUSSION

The comparison of the coefficients for the burst-corrected CR ionization with those obtained by other experimenters may be introduced by reference to a theoretical explanation of the temperature effect. Blackett[14] assumed the effect to be dependent upon meson decay, and making certain reasonable assumptions regarding the place of origin, energy, and mean life of the mesons, computed temperature coefficients of -0.16 to -0.20 percent/°C in good agreement with the value -0.18 percent/°C found by Compton and Turner,[15] and predicted the latitude effect in the temperature coefficient later found by Gill.[16] Gill found that the temperature coefficient increased with latitude, attaining its highest numerical value of -0.25 percent/°C for latitudes above 40° N and S.

Recently Duperier,[17] following Blackett,[14] has had remarkable success in explaining the differences among the temperature coefficients measured by various excellent experimenters, as well as the seasonal variations in the temperature coefficient observed by some of them, and the 12-monthly wave obtained by Forbush,[18] solely on the basis of meson decay. Duperier pointed out that Hess,[19] *et al.*, and Hogg[20] had employed daily average values in determining their average temperature coefficients of -0.09 to -0.11 percent/°C in Austria and Australia, respectively, with seasonal variations consisting of a ratio of about 2 in the first instance and 1.6 in the second, for the ratio of the barometric coefficient for winter months to that for summer months. (Hess found that the temperature coefficient changed only from -0.09 percent/°C at 2300 m altitude to -0.11 percent/°C at 600 m, both at 48.4° N geomagnetic latitude.) Duperier further pointed out that Compton and Turner,[15] Gill,[16] Schonland,[21] *et al.*, and Clay and Bruins[22] had used monthly or seasonal means in determining their temperature coefficients, and that the average of the coefficients determined by them, -0.18 percent/°C, was about twice that obtained by the first group (though the Schonland value, -0.12 percent/°C at 32.7° S geomagnetic latitude, was about equal to that of the first group).

Duperier explained that on the hypothesis of the instability of the meson, the use of daily means results in a smaller value of the (surface) temperature coefficient on account of the lag in the warming of the atmosphere relatively to the warming of the ground. Assuming that the mesons originate chiefly at the 75-mm Hg pressure level (at a mean height of 16 km; von Roka,[23] in his interesting explanation of the 27-day recurrences in CR intensity and bursts, considers that about ½ of the mesons originate at a height between 25 and 50 km) Duperier obtained $L=18.6$ km for the mean range of the mesons, and upon the basis of the temperature-dependent variations of the height of the atmospheric layer presumed to provide the principal source of the unstable mesons, he deduced the value -0.10 percent/°C for the average temperature coefficient based upon daily averages, with a seasonal variation yielding 1.6 for the ratio of the temperature coefficient for winter months to that for summer months. He also deduced -0.24 percent/°C for the temperature coefficient based on monthly averages. His 12-monthly wave deduced on this basis agreed well in both amplitude and phase with that found by Forbush. Kidnapillai[24] has deduced a barometric coefficient of magnitude 0.316 percent/mm Hg on the basis of meson decay.

Because the temperature coefficients listed in Table IV were obtained from daily average values of the variables, they should, according to Duperier, be comparable to those obtained by Hess and by Hogg. It is seen, however, that the $b_{12\cdot2}=-0.056$ percent/°C listed for all 581 days is only about half as great as the -0.10 percent/°C deduced by Duperier and measured by these experimenters, which in turn is only about half as great as the values obtained theoretically by Duperier and experimentally by the second group, for the temperature coefficient based on monthly averages. Moreover, Hogg[20] obtained $b_{12\cdot3}=-0.275$ percent/mm Hg for the average barometric coefficient during a period of five years. Hess[25] obtained an average barometric coefficient of about -0.367 percent/mm Hg in Austria, with individual 10-day values fluctuating between about 0.7 and 1.5 times this value. It is seen that the value $b_{12\cdot3}=-0.174$ percent/mm Hg listed for all 581 days in Table IV is also only about half as great as those barometric coefficients.

The disagreement of the coefficients presented here with the values obtained theoretically and experimentally by the same means by others (and at comparable latitude and altitude in the case of Hess) appears to require explanation. The simplest explanation appears to be the possibility either of an error in calibration or of radioactive contamination of the chamber or other local radiation which may have caused us to use for the average burst-corrected CR ionization a value approximately double the correct value. The probability of an error of such magnitude seems exceedingly slight for a combination of reasons. As mentioned before, the averages of the (simple)

[14] P. M. S. Blackett, Phys. Rev. **54**, 973 (1938).
[15] A. H. Compton and R. N. Turner, Phys. Rev. **52**, 799 (1937).
[16] P. S. Gill, Phys. Rev. **55**, 1151 (1939).
[17] A. Duperier, Proc. Phys. Soc. (London) **A61**, 34 (1948).
[18] S. E. Forbush, Phys. Rev. **54**, 975 (1938).
[19] V. F. Hess, Phys. Rev. **57**, 781 (1940).
[20] A. R. Hogg, Proc. Roy. Soc. (London) **A192**, 128 (1947); the valuable comprehensive report by Hogg, Memoir No. 10 (No. 5 of Vol. II), Memoirs of the Commonwealth Observatory, July, 1949, was not received by the writer until after this paper had been submitted for publication.
[21] Schonland, Delatizky, and Gaskell, Terr. Mag. **42**, 137 (1937).
[22] J. Clay and E. M. Bruins, Revs. Modern Phys. **11**, 158 (1939).
[23] E. G. v. Roka, Naturwissenschaften **36**, 24 (1949).
[24] M. Kidnapillai, Phys. Rev. **72**, 518 (1947).
[25] From a personal letter by Dr. Victor F. Hess.

barometric coefficients determined in the present series and in that of a decade earlier agreed precisely. Independent calibrations of the apparatus by Long[8] and by Whaley[6] and the writer during the earlier series agreed within 2 percent, and it appeared that the experimental error should not be greater than this. The average value of 38.2 ion-pairs cc^{-1} sec^{-1} for the CR ionization during the first 18-month series of recordings is comparable to the values 45.4 and 42.6 (corrected only for very large bursts) obtained in the same chamber with air at the same pressure during still earlier visual measurements[4] of short duration, with a 2-in. lead shield and with a 5.5- to 6-ft water shield in addition to the lead, at another location in the same building. Those visual measurements were made by manual application of varying potentials to a compensating condenser which contained no radioactive material, and depended upon a wholly independent calibration, of course. During these visual measurements the value 1.45 ion-pairs cc^{-1} sec^{-1} was obtained with both shields with air in the chamber at a pressure of 0.82 atmos, which showed that the chamber was remarkably free from radioactive contamination; and it has been protected carefully ever since. For such reasons, it appears to the writer that the value of 39 pairs of ions cc^{-1} sec^{-1} assumed for the average burst-corrected CR ionization current in the present series is probably accurate to within about 2 percent, that it is very unlikely to be in error by as much as 5 percent, and that an error of the order of 50 percent is almost unthinkable. Accuracy of the computations is believed to have been assured by having them all performed twice.

The comparison of the coefficients listed in Table IV with those obtained by other observers may be presented in a manner considerably more favorable than that adopted above. For instance, Hogg[20] found monthly mean values of the barometric coefficient to vary from -0.135 to -0.412 percent/mm Hg, the lower value being less than our $b_{12\cdot3}$ for 581 days. Also, his monthly mean values of the temperature coefficient varied from -0.011 to -0.286 percent/°C for the negative values; and two months yielded positive coefficients. The lower negative value is seen to be considerably less than our $b_{13\cdot2}$ for 581 days, and it will be recalled that each of the 19 months yielded a negative coefficient according to at least one observer. Moreover, for the entire year of 1939 Hogg obtained an average $b_{12\cdot3}=-0.239$ percent/mm Hg and an average $b_{13\cdot2}=-0.085$ percent/°C, values much closer to our 581-day values than were his averages for five years. Also, Hess[19] obtained the value $b_{13\cdot2}=-0.055$ percent/°C for the summer months, a value quite comparable to ours which displayed no seasonal effect. Hess, *et al.*, found that the use of hourly values resulted in positive temperature coefficients during late summer. Schonland,[21] *et al.*, obtained a barometric coefficient of -0.216 percent/mm Hg at Capetown and mention that Messerschmidt[26] obtained the value -0.178 percent/mm Hg at Halle and that Steinke[2] obtained the value -0.20 percent/mm Hg at Königsberg, all values more nearly comparable to our $b_{12\cdot3}=-0.174$ percent/mm Hg for 581 days, and all obtained with comparable lead shields. Forbush[27] in 1937 obtained a barometric coefficient of -0.236 percent/mm Hg and concluded that no atmospheric temperature coefficient as great as ±0.024 percent/°C exists. Clay and Bruins[22] obtained a barometric coefficient of -0.64 percent/mm Hg at Amsterdam, which is considerably larger than the values mentioned above. Using G-M tubes in vertical array, Hess,[28] *et al.*, obtained a barometric coefficient of -0.218 percent/mm Hg at New York, and temperature coefficients of -0.033 percent/°C in summer and -0.155 percent/°C in winter. Forró[29] recently found a positive temperature coefficient of 0.74 percent/°C under 1000-m water equivalent in a coal mine near Budapest, and concluded that there was no dependence upon barometric pressure there.

In view of the dependence upon the use of daily averages or monthly averages in the computation of the temperature coefficients according to Duperier, new barometric and temperature coefficients were computed on the basis of monthly averages for the burst-corrected CR ionization for the 19 full months of the present series. On this basis the following coefficients were obtained: $b_{12\cdot3}=-0.199$ percent/mm Hg, $r_{12\cdot3}=-0.505$, $t_{12\cdot3}=-2.08$, and $b_{13\cdot2}=-0.057$ percent/°C, $r_{13\cdot2}=-0.557$, $t_{13\cdot2}=-2.30$. Remarkably, the regression coefficients thus obtained are only a little higher than those obtained on the basis of the 581 daily averages as given in Table IV, and the temperature coefficients are almost identical. This leads us to wonder whether one ought not to compare the coefficients obtained by the two methods of averaging, from treatment of the data of a single experimenter rather than by employment of data obtained by two groups of experimenters as Duperier has done; possibly the situation he has emphasized could account in part for the differences between the barometric coefficients of the bursts shown in Tables II and III. In computing the partial coefficients based on monthly averages, an interesting situation regarding the simple coefficients was observed. These are $b_{12}=-0.394$ percent/mm Hg, $r_{12}=-0.879$, $t_{12}=-3.73$; $b_{13}=-0.099$ percent/°C, $r_{13}=-0.888$, $t_{13}=-3.77$; $r_{23}=0.853$, $t_{23}=3.62$. The simple barometric and temperature coefficients are seen to be closely comparable to some of the larger coefficients obtained by others as discussed above. Also, the high (simple) positive correlation between the barometric pressure and atmospheric temperature on a seasonal (monthly averages) basis serves to produce considerably lower coefficients for the partial correlation

[26] W. Messerschmidt and W. Pforte, Z. Physik **73**, 677 (1932).
[27] S. E. Forbush, Terr. Mag. **42**, 1 (1937).
[28] Altmann, Walker, and Hess, Phys. Rev. **58**, 1011 (1940).
[29] M. Forró, Phys. Rev. **72**, 868 (1947).

of the CR intensity relative to barometric pressure and to temperature than is indicated by the high, negative, individual (simple) coefficients relating CR intensity to these variables.

Comparison of the values in Tables II and IV shows that both the barometric and the temperature coefficients for the 1-mm bursts are of a higher order of magnitude than the corresponding coefficients for the burst-corrected ionization. Moreover, the reversal of sign of the temperature coefficient for the 1-mm bursts for the full period of observation (Table III) as differentiated from the coefficients for most of the individual months, has no counterpart in the burst-corrected ionization. These observations provide further confirmation of the evidence provided earlier,[1] that the small bursts and the burst-corrected CR ionization are produced by different types of penetrating radiation.

VIII. MASS ABSORPTION COEFFICIENTS

Estimates of the mass absorption coefficients of the different radiations presumed to be responsible for the small bursts and for the burst-corrected CR ionization can be made. Some years ago the writer[4] employed the chamber described here, shielded with 5.1-cm Pb, to measure by visual observations the absorption produced by a few feet of water in a large tank. Corrections were made only for large bursts observed visually, of course. Assuming exponential absorption, $I=I_0e^{-\mu x}$, limiting values of $\mu=0.0010$ and $\mu=0.0028$ cm^{-1} H_2O were obtained on the respective assumptions that the radiation was all incident vertically, and that it was incident uniformly from all directions above the horizontal. Because of the difficulty caused by the irregular shielding afforded by the heavy-walled building (the chamber was then located at a different place in the same basement where it is now located) it is not easy to make a satisfactory estimate of the actual distribution of the incoming radiation. On the assumption that the actual distribution is represented somewhat better by the first limit than by the second, we assign the first twice the weight of the second for the present purpose to obtain an average $\mu=0.0016$ cm^{-1} H_2O. This corresponds to a mass absorption coefficient or mean range or mean free path $\lambda=1/\mu=625$ g/cm^2.

An estimate may also be made from the barometric coefficient. Referring again to visual observations[30] made some time ago, a barometric coefficient of $b_{12}=-0.21$ percent/mm Hg was observed during a period of 15 days with the chamber shielded by a 5.5–6 ft shield of water. Taking account of the density of Hg and the fact that the coefficient is here expressed in percent, we obtain from this the value $\lambda=136/-b_{12}=648$ g/cm^2. Turning to Table IV of the present work, and using the multiple regression coefficient $b_{12\cdot3}=-0.174$ percent/mm Hg for all 581 days, we obtain $\lambda=136/-b_{12\cdot3}=782$ g/cm^2. The corresponding simple barometric coefficient (not listed in Table IV) for all 581 days, $b_{12}=-0.215$ percent/mm Hg yields $\lambda=633$ g/cm^2. Hogg[20] obtained a value for $\mu=0.0021$ from the barometric effect, and 0.0015 directly from absorption in lead. These values correspond to $\lambda=1/\mu=476$ and 667 g/cm^2, respectively. From their difference he deduced the value 2.8 μsec for the rest life of the meson.

Turning to Table II for the 1-mm bursts, and using $b_{12\cdot3}=-1.54$ percent/mm Hg (average of 19 monthly values) we obtain $\lambda=88$ g/cm^2 for the burst-producing radiation. Using $b_{12\cdot3}=-2.44$ percent/mm Hg (average of 10 monthly values with $t_{12\cdot3}$ above the 2 percent level) we obtain $\lambda=56$ g/cm^2. Use of the barometric coefficient given in Table III for all 581 days yields $\lambda=213$ g/cm^2; but it seems that much less confidence should be placed in this value for reasons mentioned above, particularly because it depends upon all four readers.

These values do not agree well with those obtained by Lewis[31] by shielding low pressure chambers with shields of Pb, Fe, and Al. According to him, "The mean free path changes continuously from 390 gm/cm^2 for bursts greater than 7×10^5 ion pairs to 190 gm/cm^2 for bursts greater than 2.3×10^6 ion pairs. Apparently, the absorption length approaches the geometrical one as the energy of the burst increases." Using their barometric coefficient, Jánossy[32] found $\lambda=113$ g/cm^2 for penetrating showers.

The writer desires to express appreciation of the cooperation of Dr. V. A. Long, Dr. R. M. Whaley, Dr. H. W. Boehmer, Dr. H. W. Hunter, and Mrs. F. H. Best, who assisted at various times with the modification and operation of the apparatus and with the reading of the records while the research was supported in part by the Office of Naval Research, and of the twenty-seven students who aided, chiefly with computations, then and later, when it was supported in part by grants from the Council on Research and Creative Work of the Graduate School. Appreciation is also expressed for information and suggestions provided by Professor Marcel Schein and Mr. T. G. Stinchcomb of the University of Chicago, and by Professor F. P. Stribic of the Department of Mathematics of the University of Colorado.

APPENDIX I. APPARATUS

The principal features of the high pressure CR ionization chamber were given in a paper[4] in 1931. Figure 1 of that paper is a photograph of the chamber mounted at the center of the 14-ft water tank where it was then used, with part of its lead shield in position. Figure 3 of that paper represents a longitudinal section of the chamber which shows the wall thickness and guard system, but a different central electrode from that currently employed. Figure 1 of a later paper[5] shows a very thin-walled sphere mounted concentrically with the walls of the high-pressure chamber. In that diagram the thin central sphere is shown connected to the outer wall through its thin-walled supporting tube. For the 1938–1939 and the current measurements, the

[30] Broxon, Merideth, and Strait, Phys. Rev. 43, 687 (1933).

[31] L. G. Lewis, Proceedings of the Echo Lake Cosmic Ray Symposium (Office of Naval Research), 244 (1949), unpublished.

[32] L. Jánossy, *Cosmic Rays* (Oxford University Press, 1948), p. 358.

lower end of the supporting tube of this central sphere was modified to fit into the central cone and thereby form the collecting electrode of the central system, the very small collecting electrode and its accompanying guard extension, as shown in Fig. 1, being removed. The thin sphere was supported from below as shown.

Following are the dimensions. The spherical cavity was 29.77 cm in diameter cut concentrically from a cylindrical, nickel-steel ingot 38.42 cm in diameter and 44.13 cm long. The thin-walled spherical collecting electrode had an outer diameter of 9.45 cm and a wall thickness of 0.015 cm, and weighed 33.3 g. Its supporting tube had an outer diameter of 1.35 cm and a wall thickness of 0.020 cm. The volume from which ions were collected was thus approximately 13.3 liters.

As used in the 1938–1939 and the current series of measurements, the chamber was mounted on three Bakelite legs on a brick pier with a stone top, built from the ground in the basement of a rather large building a few feet from one of its thick (30 in.) outer stone walls. The chamber was shielded with 10.2 cm of lead beneath, and 12.7 cm of lead around its sides and over the top. The lead shield was cast from old telephone-cable sheaths. An oil-cloth cover was placed over the lead shield to decrease circulation of the atmosphere through it. Whaley[6] has estimated that the shielding afforded by the building, though irregular, was roughly equivalent to 39 cm Pb. The writer[1] estimated that the shielding by the building would probably amount to some 15 cm Pb for any direction and much more than 40 cm Pb for certain directions, and pointed out that the shielding provided by the chamber walls varied from a little over 7 cm of steel for vertical rays through the center, through a maximum of over 14 cm for central rays at about 42° zenith angle to a minimum of about 4 cm for horizontal central rays. Earlier experiments[4,5,7] with the chamber at pressures extending to 0.8 atmos and various shields have shown the CR ionization chamber to be remarkably free from radioactive contamination.

As usual, the CR ionization current was nearly compensated, on the average, by a steady, contrary ionization current produced in an auxiliary chamber or compensating condenser by radioactive material. While the steady compensating current did not provide overcompensation for the total CR current in the argon-filled chamber for more than a very few days during the late summer and fall, it did provide overcompensation of the CR current after correction for bursts, for a majority of days during 5 of the months of the present series, although the CR current was generally undercompensated. The auxiliary chamber was a sealed, cylindrical air condenser. The collecting electrode in this was a well guarded cylinder of 15.4 cm length and 6.99 cm o.d. separated by a radial distance of 1.43 cm from both inner and outer coaxial cylinders at high potential. Ions were produced in it by gamma-rays from a sealed capsule containing 1.15 g of a Ra Br concentrate with a content of about 2 μg of Ra located on the axis of the condenser in a special receptacle. To diminish further the production of ions in the thick-walled, spherical, CR ionization chamber, an additional lead plate 7.6 cm thick (5.1 cm for the 1938–1939 series) was placed between the CR chamber and the compensating condenser. The CR chamber was thus shielded from the Ra gamma-rays by at least 20.3 cm Pb and the thick chamber wall. During the 1938–1939 series, positive ions were collected on the central system in the high pressure chamber, while the opposite was true during the 1947–1949 series.

The measuring instrument was a quadrant (Compton-type) electrometer of small capacity. The period of its vane was 6 sec (10 sec in 1938–1939) for a complete oscillation, or 1.5 sec for a ballistic throw. The CR records were obtained by reflecting a beam of light from the mirror on the electrometer vane, onto an 8-in.×20-in. sheet of Kodabromide F2 photographic paper on a drum which rotated once in 25 hr. The electrometer sensitivity was approximately 0.62 mm/mv for the recent observations, about 2.5 times the sensitivity used a decade earlier. The scale was very nearly linear.

In order to apply appropriate potentials and compensate for possible potential fluctuations, the ionization chambers and the electrometer were connected with two wire-wound resistors of approximately 2 and 0.5 megohms, respectively, in a balanced, capacitance-resistance bridge arrangement resembling that represented by Fig. 2 of reference 4. This provided 660 v across the spherical CR chamber and 160 v across the auxiliary chamber. Guard tubes for connecting wires were kept small and short. Long[8] found that the "dead" volume inside the guard system around connecting wires was about 175 cc in 1938–1939. This was increased by an estimated 5 cc during later modification.

Two special keys of the platinum point-to-plane-contact type were incorporated for automatic grounding of the central system and for calibration of the electrometer. The central system was insulated with amber throughout. Amber, incidentally, was the most satisfactory of the insulators tried, including the best polystyrene available. Provision was made for introducing P_2O_5 at three places to maintain dryness of the air in the guard system and of the insulators of the central system.

All the apparatus described above (apart from the light source and rotating drum) and the super-heavy-duty Burgess batteries which supplied the ion collecting potential and electrometer vane potential, were located on the pier and were surrounded by an insulating box containing a two-inch thickness of rock wool. The temperature of the room was controlled by thermostats regulating steam and electric heaters to within about 1°C, the average being 25°C during the recent series. Because of its mass and that of its lead shield, it is presumed that the temperature of the CR ionization chamber was much more nearly constant. In addition to that mentioned above, three beakers of P_2O_5 were maintained inside the insulating box.

For the 1938–1939 measurements the CR ionization chamber was filled with dry air at about 160 atmos. For the 1947–1949 measurements, it was filled with argon at 20.2 atmospheres at 25°C. According to the Linde Air Products Company, which supplied the argon, it was 99.8 percent pure, with impurities consisting of 0.2 percent nitrogen, and other impurities (consisting of oxygen, hydrogen, and carbon dioxide) not exceeding 0.01 percent. The chamber was washed upon filling, by successive insertion and release of the argon, until impurities due to the gas previously in the bomb must have been reduced far below those in the argon supplied. The auxiliary chamber was filled with dry air at the local atmospheric pressure of 62.8 cm Hg, 26°C, and sealed.

APPENDIX II. STATISTICAL PROCEDURE

In order to make quite clear what statistical procedure was employed in obtaining the coefficients listed in the tables, the formulas used in computing these are included. If x_1 represents the total number of 1-mm bursts in a day, for instance, x_2 the average barometric pressure, and x_3 the average outdoor temperature for that day (or variations of these from arbitrary values), then it is assumed that $x_1=a_1+b_{12\cdot3}x_2+b_{13\cdot2}x_3$, where $b_{13\cdot2}$ and $b_{12\cdot3}$ are the partial regression coefficients given by $b_{12\cdot3}=(b_{12}-b_{13}b_{32})/(1-b_{23}b_{32})$, etc., in terms of the simple regression coefficients, b_{12}, etc., given by equations of the form $b_{13}=[N\Sigma x_1x_3-\Sigma x_1\Sigma x_3]/[N\Sigma x_3^2-(\Sigma x_3)^2]$, where N is the number of days. The partial correlation coefficients are represented by relations of the form $r_{12\cdot3}=(r_{12}-r_{13}r_{23})/[(1-r_{13}^2)(1-r_{23}^2)]^{\frac{1}{2}}$ in terms of the simple correlation coefficients, r_{12}, etc., which are expressed in terms of the simple regression coefficients by equations of the form $r_{12}=(b_{12}b_{21})^{\frac{1}{2}}=r_{21}$, the correlation coefficient being assigned the same sign as the corresponding regression coefficient. The significance ratio (t) corresponding to any correlation coefficient is defined to be the ratio of the correlation coefficient to the standard deviation for no correlation. Thus, $t_{12}=r_{12}(N-1)^{\frac{1}{2}}$ and $t_{12\cdot3}=r_{12\cdot3}(N-2)^{\frac{1}{2}}$. $t=2.58$ at the 1 percent level. That is, a value of $t=2.58$ indicates that there is only one chance in a hundred that the correlation is fortuitous. Similarly, $t=2.33$ at the 2 percent level, 1.96 at the 5 percent level, 1.64 at the 10 percent level, 0.67 at the 50 percent level, etc. It is understood that some statisticians regard a correlation as worthy of serious consideration if its corresponding t is at the 5 percent level or higher.

The Gamma-Ray Spectrum Resulting from Capture of Negative π-Mesons in Hydrogen and Deuterium

WOLFGANG K. H. PANOFSKY, R. LEE AAMODT, AND JAMES HADLEY
*Radiation Laboratory, Department of Physics, University of California, Berkeley, California**

(Received October 6, 1950)

π^- mesons produced in an internal wolfram target bombarded by 330-Mev protons in the 184-inch cyclotron are absorbed in a high pressure hydrogen target. The resulting gamma-ray spectrum is analyzed outside the shielding of the cyclotron by means of a 30-channel electron-positron pair spectrometer. The principal results are as follows. (1) The gamma-rays result from two competing reactions: $\pi^-+p\rightarrow n+\gamma$ and $\pi^-+p\rightarrow n+\pi^0$; $\pi^0\rightarrow 2\gamma$. (2) The ratio between the π^0 yield to the single gamma-ray yield is $=0.94\pm0.20$. (3) The mass difference between the π^- meson and the π^0 meson is given by 10.6 ± 2.0 electron masses. (4) The π^- mass is 275.2 ± 2.5 electron masses. The large mass difference between π^- and π^0 precludes the conclusion that the unexpectedly small π^0 to γ ratio is due to the small amount of momentum space available for π^0 emission. It rather indicates that π^0 emission is slowed down by the nature of the coupling of the π^0 field to the nucleons. The experiment has been repeated by substituting D_2 for H_2 in the vessel. The result is that the reaction $\pi^-+D\rightarrow 2n$ and $\pi^-+D\rightarrow 2n+\gamma$ compete in the ratio 2 : 1. The reaction $\pi^-+D\rightarrow 2n+\pi^0$ is absent.

I. INTRODUCTION

THE classic experiments of Conversi, *et al.*[1] on the absorption of negative μ-mesons in matter gave the first information on the fact that the coupling of μ-mesons with nuclei is weak. On the other hand, experiments on the absorption of π^- mesons[2,3] have confirmed the fact that π-mesons are strongly coupled and that they have integral spin. This is evidenced by the fact that the process

$$\pi^-+p\rightarrow n^* \qquad (1)$$

taking place within a nucleus could not give rise to the large nuclear stars observed if an additional light particle of half-integral spin had to be emitted, as in the absorption of μ^- mesons. Other than confirming this qualitative fact, the absorption of slow π^- mesons in matter has led to no quantitative information as to the nature of the coupling of π-mesons to nuclei, since the dominant time in the capture process is the slow-down time by ionization; once a π^- meson has arrived in the K shell of an atom, absorption is presumed to take place in about 10^{-14} sec.

The case of π^- absorption in hydrogen is a singular one since clearly process (1) is forbidden by the conservation laws in the case of a free proton. Absorption of a π^- meson in hydrogen must thus lead to the emission of one or more additional particles. Excluding processes involving several spin $\frac{1}{2}$ particles which are clearly too slow to compete, the possible processes which might result are:

$$\pi^-+p\rightarrow n+\gamma, \qquad (2)$$

$$\pi^-+p\rightarrow n+2\gamma, \qquad (3)$$

$$\pi^-+p\rightarrow n+\pi^0. \qquad (4)$$

Prior to this work the possibility for process (4) rested, of course, on the possibility that the π^- might be sufficiently heavier than the π^0 to make the process energetically possible. Evidence from direct gamma-ray production in a cyclotron target bombarded by 350-Mev protons[4] points to the existence of a π^0 of mass of the order of the π^- mass, but the center of the gamma-ray spectrum cannot be localized with sufficient accuracy to decide the sign of the mass difference. Cosmic-ray evidence[5-8] and particularly the observations of gamma-gamma coincidences observed from targets bombarded in the x-ray beam of the Berkeley synchrotron[9] have shown conclusively that a π^0 exists and that it disintegrates into two gamma-rays and thus cannot have spin one. Recently, Carlson, Cooper, and King[10] have succeeded in analyzing positron-electron pairs observed in nuclear emulsions exposed at 70,000 ft in terms of neutral mesons. They show that the observed energy spectrum of such pairs is compatible with their origin from gamma-rays from a π^0 meson of mass 295 ± 20 electron masses, where only the statistical error is included in the mass estimate. Carlson, Cooper, and King also deduce the mean life, τ, of the π^0 meson to be $\tau<5\times10^{-14}$ sec.

Preliminary reports of the present experiment[11] have indicated qualitatively that both processes (2) and (4) exist. However, no accurate mass determination of the π^0 was possible and thus no very significant branching ratio between the processes could be inferred.

The evidence presented here excludes any appreciable competition from process (3). The reason is firstly a

* This work was done under the auspices of the AEC.

[1] Conversi, Pancini, and Piccioni, Phys. Rev. **68**, 232 (1945).
[2] Manon, Muirhead, and Rachat, Phil. Mag. **41**, 583 (1950).
[3] F. Adelman and S. Jones, Science **111**, 226 (1950); W. Cheston and L. Goldfarb, Phys. Rev. **78**, 320A (1950).
[4] Bjorklund, Crandall, Moyer, and York, Phys. Rev. **77**, 213 (1950).
[5] W. Fretter, Phys. Rev. **73**, 41 (1948); Phys. Rev. **76**, 213 (1949).
[6] C. Y. Chao, Phys. Rev. **75**, 581 (1949).
[7] Gregory, Rossi, and Tinlot, Phys. Rev. **77**, 299 (1949).
[8] Kaplon, Peters, and Bradt, Phys. Rev. **76**, 1735 (1949).
[9] Steinberger, Panofsky, and Steller, Phys. Rev. **78**, 802 (1950).
[10] Carlson, Cooper, and King, Phil. Mag. **41**, 701 (1950).
[11] W. K. H. Panofsky, Post Deadline Paper, New York Meeting A.P.S., 1950; Panofsky, Aamodt, and York, Phys. Rev. **78**, 825 (1950).

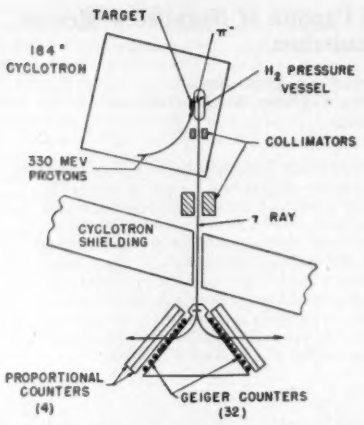

FIG. 1. Geometrical arrangement of π^- capture experiment. π^- mesons produced in a primary wolfram target of the 184-inch cyclotron are captured in the H_2 pressure vessel. The resultant gamma-rays are collimated and leave the cyclotron shielding through a hole tapering from 2 in. to 3 in. in diameter. The gamma-rays are then analyzed by a pair spectrometer.

theoretical one. It appears to be difficult to construct a selection rule which would make double gamma-emission compete effectively with single gamma-emission. Secondly, the double peaked energy distribution (see Fig. 12) of the emitted radiation practically excludes a two-gamma-process.

The details of the slowdown process of π^- in hydrogen have been discussed in considerable detail by Wightman.[12] The significant sequence of the process is as follows. (1) Slowdown of the fast meson by the ordinary stopping power mechanism ($\sim 10^{-10}$ sec). (2) Slowdown by collisions with orbital electrons of velocities comparable with that of the meson ($\sim 10^{-12}$ sec). (3) Capture of the mesons in an outer orbit leading to an excited $\pi^- - H^+$ system.[13] (4) Reduction of energy of the neutral $\pi^- - H^+$ system to the lowest quantum state. This latter process principally is not radiative but is due to collisions of the neutral system with hydrogen molecules which leads by various mechanisms to the emission of an Auger electron ($\sim 10^{-10} - 10^{-9}$ sec). In liquid or high pressure hydrogen the over-all time to enter the K shell is thus sufficiently short to compete effectively with the $\pi - \mu$ decay time.[14] This is true, however, only if the H_2 density is sufficient. This point has been verified experimentally (see Sec. VII).

Capture in flight[15] corresponds to a lifetime of the order of 10^{-4} to 10^{-5} sec, depending on assumptions as to the interaction.

We can therefore conclude that at densities approximating that of liquid hydrogen all but of the order of 10^{-3} of the secondary radiations resulting from the capture of π^- in H_2 result either from absorption of the π^- meson from an inner shell or from $\pi - \mu$-decay; the $\pi - \mu$-decay branching is small.

II. GEOMETRICAL ARRANGEMENT; THE HYDROGEN SYSTEM

The geometrical layout of the experiment is shown in Fig. 1. The 330-Mev protons circulating in the internal beam of the 184-inch cyclotron strike a wolfram target $\frac{1}{2}$ in. deep (parallel to the beam) and 0.040 in. thick (transverse to the beam). Wolfram was chosen, since the π^- cross section measurements of Weissbluth[16] showed that a heavy element favors π^- production. Also, auxiliary measurements on beam penetration and "scattering out" showed that a high density target was desirable here from the point of view of total meson yield. Finally, as discussed later, the background in this experiment is principally produced by high energy protons elastically scattered and striking the hydrogen vessel. At this energy scattering at the angles in question is principally diffraction scattering; heavy elements produce a smaller diffraction angle.

The π^- mesons enter the high pressure hydrogen through the walls of the pressure vessel shown in Fig. 2. To produce maximum yield the wall thickness is limited in order that the mesons absorbed in the hydrogen are those produced at a sufficiently low energy to correspond to a rising portion of the meson yield curve as a function of meson energy. Such considerations limit the wall thickness to ~ 4 g/cm^2. However, an H_2 density near that of the liquid phase is desirable by the capture considerations already given. The use of liquid H_2 was

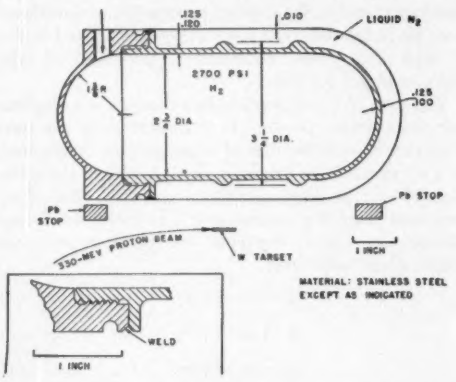

FIG. 2. High pressure vessel used for absorption of H_2 and D_2. The vessel is constructed of stainless steel machined as indicated. The load is carried by threads with the weld serving as a seal only. The outer stainless steel liquid N_2 jacket (0.010 in. thick) is soft soldered to the thick portion of the main vessel.

[12] A. S. Wightman, thesis, Princeton University, Princeton, New Jersey (June, 1949), and Phys. Rev. **77**, 521 (1950).
[13] E. Fermi and E. Teller, Phys. Rev. **72**, 399 (1947).
[14] J. R. Richardson, Phys. Rev. **74**, 1720 (1948); E. A. Martinelli and W. K. H. Panofsky, Phys. Rev. **77**, 465 (1950); Chamberlain, Mozley, Steinberger, and Wiegand, Phys. Rev. **79**, 394 (1950); M. Jakobsen, private communication.
[15] R. Marshak and A. S. Wightman, Phys. Rev. **76**, 114 (1949).
[16] M. Weissbluth, Phys. Rev. **78**, 86A (1950).

not advisable here owing to the difficulty of cooling a long horizontal filling tube required by the geometry of the cyclotron. The vessel shown in Fig. 2 operates at a factor of safety of about 2.5 when maintained at 2700 psi and at liquid N_2 temperature. The specific gravity[17] under these conditions is 0.046. The aforementioned factor of safety makes use of the appreciable increase in strength of stainless steel at low temperature.[18] The outer jacket is fed by an external liquid N_2 Dewar vessel. The pressure vessel is filled by an external oil piston pressure pump[18a] fed by commercial H_2, dried and purified in a liquid N_2 trap. A flow diagram of the arrangement is shown in Fig. 3. A similar system is used for deuterium with certain modifications to permit recovery.

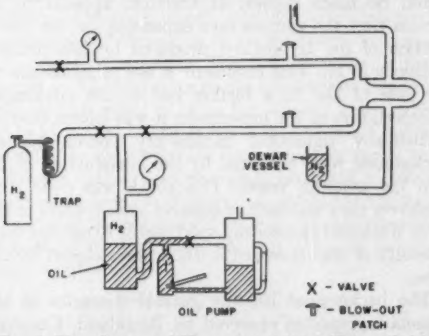

FIG. 3. Flow diagram of H_2 pressure system. H_2, purified in a liquid N_2 trap, is admitted into the pressure chamber above the pump and at tank pressure. The pressure is then raised by displacing the H_2 in the pressure chamber with oil pumped as shown.

III. THE PAIR SPECTROMETER

Since the expected pair spectra from processes (2) and (4) exhibit discontinuities, satisfactory analysis and also good signal-to-background ratio requires a spectrometer with a large number of channels. Since the counting rates in this experiment are limited entirely by absolute available intensity and not by errors introduced by accidental coincidences, etc., Geiger counters as used by Lawson[19] seem to offer the best solution to the multiple channel problem. The geometrical layout of the pair spectrometer is shown in Fig. 4. The magnet has a useful gap of 3.5 in. and a maximum field of 14,000 gauss although for this experiment only fields of the order of 5000 to 10,000 gauss were used. The pole piece is in the shape of a 90° triangle, the hypotenuse of the triangle being 30 in. The pole is widened near the converter position to improve the uniformity of the field near the converter; field uniformity is not as essential near the counters as it is near the converter. There is no specific advantage to the choice of 90° for the triangle apex angle; the angle was defined principally by arguments of size and weight. A 90° apex angle (and hence a 90° deflection angle!) provides for first-order horizontal focusing for particles of the same energy originating in different parts of the converter; this is, however, not an essential consideration if one is interested only in the sum of the energy of the two pair fragments.

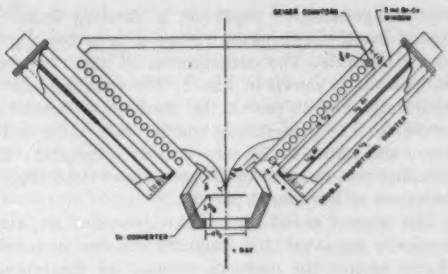

FIG. 4. Outline diagram of pair spectrometer. The converter, Geiger counter array, and the proportional counters are shown. Note the geometry of the pole piece to give a uniform field in the area of the converter.

The resolving power of a pair spectrometer of this type is essentially defined by three factors: (1) channel width; (2) multiple scattering in the converter; and (3) radiation straggling of the pair members. A feature of the triangular design is the fact that the energy width due to multiple scattering is constant. The converter thickness has been chosen such that the combination of the latter two widths approximately matches the first. This condition can only be approximately achieved, since the ratio of the radiation error to the scattering error varies as the pair energy. The choice of converter material is not critical, since pair conversion efficiency, multiple scattering, and radiation straggling depend only on the number of radiation lengths of converter used. Tantalum converters were used in this experiment. The choice of triangular shape of magnet and the analysis of the resolution of such a magnet are due to Professor Edwin McMillan. The initial design of the pair spectrometer magnet was carried out by Herbert F. York and the mechanical engineering design is due to Robert Meuser; the authors are greatly indebted to them for their contributions.

Because of the high singles rates (approximately 3 counts/sec) of the Geiger counters (Victoreen type 1B85) and the low true pair rate (approximately 30 c/hr), additional selection of events is necessary. This is provided by 4 large proportional counters (Fig. 4) backing up the counter arrangements. A pair event is selected by a quadruple coincidence count in the proportional counters; this quadruple coincidence opens a gate which passes the amplified Geiger pulses into a recorder. This recorder consists of 30 pens mark-

[17] Johnston, Berman, Rubin, Rifkin, Swanson, and Corak, MDDC-850 (to be published).

[18] E. E. Thum, *The Book of Stainless Steels* (American Society for Metals, Cleveland, 1935), second edition, p. 376.

[18a] Manufactured by the American Instrument Company, Superpressure Division, Silver Spring, Maryland.

[19] J. L. Lawson, Phys. Rev. 75, 433 (1949).

ing voltage-sensitive paper on a rotating drum. A typical event thus appears as two dots in the appropriate channels. The arrangement of the electronic components is shown in Fig. 5. The counting rate is sufficiently slow to permit this mechanical method of recording. The proportional counter gate width is 1.5 μsec; accidental counts are entirely negligible; the counting rate loss due to Geiger counter dead time is estimated at less than 2 percent.

The magnet is fed by a motor generator set, electronically regulated; the magnetic field has been calibrated against the magnetic moment of the proton; during runs the fields are monitored by current readings with a shunt and potentiometer or with a proton moment apparatus if the accuracy is needed.

The sensitivity of a pair spectrometer is not constant over the energy range covered by the instrument. This is due to (a) the variability of number of channels available to record the pair fragments of a given total energy, (b) the variation of pair production cross

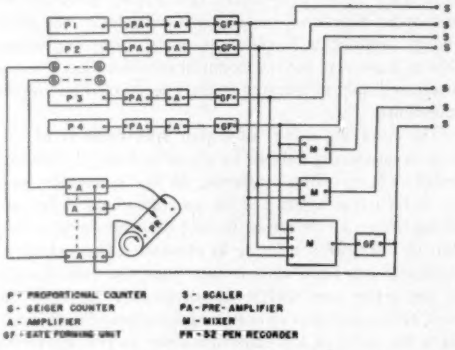

FIG. 5. Block diagram of electronic components.

section with energy, and (c) the variability of loss by scattering. It can be shown easily that (c) can be neglected in this geometry. The correction curve of the instrument due to causes (a) and (b) is given in Fig. 6.

IV. OPERATION OF RUNS

Before every run the spectrometer is checked by using gamma-rays directly produced in the cyclotron target.[4] The yield of the direct gamma-rays is sufficient to permit the plateaus of all counters to be checked with good statistics. Also, all Geiger channels are checked for singles rates by removing the gate formed by the proportional counters. The target and pressure vessel are then moved so that the primary target is well shielded from the spectrometer and the hydrogen vessel is aligned with the collimators and the spectrometer (Fig. 1).

Readings are made with the pressure vessel either evacuated or pressurized with H_2 or D_2. If the vacuum runs are to represent the true background it is necessary that no other process (e.g., scattering of protons from

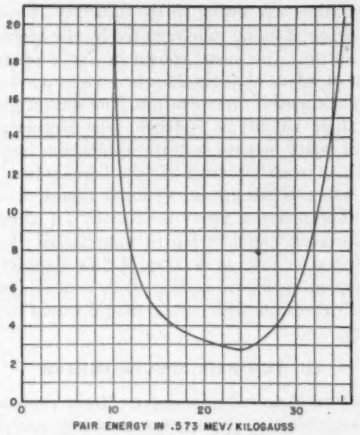

FIG. 6. Multiplication factor to be used to reduce observed counting rates to gamma-ray intensity. This factor arises from (a) variation of pair production cross section with energy and (b) number of available channels into which a given total pair energy can divide.

the target) produce gamma-rays in hydrogen. This assumption receives support from experiments by Crandall, Hildebrand, Moyer, and York,[20] indicating that the production cross section for gamma-ray production by bombardment with 345-Mev protons in hydrogen is less than 2 percent of the cross section in carbon. This means that if a sufficient number of primary protons were scattered into the hydrogen to produce gamma-rays of significant intensity, then the background due to gamma-rays hitting the steel vessel would be much higher. It therefore appears to be certain that the gamma-rays depending on the introduction of the H_2 are not produced by fast particle collisions in H_2. This argument is not as significant in the case of D_2. As a further link in the qualitative interpretation of the experiment it was shown that no statistically significant gamma-ray counts beyond background were produced by the introduction of He into the pressure vessel. This check was done with relatively poor statistics; a positive helium effect in the form of a broad gamma-ray spectrum of 10 percent total intensity of that observed in H_2 is not excluded by the data.

The background has the general character of the gamma-ray spectra observed by Bjorklund, Crandall, Moyer, and York[4] at 180° from the target. The background is almost certainly due to protons scattered by the primary target onto the steel jacket of the pressure vessel and other parts of the cyclotron. The background is negligible in the 130-Mev region but is of the same order of intensity as the H-capture gamma-rays in the 70-Mev region.

[20] Crandall, Hildebrand, Moyer, and York, private communication.

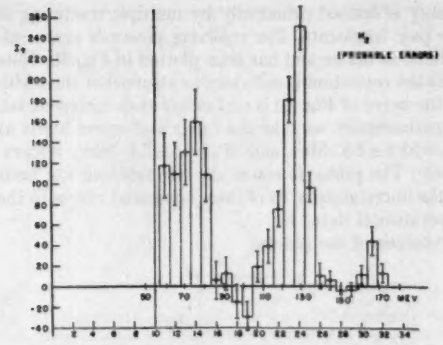

FIG. 7. Pair spectrum of gamma-rays produced by capture of π^- in H_2. Center of spectrometer set near 130 Mev.

V. GAMMA-RAY SPECTRA FROM HYDROGEN

As can be seen from the spectrometer response curve (Fig. 6) it is not possible to cover the entire spectrum of the spectrometer with good efficiency. Accordingly, different runs were made with the spectrometer set with its central point at (a) single gamma-ray peak, (b) center between the two peaks to permit easy relative area measurements, and (c) π^0 peak.

(a) The High Energy Peak; The π^- Mass

Figure 7 shows the spectrum observed with the spectrometer maximum set near the high energy peak. Note that the "π^0 peak" also appears clearly.

Since the position of the single gamma peak gives a precise measurement of the π^- mass, it is a matter of considerable interest to analyze the observed peak accurately in terms of resolving power of the pair spectrometer. Figure 8 shows plotted individually the resolving power curves due to the three principal causes of finite resolving power. The first cause is the finite channel width. This gives rise to a triangular resolution $R_1(E)$ of base equal to twice the channel width, which is 5.36 Mev. The second cause is the multiple Coulomb scattering in the converter. One can show easily that if $\langle\theta\rangle$ is the root mean square plane projected scattering angle[21] of an electron of energy of one-half the gamma-energy after having passed through the full converter thickness, then the fractional rms error in gamma-energy is given by

$$\delta = \delta E_\gamma / E_\gamma = (\sqrt{2}\langle\theta\rangle)/3. \tag{5}$$

This gives a resolving power $R_2(E)$ given by

$$R_2(E) = \exp[-(E-E_\gamma)^2/(2\delta E_\gamma^2)] \tag{6}$$

plotted in Fig. 8b.

The third cause is radiation straggling of the outgoing pair represented by a resolving power curve $R_4(E)$. Let, in the notation used by Heitler,[22] $w(y)dy$ be the probability that the energy of a single electron has decreased to e^{-y} times its initial value after traversing a thickness t. Let $W(p)dp$ be the resultant probability that an outgoing pair fragment has retained a fraction between p and $p+dp$ of its energy of formation. $W(p)$ can be generated by averaging $w(y)$ over the converter thickness. Let $P(E_1, E)dE_1$ be the probability that a pair fragment have an energy between E_1 and E_1+dE_1 for a total pair energy E_γ. It can be shown that the probability $\pi(f)df$ that the resultant pair shall have retained a fraction between f and $f+df$ of its initial energy is

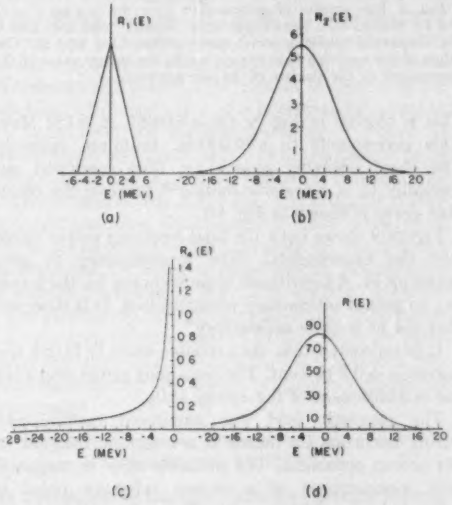

FIG. 8. Curves showing the components of the resolving power curve of the spectrometer. (a) Resolving power due to finite channel width. (b) Resolving power due to multiple scattering of pairs in converter. (c) Resolving power due to radiation straggling of outgoing pair. (d) "Fold" of a, b, and c giving total resolving power.

given by:

$$\pi(f)df = df\int_{E_A}^{E_B} dE_1\left\{\int_{1-(E_\gamma/E_1)(1-f)}^{1}\left(\frac{E_\gamma}{E_\gamma-E_1}\right)\right.$$
$$\left.\times W(p)W\left(\frac{E_\gamma f - pE_1}{E_\gamma-E_1}\right)P(E_1,E_\gamma)dp\right\}. \tag{7}$$

Here E_A and E_B are the pair fragment energy limits defined by the spectrometer. This integral has been evaluated using the forms $P(E_1, E_\gamma)dE_1 = dE_1/E_\gamma$ and $W(p) = K/(1-p)^{1-\alpha}$, where α was fitted to the computed radiation curves. The result shows that the resolving power has the approximate form:

$$\begin{aligned} R_4(E) &= 1/(E_\gamma - E)^{1-2\alpha}, & E<E_\gamma \\ &= 0, & E>E_\gamma. \end{aligned} \tag{8}$$

[21] B. Rossi and K. Greisen, Rev. Mod. Phys. 13, 240 (1941).
[22] W. Heitler, *The Quantum Theory of Radiation* (Oxford University Press, Oxford, 1936), p. 223 ff.

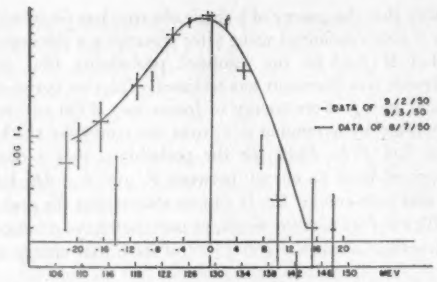

FIG. 9. Pair spectra of gamma-rays from the process $\pi^- + H \rightarrow n + \gamma$ plotted on a logarithmic scale. Plotted (solid line) also is the theoretical resolving power curve adjusted for best fit. The origin of the resolving power curve marks the energy value of the gamma-ray on the abscissa of the pair spectrum.

This is plotted in Fig. 8c for $\alpha = 0.081$, $E_\gamma = 132$ Mev. This corresponds to a 0.020-in. tantalum radiator. The three resolving powers are then combined numerically by a successive folding[22a] process; the resultant curve is shown in Fig. 8d.

Figure 9 shows both the final resolving power curve and the experimental data superimposed to give optimum fit. A logarithmic scale is chosen for the intensity to permit satisfactory normalization. It is observed that the fit is quite satisfactory.

It is estimated that the probable error in fitting the curves is ± 0.8 percent. The remaining errors deal with the establishment of the energy scale.

The magnetic field was monitored continuously during operation by means of a magnetic moment of the proton apparatus. The probable error in magnetic field measurement of a chosen reference point is estimated at ± 0.03 percent. The magnetic field was mapped with a flip coil accurate in relative measure to an accuracy of 0.1 percent probable error. Trajectories were laid out to determine the small corrections for field nonuniformity. It is estimated that the error due to uncertainty in trajectory layout is a ± 0.3 percent probable error. The geometry was laid out accurately to a ± 0.1 percent probable error. As a result the over-all probable error is ± 0.9 percent, the principal contribution being the accuracy of curve fitting. We thus obtain

$$M_{\pi^-} = 275.2 \pm 2.5 \text{ electron masses.}$$

A more accurate measurement based on this method is planned.

The excellent agreement of this result with the photographic work[23,24] confirms also the argument that we are, in fact, observing process (2).

(b) The Low Energy Peak

The spectrum in the neighborhood of the low energy peak is shown in Fig. 10. The resolving power at this energy is defined principally by multiple scattering of the pair fragments. The resolving power is again calculated as before and has been plotted in Fig. 10. Note that the resolution is sufficient to assure that the width of the curve of Fig. 10 is real rather than instrumental. Experimentally we take the lower and upper limits at $W_1 = 53.6 \pm 2.8$ Mev and $W_2 = 85 \pm 2.8$ Mev, respectively. The probable errors are estimated on the basis of the uncertainty in fit of these computed curves to the experimental data.

Analysis of the process

$$\begin{array}{l} \pi^- + p \rightarrow n + \pi^0 \\ \qquad\quad \big\lfloor 2\gamma \end{array} \tag{9}$$

is based on the following physical picture. Since essentially all the observed radiation results from π^- mesons of initial velocity $\beta \sim 1/137$, we can assume that the kinetic energy of the π^0 plus that of the neutron in process (9) are essentially equal to the mass differences involved. Since the Doppler width of the emitted gamma-ray are proportional to the momentum of the π^0, the following equation can be deduced:

$$\delta = M_{\pi^-} - (M_{\pi^-} - \Delta)\left[1 - \frac{2M_n\alpha(M_{\pi^-} + M_p)}{(M_{\pi^-} - \Delta)^2}\right]^{\frac{1}{2}}, \tag{10}$$

where

$$\alpha = (1/M_n)\{(M_n^2 + \Delta W^2)^{\frac{1}{2}} - M_n\} \approx \Delta W^2/2\,M_n^2.$$

Here δ is the mass difference between π^- and π^0, Δ is the neutron-proton mass difference,[25] and ΔW is the width of the peak: $(\delta - \Delta)$ depends thus essentially on the width of the peak of Fig. 10.

It can easily be shown statistically that the expected distribution of γ-energies is uniform on an energy scale between the two Doppler limits. The sum of the lower and upper limits of the γ-peak represents the total relativistic energy of the π^0; it is thus equal to the π^- mass less the neutron-proton mass difference and the neutron recoil energy; thus, if S is the sum of the upper and lower spectral limits,

$$S = M_{\pi^-} - \Delta - [(\Delta W)^2/2M_n]. \tag{11}$$

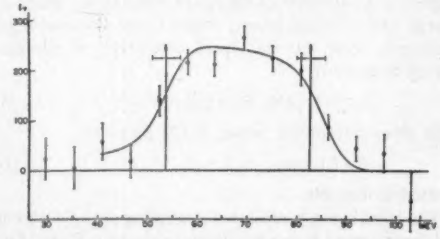

FIG. 10. Pair spectrum of gamma-rays presumably due to the process $\pi^- + H \rightarrow n + \pi^0 \rightarrow n + 2\gamma$. Plotted also is the theoretical spectral shape assuming that the spectrum lies between the limits of 53.6 Mev and 85 Mev. The estimated probable errors of these limits are indicated.

[22a] The "fold," $f(x)$, of two functions $g(x)$ and $h(x)$ is defined by the formula $f(x) = \int_{-\infty}^{+\infty} g(t-x)h(t)dt$.

[23] Gardner, Barkas, Smith, and Bradner, Science 111, 191 (1950).

[24] F. Smith, private communication.

[25] R. E. Bell and L. G. Elliott, Phys. Rev. 74, 1552 (1948).

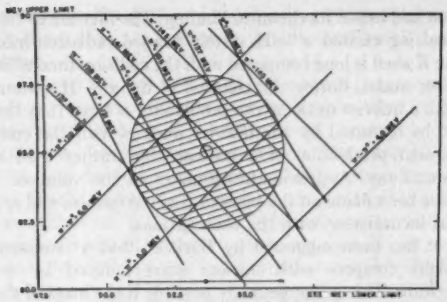

FIG. 11. Graphical representation of the relations defining the meson masses in terms of the lower and upper limit of the spectrum of Fig. 10. The ordinate and abscissa are the upper and lower limits, respectively. Plotted on this graph are: (a) The experimental values and the probable errors of the lower and upper limits. (b) The ellipse (a circle in this case) in the coordinate plane representing the area of 50 percent probability for the quoted masses. (c) The lines of constant π^- mass. (d) The lines of constant $\pi^- - \pi^0$ mass difference. (e) The curves of constant π^0 mass.

Figure 11 shows graphically the relation between the energy limits and the masses involved. The ordinates and abscissae of Fig. 11 are W_2 and W_1, the upper and lower limits, respectively, of the spectrum of Fig. 10, and the measured values are indicated. Lines of constant $\pi^- - \pi^0$ mass difference (δ) are practically of the form $W_2 - W_1 = \text{const.}$, while lines of constant π^- mass are of the form $W_2 + W_1 = \text{const.}$ Both of these functions have been plotted, in addition to the lines of constant π^0 mass. The measured values of W_1 and W_2 and their probable errors generate an ellipse of error in the $W_2 - W_1$ plane which is given here. Accordingly,

$$\delta = M_{\pi^-} - M_{\pi^0} = 5.4^{+1.0}_{-0.8}\ \text{Mev} \cong 5.4 \pm 1.0\ \text{Mev} = 10.6 \pm 2.0\ \text{electron masses.} \quad (12)$$

From the diagram:

$$M_{\pi^0} = 135 \pm 4\ \text{Mev} = 265 \pm 8\ \text{electron masses.}$$

Using the mass values already determined for the π^- mass, Eq. (12) leads to the π^0 mass:

$$M_{\pi^0} = 264.6 \pm 3.2\ \text{e.m.}$$

Further reduction of the probable errors of the π^- mass is, however, anticipated.

(c) Branching Ratio Between π^0 and γ-Emission

A run was made with the peak of the pair spectrometer intensity curve located at 100 Mev. This gives somewhat poorer statistics on either the low energy or the high energy peaks but permits a measurement of the branching ratio. The resulting curve is shown in Fig. 12. Figure 12 also shows a rectangular profile of area equal to the total intensity of the low energy group and of width equal to the width of the low energy peak in Fig. 10. Considering the fact that two photons are emitted per π^0 disintegration, we obtain a branching ratio of

$$\Gamma_{\pi^0}/\Gamma_\gamma = 0.94 \pm 0.20. \quad (13)$$

The probable error quoted is due to the statistics of the data and a reasonable allowance for the uncertainty in the spectrometer sensitivity curve. In interpreting this branching ratio it should be noted that, from Fig. 10,

$$p/M_{\pi^0}c = 0.23 \pm 0.03 \quad (14)$$

gives the momentum of the π^0 in process (4).

(d) Energy Distribution of Pair Fragments

The pair fragment energy of the pairs entering into the gamma-ray spectrum of Fig. 10 has been tabulated as a check on the performance of the pair spectrometer. Although the statistics are insufficient to provide data of interest to pair theory, it is relevant to show that the probability of division of a pair is essentially constant as a function of the division percentage.[22] Figure 13 shows a graphical representation of the number of pairs of fragment energy E_1 and E_2 plotted as a function of the division fraction $E_1/(E_1+E_2)$. The instrument does not permit recording of all possible division ratios, since (Fig. 4) the counter arrangement does not reach to the converter and is limited in radial extent. Accordingly, the scale of intensities of Fig. 13 is weighted inversely to the gamma-ray energy interval which contributes to the particular division ratio. Division ratios are given only in the range $0.2 < E_1/(E_1+E_2) < 0.8$. It is seen that within statistics the distribution is uniform as predicted theoretically.

VI. RUNS WITH MATERIALS OTHER THAN HYDROGEN OR DEUTERIUM

In the beginning stages of these experiments hydrogenous compounds were used in place of the high pressure H_2 vessel.[23] The pair spectrometer used had only a

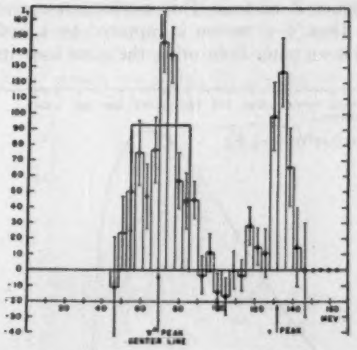

FIG. 12. Pair spectrum resulting from the absorption of π^- mesons in hydrogen. The center of the spectrometer is set near 100 Mev. The spectrum clearly shows the separation between processes (2) and (4). The branching ratio between these reactions can be derived from this spectrum.

[23] W. K. H. Panofsky and H. York, Phys. Rev. 78, 89(A) (1950).

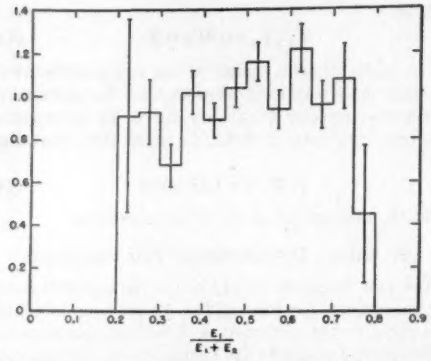

FIG. 13. Energy distribution of pair fragments. The frequency of occurrence of a given energy division is plotted against the energy fraction $E_1/(E_1+E_2)$; the measurements cover the range $0.2<E_1/(E_1+E_2)<0.8$. The ordinate does not represent the actual count but is divided by the gamma-ray energy value contributing to the particular division ratio interval. It is seen that the distribution is uniform within statistics.

single channel 30 percent, wide but the instrumentation was sufficient to show the presence or absence of gamma-ray yield within certain limits.

Let f=fraction of π^- absorbed which is finally absorbed by a hydrogen nucleus. The expected and observed intensities are tabulated in Table I.

The "expected count" was computed from evaluation of the geometry and the conversion yields. The calculations were checked by observing the gamma-rays originating directly from the target.[4] The expected count is estimated to be certainly correct to within a factor of 3. We can conclude, therefore, that $f<2\times10^{-3}$ for CH_2 and $f<6\times10^{-3}$ for LiH. It is thus clear that the absorption probability is not simply proportional[12] to Z, but that a special mechanism favors the absorption on a higher Z nucleus. This mechanism operates as follows. Once a π^- meson is captured by a hydrogen nucleus in an outer Bohr orbit, the atom loses its electron and hence its chemical binding. The lifetime of the resulting excited π^-−H system toward radiation into the K shell is long compared with the collision time with other nuclei, during the collision of the π^-−H system with a heavier nucleus, the probability is large that the π^- be captured by the heavier nucleus with the consequent production of a nuclear star, rather than a gamma-ray. Approximate estimates of the value of f have been made on the basis of this mechanism and are not inconsistent with the observations.

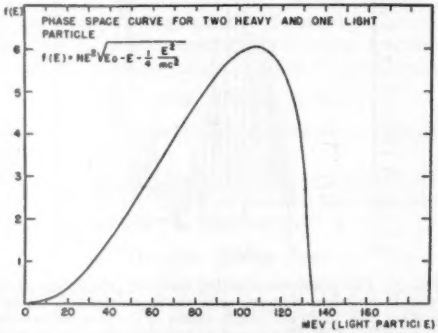

FIG. 14. Plot of the function giving the energy distribution of gamma-rays from the process $\pi^-+D\rightarrow2n+\gamma$ for a constant matrix element.

It has been suggested by Barkas[27] that π^0 emission might compete with nuclear stars induced by π^- capture. This is energetically possible if the mass of the capturing nucleus (Z, A) is less than that of the resulting $(Z-1, A)$ by less than the π^-−π^0 mass difference, δ. In particular if the corresponding β transition $(Z-1)\rightarrow Z$ is allowed, the gamma-rays from the disintegration of the resulting π^0 might be observable. This possibility is now being studied. A special case in this class is absorption in deuterium, studied theoretically by Marshak and his co-workers;[28] we shall discuss the process in the next section.

TABLE I. Tabulation of gamma-ray yield from the absorption of π^--mesons in hydrogeneous materials. (f= fraction of π^--mesons absorbed ultimately by a proton.)

Absorbing material	Gamma-ray energy (Mev)	Expected count (c/hr)	Observed count (c/hr)
CH_2	135	$5000f$	0±2
LiH	135	$1500f$	0.5±2
LiH	68	$1500f$	−1±4

VII. ABSORPTION IN DEUTERIUM

(a) Discussion of the Process

The absorption of π^- mesons in deuterium can lead to processes analogous to those previously outlined, in addition to pure heavy particle emission in the form of two neutrons. We consider thus the processes

$$\pi^-+D\rightarrow2n, \tag{15}$$

$$\pi^-+D\rightarrow2n+\gamma, \tag{16}$$

$$\pi^-+D\rightarrow2n+\pi^0. \tag{17}$$

Process (15) will lead to monoenergetic neutrons. At first sight one might expect that process (16) would lead to a very broad gamma-ray spectrum. This is actually not so, since if the gamma-ray has low energy the conservation laws are satisfied only if the neutrons are emitted nearly exactly in opposite directions. Consequently large gamma-ray energies will be favored. One can show easily that, in the absence of angular correlation between the particles, the gamma-ray distribution is given by

$$N_\gamma dE=(E_0-E-E^2/4M_nc^2)1/2^{\frac{1}{2}}E^{\frac{1}{2}}dE, \tag{18}$$

[27] W. H. Barkas, private communication.

[28] S. Tamor, Phys. Rev. 79, 221 (1950); R. E. Marshak, private communication.

where $E_0 = M_\pi - + M_D - 2M_n$. (See Fig. 14.) Actually, we shall see that the spectrum is still considerably narrower.

The spectrum of process (17) is expected again to lie between boundaries defined by the Doppler effect of the moving π^0. Because of the extra energy required in dissociating the deuteron, the peak is expected to be narrower. Using the foregoing value for the π^0 mass, the kinetic energy of the π^0 is approximately 1.9 ± 1.0 Mev. Process (17) is thus energetically permitted nominally although the π^0 mass accuracy is not sufficient to establish this fact beyond reasonable doubt.

(b) Experimental Results

Two experimental runs on deuterium were performed in the geometry, pressure, temperature, and spectrometer setting identical to the conditions under which the high energy spectrum of the absorption of π^- in H_2 was taken (Fig. 7). Accordingly, we feel safe in comparing the yields of the two processes by assuming that the same number of π^- mesons reach the K shell in the two cases for a given proton bombardment of the primary target. There might be two qualifications to this statement. Both with H_2 and D_2 we are dealing with the same number of electrons/cm^3 and thus comparable stopping power. The time required to reach an outer Bohr orbit is thus identical in the two cases. However, the time required for transition to lower states depends on collision processes;[12] the situation here is thus not quite identical in the two cases. Furthermore, possible capture from an orbit other than an S orbit depends, of course, on the process in question.

An experiment was carried out to determine whether an appreciable number of π^- mesons were lost by $\pi - \mu$ decay before reaching the K shell. If the time of the energy reduction process by collision were comparable to the $\pi - \mu$ decay time (contrary to the calculation by Wightman[12]), then the yield of gamma-ray from H_2 would fall off more rapidly with reduced density than the density itself. Table II shows the observed gamma-ray intensities at the usual operating pressure (2700 psi) and at reduced pressure.

Clearly, no significant nonlinear decrease is observed. Accordingly, we conclude that in agreement with Wightman,[12] no significant $\pi - \mu$ loss occurs; and hence, the intensity comparison between H_2 and D_2 γ-yields are valid. The evidence for process (15) (see Table III) thus rests on a good quantitative basis. A separate experiment now in progress[29] also tentatively confirms the existence of fast neutrons correlated to the presence of deuterium in the pressure vessel.

The spectrum corresponding to the spectrum of Fig. 7 is shown in Fig. 15. The first conclusion is that its spectrum does not conform to the momentum space function plotted in Fig. 14. The reason is that the two slow neutrons involved cannot be considered free but will interact to favor a small relative velocity between the neutrons. This will result in a spectrum peaked toward high energy. The effect is analogous to the high energy peak observed in the π^+ spectrum formed in $p - p$ collisions,[30] there the $n - p$ interaction favors a high π^+ energy. The low internal energy of the deuteron will also favor low relative velocities between the two neutrons.

[29] K. Crowe and H. F. York (private communication).

TABLE II. Tabulation of the relative gamma-ray yields from H_2 at 2700 psi and 1300 psi. Intensities are tabulated in terms of counts/minute. Total quadruple coincidences in the proportional counters, total number of recorded pairs, and the pairs corresponding to the high energy peak only are tabulated.

	Intensity in counts/minute		
	2700 psi	1300 psi	Ratio
Total number of quadruple coincidences	0.853 ± 0.033	0.523 ± 0.042	1.63 ± 0.14
Total number of gamma-rays recorded on multiple channel unit	0.302 ± 0.021	0.190 ± 0.027	1.60 ± 0.25
Gamma-rays recorded in the high energy peak only	0.213 ± 0.013	0.121 ± 0.017	1.74 ± 0.27
Density	0.046	0.028	1.65

The second result is the apparent absence of the π^0 peak. A separate run was made with the spectrometer centered at 70 Mev in order to place more rigid limits on the π^0 intensity. The observed counts are given in Table III. Since the H_2 spectrum shown in Fig. 7 was obtained under comparable conditions, we can directly compare the gamma-yields. This comparison is given in Table III. The intensity of the fast neutron yield (process 15) is only inferred from the intensity balance with hydrogen and does not represent direct observation.

VIII. CONCLUSIONS

In a qualitative sense the results reported here confirm some of the already reasonably well-established facts concerning π-mesons. (1) The existence of the monochromatic high energy peak from hydrogen proves that the π^- meson is a boson. (2) A π^0 meson exists[4,10]

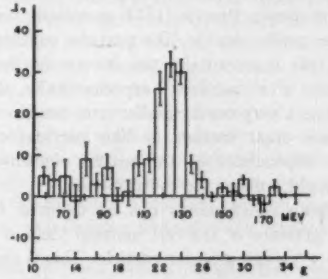

FIG. 15. Pair spectrum resulting from π^- capture in deuterium. The spectrometer center is set near 130 Mev.

[30] Cartwright, Richman, Whitehead, and Wilcox, Phys. Rev. 78, 823 (1950); V. Z. Peterson, Phys. Rev. 79, 407 (1950).

TABLE III. Summary of relative intensities of various processes obtained as a result of π^- capture in various materials. Tabulated values are given in counts per minute. In the case of single gamma-ray processes this represents the counting rate of the spectrometer; in the case of π^0 emission it represents $\frac{1}{2}$ times the spectrometer rate. The "two fast neutrons" count does not represent direct observation but only the intensity inferred by balancing counts between hydrogen and deuterium absorption.

Particle emitted \ Absorber	H	D
π^0	0.45 ±0.09 c/m	−0.007±0.020 c/m
Single γ	0.470±0.046 c/m	0.275±0.034 c/m
Two fast neutrons		0.65 ±0.11

and it disintegrates into two photons; it thus must be a spin zero particle. (3) The electrostatic self-energy or other causes make the π^- heavier than the π^0 by about 11 electron masses. (4) As long as emission of the π^0 can be in an S state only, the π^0 and π^- must be particles of identical parity properties. Considering the large kinetic energy of the π^0 emitted in process (4), this conclusion is no longer rigorous.

A quantitative result which might permit interpretation at the present time is the branching ratio between π^0 and γ-emission and the ratio between $2n$ and γ-emission in deuteron capture. By elementary notions mesons are strongly coupled to nuclei while photons are weakly coupled; therefore a branching ratio close to unity seems paradoxical, since the π^0 phase space factor $p/M_\pi c$ is as large as $\frac{1}{4}$. Processes (2) and (4) are essentially the inverse of photo meson production and of "charge exchange" scattering of π-mesons on nucleons. By a detailed balancing argument the ratio of cross section for such processes would be of the order of unity. Actually, at high energies it appears as though the photo production cross sections for mesons are well below nuclear interaction cross sections of mesons; but consideration should be given to the fact that the energies involved in the capture experiment and the inverse processes mentioned are dissimilar.

A very analogous difficulty appears in the case of the deuterium results. Process (15) is essentially the inverse of meson production in like particle collisions[30] and process (16) is essentially the inverse of the photo-production of π^- mesons;[31] experimentally, the latter process has a very much smaller cross section than the production cross section in like particle collisions. Again a dependence of the matrix elements on π^- energy could remove the contradiction.

A definite result which can be deduced from the inferred presence of the fast neutron yield is the fact that the π^- is not a scalar particle. This is clear, since the process

$$\underset{S\text{-orbit}}{\pi^-} + D \rightarrow 2n \quad \underset{}{} \quad \underset{}{} \qquad (19)$$
$$\qquad\quad {}^3S \quad {}^1S \text{ or } {}^3P$$

violates either parity or angular momentum conservation for a scalar π^-. Capture from a p-state might weaken this selection rule; however, calculations by Bruecker and Watson[32] indicate that the lifetime for radiation from a p-orbit is very short compared with the capture time, so that this effect can be neglected.

The absence of the π^0 peak in the case of π^- capture by deuterium is not surprising. If the π^- and π^0 are particles of equal parity, then in the process

$$\underset{S\text{-orbit}}{\pi^-} + D \rightarrow 2n + \underset{P\text{-wave}}{\pi^0} \qquad (20)$$
$$\qquad\quad {}^3S \quad {}^3P$$

both the π^0 and the two neutrons must be emitted in odd states of angular momentum as indicated, in order to obey conservations of parity and angular momentum and the exclusion principle. This effect[28] produces a greatly retarded yield at the small π^0 energy available.

Direct calculations of the branching ratio based on various combinations of meson character and coupling have been made by several authors.[21, 22] The formal perturbation calculations show that the number of possibilities of meson character and coupling is greatly reduced by the results of this experiment.

It has been shown quantitatively by Brueckner, Serber, and Watson[21] that the variability of the matrix element, predicted by the comparison of branching ratio measurements reported here with the inverse processes, is subject to experimental check by measurements of the excitation function of meson production in p–p collisions.

As a further remark it might be mentioned that there exists here, of course, no positive proof that the π^0 mesons as observed here are identical with the π^0 observed as produced by nuclear collisions[4–9, 10] and photo-production,[19] but the inference appears to be justified.

The authors have benefited greatly by the active cooperation of many members of this Laboratory. In particular the help of Dr. Herbert F. York during the first phases of the experiment has been indispensable. We are also indebted to Robert Meuser and Hugh Smith for mechanical design, to Mr. Alex Stripeika for assistance in electronics, and to the cyclotron crew under Mr. James Vale for the bombardments and assistance in the adjustments. The authors have also gained valuable information by discussions with Doctors Marshak, Serber, Wick, Brueckner, and Watson. Mr. Robert Phillips has actively participated in the execution of the experiment and has been of invaluable assistance.

[31] Peterson, McMillan, and White, Science **110**, 579 (1949).

[28] Brueckner, Serber, and Watson, Phys. Rev. **81**, 575 (1951).

The Capture of π-Mesons in Deuterium

K. Brueckner, R. Serber, and K. Watson
Radiation Laboratory, Department of Physics, University of California, Berkeley, California
(Received October 27, 1950)

Panofsky, Aamodt, and Hadley find that the capture of π-mesons in deuterium leads to two neutron emission in 70 percent of the cases, and to two neutrons and a γ-ray in the other 30 percent. The former process is forbidden for capture of scalar mesons from the K shell. A detailed balancing argument, based on the observed cross section for $2p\rightarrow D+\pi^+$, permits calculation of the non-radiative capture rate from orbits of higher angular momentum. It is shown that this is too small to account for the observation, and the possibility that the meson is a scalar is thus ruled out. This conclusion could only be avoided by postulating the existence of an interaction between meson and nucleons sufficiently large to alter radically the magnitude of the p-wave functions near the nucleons. For pseudoscalar mesons, non-radiative capture from the K shell is permitted, and the ratio of radiative to non-radiative transitions can be related to the ratio of meson photoproduction cross section to the cross section for $2p\rightarrow D+\pi^+$. The result is compatible with the type of meson-nucleon coupling which might be expected for pseudoscalar mesons, but uncertainties in the measured quantities are too large to permit a sharper conclusion.

I. INTRODUCTION

IN the preceding paper Panofsky, Aamodt, and Hadley[1] report that the capture of negative mesons by deuterons occurs in either of two ways, leading to the emission of two neutrons in 70 percent of the cases, and to two neutrons and a γ-ray in the other 30 percent. The first point of interest is that the two neutron process occurs at all. For if the π^- meson satisfied a scalar wave equation, and if the capture of the π^- took place from the K shell of the π^-+D system, this process would be forbidden, as Ferretti[2] has pointed out. The reason is that an s-state of the π^-+D system would have a total angular momentum $J=1$, and be an even state, whereas the only state of the two neutron system with $J=1$ is a ^3P-state, which is odd. Thus, the emission of two neutrons in about 70 percent of the captures proves either that the meson is not a scalar, or that the capture takes place from a higher Bohr orbit than the K shell, an orbit with $l\neq 0$.

To decide between these two possibilities we must estimate the rate, from the higher meson states, of capture with two neutron emission. We shall attempt to do this without recourse to an explicit meson theory, since we have learned by experience that meson theory cannot always be relied on even for orders of magnitude. In fact, we know of no meson theory which is not in gross disagreement with at least one of the presently believed experimental facts. The possibility of estimating the capture rate depends on the principle of detailed balancing. Although the cross section for the inverse of $\pi^-+D\rightarrow 2n$ has not been measured, it may reasonably be supposed that the reactions $2n\rightarrow D+\pi^-$ and $2p\rightarrow D+\pi^+$ have the same cross section. The latter reaction has been studied by Cartwright, Richman, Wilcox, and Whitehead,[3] who obtained a cross section $\sigma(2p\rightarrow D+\pi^+)=2\times 10^{-28}$ cm^2 for 340-Mev protons bombarding hydrogen. The most direct experimental support for the supposition of charge symmetry comes from work of Bradner, Bowker and Rankin,[4] who found a ratio of negative to positive mesons of 15 from carbon bombarded by 260-Mev neutrons, and the reciprocal ratio from carbon bombarded by protons of the same energy.

In the 340-Mev $2p\rightarrow D+\pi^+$ experiments the kinetic energy available in the center of mass system is 22 Mev. The principle of detailed balancing will give us the rate of $D+\pi^-\rightarrow 2n$ for 22-Mev relative energy of meson and deuteron, and we must extrapolate to lower energy to make the desired connection. The question is thus the dependence of the transition matrix element on meson momentum. Since the wave function, $\phi(\mathbf{r})$, of a meson in a p-state vanishes at the origin, we can write, for small $\mathbf{r}$,

$$\phi(\mathbf{r})=\mathbf{r}\cdot\operatorname{grad}\phi(0). \tag{1}$$

Here $\mathbf{r}$ is the coordinate of the meson relative to the center of mass of the deuteron. Thus $\phi(\mathbf{r})$, and the matrix element, will be proportional to the momentum of the meson near the deuteron, as long as (1) is adequate, which will be true as long as the wavelength of the meson is large compared to the distances, $\mathbf{r}$, which contribute to the process. The values of $\mathbf{r}$ in question are certainly not larger than the radius of the deuteron (which is about the same as the wavelength of a 20 Mev meson), but in fact will be considerably smaller because of the high relative energy (μc^2) which must be transferred to the nucleons. Such high energy transfers will occur only in intimate collisions of the nucleons; if the

[1] Panofsky, Aamodt, and Hadley, Phys. Rev. **81**, 565 (1951).
[2] B. Ferretti, *Report on the International Conference on Low Temperatures and Fundamental Particles* (Cambridge, 1946), p. 75. S. Tamor, Phys. Rev. **78**, 221 (A) (1950).
[3] Cartwright, Richman, Wilcox, and Whitehead (private communication). Although the experimental energy resolution is not good enough to establish conclusively the high energy meson peak as due to $2p\rightarrow D+\pi^+$ rather than $2p\rightarrow p+n+\pi^+$, we shall clearly overestimate the rate of capture in deuterium if we ascribe the observed cross section to the former process.
[4] H. Bradner (private communication).

transfer takes place in a single collision of the nucleons the distance would be about the wavelength of the neutrons, $r\sim\hbar/(M\mu)^{\frac{1}{2}}c=4\times10^{-14}$ cm. Since the wavelength of a 20 Mev meson is about five times larger, the proportionality of the matrix element to meson momentum would be expected to hold over the energy range in question.[5]

In addition to its dependence on the relative momentum of meson and deuteron, the matrix element will also depend on the neutron momenta. However, as the meson energy changes from 20 Mev to zero, the neutron momenta change by only 7 percent. We shall therefore neglect this dependence. In fact, quite apart from questions of the trustworthiness of meson theory, one of the advantages of using the detailed balancing argument is that in the calculation of the capture rate one avoids the question of the magnitude of high frequency Fourier components of the deuteron wave function, since nearly the same Fourier components are involved in the production process.

Finally, it should be pointed out that the foregoing argument assumes that there does not exist an interaction between meson and nucleons sufficiently strong to radically change the form of the p wave-function near the nucleons. Were such an interaction present, the argument would, of course, be invalidated.

II. THEORY

Let us denote by $R(\pi^-+D\rightarrow 2n)$ the rate of capture from a bound p-state, and by $\sigma(\pi^-+D\rightarrow 2n)$ the cross section of this process for an unbound meson. In the latter case let v_π and p_π be the relative velocity and momentum of meson and deuteron, v_n and p_n those of the two neutrons. According to the argument following (1), the ratio of the capture rate, $R(\pi^-+D\rightarrow 2n)$, from the bound state to the capture rate, $v_\pi\sigma(\pi^-+D\rightarrow 2n)$, from a plane wave of unit amplitude should be the ratio of the square of the gradient of the bound state function, $|\nabla\phi(0)|^2$, to the square of the same quantity for the plane wave, $p^2/\hbar^2$. Thus

$$R(\pi^-+D\rightarrow 2n)=\hbar^2 v_\pi\sigma(\pi^-+D\rightarrow 2n)|\nabla\phi(0)|^2/p_\pi^2. \quad (2)$$

TABLE I. A comparison is given of the transition rates for meson absorption and radiation to the ground state from the lower p state Bohr orbits.

Transition from the state	Transition rates in units of 10^{10} sec^{-1} Decay by fast neutron emission	Radiation to ground state
$2p$	0.94	17.2
$3p$	0.33	5.1
$4p$	0.15	2.2

[5] For states with $l>1$, the matrix element will fall off even more rapidly as the momentum is reduced. Use of a linear momentum dependence, which is tantamount to assuming the entire production process takes place from p-states, can therefore only overestimate the rate of meson capture.

The principle of detailed balancing gives

$$\sigma(\pi^-+D\rightarrow 2n)=\tfrac{2}{3}p_n^2\sigma(2n\rightarrow D+\pi^-)/p_\pi^2. \quad (3)$$

The factor $\frac{2}{3}$ is the product of 4/3, for the statistical weight of the spin states, and $\frac{1}{2}$, to allow for the indistinguishability of the two neutrons. Combining (2) and (3) we find

$$R(\pi^-+D\rightarrow 2n)=\tfrac{2}{3}\hbar^2 p_n^2\sigma(2n\rightarrow D+\pi^-)|\nabla\phi(0)|^2/\mu p_\pi^3,$$

where μ is the reduced meson mass, or using the approximate energy relation, $p_n^2/M=\mu c^2$, with M the neutron mass, and the assumption of charge symmetry,

$$R(\pi^-+D\rightarrow 2n)=\tfrac{2}{3}\hbar^2 Mc^2\sigma(2p\rightarrow D+\pi^+)|\nabla\phi(0)|^2/p_\pi^3. \quad (4)$$

If we put in the value of $|\nabla\phi(0)|^2$ for a p-state of principal quantum number, n, we find

$$R(\pi^-+D\rightarrow 2n)=(2/9\pi)\hbar^2 Mc^2(n^2-1)\sigma(2p\rightarrow D+\pi^+)/n^5a^5p_\pi^3, \quad (5)$$

where a is the mesonic Bohr radius, $a=\hbar^2/\mu e^2$. With the measured value of $\sigma(2p\rightarrow D+\pi^+)$, (5) gives

$$R(\pi^-+D\rightarrow 2n)=1.0\times10^{11}(n^2-1)/n^5 \text{ sec}^{-1}.$$

In Table I this transition rate is compared with that for the radiative transition of the meson from the np-state to the $1s$-state. For $n>3$ it is estimated that the transition rate by molecular collisions should predominate over that for radiation. The table shows that the rate of the two neutron process is at least thirty times too small to account for the observed ratio of $\pi^-+D\rightarrow 2n$ to $\pi^-+D\rightarrow 2n+\gamma$.

The supposition that the meson is a scalar can, thus, be excluded, unless, indeed, the alternative of a large meson-nucleon interaction is the true one. If we imagine such an interaction to be representable by a short range potential well, it is evident that, in order to greatly change the p-wave function near the nucleon, the strength of the interaction must be nearly great enough to contain a bound p-state in the well; that is, nearly great enough to produce an isobaric state of the nucleon.

If the π-meson is a pseudoscalar particle, the angular momentum and parity selection rules allow non-radiative capture from the K shell of the π^-+D system. The question then is whether the observed ratio of the radiative and non-radiative processes can be easily understood.

If we suppose that s-states alone, rather than p-states, are involved in the reactions $\pi^-+D\rightarrow 2n$ and $2p\rightarrow D+\pi^+$, the relation (4) would have the factor $\hbar^2|\nabla\phi(0)|^2/p_\pi^2$ replaced by $|\phi(0)|^2$. There is, however, no reason to exclude p-states from the production process, and we shall write

$$R(\pi^-+D\rightarrow 2n)=\frac{2}{3}\frac{Mc^2\sigma(2p\rightarrow D+\pi^+)|\phi(0)|^2}{p_\pi(1+bp_\pi^2/\mu^2c^2)}, \quad (6)$$

where the term in the denominator proportional to p_π^2

represents the p-state contribution (relative to that of the s-state) to $\sigma(2p\rightarrow D+\pi^+)$. Indeed, it is characteristic of pseudoscalar meson theory that it describes the meson-nucleon interaction as primarily taking place in the p-state, the s-state coupling arising only from "small" relativistic correction terms. The smallness of these terms is characterized by the mass ratio μ/M, which is not, in truth, a very small parameter. According to the theory, the constant b would be of order M/μ.

To obtain the rate of the $\pi^-+D\rightarrow 2n+\gamma$ reaction, we shall again appeal to the principle of detailed balancing, making use of the information available on the photoproduction process, $\gamma+n\rightarrow p+\pi^-$. This can be regarded as the inverse of the radiative capture in deuterium to the extent that the presence of the additional neutron does not affect the capture rate. We have calculated the effect to be expected because of the exclusion principle and the existence of n-n forces in the final state, and conclude that the capture rate in deuterium will be reduced by a factor, f, of approximately two-thirds.[6] In analogy with (2), we now have

$$R(\pi^-+D\rightarrow 2n+\gamma)=fv_\pi'\sigma(\pi^-+p\rightarrow n+\gamma)|\phi(0)|^2,$$

where $\sigma(\pi^-+p\rightarrow n+\gamma)$ is the cross section for this reaction for very slow mesons, of velocity v_π'. From detailed balancing,

$$\sigma(\pi^-+p\rightarrow n+\gamma)=2\mu c^2\sigma(n+\gamma\rightarrow p+\pi^-)/p_\pi'^2,$$

so

$$R(\pi^-+D\rightarrow 2n+\gamma)=2f\mu c^2\sigma(n+\gamma\rightarrow p+\pi^-)|\phi(0)|^2/p_\pi'. \quad (7)$$

In this equation, $\sigma(n+\gamma\rightarrow p+\pi^-)/p_\pi'$ is to be evaluated just above threshold.

The experiments of Steinberger and Bishop[7] on photoproduction in hydrogen give an approximate value of the cross section $\sigma(\gamma+p\rightarrow n+\pi^+)=7\times 10^{-29}$ cm^2 for a γ-ray of 180 Mev, corresponding to 23-Mev relative energy of meson and neutron in the center of mass system. According to an argument of Brueckner and Goldberger,[8] the cross section for $\gamma+n\rightarrow p+\pi^-$ would be expected to be larger, for non-relativistic meson energies, in the ratio $1/(1-\mu/M)^2=1.3$. The existence of a negative excess in the photoproduction from carbon has been demonstrated experimentally by McMillan, Peterson, and White[9] and Peterson.[10] While there is some doubt as to how well the observations agree in detail with the predictions of Brueckner and Goldberger, there is no doubt that the negative to positive ratio is at least as large as is indicated above. We shall accordingly take $\sigma(\gamma+n\rightarrow p+\pi^-)=10^{-28}$ cm^2. Since the lowest energy for which experimental data is available is that just quoted for production of 23 Mev mesons, while (7) requires the cross section just above threshold, an assumption about the energy dependence of the photoproduction cross section is necessary. If the matrix element for the process is a constant (i.e., if the variation of the cross section is determined solely by the available phase space), over this energy range, $\sigma(n+\gamma\rightarrow p+\pi^-)p_\pi'$ will be independent of energy, and the 23 Mev value can be used in (7). While this assumed energy dependence is the one to be expected on the basis of pseudoscalar meson theory, it should be emphasized that it is not based on any direct experimental information: our present knowledge of the excitation function for the photoproduction of mesons is not sufficiently accurate to permit an unambiguous extrapolation to zero energy.

The ratio of (7) to (6) gives

$$\frac{R(\pi^-+D\rightarrow 2n+\gamma)}{R(\pi^-+D\rightarrow 2n)}=3f\frac{\mu p_\pi'\sigma(n+\gamma\rightarrow p+\pi^-)}{Mp_\pi\sigma(2p\rightarrow D+\pi^+)}(1+bp_\pi^2/\mu^2c^2). \quad (8)$$

Inserting 3/7 for the ratio of the R's, $f=\frac{3}{4}$, $\mu/M=1/7$, $p_\pi'/p_\pi=1$, $\frac{1}{2}$ for the ratio of the σ's, we find $(1+bp_\pi^2/\mu^2c^2)=3$. This evaluation, in view of the uncertainties in the measurements of the various quantities appearing in (8), can hardly be trusted to better than a factor of two. However, the result is quite compatible with the notions one has as to the proper behaviour of a pseudoscalar field; since $p_\pi/\mu c=1/2$, a value of b of the order M/μ is indeed permissible. Quite apart from the uncertainties in the measured quantities, it should also be pointed out that the value found here is in the nature of an upper limit for the s-state contribution, since if the photoproduction cross section decreases more rapidly with decreasing meson momentum than we have assumed, the s-wave coupling will be correspondingly reduced. Cartwright, Richman, Whitehead, and Wilcox[3] and Peterson[11] have found that mesons from the $2p\rightarrow D+\pi^+$ reaction have a markedly non-uniform angular distribution in the center of mass system, which shows quite definitely the existence of coupling to other than s states.

The absolute value of the capture rate given by (7), found by inserting $|\phi(0)|^2=1/\pi a^3$ and the previously quoted value of the cross section, is

$$R(\pi^-+D\rightarrow 2n+\gamma)=2.7\times 10^{14}\ \text{sec}^{-1}.$$

The capture of π^- mesons in elements heavier than deuterium leads characteristically to stars, rather than high energy γ-emission. Panofsky, Aamodt and Hadley[12] give as upper limits for the fraction of high energy γ-emissions 10 percent in helium and 0.5 percent in carbon. As we have previously remarked, the non-

[6] The effect of n-n forces, while modifying the γ-ray spectrum, does not appreciably influence the capture rate.
[7] J. Steinberger and A. S. Bishop, Phys. Rev. 78, 494 (1950).
[8] K. Brueckner and M. Goldberger, Phys. Rev. 76, 1725 (1949).
[9] McMillan, Peterson, and White, Science 110, 579 (1949).
[10] J. Peterson, Dissertation, University of California (1950).
[11] V. Z. Peterson (private communication).
[12] Panofsky, Aamodt, and Hadley (private communication).

radiative capture in deuterium depends on the probability of finding a high relative momentum of the nucleons in the deuteron. In more tightly bound systems this probability will be considerably larger. Crude estimates, based on a semi-empirical momentum distribution for the nucleons in carbon given by Chew and Goldberger,[13] indicate that an increase in the non-radiative capture rate by a factor as large as 30 may be expected. On the other hand, the rate of emission of high energy γ-rays will be reduced in the more tightly bound systems relative to deuterium, because of the greater inhibiting effect of the exclusion principle in the final state. The experiments of Peterson and White[14] and of Mozley,[15] on the photoproduction of mesons show that a proton bound in carbon has only one-third as large a photoproduction cross section, at 260 Mev photon energy, as a free proton. Calculations by Bruno[16] indicate that a similar reduction by a factor of three is to be expected in the radiative capture rate in carbon. The γ-ray emission rate can thus be expected to be reduced, relative to deuterium, by a factor two. The combination of these two effects leads to the expectation that the 30 percent of γ-emission found in deuterium will be reduced to something of the order of 0.5 percent in heavier elements.

Finally, it may be mentioned that if it be supposed that the π^- meson has spin one (despite the fact that the π^0 certainly has not, since it decays to two γ-rays), an explanation of the observed ratio of the $\pi^-+D\rightarrow 2n$ and $\pi^-+D\rightarrow 2n+\gamma$ processes can be based solely on selection rules. A vector meson in the K-shell would have odd parity, and $J=0$, 1, or 2. It could thus decay to the ${}^3P_{0,1,2}$ states of the two neutron system. However, a pseudovector meson would give states of even parity; those with $J=0$ and 2 could decay to the ${}^1S_0$ and ${}^1D_2$ two neutron states, but decay from the $J=1$ state would be forbidden. If we suppose the states are occupied in proportion to their statistical weights, a ratio of radiative to non-radiative transitions of 1/2 is thus to be expected.

[13] G. F. Chew and M. L. Goldberger, Phys. Rev. **77**, 470 (1950).
[14] J. M. Peterson and S. R. White, Phys. Rev. **78**, 84 (A) (1950).
[15] R. Mozley, Phys. Rev. **80**, 493 (1950).
[16] B. Bruno, private communication.

On the Density Spectrum and Structure of Extensive Air Showers*†

S. F. Singer
Applied Physics Laboratory, Johns Hopkins University, Silver Spring, Maryland
(Received July 19, 1950)

Experiments on the particle density spectrum and structure of extensive air showers were conducted in the Arctic regions by means of a G-M counter arrangement which allowed simultaneous measurements on showers of high and low densities. The mean densities investigated ranged from about 40 to 1000 particles/m². The integral density spectrum of shower particles at sea level was found to be $N(>\rho)=562\rho^{-1.4}$ hr^{-1} (ρ in particles/m²). With this spectrum it was possible to satisfy all the experimental data obtained with arrangements of various counter areas and multiplicities of coincidences. The decoherence curve of two counters, where extensive showers were first selected by a master coincidence, was found to be flat for small separations down to 7 cm, in disagreement with the results of other workers who did not select extensive showers. This result provides evidence against the existence of a large number of "cores" distributed throughout the extent of the shower.

No latitude dependence of extensive showers was found between geomagnetic latitudes $\lambda=50°$ and $\lambda=80°$ to 90°.

I. INTRODUCTION

EXTENSIVE air showers (Auger showers) are ascribed to the very high energy component of the cosmic radiation (10^{13}–10^{17} ev), and manifest themselves by blanketing areas of the order of 100 m radius with thousands, and even millions, of time-correlated particles. Their discovery by Auger[1] and his collaborators first provided evidence for the existence of cosmic-ray primary particles possessing nearly macroscopic energies (10^{17} ev is about 4 millicalories). In their initial experiments, Auger and his collaborators obtained estimates of the density and energy of air showers, and also described their principal features: the large number of particles, predominantly electrons produced in a cascade process; the existence of a heavy concentration of particles in the center of the shower forming the shower core; the penetrating quality of some of the shower particles.

The high energies of the shower-originating primary particles make the subject of considerable interest from the astrophysical point of view. Their presence must be explained by any successful theory of the origin of cosmic rays. It is also of importance to establish whether there exists an *upper limit* to the energy of cosmic-ray particles. It has been suggested[2] that our galaxy has a magnetic field of the order of 10^{-12} to 10^{-9} gauss extending over a distance of 10,000 parsecs. If cosmic rays originate in the galaxy, then there exists a critical energy (10^{13}–10^{16} ev) below which recirculating cosmic-ray particles will have a finite chance of hitting the earth. Particles of energy higher than critical will escape from the galaxy and hence will not be detected.

In practically all cosmic-ray studies the question of the existence or absence of a *geo*magnetic effect is of fundamental interest since it provides a means of establishing the ratio of momentum to charge of the primary particles responsible for the phenomenon under study. The normal latitude effect displayed by the total cosmic radiation, which is caused by the geomagnetic cutoff at lower latitudes of particles with energies in the range of 10^{10} ev or less, is not expected to be observed for extensive air showers. However, the possibility has been pointed out[3] of observing a latitude effect at high latitudes produced by a cutoff (due to radiation loss in the earth's magnetic field) at the high energy end of the primary particle spectrum (10^{17} ev).

Of great physical interest are studies which bear on the mode of origin of the extensive showers in the upper portion of the atmosphere. The complete description of their initiation process constitutes perhaps the central problem in the study of showers. The application of experimental techniques to this problem involves the study of certain properties of showers at relatively low altitudes sufficiently far removed from their place of origin so they can be termed "extensive." To allow discrimination between various types of proposed initiation mechanisms, a rather high degree of precision is necessary in certain of these measurements in view of the extrapolation involved in applying data obtained at low altitudes to processes occurring near the top of the atmosphere.

To gain more information on some of the problems just mentioned, it was decided to carry out a shower experiment along with other investigations conducted in connection with a U. S. Navy expedition into the Arctic during the summer of 1947. The following objectives were to be accomplished:

(1) A very careful absolute redetermination of the particle density spectrum of extensive air showers at sea level, and the extension of these measurements to a wider range of densities.

* Supported by the Navy Bureau of Ordnance.
† Based on a dissertation submitted to Princeton University, June, 1948, in partial fulfillment of the requirements for a Ph.D. degree.
[1] Auger, Maze, and Grivet-Meyer, Compt. rend. **206**, 1721 (1938).
[2] H. Alfvén, Z. Physik **107**, 579 (1937); L. Spitzer, Jr., Phys. Rev. **70**, 777 (1946).
[3] I. Pomeranchuk, J. Phys. (U.S.S.R) **2**, 65 (1940). See also Sec. VI.

(2) Verification of the concept of shower density over a variety of experimental arrangements to help resolve discrepancies in earlier work of other investigators.

(3) A new determination of the decoherence curve of two counters for small separations in order to gain more information about the structure of showers.

(4) Investigation of the existence of a latitude effect; in particular the "inverse" latitude effect suggested by Pomeranchuk.[3]

Experimentally, showers can be detected by coincidence counts between Geiger-Müller counters, generally located in a horizontal plane and separated by several meters, but so disposed that they cannot all be set off by a single particle. Care must be taken to insure that there is a minimum of material above the counters to avoid the effects of "local showers" which may be produced in the material by single particles. In the present experiments these precautions were carefully observed, the efficiencies and effective areas of the G-M counters used were measured in separate experiments, and considerable effort was spent in making the whole system completely reliable in order to assure an accurate measurement of the particle density spectrum. An improvement in technique was obtained by designing the equipment to collect data on showers of high and low densities simultaneously through use of a system of master and subsidiary coincidences. Then, in reduction of the data, counters could be considered in various parallel or multifold coincidence arrangements. The results obtained in this manner, in agreement with the findings of other workers, indicate that the *density spectrum* of particles in extensive showers can be expressed quite well in the form of an *inverse power law*. Furthermore, the *same* spectrum satisfies all the data obtained with *different* experimental arrangements. The results of the decoherence experiment clearly favor the existence of a single *central* shower core as opposed to a large number of subsidiary cores *distributed* throughout the extent of the shower. Comparison of the results obtained at $\lambda=50°$ with those obtained in the Arctic regions ($\lambda=80°$–$90°$) show an *absence* of any *latitude dependence*. As far as we can determine there are no comparable results of other investigators in this range of latitudes. The Pasadena group[4] in recent experiments at lower latitudes has similarly found no evidence for geomagnetic effects of extensive showers; their results may be regarded as complementary to ours.

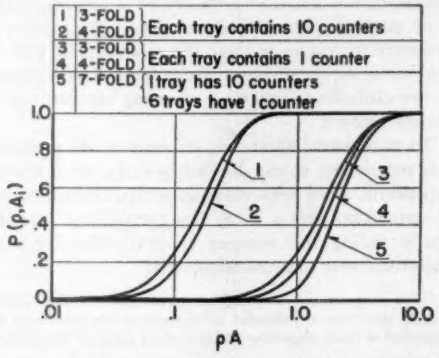

FIG. 1. Probability of obtaining a coincidence *vs* ρA (the number of particles per counter tube area A) for G-M counter arrangements of various areas and multiplicities of coincidence.

II. ANALYSIS OF COUNTER EXPERIMENTS ON SHOWER DENSITY[4a]

The utility of the concept of shower density (particles per unit surface area) is well known[5] and has been applied extensively to the analysis of counter experiments.[6–8] In analogy with the concept of intensity in telescope experiments, it enables one to express results in a manner which does not depend very strongly on the dimensions of the equipment, and thus provides a means of comparing the shower experiments of different workers. The concept is meaningful because (a) extensive showers contain a very large number of particles, and (b) the density does not vary appreciably over the dimensions of the usual experimental set-up (2 to 4 meters), i.e., distances which are a small fraction of the shower radius[9] (75 m at sea level), but large enough to assure that narrow showers which originate in the vicinity of the apparatus are not detected. Point (b) is perhaps subject to criticism if the equipment should be located near the core of the shower where a large density gradient exists; however, it has already been shown experimentally[6] that these events can be neglected. With the assumption of uniform density[9a] in the vicinity of the apparatus subject only to statistical fluctuations, the classical probability argument[5] can be applied to counter experiments. Assuming a shower density ρ particles/m^2, we find that the probability of missing a counter of area A m^2 is $\exp(-\rho A)$. The probability for the counter to be hit by one or more particles is

$$p(\rho, A)=1-\exp(-\rho A). \qquad (1)$$

The probability for n counters, of areas A_i, to be set

[4] Biehl, Neher, and Roesch, Phys. Rev. **76**, 914 (1949).

[4a] More precisely: *Local* particle density of an extensive air shower. The expressions "high density shower" and "low density shower" are not strictly correct. It is well known that the concept of "density of a shower" is not meaningful, since particle densities ranging from very low to very high values may be observed in the same shower depending on the distance of the point of observation from the shower core (see Appendix).

[5] C. G. Montgomery and D. D. Montgomery, Phys. Rev. **48**, 786 (1935).

[6] Cocconi, Loverdo, and Tongiorgi, Nuovo cimento **2**, 14 (1944); Phys. Rev. **70**, 841 (1946).

[7] P. Auger and J. Daudin, J. phys. radium **6**, 233 (1945).

[8] G. Cocconi and V. Cocconi-Tongiorgi, Phys. Rev. **75**, 1058 (1949).

[9] Defined as $E_s X_0/\epsilon$, where $E_s=21$ Mev, ϵ=critical energy, X_1=radiation length. See B. Rossi and K. Griesen, Revs. Modern Phys. **13**, 240 (1941).

[9a] The requirement of uniform density can be relaxed if in order to determine the shower density spectrum only the effective areas of the counter trays are changed in a proportional manner. It can be shown that it is then only necessary to assume that all showers—irrespective of the number of particles in the shower—have the same lateral structure function (see Appendix).

off by a shower with average density ρ at the location of the counters is the product of the independent probabilities

$$P(\rho, A_i)=\prod_{i=1}^{n}[1-\exp(-\rho A_i)]. \quad (2)$$

This expression also gives the probability of a coincidence count for a certain counter arrangement due to a shower of density ρ; in Fig. 1 $P(\rho, A_i)$ is plotted as a function of ρ for various combinations of n and A_i.

In general, the equipment will experience particle densities ranging from very low to very high values and occurring with frequencies given by a certain distribution of densities $\nu(\rho)$. The quantity $\nu(\rho)d\rho$ represents the number of showers per unit time with densities between ρ and $\rho+d\rho$ at the point of observation. The coincidence rate is then given as

$$C_n=\int_0^\infty P(\rho, A_i)\nu(\rho)d\rho. \quad (3)$$

Since $P(\rho, A_i)$ is a function which rises from zero to unity over a narrow interval of ρ, while $\nu(\rho)$ is found to be a rapidly decreasing function of ρ, the integrand of (3) shows a rather sharp maximum at a particular value of ρ. Thus, a specific experimental arrangement records predominantly events occurring with a particular value of density.[6,7] An integrand of the form in (3), computed for a certain density spectrum and coincidence arrangement, is shown in Fig. 2.

Integral (3) can be evaluated in closed form in certain special cases. Let the experimental density spectrum be represented by a power law of the form

$$\nu(\rho)d\rho=K\rho^{-\gamma}d\rho. \quad (4)$$

On substitution into (3) we find

$$C_n=\int_0^\infty \prod_{i=1}^{n}[1-\exp(-\rho A_i)]K\rho^{-\gamma}d\rho. \quad (3')$$

Expanding integral (3') we get

$$C_n=K\int_0^\infty \{1-[\exp(-\rho A_1)+\exp(-\rho A_2)+\cdots]$$
$$+[\exp(-\rho A_1-\rho A_2)+\exp(-\rho A_1-\rho A_3)$$
$$+\exp(-\rho A_2\rho-A_3)+\cdots]$$
$$-[\exp(-\rho A_1-\rho A_2-\rho A_3)+\exp(-\rho A_1-\rho A_2$$
$$-\rho A_4)+\cdots]+[\cdots]\}\rho^{-\gamma}d\rho.$$

Even though individual terms of the integral diverge, we can make use of the formula

$$\int_0^\infty x^n\exp(-Ax)dx=A^{-(n+1)}\Gamma(n+1)$$

and evaluate the integral (3') formally;[10] we find for the rate of coincidences

$$C_n=K\Gamma(1-\gamma)\{-[A_1^{\gamma-1}+A_2^{\gamma-1}+A_3^{\gamma-1}+\cdots]$$
$$+[(A_1+A_2)^{\gamma-1}+(A_1+A_3)^{\gamma-1}+(A_2+A_3)^{\gamma-1}+\cdots]$$
$$-[(A_1+A_2+A_3)^{\gamma-1}+(A_1+A_2+A_4)^{\gamma-1}+\cdots]\}. \quad (5)$$

We can apply expression (5) to our experimental results; the coincidence rates C_n are known for different experimental arrangements of counters, and we would like to determine whether the data can be correlated with a power law spectrum of particle densities $K\rho^{-\gamma}$. In other words, can we find a value for γ in (5) which will make the calculated coincidence rates fit the observed rates over the whole range of densities? After γ has been determined, the constant K can be normalized to the most precisely known experimental point.

Having obtained numerical values for K and γ, it is of some interest to determine the mean density of showers $\bar{\rho}$ as recorded by different arrangements of counters, and as defined by

$$\bar{\rho}\equiv C_n^{-1}\int_0^\infty \prod_{i=1}^{n}[1-\exp(-\rho A_i)]K\rho^{-(\gamma-1)}d\rho. \quad (6)$$

It is evident that (6) can be evaluated from expression (5) by substituting $(\gamma-1)$ for γ throughout.

Another arrangement of interest is that of n separate counters of equal area A which experience a shower of density ρ. The probability for particles striking any k counters and missing the remaining $(n-k)$ counters is from (2) and (1):

$$P_n(k)=\{n!/[k!(n-k)!]\}$$
$$\times[1-\exp(-\rho A)]^k[\exp(-\rho A)]^{n-k}. \quad (7)$$

$P_n(k)$ has been computed for $n=4$ and is plotted as a function of k in Fig. 3 for different values of ρ. In the experiment the densities involved are given by the spectrum (4) selected by a coincidence arrangement

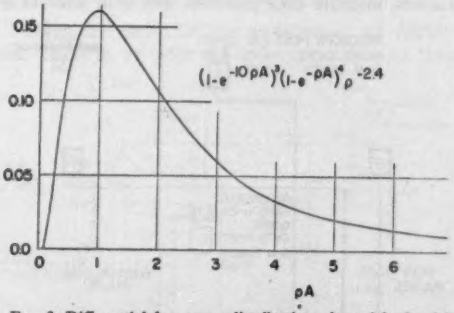

FIG. 2. Differential frequency distribution of particle densities in showers recorded with experimental arrangement ($ABCd^4$) (sevenfold coincidence between trays A, B, and C, each containing 10 counters, and 4 single counters in tray D). The "differential response function" of this particular experimental arrangement has been calculated using the density spectrum $\nu(\rho)\propto\rho^{-2.4}$. Note the sharp maximum corresponding to $\rho A\sim 1$, i.e., for a density of the order of one particle per counter area.

[10] The mathematical justification for this procedure is given by D. Broadbent and L. Jánossy, Proc. Roy. Soc. (London) **192**, 364 (1948).

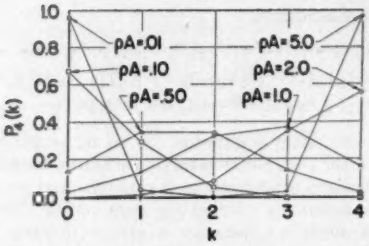

FIG. 3. Probability $P_k(k)$ for setting off a number k ($k=0, 1, 2, 3, 4$) out of 4 counters as a function of k for different average densities of shower particles.

and, therefore, modified by a probability function of the form (2): i.e.,

$$\nu'(\rho)d\rho = P(\rho, A_i)\nu(\rho)d\rho. \tag{8}$$

This expression might be termed the "differential response function" of the particular experimental arrangement described by (2); an example is shown in Fig. 2. If we select showers by means of a set of i counters of areas A_i in coincidence, the rate at which k counters out of n additional counters of equal area A are set off, is then given by the expression

$$C_n(k) = \int_0^\infty P_n(k)\nu'(\rho)d\rho. \tag{9}$$

These integrals can be evaluated by the procedure used to obtain Eq. (5).

The results of this section which are contained in Eqs. (3′), (6), and (9) will be used to interpret the experimental data in terms of a power law spectrum of particle densities and to establish the range of densities over which the power law is valid.

III. EXPERIMENTAL ARRANGEMENT

The arrangement which was used to detect the Auger showers, measure their densities, and gain some information concerning their structure was laid out on the signal deck of the USS Wyandot (AKA 92) as shown in Fig. 4. It consisted of four trays, each containing 10 G-M counters; they were designated, respectively, G-M trays A, B, C, and D, and located at the corners of a 2 m rhomboid. The equipment was designed to gather a large amount of data about individual showers, essentially by sampling each shower at twenty locations by means of twenty G-M counters. By analyzing the data so as to obtain the effects of various counter areas or multiplicities of coincidences, it was possible to determine the frequency distribution of densities $\nu(\rho)$.

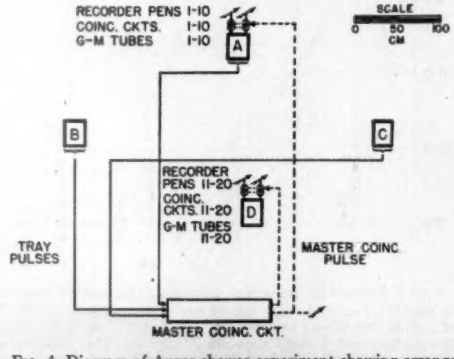

FIG. 4. Diagram of Auger shower experiment showing arrangement of G-M counter trays. Trays A, B, and C produce a master coincidence which is then used to establish subsidiary coincidences with the ten counters of tray A and the ten counters of tray D.

As has been shown by Cocconi, Loverdo, and Tongiorgi,[9] the counting rate of an arrangement of this type does not depend appreciably on the counter tray separation for distances of the order of two to eight meters. As can be seen from Fig. 4, the separation between trays B and C was about four meters. Furthermore, the trays were arranged so that no particle traveling in a straight line could set off more than two counter trays. The trays were housed in individual wooden boxes, whose temperatures were thermostatically controlled. Each tray was placed directly beneath the wooden cover which had a thickness of 0.6 g/cm². No other material was located above the trays.

The equipment operated in the following manner. In G-M trays A, B, and C, the outputs of the G-M counters were connected *in parallel* into the master coincidence circuit. An extensive shower which set off at least one counter in each of the three trays would operate the master coincidence circuit and produce a master coincidence pulse at the output of the circuit. Subsidiary coincidences were then formed between the master coincidence pulse and the twenty *individual* G-M counters of trays A and D. A 20-pen recorder indicated the counters in trays A and D which were set off by the Auger shower.

A detailed description of the experimental arrangement follows:

(a) Each G-M tray held ten self-quenching G-M counters, arranged side by side and touching, so as to form a large rectangular area. The counters were matched as to G-M threshold and flatness of plateau as determined by tests of counting rate *vs* voltage on exposure to a radium source. The threshold was around 960 volts; the counters were operated at 1100 volts. The counters were of the "all-metal" type with 0.8-mm thick copper walls, 0.10-mm tungsten wires, filled with a mixture of 10 cm argon and 1 cm absolute ethyl alcohol. In auxiliary experiments, the effective length of the counters was measured with an arrangement similar to that of Street and Woodward.[11] The active volume of the counters was found to be a cylinder 2.38 cm in diameter and 29.2 cm long, and effective area of 69.5 cm². The efficiency of these counters for cosmic-ray particles was tested in coincidence telescopes and found to be greater than 99.3 percent. The recovery time as measured on a cathode-ray oscilloscope was about 3×10^{-4} sec. No appreciable variation in the counting rate was found for temperatures between 10° and 100°C.

(b) The pulses of each G-M tube were fed into individual cathode followers, and then added into a common tray output by means of a crystal diode mixing circuit (Fig. 5). In the case of trays A and D, the outputs of the cathode followers were also connected to individual coincidence circuits to be described later.

[11] J. C. Street and R. H. Woodward, Phys. Rev. 46, 1029 (1934).

The tray counting rate due to radioactive background and cosmic rays was approximately 16 counts/sec for each of the four trays.

(c) In trays *B* and *C* provision was made for changing the tray counting area from its full value (10 counters) to one-tenth of the full value (one counter) by disconnecting nine counters from the high voltage supply.

(d) The master coincidence (MC) circuit (Fig. 6) was a Rossi-type triple coincidence circuit fed from trays *A*, *B*, and *C*. By measuring the accidental coincidence rate of two counter trays when they were exposed to radium sources, the resolving time of the MC circuit was determined to be 3×10^{-6} sec. The bias on the 6AQ5 output tube was set to give complete discrimination against double coincidences. The output (MC pulse) was a shaped negative 80 v square pulse, 8×10^{-6} sec wide, fed from a low impedance circuit to the twenty subsidiary coincidence circuits. To allow rapid testing of the G-M counters and coincidence and recorder circuits of trays *A* and *D*, a negative dc voltage ($-22\frac{1}{2}$ v) could be switched into the output of the MC circuit by the Operate-Test switch. It was effectively an artificial MC pulse, which was on continuously. The actual counting rates of the G-M counters of trays *A* and *D* were thereby recorded.

(e) Coincidence and recorder circuit trays were attached to G-M trays *A* and *D* (Fig. 7). Each had 10 independent sections—one for each G-M tube—consisting of a two-pentode coincidence

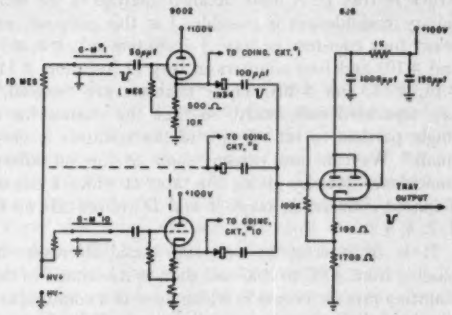

FIG. 5. Circuit for G-M trays *A* and *D*. In the circuits for trays *B* and *C* the outputs to the subsidiary coincidence circuits are omitted.

circuit and a thyratron driver for the recorder. The grid of the first pentode was connected to the corresponding G-M tube cathode follower in the G-M tray, the grid of the second pentode was fed from the MC circuit. These coincidence circuits had a resolving time of about 10×10^{-6} sec.

(f) An Esterline-Angus 20-pen operations recorder indicated by markings on paper tape the G-M counters set off by a shower. MC pulses were recorded directly through a thyratron driver circuit on the MC circuit chassis by a second tape recorder which was monitoring other experiments conducted on the same expedition.

(g) The resolving time in all coincidence circuits was sufficiently short to allow us to neglect all chance coincidences without further correction. At the same time, it was ample to allow for differences in the arrival time of pulses caused by spurious delays in G-M counters, fixed delays in circuits and cables, and possible differences in rise times of pulses.

For equipment to be used in the field which required stable operation over an extended period of time, reliability, coupled with a simple procedure for operational checks, was a most important requirement. Consequently, the following program was adopted:

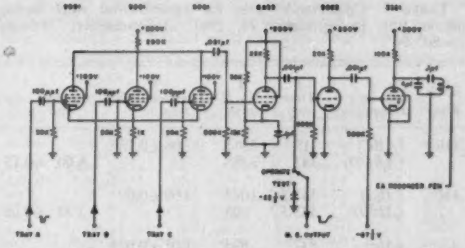

FIG. 6. Master coincidence circuit. With the switch in the TEST position the individual G-M counters and coincidence circuits of trays *A* and *D* are automatically checked for proper operation.

(a) In the original design of the circuits a large factor of safety was allowed for, so that variations in supply voltages, aging of vacuum tubes and components, temperature changes, etc., would not affect the proper operation of the experiment.

(b) Over-all checks were made on the system with an artificial pulser to establish the operating ranges of supply voltages and their interdependence. It was found, for example, that outside of this operating range, crosstalk caused by capacitive coupling between adjacent tray circuits would actuate recorder pens; or conversely, pens would fail to be actuated by genuine pulses.

(c) Detailed checks were made at every point of the system with artificial pulser and cathode-ray oscilloscope to establish critical levels of pulse height in the various circuits. With G-M counters active, the G-M pulses were later verified to be well above the critical levels.

(d) G-M counter rates were checked daily by means of a pulse scaling circuit and oscilloscope. A set of simple tests was evolved which were used for rapid trouble shooting but which were also applied daily to check the operation of all circuits and recorders.

(e) The problem of outside interference (electrical pick-up) was solved by proper electrical shielding and by making solid ground connections everywhere, particularly to the G-M counter shells and the negative side of the high voltage supply. Coaxial cable was used for all high voltage and pulse cables. To check absence of electrical pick-up, the high voltage on the G-M counters was reduced from 1100 v to 810 v (150 v below the G-M threshold). No coincidence counts were observed even when severe electrical interference was produced by operating a Tesla coil close by. Runs with reduced voltage were carried out periodically.

During the course of the experiments, all circuits were found to be quite stable in operation and their

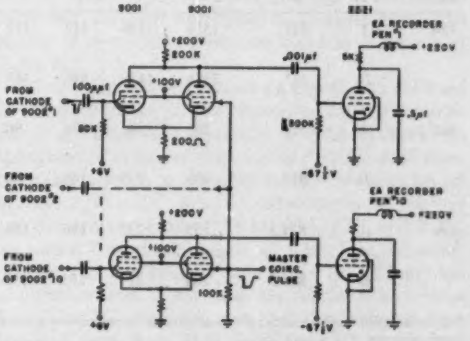

FIG. 7. Subsidiary coincidence and recorder circuits for trays *A* and *D*.

TABLE I. Coincidence rates for experimental runs during period July 16–September 24, 1947, at geomagnetic latitude $\lambda = 80°$–$90°$.

1 Run	2 Coincidence arrangement	3 Time (hr)	4 No. of coinc.	5 Threefold coinc. rate (hr^{-1})	6 Fourfold coinc. rate (hr^{-1})
ABC	(*ABC*)	410	5362	13.08±0.18[a]	
	(*ABCD*)	382	3286		8.60 ±0.15
AbC	(*AbC*)	347.5	1072	3.09±0.09	
	(*AbCD*)	345.5	805		2.33 ±0.08
Abc	(*Abc*)	847	893	1.05±0.035	
	(*AbcD*)	847	793		0.936±0.033

[a] All rates are corrected for accidental coincidences, counter efficiency, and counter dead time. All errors quoted are standard deviations assigned only on the basis of the number of counts, i.e., square root of number of counts divided by time.

characteristics did not have to be readjusted. It was not necessary to replace any of the G-M counters.

As a further check on the reasonableness of the results, a plot of the differential frequency distribution of time intervals between showers was prepared for certain portions of the experimental runs. As anticipated, it gave the exponential relation expected from random events.

IV. DENSITY SPECTRUM OF PARTICLES IN EXTENSIVE AIR SHOWERS

The experimental data will now be summarized and applied to the computation of a density spectrum. In 70 days of data collecting, about 7500 master coincidences produced by trays *A*, *B*, and *C* were observed, each accompanied by up to twenty subsidiary coincidences with the counters of trays *A* and *D*. Three types of experimental runs were carried out:[12]

(i) *ABC* Run: Trays *A*, *B*, and *C* each contain 10 counters.

(ii) *AbC* Run: Trays *A* and *C* each contain 10 counters, tray *B* only one active counter.

(iii) *Abc* Run: Tray *A* contains 10 counters, trays *B* and *C* only one active counter each.

Columns 5 and 6 of Table I show the striking change in counting rate when the area of a counter tray is changed, which reflects the rapid fall-off with density of the number of events of a given density. This decrease may be deduced from the consideration that the *ABC* arrangement is quite sensitive to low density events, which would thus appear to be very numerous; it also records all high density events, but their number is comparatively small. For *Abc* runs, however, it is only this small number of high density events which gives rise to the observed coincidences, since the sensitivity of the *Abc* arrangement to the low density events is practically zero (see Fig. 1).

In Table I the threefold coincidences are, of course, the master coincidences. The fourfold coincidences correspond to cases in which at least one counter was struck in tray *D*. A more detailed analysis of the subsidiary coincidences is possible. For this purpose, we select four counters in tray *A* (counters #1, #4, #7, and #10) and four counters in tray *D* (counters #11, #14, #17, and #20). These counters are "spaced," i.e., separated sufficiently, so that the chance for a single particle to set off two of the counters is very small.[13] We can now present some of the subsidiary coincidence data by giving the rates at which k out of 4 spaced counters in trays *A* and *D* are set off: $k = 0, 1, 2, 3, 4$.

It is of interest to note the rapid decrease—in passing from *ABC* to *AbC* and then to *Abc* runs—in the counting rate for events in which none of 4 counters are hit. At the same time we notice the very slight decrease in the rate for all out of 4 counters going off in the event of a shower. Another interesting fact is apparent

TABLE II. Rates with which k out of 4 spaced counters are set off in trays *A* and *D* for *ABC*, *AbC*, and *Abc* runs.

1 Run	2 Tray	3 Time (hr)	4 Number of counts $k=0$	1	2	3	4	5 Rates (hr^{-1}) $k=0$	1	2	3	4
ABC	*A*	317	1554	1769	519	232	140	4.87 ±0.12	5.58 ±0.13	1.64 ±0.07	0.73 ±0.05	0.44 ±0.04
	D	317	2331	1138	446	185	108	7.35 ±0.15	3.59 ±0.11	1.41 ±0.07	0.58 ±0.04	0.34 ±0.03
AbC	*A*	317	267	341	174	96	106	0.84 ±0.05	1.08 ±0.06	0.55 ±0.04	0.30 ±0.03	0.33 ±0.03
	D	317	403	255	161	86	78	1.27 ±0.06	0.80 ±0.05	0.51 ±0.04	0.27 ±0.03	0.25 ±0.03
Abc	*A*	831.5	152	222	146	154	207	0.183 ±0.015	0.267 ±0.018	0.176 ±0.015	0.185 ±0.015	0.249 ±0.018
	D	831.5	204	214	152	137	174	0.245 ±0.017	0.257 ±0.018	0.183 ±0.015	0.165 ±0.014	0.210 ±0.016

[12] Lower case letters indicate *one* active counter in the corresponding tray, upper case letters *ten* active counters.
[13] It will be shown in Sec. V that this assertion is indeed correct.

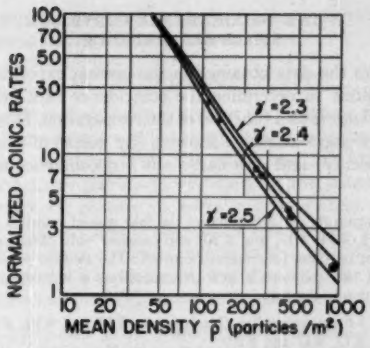

FIG. 8. Normalized coincidence rates vs mean density. The coincidence rates of nine experimental arrangements are plotted as circles. The size of the circle indicates the experimental error. These values are compared with the expected coincidence rates computed under the assumption of a differential density spectrum of the form $\nu(\rho)d\rho = K\rho^{-\gamma}d\rho$. It is seen in Table III that the exponent $\gamma = 2.4$ gives the best fit to the experimental points. The mean densities corresponding to the various experimental arrangements have been computed using $\gamma = 2.4$; their use as abscissa serves only the purpose of graphical presentation of the comparison in Table III.

from the data in Table II: the rate for all out of 4 counters is about 70 percent lower than the rate for 3 out of 4 counters in the case of *ABC* runs, about the same in the case of *AbC* runs, and about 20 percent *higher* in the case of *Abc* runs. The explanation, of course, rests on the fact that *Abc* runs, and to a lesser degree *AbC* runs, are sensitive only to high particle densities. The difference in the rates between trays *A* and *D* arises because at least one counter (out of 10) had to fire in tray *A* to produce a shower count, whereas tray *D* did not contribute to the master coincidence.

One can now select from the data coincidence combinations which are sensitive to even higher densities:

(i) (*abc*): Coincidence rate observed with one active counter in trays *A*, *B*, and *C*. This requirement is partially satisfied by *Abc* runs (*Abc*); to obtain the effect of a single counter in tray *A*, we fix our attention on one particular counter of tray *A* out of the four spaced counters and determine the rate at which it is hit by showers selected in *Abc* runs. (We have, of course, the data to get this rate directly; however, the procedure given below is more convenient to apply.) Clearly, if all 4 spaced counters of tray *A* are set off, our chosen counter is fired with a probability of 1; if 3 out of 4 counters fire, the probability for our counter is 3/4; for 2 counters the probability is 1/2, for 1 counter going out of 4, the chance for our counter is 1/4. Applying these weighting factors to the data of Table II, we get for the coincidence rate of three single counters

$$(abc) = 0.547 \pm 0.026/\text{hr}.$$

(ii) (*Abcd*): Using the procedure described above, we consider *Abc* runs and select one counter in tray *D*.

$$(Abcd) = 0.488 \pm 0.024/\text{hr}.$$

(iii) ($Abcd^4$): We consider *Abc* runs and require all four spaced counters in tray *D* to be struck.

$$(Abcd^4) = 0.210 \pm 0.016/\text{hr}.$$

TABLE III. Observed coincidence rates, and coincidence rates calculated using a power law density spectrum of the form $K\rho^{-\gamma}d\rho$. Mean densities $\bar{\rho}$ calculated using spectrum $787\rho^{-2.4}d\rho$ hr^{-1}.

1	2	3	4			5
Counter combination	Obs. coinc. rate (hr^{-1})	Obs. coinc. rate (normalized to $(ABC)=100$)	Calc. coinc. rate (normalized) $\gamma=2.3$	$\gamma=2.4$	$\gamma=2.5$	Mean density (No. of particles/m²)
(*ABC*)	13.08 ±0.18	100 ±1.4	100	100	100	45.7
(*ABCD*)	8.60 ±0.15	65.7 ±1.1	70.5	67.5	64.1	63
(*AbC*)	3.09 ±0.09	23.6 ±0.7	24.2	22.6	21.1	118
(*AbCD*)	2.33 ±0.08	17.8 ±0.6	20.2	17.6	16.3	144
(*Abc*)	1.05 ±0.035	8.0 ±0.27	9.0	7.7	6.6	268
(*AbcD*)	0.936 ±0.033	7.15 ±0.25	8.4	7.1	5.8	291
(*abc*)	0.547 ±0.026	4.18 ±0.20	5.0	4.0	3.2	457
(*Abcd*)	0.488 ±0.024	3.73 ±0.18	4.9	3.9	3.1	478
($Abcd^4$)	0.210 ±0.016	1.60 ±0.12	2.44	1.76	1.3	975

It is now possible to determine (a) whether the observed coincidence rates can be checked by calculation on the assumption of a power law density spectrum of the form $K\rho^{-\gamma}$, and (b) if such a spectrum exists, what are the values for K and γ.

It can be seen from Table III and Fig. 8, which incorporates the data of Table III, that the differential density spectrum can indeed be represented by a power law expression of the form $K\rho^{-\gamma}$. The calculated coincidence rates C_n were obtained from Eq. (3′) using the following values for the differential spectrum exponent: $\gamma = 2.3$, $\gamma = 2.4$, $\gamma = 2.5$. It is seen that the experimental values (column 3) agree very closely with the $\gamma = 2.4$ results. They differ considerably from the $\gamma = 2.3$ and the $\gamma = 2.5$ results. This comparison indicates the sensitivity of the agreement between experimental and calculated coincidence rates to the value of the spectrum exponent γ. On comparison of the absolute observed coincidence rate per hour with the value of the integral (3′) calculated using $\gamma = 2.4$, we find K to be 787 hr^{-1}, so that finally we obtain as the differential density spectrum of extensive air showers at sea level

$$\nu(\rho)d\rho = 787\rho^{-2.4}d\rho \text{ hr}^{-1}, \tag{10}$$

where ρ is given in particles/m².

It is now of some interest to calculate with the help of our experimentally determined density spectrum and Eq. (6) the mean particle densities which were recorded with the different experimental arrangements. The results of these calculations are listed in column 5 of Table III.

We next want to make use of a group of data obtained in this experiment, but not employed for the determination of the density spectrum, in order to check the spectrum law independently. Let us consider *ABC* runs, i.e., cases in which at least one counter has been set off in trays *A*, *B*, and *C*. If we fix our attention on the four spaced counters of tray *D* (#11, #14, #17, and #20), we notice that combinations of them (i.e., (i) none, (ii) one, (iii) any two, (iv) any three, (v) all four) fire at different rates. These rates are tabulated in column 5 of Table II, where it is seen that they decrease by a factor of more than 20 in going from (i) no counters firing to (v) all counters firing. It is now possible to

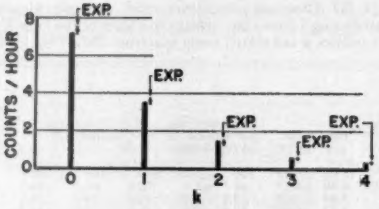

FIG. 9. Rates for setting off k out of four spaced counters (counters #11, #14, #17, and #20 of tray D), when extensive showers are selected by coincidences between trays A, B, and C, each containing 10 counters. The experimental points are as indicated. The calculated rates are shown by the heights of the solid bars; they were computed with the use of the density spectrum $N(\rho)d\rho = 787\rho^{-2.4}d\rho$, obtained independently through other data of this experiment.

check these rates by calculation. We have earlier derived an expression (9) giving the rate at which k out of n counters go off. It remains now to substitute $n=4$ and to put our observed density spectrum $787\rho^{-2.4}$ hr^{-1} inside the integral. The excellent agreement between observed and calculated values is evident from Fig. 9.

Our result (10) for the particle density spectrum of extensive air showers at sea level and geomagnetic latitude[14] 80° to 90° N can also be expressed in the integral form

$$N(>\rho) = 562\rho^{-1.4}\ \text{hr}^{-1}. \qquad (11)$$

Very roughly, this spectrum corresponds to:

~20 events per hour with density greater than 10 particles/m²;
~ 1 event per hour with density greater than 100 particles/m²;
~ 1 event per day with density greater than 1000 particles/m².

The experimental results can be stated in a different manner by giving the twofold, threefold, and fourfold coincidence rates of an arrangement of counters, each of area A m²:

$$C_2(A) = 1330A^{1.4}\ \text{hr}^{-1},$$
$$C_3(A) = 546A^{1.4}\ \text{hr}^{-1},$$
$$C_4(A) = 360A^{1.4}\ \text{hr}^{-1}.$$

These expressions are applicable to counters located in a horizontal plane at sea level, separated about 2 to 4 m, and with areas of the order of 0.0010 to 0.0700 m².

The results given in this section provide corroboration for the validity of an analysis in terms of a density spectrum of showers over a wide range of densities. Such confirmation of the validity of the density concept tends to increase our confidence in the general picture of an air shower as we think of it now.

[14] And, hence, at any latitude between 50° and 90° N, as the latitude effect is negligible between these regions according to results given in Sec. VI.

V. THE DECOHERENCE CURVE FOR SMALL SEPARATIONS

From the data obtained in the present experiment it is possible to determine the coincidence rate between two counters as a function of their separation. However, we *first select* extensive showers (by means of a master coincidence) and *then* carry out a decoherence experiment.

We again fix our attention on the four spaced counters of tray D (#11, #14, #17, and #20) and consider only cases in which two out of these four counters go off. The twofold coincidence rate of two counters is now determined as a function of their separation in the tray:

(i) 7.6-cm separation (for counters #11 and #14, #14 and #17, #17 and #20).
(ii) 15.2-cm separation (for counters #11 and #17, #14 and #20).
(iii) 22.8-cm separation (for counters #11 and #20).

The results are listed in column 5 of Table IV after applying proper weight factors to the data of column 4.

We can obtain one additional point on the decoherence curve by computing the rate which corresponds to a separation of the order of the extension of the experimental set-up, about 2 to 4 meters. We consider the case in which the three master coincidence trays A, B, and C each have ten active counters (ABC). There are also four single counters connected to subsidiary coincidence circuits (D); the rate with which two particular counters (and only these two) are set off, is just given by:

$$(ABCd_1d_2) = \int_0^\infty \{[1-\exp(-\rho A)]^3[\exp(-\rho A)]^2\} \times \{[1-\exp(-10\rho A)]^2 K\rho^{-\gamma}\}d\rho. \qquad (12)$$

On evaluating this expression using $A=0.00695$ m² and our experimental spectrum (10) we obtain for $(ABCd_1d_2)$ 0.24 hr^{-1} for a separation of 2 to 4 m. This is very closely the same as the experimental rate of 0.22 ± 0.02 hr^{-1} for small separations of the order of 10 to 20 cm.

We find then that when extensive showers are *first selected* by a group of counters, the coincidence rate between two additional counters located in the vicinity of the selector—within our experimental error—is independent of their separation for distances of the order of a few meters down to 7 cm. From the observations of other workers[1] in a different region of separations, the coincidence rate can be expected to decrease

TABLE IV. Coincidence rate as a function of counter separation of spaced counters in tray D.

1	2	3	4 No. of coinc. for counter separation of			5 Coinc. rate/hr for counter separation of		
Run	Coinc. arrangement	Time (hr)	(i) 7.6 cm	(ii) 15.2 cm	(iii) 22.8 cm	(i) 7.6 cm	(ii) 15.2 cm	(iii) 22.8 cm
ABC	$(ABCd_1d_2)$	233	155	94	47	0.22 ±0.02	0.20 ±0.02	0.20 ±0.03
AbC	$(AbCd_1d_2)$	227	54	41	21	0.08 ±0.01	0.09 ±0.01	0.09 ±0.02
Abc	$(Abcd_1d_2)$	565	53	30	20	0.031 ±0.004	0.027 ±0.005	0.035 ±0.008
All runs			262	165	88	1.00 ±0.06[a]	0.95 ±0.07[a]	1.01 ±0.11[a]

[a] The coincidence rates averaged over all runs are normalized by a factor 3/262.

for separations large enough so as to constitute an appreciable fraction of a shower radius.

VI. LATITUDE DEPENDENCE

Pomeranchuk[3] has pointed out that primary electrons will lose energy by radiation on being accelerated in the earth's magnetic field. The effect becomes important for electrons coming in vertically in the plane of the geomagnetic equator at energies greater than 10^{17} ev. The radiation loss is zero at all energies for electrons entering along the geomagnetic axis. A variation with geomagnetic latitude could, therefore, exist for showers provided two conditions are satisfied:

(i) There exist in the primary radiation electrons of energy 10^{18} ev and higher. However, it has been pointed out recently[16,16] that electrons traversing intergalactic space cannot maintain an energy greater than about 10^{19} ev because of Compton collisions with photons; primary particles of higher mass would not be latitude-sensitive even at the extremely high energy of 10^{19} ev.

(ii) But even assuming the presence of electrons of energies as high as 10^{18} ev in the primary radiation, the experimental consequences of the radiation loss may not be easily observable. Tzu[17] has shown that the excess energy of these electrons would be radiated in the form of some 600 high energy photons, all of comparable energy, which would give rise to extensive showers at sea level. These showers will be practically superimposed on the original shower and will, therefore, be experimentally indistinguishable from it. The main effect would consist in shifting the shower maximum to a higher altitude. This shift might be difficult to demonstrate experimentally.

On the basis of the foregoing considerations we do not expect to find a latitude dependence, particularly so in view of the fact that only a very small fraction of the events observed in the present experiment are caused by primaries of energy greater than 10^{17} ev. Experimentally, no evidence of a latitude effect was found between 50° and 90°, as shown in Table V, which compares data at 50° with the data of Table I which were obtained almost entirely at geomagnetic latitudes between 80° and 90°. Every effort was made to keep other experimental conditions as nearly identical as possible. Comparison of coincidence rates shows the absence of a dependence on latitude within the limits of experimental error.

TABLE V. Coincidence rates for experimental runs at Silver Spring, Maryland ($\lambda = 50°$).

1 Run	2 Coincidence arrangement	3 Time (hr)	4 Number of coincidences	5 Coincidence rate (hr^{-1})
ABC	(*ABC*)	145	1881	13.0 ±0.3
Abc	(*Abc*)	339	338	1.00±0.05
	From Table I: Coincidence rates at $\lambda = 80°$–90°			
ABC	(*ABC*)	410	5362	13.08±0.18
Abc	(*Abc*)	847	893	1.05±0.035

VII. DISCUSSION

This section is devoted to relating the results of the present experiment on the particle density spectrum and the structure of showers to the general experimental picture of showers, in particular to the question of what type of process in the upper atmosphere is responsible for the initiation of extensive showers.

Origin of Extensive Showers

It has now been established that 98 to 99 percent of the ionizing particles in extensive showers at low altitudes consist of electrons which have been produced by cascade multiplication. The remainder, the so-called "penetrating component" of showers, is presumably made up of μ-mesons;[18] there is also a small admixture of nucleonic component.[19]

Initially it was believed that Auger showers were originated by high energy primary electrons, the presence of penetrating particles (mesons) being explained by assuming them to be produced by energetic γ-rays. At present, however, there exists direct experimental evidence from cloud chamber measurements,[20] specific ionization,[21] and burst measurements[22] at very high altitudes against the presence of an appreciable fraction of primary electrons in the 10-Bev energy range. The lowest upper limit given is about 1 percent.[20] There is evidence against the existence of primary electrons with energies of 10^{18} to 10^{17} ev, which might lead to production of extensive showers, but the conclusion is indirect[14,16] and the possibility of having a few electrons of such high energies in the primary radiation cannot be completely excluded.

Nevertheless, it is now generally supposed that the electronic component of showers originates in the nuclear interactions of primary protons or heavier nuclei with air molecules in the upper atmosphere. The mesons present in showers can then be explained quite naturally as being produced in the same interaction. There is a good deal of experimental evidence from experiments in the lower atmosphere[23] for the production of electrons and/or photons with mesons.

The interactions observed so far in the experiments cited involve energies very much lower than those encountered in the initiation of air showers; however, they are suggestive of the higher energy processes. The detailed mechanism for the production of the electronic

[16] J. W. Follin, Jr., Phys. Rev. **72**, 743 (1947).
[16] E. Feenberg and H. Primakoff, Phys. Rev. **73**, 449 (1948).
[17] H. Y. Tzu, Proc. Roy. Soc. (London) **192**, 231 (1948).
[18] Cocconi, Cocconi-Tongiorgi, and Greisen, Phys. Rev. **75**, 1063 (1949); W. W. Brown and A. S. McKay, Phys. Rev. **76**, 1034 (1949).
[19] Cocconi, Cocconi-Tongiorgi, and Greisen, Phys. Rev. **74**, 1867 (1948).
[20] Critchfield, Ney, and Oleksa, Phys. Rev. **79**, 402 (1950).
[21] S. F. Singer, Phys. Rev. **76**, 701 (1949).
[22] Schein, Jesse, and Wollan, Phys. Rev. **59**, 615 (1941); R. I. Hulsizer, Echo Lake Conference (June, 1949); J. A. Van Allen, Echo Lake Conference (June, 1949).
[23] B. Rossi, Revs. Modern Phys. **20**, 537 (1948); Bridge, Hazen, Rossi, and Williams, Phys. Rev. **74**, 1083 (1948); C. Y. Chao, Phys. Rev. **75**, 581 (1949); W. B. Fretter, Phys. Rev. **76**, 511 (1949); B. P. Gregory and J. H. Tinlot, Phys. Rev. **79**, 205 (1950).

component is not known, and constitutes one of the outstanding problems of shower theory. Some of the mechanisms considered have been of the electromagnetic type, e.g. γ-rays produced in the deceleration of primary protons near an air nucleus[24] analogous to the bremsstrahlung of electrons, also γ-rays emitted in the acceleration of charged mesons[25] as they are generated in a nuclear interaction. In distinction, processes have been considered which are of the nuclear type. Lewis, Oppenheimer, and Wouthuysen[26] have proposed production of neutral mesons along with charged mesons. The neutral meson is assumed to be extremely unstable, decaying into two γ-rays which then initiate electronic cascades. There appears to be now firm experimental evidence for the existence of neutral mesons from experiments at Berkeley.[27] Independently, a very remarkable star[28] showing the interaction of a primary alpha-particle of about 10^{12} ev with an Ag or Br nucleus in a photographic emulsion, lends much support to this hypothesis for the origin of Auger showers. Bethe[29] has recently put forth a qualitative but very suggestive picture of the development of an extensive shower to fit the present experimental situation; it is based on the neutral meson hypothesis, and incorporates ideas on cascade multiplication of the N-component (nucleons and π-mesons).

Experimental Approach and Difficulties

The present experimental evidence on extensive showers is not sufficient to give a description of the initiating process or even to discriminate between various possibilities. One promising approach seems to be the study of some of the gross properties of extensive showers, the particle densities and structure of showers, as functions of the altitude. For all practical purposes this approach entails a study of the electronic component, which should behave in accordance with cascade theory. A complete analysis of such data on the basis of cascade theory gives in principle some information about the initial multiplicity and angular divergence of the cascade-initiating γ-rays or electrons. However, many factors enter in to complicate the simple picture.

One of the principal difficulties in the interpretation of high altitude data on showers arises from the contribution of nonvertical showers; at sea level, however, the showers detected arrive predominantly from the vertical direction if—as in the present experiment—the counter separations are not very large.[30]

In order to compare experimental data obtained at different altitudes, the results should be expressed in units which are independent of the local air density. Accordingly, the integral density spectrum (11) obtained in the present experiment should be stated as

$$N(>\rho)=1.0\times10^{8}\rho^{-1.4}\ \text{hr}^{-1}, \qquad (13)$$

where ρ is now expressed in particles per shower radius[9] squared.

From the experimental density spectrum, we can compute immediately an expression for the frequency distribution of showers as a function of the number of particles in the shower, under the assumption that the particles are distributed in every shower according to a certain structure function (see Appendix). Using this result together with certain expressions from cascade theory,[9] we have carried out a computation for the primary spectrum based on the early model of primary electrons initiating extensive showers at the top of the atmosphere. The results of this computation[31] give a primary spectrum about thirty times larger than that obtained by other workers;[32] the discrepancy arises mainly from the fact that we used a corrected value for the radiation length in air in order to take into account the bremsstrahlung and pair production effects of the atomic electrons.[33]

Comparison of Experimental Results on the Density Spectrum

Figure 10 shows a comparison of some integral density spectra determined from G-M counter and ionization chamber measurements near sea level. The three sets of counter data[6,8] are seen to be in good agreement with one another. Our spectrum is in excellent accord with Cocconi's recent measurements.[8] In agreement with his result, a trend toward a slightly higher value of γ is discernible in our data (in Table III and Fig. 8) for the point corresponding to our highest mean density (about 1000 particles per square meter). This increase in γ is very pronounced at even higher mean densities, which are more accessible to measurement by means of ion chambers. The results of Montgomery and Lapp shown in Fig. 10 were taken from Montgomery's[34] summary paper. The use of high pressure chambers in their burst measurements tends to minimize the effects of stars and local showers, and therefore leads to quite a reasonable value for γ. Nevertheless, a large discrepancy exists between G-M counter and ion chamber results at intermediate shower densities, possibly due to the fact—as pointed out by Cocconi[35]—that ion chambers do not measure particle densities directly but rather total ionization of the shower particles, which includes secondary electrons and possibly nuclear events.

[24] J. L. Powell, Phys. Rev. **75**, 32 (1949).
[25] L. I. Schiff, Phys. Rev. **76**, 89 (1949).
[26] Lewis, Oppenheimer, and Wouthuysen, Phys. Rev. **73**, 127 (1948).
[27] Bjorklund, Crandall, Moyer, and York, Phys. Rev. **77**, 213 (1950).
[28] Kaplon, Peters, and Bradt, Phys. Rev. **76**, 1735 (1949); see also discussion by R. E. Marshak, Phys. Rev. **76**, 1736 (1949).
[29] H. A. Bethe, Echo Lake Conference (June, 1949).
[30] G. Cocconi, Phys. Rev. **72**, 350 (1947); S. F. Singer, Phys. Rev. **74**, 844 (1948). A very strong zenith angle dependence (as great as $\cos^{8}\theta$) has been deduced for air showers by various observers: J. Daudin, J. phys. radium **6**, 302 (1945); W. W. Brown and A. S. McKay, Phys. Rev. **76**, 1034 (1949); H. L. Kraybill, Phys. Rev. **77**, 410 (1949).
[31] S. F. Singer, thesis, Princeton University, 1948.
[32] A. Migdal, J. Phys. (U.S.S.R.) **9**, 183 (1945); Cocconi, Loverdo, and Tongiorgi, Phys. Rev. **70**, 846 (1946).
[33] J. A. Wheeler and W. E. Lamb, Phys. Rev. **55**, 858 (1939).
[34] C. G. Montgomery and D. D. Montgomery, Phys. Rev. **72**, 131 (1947).
[35] G. Cocconi, Phys. Rev. **70**, 975 (1946).

Significance of the Density Spectrum Exponent γ

It is evident from Table III and Fig. 9 that the same spectrum can be used to compute the coincidence rates of all types of counter arrangements used in our experiments; in other words, the value of γ is the *same* in our experiment whether determined by variation of counter areas or by varying the multiplicity of coincidences. This, we feel, should certainly be the case if our concept of shower density (Sec. II) is correct; it is the result anticipated with the symmetrical arrangement of counter trays used in the present experiment.

Other experimenters who have not found such agreement have accounted for the discrepancy in various ways: (1) The applicability of Poisson's law to the analysis of counter experiments on showers may be doubtful in view of correlations existing between shower particles, according to Daudin.[36] We believe that while a correlation effect certainly exists,[37] it is not of great importance experimentally. This conclusion is drawn from our data on the decoherence curve at small separations (Sec. V). It is rather difficult to draw unambiguous conclusions from the experiments presented by Daudin, since in some cases showers were detected by only a twofold coincidence. (2) Treat and Greisen[38] have expressed the opinion that the discrepancy arises from extraneous causes, such as changes in barometric pressure, etc. Effects of this sort would not have affected our results appreciably since in our master coincidence arrangement essentially both methods for determining γ were carried on simultaneously. (3) Recently, Ise[39] has pointed out that in general one should not obtain a unique value for γ, since even in a counter arrangement of moderate extension most showers detected have their cores located close enough to give an appreciable density gradient over the extension of the equipment. This gradient should not affect the value of γ as determined by variation of counter areas (see Appendix), but would increase the value of γ obtained by adding additional counters for multifold coincidences. No estimate of the magnitude of the effect is given; in any case only an estimate of an upper limit of the increase may be meaningful since the assumptions on which the calculations are based are open to some question (see Appendix). We cannot check this effect by means of our experimental results since we used the additional tray (tray *D*) in a very symmetrical arrangement and quite close to tray *A* (Fig. 4). Because of this symmetrical set-up, one would expect that the concept of a distribution-in-density (which neglects the density gradients which actually exist) would be a good first approximation. This is what we find experimentally. On the other hand, Ise's arrangement—consisting of three counter trays in a straight line, with a fourth one at right angles—is much less symmetric, and the assumption of constant density over this arrangement is much less adequate.

In any case, we feel reasonably certain that the concept of shower density can now be considered well confirmed, and that it provides an adequate basis for the expression and comparison of results obtained with different experimental arrangements.

Structure of Extensive Showers

The existence of a large number of shower cores distributed throughout the extent of the main shower has been suggested by some authors,[40] but no clearcut experimental evidence has been brought forth on this point. Recently, this question has assumed added importance because of a theory concerning the origin of extensive showers involving neutral mesons of very short lifetime.[26] According to the authors, the neutral mesons are produced with an angular divergence of $(2M/E_0)^{\frac{1}{2}}$, a divergence sufficiently great to effect appearance of a multiple core structure in the shower, with a core separation—near sea level—of the order of 10 m. Furthermore, the possibility cannot be ruled out *a priori*, that individual penetrating particles have associated with them clusters of electrons (genetically related to them) so as to give a type of "fine structure"

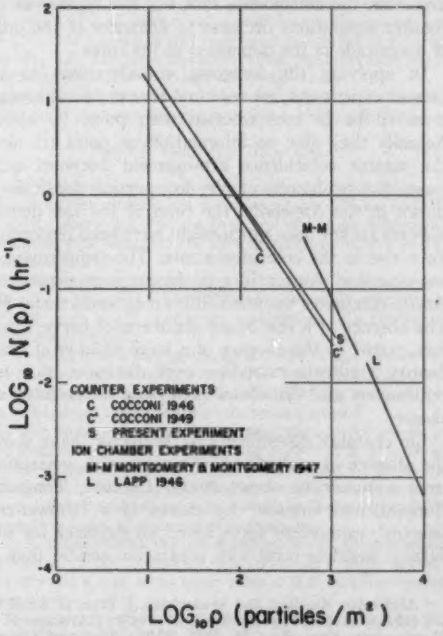

FIG. 10. Integral density spectrum of extensive air showers at sea level. A comparison of results obtained with counters and with thin-walled high pressure ionization chambers.

[36] J. Daudin, J. phys. radium **10**, 65 (1949).
[37] V. Berestetzky, J. Phys. (U.S.S.R.) **9**, 197 (1945).
[38] J. E. Treat and K. I. Greisen, Phys. Rev. **74**, 414 (1948).
[39] J. Ise, Jr., and W. B. Fretter, Phys. Rev. **76**, 933 (1949).
[40] J. Clay, Physica **9**, 897 (1942).

to the well-known distribution function; this structure would be revealed only upon detailed examination.

It is possible to determine how our result of Sec. V, namely *no rise in the decoherence curve for small separations when extensive showers are first selected*, bears on this question of the existence of local condensations of particles or "cores." We will first examine the behavior of the decoherence curve of two counters for small separations where no selection of extensive showers is involved. Experimentally, the coincidence rate has been found to rise very rapidly as the counters are brought together.[41] This increase can be ascribed to a number of causes:

(i) The coincidence rate may rise just due to the effect of the core of extensive showers, as has been pointed out by Blatt.[42] However, the same basic assumptions which occur in Ise's calculations are involved here to an even greater degree and are open to some question (compare Appendix).

(ii) At small separations, the coincidence rate will also be affected by "narrow showers," knock-on processes, and possibly other phenomena not directly connected with extensive showers. This is thought to be the principal cause for the rise in the coincidence rate.[41]

(iii) Furthermore, if a large number of cores exist in a shower, the coincidence rate will rise rapidly as the counter separations decrease to distances of the order of magnitude of the dimension of the cores.

In applying the foregoing considerations to the present experiment, we note first that our results might seem to be in contradiction with point (i) above. Actually they give no information on point (i), since the master coincidence arrangement becomes quite insensitive to showers of very low particle densities; as shown in the Appendix, the cores of the low density showers are the ones which might have been responsible for a rise in the coincidence rate. The requirement of an extensive shower in our decoherence experiment clearly eliminates the possibilities mentioned under (ii). The absence of a rise in our decoherence curve, therefore, points to the absence of a large number of sharp density gradients extending over distances of a few centimeters and *distributed throughout the extent of the shower*.

Ion chamber experiments by Williams[43] have shown the absence of multiple shower cores with separations from a meter to about 30 m. Cocconi, Tongiorgi-Cocconi, and Greisen[44] by means of a "shower-core selector" experiment have found no evidence for subsidiary, multiple cores with separation greater than 10 meters, but rather a monotonic decrease in density with distance from the main shower core. This absence of widely separated cores is in disagreement with the anticipated results of the neutral meson theory as quoted in reference 26. However, it has been pointed out by one of its authors[45] and others that the essential features of the theory would not be affected by assuming that the neutral mesons are produced with a much smaller angular divergence, possibly of the order of M/E_0, analogous to photon pair production.

Taken together, all experimental evidence tends to exclude the presence of local condensations or cores *distributed throughout the extent of the shower*. We cannot, however, exclude the presence of a number of multiple cores—separated by a few centimeters—*located within the main core* of the shower; indeed their existence is to be expected in view of some of the initiation mechanisms proposed.

The author is greatly indebted to the Navy Bureau of Ordnance for providing the opportunity for this investigation, and to the officers and men of the USS Wyandot (AKA 92) for their excellent cooperation.

He wishes to express his appreciation to his associates at the Applied Physics Laboratory, particularly Drs. H. E. Tatel (now with the Department of Terrestrial Magnetism, Carnegie Institution of Washington) and J. A. Van Allen, to Drs. D. J. X. Montgomery and John Blatt for valuable comments, and to Professor John A. Wheeler for his guidance in many phases of this work.

APPENDIX

We are interested in computing from our experimental particle density spectrum $\nu(\rho)d\rho$ the distribution $f(\Pi)d\Pi$; $f(\Pi)d\Pi$ can be interpreted as the number of showers per hour, whose centers strike within a horizontal area of one square meter at the place of observation, and which contain a total number of particles between Π and $\Pi+d\Pi$. We will assume that the particles in showers of all sizes are distributed according to the same lateral structure function $\phi(r)$, computed by Molière[46] for the lateral distribution of particles at the plane of the cascade maximum. An analytical approximation to the Molière function has been given by Bethe (and quoted by Williams[43]):

$$\phi(r)=[2.85/(2\pi r_0^2)](1+4r/r_0)\exp[-4(r/r_0)^{\frac{1}{2}}], \qquad (14)$$

where r_0 is the shower radius defined earlier.[9] $2\pi\phi(r)dr$ can be interpreted as the probability for a shower particle to fall between distance r and $r+dr$ from the shower center. From this definition it follows that

$$\rho(r)=\phi(r)\cdot\Pi. \qquad (15)$$

Let us consider now the apparatus which measures shower densities located at the origin of a polar coordinate system. A shower containing Π-particles and centering at a distance r from the apparatus will produce at the origin a particle density given by (15) and (14). A distribution $f(\Pi)$ will, therefore, lead to a distribution of densities

$$\nu(\rho)\Delta\rho=2\pi\int_0^\infty f(\Pi)(\Delta\Pi)r\,dr, \qquad (16)$$

[41] Alichanian, Asatiani, and Alexandrian, J. Phys. (U.S.S.R.) **9**, 175 (1945); **10**, 296, 518 (1946); **11**, 16 (1947); J. Wei and C. G. Montgomery, Phys. Rev. **76**, 1488 (1949); Keck and Greisen, Echo Lake Conference (June, 1949).

[42] J. Blatt, Phys. Rev. **75**, 1584 (1949).

[43] R. W. Williams, Phys. Rev. **74**, 1689 (1948).

[44] Cocconi, Tongiorgi-Cocconi, and Greisen, Phys. Rev. **76**, 1020 (1949).

[45] J. R. Oppenheimer, private communication; see also p. 136 of reference 26.

[46] G. Molière, *Cosmic Radiation*, edited by W. Heisenberg (Dover Publications, New York, 1946).

where Π must satisfy (15), so that

$$\nu(\rho)\Delta\rho = 2\pi\int_0^\infty f[\rho/\phi(r)][\Delta\rho/\phi(r)]rdr. \quad (16')$$

If we assume a power law distribution for $f(\Pi)$

$$f(\Pi)d\Pi = k\Pi^{-\gamma}d\Pi,$$

we obtain

$$\nu(\rho)\Delta\rho = 2\pi k\int_0^\infty [\rho/\phi(r)]^{-\kappa}[\Delta\rho/\phi(r)]rdr$$
$$= 2\pi k\rho^{-\kappa}\Delta\rho\int_0^\infty [\phi(r)]^{\kappa-1}rdr. \quad (17)$$

We can now compare this result with our experimental density distribution $\nu(\rho)d\rho = K\rho^{-\gamma}d\rho$. For agreement κ must equal γ, a result which is seen to be independent of the form of the structure function $\phi(r)$ and depends only on the assumption that the structure function is the same for all showers. The final result for $f(\Pi)$ based on our experimental spectrum $787\rho^{-2.4}$ hr^{-1} is

$$f(\Pi)d\Pi = 2.5\times 10^4\Pi^{-2.4}d\Pi \text{ hr}^{-1}\text{ m}^{-2}. \quad (18)$$

When the shower radius[9] is used as the unit of length, Eq. (18) becomes:

$$f(\Pi)d\Pi = 1.4\times 10^6\Pi^{-2.4}d\Pi \text{ hr}^{-1}(r_0)^{-2}. \quad (18')$$

In the calculation above it has been assumed implicitly that the dimensions of the experimental arrangement are small enough so that the particle density may be considered as uniform over the extension of the apparatus. In reality, however, the counter trays are separated by an appreciable fraction of a shower radius. The coincidence rate C_n of a set of n Geiger counters of areas A_i and located at distances r_i from the shower core is given by

$$C_n = \int_0^\infty\int_0^\infty\int_0^{2\pi} k\Pi^{-\gamma}d\Pi rdrd\theta\cdot\prod_i\{1-\exp[-\Pi A_i\phi(r_i)]\}. \quad (19)$$

By making the substitution $\Pi' = \Pi A$, and taking $A_i = a_i A$, we can see immediately that $C_n \propto A^{\gamma-1}$; i.e., the counter areas need not be equal, but if they are changed in a proportional manner, the exponent of the distribution-in-number $f(\Pi)$ can be obtained directly from the coincidence rates C_n.

A numerical integration of expression (19) has been carried out by Ise[39] for a very useful experimental case, namely that of three counter trays of equal area A, located on a straight line with a spacing $a = 0.05r_0$. The integral then becomes[39]

$$C_3(A) = \int_0^\infty\int_0^\infty\int_0^{\pi/2} k\Pi^{-\gamma}d\Pi\cdot 2\pi rdr\cdot 2d\theta/\pi\{1-\exp[-\Pi A\phi(r)]\}$$
$$\times\{1-\exp[-\Pi A\phi(r_1)]\}\{1-\exp[-\Pi A\phi(r_2)]\}, \quad (19')$$

where $r_{1,2} = (a^2+r^2\pm 2ar\cos\theta)^{\frac{1}{2}}$; all distances are expressed in units of r_0.

It is a rather trivial problem to extrapolate these calculations to the case of $a = 0$, but comparison of the case $a = 0$ with the case $a = 0.05r_0$ gives considerable insight into the assumptions underlying these calculations, and is also of importance in the interpretation of decoherence experiments involving small separations. We first note that the probability of a coincidence is a maximum when the center of the shower coincides with the center tray.[47] Ise shows that (for $a = 0.05$) this maximum probability is 1.0 for values of ΠA down to about 1.0, and then falls off, the probability being about 0.22 for $\Pi A = 0.1$. In our case ($a = 0$) the probability remains 1.0 for all values[48] of ΠA. This difference accounts for the discrepancy between the two sets of curves in Fig. 11 for small values of ΠA. There we have plotted the function $I(r)$, obtained through one integration (over θ) of a portion of the integrand of Eq. (19'):

$$I(r) = r\int_0^{\pi/2}\{1-\exp[-\Pi A\phi(r)]\}\{1-\exp[-\Pi A\phi(r_1)]\}$$
$$\{1-\exp[-\Pi A\phi(r_2)]\}d\theta. \quad (20)$$

[47] The dimensions of the counter trays are neglected in this discussion. This will tend to overemphasize the difference between $a = 0$ and the $a = 0.05$ plots in Figs. 11 to 13.

[48] This no longer holds true for very small values of Π, as will be discussed later.

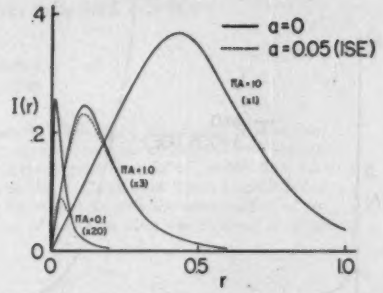

FIG. 11. Probability $I(r)$ of a threefold coincidence due to all showers striking at a distance r from the central counter tray for various values of ΠA.

This function represents the probability of a threefold coincidence due to all showers which strike at a distance r from the central counter for various values of πA.

The next step in the evaluation of Eq. (19') can be the integration over r, yielding the function

$$R'(\Pi A) = 2\pi\Pi^{-\gamma}\int_0^\infty I(r)dr. \quad (21)$$

A graph of this function *vs* the logarithm of ΠA is shown in Fig. 12 for the two values of a and for $\gamma = 2.5$. From the relation

$$R'(\Pi A) = dC_3(A)/d\Pi \quad (22)$$

it is possible to interpret $R'(\Pi A)$ as the differential distribution with respect to Π of showers which contribute to the coincidence rate (19'). The function $R'(\Pi A)$ can be plotted *vs* ΠA on a linear basis (Fig. 12). The areas under the curves represent the coincidence rates (19') for $a = 0.05$ and $a = 0$, respectively.

Instead of integrating over r, the second step in the evaluation of (19') could also be an integration over ΠA, yielding the function

$$P(r) = \int_0^\infty (\Pi A)^{-\gamma}I(r, \Pi A)d(\Pi A). \quad (23)$$

A graph of this function *vs* r is shown in Fig. 13. Again the areas under the curves represent the coincidence rates (19') for $a = 0.05$ and $a = 0$, respectively. $P(r)$ can be interpreted as the differential distribution with respect to r of showers which contribute to the coincidence rate (19').

Several interesting conclusions may be drawn from the comparisons shown[49] in Figs. 12 and 13, subject to certain reservations as stated below which involve the assumptions on which these calculations are based:

(i) In going from a tray separation of $0.05r_0$ to zero separation, the coincidence rate increases by not more than about 50 percent. To evaluate this increase precisely, it is definitely necessary to take into account the finite size of the counter trays.[50]

(ii) The counter arrangement with separation $a = 0.05$ shows a sharp maximum at $\Pi A = 0.04$ according to Ise[39] (Fig. 12), but a very *flat* maximum (Fig. 13) around $r = 0.1$ (about 7.5 m at sea level). One is, therefore, not justified in assuming that the centers of most showers detected by counters with moderate separations strike within about 10 meters of the apparatus.

(iii) As anticipated for the case of zero separation, the maximum contribution to the coincidence rate occurs at a much smaller value of r and a very much lower value of ΠA. In other words,

[49] No great accuracy is implied in the curves presented in Figs. 11 through 13.

[50] Qualitatively, the finite size of the counters serves to exclude the extremely small showers, which lead to the very steep rise in the $a = 0$ curves, e.g., in Figs. 12 and 13. The effect of the finite dimension of a detector has been considered in the case of ion chambers by Blatt (reference 42).

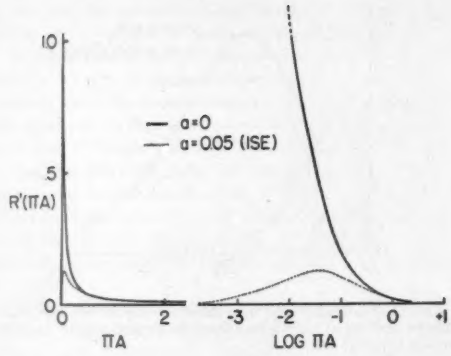

FIG. 12. Contribution to threefold coincidence rate by showers of various total numbers ΠA of electrons striking at all distances from the central counter.

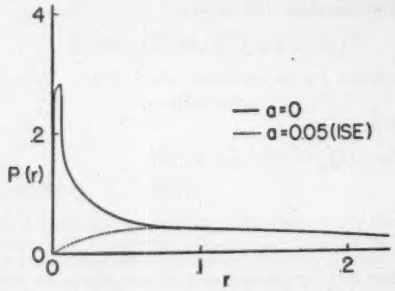

FIG. 13. Contribution to threefold coincidence rate by all showers (taking account of their distribution-in-number) at various distances r of shower core to central tray.

with very small counter separations a large fraction of the coincidence rate is due to showers, containing relatively few particles, whose cores strike a short distance away from the counter arrangement.

(iv) These considerations lead to ideas on the construction of a core selector based purely on the structure of showers. It would consist of two identical sets of counters. The first set of, say, three counters would be very closely spaced, the second set moderately spaced and in anticoincidence with the first set. A combination, such as shown in Fig. 13, would select showers whose cores are about one meter from the center of the counter arrangement. The area A of the counters would determine the mean size $\bar{\Pi}$ of the showers selected.

We finally wish to discuss briefly some of the assumptions on which the above considerations have been based.

(i) With a counter tray area of about $10^{-5}r_0^3$, most of the showers registered by our equipment contain in the neighborhood of $0.04\times10^6\sim4000$ particles (see Fig. 12). A shower with $\Pi\sim4000$ particles at sea-level can be expected to be an "old" shower,[9] i.e., to have passed through its stage of maximum development at a much higher altitude. Its structure *near the core* would not be as steep as given by the Molière function.[41] Furthermore, if Auger showers originate in a multiple process, as seems likely, the structure function would again be much flatter near the core of the shower.

(ii) In addition, we suspect that the distribution-in-number of showers does not follow a pure power law, but becomes much flatter for smaller values of Π (as it certainly must, in order not to exceed the total cosmic-ray intensity). Some evidence for this is already available from shower experiments.[8]

(iii) Finally, for very small values of Π the probability expressions we have been using become inaccurate and break down. This arises from the fact that the probability of a coincidence is no longer the product of the separate probabilities. Effectively, when one counter is hit by a particle, it "robs" the other counters of that particle, decreasing Π and, therefore, their probabilities to be hit.

These points have various degrees of importance, depending on the exact nature of the experimental arrangement (areas, separation, etc.). Broadly speaking, their effect will be to minimize the influence of the shower core; e.g., on the rise of the decoherence curve at small separations,[42] and on the discrepancy of the determination of the density spectrum exponent γ by different methods.[39] The above considerations, we believe, tend to bring experimental results into harmony with theory.

[41] The recent experiments of the Cornell group (reference 44) give information on the structure function only at some distance from the core.

Proton-Proton Scattering at 3.4, 6.8, and 7.5 Mev

JAMES ROUVINA*
University of Rochester, Rochester, New York
(Received August 28, 1950)

Using a gas target and photographic plates as detectors, absolute differential p-p scattering cross sections in the angular range of 45° to 10° at 6.8 and 7.5 Mev were measured with an accuracy of two percent. The apparatus was checked by obtaining data at 3.4 Mev in the angular range of 15° to 45°. The data obtained at this energy range were in agreement with the precise Van de Graaff data. The 6.8- and 7.5-Mev data show that the S-wave cross sections at these energies are consistent with the extrapolation of the precise Van de Graaff data to this energy region. No indication of a P-wave effect was observed in either the low or high energy data.

I. INTRODUCTION

THE status of p-p scattering at the beginning of this investigation was somewhat confused. P-p scattering experiments had been performed[1] in the energy range from 200 kev to 3.5 Mev using Van de Graaff generators.[2] These data were self-consistent and no appreciable P-wave effect was observed. Experiments had been performed by Wilson and his collaborators[3] at 8, 10, and 14 Mev using cyclotrons. The S-wave data of these cyclotron experiments, in view of the large uncertainty assigned them, could be regarded as being in agreement with the extension of the accurate low energy data. This data gave an indication of a repulsive central P wave. Other experiments on p-p scattering were carried out by May and Powell[4] and Dearnley, Oxley, and Perry.[5] May and Powell made an absolute measurement of the cross section at 45° in the laboratory system at 4.2 Mev, which measurement was good to ±6 percent and was in agreement with the extension of the low energy S-wave data. Dearnley *et al.* performed a fairly precise cyclotron experiment at 7 Mev. They obtained an S-wave cross section which was about 10 percent lower than the cross section extrapolated from the low energy data. This low cross section could not be explained in any reasonable fashion. Some indication of a P-wave effect was also observed by these workers.

In order to clarify the situation at 7 Mev, the present investigation was undertaken with a completely different scattering chamber. Our aim was to determine the consistency of the S-wave data in the 7-Mev region with the low energy data and to settle whether or not the P-phase shift was real. Our aim was achieved by first checking the apparatus at 3.4 Mev through measurements of the absolute differential scattering cross sections in the angular range 15° to 45°. When it was found that the data at 3.4 Mev were in excellent agreement with the precise Van de Graaff data, absolute differential scattering cross sections for incident proton energies of 6.8 and 7.5 Mev in the angular range 10° to 45° were measured.

II. DESCRIPTION OF APPARATUS

During the course of the work of Dearnley, *et al.*[5] it became apparent that certain important improvements could be made in the apparatus used by them and that these could be achieved by simply increasing the physical dimensions of the scattering chamber. The principal improvement was that the slit edge penetration correction decreased because the ratio of slit translucent area to slit transparent area was decreased. In the worst case for the present apparatus, this correction amounted to only 0.6 percent as compared with 15 percent for their apparatus. The increased size of the camera also made possible more precise measurements of its geometry.

The scattering apparatus can best be described by referring to Figs. 1 and 2. Protons emerge from the exit port of the cyclotron through a 0.25-mil aluminum window 2 mm in diameter at S 1. Further collimation of this beam is achieved with circular openings of 2-mm diameter each at S 2, 3, and 4 mounted in the sections of flexible tubing. The fringing field of the cyclotron passes through the flexible tubing and hence a fairly

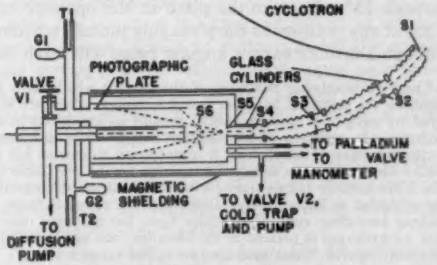

FIG. 1. General schematic drawing of the scattering camera attached to the cyclotron.

* AEC Predoctoral Fellow, 1948–1950.

[1] Ragan, Kanne, and Taschek, Phys. Rev. **60**, 628 (1941). These measurements were made in the 200 to 300 kev region using a Cockcroft-Walton machine.

[2] J. M. Blatt and J. D. Jackson, Revs. Modern Phys. **22**, 77 (1950). A complete bibliography of p-p scattering experiments is given in this paper.

[3] R. R. Wilson and E. C. Creutz, Phys. Rev. **71**, 339 (1947). R. R. Wilson, Phys. Rev. **71**, 384 (1947). Wilson, Lofgren, Richardson, Wright, and Shankland, Phys. Rev. **72**, 1131 (1947).

[4] A. N. May and C. F. Powell, Proc. Roy. Soc. (London) **A190**, 170 (1947).

[5] Dearnley, Oxley, and Perry, Phys. Rev. **73**, 1290 (1948).

monoenergetic beam of protons emerges from S 5 into the scattering volume V. The scattering volume is at a hydrogen pressure of one cm of mercury during a gas run.[6] The hydrogen is admitted to the system through a palladium valve and passes through a 20-ft length of coiled copper tubing which serves to bring the hydrogen temperature into equilibrium with that of the surroundings before it enters the scattering volume. A thermometer in intimate contact with the chamber end of the copper tubing measures this temperature with an accuracy of ± 0.16 percent for runs in which no liquid nitrogen[7] is used in trap T 1, Fig. 1. During either kind of run,[7] valve V 1 is kept closed and the chamber is pumped out by a fore pump via V 2 and a dry ice-acetone trap. The pressure is measured by means of a butyl-phthalate manometer. One arm of the manometer is connected to the scattering volume, the other arm is connected to a fore pump. The pressure is measured by reading the difference in manometer column heights h with a cathetometer and determining the density ρ of the manometer oil by measuring the temperature of the oil. Both h and ρ can be measured with an accuracy of ± 0.10 percent.

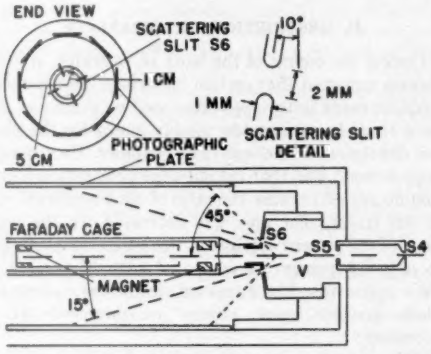

FIG. 2. Detailed drawing of the scattering camera.

Figure 2 shows that protons scattered through the scattering slit S 6 at an angle of 45° will enter the photographic plate at one end and protons scattered through 15° will enter the plate at the opposite end. Thus at any position on the plate only protons scattered through a definite narrow angular range will reach that position. The purpose of S 5, which is a circular hole 2.5 mm in diameter, is to prevent protons scattered by the edge of S 4 from reaching the photographic plates. The proton beam impinges in the collecting cup of the Faraday cage after passing through the scattering volume.

Eight photographic plates are used simultaneously in this scattering camera. They are arranged coaxially with the beam as shown in Fig. 2. The cyclotron beam is monitored during a run by measuring the beam current incident on the insulated slit S 2. The slit jaws of the scattering slit S 6 are fully rounded with a radius of 0.5 mm in order to reduce the slit edge penetration. The angle of the slit was chosen to be 10° in order to favor the number of tracks observed at 10° on the plate. The slit width is 2 mm.

The Faraday cage is kept at a pressure of 10^{-6} mm of mercury during a run with an oil diffusion pump and this pressure is measured with ion gauge G 2. During a run, trap T 2 of the Faraday cage vacuum system is kept filled with liquid nitrogen. The proton beam in passing through the 0.35-mil aluminum window over the entrance to the cage will knock out electrons which can reach the collecting cup and neutralize part of the proton charge collected. To avoid this, a small cyclotron-shaped magnet is placed at the back of the aluminum window. The field in the gap is about 1.8 kilogauss. The magnet has no appreciable effect on the proton beam but the recoil electrons from the window are deflected so that none can reach the collecting cup. The computed safety factor of the magnetic field in the gap is about three. Another similar magnet is placed at the back of the collecting cup. The purpose of this magnet is to prevent electrons produced by the proton beam from leaving the cup. The probability of protons scattering out of the cup is reduced by partially closing the opening of the collecting cup. The Faraday cage is so designed that it can be opened easily and photographic films inserted to check whether all of the proton beam is entering the collecting cup. The charge collected by the Faraday cage is fed through a coaxial cable to a polystyrene insulated condenser in the cyclotron control room. There it is discharged through a ballistic galvanometer by an integrating circuit[8] and the deflection recorded.

The charge was corrected for leakage of the circuit during both the scattering run and calibration of the ballistic galvanometer. The correction for leakage during calibration varied between 0.02 and 0.07 percent. The leakage correction during the run amounted to 0.8 percent in the worst case and 0.5 percent in most other cases. These corrections are known to ± 10 percent. Each discharge of the condenser amounted to 0.18 microcoulombs, a run consisted of at least 30

[6] In a gas scattering run most of the protons which enter the emulsion are scattered by other protons, though a few are scattered by oxygen or nitrogen nuclei present as impurities in the hydrogen. In order to obtain relative and absolute differential scattering cross-section curves, it is necessary to correct for the tracks which appear to satisfy the criterion for the p-p tracks but which are actually tracks arising from the neutron background of the cyclotron or impurity scattering. This correction is made by making scattering runs which differ from the gas runs only in that no hydrogen is present in the chamber, but are identical in all other respects. These runs are here called vacuum runs.

[7] Runs in which trap T 1 was filled with liquid nitrogen were called liquid nitrogen runs. Non-liquid nitrogen runs are runs in which trap T 1 was left empty.

[8] The integrating circuit is an automaton which discharged the polystyrene insulated condenser through the ballistic galvanometer whenever the voltage across the condenser reached 12 volts.

discharges and lasted about two and one half hours. The dielectric soakage of the charge measuring circuit amounted to about 0.16 percent. The soakage introduced no errors in either the calibration of the circuit or the measurement of the charge during a run. During a run the soakage is compensated for by reading the residual deflection at the conclusion of the run. By allowing the circuit to discharge several times before calibration, the soakage effect is compensated for in the calibration. The total rms error in the charge measurement for the different runs varied between ± 0.31 and ± 0.55 percent.

In aligning the scattering apparatus a special back with centered cross lines was used in place of the Faraday cage back. The beam was first aligned on the slit system of the flexible tubing and finally on the centered cross lines of the alignment back. The alignment was further checked by exposing a film at the entrance to the Faraday cage. In all cases the beam was well centered on the Faraday cage opening when it was well centered on the cross lines. One additional check on the alignment was to observe the distribution in tracks at a given angle, preferably 10°, as a function of the plate position in the camera.

In order to obtain data down to 10° an extension back was employed which moved the Faraday cage back about 4 in. Using the extension back, films exposed within the Faraday cage showed the proton beam to be well centered in the collecting cup at proton energies of 7.5 and 6.8 Mev; however at 3.4 Mev it appeared as though there were a slight possibility of the beam not clearing the entrance to the collecting cup. Films exposed within the Faraday cage with the extension back omitted at 3.4 Mev showed the beam to be well centered in the collecting cup, thus absolute data could only be obtained in the angular range 15° to 45° at 3.4 Mev.

The photographic plates used in this experiment were Kodak NTA nuclear emulsion plates. They were 10 in. $\times 0.75$ in. $\times 1$ mm with a 25μ-emulsion. The plates were prepared for use as follows. Using a reticule, two lines each spaced 2 mm from the longitudinal center line were photographed on the plates. The track counting was confined to the region between the two reticule lines. After the lines were photographed, the plates were taped about the edges with Scotch tape to prevent the emulsion from peeling off of the glass during evacuation. The plates were processed in the manner prescribed by Kodak.

The p-p differential scattering cross section $\sigma(\theta)$ is given by:

$$\sigma(\theta) = Y(\theta) A S(\theta),$$

where $Y(\theta)$ is a geometrical factor, A is the run constant and $S(\theta)$ is the corrected number of tracks per swath. The swath will be defined and $S(\theta)$ will be discussed in a subsequent section on surveying of plates.

The run constant A is given by:

$$A = T/M\rho h,$$

where T is the temperature of the hydrogen, M is the total charge collected and ρ and h have been previously defined. The computation of A (A is denoted as $1/R$ in reference 5) has been discussed by Dearnley, *et al.*[5]

The geometric factor $Y(\theta)$ involves the universal constants entering into the expression for the cross section and depends inversely on $L(\theta)w(\theta)$ where $L(\theta)$ is the scattering length or effective thickness of target and $w(\theta)$ is the solid angle defined by the area of a swath. $Y(\theta)$ has been evaluated for the angles of interest. The rms errors in the geometric factor $Y(\theta)$ due to errors in the measurement of the geometry vary between ± 0.30 and ± 0.42 percent. The angle θ is determined to an accuracy of between ± 0.02 and ± 0.04 percent.

III. RUN PROCEDURE

A check on the impurity scattering in every run was made by covering two of the eight plates with a thickness of aluminum foil sufficient to stop protons which were scattered by protons, but would allow protons scattered by heavier nuclei to pass through. The aluminum covered plates gave information about impurity scattering in the angular interval 30° to 45°.

In the preliminary stages of this experiment it was found that the background pressure (as read with ion gauge G 1) of the scattering chamber, when loaded with plates, could be reduced by a factor of 5 or 10 by adding liquid nitrogen to trap T 1, Fig. 1. The removal of impurities also manifested itself in the comparison of the number of proton tracks observed at small angles in uncovered plates from liquid nitrogen and non-liquid nitrogen vacuum runs. The vacuum track corrections for both types of runs were essentially the same down to angles of about 20°; that is, it varied from about one percent at 45° to about two percent at 20°. However in the range 20° to 10° there was a marked difference in the magnitude of the vacuum track correction between the two types of runs. In the case of non-liquid nitrogen runs it amounted to about 10 percent at 10°, whereas in the case of liquid nitrogen runs it amounted to only two percent at 10°.

With the object of reducing corrections as much as possible it was decided to make runs for the relative cross section from 45° to 10° using liquid nitrogen in trap T 1. Because of the possible cooling of the gas in the scattering volume due to T 1 during a liquid nitrogen run, the absolute cross section was to be determined from data obtained from non-liquid nitrogen runs in the angular range of 30° to 45°. This range was used because an impurity check using aluminum-covered plates could be made.

The system was pumped down for 45 hr for non-liquid nitrogen runs, 24 hr for liquid nitrogen runs and was leak tested before each run. After the system was

found to be tight it was isolated from the diffusion pump by closing valve $V1$ and connected to the hydrogen flushing fore pump by opening valve $V2$. Shielding prevented air from the cyclotron cooling system, the liquid nitrogen traps and the diffusion pump blower from reaching the chamber proper or the coiled tubing introducing hydrogen into the system. The palladium valve was turned on and valve $V2$ was adjusted until an equilibrium hydrogen pressure of one cm of mercury was reached in the scattering chamber. The setting of $V2$ determined the pumping speed of the chamber. This same pumping speed of 6.4 cc/sec at a pressure of one cm of mercury was used throughout all of the runs.

The resistance of the charge measuring circuit and the ballistic constant of the galvanometer used for charge measuring were measured. The charge was measured during the run by recording the individual deflections of the ballistic galvanometer. During the run, readings of the pressure and temperature of the hydrogen were taken every five minutes. At the conclusion of the run, the resistance was remeasured and the ballistic constant of the galvanometer redetermined. The time for charging between successive discharges of the condenser was recorded. The resistance of the charge measuring circuit was about 5×10^{12} ohms.

In the case of a vacuum run, the same initial procedure was followed. No final measurement of the resistance or of the ballistic constant was made since knowing the total charge within several percent was sufficient for making the track background correction.

TABLE I. Summary of energy data.

Energy run no.	High energy component of beam (Mev)	Percentage of high energy component of beam	Low energy component of beam (Mev)	Percentage of low energy component in beam	Average energy for run (Mev)	Average energy for set of runs with assigned rms errors (%)
1	3.399	87.05	3.272	12.95	3.383	3.384 Mev±1.42
2	3.400	85.47	3.290	14.53	3.384	
3	3.453	87.86	3.301	12.14	3.435	3.435 Mev±1.40
4	6.839	100			6.839	6.846 Mev±0.58
5	6.860	95.67	6.705	4.33	6.853	
6	7.528	92.73	7.370	7.27	7.517	7.514 Mev±0.53
7	7.527	93.99	7.360	6.01	7.517	
8	7.508	100			7.508	

IV. ENERGY MEASUREMENT

Runs were made at cyclotron energies of 3.4, 6.8, and 7.5 Mev. The various energies were obtained by changing the resonance conditions of the cyclotron. The energy was measured by running Bragg curves in air as described by Dearnley, *et al.*[8] The points of the Bragg curve were corrected for temperature, pressure and humidity. The energy was evaluated using recent curves given by Bethe.[9] Table I is a summary of the energy measurements with the assigned rms errors.

[9] H. Bethe, *Properties of Atomic Nuclei*, No. 2 (Brookhaven National Laboratory, 1949), unpublished.

V. SURVEY OF PLATES

Binocular microscopes with 10× eyepieces, 43× objectives and dark field illumination were used for surveying the plates. One ocular of the microscope was fitted with a Howard disk[10] to define a given area on the plate being surveyed. The microscopes were fitted with special stages to handle 10-in. plates. The stages were fitted with a longitudinal travel which could be set to ±0.005 cm and an ordinary lateral travel.

A plate was set on the stage so that the longitudinal scale would read the distance from the 45° end of the plate to one edge of the Howard disk. The track counting was confined to the area enclosed between the two reticule marks photographed on the plate. The large square of the Howard disk defined an area of plate about 270μ square which was called a field. The track counting was done in units of one swath, the swath being defined as 16 fields across the plate but confined within the two reticule marks. In all cases more than one swath per plate was counted at a given angle in order to obtain sufficient numbers of tracks.

TABLE II. Liquid nitrogen p-p differential scattering cross sections at 3.38 and 6.85 Mev in the laboratory system in units of 10^{-24} cm^2.

θ (%)	$\sigma(\theta)$ at 3.38 Mev	$\sigma(\theta)$ at 6.85 Mev
45.199°±0.04	37.89±0.70	21.23±0.40
40.174°±0.04	40.82±0.76	22.67±0.44
35.142°±0.05	43.42±0.81	24.81±0.48
30.117°±0.05	43.63±0.85	25.29±0.48
25.078°±0.04	45.81±0.84	26.06±0.49
20.062°±0.05	48.50±0.92	26.48±0.51
15.040°±0.04	59.74±1.09	29.03±0.55
12.534°±0.04		34.64±0.68
10.062°±0.02		51.76±1.00

The errors given are rms errors.

The swaths were counted symmetrically about a center swath used for computing the angle θ.

The binocular microscope was adjusted to the proper interpupillary distance of the person counting. The area subtended on the plate by the Howard disk was a function of the interpupillary setting, consequently the average number of tracks per swath obtained by a surveyor had to be corrected. This correction amounted to as much as eight percent in the case of one surveyor. The following criteria were used in surveying the plates. For incident proton energies in the range 3.4 to 7.5 Mev the proton scattered protons penetrate the emulsion in the angular range 45° to 20°. For incident proton energies of 6.8 Mev or greater, the proton scattered protons penetrate the emulsion in the angular range 20° to 10°. For 3.4 Mev incident protons, the proton scattered protons are just able to penetrate at 20°, at 10° they can pass through about 70 percent of the emulsion. Because of the slit edge penetration, the

[10] The Howard disk is a reticule consisting of a large square subdivided into sixteen equal squares.

length criterion was chosen as follows. All tracks with lengths greater than 25 percent of the expected length of a proton scattered proton at a given angle were counted. In addition, the initial part of the track had to be parallel to the reticule lines and inclined at an angle θ to the surface of the emulsion. Finally, only tracks beginning in the field defined by the Howard disk were counted. The same criteria as applied to the counting of gas runs were applied to the vacuum runs. The plates were surveyed by five readers. Frequent checks were made and they showed consistency in the counting amongst the five.

In this experiment the minimum number of tracks on which a cross section is based is greater than 7000 and the maximum is about 20,000, with most points based on about 10,000. This gave a spread in the rms error in $S(\theta)$ of a purely statistical nature of from ± 1.20 to ± 0.71 percent. The counting criteria were doubtfully satisfied by about one percent of the total number of tracks observed. This introduced an additional rms error of ± 1 percent in $S(\theta)$. The total rms error in $S(\theta)$ for the various cross sections was in the range of ± 1.22 to ± 1.56 percent.

TABLE III. Non-liquid nitrogen p-p differential scattering cross sections at 3.44, 6.85, and 7.51 Mev in the laboratory system in units of 10^{-26} cm^2.

θ (%)	$\sigma(\theta)$ at 3.44 Mev	$\sigma(\theta)$ at 6.85 Mev	$\sigma(\theta)$ at 7.51 Mev
45.199°±0.04	37.74±0.68	21.35±0.41	19.48±0.37
40.174°±0.04	40.32±0.74	23.23±0.45	20.92±0.40
35.142°±0.05	41.89±0.76	24.74±0.48	22.81±0.44
30.117°±0.05	44.28±0.82	25.84±0.52	23.71±0.46
25.078°±0.04	45.10±0.82	26.06±0.50	23.96±0.44
20.062°±0.05	46.22±0.86	27.00±0.53	24.66±0.48
15.040°±0.04	55.02±1.05	28.44±0.56	25.35±0.48
13.611°±0.04		30.82±0.63	26.08±0.52
12.534°±0.04		32.43±0.67	28.38±0.53
11.260°±0.04		38.12±0.82	33.75±0.63
10.062°±0.02		48.58±1.04	42.15±0.86

The errors given are rms errors.

VI. SMALL CORRECTIONS

In deriving the expressions for $L(\theta)$ and $w(\theta)$ the assumption was made that an ideal geometry prevailed and consequently certain small effects and their corrections were ignored. These corrections were first considered by Breit, *et al.*[11] and subsequently by Dearnley, *et al.*[5] for apparatus similar to the present apparatus.

The fringing field of the cyclotron was expected to affect the protons within the chamber. The field was measured and its effect computed and found to be negligible for the energies of this experiment. This was also evident experimentally from observations of the uniformity of the distribution of protons at a given angle θ in all of the plates from any run.[12]

The effect of the slit edge penetration was to increase the effective scattering length. The correction to the cross section for the increase in scattering length was computed on the assumption that tracks with lengths greater than 25 percent of the maximum track length were counted and amounted to less than 0.54 percent. The justification for computing this correction is given by Dearnley, *et al.*[5]

In deriving expressions for $L(\theta)w(\theta)$ and θ the finite size of the beam, scattering slit and total area of plate surveyed per angle were disregarded. To correct for this, $L(\theta)w(\theta)$ and θ were averaged over the scattering volume and total area of plate surveyed per angle. The corrections to the cross section and θ were less than 0.4 and 0.1 percent, respectively.

The cross section was also corrected for the curvature of the cross section (laboratory system of coordinates) over the angular interval of observation. This correction amounted to 0.5 percent in the worst case.

VII. P-P DIFFERENTIAL SCATTERING CROSS SECTIONS

The data obtained at 3.44 and 6.85 Mev are the results of two gas scattering runs, the data at 7.51 Mev are the results of three gas scattering runs and that at 3.38 Mev of only one such run. Using the data from the individual scattering runs, the uncorrected cross sections were computed for the purpose of determining any inconsistency in the values obtained from the separate runs. In nearly all cases, the individual cross sections obtained agreed with each other within the statistical errors in $S(\theta)$. The experimental cross sections given in Tables II and III are completely corrected for all of the corrections discussed in the preceding section. The total rms errors assigned to the cross sections are also given. Using the S phase shifts from the non-liquid nitrogen data at 7.51, 6.85, and 3.44 Mev and the liquid nitrogen data at 3.38 Mev, S wave scattering cross sections were computed. These theoretical curves together with the experimental data are plotted in Figs. 3 through 7.

For a central force, the repulsive P wave will tend to increase the cross section over the pure S wave cross section for small scattering angles, and go to zero at 90° in the cg system. This P wave contribution is expected to become appreciable at 7 Mev if present. It is not expected to have any observable effect at 3.4 Mev. If impurities are present in the scattering volume, then the Coulomb scattering from the impurities will simulate a repulsive central P wave effect at small scattering angles.

When the liquid nitrogen data at 6.85 Mev were first obtained and analyzed, an increase in the cross section for small scattering angles was noted. At first this was interpreted as indicating a repulsive central P wave

[11] Breit, Thaxton, and Eisenbud, Phys. Rev. **55**, 1018 (1939).

[12] An asymmetry in the track distribution was observed in one case at 3.17 Mev in which the back of the scattering chamber was out of alignment by 0.5 mm. The cross-section curve obtained from this data was a pure S wave curve from 10° to 45°. This did show experimentally that the effect of a slight off-centering of the apparatus cancels out in the final result because of the symmetry of the geometry.

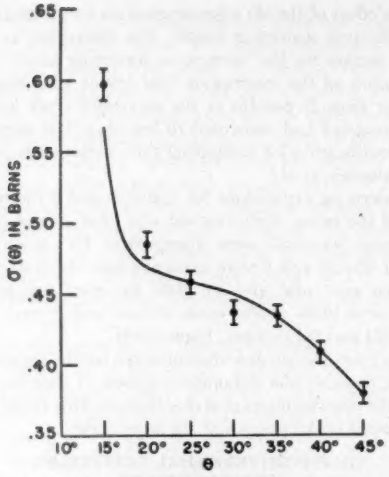

FIG. 3. Liquid nitrogen p-p differential scattering cross sections in the laboratory system with assigned rms errors at 3.38 Mev and S wave curve for S phase shift of 52.54°.

effect of −0.5°. The non-liquid nitrogen data at 6.85 Mev were evaluated later and showed no increase over the S wave curve at small angles. The liquid nitrogen runs at 3.38 Mev also indicated an increase in the cross section for small angles whereas the non-liquid nitrogen runs at 3.44 Mev indicated no such effect. This was interpreted to mean that while the liquid nitrogen in trap $T1$ was very efficient in removing impurities in vacuum runs it was inefficient during gas runs. This led to an undercorrection for the vacuum track background at small angles. Thus the conclusion was reached

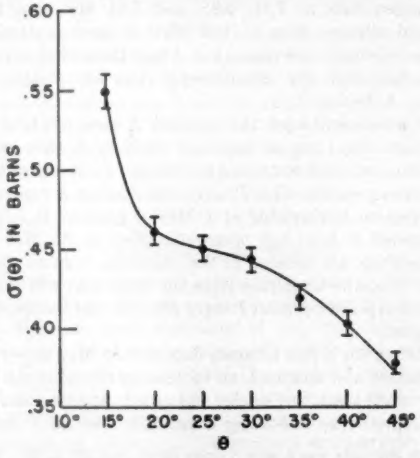

FIG. 4. Non-liquid nitrogen p-p differential scattering cross sections in the laboratory system with assigned rms errors at 3.44 Mev and S wave curve for S phase shift of 52.46°.

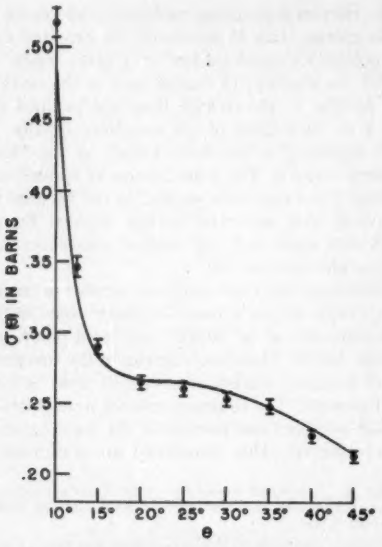

FIG. 5. Liquid nitrogen p-p differential scattering cross sections in the laboratory system with assigned rms errors at 6.85 Mev and S wave curve for S phase shift of 55.82°.

that all data must be obtained from non-liquid nitrogen runs.

Referring to the data, one notes that the scattering appears to be wholly S wave. The S phase shifts were computed using the exact expression for the S phase shift

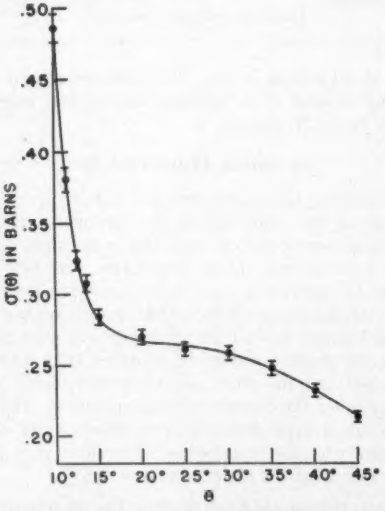

FIG. 6. Non-liquid nitrogen p-p differential scattering cross sections in the laboratory system with assigned rms errors at 6.85 Mev and S wave curve for S phase shift of 55.82°.

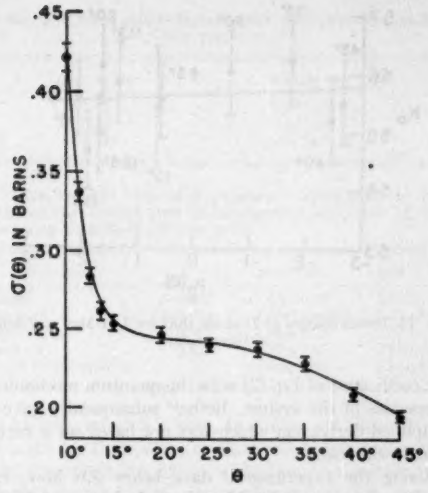

FIG. 7. Non-liquid nitrogen p-p differential scattering cross sections in the laboratory system with assigned rms errors at 7.51 Mev and S wave curve for S phase shift of 55.78°.

given by Critchfield and Dodder.[13] Because of the false P wave effect observed in the liquid nitrogen data and the lack of an appreciable P wave effect in the non-liquid nitrogen data, the final S phase shifts obtained from the non-liquid nitrogen data were computed as follows. At 3.44 Mev the final S phase shift was the average of the phase shifts obtained for $\theta \geqslant 25°$. This cut-off angle was chosen because the 3.38-Mev liquid nitrogen data for $\theta \leqslant 20°$ showed an appreciable increase in cross section over the S wave cross section. The final S phase shift for 3.44 Mev was computed in this manner in order to be certain that no impurity scattering could affect it. Using the same criterion, the final S phase shifts for the 6.85 and 7.51 Mev non-liquid nitrogen data were computed for a cut-off angle of 15° which was determined from the 6.85-Mev liquid nitrogen data. The S phase shifts for the liquid nitrogen data were

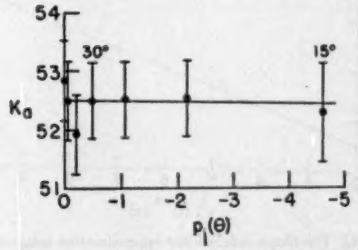

FIG. 8. Determination of central P phase shift for 3.44-Mev non-liquid nitrogen data.

[13] C. Critchfield and D. Dodder, Phys. Rev. 75, 419 (1949).

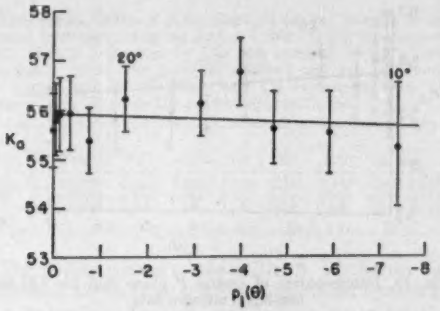

FIG. 9. Determination of central P phase shift for 6.85-Mev non-liquid nitrogen data.

computed in identically the same manner. The S phase shifts obtained are given in Table IV.

The data were analyzed for central P wave effects using the method of apparent S phase shifts described by Blatt and Jackson.[2] This analysis is shown in Figs. 8, 9 and 10. The P phase shifts obtained are given in Table V. Figure 11 is the analysis of the 6.85-Mev liquid nitrogen data.

The 7.51-Mev data were analyzed for a D phase shift using this method. A D phase shift of $-0.05°\pm0.1°$ was obtained. This analysis is shown in Fig. 12.

The lack of P and D wave effects at 7.51 Mev is consistent with the 29- and 32-Mev p-p scattering data obtained at Berkeley[14] which showed no appreciable P or D wave contributions although one would expect large contributions at these energies.

VIII. ANALYSIS OF THE DATA

The S wave data were analyzed using the function $f(E)$ defined by:

$$f(E)=\pi \cot K_0/(e^{2\pi\eta}-1)+h(\eta), \qquad (1)$$

where

$$\eta=e^2/\hbar v,$$

and

$$h(\eta)=-\ln\eta+0.5772\cdots+\eta\sum_{s=1}^{\infty}1/s(s^2+\eta^2).$$

$0.5722\cdots$ is Euler's constant and v is the relative

TABLE IV. S phase shifts obtained from all data with rms errors.

Type of run	Energy in Mev	S phase shift
Liquid nitrogen[a]	3.38	52.54°
Non-liquid nitrogen	3.44	52.46°±0.6°
Liquid nitrogen[a]	6.85	55.42°
Non-liquid nitrogen	6.85	55.82°±0.6°
Non-liquid nitrogen	7.51	55.78°±0.6°

[a] No errors are assigned the liquid nitrogen data because of the uncertainty in the temperature measurement of the hydrogen gas.

[14] Panofsky and Fillmore, UCRL 481 (University of California) (1949), unpublished. Richman, Cork, and Johnston, UCRL 482 (University of California) (1949), unpublished.

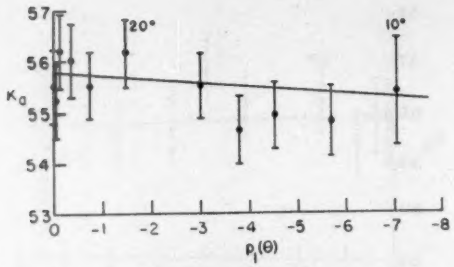

FIG. 10. Determination of central P phase shift for 7.51-Mev non-liquid nitrogen data.

velocity of the two protons. The function $f(E)$ allows a power series expansion in the energy k^2, thus giving

$$f(E)=R(-a^{-1}+0.5r_0k^2-Pr_0^3k^4\cdots) \qquad (2)$$

where $R=\hbar^2/Me^2$ is the Bohr radius of a proton bound to a fixed center of electrostatic attraction, $k^2=ME_{\text{lab}}/2\hbar^2$, a is the Fermi scattering length[15] for two protons evaluated at zero energy, r_0 is the effective range of nuclear forces and P is a coefficient depending upon the tail of the nuclear potential. The approximation to $f(E)$ afforded by taking only the first two terms of Eq. (2) is called the "shape independent" approximation. Every type of interaction determines a set of coefficients a, r_0, P, $\cdots$. The coefficients of the k^4 and higher order terms are very small for the potentials commonly assumed.

Breit, Condon, and Present[16] first defined the function $f(E)$. Subsequently, Landau and Smorodinsky[17] used $f(E)$ to prove the non-existence of the di-proton. Schwinger[18] was the first to give a rigorous derivation of $f(E)$ based on a variational principle and to correlate

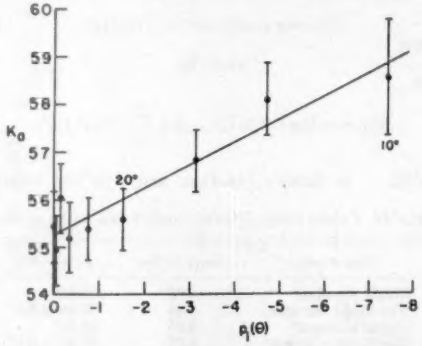

FIG. 11. Determination of central P phase shift for 6.85-Mev liquid nitrogen data.

[15] E. Fermi and L. Marshall, Phys. Rev. 71, 666 (1947).
[16] Breit, Condon, and Present, Phys. Rev. 50, 825 (1936).
[17] L. Landau and J. Smorodinsky, J. Phys. USSR 8, 154 (1944).
[18] J. Schwinger, Nuclear Physics Notes (Harvard, 1947), unpublished.

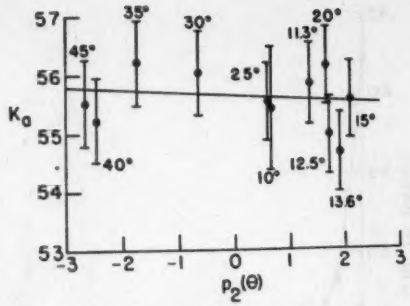

FIG. 12. Determination of D phase shift for 7.51-Mev non-liquid nitrogen data.

the coefficients of Eq. (2) with the quantum-mechanical properties of the system. Bethe[19] subsequently gave a simplified derivation which was not based on a variational principle.

Using the experimental data below 3.6 Mev, excluding the present 3.4-Mev data, Jackson and Blatt[2] have made a best weighted least-squares fit to the data for the four potentials commonly used and the shape independent approximation and determined the variational and well parameters. The variational parameters obtained by them are given in Table VI.

The shape independent approximation using the parameters of Table VI and the present experimental data with rms errors are shown in Fig. 13. Also shown in Fig. 13 is the Dearnley, *et al.*[5] point with its rms error.

Using the data of Table VI, $f(E)$ was computed for the four potentials and the shape independent approximation for the energies at which data were obtained in the present experiment. These values of $f(E)$ plus the experimentally determined values of $f(E)$ with their rms errors are given in Table VII. From Table VII one can see that all four potential shapes are consistent with the experimental data obtained.

The present data shows no appreciable P wave effect

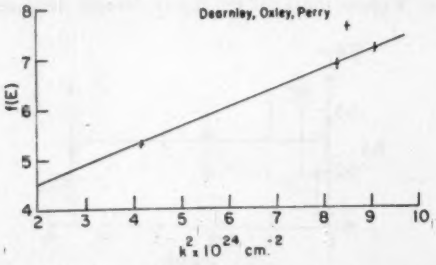

FIG. 13. The shape independent approximation using constants of Table VI. The Dearnley, *et al.* (reference 5) point and the present experimental points with assigned rms errors to $f(E)$ and k^2 are shown.

[19] H. Bethe, Phys. Rev. 76, 38 (1949).

TABLE V. P phase shifts obtained from non-liquid nitrogen data with rms error.

Energy in Mev	P phase shift
3.44	0.01°±0.1°
6.85	0.03°±0.1°
7.51	0.07°±0.1°

TABLE VI. The variational parameters which give the best weighted least-squares fit to the experimental data below 3.6 Mev (excluding the present 3.4-Mev data).

Well shape	P	$a(10^{-13}$ cm)	$r_0(10^{-13}$ cm)
Square	−0.033	−7.66±0.05	2.60±0.07
Gaussian	−0.019	−7.66(5)±0.05	2.62±0.07
Exponential	0.009	−7.68±0.05	2.67±0.07
Yukawa	0.055	−7.70±0.05	2.76±0.07
Shape indep. approx.		−7.67±0.05	2.64±0.07

up to energies of 7.5 Mev. It is also not inconsistent with the predictions of the Christian-Noyes potential[20] used to explain the 32- and 340-Mev p-p scattering.[21] The Christian-Noyes potential predicts an overall increase of less than two percent at 7.5 Mev to the S wave curve due to the tensor P wave contribution.

[20] Christian and Noyes, UCRL 554 (University of California) (1949), unpublished.

[21] Chamberlain and Wiegand, UCRL 553 (University of California) (1949), unpublished.

TABLE VII. Values of $f(E)$ computed for the energies of the present experiment using the data of Table VI. The experimental value of $f(E)$ is denoted by f_{exp}. The numbers in the column headings f denote the potential assumed and are as follows: (1) square well, (2) Gaussian well, (3) exponential well, (4) Yukawa well, (5) shape independent approximation.

E (Mev)	$k^2(10^{26}$ cm$^{-2})$	$f(1)$	$f(2)$	$f(3)$	$f(4)$	$f(5)$	f_{exp}
3.44	4.142±0.06	5.340	5.341	5.336	5.333	5.333	5.302±0.067
6.85	8.254±0.05	6.966	6.943	6.893	6.798	6.897	6.859±0.122
7.51	9.060±0.05	7.291	7.261	7.196	7.072	7.204	7.177±0.130

The author wishes to thank Dr. S. W. Barnes for suggesting the problem and for his continued interest in the experiment. The apparatus was designed by Dr. Barnes and constructed under his supervision and that of Mr. E. Chandler of the 130-in. laboratory. Modifications were made on the apparatus by Mr. M. Winchell of the 130-in. laboratory and Mr. A. Gibson of the Physics Dept. Dr. J. Wallace Moyer and Mr. A. M. Perry were collaborators in the preliminary stages of this experiment. Mr. R. Vanselow and Misses M. Carroll and N. Dunkelberg and Mrs. M. Torrebara assisted in obtaining data. The author wishes to thank Dr. G. Breit of Yale University and Drs. Barnes, C. Oxley and R. Marshak for many discussions and suggestions. This research was supported in full by two grants to Dr. Barnes from the Research Corporation.

The Relative Probabilities and Absolute Cross Sections of the D−D Reactions

K. G. McNeill* and G. M. Keyser†
Clarendon Laboratory, Oxford University, Oxford, England
(Received October 13, 1950)

Measurements with a gas target have been made of the relative probabilities and absolute cross sections of the two possible D−D reactions, by simultaneously counting the helium and hydrogen nuclei produced by the reactions. The counters were separated from the target by a thin silica window. The ratio of the cross section of the neutron-producing reaction to that of the proton-producing reaction was found to increase from 0.95 at 120 kev to 1.06 at 250 kev. The "neutron" cross section was 0.019 barn at 120 kev and 0.038 barn at 250 kev while the "proton" cross section increased from 0.020 barn at 120 kev to 0.049 barn at 300 kev. The results can be fitted to an expression of the form $\sigma E=\sum a_l P_l$ and the values of the coefficients a_l are given.

I. INTRODUCTION

WHEN deuterium is bombarded with deuterons of any energy two nuclear reactions are possible:

$$D^2+D^2\rightarrow H^3+H^1$$
$$\rightarrow He^3+n.$$

Many investigations have been carried out on the first of these reactions but the other has been relatively neglected. This is mainly due to the circumstance that either the He particles or the neutrons must be counted, and the first is troublesome owing to the short range of the He nuclei, the second owing to scattering and to the necessity of calibrating the neutron counter. Theoretically, it has usually been considered that the two reactions would have the same probabilities.

The experimental results, however, indicate that the ratio of the cross section of the second reaction (the neutron-producing reaction), to the cross section of the first (the proton-producing one), hereafter called the branching ratio, does not in general equal unity, nor does it remain constant with energy. The experiments of Blair and his co-workers[1] in the range 1 to 3.5 Mev indicate a tendency for the branching ratio to fall with energy while Manley, Coon, and Graves and Graves, Graves, Coon and Manley[2,3] found that the branching ratio increased with energy in the energy range 100 to 300 kev. Pepper[4] concludes that the branching ratio is constant below 60 kev. Previous work in this laboratory[5] appeared to shown that the branching ratio increased with energy in the region 70 to 160 kev. Of these authors, only Blair and his associates used a gas target.

Again, the values for the absolute cross section of the proton reaction given by Sanders, Moffat, and Roaf[6] and by Bretscher, French, and Seidl[7] do not agree.

In view of these inconsistencies, it appeared important to redetermine the variation of the branching ratio with voltage using a gas target. This approximates to an ideally thin target in which there can be no dispute as to the energy of the incident particles when a reaction takes place. Moreover, the use of a gas target enables absolute cross sections to be determined without the necessity of knowing, for example, the rate of loss of energy of deuterons in heavy ice.

II. APPARATUS

The high voltage was provided by a Philip's type generator, capable of giving voltages up to 500 kev. An rf ion source was employed.[8] The beam was analyzed magnetically, to ensure that only D^+ ions of definite energy caused reactions. At first a 90° analyzer was used, but later this was replaced by a 10° analyzer, which had a smaller defocusing action on the beam. The beam passed into the target through the two canals of a differential pumping system. A diagram of the canal system and the target is given in Fig. 1.

In lining up the beam the following procedure was adopted. First a maximum current was obtained through the analyzer. The first canal section was then bolted to the analyzer, and an observation chamber placed at its far end. The beam was centered on the entrance port of the canal, as seen through a window. The canal was pivoted about an axis through the entance port with ball and socket joint, and could be rotated in any direction (±15°), by means of the threaded rods and flexible section contained in its construction. Its orientation was adjusted until a

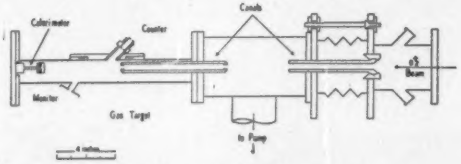

FIG. 1. Differential pumping system and gas target.

* At present at Yale University, New Haven, Connecticut.
† On leave from the National Research Council of Canada, Ottawa, Canada.
[1] Blair, Freier, Lampi, Sleater, and Williams, Phys. Rev. **74**, 553 (1948).
[2] Manley, Coon, and Graves, Phys. Rev. **70**, 101A (1946).
[3] Graves, Graves, and Manley, Phys. Rev. **70**, 101A (1946).
[4] T. P. Pepper, Can. J. Research **27**, 143 (1949).
[5] McNeill, Thonemann, and Price, Nature **166**, 28 (1950).
[6] Sanders, Moffat, and Roaf, Phys. Rev. **77**, 754A (1950).
[7] Bretscher, French, and Seidl, Phys. Rev. **73**, 815 (1948).
[8] Thonemann, Moffat, Roaf, and Sanders, Proc. Phys. Soc. (London) **61**, 483 (1948).

maximum current passed through the canal, and the rods were then locked. The target, to which the second canal was rigidly attached, was then screwed to the T-piece joining the diffusion pump to the target system, and the T-piece attached to the pump through a bellows section. A lattice-work sleeve fitted over the second canal, to ensure that when the target section was screwed to the first canal section the two canals would be parallel, and that therefore a maximum beam would pass through the second canal into the target. This sleeve is not shown in the figure.

The diffusion pump used was an Edwards 403, which has a nominal baffled speed for air of 200 liters/sec. It was found possible to maintain a pressure of about 0.1 mm Hg in the target without the pressure in the accelerator tube rising appreciably. About 200 cc of deuterium at NTP were used per hour, and this was ejected to the air and wasted. At this target pressure the loss of energy of the incident deuteron beam is negligible. The deuterium flow into the target was controlled by a needle valve, and a McLeod gauge was used to measure the target pressure. A reading of the gauge was taken every few minutes during a run, and the average pressure at any particular time was obtained from a pressure-time graph. After each run the gas from the target was sampled. K. I. Mayne very kindly analyzed the samples in a mass spectrometer to determine the relative amounts of deuterium and other gases present.

The beam intensity was measured by means of a calorimeter,[9] similar to that used by Moffat, Roaf, and Sanders[10] and had a sensitivity of about 0.3 mv/watt.

The beam current measurement is dependent directly on the beam voltage measurement, as the calorimeter measures watts, rather than amperes. The voltage was measured by the current flow through a high resistance of approximately 200 megohms. The value of the resistor was determined by a condenser discharge method with an accuracy of 1 percent. During the long runs necessary with the gas target, it was found that the high voltage tended to fluctuate, owing to the variations in the current drawn from the set. The resolving power of the magnet plus the canal system was such that a variation of 1.5 percent in the beam voltage would stop the beam entering the target, and if the voltage altered by more than 0.5 percent it was noticed by a fall in the current and returned to its original value. The ripple on the set did not exceed 0.5 percent of the steady potential.

The gas target is shown in Fig. 1. The main body was made from a section of rectangular wave-guide tubing of cross section 4 in.×2 in. and length 12 in. Both ends had flanges soldered to them, in one of which was pushed the target canal, and through a hole in the other was inserted the beam measuring calorimeter. The beam passed close to the top of the wave guide, so that the solid angle subtended by the beam to the counters was as large as possible. The deuterium gas entered the target through a tube in the bottom of the wave guide, and through a similar tube a lead was taken to the McLeod gauge. On the top surface of the guide was hard-soldered a flange which served as a bed for the counter turn-table. Finally, provision was made for the attachment of a subsidiary counter to the bottom of the guide to act as a monitor for the beam. All vacuum seals throughout the target and the rest of the system were made with rubber gaskets, or, where this was impracticable, with wax.

[9] J. Sanders, J. Sci. Instr. 26, 36 (1949).
[10] Moffat, Roaf, and Sanders (to be published).

III. EXPERIMENTAL PROCEDURE

The three charged particles produced by the D−D reaction have widely different rates of loss of energy, and it is thus possible to differentiate among them using a single proportional counter. As the proton pulses, in the counters used, were very small compared with those produced by the He^3 nuclei (about $\frac{1}{10}$ as large), it was found better to count the protons in a second chamber, separated from the first by an Al foil. The counting of the protons was done simultaneously with the counting of the heavier particles in the first chamber.

The twin counters used were screwed on to a threaded tube mounted on the counter turn-table, and thus could be rotated about the beam. For simplicity the two counters were made as a single unit, and filled to the same pressure. They were both of the side-on type, the counter wires, of 100μ tungsten, being terminated in small glass beads. The first counter, in which He^3 and H^3 nuclei were counted, was of width 1 cm, whereas the path length of the protons in the second counter was 5 cm, to compensate for their smaller rate of loss of energy. As described in a previous letter,[5] a thin Si window was used between the target and the first counter, this window allowing all of the charged reaction particles to pass through it. The partition between the twin counters, which was removable, had an insert for receiving an Al foil, which was held taut and in place by a spring washer. This foil was of sufficient thickness to stop the He^3 and H^3 nuclei entering the second chamber. A number of holes around the outside edge of the partition allowed free passage for the counter gas. The counters could be filled to any desired pressure with a 10:1 argon-alcohol mixture. It was found that 12 cm of this mixture gave optimum conditions for resolution between the different particles. A copper plate, sufficiently thick to stop all of the charged particles, could be moved across the entrance to the collimating system by means of a rod passing through a Wilson seal, to enable backgrounds to be measured. In previous experiments, when an end-on counter was used to count the protons, difficulties had been experienced, owing to the fact that the number of tritons counted in the first chamber was not equal to the number of protons in the second counter. This was probably

due to the end-on counter not being equally efficient at different distances from the wire, but to check that this was not the case with the present arrangement, the counters and collimating system were tested with alpha particles before being used on the D−D reaction. For this experiment the Al foil was removed from the partition.

Conventional electronic circuits were employed, with a head and main amplifier, cathode-ray oscillograph monitor, and pulse-height discriminator and scaler, or pulse-height selector and scaler, connected to each counter. With the counting rates used, there was negligible error caused by the finite resolving time of the counters or the electronic equipment.

The optimum counter conditions were first found using an Al target; i.e., a target in which deuterium gas from the beam is occluded. This conserved deuterium, and also enabled the best conditions of counter pressure, wire potential, etc., to be found rapidly, owing to the large yield obtained from this type of target.

Owing to the time lag in the current measurement caused by the use of a calorimeter, a GEC G-M4 counter was used to monitor the beam. This was attached to the underside of the wave guide. If the count registered by the monitor during a run was very high or very low, the run was rejected, as it indicated that a large fluctuation in the beam current had taken place. The calorimeter had a half-period of 1 minute, and during the experiment the millivoltmeter attached to the thermocouples was read every minute. Alternate "direct" and background runs were taken, to avoid any errors due to fluctuations in the background. The background in the counters was almost entirely caused by neutrons which were due to the D−D reaction taking place at solid parts of the target; e.g., the calorimeter and canals, where deuterium was occluded.

TABLE I. Values of the branching ratio of the D−D reactions.

Voltage	Branching ratio σ_n/σ_p	Statistical error
120 kev	0.95	0.04
140	1.00	0.07
160	1.00	0.04
250	1.06	0.04

Counting rates of about one per second were obtained during the direct runs, and normally about 4000 counts were taken. The background was of the same order as the hydrogen count, and about a third of the actual count in the counting of the He^3 particles (the difference is caused by the fact that the He^3 pulses were much bigger than the H pulses). This causes the statistical errors to be much larger than the figure 4000 would lead one to expect. It was not found possible to reduce the background appreciably by the introduction of paraffin wax, owing to the small distance between the counters and the target.

To ensure that all particles were being counted, both pulse height discriminator bias curves and pulse height selector (kick-sorter) bias curves were taken. The equality of the triton and proton counts was checked. To guard against the possibility that the counter system was not symmetrical about the beam, the counters were turned through 180° and the equality, within the statistical error, of the proton counts in the two positions checked.

IV. RESULTS

For comparison, all data were transformed from the observation angle of 90° in the laboratory system to an angle of 90° in the center of gravity system, assuming an angular asymmetry of the form

$$\sigma_\phi = \sigma_{90}(1+A\cos^2\phi). \quad (1)$$

To make the comparison, all counts were multiplied by the expression

$$g(\phi)/(1+A\cos^2\phi).$$

The factor $g(\phi)$ is due to the change in solid angle in turning from one system to another, and is equal to $[\sin^2\theta/\sin^2\phi]\cos(\phi-\theta)$, where θ is the laboratory angle, 90° in this case, and ϕ is the center of mass angle.[11] The values of A were taken from the work of Manning, Huntoon, Myers, and Young.[12]

All readings were normalized to unit current, time, and pressure in the target. In dividing any particular reading by the current, account had to be taken of the fact that the calibration of the calorimeter altered with different target pressures. As the background was virtually independent of the gas pressure, the actual normalizing formula was

$$\left\{\frac{\text{count}}{\text{current}\times\text{time}}-\frac{\text{background}}{\text{current}\times\text{time}}\right\}\Big/\text{pressure}.$$

By a comparison of the He and H counts for the same number of reactions, i.e., with unit beam current, unitary target pressure and in unit time, the ratio of the cross sections, the branching ratio, is directly obtained. The results are given in Table I. The errors indicated are statistical. In addition, there are measurement errors which are considered to have a maximum value of 2.7 percent. These enter from the reading of the pressure (½ percent), and the thermocouple emf (½ percent) (both readings are averaged over a run), and from the fact that inaccuracies in the reading of, or variations in, the beam voltage will introduce an error directly into the determination of the current from the calorimeter readings (1.5 percent) and also indirectly into the branching ratio values as the branching ratio is a function of the high voltage (0.2 percent). In the graph of the results, Fig. 2, the statistical errors are indicated. For comparison, the values of the branching ratio found previously using a solid target are given.

[11] Haxby, Allen, and Williams, Phys. Rev. **55**, 140 (1939).
[12] Manning, Huntoon, Myers, and Young, Phys. Rev. **61**, 371 (1941).

From the readings obtained in the branching ratio experiments it is possible to obtain the absolute cross sections of the two reactions. This entails the calibration of the calorimeter and the McLeod gauge and the calculation of the solid angle subtended by the collimating system. The calibration of the calorimeter was carried out using a Metrosil resistor as a heating unit, the wattage dissipated in the heater being measured by a potentiometer method. As with gas in the target gaseous conduction of heat competes with the metallic conduction down the thin walled tube, the calibration depends on the gas target pressure, and this variation was also determined. The McLeod gauge was calibrated by the normal technique of expanding small volumes of gas at pressures of 10 cm or so, which can be measured accurately by an Hg manometer and vernier microscope, into large volumes.

The collimating system consisted of two circular apertures, A and B, of diameters $2\frac{1}{2}$ and 4 mm separated by a distance of 2 cm. The direct calculation of the solid angle with such a system is difficult, and therefore an indirect method was employed. It was assumed for a first approximation that the hole nearer the beam was a slit. With such a system the calculation is straightforward.[13] The expression for the solid angle thus obtained was multiplied by a factor G, to correct for the use of a circular aperture. G was determined graphically, with an estimated error of less than 2 percent. Apart from all possible errors introduced in the measurement of the solid angle, there is a possibility that there may be a central core to the beam, which is not necessarily in the geometric center of the target area. Although optical observation did not indicate the presence of such a core, the possibility may not be excluded when the maximum errors are being considered. With the canal diameters and the distance of the beam from the counters used, this would introduce a maximum error of 5 percent, on top of the purely measurement errors (including that in G), of another 5 percent.

The readings taken will give the differential cross sections at 90° to the beam. The total cross section can be obtained by multiplying the differential cross section by $4\pi(1+A/3)$, assuming an angular asymmetry of the form of Eq. (1). As before, the values of A at different voltages are taken from the work of Manning *et al.* In Table II the differential and total cross sections of the two possible reactions are given between 120 and 300 kev, with the assumed value of A recorded. The errors indicated are statistical. In addition, errors in calibration and measurement, amounting to a maximum possible value of 20 percent, must be considered. This figure is made up of a 10 percent geometric error, $3\frac{1}{2}$ percent from the calibration and reading of the McLeod, $4\frac{1}{2}$ percent from the current measurement (2 percent from the wattage calibration, 2 percent from beam voltage uncertainty and $\frac{1}{2}$ percent reading error), $\frac{1}{2}$ percent from the estimation of the deuterium content of the target gas, and $1\frac{1}{2}$ percent from the high voltage. This comes from the variation of cross section with voltage. In the graphs of the results, Figs. 3 and 4, 20 percent errors are indicated.

[13] Herb, Kerst, Parkinson, and Plain, Phys. Rev. **55**, 998 (1939).

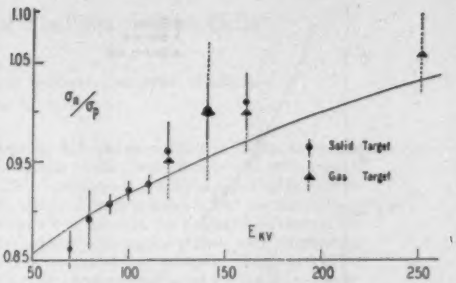

FIG. 2. The ratio of the cross sections of the D(d, n)He^3 and the D(d, p)H^3 reactions (branching ratio) as a function of voltage. The solid target results are taken from reference 5.

V. DISCUSSION

Following Konopinski and Teller,[14] an attempt was made to fit the results to an expression of the form $\sigma E=\sum_l a_l P_l$ where σ is the total cross section at energy E, P_l is the interpenetrability of two deuteron waves with relative angular momentum l, and a is a constant, equal to $\pi(2l+1)\cdot|\alpha_l|^2\cdot\hbar^2/2m$ where $|\alpha_l|$ is the intrinsic probability of a particular reaction taking place. In the voltage range considered only three terms of the expansion need be considered, owing to the rapid decrease of P_l with E. The values of P_l are given in a paper by Hunter and Richards,[15] and have been independently computed by Spiers.[16] In fitting the proton cross-section curve, consideration has been given to the values obtained by Blair, *et al.*, in the Mev range,[1] and by Sanders, Moffat, and Roaf in the 0- to 50-kev region,[6] as well as to the present results. In fitting the D(d, n)He^3 cross-section curve, consideration was

TABLE II. Differential and total cross sections of the D−D reactions at various voltages.

Voltage (kev)		Diff. σ (barns)	Total σ (barns)	(A)	Stat. error (percent)
120	σ_p	0.0013	0.020	(0.55)	3
	σ_n	0.0012	0.019		3
140	σ_p	0.0017	0.026	(0.63)	5
	σ_n	0.0017	0.026		5
160	σ_p	0.0016	0.026	(0.70)	3
	σ_n	0.0016	0.026		3
250	σ_p	0.0021	0.036	(1.00)	3
	σ_n	0.0022	0.038		3
300	σ_p	0.0023	0.049	(1.18)	6

[14] E. J. Konopinski and E. Teller, Phys. Rev. **73**, 822 (1948).
[15] G. T. Hunter and H. T. Richards, Phys. Rev. **76**, 1445 (1949).
[16] J. A. Spiers, private communication.

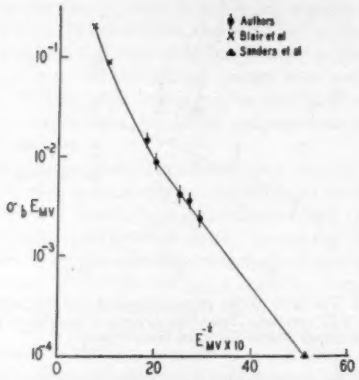

FIG. 3. A Gamow plot, $\log\sigma \cdot E$ vs $E^{-\frac{1}{2}}$, of the cross section of the reaction $D(d, p)H^3$.

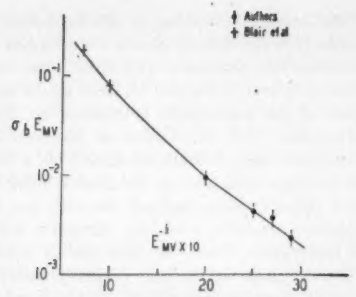

FIG. 4. A Gamow plot, $\log\sigma \cdot E$ vs $E^{-\frac{1}{2}}$, of the cross section of the reaction $D(d, n)He^3$.

taken of the results of Blair, *et al.*, Hunter and Richards, and of the present work. All these authors used gas targets. The best fit was obtained with the coefficients listed below. a_0, a_1, a_2, have been used to denote the coefficients a_l with l equal to 0, 1, and 2 in the $D(d, p)H^3$ reaction, and b_0, b_1, b_2, the corresponding coefficients in the neutron reaction.

$$a_0=0.006 \qquad b_0=0.0045$$
$$a_1=0.12 \qquad b_1=0.15$$
$$a_2=0.26 \qquad b_2=0.26.$$

The theoretical curve based on these coefficients is included in the graphs of the results.

The branching ratio (BR) will be given at any voltage by the expression

$$BR=(b_0P_0+b_1P_1+b_2P_2)/(a_0P_0+a_1P_1+a_2P_2)$$

where the P_l correspond to that voltage. Using the above values of the coefficients, the values of the branching ratio at various voltages have been calculated, and the theoretical line based on these figures is included in Fig. 3. It is of particular interest to note that there is very close agreement between the values of the branching ratio obtained using an occluded target and those using the gas target. This may be due to a thin layer of deuterium absorbed on the surface of the copper block acting as the main target.

It will be seen from the graphs, that there is good agreement of the present work with the results obtained by other workers using a gas target. There is, however, considerable disagreement with the results of Bretscher, French, and Seidl, who used a heavy ice target. An incorrect value for the rate of loss of energy of deuterons in heavy ice could account for the discrepancy.

We wish to express our thanks to Professor Lord Cherwell for extending to us the facilities of the laboratory, to Mr. C. H. Collie for his continued interest and advice, and to all the members of the HT group for their generous support. Mr. J. A. Spiers is to be thanked for many valuable discussions. One of us (K. G. McN.), is indebted to the Harmsworth Trust of Merton College, Oxford, and to the Department of Scientific and Industrial Research for financial support at different times, and the other of us (G. M. K.), wishes to thank the Physics Department of the National Research Council of Canada for similar assistance.

On the Photo-Conductivity of Thallous Sulfide Cells*

A. W. EWALD†
Randall Laboratory of Physics, University of Michigan, Ann Arbor, Michigan
(Received October 16, 1950)

An investigation of the rise and decay of the photo-current in Tl_2S cells shows that the simple bimolecular recombination theory on which previous quantitative discussions of the photo-effect in Tl_2S were based is inadequate for the complete explanation of these curves. The dependence of the initial slopes of the response curves on light intensity is that to be expected for a homogeneous photo-conductor, but the temperature dependence of these slopes suggests the presence of barriers which influence the conductivity through the mobility. The variation of both the initial slopes and the steady-state photo-conductivity with temperature indicate an exponential dependence of the mobility upon temperature with an activation energy of 0.19 ev. These results indicate that Tl_2S conforms to neither the strictly homogeneous model nor the sharp barrier picture but possesses features of both of these models; the photo-effect corresponds to the homogeneous model, but the charge carriers move with a mobility determined by light-insensitive barriers.

I. INTRODUCTION

THE development of highly sensitive thallous sulfide and lead sulfide infrared detectors during the war, together with the later development of lead selenide and lead telluride cells,[1–4] has aroused a general interest in photo-conductive materials. Systematic investigations of the properties of these cells have been undertaken for the most part only recently, and at present the mechanism of the photoelectric process in these materials is still under discussion. The earliest attempts at an explanation[5,6] were based on a homogeneous model in which the photoconductivity was attributed to the liberation by the light of charge carriers which recombine according to a bimolecular law. In the case of Tl_2S the square root dependence of the steady-state photo-current on the light intensity has been taken as strong evidence in favor of this picture. However, other properties such as the high resistance of the sensitive layers, and the disappearance of the photo-sensitivity with increasing frequency of an applied ac voltage (observed in PbS layers[7]) are not readily explained in terms of this model. To account for these and other properties various barrier pictures have been proposed[8,9] in which the photo-conductivity is attributed to a modification in the charge distribution of the barriers by the exciting radiation. These barrier pictures have proved to be more satisfactory for the explanation of the properties of PbS cells. Yet it now appears that neither the barrier model nor the homogeneous model is sufficiently general to allow a complete explanation of all of the photo-conductivity properties observed in the various types of cells and that these pictures represent only two extreme limiting cases of a more general behavior.[10]

In the present work the photo-conductivity of Tl_2S has been investigated both with modulated light and under steady excitation at various light intensities and temperatures. It is found that the cell behavior as revealed by even this limited investigation does not conform to the homogeneous model using a bimolecular recombination law. An analysis of the data in terms of a more general homogeneous model indicates that the photo-effect is probably due to the liberation of charge carriers but that the mobility of the carriers is affected by the presence of barriers.

II. EXPERIMENTAL METHOD AND RESULTS

To simplify the interpretation of the modulated light experiments the rise and decay of the photo-current were recorded between steady states in the dark and in the light. With the cell in the dark the excitation was initiated suddenly by means of a motor-driven, rotating shutter having an onset time of the order of 0.1 msec. Similarly, for the decay curves, with the cell initially exposed to the steady radiation, the excitation was interrupted suddenly. To make possible the amplification of the resulting relatively slow variations in cell conductance with a conventional ac amplifier, the usual dc cell voltage supply was replaced by an audio oscillator tuned to 1000 cps. The cell response then produced a modulation of the amplitude of the ac cell current. Strict proportionality between cell conductance and amplified signal was insured through the use of a sufficiently small cell load resistor in the input circuit to the linear amplifier, which had a flat frequency response in the vicinity of 1000 cps. The amplified signal was

* Part of a dissertation submitted in 1948 in partial fulfillment of the requirements for the degree of Doctor of Philosophy at the University of Michigan.
The thallous sulfide cells used in this research were developed by Dr. R. J. Cashman. The research was assisted by a Bureau of Ships, Navy Department, contract.
† Now at Northwestern University, Evanston, Illinois.
[1] R. J. Cashman, OSRD Report No. 5997 NDRC Div. 16.4 (1945) (unpublished).
[2] R. J. Cashman, OSRD Report No. 5998 NDRC Div. 16.4 (1945) (unpublished).
[3] Blackwell, Simpson, and Sutherland, Nature **160**, 793 (1947).
[4] Simpson, Sutherland, and Blackwell, Nature **161**, 281 (1948).
[5] A. Von Hippel and E. S. Rittner, J. Chem. Phys. **14**, 370 (1946).
[6] Ewald, Hole, and Uhlenbeck, Special Report No. 26 NDRC Div. 16.4 (1945) (unpublished).
[7] R. P. Chasmar, Nature **161**, 281 (1948).
[8] Sosnowski, Starkiewicz, and Simpson, Nature **159**, 818 (1947).
[9] W. James, Science **110**, 254 (1949).
[10] E. S. Rittner, Science **111**, 685 (1950).

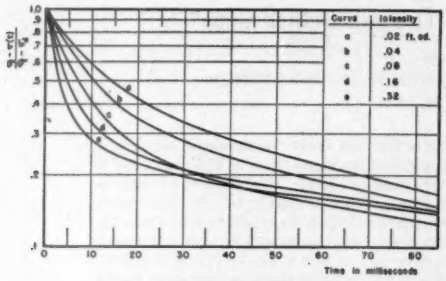

FIG. 1. Experimentally determined rise characteristics at five different light intensities.

applied to the horizontal plates of a cathode ray oscillograph. Sweep action in the vertical direction was provided through the use of a moving film camera in which the photographic recording paper was wrapped around a rotating drum driven at constant speed by a synchronous motor. An effective sweep length of 30 in. was obtained in this way. An extended sweep is quite essential in recording these rise and decay curves for which, as will be seen, the initial and final slopes are widely different.

A representative set of rise and decay characteristics[10a] for a particular cell (No. 661) taken at five different light intensities ranging from 0.02 to 0.32 ft.-c. is shown in Figs. 1 and 2. It will be noted that the initial slopes of both rise and decay characteristics increase with increasing light intensity. In this respect the behavior of these cells is essentially different from that of PbS cells for which Gibson[11] has recently found that the time for the response to decay to $(1/e)$th of the peak value (which corresponds very nearly to the reciprocal of the initial slope of the decay characteristic) increases slightly with increasing light intensity.

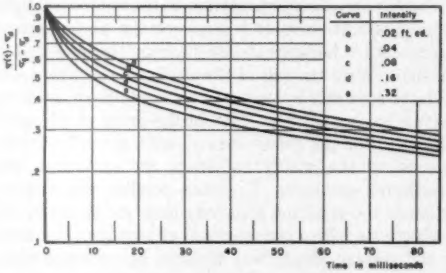

FIG. 2. Decay characteristics at various light intensities.

[10a] The plots of $\ln\{[\sigma_l-\sigma(t)]/[\sigma_l-\sigma_d]\}$ and $\ln\{[\sigma(t)-\sigma_d]/[\sigma_l-\sigma_d]\}$ vs time will be referred to as the rise and decay "characteristics," respectively, to distinguish them from the linear plots of conductivity vs time. σ_l and σ_d are the steady-state conductivities in the light and in the dark, and $\sigma(t)$ is the instantaneous conductivity. The experimental data are plotted in this way to facilitate the accurate measurement of the slopes which are simply related to the characteristic times.

[11] A. F. Gibson, unpublished memorandum of the T.R.E.

It will be shown below that, on the basis of a general homogeneous model in which the photo-conductivity is caused by the liberation of charge carriers, one would expect equality of the initial slopes of the rise and decay characteristics obtained under the same conditions, and also that these initial slopes would be proportional to the ratio of the light intensity to the steady-state photocurrent. The values of the initial slopes of the corresponding rise and decay characteristics for three typical cells are compared in Table I. The uncertainty in these values is estimated to be ± 5 percent for the rise and ± 10 percent for the decay; the latter being the greater because of the curvature in these characteristics for even small values of the time. Within these limits the predicted equality of the initial slopes is found to hold. The dependence of the initial slope of the rise characteristics upon light intensity is shown graphically in Fig. 3. It appears that for two of the cells the initial slope increases more rapidly than in direct proportion to the quantity plotted as abscissa, and the discrepancy is greater than the estimated uncertainty in the measurement of the slopes. The other possible source of error is in the values assigned to σ_l. The accuracy here can

TABLE I. Comparison of the initial slopes of rise and decay characteristics.

Cell No.		583		661		1366	
Intensity in foot-candles	Initial slopes in sec^{-1}	Rise	Decay	Rise	Decay	Rise	Decay
0.02		119	130	69	67	68	79
0.04		148	156	82	81	104	109
0.08		180	180	115	103	161	171
0.16		222	229	173	151	250	246
0.32		316	323	245	226		

readily be checked since previous steady state measurements on Tl_2S have established that the conductivity varies with the light intensity according to the following square-root relation based upon a bimolecular recombination law:[5,6]

$$\sigma_l=\sigma_d(1+kI)^{\frac{1}{2}}.$$

To verify this relationship under the present experimental conditions the quantity $(\sigma_l/\sigma_d)^2-1$ has been plotted against I, the light intensity, in Fig. 4. The deviations from direct proportionality which do exist are not large enough nor in the right direction to account for the above discrepancy. We conclude, therefore, that in regard to the dependence of the initial slope on light intensity there is approximate but not perfect agreement between experiment and the deductions from a general, homogeneous model.

The effect of temperature on the rise of the response is shown in Fig. 5, in which the rise characteristics at the two temperatures of 250°K and 300°K are compared for a fixed light intensity of 0.16 ft-c. It is seen that a decrease in temperature results in a decrease in the initial slope. The implications of this strong temperature dependence with regard to the variation of the

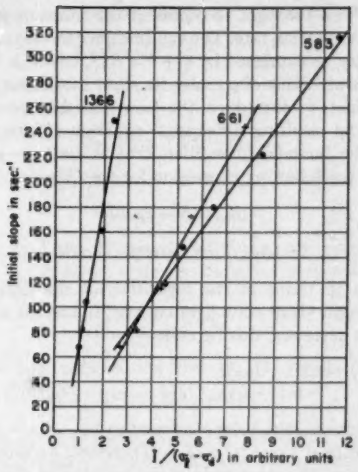

FIG. 3. Initial slopes of the rise characteristics of three cells plotted against the ratio of light intensity to photo-conductivity, showing the approximate direct proportionality.

mobility will be discussed in the next section and this will be related to the temperature dependence of the steady-state conductivity shown in Fig. 6. This plot shows the variation of the conductance (as determined by dc resistance measurements) of cell No. 661 in the dark and for several light intensities over a temperature range in which the photo-excitation of charge carriers can be made large in comparison with the thermal excitation. It may be noted here that throughout the low temperature range the photo-conductivity is proportional to the square root of the light intensity. This relationship, which previously has been well established at higher temperatures, is the principal experimental evidence for a bimolecular recombination process.

III. DISCUSSION

Because of the square root dependence of the steady-state photo-current on light intensity, it is natural to

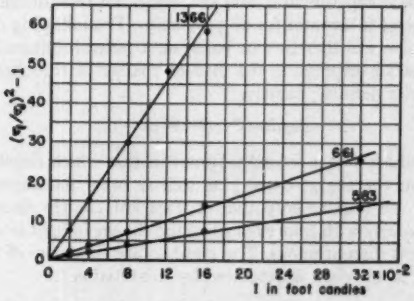

FIG. 4. Verification of the square root dependence of the photo-conductivity on light intensity under the conditions of the present experiments.

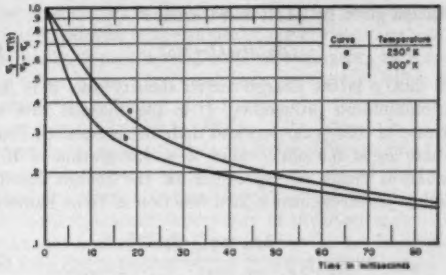

FIG. 5. Rise characteristics at two different temperatures.

assume that the photo-effect in Tl_2S might be explained in terms of a homogeneous model in which the charge carriers created by the irradiation recombine according to a bimolecular law. On the basis of this model one can also deduce expressions for the rise and decay of the photo-current when the irradiation is discontinuous. A comparison of the calculated expressions with the experimental data, however, shows a lack of agreement. For the decay this disagreement is serious only for strong excitation, but for the rise there is qualitative disagreement even at moderate light intensities. To indicate the magnitude of the discrepancies encountered we will outline briefly the calculations and compare the resulting expressions with our experimental results.

The previously derived expression for the decay of the photo-current[5,6] is based on the following differential equation, which is a simple extension of the steady-state

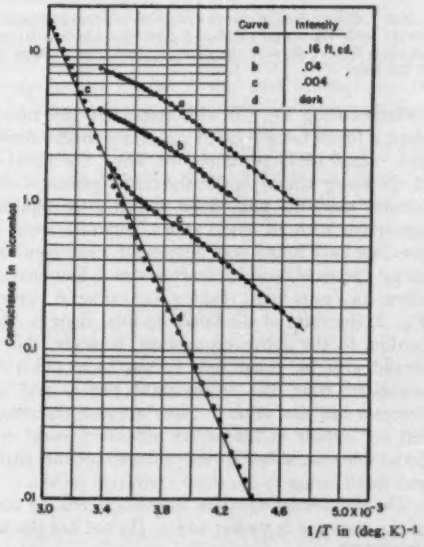

FIG. 6. Temperature dependence of the steady-state dark and photo-conductance.

relation given by Mott and Gurney:[12]

$$d\rho/dt = Q - B\rho^2. \tag{1}$$

In this, ρ is the charge carrier density and B is the recombination probability. Q is the thermal rate of release of charge carriers and therefore is equal to $B\rho_d^2$, where ρ_d is the dark value of ρ. Integration of this equation yields an expression for the charge density due to photo-excitation as a function of time, namely,

$$\Delta\rho = \frac{\Delta\rho_m \exp(-2\rho_d Bt)}{1+(\Delta\rho_m/2\rho_d)[1-\exp(-2\rho_d Bt)]}, \tag{2}$$

in which $\Delta\rho = \rho - \rho_d$, and $\Delta\rho_m$ is the value of $\Delta\rho$ at the instant the irradiation is interrupted. Since the current is proportional to the charge carrier density, the logarithm of the photo-current is given by

$$\ln\Delta i = \ln\Delta i_m - 2\rho_d Bt - \ln\{1+(\Delta\rho_m/2\rho_d)[1-\exp(-2\rho_d Bt)]\}. \tag{3}$$

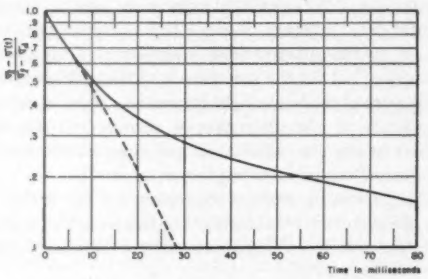

FIG. 7. Comparison of the experimental rise characteristic (solid curve) with the curve calculated from the bimolecular recombination theory, showing the divergent behavior at large values of the time.

Differentiating Eq. (3) with respect to the time, the slope is found to be $-(2\rho_d+\Delta\rho_m)B$ for small values of t, and $-2\rho_d B$ for large values of t. Thus, the initial slope of the decay characteristic should be greater (in magnitude) than the final slope, which is in qualitative agreement with all observations. Quantitatively, however, we have found poor agreement, especially for the decay curves obtained following strong illumination or when $\Delta\rho_m/\rho_d$ is large. Taking, for example, curve *e* of Fig. 2, the ratio of the initial to final slope is 34. According to the above expressions, however, this ratio should also be equal to $1+(\Delta\rho_m/2\rho_d)$, which when evaluated from the steady-state photo- and dark-currents has the value 3. Such extreme discrepancies did not appear in the earlier published work[5] on the decay following short flashes, probably because $(\Delta\rho_m/\rho_d)$ was small owing to the short excitation period.

The differential equation used in calculating the rise of the response is similar to Eq. (1) but has the added term, P, on the right to represent the constant photo-electric excitation rate. The equilibrium condition in the light may be expressed by $Q+P=B\rho_l^2$, where ρ_l is the steady-state value of ρ under constant irradiation. It is convenient to introduce the new variable $z=\rho_l-\rho$. When the resulting differential equation is integrated using the boundary condition that at $t=0$, $z=\rho_l-\rho_d=\Delta\rho_m$, the following expression for z is obtained:

$$z = \frac{\Delta\rho_m \exp(-2\rho_l Bt)}{1-(\Delta\rho_m/2\rho_l)[1-\exp(-2\rho_l Bt)]}. \tag{4}$$

Written in terms of the logarithm of the difference between the stead-state light current, i_l, and the instantaneous current i, this becomes

$$\ln(i_l-i) = \ln\Delta i_m - 2\rho_l Bt - \ln\{1-(\Delta\rho_m/2\rho_l)[1-\exp(-2\rho_l Bt)]\}, \tag{5}$$

for which the initial slope is found to be $-(2\rho_l-\Delta\rho_m)B$ and the final slope is $-2\rho_l B$. Therefore, according to this theory, the magnitude of the initial slope should be less than that of the final slope. Actually, just the reverse is found experimentally; the initial slope is considerably greater than the final slope. To show the marked discrepancy in this case, an experimentally determined rise characteristic is given in Fig. 7 together with the plot of Eq. (5). The parameters in the equation were determined from the initial slope of the experimental curve and the steady-state values of the photo- and dark currents.

In view of these results it is evident that the simple bimolecular recombination law can not account for the rise and decay characteristics of the Tl_2S cell. The relatively long "time constants" involved in the rise and decay of the response suggest a secondary process which delays the recombination of the charge carriers, and consequently a suitably modified recombination function is required. However, this function must reduce to the quadratic form in the steady-state case. With the present limited knowledge of the cell properties it seems desirable to avoid detailed models of the photo-conductive mechanism which might fully explain the present experimental data but would not be sufficiently general to account for all properties. The following discussion will therefore be based on a general differential equation expressing the rate of change of the charge carrier density; namely,

$$d\rho/dt = P+Q-F(\rho\cdots), \tag{6}$$

in which F is a recombination function which depends upon the charge density as well as other parameters; but we require only that it does not change discontinuously with time even when the change in light intensity is discontinuous. The steady-state condition of the cell in the dark is expressed by the relation

$$d\rho/dt = O = Q - F(\rho_d\cdots). \tag{7}$$

Similarly, after equilibrium has been reached under

[12] N. F. Mott and R. W. Gurney, *Electronic Processes in Ionic Crystals* (Oxford University Press, New York, 1940), p. 191.

constant illumination, the above expression becomes

$$d\rho/dt=O=P+Q-F(\rho_l\cdots). \tag{8}$$

The initial rate of increase of ρ when the excitation is started is given by

$$(d\rho/dt)_r=P+Q-F(\rho_d\cdots), \tag{9}$$

which upon substitution from Eq. (7) yields

$$(d\rho/dt)_r=P. \tag{10}$$

The initial rate of decrease of ρ when the excitation is interrupted (after a steady state has been reached) is given by

$$(d\rho/dt)_d=Q-F(\rho_l\cdots), \tag{11}$$

which upon substitution from Eq. (8) yields

$$(d\rho/dt)_d=-P. \tag{12}$$

Assuming that the mobility, μ, is independent of the excitation rate, it follows directly from relations (10) and (12) that the initial slopes, S_i, of the rise and decay characteristics should be equal and given by the relation

$$S_i=-\mu eP/(\sigma_l-\sigma_d), \tag{13}$$

in which e is the electronic charge. Conversely, the equality of the initial slopes for rise and decay as found experimentally supports the assumption about μ, as it is easily shown that a dependence of μ on the light intensity tends to cause the initial slopes for rise and decay to be different. Setting the photo-excitation rate proportional to the light intensity, I, yields the following relation, which was used above in the discussion of the experimental results as plotted in Fig. 3:

$$S_i=-K\mu I/(\sigma_l-\sigma_d). \tag{14}$$

This relation can also be used to investigate the variation of the mobility with temperature. The ratio of the mobilities at two temperatures, T_1 and T_2, will be

$$\mu_2/\mu_1=S_2[(1-\sigma_d/\sigma_l)\sigma_l]_2/\{S_1[(1-\sigma_d/\sigma_l)\sigma_l]_1\} \tag{15}$$

if the intensity of illumination used in measuring the response curves is the same at the two temperatures. On substitution of the values of the initial slopes found from Fig. 5 together with the corresponding values of σ_d and σ_l from Fig. 6 one finds that the mobility increases by a factor of 4.3 when the temperature is raised from 250°K to 300°K. This strong variation suggests an exponential dependence of the mobility on temperature with an activation energy of 0.19 ev. Further evidence for this exponential behavior is found in the temperature dependence of the stead-state conductance under strong illumination. On the basis of a strictly homogeneous model in which the mobility is temperature independent, one would expect a temperature independent conductivity for light intensities and temperatures such that the photo-conductivity is large compared with the dark conductivity. This is not the case for Tl_2S cells; the photo-conductivity increases with increasing temperature as shown in Fig. 6. If the increase is attributed to an exponential temperature dependence of the mobility, the slopes of the high temperature portions of curves *a* and *b* again yield a value of 0.19 ev for the activation energy. This indicated behavior of the mobility strongly suggests the presence of barriers. However, in view of the reasonably good agreement between the fixed temperature data and a homogeneous model, in particular, the equality of initial slopes for rise and decay curves, it would appear that the barriers do not play an essential role in the photo-effect; that is, the barrier height must be insensitive to the light.

Whether or not these ideas are correct cannot be decided on the basis of the present data alone. Further measurements, especially the determination of the photo- and dark conductivity at high frequencies of an applied ac voltage, should be made on Tl_2S. If the present interpretation is correct, one would expect an increase in both the photo- and dark conductivity over the dc values and the photo-sensitivity should not disappear at high frequencies as it does in PbS.

The author wishes to thank Professors G. E. Uhlenbeck and E. Katz for many helpful discussions and valuable suggestions in connection with this work.

New Aspects of the Photoelectric Emission from Na and K

JEAN DICKEY
General Electric Research Laboratory, Schenectady, New York
(Received September 18, 1950)

The external photoelectric effect for Na and K in the form of thick evaporated layers was investigated with photon energies $h\nu$ up to 6.71 ev. When $h\nu$ was within 1.5 ev of the threshold, the energy distributions of the emitted electrons were like those derived by DuBridge for a simple photoelectric effect involving an ideal metal. For larger $h\nu$, there was a growing preponderance of low velocity electrons. Their appearance could not be correlated, on the basis of a simple emission process, with the assumed parabolic shapes and approximately known widths of the valence bands. The following complications were therefore considered: (a) scattering by other electrons, causing the excited electron to lose energy before escape; (b) absorption of the recoil momentum by a second electron rather than by the entire crystal, resulting in the transfer of only a portion of the photon energy to the photo-electron; (c) modifications of the simple Fermi band by electron interactions, giving the effect of initial energy states much farther below the surface barrier than had been assumed.

The spectral distributions showed no evidence of a sharply defined "volume effect" such as might be due to optical transitions between zones. The form of these spectral curves was notably sensitive to variations in the structure of the evaporated films. Either matte or specular Na surfaces could be produced merely by controlling the deposition rate. There was no appreciable difference in the *energy* distributions for electrons from the two types of sufaces.

I. INTRODUCTION

PHOTOELECTRIC emission from metals has usually been treated as a simple process in which a single electron absorbs the full energy, $h\nu$, of a quantum, and appears outside the surface barrier with a kinetic energy

$$E=h\nu-(\mu-\epsilon)-\varphi. \quad (1)$$

Here ϵ is the total energy of the electron before excitation, μ is the Fermi level, and φ is the work function. (Both ϵ and μ are referred to the same arbitrary level.) To a first approximation, the excitation probability may be assumed independent of ϵ and $h\nu$. The probability that an excited electron will escape may be assumed proportional[1] to E. This elementary picture describes quite accurately the experimental results on metals when $h\nu$ is not too much greater than φ. Because intense sources of high energy photons were lacking, most observers in the past have confined their attention to this region relatively near the photoelectric threshold.

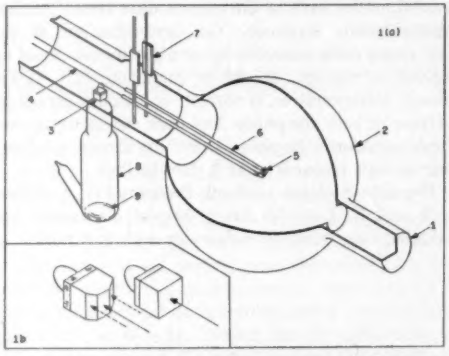

FIG. 1. (a) Cut-away sketch of photo-tube: (1) quartz window; (2) graphite coated collector sphere 6 in. in diameter; (3) movable bucket-type emitter; (4) tungsten hairpin; (5) bucket-support connected to hairpin; (6) sleeves of nickel tubing insulated from central hairpin by glass beading; (7) nickel armatures enabling one to pull spring-contact wires away from sleeves and shake buckets past; (8) last evaporation chamber, sealed off from rest of distillation train; (9) pool of alkali metal. (b) Bucket-shaped emitters drawn to a larger scale. They are shown in position for measurement, with arrows indicating the direction of the incident light. On the left is a glass bucket with polished facets allowing 0°, 45°, and 60° angles of incidence. (A strip of platinum paint on the glass around the top, and inside, provided conductivity.) On the right is a standard square metal bucket for which the angle of incidence is seen to be 0°.

For $h\nu>5.0$ ev, the behavior of the photo-emission from the alkali metals can give an interesting check on the range of validity of the theories outlined above. These elements possess the lowest work functions known for pure metals, as well as the narrowest Fermi bands. For Na, the band width given by the Sommerfeld free electron model is about 3.0 ev, a value which has been corroborated by the soft x-ray emission work of Skinner[2] and of Cady and Tomboulian.[3] The work function of Na is about 2.3 ev. Thus, the lowest occupied state, in the simple band structure, lies below the vacuum potential by 5.3 ev. This is considerably less than the highest photon energies now in use.

If we denote by ϵ_1 the energy of an electron at the bottom of the conduction band, then $\mu-\epsilon_1=W$, the width of this band. For $h\nu$ greater than $\varphi+W$ in Eq. (1), we should expect to find no photo-electrons with kinetic energies smaller than $h\nu-(\varphi+W)$, since electrons obviously cannot originate in levels *below* the lowest occupied state.

The shape as well as the width of the Fermi band might be expected to influence the form of the energy distributions. In an ideal metal, the density of states rises as $(\epsilon-\epsilon_1)^{\frac{1}{2}}$. According to Mitchell[4] and to Makinson,[5] the excitation probability at the bottom of the

[1] The original assumptions of Fowler and DuBridge are treated in slightly modified form by Apker, Taft, and Dickey, Phys. Rev. **74**, 1462 (1948).
[2] H. W. B. Skinner, Trans. Roy Soc. (London) **239**, 95 (1940).
[3] W. M. Cady and D. H. Tomboulian, Phys. Rev. **59**, 381 (1941).
[4] Mitchell, Proc. Roy. Soc. (London) **146A**, 442 (1934).
[5] Makinson, Proc. Roy. Soc. (London) **162**, 367 (1937).

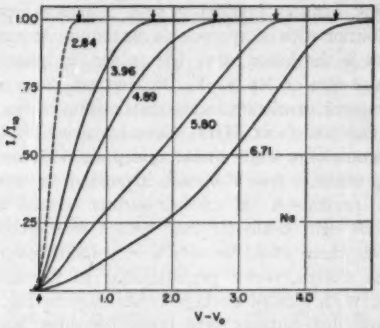

FIG. 2. Current-voltage characteristics for Na with $h\nu = 2.84$, 3.96, 4.89, 5.80, and 6.71. Currents are normalized with $I = 1.0$ at applied voltage $V = +10$ volts. The curves are set coincident at V_0, the stopping potential for 0°K. No reverse-current corrections were necessary. The position of V_0, the voltage required for saturation of the photo-current, is marked by an arrow in each case. The corresponding value of the work function of this particular Na surface is 2.27 ev.

band is approximately proportional[6] to $(\epsilon - \epsilon_1)$. Let us again take the escape probability proportional to E. Then for the specialized case in which $h\nu$ is just sufficient to eject electrons from the lowest state, $E = (\epsilon - \epsilon_1)$. The resultant energy distribution would rise as $E^{3/2}$. This should apply to the emission from Na at $h\nu \sim 5.3$ ev. The relative sparsity of slow electrons so indicated was not found in the experiments described here. In fact, just the opposite of this trend was observed.

As one might have surmised, the theory of the preceding paragraphs is not nearly complex enough to account for the behavior of the photo-emission from Na and K when $h\nu - \varphi$ is greater than about 1.5 ev. In a later section, some possibilities will be suggested to explain the large percentages of low velocity photo-electrons obtained.

II. EXPERIMENTAL DETAILS

Most of the methods and apparatus used in this experiment have been described in previous papers.[7] Figure 1 is a sketch of a typical photo-tube showing the features of chief interest. The collecting sphere was coated with a graphite-bentonite mixture and thoroughly baked, first in nitrogen, then in high vacuum. Each alkali metal was subjected to four or five preliminary distillations before being sealed (at a pressure of about 5×10^{-7} mm Hg) into $\frac{1}{2}$-in. diameter Pyrex pellets. These were broken in vacuum by glass-sheathed nickel armatures, and further distillation was carried out in a Pyrex evaporation train connected directly to the photo-tube. The metal was finally deposited on the movable bucket-type emitters when the last evaporation chamber was gently torched. This was done in the sealed-off tubes at pressures ranging from 2×10^{-9} to 4×10^{-7} mm Hg.

With an emitter in place for measurement, an arbitrary potential could be applied between it and the insulated sleeves of the supporting hairpin. This compensated for the difference in the work functions of the sleeve material and the emitting surface. As illustrated in the first paper of reference 7, results may be distorted seriously by stray fields if this point is ignored.

In four separate photo-tubes, 24 Na surfaces were prepared on buckets of Ni, Ta, Pt, Ag, and glass. For K, only one tube was constructed; Ni, Ta, and Pt served as substrates for the 4 surfaces investigated.

III. RESULTS

Figure 2 shows retarding-potential curves for the photoelectric emission from Na with values of $h\nu - \varphi$ ranging from about 0.5 to 4.4 ev. The corresponding energy distributions are given in Fig. 3. For $h\nu = 3.96$ the results resemble the parabolic current-voltage characteristic and linear energy distribution predicted by DuBridge's simple theory. However, for $h\nu$ near 5.0 ev, there is no suggestion that the energy distributions rise as $E^{3/2}$. (Note that kinetic energy increases to the *left* in Figs. 2 to 5.) Moreover, for $h\nu > 5.3$ ev the minimum photo-electron energy is zero, not $h\nu - (\varphi + W)$ as mentioned in the introduction. Also, photo-electrons with energies close to zero are much more numerous than was expected.

Measurements on Na with accelerating potentials up to 900 v gave more evidence of the importance of slow

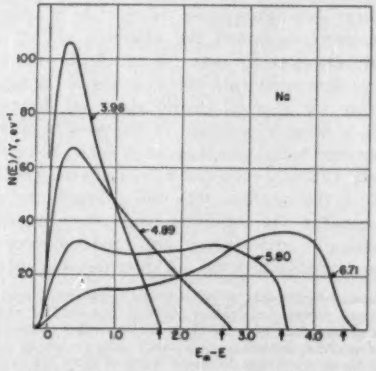

FIG. 3. Energy distributions, $N(E)/Y$, obtained by differentiating four of the curves in Fig. 2. (Y represents the yield in electrons per quantum. As defined in reference 1, $N(E)$ implicitly contains the factor Y. Hence, the differentiation of *normalized* current-voltage curves gives $N(E)/Y$.) The ordinate scale is given in percent normalized current per electron volt. Zero on the abscissa scale corresponds to the maximum kinetic energy (E_m) at 0°K. Energies *decrease* toward the right, and the arrows mark the points at which $E = 0$ for each value of $h\nu$.

[6] For electrons near the top of the conduction band, there is no great error involved in assuming the excitation probability independent of ϵ, as in the first paragraph of this section. The larger W, the smaller this error.

[7] Apker, Taft, and Dickey, Phys. Rev. 73, 46 (1948); 74, 1462 (1948); Taft and Apker, Phys. Rev. 75, 344 (1949); J. A. Becker, Elec. Eng. 68, 937 (1949).

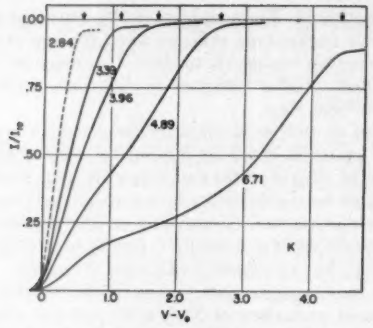

FIG. 4. Current-voltage characteristics for K, presented in the same manner as the curves for Na in Fig. 2. Corrections have been made for back currents amounting to five to eight percent of I_{10}. Values of $h\nu$ are indicated beside each curve. The dotted characteristic was included to show the fairly sharp saturation point which determined the work function (2.27 ± 0.03) of this K surface.

photo-electrons for $h\nu > 5.0$ ev. For values of $h\nu$ from 2.84 to 4.89, the percentage increase of photo-current at 900 v (over that at 10 v) became steadily lower, in the manner typical of a simple Schottky effect. For higher $h\nu$, the slopes of the saturation curves became steeper, thus indicating the collection of greater numbers of electrons emerging with extremely low kinetic energies.

Curves analogous to those for Na are shown for K in Figs. 4 and 5. Again we find increasingly higher percentages of low energy electrons as $h\nu$ becomes larger. (The results are distinguishable from those of Na because of the fairly large fraction of the electrons that retain energies within 0.5 ev of the maximum ($E_m = h\nu - \varphi$) even when $h\nu = 6.71$ ev.)

Energy data taken at six values of $h\nu$ in addition to those listed confirmed the existence of the effects already described for both Na and K; for the sake of clarity, these results are not presented in the figures.

Before the spectral distributions are discussed in detail, a short description of the results of various evaporation techniques may be of value. Layers of Na deposited rapidly (in a few minutes) were smooth and shiny; if the substrate was well polished, the deposit was specular. On the other hand, slow evaporations (requiring 15 minutes or more) produced very white, frosty deposits which did not show metallic luster.[8]

[8] No correlation was noted between pressure (as read by the ion-gauge) during evaporation and the formation of either type of Na surface. Likewise, the phenomenon seemed to be indifferent to the substrate except in one instance: all attempts to evaporate frosty Na on previously deposited layers of shiny Na were unsuccessful; the reverse process was easily carried out for sufficiently heavy layers, however. In all cases, the substrates were at room temperature, except for heating effects due to condensation of the Na atoms or to radiation from the warm evaporator bulb. These effects were greater during the fast evaporations, of course.

A pertinent paper dealing with the influence of evaporation rates on the formation of thin metal films has been published recently by R. S. Sennett and G. D. Scott, J. Opt. Soc. Am. 40, 203 (1950).

Shiny surfaces invariably gave a smooth spectral distribution with no appreciable maximum. An example of this is the lower curve (B) in Fig. 6, taken on a specular film of Na on Ta. In contrast, there was a pronounced maximum in the distribution of the yield from frosty surfaces. This is shown by curve A in Fig. 6, taken on a very white sparkling deposit of Na on Ta.

The ordinary type of bucket, in position for measurement, presents a flat emitter surface normal to the incident light beam. If this surface were extremely smooth, there would be only a very small component of the electric vector perpendicular to the emitting areas. With faceted buckets as sketched in Fig. 1(b), spectral distributions were taken for shiny Na with unpolarized light at various angles of incidence. Although the yields at angles of 45° and 60° were as much as 3 or 4 times higher than those at 0°, the maximum in the spectral distribution obtained for shiny surfaces in this manner was broader and lower than the peak of curve A in Fig. 6. Since contamination had raised the work function of these surfaces to about 2.5 ev, the experiment did not give a conclusive answer to the question of whether the high maximum found for frosty Na on flat buckets was entirely due to the high angles of incidence at which light struck the elemental emitting areas of the matte surface.

A reproducible feature of the data for shiny Na deposits on the faceted emitters is shown in the inset of Fig. 6. For light incident at 0° the curve continued downward as $h\nu$ increased to 6.19 ev, but at 45° and 60° the yields went through a minimum at $h\nu \cong 5.7$ ev. The same minimum was found in the spectral distributions

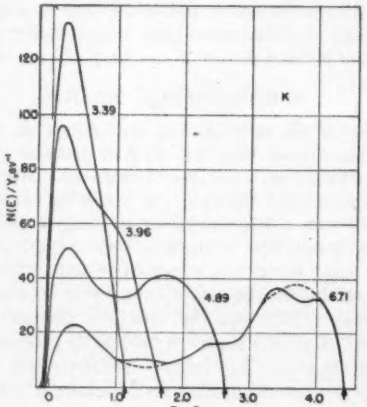

FIG. 5. Energy distributions for K, obtained by differentiating the curves in Fig. 4. Because of low yield, data at $h\nu = 6.71$ are not as trustworthy as those at other values of $h\nu$. The dotted sections of this energy distribution show results obtained on another K surface. The corresponding current-voltage curve is not given in Fig. 4.

for *all* the frosty surfaces, whatever the angle of incidence.[9]

The results on matte Na are in reasonable agreement with those described by Maurer,[10] although the surfaces were not as stable. Contamination shifted the threshold to higher $h\nu$ values and lowered the yields slightly. Curve *A* of Fig. 6, was taken on a surface only 45 minutes old. Except for a shift of about 0.1 ev to the right, it compares fairly well with Maurer's "Na D" spectral distribution shown in Figs. 4 and 5 of his paper.

Hill's[11] energy-distribution for Na at 2536A ($h\nu = 4.89$), showing a relative abundance of slow electrons, is in agreement with the results examined in the first paragraph of this section. The minor deviations from simple theory which he found for smaller values of $h\nu$ can probably be attributed to a contact potential difference between the spherical emitter and its supporting rod.

That optical effects can account for most of the differences between the spectral distributions for shiny and for frosty Na surfaces is supported by the fact that energy distributions at a given value of $h\nu$ for the two types of Na were nearly the same. Shiny surfaces consistently yielded a slightly smaller percentage of slow electrons than did frosty surfaces. (All energy data were taken with an angle of incidence of about 0°.) Contamination or aging effects were much less noticeable on the current-voltage curves than on the spectral distributions. The curves of Fig. 2 were all taken within 5 minutes to 2 hours after deposition of a frosty surface.

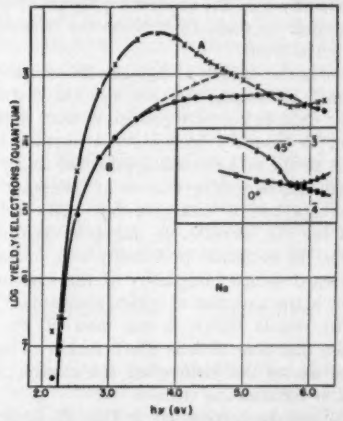

FIG. 6. Spectral distributions of the photoelectric yield from Na. (The characteristics of the logarithms of the yield are negative.) Curves *A* and *B* were taken with unpolarized light (at 0° angle of incidence with the polished Ta substrates) on matte and specular deposits, respectively. Fowler's theoretical distribution (dotted curve) fits the lower characteristic for about 1.0 ev near the threshold, giving a work function of 2.30. In the inset are shown sections of two spectral distributions taken on a shiny surface of Na on glass with unpolarized light at the two angles of incidence indicated. Note that the ordinate scale here has been shifted down one decade, but that the abscissa scale is unchanged.

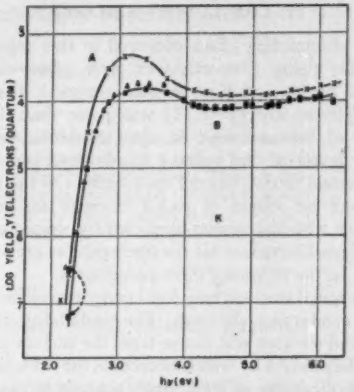

FIG. 7. Spectral distributions of the photoelectric yields from two slightly different surfaces of K on Ni (see text). Unpolarized light at 0° angle of incidence was used in each case. The triangles on the lower curve represent data taken with a tungsten lamp immediately after deposition of the K. All other points were taken with a 1-atmosphere mercury arc. The intensity of the source of 6.71-ev radiation was not accurately known, so no yields are given for this value of $h\nu$. The dotted arrow shows the decrease in yield at $h\nu = 2.27$ when a suitable bias-voltage suppressed photo-current caused by scattered light striking the thin film of K on the sleeves of the bucket support.

The spectral distributions for K, given in Fig. 7, are for uniform matte surfaces on flat metal buckets with incident light normal to the substrate. K layers which looked rather frosty immediately after deposition acquired a shiny even-textured graininess in a few hours. Curve *A* was taken on the frostier of the two surfaces represented here. It is similar in shape to Klauer's[12] spectral distribution for a fresh K deposit; his highest value of $h\nu$ was 3.39 ev. His yields were given only in order of magnitude; the estimate was 10^{-4} electrons/quantum or less, at the peak, which occurred at a slightly lower value of $h\nu$ than that for the maximum in curve *A*. Contamination effects in the K tube were of the same type as those described for Na. Surfaces produced under the best vacuum conditions had work-functions of ~2.20. This is a slightly lower value than the one given in Fig. 4, and is probably closer to the value for clean K.

Tentative values of the photoelectric yields for Rb were about the same as those for K, and the spectral distributions showed the same slight maximum and minimum as seen in curve *B* of Fig. 7.

[9] Increasing the angle of incidence from 0° to 70° on frosty surfaces almost doubled the yields but did not change the general shape of the spectral distributions.

[10] R. J. Maurer, Phys. Rev. **57**, 653 (1940). The writer is indebted to Dr. Maurer for a more detailed description of his method of depositing Na.

[11] A. G. Hill, Phys. Rev. **53**, 184 (1938).

[12] Klauer, Ann. Physik **20**, 909 (1934).

IV. CONCLUDING REMARKS

The outstanding effect observed in this experiment was the rising proportion of slow photo-electrons emitted by Na and K as $h\nu$ was increased. The maximum photon energy (6.71) was more than 1 ev in excess of that required to eject electrons from the lowest levels of the valence bands described by the Sommerfeld model. Energy distributions of the emitted electrons for values of $h\nu > 4$ ev were markedly at variance with the results predicted by simple theories. Some possible reasons for the discrepancies are set down briefly in the following three paragraphs.

An excited electron may lose energy by collisions with other conduction electrons. The probability that the scattered electron will escape from the surface increases with the amount by which $h\nu$ exceeds the work function. The applicability of DuBridge's analysis to the energy data at low $h\nu$ must depend on the fact that few of the scattered electrons appear externally when

$$h\nu - \varphi < 1.5 \text{ ev}.$$

A photo-electron may acquire considerably less than the entire energy of an exciting photon because a second electron, instead of the crystal as a whole, receives the recoil momentum.[13]

The actual distribution of the initial energy states doubtless differs somewhat from the ideal parabolic form that has been assumed. The extent to which electron interactions may alter the simple picture is difficult to assess accurately.[14] It is conceivable that levels near the bottom of the conduction band are broadened by a phenomenon analogous to the Auger effect described by Skinner.[2,15] The low energy tail on the soft x-ray emission spectrum represents a decidedly smaller deviation from the ideal band shape than would be necessary for a complete explanation of the photo-electric results on Na, however.

It should be noted that the three mechanisms discussed separately above are probably not independent. The interrelations and similarities which may exist will not be considered here.

In the case of a metal with a slightly higher work function and wider Fermi band, it seems likely that the simple photoelectric effect should account for most of the yield in the range of $h\nu$ considered here. Skinner's experimental value of the band width W for Li is about 4.0 ev. A Li surface of work function $\varphi = 2.6$ ev was prepared by E. A. Taft of this laboratory. Tentative energy distributions of the photo-electrons at $h\nu = 6.7$ ev showed a considerably lower percentage of slow electrons than found for Na and K at the same $h\nu$. This strengthens the supposition that complicating effects play a less prominent part in the photo-emission when $h\nu \gtrsim \varphi + W$.

The spectral distributions are presented as subsidiary data. Their behavior was quite dependent on the physical structure of the evaporated surfaces; this was presumably due to differences in the optical properties of the various types of deposits. Thus it seems hazardous to try to correlate any features illustrated in Figs. 6 and 7 with factors influencing the form of the energy distributions.

The spectral data gave no clearcut evidence of a "volume effect" like that discussed by Tamm and Schubin.[16] One might expect such a phenomenon to produce an increase in yield starting at some critical frequency dictated by the zone scheme of the metal.[17] This type of effect need not show up at all in the energy distributions. It would not give rise to a disproportionate number of slow photo-electrons unless the allowed transitions were especially probable for electrons near the bottom of the conduction band. Even this possibility does not account for the many electrons which appear to come from *below* the bottom of the simple Fermi band.

Except in the case of shiny surfaces struck by light at normal incidence, the Na spectral distributions showed a definite but very gradual upward slope in the range of $h\nu$ from 5.7 to 6.2 ev. An estimate of the intensity of the 6.71-ev source indicated that the total yield was still increasing with $h\nu$ at this point. Photo-electric experiments can give few clues as to the reasons for the increase. It might be ascribed to a change in the excitation probability with frequency, to an increased escape probability of the scattered electrons, or to the variation of optical constants.[18] Judging from the results shown in the inset of Fig. 6, one concludes that none of these effects makes an important contribution to the yield when the electric vector is *parallel* to the emitting surface.

I am very much indebted to Drs. H. A. Bethe, H. Brooks, M. H. Hebb, and H. B. Huntington for their interest in discussing the theoretical problems involved in this work. I wish to express my sincere thanks to Dr. L. Apker for encouragement and advice, and to Mr. E. Taft for experimental assistance.

[13] This mechanism was proposed by Dr. Harvey Brooks and Professor H. A. Bethe in helpful discussions for which the writer is very grateful.

[14] E. Wigner, Trans. Faraday Soc. **34**, 678 (1938).

[15] See P. T. Landsberg, Proc. Phys. Soc. (London) **A62**, 806 (1949) for a theoretical treatment of this problem. E. P. Wohlfarth [Phil. Mag. **41**, 534 (1950)] finds that Landsberg's approach can also be used successfully in the theory of the specific heat of Na.

[16] Tamm and Schubin, Z. Physik **68**, 97 (1931).

[17] H. Y. Fan concludes from his calculations [Phys. Rev. **68**, 43 (1945)] that the volume effect should become important not far from the threshold of the surface photoelectric effect.

[18] According to Wood [Phys. Rev. **44**, 353 (1933)], Na becomes transparent at $h\nu \sim 5.9$, K at $h\nu \sim 3.9$.

On the First Passage Time Probability Problem

ARNOLD J. F. SIEGERT
Physics Department, Northwestern University, Evanston, Illinois
(Received July 12, 1950)

We have derived an exact solution for the first passage time probability of a stationary one-dimensional Markoffian random function from an integral equation. A recursion formula for the moments is given for the case that the conditional probability density describing the random function satisfies a Fokker-Planck equation. Various known solutions for special applications (noise, Brownian motion) are shown to be special cases of our solution. The Wiener-Rice series for the recurrence time probability density is derived from a generalization of Schrödinger's integral equation, for the case of a two-dimensional Markoffian random function.

I. INTRODUCTION

A STATIONARY Markoffian random function, $y(t)$, such as a velocity component of a colloidal particle in Brownian motion or of a star in a cluster, or the noise current in an R-L circuit as functions of the time, is defined by $P(y_0|y,t)dy$, the probability that $y \leqslant y(t) < y+dy$, if $y(0)=y_0$. For a continuous function, $y(t)$, the first passage time probability $\mathcal{P}(y_0|t,a)dt$ is defined as the probability that $y(t)$ passes the value a for the first time in the time interval $(t, t+dt)$ if $y(0)=y_0$.

The problem of determining $\mathcal{P}(y_0|t,a)$ has been solved for certain special cases by Schrödinger,[1] Smoluchowski,[2] Chandrasekhar,[3] and Wang and Uhlenbeck.[4] Schrödinger and Smoluchowski found the probability that a free particle in Brownian motion in a medium of high viscosity reaches a marker at a for the first time in $(t, t+dt)$ after starting from y_0 at $t=0$. For high viscosity the coordinate of the particle can be treated as a Markoffian random function (for times large as compared with the relaxation time),[5] and $P(y_0|y,t)$ is the well known expression determined by Einstein, which satisfies the ordinary diffusion equation. $\mathcal{P}(y_0|t,a)$ was obtained by observing that for $y_0<a$

$$\mathcal{P}(y_0|t,a) = -\frac{\partial}{\partial t}\int_{-\infty}^{a} P_a(y_0|y,t)dy, \tag{1.1}$$

where $P_a(y_0|y,t)dy$ is the probability that the particle is in $(y, y+dy)$ at t and that at no time between 0 and t the particle has reached the marker at a. The probability $P_a(y_0|y,t)dy$ can be visualized as the probability of finding the particle in $(y, y+dy)$ at t if an absorbing barrier is present at a, and can thus be obtained as the fundamental solution of the diffusion equation with boundary conditions

$$P_a(y_0|-\infty, t) = P_a(y_0|a,t) = 0. \tag{1.2}$$

Schrödinger pointed out that his expression for $\mathcal{P}(y_0|t,a)$ can be checked by means of an integral equation obtained by the following argument. The probability

$$\phi(y_0|t,a) = \int_{-\infty}^{a} P(y_0|y,t)dy$$

that the particle is at t in $(-\infty, a)$ is the sum of the probability $f(y_0|t,a)$ that the particle did not pass a in $(0,t)$, and the probability that it passed a for the first time at some time $\vartheta(0<\vartheta<t)$ but returned. Since

$$\mathcal{P}(y_0|t,a) = -\partial f(y_0|t,a)/\partial t, \tag{1.3}$$

this yields an integral equation for $\mathcal{P}(y_0|t,a)$. Chandrasekhar estimated the rate of escape of stars from clusters by determining the probability that a star with given initial velocity will reach a chosen velocity for the first time in $(t, t+dt)$. He obtained this probability using the first method described above with the appropriate differential equation of the Fokker-Planck type instead of the ordinary diffusion equation. Uhlenbeck and Wang gave an explicit function for the probability that a velocity component of a free particle in Brownian motion (or the noise current in an L-R circuit) passes the value zero for the first time in $(t, t+dt)$.

The problem of the distribution of the absolute maximum of $y(t)$ in an interval is closely related to the first passage time problem. The probability $M(a,t)da$ that the absolute maximum of y in the interval $(0,t)$ lies between a and $a+da$ is given by

$$M(a,t) = \frac{\partial}{\partial a}\int_{-\infty}^{a} W(y_0)dy_0 f(y_0|t,a) \tag{1.4}$$

where

$$W(y) = \lim_{t\to\infty} P(y_0|y,t). \tag{1.5}$$

Problems of this type arise in engineering applications since circuits have been designed which register the absolute maximum of a current in a time gate, with the purpose of improving discrimination between signals and noise.

Apart from applications, the first passage time problem seemed of interest since it can be considered as the problem of finding the statistical properties of a branch of the inverse function $t(y)$ if the statistical properties of $y(t)$ are known.

[1] E. Schrödinger, Physik. Z. 16, 289 (1915).
[2] M. v. Smoluchowski, Physik. Z. 16, 318 (1915).
[3] S. Chandrasekhar, Astrophys. J. 97, 263 (1943).
[4] M. C. Wang and G. E. Uhlenbeck, Revs. Modern Phys. 17, 323 (1945).
[5] H. A. Kramers, Physica 7, 284 (1940).

In Sec. II we have given an integral equation for $\mathcal{P}(y_0|t, a)$ without making the assumption that $P(y_0|y, t)$ satisfies a Fokker-Planck equation. The integral equation yields an exact expression for $\mathcal{P}(y_0|t, a)$ in terms of $P(y_0|y, t)$. Schrödinger's integral equation is shown to follow from our simpler integral equation. A simple expression for $\mathcal{P}(y_0|t, a)$ has been obtained for the case in which a is a point of symmetry of the problem. The formula given by Uhlenbeck and Wang for the Gaussian case is a special case of this result. In Sec. III we have derived the differential equation method from our result in case $P(y_0|y, t)$ satisfies a Fokker-Planck equation and have given a recursion formula for the moments of the first passage time. In Sec. IV we have discussed $\mathcal{P}(y_0|t, a)$ and $f(y_0|t, a)$ as solutions of the adjoint of the Fokker-Planck equation. In order to show the connection between the integral equation method and the approach of Wiener and Rice leading to the Wiener-Rice series[6] for the recurrence time probability of a random function in Sec. V we have derived the series from an integral equation for the case of a two-dimensional stationary Markoffian random function.[7]

II. THE INTEGRAL EQUATION

The fundamental integral equation is obtained by classifying the functions $y(t')$ for which $y(0)=y_0$ and $y \leqslant y(t)<y+dy$ according to the time $\vartheta>0$ at which they pass the value a for the first time ($y_0<a \leqslant y$). One thus obtains:

$$P(y_0|y, t)=\int_0^t \mathcal{P}(y_0|\vartheta, a)P(a|y, t-\vartheta)d\vartheta. \quad (2.1)$$

This integral equation is solved by a Laplace transformation. Using the notation f_L for the Laplace transform of a function f, we have

$$P_L(y_0|y, \lambda)=\int_0^\infty e^{-\lambda t}P(y_0|y, t)dt \quad (2.2)$$

and

$$\mathcal{P}_L(y_0|\lambda, a)=\int_0^\infty e^{-\lambda t}\mathcal{P}(y_0|t, a)dt, \quad (2.3)$$

and from (2.1)

$$P_L(y_0|y, \lambda)=\mathcal{P}_L(y_0|\lambda, a)P_L(a|y, \lambda) \quad (2.4)[8]$$

and

$$\mathcal{P}(y_0|t, a)=\frac{1}{2\pi i}\int_{\gamma-i\infty}^{\gamma+i\infty} e^{\lambda t}\frac{P_L(y_0|y, \lambda)}{P_L(a|y, \lambda)}d\lambda, \quad (2.5)$$

with $\gamma>0$ and otherwise arbitrary real, and $y_0<a \leqslant y$.

From (2.3) and (2.4) it follows that

$$\mathcal{P}(a|t, a)=0 \text{ for } t>0 \quad (2.6)$$

with

$$\int_0^\epsilon \mathcal{P}(a|t, a)=1 \text{ for any real } \epsilon>0 \quad (2.7)$$

which is in agreement with (2.1) and (2.8).

From our solution follows a property of $\mathcal{P}(y_0|ta)$ which can also be obtained directly from the argument leading to (2.1); i.e.,

$$\mathcal{P}(y_0|t, b)=\int_0^t \mathcal{P}(y_0|\vartheta, a)\mathcal{P}(a|t-\vartheta, b)d\vartheta \quad (2.8)$$

for $y_0<a<b$.

Schrödinger's integral equation[1] can be derived from (2.1) by integration over y from a to ∞. We define $f(y_0|t, a)$ as in Sec I and notice that $f(y_0|0, a)=1$ for $y_0 \leqslant a$, and that

$$\mathcal{P}(y_0|t, a)=-\partial f(y_0|t, a)/\partial t. \quad (2.9)$$

Defining further

$$\phi(y_0|t, a)=\int_{-\infty}^a P(y_0|y, t)dy \quad (2.10)$$

and making use of

$$\int_{-\infty}^\infty P(y_0|y, t)dy=1, \quad (2.11)$$

we have

$$1-\phi(y_0|t, a)=\int_0^t d\vartheta\mathcal{P}(y_0|\vartheta a)[1-\phi(a|t-\vartheta, a)]$$

$$=f(y_0|0, a)-f(y_0|t, a)$$

$$-\int_0^t \mathcal{P}(y_0|\vartheta, a)\phi(a|t-\vartheta, a)d\vartheta$$

or

$$f(y_0|t, a)=\phi(y_0|t, a)$$

$$-\int_0^t \mathcal{P}(y_0|\vartheta, a)\phi(a|t-\vartheta, a)d\vartheta \quad (2.12)$$

or, since $\phi(a|0, a)=\frac{1}{2}$,

$$\mathcal{P}(y_0|t, a)=2\left\{-\frac{\partial}{\partial t}\phi(y_0|t, a)\right.$$

$$\left.+\int_0^t \mathcal{P}(y_0|\vartheta, a)\frac{\partial\phi(a|t-\vartheta, a)}{\partial t}d\vartheta\right\}. \quad (2.12')$$

The integral equation (2.12) can also be solved by finding the Laplace transform. We obtain

$$f_L(y_0|\lambda, a)=\phi_L(y_0|\lambda a)-\mathcal{P}_L(y_0|\lambda a)\phi_L(a|\lambda, a) \quad (2.13)$$

[6] S. O. Rice, Bell System Tech. J. **24**, 46, 64 (1945).

[7] The main results of our calculations have been stated in the following abstracts: A. J. F. Siegert, Phys. Rev. **70**, 449 (1946); **71**, 469 (1947); **71**, 485 (1947); **73**, 1271 (1948).

[8] Moments of $\mathcal{P}(y_0|t, a)$ can be obtained by expanding $P_L(y_0|y, \lambda)/P_L(a|y, \lambda)$ in powers of λ.

or since

$$\mathcal{P}_L(y_0|\lambda, a)=1-\lambda f_L(y_0|\lambda, a) \tag{2.13'}$$

we have

$$\mathcal{P}_L(y_0|\lambda, a)=[1-\lambda\phi_L(y_0|\lambda, a)]/[1-\lambda\phi_L(a|\lambda, a)] \tag{2.14}$$

and

$$f_L(y_0|\lambda, a)=\frac{\phi_L(y_0|\lambda, a)-\phi_L(a|\lambda, a)}{1-\lambda\phi_L(a|\lambda, a)}. \tag{2.15}$$

If specially the problem has a point of symmetry s defined by

$$P(s|y, t)=P(s|2s-y, t), \tag{2.16}$$

one has immediately an explicit solution for the probability density of the first passage time through s, since then

$$\phi(s|t, s)=\tfrac{1}{2} \text{ for all } t \tag{2.17}$$

and, therefore,

$$\mathcal{P}(y_0|t, s)=-2(\partial/\partial t)\int_{-\infty}^{s} P(y_0|y, t)dy. \tag{2.18}$$

The result of Wang and Uhlenbeck [reference 4, Eq. (82)] is a special case of (2.18) obtained by taking for $P(y_0|y, t)$ the Gaussian distribution defined by Eq. (36) of reference 4, for which $s=0$.

It is to be expected that the existence of the first passage time probability density $\mathcal{P}(y_0|t, a)$ imposes certain limitations on the choice of $P(y_0|y, t)$. We note that the expression $P_L(y_0|y, \lambda)/P_L(a|y, \lambda)$ must be independent of y for $y_0<a<y$.

III. THE SOLUTION WHEN $P(y_0|y, t)$ SATISFIES A FOKKER-PLANCK EQUATION. RECURSION FORMULA FOR THE MOMENTS OF $\mathcal{P}(y_0|t, a)$

If the limits of the first and second moments

$$A(z)=\lim_{\Delta t\to 0}\frac{1}{\Delta t}\int_{-\infty}^{\infty} dy(y-z)P(z|y, \Delta t)$$

and

$$B(z)=\lim_{\Delta t\to 0}\frac{1}{\Delta t}\int_{-\infty}^{\infty} dy(y-z)^2P(z|y, \Delta t)$$

exist and all higher moments tend to zero faster than Δt for $\Delta t\to 0$ $P(y_0|y, t)$ satisfies the two differential equations[9]

$$\frac{\partial P}{\partial t}=-\frac{\partial}{\partial y}[A(y)P]+\frac{1}{2}\frac{\partial^2}{\partial y^2}[B(y)P]\equiv LP \tag{3.1}$$

and

$$\frac{\partial P}{\partial t}=A(y_0)\frac{\partial P}{\partial y_0}+\tfrac{1}{2}B(y_0)\frac{\partial^2 P}{\partial y_0^2}\equiv L_0^+P \tag{3.1'}$$

with initial condition $P(y_0|y, 0)=\delta(y-y_0)$ and boundary conditions $P(y_0|\pm\infty, t)=0$ for finite y_0, and $P(\pm\infty|y, t)=0$ for finite y. The Laplace transform $P_L(y_0|y, \lambda)$, therefore, satisfies the differential equations

$$(L-\lambda)P_L=-\delta(y-y_0) \tag{3.2}$$

and

$$(L_0^+-\lambda)P_L=-\delta(y-y_0). \tag{3.2'}$$

To derive the differential equation method of references 1 and 2 we construct a function $P_a(y_0|y, t)$ which satisfies Eq. (3.1) for $y<a$ with initial condition $P_a(y_0|y, 0)=\delta(y-y_0)$ and boundary conditions

$$P_a(y_0|-\infty, t)=P_a(y_0|a, t)=0,$$

by writing its Laplace transform as

$$P_{aL}(y_0|y, \lambda)=P_L(y_0|y, \lambda) -P_L(y_0|a, \lambda)P_L(a|y, \lambda)/P_L(a|a, \lambda). \tag{3.3}$$

Using Eq. (2.4) and integrating we get

$$\int_{-\infty}^{a} P_a(y_0|y, \lambda)dy=\phi_L(y_0|\lambda a)-\mathcal{P}_L(y_0|\lambda, a)\phi_L(a|\lambda, a) =f(y_0|\lambda, a) \tag{3.4}$$

according to Eq. (2.13) and further

$$-\frac{\partial}{\partial t}\int_{-\infty}^{a} P_a(y_0|y, t)dy=-\frac{\partial f(y_0|t, a)}{\partial t}=\mathcal{P}(y_0|t, a).$$

The differential equation method of references 1 and 2 thus leads to the same result as our method, if $P(y_0|y, t)$ satisfies the Fokker-Planck Eq. (3.1).

The function $P_a(y_0|y, t)dy$ is to be interpreted for $y\lesseqgtr a$ as the probability that the random function $y(t')$, having started as $y(0)=y_0$, reaches a value between y and $y+dy$ at t without having assumed the value a at any time $t'(\geqslant 0)$ before t. The validity of this interpretation is shown by Laplace transformation of Eq. (3.3) which results in

$$P_a(y_0|y, t)=P(y_0|y, t) -\int_0^t \mathcal{P}(y_0|\vartheta, a)P(a|y, t-\vartheta)d\vartheta. \tag{3.5}$$

If $P(y_0|y, t)$ satisfies the adjoint Fokker-Planck equation (3.1') an integral recursion formula for the moments is obtained as follows. Equation (3.1') may be written in the form

$$\frac{\partial P(y_0|y, t)}{\partial t}=\frac{1}{2W(y_0)}\frac{\partial}{\partial y_0}\left\{B(y_0)W(y_0)\frac{\partial P(y_0|y, t)}{\partial y_0}\right\}, \tag{3.6}$$

where $W(y)$ is the stationary distribution

$$W(y)=\frac{\text{Const}}{B}\exp\left[\int^{y} 2(A/B)dy\right]. \tag{3.7}$$

[9] Equation (3.1) is derived in reference 4, Eq. (3.1') by an obvious variant of this derivation. Both equations are special cases of Kolmogoroff's equations [A. Kolmogoroff, Math. Ann. **104**, 415 (1931)].

If $B(y_0)W(y_0)\partial P(y_0|y,t)/\partial y_0 \to 0$ for $y_0 \to -\infty$ we have

$$B(y_0)W(y_0)\frac{\partial P(y_0|y,t)}{\partial y_0} = \int_{-\infty}^{y_0} 2W(x)dx \frac{\partial P(x|y,t)}{\partial t}. \quad (3.8)$$

We further obtain

$$P(y_0|y,t) - P(a|y,t) = \int_a^{y_0} \frac{2dz}{B(z)W(z)} \int_{-\infty}^{z} W(x)\frac{\partial P(x|y,t)}{\partial t}dx. \quad (3.9)$$

Since, for $\lambda \neq 0$

$$\int_0^\infty e^{-\lambda t}\frac{\partial P(x|y,t)}{\partial t}dt = -\delta(y-x) + \lambda P_L(x|y,\lambda) \quad (3.10)$$

we have for $y > y_0$

$$P_L(y_0|y,\lambda) - P_L(a|y,\lambda) = \lambda \int_a^{y_0} \frac{2dz}{B(z)W(z)} \int_{-\infty}^{z} W(x)P_L(x|y,\lambda)dx. \quad (3.11)$$

With the moments denoted by $t_n(y_0|a)$ and

$$\mathcal{P}_L(y_0|\lambda,a) = P_L(y_0|y,\lambda)/P_L(a|y,\lambda) = \sum_0^\infty (-\lambda)^n t_n(y_0|a)/n!, \quad (3.12)$$

one obtains

$$\sum_{n=0}^{\infty}\frac{(-\lambda)^n}{n!}\int_{y_0}^{a}\frac{2dz}{B(z)W(z)}\int_{-\infty}^{z}W(x)t_n(x|a)dx = \frac{1}{\lambda}[1 - P_L(y_0|y,\lambda)/P_L(a|y,\lambda)] = -\frac{1}{\lambda}\sum_1^\infty \frac{(-\lambda)^n}{n!}t_n(y_0|a), \quad (3.13)$$

since $t_0(y_0|a) = 1$. We thus have the recursion formula

$$t_n(y_0|a) = n\int_{y_0}^{a}\frac{2dz}{B(z)W(z)}\int_{-\infty}^{z}W(x)t_{n-1}(x|a)dx. \quad (3.14)$$

Specially for the average first passage time we have

$$t_1(y_0|a) = \int_{y_0}^{a}\frac{2dz}{B(z)W(z)}\int_{-\infty}^{z}W(x)dx. \quad (3.15)$$

Since $(BW)' = 2AW$, this can be written as

$$t_1(y_0|a) = \int_{y_0}^{a} dz/\bar{A}(z),$$

where $\bar{A}(z)$ is defined as an average drift velocity:

$$\bar{A}(z) = \int_{-\infty}^{z} A(x)W(x)dx \Big/ \int_{-\infty}^{z} W(x)dx. \quad (3.16)$$

IV. DISCUSSION OF $f(y_0|t,a)$ AS SOLUTION OF THE ADJOINT FOKKER-PLANCK EQUATION

In the preceding section we have derived the differential equation method of references 1 and 2, which uses the ordinary Fokker-Planck equation, from our integral equation. We now show that $f(y_0|t,a)$ and $\mathcal{P}(y_0|t,a)$ are solutions of the adjoint Fokker-Planck equation and, by means of a heuristic derivation, give an interpretation of this fact. We shall also show how $f(y_0|t,a)$ and $\mathcal{P}(y_0|t,a)$ are obtained in terms of a solution $v_\lambda(y_0)$ of the homogeneous equation

$$(L_0^+ - \lambda)v_\lambda = 0, \quad (4.1)$$

where $v_\lambda(y_0)$ is that solution which is regular for $y_0 \to -\infty$. The solution for the Gaussian case is given as an example.

From (3.2′) and (2.10) it follows that

$$(L_0^+ - \lambda)\phi(y_0/\lambda, a) = -1 \text{ for } y_0 < a, \quad (4.2)$$

and, therefore, using (2.15)

$$(L_0^+ - \lambda)f_L(y_0|\lambda,a) = -1 \quad (4.2')$$

so that

$$L_0^+ f(y_0|t,a) = \partial f(y_0|t,a)/\partial t \quad (4.3)$$

with initial condition

$$f(y_0|0,a) = 1, \quad y_0 < a. \quad (4.4)$$

If we demand the validity of (2.1) for $y_0 \leqslant a < y$ we must extend the initial condition to include $y_0 = a$. From (2.15) follows the boundary condition

$$f(a|t,a) = 0, \quad t > 0$$

and since

$$\phi_L(y_0|\lambda,a) \to 1/\lambda \text{ for } y_0 \to -\infty,$$
$$f_L(y_0|\lambda,a) \to 1/\lambda \text{ for } y_0 \to -\infty$$

or

$$f(y_0|t,a) \to 1 \text{ for } y_0 \to -\infty. \quad (4.5)$$

These boundary and initial condition are easily understood on the basis of the meaning of $f(y_0|t,a)$ as the probability that $y(t') \leqslant a$ for all t' in the interval $0 \leqslant t' < t$ if $y(0) = y_0$.

Conversely, a function $f(y_0|t,a)$ which is a solution of (4.3) with the above boundary conditions is also a solution of (2.12). To show this we consider the problem of finding $\phi(y_0|t,a)$ as a solution of the Fokker-Planck equation with boundary condition

$$\phi(y_0|t,a) < \infty \text{ for } y_0 \to -\infty,$$
$$\phi(y_0|t,a) = \phi(a|t,a) \text{ for } y_0 = a \quad (4.6)$$

and initial condition

$$\phi(y_0|0,a) = 1 \text{ for } y_0 < a,$$

where $\phi(a|t, a)$ is considered given. Using

$$\mathcal{P}(y_0|t, a) \equiv -\partial f(y_0|t, a)/\partial t$$

as source function we can construct $\phi(y_0|t, a)$ as

$$\phi(y_0|t, a) = f(y_0|t, a) + \int_0^t \mathcal{P}(y_0|\vartheta, a)\phi(a|t-\vartheta, a)d\vartheta \tag{4.7}$$

which is identical with (2.12).

To understand the reason why $f(y_0|t, a)$ satisfies the adjoint to the Fokker-Planck equation we give a heuristic derivation of this property, by subdivision of the time interval $(0, t)$. Consider the function $f_n(y_0|t, a)$ defined as the conditional probability that if $y(0) = y_0 \leqslant a$—also $y(kt/n) \leqslant a$, where $k = 1, 2 \cdots n$ and $t > 0$. The function $f_n(y_0|t, a)$ is given by

$$\begin{aligned} f_n(y_0|t, a) &= \int_{-\infty}^{a} P(y_0|y_1, t/n)dy_1 \\ &\quad \times \int_{-\infty}^{a} P(y_1|y_2, t/n)dy_2 \cdots \\ &\quad \times \int_{-\infty}^{a} P(y_{n-1}|y_n, t/n)dy_n \\ &= [\Lambda(t/n)]^n \chi(y_0) \end{aligned} \tag{4.8}$$

where $\chi(y_n) = 1$ for $y_0 \leqslant a$ and Λ is the operator defined by

$$\Lambda(t/n)g(y_0) = \int_{-\infty}^{a} P(y_0|y, t/n)g(y)dy.$$

Replacing n by $n+1$ and t by $(1+1/n)t$ in (4.8), we have

$$\begin{aligned} &f_{n+1}(y_0|(1+1/n)t, a) \\ &\quad = [\Lambda(t/n)]^{n+1}\chi(y_0) = \Lambda(t/n)f_n(y_0|t, a). \end{aligned} \tag{4.9}$$

Expanding we have

$$\begin{aligned} f_{n+1}(y_0|t, a) + \frac{t}{n}\frac{\partial f(y_0|t, a)}{\partial t} + \cdots \\ = \Lambda(t/n)f_n(y_0|t, a). \end{aligned} \tag{4.10}$$

If the sequence f_n converges we have

$$\begin{aligned} &\partial f(y_0|t, a)/\partial t \\ &= \lim_{n\to\infty}\left\{\frac{n}{t}[\Lambda(t/n) - 1]f(y_0|t, a)\right\} \\ &= \lim_{n\to\infty}\left\{\frac{n}{t}\left[\int_{-\infty}^{\infty} P(y_0|y, t/n)dy f(y|t, a) - f(y_0|t, a)\right]\right\} \\ &\quad + \lim_{n\to\infty}\left\{\frac{n}{t}\int_{a}^{\infty} P(y_0|y, t/n)f(y|t, a)\right\}. \end{aligned} \tag{4.11}$$

If the moment conditions for the derivation of the Fokker-Planck equation are fulfilled, the first term on the right-hand side becomes

$$A(y_0)\partial f/\partial y_0 + B(y_0)\partial^2 f/\partial y_0^2.$$

For any fixed $y_0 < a$ the second term vanishes, since

$$\begin{aligned} \int_a^{\infty} P(y_0|y, t/n)f(y|t, a)dy &\leqslant \int_a^{\infty} P(y_0|y, t/n)dy \\ &\leqslant \int_a^{\infty} [(y-y_0)/(a-y_0)]^4 P(y_0|y, t/n)dy, \\ &\leqslant \int_{-\infty}^{\infty} [(y-y_0)/(a-y_0)]^4 P(y_0|y, t/n)dy \end{aligned} \tag{4.12}$$

and

$$\lim_{n\to\infty}\frac{n}{t}\int_{-\infty}^{\infty}(y-y_0)^4 P(y_0|y, t/n)dy = 0. \tag{4.13}$$

For any value of $y_0 < a$ the function $f(y_0|t, a)$ thus satisfies the adjoint Fokker-Planck Eq. (3.2). For $y_0 = a$, $t > 0$ we have $f(a|t, a) = 0$; for $t = 0$, $y_0 < a$ we have $f(y_0|0, a) = 1$ directly from (4.8). The inequality $f(y_0|t, a) \leqslant 1$ also follows from this equation.

If a solution $v_\lambda(y_0)$, regular for $y_0 \to -\infty$, of the homogeneous equation

$$(L_0^+ - \lambda)v_\lambda = 0 \tag{4.14}$$

is known, one obtains $f_L(y_0|\lambda, a)$ in the form

$$f_L(y_0|\lambda, a) = \lambda^{-1}\{1 - v_\lambda(y_0)/v_\lambda(a)\}, \tag{4.15}$$

since this expression satisfied (4.2′) and vanishes for $y_0 = a$. Using (2.13′) one then obtains

$$\mathcal{P}_L(y_0|\lambda, a) = v_\lambda(y_0)/v_\lambda(a). \tag{4.16}$$

For the one-dimensional Gauss-Markoff function[10] ($A(y_0) = -y_0$; $B/2 = 1$) one has, for example,

$$v_\lambda(y_0) = \exp(y_0^2/4)D_{-\lambda}(-y_0) \tag{4.17}$$

and thus

$$\begin{aligned} \mathcal{P}_L(y_0|\lambda, a) &= \exp[\tfrac{1}{4}(y_0^2 - a^2)] \\ &\quad \cdot D_{-\lambda}(-y_0)/D_{-\lambda}(-a), \end{aligned} \tag{4.18}$$

where $D_\nu(z)$ is the solution of Weber's equation defined by Whittaker and Watson [*Modern Analysis*, p. 347 ff]. This result can also be obtained from Eq. (2.4) using

$$\begin{aligned} P_L(y_0|y, \lambda) &= (2\pi)^{-\frac{1}{2}}\Gamma(\lambda)\exp[\tfrac{1}{4}(y_0^2 - y^2)] \\ &\quad \cdot D_{-\lambda}(y)D_{-\lambda}(-y_0) \end{aligned} \tag{4.19}$$

(valid for $y_0 < y$). This expression follows from (3.2) and (3.2′) and can be checked by means of the series expansion for $P(y_0|y, t)$ given by Uhlenbeck and Ornstein.[11]

[10] The recurrence time problem for the corresponding random process (Ehrenfest model) has been solved by R. Bellman and T. E. Harris, Ann. Math. Statistics (in print).

[11] G. E. Uhlenbeck and L. S. Ornstein, Phys. Rev. **36**, 823 (1930).

For $y_0 \ll a \ll -1$ one expects the first passage time to approach the value $\ln(y_0/a)$. Actually one obtains $\mathcal{P}(y_0|t, a) \sim \delta(t - \ln y_0/a)$, by using the asymptotic form of the Weber function

$$D_{-\lambda}(-y_0) \sim (-y_0)^{-\lambda} \exp(-y_0^2/4) \text{ (for } y_0 \to -\infty). \quad (4.20)$$

For a and t both of the order of unity, or greater, the smallest root λ_0 of $D_{-\lambda}(-a)$ dominates the behavior of $\mathcal{P}(y_0|t, a)$, and λ_0 can be estimated by analogy with the quantum-mechanical problem of an oscillator with a reflecting wall at a.

V. DERIVATION OF THE WIENER-RICE SERIES FROM AN INTEGRAL EQUATION

Let $y(t)$ be Markoffian in y and $\dot{y}$, and be stationary and characterized by the conditional probability

$$P_2(y_0, \dot{y}_0; y_1, \dot{y}_1; t_1 - t_0)dy_1 d\dot{y}_1 = \text{cond. prob.}$$
$$\{\text{if } y(t_0) = y_0, \dot{y}(t_0) = \dot{y}_0, \text{ then } y_1 < y(t_1) < y_1 + dy_1, \quad \dot{y}_1 < \dot{y}(t_1) < \dot{y}_1 + d\dot{y}_1\}. \quad (5.1)$$

Let further $\mathcal{P}_k(t_0, \dot{y}_0|t, \dot{y})dtdy$ be the conditional probability that, if $y(t_0) = 0$ and $\dot{y}(t_0) = \dot{y}_0$, then y will go through zero with slope between $\dot{y}$ and $\dot{y} + d\dot{y}$ in the interval $(t, t + dt)$ and will have k other roots between t_0 and t. Because y is assumed to be two-dimensional Markoffian, there is the following recursion formula for $\mathcal{P}_k$:

$$\mathcal{P}_{k+1}(t_0, \dot{y}_0|t, \dot{y}) = \int_{t_0}^{t} d\vartheta \int_{-\infty}^{\infty} d\dot{\eta} \mathcal{P}_0(t_0, \dot{y}_0|\vartheta, \dot{\eta}) \mathcal{P}_k(\vartheta, \dot{\eta}|t, \dot{y}). \quad (5.2)$$

If we define the function $\Omega F(t_0, \dot{y}_0|t, \dot{y})$ by

$$\Omega F(t_0, \dot{y}_0|t, \dot{y}) = \int_{t_0}^{t} d\vartheta \int_{-\infty}^{\infty} d\dot{\eta} \mathcal{P}_0(t_0, \dot{y}_0|\vartheta, \dot{\eta}) F(\vartheta, \dot{\eta}|t, \dot{y}) \quad (5.3)$$

we have

$$\mathcal{P}_k(t_0, \dot{y}_0|t, \dot{y}) = \Omega^k \mathcal{P}_0(t_0, \dot{y}_0|t, \dot{y}). \quad (5.4)$$

We now define $p(t_0, \dot{y}_0|t, \dot{y})dtd\dot{y}$ as the conditional probability that y goes through zero between t and dt, with a slope between $\dot{y}$ and $\dot{y} + d\dot{y}$ if $y(t_0) = 0$, $\dot{y}(t_0) = \dot{y}_0$, without regard to other roots. We then have

$$p(t_0, \dot{y}_0|t, \dot{y}) = \sum_{k=0}^{\infty} \mathcal{P}_k(t_0, \dot{y}_0|t, \dot{y}) = \sum_{k=0}^{\infty} \Omega^k \mathcal{P}_0(t_0, \dot{y}_0|t, \dot{y})$$
$$= (1 - \Omega)^{-1} \mathcal{P}_0(t_0, \dot{y}_0|t, \dot{y}) \quad (5.5)$$

or

$$\mathcal{P}_0(t_0, \dot{y}_0|t, \dot{y}) = p(t_0, \dot{y}_0|t, \dot{y}) - \int_{t_0}^{t} d\vartheta \int_{-\infty}^{\infty} d\dot{\eta} \mathcal{P}_0(t_0, \dot{y}_0|\vartheta, \dot{\eta}) p(\vartheta, \dot{\eta}|t, \dot{y}). \quad (5.6)$$

This can now be considered as an integral equation for $\mathcal{P}_0$. It expresses the fact that to obtain $\mathcal{P}_0$ one must *deduct* from $p(t_0, \dot{y}_0|t, \dot{y})$ the probability that y has gone through zero for the first time after t_0 at some time $\vartheta < t$ with any slope $\dot{\eta}$, and passes again through zero (after an arbitrary number of passages) in the time interval $(t, t + dt)$ with slope $(\dot{y}, \dot{y} + d\dot{y})$. This integral equation is thus obtainable by a direct generalization of a method applied first by Schrödinger to the first passage time problem for particles in Brownian motion. The function $p(t_0, \dot{y}_0|t, \dot{y})$ can be expressed in terms of $P_2(y_0, \dot{y}_0|y_1, \dot{y}_1; t_1 - t_0)$ since

$$p(t_0, \dot{y}_0|t, \dot{y})dtd\dot{y} = P_2(0, \dot{y}_0|0, \dot{y}, t - t_0)|\dot{y}|dtd\dot{y}. \quad (5.7)$$

To derive the Wiener-Rice series we define

$$\Delta F(t_0, \dot{y}_0|t, \dot{y})$$

by

$$\Delta F(t_0, \dot{y}_0|t, \dot{y}) = \int_{t_0}^{t} d\vartheta \int_{-\infty}^{\infty} d\dot{\eta} F(t_0, \dot{y}_0|\vartheta, \dot{\eta}) p(\vartheta, \dot{\eta}|t, \dot{y})$$

and write (5.6) in the form

$$(1 + \Delta)\mathcal{P}_0(t_0, \dot{y}_0|t, \dot{y}) = p(t_0, \dot{y}_0|t, \dot{y}) \quad (5.8)$$

or

$$\mathcal{P}_0(t_0, \dot{y}_0|t, \dot{y}) = \sum_{k=0}^{\infty} (-)^k \Delta^k p(t_0, \dot{y}_0|t, \dot{y}), \quad (5.9)$$

where

$$\Delta^k p(t_0, \dot{y}_0|t, \dot{y}) = \int_{t_0}^{t} dt_k \int_{-\infty}^{\infty} d\dot{y}_k \int_{t_0}^{t_k} dt_{k-1} \int_{-\infty}^{\infty} d\dot{y}_{k-1} \cdots$$
$$\cdots \int_{t_0}^{t_2} dt_1 \int_{-\infty}^{\infty} d\dot{y}_1 p(t_0, \dot{y}_0|t_1, \dot{y}_1) \cdots p(t_k, \dot{y}_k|t, \dot{y}). \quad (5.10)$$

We now define, with $t_0 < t_j' < t$

$$w_k(t_0, \dot{y}_0|t_1', t_2', \cdots t_k', t) = \int_{-\infty}^{\infty} d\dot{y} \int_{-\infty}^{\infty} d\dot{y}_2 \cdots \int_{-\infty}^{\infty} d\dot{y}_1 p(t_0, \dot{y}_0|t_1, \dot{y}_1)$$
$$\times p(t_1, \dot{y}_1|t_2, \dot{y}_2) \cdots p(t_k, \dot{y}_k|t, \dot{y}), \quad (5.11)$$

where $t_1, t_2, t_3 \cdots t_k$ is the same set of values as $t_1', t_2' \cdots t_k'$, only rearranged, such that

$$t_1 < t_2 < t_3 \cdots < t_k.$$

w_k is thus symmetric in the variables t_j', because whatever the order of the t_j' may be, they appear in order of size on the right hand side. We note that

$$w_k(t_0, \dot{y}_0|t_1', \cdots, t_k', t)dt_1' \cdots dt_k'dt$$

is the conditional joint probability that, if $y(t_0) = 0$ and

$\dot{y}(t_0)=\dot{y}_0$, then the function $y(t')$ has roots in the intervals $(t_1', t_1'+dt_1')\cdots(t_k', t_k'+dt_k')$, $(t, t+dt)$, regardless of any other roots in the interval (t_0, t). Because of the symmetry of w_k, we have

$$\int_{t_0}^{t} dt_1' \int_{t_0}^{t} dt_2' \cdots \int_{t_0}^{t_{k-1}'} dt_k' w_k(t_0, \dot{y}_0 | t_1', t_2', \cdots t_k', t)$$

$$= k! \int_{t_0}^{t} dt_k' \int_{t_0}^{t_k'} dt_{k-1}' \cdots \int_{t_0}^{t_2'} dt_1' w_k(t_0, \dot{y}_0 | t_1', \cdots t_k', t)$$

$$= k! \int_{-\infty}^{\infty} d\dot{y} \Lambda^k p(t_0, \dot{y}_0 | t, \dot{y}). \quad (5.12)$$

Integration of (5.9) over $\dot{y}$ and use of (5.12) yields

$$\int_{-\infty}^{\infty} d\dot{y} \mathcal{P}_0(t_0, \dot{y}_0 | t, \dot{y}) = \sum_{k=0}^{\infty} \frac{(-)^k}{k!} \int_{t_0}^{t} dt_1 \int_{t_0}^{t} dt_2 \cdots$$

$$\cdots \int_{t_0}^{t} dt_k w_k(t_0, \dot{y}_0 | t_1, t_2 \cdots t_k, t). \quad (5.13)$$

We now define $W_0(t_0|t)$ by the relation

$$W_0(t_0|t) = \int_{-\infty}^{\infty} d\dot{y}_0 W_2(0, \dot{y}_0) \int_{-\infty}^{\infty} d\dot{y} \mathcal{P}(t_0, \dot{y}_0 | t, \dot{y}) \quad (5.14)$$

and $\hat{w}_k(t_0 t_1, \cdots, t_k, t)$ by the relation

$$\hat{w}_k(t_0 | t_1, \cdots, t_k, t) = \int_{-\infty}^{\infty} d\dot{y}_0 W_2(0, \dot{y}_0) w_k(t_0, \dot{y}_0 | t_1, t_2, \cdots, t_k, t). \quad (5.15)$$

Then $W_0(t_0|t)dt$ is the conditional probability that, if $y(t_0)=0$, then there is a root of y in the interval $(t, t+dt)$ and no root between t_0 and t, while $\hat{w}_k(t_0|t_1, \cdots, t_k, t)dt_1 \cdots dt_k dt$ is the conditional probability that, if $y(t_0)=0$, then y has roots in the intervals (t_j, t_j+dt_j) $[j=1, 2, \cdots, k]$ and in $(t, t+dt)$, regardless of other roots. With these definitions we obtain from (5.13)

$$W_0(t_0|t) = \sum_{k=0}^{\infty} \frac{(-)^k}{k!} \int_{t_0}^{t} dt_1 \int_{t_0}^{t} dt_2 \cdots \int_{t_0}^{t} dt_k \times \hat{w}_k(t_0 | t_1, \cdots, t_k, t), \quad (5.16)$$

which is the Wiener-Rice series for our case.

These considerations can obviously be generalized immediately to the case of a function y which is Markoffian in $y, \dot{y}, \ddot{y}, \cdots, y^{(n)}$ by replacing $\dot{y}$ by $\{\dot{y}, \ddot{y}, \cdots, y^{(n)}\}$ and $d\dot{y}$ by the volume element in the space $\{\dot{y}, \ddot{y}, \cdots, y^{(n)}\}$, whereby, however, $|\dot{y}|$ retains its original meaning in Eq. (5.7).

We wish to thank Professor G. E. Uhlenbeck and Professor M. Kac for interesting discussions, Dr. M. Rosenblatt for checking some of the derivations and the Graduate School of Northwestern University for a grant to cover travel expenses for two trips to Cornell University.

Letters to the Editor

PUBLICATION of brief reports of important discoveries in physics may be secured by addressing them to this department. The closing date for this department is five weeks prior to the date of issue. No proof will be sent to the authors. The Board of Editors does not hold itself responsible for the opinions expressed by the correspondents. Communications should not exceed 600 words in length.

The Atomic Masses of H^1, C^{12}, and S^{32}

ALFRED O. NIER
Department of Physics, University of Minnesota, Minneapolis, Minnesota*
December 6, 1950

THE masses of H^1, C^{12}, and S^{32} have been determined relative to O^{16} by the doublet method with the double-focusing mass spectrometer developed in this laboratory.[1] Table I lists the

TABLE I. Mass doublets from which masses of H^1, C^{12}, and S^{32} are calculated.

Doublet	Source of ions	No. of runs	$\Delta M \times 10^4$amu
a. $(C^{12})_4-S^{32}O^{16}$	C_4H_8 SO_2	4	331.82±0.07
b. $C^{12}(O^{16})_2-C^{12}S^{32}$	CO_2 CS_2	6	177.82±0.25
c. $(C^{12})_2(H^1)_8-C^{12}(O^{16})_2$	C_2H_8 CO_2	6	729.67±0.41
d. $(C^{12})_6(H^1)_4-C^{12}(S^{32})_2$	C_6H_4 CS_2	4	873.26±0.58

doublets studied together with the number of runs on each and the results obtained. As in previous work, each run consists of ten determinations. Mass differences involving hydrocarbon ions of the form $(C^{12})_n(H^1)_m$ are corrected for the presence of unresolved $(C^{13})_{n-1}C^{12}(H^1)_{m-1}$ ions. The probable error given indicates the consistency between runs. From the data in Table I, one finds:[2]

$$S^{32}=32-b=31.982218\pm25$$
$$C^{12}=12+(a-b)/4=12.003850\pm6$$
$$H^1=1+(a+7b+8c-4d)/48=1.0081685\pm90$$

or

$$H^1=1+(5c+4b-2d)/32=1.008166\pm8$$

or

$$H^1=1+(2d+3c-4a)/32=1.008151\pm6.$$

The result for S^{32} substantiates the value 31.9823±3 given by Aston[3] rather than that of Okuda and Ogata,[4] 31.98089±7. The new value is consistent with 31.98199±21 computed by Penfold[5] from disintegration and some mass spectrographic data, and the number 31.9823±10 found by Smith[6] in his new "synchrometer" mass spectrometer.

The weighted average of the three values for H^1 is 1.008159±4. An examination of the computations which lead to the three individual values shows that all three depend rather strongly upon the value of the doublet c, the first two more so than the last. If one arbitrarily weights the three in the ratio 1:1:2, respectively, in computing the average, one again obtains 1.008159. Because of the strong dependence of the three separate errors upon the error in the common doublet c it may be safer to assume 6, the lowest probable error of the three separate values, as the probable error in the final answer. This has been done in the computations which follow.

The present values for H^1 and C^{12} are in good agreement with the values 1.0081686±52 and 12.003803±13, respectively, found by Roberts while considering an entirely different cycle. His results are given separately.[7] The weighted averages of his and the present results for H^1 and C^{12} are given in Table II. Also given in Table II are masses for other isotopes based upon doublet measurements

TABLE II. Summary of atomic masses determined by mass spectrometry.

H^1	1.008165±4
H^2	2.014778±8[a]
He^4	4.003944±19[b]
C^{12}	12.003842±6
N^{14}	14.007564±7[c]
Ne^{20}	19.998835±43[d]
S^{32}	31.982218±25
A^{36}	35.97926 ±8[e]
A^{40}	39.97524 ±3[f]

[a] From $H_2-D=(15.519\pm0.017)\times10^{-4}$amu.
[b] From $D_2-He^4=256.12\pm0.09$.
[c] Weighted average from $C^{13}H_2-N^{14}=125.86\pm0.13$; $(N^{14})_2-C^{12}O^{16}=112.80\pm0.13$; $(C^{13})_4H_8-(N^{14})_2O^{16}=617.6\pm0.9$.
[d] From $D_2O^{18}-Ne^{20}=307.21\pm0.39$.
[e] From $H_2O^{18}-A^{36}/2=267.02\pm0.40$.
[f] Weighted average from $Ne^{20}-A^{40}/2=112.80\pm0.18$; $(C^{13})_4H^4-A^{40}=688.77\pm0.35$; $D_2O-A^{40}/2=419.67\pm0.18$.

reported in the present two letters and in the paper referred to under reference 1.

The assistance of Walter H. Johnson and Ruth C. Boe in making the determinations is gratefully acknowledged. The construction of the apparatus used in this research was aided by grants from the Graduate School and the Minnesota Technical Research Fund subscribed to by General Mills, Inc., *Minneapolis Star* and *Tribune*, Minnesota Mining and Manufacturing Company, Northern States Power Company, and Minneapolis Honeywell Regulator Company.

* This work supported by joint program of the ONR and AEC.

[1] Preliminary reports on the apparatus and some results already have been given: Phys. Rev. **75**, 346 (1949); **77**, 746 (1950). A more complete report on the apparatus and measurements on 13 mass doublets will be found in a paper appearing elsewhere in this issue, Phys. Rev. **81**, 507 (1951).

[2] Except in Table I, probable errors given in this letter apply to the last significant figures in the values to which the probable errors are attached.

[3] F. W. Aston, Nature **138**, 1094 (1936); Proc. Roy. Soc. (London) **A163**, 391 (1937).
[4] T. Okuda and K. Ogata, Phys. Rev. **60**, 690 (1941).
[5] A. S. Penfold, Phys. Rev. **80**, 116 (1950).
[6] L. G. Smith, Phys. Rev. **81**, 295 (1951).
[7] T. R. Roberts, Phys. Rev. **81**, 624 (1951).

The H_2-D Mass Difference and the Determination of Secondary Atomic Mass Standards*

T. R. ROBERTS
Department of Physics, University of Minnesota, Minneapolis, Minnesota
December 6, 1950

THE physical table of isotopic weights is determined relative to O^{16}. As summarized by Tollestrup, Fowler, and Lauritsen[1] key light elements H, C^{12}, and N^{14} have not yet been compared directly with O^{16} by nuclear reactions and are dependent only upon mass doublet measurements. The low probable errors of Mattauch's and Jordan's fundamental doublets H_2-D, $C^{12}H_4-O^{16}$, and $D_3-C^{12}/2$ have weighted their data predominantly in the mass values recommended by Bainbridge,[2] and are shown in Table I.

TABLE I. Secondary atomic mass standards.

Isotope	Bainbridge report[a]	Present results
H	1.0081283 ±0.0000026	1.0081686 ±0.0000052
D	2.0147186 ±0.0000055	2.014785 ±0.000010
C^{12}	12.003856 ±0.000019	12.003803 ±0.000013
N^{14}	14.007536 ±0.000022	14.007544 ±0.000010
n	1.0089383 ±0.0000057	1.0090087 ±0.0000056

[a] See reference 2.

The H_2-D doublet can be combined with the deuteron binding energy to give the neutron-proton mass difference. Recently Bell and Elliott[1] have reported a new and considerably different value for the deuteron binding energy. In addition the $T(p, n)$ threshold of Taschek, *et al.*[2] combined with the tritium beta-decay end point gives the $n-H$ difference directly. The nuclear data thus indicates a H_2-D difference of 15.55 ± 0.08 (expressed in units of 10^{-4} atomic mass units in this paper). This figure differs from Mattauch's mass spectrographic value[3] of 15.380 ± 0.021 by eight times the latter's probable error.

In an attempt to resolve this discrepancy and also to recheck the secondary atomic mass standards, H, D, and C^{12}, various doublets have been measured with the double-focusing spectrometer described elsewhere.[4] For H_2-D measurements, D ions were obtained from D_2O vapor admitted through an adjustable leak. A preliminary value[7] for this doublet was based on data with the D peaks about 10 percent broader than those of H_2 at the half-height. Subsequent studies have shown this shape difference to be caused by the initial lateral kinetic energy spread of the D ions. This effect has been minimized and the average of runs obtained on fourteen different days over an eight-month period is 15.519 ± 0.017.

To obtain the secondary mass standards the following doublets are used:[5]

$$a=H_2-D$$
$$b=C^{12}H_4-O^{16}=364.78\pm0.22$$
$$c=2(D_2O^{16}-A^{40}/2)-(C_2H_4-A^{40})=150.57\pm0.50.$$

Solution for the masses yields the results in Table I:

$$H=1+(4a+3b+c)/16$$
$$D=2-(4a-3b-c)/8$$
$$C=12-(4a-b+c)/4.$$

The N^{14} mass is obtained using the $N_2^{14}-C^{12}O$ and $C^{12}H_3-N^{14}$ doublets previously reported. The values in the table for H, D, and n differ by about ten times the probable errors assigned.

Recent mass spectrographic studies by Ewald[6] have shown that the spacing of doublets containing fragment ions such as O^+ could be changed by very slight instrument misalignments. Results of Dempster and Shaw[9] indicate that inaccuracies may arise in instruments at pressures greater than 10^{-5} mm. With the exception of doublet a, the present results are based primarily on doublets involving only molecular ions. All data are taken at pressures below 5×10^{-6} mm. Measurement of the $(C^{12})_3H_9-(C^{12})_3H_7$ mass difference indicates that systematic errors in a doublet measurement are not likely to exceed 0.1 percent.

The construction of the apparatus used in this research was aided by grants from the Graduate School and the Minnesota Technical Research Fund subscribed to by General Mills, Inc., *Minneapolis Star* and *Tribune*, Minnesota Mining and Manufacturing Company, Northern States Power Company, and Minneapolis Honeywell Regulator Company.

[*] Assisted by the joint program of the ONR and AEC.
[1] Tollestrup, Fowler, and Lauritsen, Phys. Rev. **78**, 372 (1950).
[2] K. T. Bainbridge, National Research Council Preliminary Report No. 1, Nuclear Science Series (1948).
[3] R. E. Bell and L. G. Elliott, Phys. Rev. **79**, 282 (1950).
[4] Taschek, Argo, Hemmendinger, and Jarvis, Phys. Rev. **76**, 325 (1949).
[5] J. Mattauch and A. Flammersfeld, *(Isotopic) Report—1948* (Verlag d. Zeits. f. Natur., Tubingen, Germany, 1949).
[6] A. O. Nier and T. R. Roberts, Phys. Rev. **81**, 507 (1951).
[7] T. R. Roberts and A. O. Nier, Phys. Rev. **77**, 746 (1950).
[8] H. Ewald, Z. Naturforsch. **2a**, 384 (1947); **3a**, 114 (1948).
[9] A. J. Dempster and A. E. Shaw, Phys. Rev. **77**, 746 (1950).

Beta-Decay and Meson Decay

EDUARDO R. CAIANIELLO
University of Rochester, Rochester, New York
December 4, 1950

THE question has been raised recently[1,2] of whether it is possible to re-establish Yukawa's scheme of β-decay by assuming the decay to occur through the creation of a virtual pseudoscalar π-meson, which subsequently gives rise to an electron-neutrino pair. This would be of great interest, since the experimental data on the π-meson (induced disintegration of deuterium[3] and considerations of parity and selection rules[4]) rule out a scalar and a vector π-meson. The results quoted in reference 1 tend to favor this possibility, while an earlier study by Nelson[5] rejects it, so that it has seemed to be appropriate to investigate the question further. Our calculation confirms Nelson's result completely, the conclusion being that only a virtual vector meson (τ-meson?) can fit the Yukawa scheme.

We have considered the decay of a free neutron, since uncertainties arising from our lack of knowledge of the true nuclear wave functions are thereby eliminated. Let r_μ be the ratio m_μ/m_π, M be the nucleon mass, g_1, f_1, g_2, f_2, g_2', f_2' be pseudoscalar (g) and pseudovector (f) constants coupling a pseudoscalar π-meson respectively with nucleons, electron-neutrino, and μ-meson, and neutrino. We assume the neutrino mass to be zero and define

$$G_1=g_1+2Mf_1/m_\pi,\quad G_2=g_2+m_\mu f_2/m_\pi,\quad G_2'=g_2'+m_\mu f_2'/m_\pi.$$

Then a standard quantization procedure for the π-meson field yields the following relations among the lifetimes τ_e, τ_μ, τ_β for the processes ($\bar\nu$ represents the antineutrino):

$$\pi\to e+\nu,\quad \pi\to\mu+\nu,$$
$$P+\pi^-+\bar\nu$$
$$N+\bar\nu \qquad\qquad P+e,$$
$$N+\pi^++e$$

$$1/\tau_\mu=(1-r_\mu^2)^2(G_2'/G_2)^2/\tau_e,$$
$$1/\tau_\beta=(13.84/\pi)(m_e/m_\pi)^2(m_e/M)^2(G_1^2/\hbar c)\cdot(1/\tau_e),$$

to the first significant power of m_e/M, where

$$1/\tau_e=(m_\pi c^2/2\hbar)(G_2^2/\hbar c).$$

Normalization of the interaction Hamiltonian as in reference 5 would double the value of $1/\tau_e$.

As pointed out by d'Espagnat, the assumptions $g_2=g_2'=0$, $f_2=f_2'$ lead to $\tau_e\gg\tau_\beta$, in agreement with experiment; but evaluation of τ_e, using the values $m_\pi=280m_e$, $\tau_\beta=(10$ to 20 min$)/0.693$ and $(G_1^2/\hbar c)\cong1$, gives $\tau_e\cong10^{-12}$ sec, a value which is completely unacceptable. This is largely due to the fact, overlooked in reference 2, that the γ_5 appearing in the pseudoscalar interaction Hamiltonian brings an additional momentum into the expression for the transition probability. A similar momentum factor appears also if one considers the β-decay of complex nuclei; this effect would itself rule out the Yukawa scheme for a pseudoscalar meson because it leads to a W_0^7 (W_0 is the maximum β-ray energy) dependence of the lifetime rather than the experimentally established W_0^5.

We may then ask whether a Yukawa scheme for β-decay is possible at all, foregoing identification of the virtual meson with the π-meson, if we require only that we should obtain a W_0^5 law, together with Gamow-Teller selection rules. It turns out, as is well known, that only a virtual vector meson can satisfy the Yukawa scheme. If we use the lifetime expression for a vector meson given by Bethe and Nordheim,[6] a lifetime of 10 minutes for the neutron decay, a meson mass $\mu=1000m_e$, and a value $F_1^2/\hbar c\cong1$ for the constant coupling the meson with nucleons (retaining only the part of the interaction that gives Gamow-Teller selection rules), we find $\tau_e\cong2.5\times10^{-11}$. Such a vector π-meson may still be found and validate the Yukawa scheme.

This research has been suggested and supervised by Dr. R. E. Marshak; to him and to Dr. J. Ashkin the author is indebted for many valuable discussions.

[1] B. d'Espagnat, Compt. rend. **228**, 744 (1949).
[2] H. Yukawa, Revs. Modern Phys. **21**, 474 (1949).
[3] Panofsky, Aamodt, Hadley, and Phillips, Phys. Rev. **80**, 94 (1950).
[4] Brueckner, Tamor, and Marshak (to be published).
[5] E. C. Nelson, Phys. Rev. **60**, 830 (1941).
[6] H. A. Bethe and L. W. Nordheim, Phys. Rev. **57**, 998 (1940).

Low Energy Electron Resulting from a Stopped μ-Meson*

GERHART GROETZINGER,† LEWIS B. LEDER, AND FRED L. RIBE
Institute for Nuclear Studies, University of Chicago, Chicago, Illinois
November 24, 1950

IN the course of experiments in this laboratory, using a cloud chamber expanded at random, we have incidentally observed in approximately 10,000 expansions a stopped μ-meson resulting in the emission of a negative electron with an energy of 70 kev. The electron track is unfortunately so faint in both stereoscopic views that it does not lend itself to reproduction. A total of three stopped mesons were observed, of which only one was accompanied by the emission of a charged particle. The cloud chamber was horizontal, filled with 0.6 atmos helium and 0.4 atmos argon, and had a diameter of 24 cm and an illuminated region 3 cm deep. The magnetic field strength was 350 gauss, so that no statement can be made concerning the charge of any one of the stopped mesons.

The emission of electrons of such a low energy accompanying the stoppage of mesons could not have been observed in cloud-chamber experiments designed to study μ-meson decay, since magnetic fields of the order of 10,000 gauss have been used in investigations of this kind.

It seems to us worth while to report our finding in view of the frequent appearance of electrons of energies between 10 and 60 kev at the end of μ-meson tracks in photographic emulsions reported, among others, by Frey,[1] who interpreted them as atomic electrons ejected from the heavy elements in the emulsions during the capture of the meson. In the case of the evidence obtained from photographic emulsions there might, however, exist an alternative explanation for the appearance of at least a part of these electrons; namely, that they are internal conversion electrons or beta-decay of radioactive isotopes formed by the capture of μ-mesons in bromine or silver.

* This research was supported in part by the joint program of the ONR and AEC.
† Now at the National Advisory Committee for Aeronautics, Cleveland, Ohio.
[1] W. F. Frey, Phys. Rev. 79, 893 (1950).

Production of Highly Polarized Neutron Beams by Bragg Reflection from Ferromagnetic Crystals

C. G. SHULL
Oak Ridge National Laboratory, Oak Ridge, Tennessee
December 8, 1950

THE theory of magnetic scattering of neutrons, as given for instance by Halpern and Johnson,[1] predicts a polarization in the neutrons scattered by a lattice containing aligned atomic magnetic moments. For the particular case where the magnetization vector is perpendicular to the plane of scattering, the intensity of scattering for the two neutron spin states, respectively parallel and antiparallel to the magnetic field, is given as

$$I_1 = b(C-D)^2$$
$$I_2 = b(C+D)^2,$$

where C is the nuclear scattering amplitude, D is the magnetic scattering amplitude, and b is a proportionality constant. The greatest difference between I_1 and I_2, and hence the highest polarization, will be obtained when $C=D$, for which there will be scattered intensity for only a single spin state. This situation of balanced nuclear and magnetic amplitudes has been found in the (220) reflection of Fe_3O_4 described earlier,[2] for which $C=0.95\cdot10^{-12}$ cm and $D=0.97\cdot10^{-12}$ cm, and hence a very high polarization would be expected in this reflection.

We have looked for this polarization and find it to be indeed very high. A thin slice of Fe_3O_4 approximately one square centimeter in area and 0.1 cm in thickness was cut along the (220) planes in a natural, single crystal of magnetite. This slice was magnetized in the gap of a permanent magnet ($H=4500$ oersteds), and a monochromatic beam of neutrons ($\lambda=1.204$A) was reflected from the (220) planes with the crystal slice set in transmission orientation and with the magnetization vector perpendicular to the plane of scattering. The degree of polarization in the reflected beam was determined by passage through an analyzing block of polycrystalline iron which could be magnetized with a field of 8000 oersteds in the gap of an electromagnet. Single transmission measurements were taken of the analyzing block with analyzing field off and on (with field always parallel to the polarizing field in order to avoid any depolarization of the neutron beam in the intervening space) for both the polarized beam from Fe_3O_4 and an unpolarized beam from a copper crystal. These measurements permit evaluation of the degree of polarization after allowance for depolarization effects in the analyzing block according to formulas of Halpern and Holstein.[3] Analysis of the data showed the polarization in the (220) Fe_3O_4 reflection to be 100 percent within the experimental uncertainty of perhaps 5 percent. This means that the relative intensities of the two neutron spin states are in ratio at least 40 to 1.

Other crystal reflections are of interest as possible polarizing reflections. Some reflections from Co have very favorable amplitudes for this purpose; but this material is difficult to magnetize, and there may result internal depolarization of the beam. The (110) reflection from an Fe crystal is not too favorable for polarization purposes, since by calculation the expected polarization is only about 60 percent. We have studied this reflection with an Fe crystal (5 percent silicon) in the same fashion as for Fe_3O_4 above and find it to be about 41 percent polarized. This value, which is lower than calculated, could be explained on the basis of extinction effects, depolarization, or silicon impurity within the crystal lattice.

The above Fe_3O_4 (220) reflection is also interesting because *the polarization direction is just reversed from that obtained in the (110) Fe reflection.* This shows up in the sign of the single transmission effect in the analyzing block and results because only Fe^{+++} ions at tetrahedral positions in the magnetic lattice contribute to the intensity in the (220) Fe_3O_4 reflection. The iron atoms at the tetrahedral positions are coupled antiferromagnetically to those at the octahedral positions; and since the latter are in the majority and consequently will be aligned in the applied field direction, the tetrahedral ions will be aligned antiparallel to the external field. The polarization observation constitutes direct proof of the antiferromagnetic nature of the Fe_3O_4 lattice. Other Fe_3O_4 reflections, also highly polarized, are normal with respect to showing polarization parallel to the applied field direction.

It is possible by this method to produce a collimated beam of monochromatic, completely polarized neutrons with an intensity of about 10^5 neutrons/sec. The beam can also be pulsed as suggested earlier.[2]

[1] O. Halpern and M. H. Johnson, Phys. Rev. 55, 898 (1939).
[2] Shull, Wollan, and Strauser, Phys. Rev. 81, 483 (1951).
[3] O. Halpern and T. Holstein, Phys. Rev. 59, 960 (1941).

Thermal Expansion at Low Temperatures

S. VISVANATHAN
Harvard University, Cambridge, Massachusetts
November 24, 1950

IN the customary derivation of the Gruneisen[1] relation between the thermal expansion and the atomic heat of an isotopic solid, namely,

$$3\alpha V/\chi = \gamma(C_V)_D, \quad \text{where} \quad \gamma = -d(\ln\theta)/d(\ln V), \tag{1}$$

one neglects the temperature dependence of the kinetic energy of the conduction electrons. It is fairly obvious that this is invalid at low temperatures as the electronic specific heat of the solid at these low temperatures becomes comparable with the Debye atomic heat.

We have

$$3\alpha/\chi = -\partial/\partial T[(\partial\Phi/\partial V)_T], \tag{2}$$

where Φ is the free energy of the system. In order to take into account the contribution of the conduction electrons at low temperatures, we regard the electrons as a Fermi gas and include the free energy thereof in the free energy of the whole system. We regard the contributions from the ionic lattice and the electron gas as independent.

The total free energy of the system Φ is given by

$$\Phi(V,T)=\Phi_0(V)+\Phi_D(V,T)+\Phi_e(V,T) \tag{3}$$

and consequently

$$\frac{3\alpha}{\chi}=-\frac{\partial}{\partial T}\left(\frac{\partial\Phi_D}{\partial V}\right)_T-\frac{\partial}{\partial T}\left(\frac{\partial\Phi_e}{\partial V}\right)_T. \tag{4}$$

The first term on the right-hand side leads to the usual Debye term $\gamma(C_V)_D/V$. Now to evaluate the second term, we must know the free energy of the electron gas. The free energy Φ_e of the electron gas is given[2] by

$$\Phi_e(V,T)=NkT\mu-\Omega, \tag{5}$$

where

$$\Omega=-kTZ=-V\int_0^\infty g(\epsilon)\ln(1+e^{\mu-\epsilon/kT})d\epsilon. \tag{6}$$

Here $g(\epsilon)$ is the density of electron states per unit volume of the metal as a function of the energy and μ is essentially the thermodynamic potential in the Fermi-Dirac distribution function

$$f(\epsilon)=\frac{1}{\{\exp[(\epsilon/kT)-\mu]+1\}}, \quad \text{and} \quad N=\partial Z/\partial\mu. \tag{7}$$

From (6) and (7), we have

$$-\frac{\partial}{\partial T}\left(\frac{\partial\Phi_e}{\partial V}\right)_T=-\frac{\partial}{\partial T}(kTZ/V) \tag{8}$$

Defining $G(\epsilon)=\int_0^\epsilon g(\epsilon)d\epsilon$,

$$kTZ/V=\int_0^\infty g(\epsilon)\ln(1+e^{\mu-\epsilon/kT})d\epsilon=\int_0^\infty G(\epsilon)f d\epsilon. \tag{9}$$

Now[3]

$$\begin{aligned}\frac{\partial}{\partial T}\left(\frac{\partial\Phi_e}{\partial V}\right)_T&=-\frac{\partial}{\partial T}(kTZ/V)=-\frac{\partial}{\partial T}\int_0^\infty G(\epsilon)f d\epsilon\\&=G(\mu')(\pi^2k^2T/3)g'(\mu')/g(\mu').\end{aligned} \tag{10}$$

The electronic specific heat per gram atom of the metal

$$(C_V)_e=V\frac{\partial}{\partial T}\int_0^\infty \epsilon g(\epsilon)f d\epsilon=\tfrac{1}{3}\pi^2k^2Tg'(\mu')V\mu'. \tag{11}$$

Expressing (10) in terms of (11), we are led to

$$-\frac{\partial}{\partial T}\left(\frac{\partial\Phi_e}{\partial V}\right)_T=-\frac{\partial}{\partial T}(kTZ/V)=\frac{1}{V}\frac{d(\ln\mu')}{d[\ln G(\mu')]}(C_V)_e. \tag{12}$$

Finally we have the modified Gruneisen relation as

$$\frac{3\alpha V}{\chi}=\gamma(C_V)_D+\frac{d(\ln\mu')}{d[\ln G(\mu')]}(C_V)_e. \tag{13}$$

In the free electron case (alkali metals) $g(\epsilon)=A\epsilon^{\frac{1}{2}}$ and (13) reduces to

$$3\alpha V/\chi=\gamma(C_V)_D+\tfrac{2}{3}(C_V)_e. \tag{14}$$

Equation (13) can also be written as

$$3\alpha V/\chi=\gamma(C_V)_D+(aNT/\mu'), \tag{15}$$

where a is a numerical factor emerging from the reduction of the second term in (13).

The electronic specific heat at low temperatures is $(C_V)_e=\frac{1}{3}\pi^2k^2TVN(\mu_0)$; and so from (12) above, we expect a similar proportionality to T, also obvious from (14), for the thermal expansion provided we can neglect the temperature variation of α. On account of the second term of (13) the thermal expansion of a metal at liquid helium temperatures falls more slowly than expected from the behavior at moderate temperatures; and, therefore, the measurement of α seems to be plausible even at very low temperatures. In the case of transition metals which show a large electronic specific heat or have a low thermodynamic potential (μ'), the effect of the conduction electrons on the thermal expansion should be considerable. Keesom and Kurrelmeyer[4] found from their experiments on α-iron, the relation

$$C_V=0.60\times10^{-3}RT+2.36\times10^{-4}RT^3. \tag{16}$$

We readily see that $(C_V)_e>(C_V)_D$ and the two become equal at about 15°K, so that the effect of the conduction electrons should be noticeable around this temperature.

It is a pleasure to thank Professor H. Brooks for his suggestions and illuminating discussions.

[1] Gruneisen, *Handbuch der Physik*, Vol. X.
[2] E. C. Stoner, Phil. Mag. 21, 145 (1936).
[3] F. Seitz, *Modern Theory of Solids* (McGraw-Hill Book Company, Inc., New York, 1940).
[4] W. H. Keesom and Kurrelmeyer, Physica 6, 364 (1939).

The Directional Distribution of Photo-Electrons Ejected by Polarized Quanta*

FRANK L. HEREFORD
University of Virginia, Charlottesville, Virginia
December 4, 1950

AN earlier Letter[1] reported an azimuthal asymmetry in the directional distribution of photo-electrons ejected coincidentally by annihilation radiation. If the cross-polarization of the quanta is accepted on the basis of previous theoretical and experimental results,[2] then these data bear upon the directional distribution of photo-electrons produced by polarized quanta. Previous data[3] in this regard were for low energy photons (<40 kev) and involved a distinction between polarized and unpolarized photons by somewhat indirect means.

In order to interpret the results in the present case, it is necessary to carry through a computation of the expected coincidence asymmetry for cross-polarized quanta, employing some distribution function for photo-electrons ejected by polarized photons. For the nonrelativistic case this distribution is of the form,[4]

$$J_1(\theta,\phi)=A+B(\theta)\cos^2\phi, \tag{1}$$

where ϕ is the angle between the plane containing the beam of photons and the electric vector and the plane containing the beam and the direction of the photo-electron, and θ is the angle between the direction of the beam and that of the photo-electron. The second member, containing the factor $\cos^2\phi$, arises principally from photo-electrons ejected from the K and L_1 levels, and the first from those from higher levels. The asymmetry with respect to ϕ is involved in the experiment under consideration.

From such a distribution the coincidence rate expected for cross-polarized annihilation quanta and for ideal geometry can be obtained following the method of Snyder, Pasternack, and Hornbostel[5] in their consideration of the experiment where the scattered quanta are detected. By analysis of each beam into two orthogonal components of polarization, one finds for the total coincidence rate for fixed θ_1 and θ_2, and for relative azimuthal orientation of the counters, $\phi_2-\phi_1$,

$$J_2(\phi_2-\phi_1)=2(A^2+AB)+B^2\sin^2(\phi_2-\phi_1). \tag{2}$$

For the case of finite counter geometry, one must integrate with respect to θ_1, θ_2, ϕ_1, and ϕ_2 over the finite spans of the counters.

For annihilation radiation, however, relativistic expressions for A and B are required in Eq. (1). This calculation has been performed for K-shell electrons by Sauter[6] employing the Dirac theory. However, even without correction for finite geometry, his result cannot be reconciled with the data reported in reference 1, nor does it seem to be physically reasonable.

For $\theta=\pi/2$, Sauter's result for the K-shell electron distribution may be written,

$$\begin{aligned}J_1(\tfrac{1}{2}\pi,\phi)=\text{const}\Big[&\cos^2\phi\left\{(1-\beta^2)^{\frac{1}{2}}-\frac{1-(1-\beta^2)^{\frac{1}{2}}}{2(1-\beta^2)^{\frac{1}{2}}}\right\}\\&+\tfrac{1}{2}\left(\frac{1-(1-\beta^2)^{\frac{1}{2}}}{(1-\beta^2)^{\frac{1}{2}}}\right)^2\Big].\end{aligned} \tag{3}$$

For annihilation quanta $[(1-\beta^2)^{\frac{1}{2}}=\frac{1}{2}]$ the first term vanishes yielding complete azimuthal symmetry. For higher energies this term is negative with the second term predominating (since it contains the square of the energy which the first term does not). Thus, in this region the preferred electron emission is at right angles to the electric vector, which result seems to be at variance with the known mechanisms which are operative in the photoelectric process.

As regards the data presented in reference 1, they fail to confirm the symmetrical azimuthal distribution predicted by Eq. (3) for annihilation quanta. Moreover, integration of Sauter's general expression, $J_1(\theta, \phi)$, over the finite spans of the counters does not introduce sufficient dependence on ϕ to account for the observed asymmetry.

It is worth while to point out that the experimental results do confirm the rough estimate of the expected asymmetry given by Pryce and Ward.[7] They argue that the K-shell electrons, comprising some 80 percent of all electrons ejected should show strong asymmetry. Setting $A=0.2$ and $B=0.8$ in Eq. (2), and correcting approximately for finite geometry by integrating over the finite azimuthal spans only, one obtains $C_\perp/C_{11}=2.12$. Agreement with the observed value, $C_\perp/C_{11}=1.94\pm0.14$, is satisfactory in view of the approximate nature of the expected value. However, the failure of the relativistic result to predict the asymmetry remains unexplained.

Thanks are due to Dr. J. Hornbostel of Brookhaven National Laboratory for several helpful discussions concerning the proper method of correction for counter geometry.

* Supported in part by Navy Bureau of Ordnance.

[1] F. L. Hereford, Phys. Rev. **81**, 482 (1951).
[2] J. A. Wheeler, Ann. N. Y. Acad. Sci. **48**, 219 (1946); E. Bleuler and H. L. Bradt, Phys. Rev. **73**, 1398 (1948); R. C. Hanna, Nature **162**, 332 (1948); C. S. Wu and I. Shaknov, Phys. Rev. **77**, 136 (1950).
[3] P. Kirkpatrick, Phys. Rev. **38**, 1938 (1931). References to earlier work are given in this paper.
[4] A. Sommerfeld and G. Schur, Ann. Physik **4**, 409 (1930); G. Schur, Ann. Physik **4**, 433 (1930).
[5] Snyder, Pasternack, and Hornbostel, Phys. Rev. **73**, 440 (1948).
[6] F. Sauter, Ann. Physik **11**, 454 (1931). The result is given also by H. Bethe [*Handbuch der Physik* (Verlag. Julius Springer, Berlin, 1933), Vol. 24, p. 487], but a factor $(1-\beta^2)^{-1}$ has apparently been omitted in the second term.
[7] M. H. L. Pryce and J. C. Ward, Nature **160**, 435 (1947).

On the Production of Polarized High Energy X-Rays

M. May and G. C. Wick
Department of Physics, University of California, Berkeley, California
December 12, 1950

THE purpose of this note is to examine the possibility of experiments with *polarized* x-rays of high energy, the polarization being obtained by using only a portion of the x-ray beam emitted (by a betatron, synchrotron, or linear-accelerator target) at an angle θ to the direction of the electron beam. The optimum angle, neglecting certain secondary phenomena to be mentioned later, is $\theta=mc^2/E$, the ratio of the rest energy to the full energy of the electrons. The smallness of θ imposes rather stringent but perfectly possible conditions on the geometry.

The polarization expected in this off-center radiation is in a sense the analog of the well-known polarization of ordinary bremsstrahlung[1] when observed at right angles to the electron beam. At relativistic energies, however, the polarization and frequency dependence thereof are exactly reversed, as the formulas given later show; the dominant direction of the electric polarization vector is perpendicular, instead of parallel, to the emission plane (the plane containing the incident electron and the direction of observation); and the degree of polarization goes to zero at the short-wave limit, instead of being a maximum there.

The angular distribution and polarization of high energy bremsstrahlung can be derived by an easy extension of Weizsäcker's analysis[2] of the radiative collision between an electron and a nucleus. Namely, one exploits the approximate equivalence (in the rest system of the incident electron) between the actual electromagnetic field of the nucleus and a purely transverse field, corresponding to virtual quanta with a frequency distribution $Cd\nu/\nu$. Scattering of these quanta by the electron gives rise to the bremsstrahlung. The polarization of the bremsstrahlung is then simply an indirect application of the well-known fact that an initially unpolarized radiation—in our case, the virtual quanta—becomes partially polarized after being scattered. A *direct* application of this fact is made in the other classical method for obtaining polarized x-rays, namely, by scattering. While this method fails, however, to give any significant polarization as soon as $h\nu\gg mc^2$ (as a simple inspection of the Klein-Nishina formula will show), it is indeed remarkable that a similar difficulty does *not* arise in the *indirect* application. The reason is that, in the electron's rest system where the polarization by scattering is computed, the energy of the bremsstrahlung-quanta can be comparable to mc^2, even though it is much larger in the laboratory system.

Omitting further details, here is then the result of the calculation of the bremsstrahlung cross section $d\sigma$ for electrons of energy E and velocity βc and a nucleus of charge Ze. Let $\sigma_0=(Ze^2/mc^2)^2(137)^{-1}\ln(137Z^{-\frac{1}{3}})$, $f(\theta)=[mc^2/E(1-\beta\cos\theta)]^2$, a function sharply peaked in the forward direction, x the Compton-shift ratio (frequency after/frequency before scattering) in the electron's rest system. Then the cross section for the production of quanta polarized at an angle ϕ to the plane of observation is

$$d\sigma=\sigma_0(d\nu/\nu)f(\theta)[1+x^2-2xf(\theta)\sin^2\theta\cos^2\phi]\sin\theta\cdot d\theta.$$

Using the Lorentz-transformation of the frequencies one finds that $x\approx1-h\nu(1+\cos\theta)/2E$; $f(\theta)\sin^2\theta$ has a maximum value of unity at the previously mentioned optimum angle. All the previous statements can be easily verified on the formula. If, for example, $h\nu=E/2$, $x=0.5$, the ratio of the perpendicular to the parallel component is 5:1. Quantitatively, these conclusions may be slightly changed if the more exact Bethe-Heitler formulas are used. Work on this is in progress.

The most serious obstacle opposing an application of these ideas seems to be the extreme thinness of the target which is required in order to keep the direction of the electrons sufficiently well defined within the target. With a 1-mil thick Pt target, for instance, the angular spread of the beam due to multiple scattering is already two or three times the optimum angle of observation, so that a very considerable reduction of the polarization effect is expected. Also the angle at which maximum polarization is expected can be affected considerably. Numerical data on these effects are being prepared.

[1] A. Sommerfeld, *Atombau und Spektrallinien*, Vol. II, Chapter 7.
[2] C. F. v. Weizsäcker, Z. Physik **88**, 612 (1934).

The Integral Multiplicity of Meson Production*

Kurt Sitte
Department of Physics, Syracuse University, Syracuse, New York
December 6, 1950

IN an attempt to obtain additional information on the total number of mesons produced per primary cosmic-ray particle of given energy, the geomagnetic effects of the hard component have been analyzed by a method similar to that described previously.[1] The experimental data most suitable for the analysis are the height-intensity curves obtained by Barber[2] under 14.5-cm Pb at 41°, between atmospheric depths of 231 and 955 g/cm², and of Biehl, Neher, and Roesch[3] under 10.4- and 20.8-cm Pb at the geomagnetic equator, and at 53°N up to 310 g/cm² atmospheric depth.

At airplane altitudes the hard component recorded in these experiments includes a quite appreciable fraction of nucleons, and can certainly not be identified with the meson component, which is the subject of this discussion. However, the analysis makes use only of the *differences* between the intensities at the various latitudes, and it seems plausible to expect very little latitude dependence of the hard component protons at a depth corre-

sponding to about 3 to 4 collision mean free paths. The "filling-in" of the cut-off spectrum should be nearly complete, and the differences be due only to the fraction of the primaries that escaped collision. Hence the difference between the intensities of the hard component is a reasonably good approximation to the difference of the meson intensities. (Incidentally, when an attempt was made to construct the meson intensity curves, taking the observed intensities below 500 g/cm² as arising from mesons only and calculating the intensities expected at higher altitudes, the results were found to be identical within the accuracy of the computations.)

The next step in the analysis is subject to stronger criticism. It was assumed that the bulk of the mesons recorded were produced near the top of the atmosphere, so that a minimum energy at production can be ascribed to a particle recorded at a given depth, and under a known absorber. This procedure is satisfactory at large depths, while in the upper atmosphere local production even of hard component mesons becomes appreciable. Still, this holds only for the low energy part of the recorded intensity, and hence the error introduced by the suggested summary treatment is not critical. In this way the altitude-intensity curves at various latitudes can be transformed into "integral intensity" spectra, and their differences into the "integral spectra" produced by primary particles of various energies.

If the meson spectrum is known at a given altitude, a correction for decay in flight can be made. This was done by assuming in the customary way an exponential absorption of the primary radiation with a mean free path of 120 g/cm², and a constant cross section for meson production throughout the atmosphere. In a manner similar to that used in the earlier note[1] it can be argued that the latter assumption is not seriously in error for fast mesons, although its application to slow mesons would hardly be justified.

The differences between the meson intensities thus corrected, and divided by the differences between the primary intensities at the latitudes 53° and 41°, and 41° to 0°, represent the total number of meson with energies exceeding a certain minimum value, produced per primary particle in the energy intervals of about 1.5 to 4 Bev, and 4 to 14 Bev. The results are shown in Fig. 1, where the upper curve (b) represents the integral multiplicity of meson production for the more energetic, and the lower curve (a) that for the slower primaries. If one attempts to extrapolate these curves to include all relativistic mesons, which is a somewhat dubious procedure in view of the low degree of reliability of both the experimental values and the method of computation for the highest altitudes, he finds a total of 1 to 2 mesons in the lower, and 2 to 3 mesons in the higher energy interval. The agreement with the data from photographic plates[4] is satisfactory.

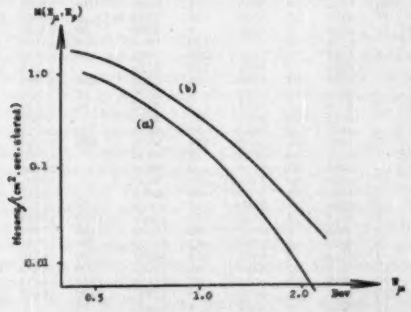

FIG. 1. The integral multiplicity $M(E_\mu, E_p)$, defined as the number of mesons with energies exceeding E_μ, produced per primary of energy E_p. Curve (a): 1.5 Bev $\leqslant E_p \leqslant$ 4 Bev. Curve (b): 4 Bev $\leqslant E_p \leqslant$ 14 Bev.

The apparent slow variation with primary energy of the total number of relativistic mesons produced per primary particle, together with the marked energy dependence of the differential multiplicity,[1] gives us some indication as to the spectral distribution of the mesons produced in a collision. Certainly the frequently used law of the form dE/E, predicting equal contributions from all primaries of sufficiently high energies at any meson energy, seems to be a rather poor approximation even at meson energies as low as 0.5 Bev. However, reliable quantitative conclusions cannot be reached until more complete experimental data are available.

* This work was supported in part by the AEC.

[1] K. Sitte, Phys. Rev. 81, 484 (1951).
[2] W. C. Barber, Phys. Rev. 75, 590 (1949).
[3] Biehl, Neher, and Roesch, Phys. Rev. 79, 914 (1950).
[4] Salant, Hornbostel, Fisk, and Smith, Phys. Rev. 79, 184 (1950).

Delays of Penetrating Particles in Atmospheric Showers

L. MEZZETTI, E. PANCINI, AND G. STOPPINI
Istituto di Fisica dell'Università, Centro di Studio per la Fisica Nucleare del C.N.R., Rome, Italy

November 20, 1950

WE report the preliminary results of an experiment which is in progress at the Laboratorio della Testa Grigia (3500 m, mean pressure 675 g/cm²) to study the relative delays among the particles of an atmospheric shower in reaching the recording device.

The experimental arrangement is sketched in Fig. 1. In the counter groups T_1, T_2, T_3, each of 8 counters of 2 cm diameter

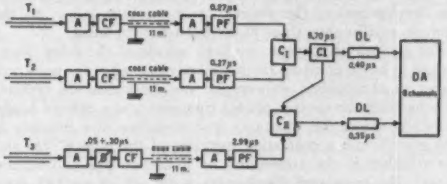

FIG. 1. Experimental arrangement. A = amplifier, CF = cathode follower, PF = pulse forming circuit, CI = clipping circuit, DL = delay line, D (arrow) = adjustable delay, DA = delay analyzer, C = coincidence circuit, T = counter tray.

and 50 cm effective length are placed at the vertices of an almost equilateral triangle with sides about 5.5 m. The counter pulses, after high amplification, are fed into the coincidence circuit C_I between trays T_1 and T_2, and into the coincidence circuit C_{II} (resolving time 8.70 μsec) between the output of C_I and the tray T_3. The output pulses from C_I and C_{II} are fed into the delay-analyzer, which discriminated all of the threefold coincidences (123) into 8 delay-channels according to the relative delay (positive and negative) between the outputs of C_I (12) and C_{II} (123). The apparatus[1] is so adjusted that a threefold coincidence is recorded in the first channel when the delay of the input pulse to the third coincidence branch, relative to the latter of the input pulses of branches 1 and 2, has a value in the interval -3.25 to $+0.05$ μsec, and in successive channels when the delay exceeds $+0.05$ μsec.

Measurements were taken with trays T_1 and T_2 always unshielded and tray T_3 alternately shielded and unshielded (the shielding used was 17.5 or 22.5 cm of lead). The results are plotted in Fig. 2. The time scale for the abscissae is a "mean" scale, which takes into account the fluctuations due to the counters, the spread of the resulting distribution being ± 0.17 μsec. The rates recorded by the 8th channel are well accounted for, within the limits of experimental errors, by chance coincidences; the contribution of the latter to the counting rates of the remaining channels is in every case negligible.

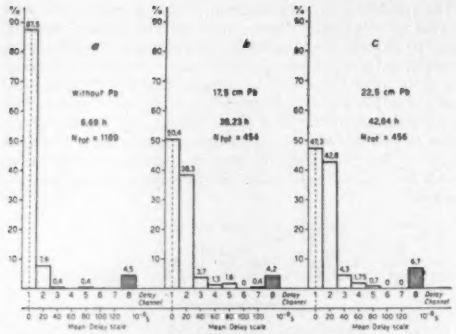

FIG. 2. Experimental results. The true scale for the abscissa is a "mean" scale, which takes into account the spreading due to the counter fluctuations.

One can calculate readily that under our experimental conditions the time origin is given, in more than 98 percent of the cases, by the arrival of an electron. Thus, the histograms (b) and (c) can be assumed to give the actual distributions of penetrating events relative to the electrons. They are in fairly good agreement with the results of McCusker and his co-workers,[2] who rule out the existence of delays greater than about 1.5 μsec. As it is reasonable to assume that the electron-photon component travels with the velocity of light throughout the whole development of the shower, the most plausible interpretation of the delays found is that they are due to the velocities of the penetrating particles produced in the development of the shower, these velocities being, on the average, smaller than those of the electron-component.

For a rough comparison, we have calculated the delay distribution to be expected on the hypothesis that all of the pairs produced in atmospheric showers are mesons which are created, together with the electron-photon component, at a definite height vertically above the apparatus (corresponding to a pressure of 100 g/cm²) with a generation spectrum of the type $E^{-3}dE$, and are absorbed in the atmosphere by ionization loss and natural decay. The calculated distribution is cut off at $\tau=0.45$ μsec, owing to the lead shield; this is obviously independent of the generation spectrum and practically independent of the height of formation chosen, at least for heights greater than that chosen. The cut-off time is thus an upper limit for the delays due to a penetrating particle, always in the form of a meson or particle of lighter mass, which can be traced back from the apparatus to the origin of the shower. The counting rates of the delay channels 4 to 7 (about 2 to 3 percent of the total number of penetrating events) must therefore be due to pairs which have traveled for a noticeable fraction of their paths from the origin of the shower, as particles with a mass much larger than that of the meson. The experimental results are in rough agreement with the calculated distribution for $\tau \lesssim 0.45$ μsec, but no great significance can be attached to this agreement as an indication of the accuracy of the hypothesis made.

[1] A detailed description of the electronics employed, as well as a discussion of the effect of the fluctuations in the times of discharge of the counters will appear shortly in *Nuovo Cimento*. For the method used in the calibration of the time axis see *Energia Elettrica*, November, 1950.
[2] McCusker, Ritson, and Nevin, Nature **166**, 400 (1950).

Microwave Spectra of Deutero-Ammonias

HAROLD LYONS, L. J. RUEGER, R. G. NUCKOLLS, AND M. KESSLER
National Bureau of Standards, Washington, D. C.
December 1, 1950

APPROXIMATELY 125 lines of ND_3, ND_2H, and NDH_2 have been found[1] in the region from 2000 to 17,000 Mc. This work is part of a program to provide precise reference standards for frequency and intensity to lower frequencies than previously available as an adjunct to compilation of microwave spectra tables.[2]

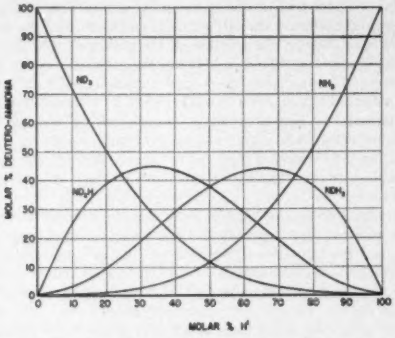

FIG. 1. Deutero-ammonia equilibrium ratios *vs* H^1 contamination.

All measurements were made using a 5-kc, zero-based, square-wave-modulated Stark spectrograph employing a synchronous detector.[3] A new design of mica and metal *S*-band absorption cell allowed high temperature outgassing.[4] Hyperfine spacings were found to be somewhat different from NH_3; hyperfine lines are not included in Table I.

The source of the deutero-ammonias for this work was a high pressure bomb of ND_3 containing up to 5 or 10 percent H^1. In the presence of other H^1 containing molecules, the partially deuterated ammonias are known to be formed rapidly[4] in the ratios indicated in Fig. 1. This effect was utilized to generate the partially deuterated ammonias and to provide a means of isotopic assignment of the lines on the basis of intensity growth. Excluding the NH_3 lines, measurements showed that there were three qualitatively distinct types of lines. Within one-half hour after insertion of a fresh sample of ND_3, type (0) lines decreased perhaps 10 percent or more of their initial strong values; type (1) lines increased by 10 to 100 percent above the initial strong intensity; and type (2) lines increased from essentially zero to an intensity many times the initial value. A reference to Fig. 1 indicates that, in a system where the hydrogen contamination drives the equilibrium from

TABLE I. Deutero-ammonia microwave spectrum.[a]

Freq. (Mc)	Rel. int.	Freq. (Mc)	Rel. int.	Freq. (Mc)	Rel. int.	Freq. (Mc)	Rel. int.	Freq. (Mc)	Rel. int.
2094[0]	43	4161	8	5236	3	7104	10	12620	40
2186[0]	75	4199	12	5364	99	7238[1,b]	3	12778	1290
2290[0]	15	4216	8	5368	5	7388[1]	90	13065	169
3261		4219	9	5392	120	7562[2]	350	13119	523
2403[0]	5	4241	7	5415	200	7803	185	13175	23
2408		4282	2	5495	210	8278		13210	1200
2431		4407	105	5508[1]	84	8283	470	13316	400
2480		4410	30	5549	2	8778	60	13488	234
2533[0]	5	4511	25	5574	3	8903	54	13626	580
2599		4721	36	5582[1]	320	8922		13657	106
2614	4	4850	72	5632[1]	55	9014	220	13923	586
2652	7	4859	141	5635[1]	114	9521	600	14067	620
2668		4907	90	5689	1	9636		14102	700
2699		4915	23	5726	2	9829		14566	530
2746		4938	14	5786[1,b]	110	9967		15004	18
2786		4948	96	5787[1,b]	120	10091		15132	384
2800	4	4956	37	5964[1,b]	126	10660	50	15524	35
2900	3	5025	27	6105[1,b]	132	10844	1750	15634	9
2939	3	5030	7	6164[1,b]	120	11400	100	15772	280
2978	3	5122	3	6390[1,b]	45	11975	250	15935	20
3010	3	5124	6	6463	153	11983	250	16320	134
3187	17	5192	42	6598	46	12147	500	16455	210
3470[1]	29	5199[1]	290	6641[1,b]	27	12150	1833	16493	153
3865[1]	290	5213	2	6922[1,b]	13	12392	700	16497	34
4086[1]	13	5230	5	6975	1	12444	75		

[a] Superscripts 0, 1, 2 denote, respectively, line types 0, 1, 2.
[b] Assignments subject to further tests.

the most deuterated condition toward a more nearly equal concentration of H^1 and H^2, the intensity changes of type (0), (1), and (2) lines are to be associated respectively with 0, 1, and 2, hydrogen replacements per molecule of ND_3. From a measure of the type and amount of intensity drift observed for a given type line, a quantitative estimate was made as to the instantaneous location on the ratio curves. From this position a prediction could be made as to the intensity change to be expected by driving the assumed equilibrium slightly toward NH_3 or ND_3 by addition of a small amount of the appropriate gas. In every instance both the initial change and the rate of the line intensity confirmed the indicated correlation between line type and deutero-hydrogen assignment. The complete assignment of all observed lines by these techniques awaits further work.

Table I lists the lines so far measured. Rough frequency measurements for this preliminary survey were made by means of cavity frequency meters with precision measurements to be made later directly against the NBS frequency standards. Relative intensities expressed, as recorder line-heights, are shown in Table I when intensity measurements were made and are uncorrected for the unknown isotopic abundance. Line intensities in restricted frequency regions were reproducible for a given type line. However, variations of equipment sensitivity with line-height and frequency correspondingly limit the ranges within which these values have significance.

Helpful discussions with C. H. Townes during the course of this work are gratefully acknowledged.

* Now at Brandeis University, Waltham, Massachusetts.
[1] Harold Lyons, Phys. Rev. 76, 161 (1949); J. Appl. Phys. 21, 59 (1950). Lyons, Kessler, Rueger, and Nuckolls, Phys. Rev. 81, 297 (1951).
[2] P. Kisliuk and C. H. Townes, J. Research Nat. Bur. Stand. 44, 611 (1950).
[3] Strandberg, Wentink, and Kyhl, Phys. Rev. 75, 270 (1949); McAfee, Hughes, and Wilson, Jr., Rev. Sci. Instr. 20, 821 (1949); A. H. Sharbaugh, Rev. Sci. Instr. 21, 120 (1950).
[4] A description of this cell is to be submitted soon to the Rev. Sci. Instr.
[5] See also an account of similar difficulties with the deutero-ammonias in the infrared by J. S. Burgess, Phys. Rev. 76, 1267 (1949).

The Enhanced Photoelectric Emission Effect in Barium Oxide*

B. D. McNary
Department of Physics, University of Missouri, Columbia, Missouri
November 29, 1950

THE activation effect of ultraviolet radiation on the photoelectric emission from BaO recently reported by Dickey and Taft[1] has been studied in this laboratory. Since the reported effect was found for thin films of the oxide, whereas our observations have been made on thermionically active oxide cathode coatings, and since the pronounced wavelength dependence of this effect was not described, it seems desirable to report at this time the results of our study.

Figure 1 (A) shows the spectral distribution of photoelectric emission from a normal sample of pure[2] BaO. This cathode was activated for thermionic emission by drawing current to a movable tantalum anode. A Richardson plot gave thermionic constants of $\varphi = 1.44$ ev and $A = 0.026$ amp/cm^2 °K^2. Maxima in the photoelectric response curve between $h\nu = 3.6$ and 4.0 ev have been found for all samples, although the exact shape in this region differs. These maxima for BaO were previously reported by Apker[3] and are not unlike the maxima found[4] for KI and attributed to exciton production. Curve B was obtained after allowing 3700A radiation ($h\nu = 3.37$ ev) to fall on the sample for 30 minutes. In the region of the photoelectric threshold, below 1.5 ev, the photoemission was doubled, whereas in the region of the exciting wavelength the increase was only about 30 percent.

Measurement of the photo-current in the ultraviolet region from unactivated samples could not be carried out without the radiation used in this measurement changing the state of photoelectric activation, particularly for photo-emission near the threshold. An attempt was made to determine the wavelength range over which photoelectric activation could be produced. All ultraviolet wavelengths down to and including 2537A produced the effect as did wavelengths in the visible. A sample in a low state of activity for enhanced photo-emission could be activated by 7000A radiation, whereas a partially activated sample, e.g., that of Fig. 1, could not be activated further by 4000A. Although the relative efficiencies for these activating wavelengths have not yet been investigated thoroughly, it is clear that the efficiency increases with higher energies but that irradia-

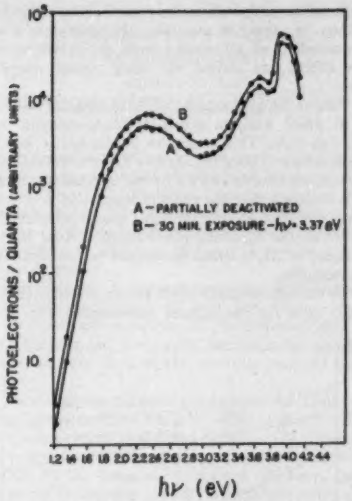

FIG. 1. (A) Spectral distribution of photo-emission from BaO sample. (B) Spectral distribution resulting following 30-minute irradiation at $h\nu = 3.37$ ev.

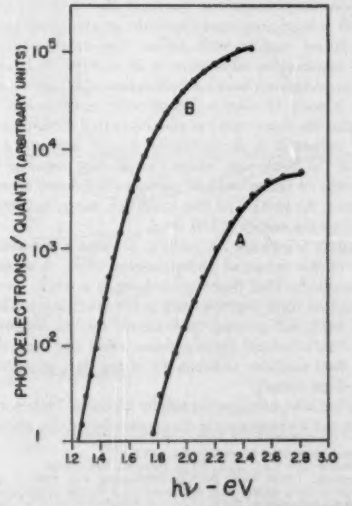

FIG. 2. Spectral distribution of photo-emission from BaO near the threshold, (A) initial unactivated state, (B) after 30 minutes irradiation at $h\nu = 3.37$ ev.

tion in the fundamental absorption band[5] is not required. In order to keep the sample in essentially the same state of activity for photo-emission, all subsequent work on activation and deactivation effects was carried out using photon energies less than 3.0 ev.

Figure 2 shows the enhancement of photo-emission starting from a state (A) which was less active for photo-emission than the sample in Fig. 1(A). Thirty minutes irradiation at $h\nu = 3.37$ ev changed the sample to state (B). At $h\nu = 1.8$ ev a 1000-fold increase was observed, whereas at $h\nu = 2.5$ ev the increase was by a factor of 30. It is apparent that the effect of irradiation is considerably greater near the photoelectric threshold than for higher energies. This feature of the enhanced photo-emission from BaO differs from the effect[4] in KI, in which the increase occurs simultaneously for all wavelengths.

At 300°K the enhancement effect decays slowly with time but at different rates for the various wavelengths, Fig. 3. Wavelengths near the photoelectric threshold for which the enhancement effect is most pronounced have the greater decay rate. This decay increases rapidly with higher temperatures; at 600°K complete deactivation takes place in 30 minutes. It is apparent that the decay does not have a simple exponential time dependence nor does it seem to obey a second-order reaction law. If one assumes that the decay rate has an initial exponential dependence on E/kT, where E is the activation energy, and uses $1/t$, as a measure of the decay rate, where t is the time required for the photo-current to fall to one-half value, an activation energy may be evaluated. At $h\nu = 1.8$ ev this activation energy is 0.92 ev and at $h\nu = 2.5$ ev the energy is 1.07 ev.

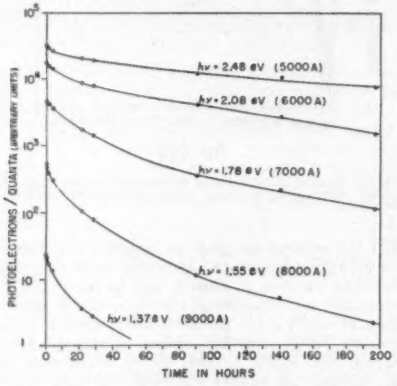
PHOTOELECTRONS / QUANTA (ARBITRARY UNITS)
TIME IN HOURS
hν = 2.48 eV (5000A)
hν = 2.08 eV (6000A)
hν = 1.78 eV (7000A)
hν = 1.55 eV (8000A)
hν = 1.378 V (9000A)

FIG. 3. Decay of enhanced photo-emission from BaO at 300°K at various wavelengths.

Although it is perhaps too early to attempt a complete interpretation of this enhanced photo-emission effect, it seems likely that incompletely filled donor levels lying in a region 1 ev below the conduction band together with a few low lying levels above the filled band will account qualitatively for the observed phenomena. This enhanced photo-emission effect has been observed on three BaO cathodes although all of the data presented here are for a single sample.

The author acknowledges the helpful advice of Professor Albert Eisenstein and his assistance in the preparation of this manuscript.

* This work supported in part by the ONR.
[1] J. E. Dickey and E. A. Taft, Phys. Rev. **80**, 308 (1950).
[2] Mallinckrodt Ultra Pure $BaCO_3$, containing less than 1 ppm Sr, sprayed onto a pure nickel base and converted to the oxide in vacuum. Coating thickness about 10^{-3} cm.
[3] L. Apker, Phys. Rev. **78**, 352 (1950).
[4] L. Apker and E. Taft, Phys. Rev. **79**, 964 (1950).
[5] W. W. Tyler, Phys. Rev. **76**, 1887 (1949).

Angular Distributions of Neutrons from (α, n) and (d, n) Reactions

BERNARD L. COHEN*
Carnegie Institute of Technology, Pittsburgh, Pennsylvania
July 13, 1950

BEFORE interpreting the data of Allen, *et al.*[1] on the angular distributions of the neutrons from (α, n) and (d, n) reactions, as measured with sulfur detectors, two very important corrections must be applied: (1) a correction for the variation of the solid angle in the center-of-mass system, and (2) a correction for the fraction of the neutrons detectable by a threshold detector at various angles.

The first of these is described by Taschek and Hemmendinger,[2] and their formulas can be used. The second arises as follows. A neutron produced in an (α, n) reaction on element A will have different energies in the laboratory and the center-of-mass systems. These are related by the formula (with the masses in atomic units)

$$E_c = \tfrac{1}{2}\left[(2E_L)^{\frac{1}{2}} - \left(\frac{M_c}{M_c+M_A}\right)(2E_a/M_a)^{\frac{1}{2}}\cos\theta_c\right]^2. \quad (1)$$

An ideal threshold detector detects all neutrons with E_L greater than its threshold, B. Assuming the neutrons to be emitted with an energy distribution

$$I(E) \propto e^{-E/T}, \quad (2)$$

the total number of neutrons detected is

$$N \approx \int_{E_{\min}}^{E_{\max}} E e^{-E/T} dE, \quad (3)$$

where

$$E_{\min} = \tfrac{1}{2}\left[(2B)^{\frac{1}{2}} - \frac{M_c}{M_c+M_A}\cdot(2E_a/M_a)^{\frac{1}{2}}\cos\theta_c\right]^2, \quad (4)$$

$E_{\max}$ = maximum energy in the center-of-mass system.

On integrating (3) and assuming that $E_{\max} \gg T$, we find that

$$N \approx (E_{\min}+T)\exp(-E_{\min}/T). \quad (5)$$

Use of (4) in (5) gives a large correction factor in many cases. As an example, Fig. 1 shows the correction to the intensities at 90° and 180° with respect to 0° using sulfur detectors ($B \sim 3$ Mev), plotted against the parameter T (effective nuclear temperature).[3,4]

Table I shows the result of applying these corrections to the (α, n) data of reference 1. Column 4 shows the value of T required

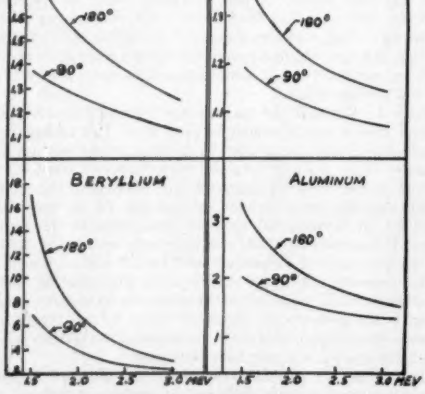

FIG. 1. Correction factors for detector activities at 90° and 180° with respect to 0° activity for (α, n) angular distributions. Abscissa is the effective nuclear temperature of the outgoing neutrons.

TABLE I. Relative neutron yields from (α, n) reactions at 0°, 90°, and 180°.

(1) Target element	(2) Yield at 180°/Yield at 0° Observed ratio[a]	(3) Corrected for CM solid angle[b]	(4) T required to remove asymmetry	(5) Yield 90°/Yield 0° (corrected)
Beryllium	0.13	0.60	>4.0 Mev[c]	~0.7
Manganese	0.55	0.70	1.5–2.0	0.77
Silver	0.76	0.87	1.4–2.3	0.80
Gold	0.93	0.99	1.0–∞	0.74
Bismuth	0.98	1.03	1.0–∞	0.81
Columbium	0.78	0.92	1.5–2.8	0.81
Aluminum	0.39	0.67	2.3–2.8	0.80
Copper	0.70	0.89	2.2–4.0	0.81
Cadmium	0.74	0.84	1.4–2.1	0.81
Cobalt	0.82	1.05	>3.5	0.73
				Av. $=0.79\pm0.04$

[a] See reference 1. [b] See reference 2.
[c] This is much larger than the observed value of 2.3 Mev (reference 5). It is probably caused by the fact that the 180° intensity is so small that the effect of scattered neutrons is important. Beryllium was neglected in obtaining the average in column (5).

to make the ratio of the intensities at 180° and 0° equal to 1.0 ± 0.1. The values are in good agreement with the measured values[5] and theoretical estimates of the effective nuclear temperature.[4] This, taken together with column 5 of Table I, gives strong support to Wolfenstein's theory[6] of the angular distributions from compound nucleus reactions, which predicts[6] symmetry about 90°, maxima at 0° and 180°, and minima at 90°.

The correction factors are so sensitive to the value of T that the assumption of equal intensities at 0° and 180° provides a quick method of determining T. This can be done much more accurately using higher energy threshold detectors (e.g., the 24.5-min activity in silver, $B\sim11$ Mev), since the center-of-mass solid angle correction is smaller and the dependence on temperature is stronger.

Table II shows the observed[1] 180°/0° intensity ratio for (d, n)

TABLE II. Relative neutron intensities at 180° and 0° from deuteron bombardment.

Element	Observed[a]	Corrected
Beryllium	0.06	0.56
Aluminum	0.12	0.26
Titanium	0.38	0.60
Chromium	0.28	0.40
Manganese	0.24	0.35
Cobalt	0.31	0.43
Copper	0.29	0.39
Columbium	0.34	0.40
Molybdenum	0.27	0.32
Cadmium	0.31	0.37
Tantalum	0.33	0.34
Gold	0.42	0.46
Lead	0.44	0.48
Bismuth	0.45	0.49
		0.42 ± 0.07

[a] See reference 1.

reactions and the corrected ratio using plausible and in some cases, measured values of T. It is evident that some process other than compound nucleus interaction is effective, and some sort of a deuteron stripping process is suggested.[7]

* Present address: Oak Ridge National Laboratory, Oak Ridge, Tennessee.

[1] Allen, Nechaj, Sun, and Jennings, Phys. Rev. 81, 536 (1951).
[2] R. Taschek and A. Hemmendinger, Phys. Rev. 74, 373 (1948).
[3] V. Weisskopf, *Lecture Series in Nuclear Physics* (U. S. Govt. Printing Office, Washington, D. C., 1947).
[4] The effective nuclear temperature in this case is the nuclear temperature (reference 3) at an excitation of $(E_{max}-E)$, where E is the energy (in the center-of-mass system) which will be most effective in exciting the threshold detectors (reference 5).
[5] B. Cohen, Carnegie Inst. of Tech. Technical Report No. 4 (May 20, 1950), unpublished.
[6] L. Wolfenstein, Phys. Rev. 78, 322 (1950).
[7] R. Serber, Phys. Rev. 72, 1017 (1947); S. Dancoff, Phys. Rev. 72, 1008 (1947).

Photo-Luminescence Efficiency of ZnS:Cu Phosphors as a Function of Temperature*†

RICHARD H. BUBE
Radio Corporation of America, RCA Laboratories Division, and Princeton University, Princeton, New Jersey
December 21, 1950

IN recent communications by the author, the luminescence and trapping of a series of cubic and hexagonal ZnS:[Zn]:Cu(0.0–0.3), [NaCl(2)] phosphors,[1] and the effects of infrared on these phosphors,[2] have been discussed. This letter presents additional data on the variation with operating temperature of the photo-luminescence efficiency of these phosphors during 3650A ultraviolet excitation.

The blue and green luminescence emission intensities have been recorded through Wratten 47 and 58A filters, respectively. Figure 1 shows the variation of photo-luminescence emission intensity through the green filter for the cubic and hexagonal phosphors, and Fig. 2 shows the variation obtained through the blue filter.

The curves of these figures show that the temperature for maximum green intensity starts to shift to lower temperatures with increasing copper proportion between 0.01 and 0.03 weight percent copper for the cubic phosphors, and between 0.03 and 0.1 percent Cu for the hexagonal phosphors. Similarly, the blue intensity starts to decrease rapidly and continuously to zero for copper proportions between 0.01 and 0.03 percent for the cubic phosphors, and between 0.03 and 0.1 percent for the hexagonal phosphors.

These results are further evidence of the critical change previously reported in the nature of the copper imperfection when the amount of copper activator has reached a certain amount. Between 0.01 and 0.03 percent copper for the cubic phosphors,

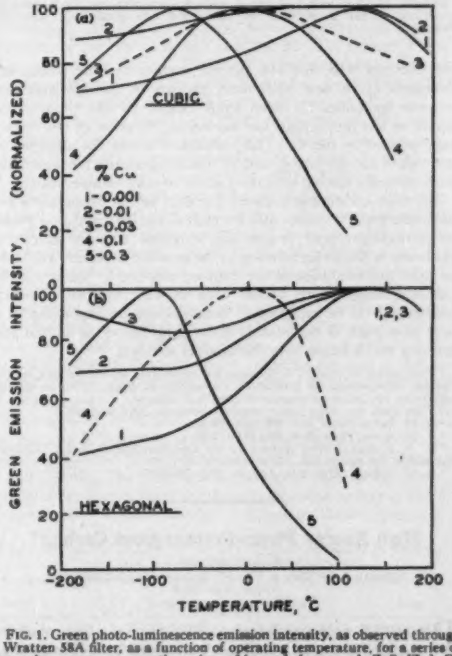

FIG. 1. Green photo-luminescence emission intensity, as observed through a Wratten 58A filter, as a function of operating temperature, for a series of increasing copper proportions in cubic and hexagonal ZnS:[Zn]:Cu phosphors.

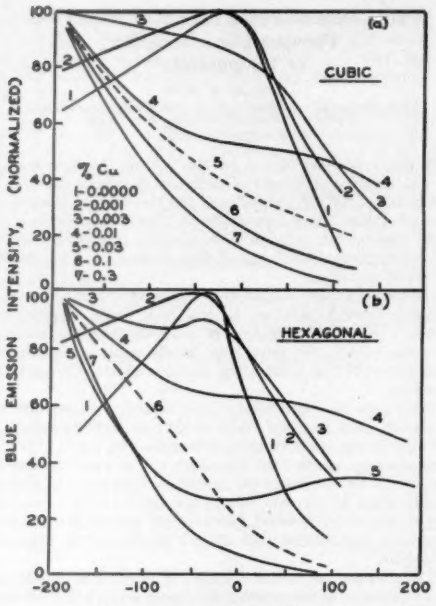

FIG. 2. Blue photo-luminescence emission intensity, as observed through a Wratten 47 filter, as a function of operating temperature, for a series of increasing copper proportions in cubic and hexagonal ZnS:[Zn]:Cu phosphors.

and between 0.03 and 0.1 percent copper for the hexagonal phosphors (1) a new blue band appears in the luminescence emission spectrum, (2) deep traps caused by the presence of copper in low proportions are destroyed, (3) some of the deeper traps present in the ZnS:[Zn] phosphor before the addition of any copper are destroyed, and (4) the temperature for maximum green intensity during excitation shifts to lower temperatures.

The close correlation between the shift of the temperature for maximum green intensity and the shift of the principal glow peaks for increasing copper proportions indicates that the efficiency maximum is due to an increase in the number of centers available for repetitive excitation as the traps are emptied by increasing the operating temperature. It has been shown[3,4] that an efficiency maximum is to be expected at temperatures corresponding to a large glow peak, if the number of excitable centers is limited and not very much larger than the number of traps.

* This letter is part of a dissertation presented to the faculty of the Physics Department of Princeton University in May, 1950, as partial fulfillment for the requirements of the Ph.D. degree.
† This work was done under contract between ONR and RCA.
[1] R. H. Bube, Phys. Rev. **80**, 655 (1950).
[2] R. H. Bube, Phys. Rev. **80**, 764 (1950).
[3] F. A. Kroeger, *Some Aspects of the Luminescence of Solids* (Elsevier Publishing Company, Inc., New York, 1948).
[4] R. H. Bube, J. Opt. Soc. Am. **39**, 681 (1949).

High Energy Photo-Protons from Carbon*

DARCY WALKER
Newman Laboratory of Nuclear Studies, Cornell University, Ithaca, New York

December 15, 1950

PROTONS with energies up to 124 Mev have been observed coming from a carbon target bombarded by γ-rays from an electron synchrotron operated at 195 Mev.

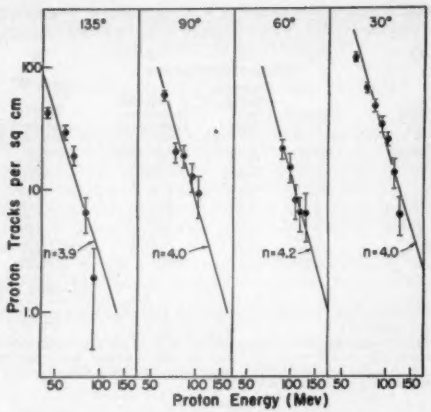

FIG. 1. Log-log plots of the density of proton tracks (N) in the emulsions of successive photographic plates against the proton energy (E) required for a proton to pass through each emulsion layer. Results are given for protons emitted at angles in the laboratory system of 135°, 90°, 60°, and 30° to the γ-ray beam. The track density is normalized to a target-emulsion distance of 22.8 cm. The errors shown are probable errors.

The γ-ray beam was passed through a 1.3-cm diameter hole in a lead block and allowed to impinge on a carbon plate 0.26 g/cm² thick placed at 45° to the beam. Disposed about the carbon target were four stacks of Ilford C-2 Nuclear Research plates interleaved with aluminum absorbers. These stacks recorded protons emitted from the target at angles of 135°, 90°, 60°, and 30° to the γ-ray beam, the over-all angular resolution being ±6°. The planes of the photographic plates were inclined at 30° to a line joining plate and target centers.

Figure 1 shows the form of the experimental results. The plots represent integral energy spectra. The lines give mean values of n, the spectra being represented by the form $N=N_0E^{-n}$. The value of n is about 4. This is a minimum value because the track counts corresponding to the lower energies tend to be too small, since (a) C-2 emulsions will not record protons with residual energies less than about 50 Mev and (b) blackening of the emulsion by

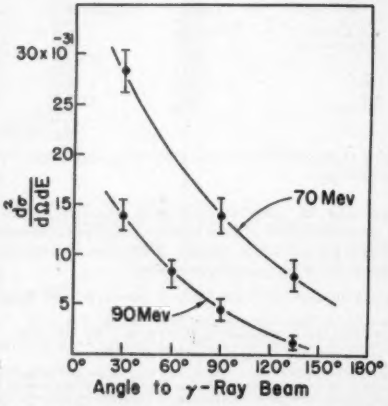

FIG. 2. Differential nuclear cross section of carbon for the production of protons plotted as a function of the angle of proton emission in the laboratory system. The differential nuclear cross section is expressed as square cm per steradian per Mev of proton energy (E) per unit Q. Results are shown for $E=70$ Mev and $E=90$ Mev.

electrons from the target becomes progressively more marked the nearer a plate to the target. The loss of counts due to (a) can be allowed for approximately; and if this is done, the value of n is increased from 4 to about 5. This value $n=5$ means that the number of protons per Mev of proton energy decreases as E^{-6}.

To derive absolute cross sections, a method due to Wilson[1] has been used. For the range of γ-ray energies in which we are interested, the average number of electrons produced by the cascade shower mechanism at a depth of 1 cm in lead is approximately $W/50$ for a γ-ray quantum of energy W Mev incident on the surface of the lead. The γ-ray beam, after passing through the target, impinged on a sheet of lead 1 cm thick, behind which was a flat aluminum ionization chamber 2.5 cm thick. If the number of quanta in the incident γ-ray spectrum between W and $W+dW$ is assumed to be QdW/W up to the maximum energy W_0, then the number of electrons traversing the ionization chamber is

$$\int_0^{W_0}(W/50)(Q/W)dW=QW_0/50.$$

These electrons traverse the ionization chamber at close to minimum ionization. Thus, the charge collected in the ionization chamber yields a value of Q, which is considered to be accurate to within a factor of 2.

Figure 2 shows the differential nuclear cross section plotted against the angle of emission of the protons for proton energies of 70 Mev and 90 Mev. These cross sections have been derived from the data of Fig. 1, allowance being made for protons not recorded owing to the limited sensitivity of C-2 emulsions. The probable errors shown relate to the relative values of the cross section at the various angles. The absolute values of the cross sections could be in error by as much as a factor of 3 when all sources of error are considered.

The strong forward bias in the angular distribution is inconsistent with a compound nucleus model. It agrees qualitatively with a two-nucleon model.[2] The strong decrease in cross section with increasing proton energy in the vicinity of 100 Mev, which is approximately half the maximum γ-ray energy, also lends support to a two-nucleon model.

The author would like to express his appreciation to Professor R. R. Wilson for the privilege of working in his laboratory and to the Commonwealth Fund for support.

* This work made use of facilities provided under a contract with the ONR.

[1] R. R. Wilson, private communication.

[2] J. Levinger, private communication.

The Nuclear Spin of Be^9

H. S. Gutowsky, R. E. McClure, and C. J. Hoffman
Noyes Chemical Laboratory, University of Illinois, Urbana, Illinois*
December 18, 1950

THE theoretically predicted and generally accepted value of 3/2 for the nuclear spin of Be^9 has had little experimental confirmation.[1] We have eliminated 1/2 as a possible value by observing the detailed line shape of the F^{19} magnetic resonance in vitreous BeF_2. Similar observations for K_2BeF_4 make a value of 5/2 unlikely. The nonappearance of hyperfine structure is further evidence[2] against this value. Thus, it appears that a value of 3/2 can now be assigned from experimental data.

The broadening of the F^{19} magnetic resonance in powdered beryllium compounds is predicted quantitatively by the second-moment equation[2]

$$\Delta H_f^2=(9/20)g_0^2\beta^2\Sigma_k r_{0k}^{-6}+(4/15)g_f^2\beta^2I_f(I_f+1)\Sigma_f r_{0f}^{-6}.$$

The subscripts 0, k, and f refer to a given fluorine nucleus, its fluorine, and its beryllium neighbors, respectively. In principle, I_f is obtained by the comparison of experimental second moments with the second moments computed from crystal structures and gyromagnetic ratios.

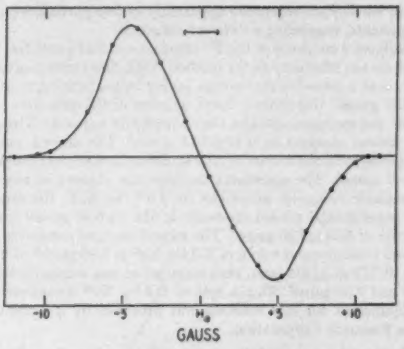

FIG. 1. The observed first derivative of the F^{19} magnetic resonance absorption line in vitreous BeF_2. The modulation is indicated by the horizontal arrow. The ordinate is in arbitrary units of intensity. H_0 is 6365 gauss.

The equipment and procedure used are similar to published accounts.[3,4] Vitreous BeF_2 was prepared by the thermal decomposition[5] of $(NH_4)_2BeF_4$. A typical derivative of the F^{19} magnetic resonance absorption line observed for this sample is given in Fig. 1. Four separate line plots gave second moments from 11.25 to 11.75 gauss[2], averaging 11.55 gauss[2], with a probable error of ± 0.15 gauss[2]. No complete structural analysis appears to be available for BeF_2. The x-ray scattering curve for vitreous BeF_2 is compatible[6] with a random network structure and an assumed Be—F distance of 1.60A. However, Brandenberger[6] has made a determination of the unit cell size and symmetry of crystalline BeF_2 and suggests a Be—F distance of 1.53A. Lacking more detailed information, the spatial arrangement of Warren and Hill[6] was assumed; and theoretical second moments were computed as a function of the Be^9 spin and also the Be—F distance. These values are given in Table I. The Be—F distance of 1.46A required for agreement with a spin of 1/2 is impossibly small. The 1.53A distance[6] gives a spin of 3/2, while the 1.60A value[6] gives 5/2.

Observations were made on K_2BeF_4 to resolve the 3/2 *versus* 5/2 question. Three second moments were measured, ranging from 6.25 to 6.90 gauss[2], with an average of 6.65 gauss[2]. In a partial analysis of the crystal structure[7] of $(NH_4)_2BeF_4$, tetrahedral $BeF_4^=$ groups were found, and a Be—F distance of 1.61A was suggested. When a Be^9 spin of 3/2 is used, the computed second moment for the $BeF_4^=$ group alone is 3.78 gauss[2]. The broadening by nuclei outside the $BeF_4^=$ contributes an additional approximate[2] 2 gauss[2]. Agreement between computed and experimental second moments can be achieved either by using a Be^9 spin of 5/2 or by decreasing the Be—F distance to about 1.57A. However, because of charge effects, the Be—F distance in the $BeF_4^=$ group should be slightly larger than in BeF_2. This criterion and the second-moment data can be satisfied most simply by assigning the spin of Be^9 as 3/2, and the Be—F distances as 1.57 and 1.52A in $BeF_4^=$ and BeF_2, respectively.

The desirability of further x-ray analysis of some of the beryllium fluorides is indicated by the above discussion. In addition, Rb_2BeF_4 is reported[8] to have the same crystal structure as K_2BeF_4 and $(NH_4)_2BeF_4$. The F^{19} magnetic resonance lines in the latter compounds are simple, being quite similar in shape to that in BeF_2 indicated by the derivative in Fig. 1. However, the F^{19} resonance

TABLE I. The second moment of the F^{19} magnetic resonance in vitreous BeF_2 as a function of Be^9 spin and Be-F distance.

r of Be-F		1.60A	1.515A	1.46A
I of Be^9	1/2	6.75 gauss[2]	9.40 gauss[2]	11.55 gauss[2]
	3/2	8.30	11.55	14.20
	5/2	10.85	15.15	18.55

line in Rb_3BeF_4 is composed apparently of five partially resolved components, suggesting a different structure.

Analyses were made of the F^{19} resonance in CaF_2 and NaF as a check on the reliability of the method. Eight lines were plotted for CaF_2 over a period of six months, giving values ranging from 6.00 to 6.85 gauss[2]; this range is large, as some of the data were taken before the electronic circuits were completely adjusted. The average second moment is 6.42 ± 0.13 gauss[2]. The second moment computed from the known crystal structure and nuclear properties is 6.47 gauss[2]. The agreement confirms the absence of any very appreciable magnetic properties for Ca^{40}. In NaF, the range of five experimental second moments is 6.05 to 6.40 gauss[2] with an average of 6.21 ± 0.05 gauss[2]. The second moment computed from crystal structure and a spin of 3/2 for Na^{23} is 6.16 gauss[2]. If a Na^{23} spin of 1/2 or 5/2 is used, the computed second moments become 4.23 and 9.36 gauss[2]. Thus a spin of 3/2 for Na^{23} is confirmed.

Equipment for this research was provided by a grant-in-aid from Research Corporation.

* Supported in part by ONR.

[1] J. E. Mack, Revs. Modern Phys. 22, 64 (1950).
[2] W. Paul, Z. Physik 117, 774 (1941).
[3] Gutowsky, Kistiakowsky, Pake, and Purcell, J. Chem. Phys. 17, 972 (1949).
[4] G. E. Pake, J. Chem. Phys. 16, 327 (1948).
[5] B. E. Warren and C. F. Hill, Z. Krist. 89, 481 (1934).
[6] E. Brandenberger, Schweiz. mineralog. petrog. Mitt. 12, 243 (1932).
[7] R. Hultgren, Z. Krist. 88, 233 (1938).
[8] P. L. Mukherjee, Indian J. Phys. 18, 148 (1944). The approximation of the external broadening used the unit cell dimensions for K_3BeF_4 cited in this reference and the lattice positions (reference 7) in $(NH_4)_3BeF_4$. This procedure appears reasonable, as the crystals are isomorphous (reference 7) and unit cell dimensions are quite similar.

On the Hard Sphere Model of the Nucleon*

ROBERT JASTROW
Radiation Laboratory, Department of Physics, University of California, Berkeley, California

December 28, 1950

IT has been suggested that the evidence from p–p scattering experiments[1] at 340 Mev for large momentum transfers in nucleon-nucleon collisions can be explained by the assumption of a strong short-range repulsion between nucleons.[2] Since the completion of calculations based on this assumption, additional experimental results have been reported at 340 Mev and at lower energies.

The experiments at intermediate energies are of special interest because the assumption of a hard sphere repulsion in the nucleon-nucleon interaction results in the appearance of a pronounced minimum in the singlet cross section at energies in the neighborhood of 170 Mev, as a result of interference between the repulsion

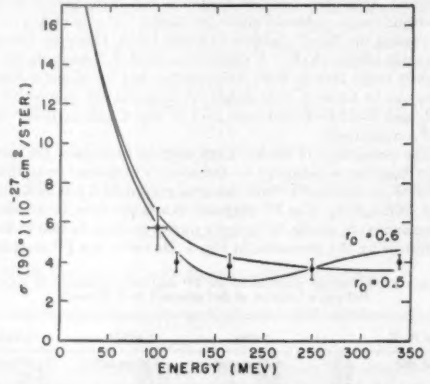

FIG. 1. p–p cross sections at 90°. The experimental values at 100 Mev are taken from reference 3, the remainder from reference 4.

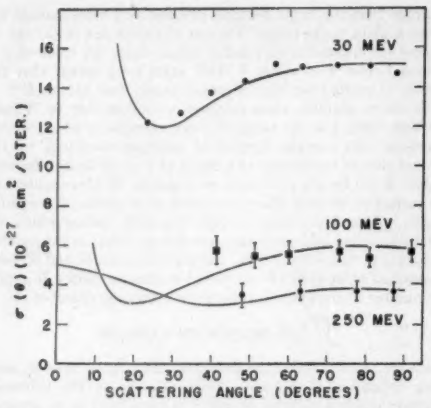

FIG. 2. p–p cross sections at 30 Mev, 100 Mev, and 250 Mev compared with calculations assuming a radius of repulsion 0.60×10^{-13} cm.

and the surrounding attractive well. This minimum is partially masked by a maximum in the tensor contribution to the complete cross section at corresponding energies; but, nevertheless, its effect becomes appreciable for sufficiently large radii of repulsion.

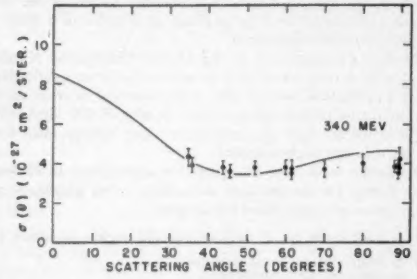

FIG. 3. p–p cross sections at 340 Mev compared with the same model.

In Fig. 1, values of the p–p cross section at 90° for energies between[3] 100 Mev and[4] 340 Mev are compared with calculations in which the repulsion is represented by a hard sphere, using radii of 0.50 and 0.60×10^{-13} cm. From Fig. 1, one can conclude that a radius greater than 0.60×10^{-13} cm would lead to a minimum in the p–p cross section incompatible with present experimental values.

The angular dependence of the p–p cross section at intermediate energies has also been measured recently and is compared in Fig. 2 at[3] 100 Mev and[4] 250 Mev with curves calculated on the assumption of a hard sphere repulsion of radius 0.60×10^{-13} cm. Previously published values at 30 Mev are also shown.[5]

Revised values at 340 Mev are shown in Fig. 3 on a plot of the p–p cross section calculated from the same model.

The indicated experimental uncertainties include both statistical and estimated systematic errors, with the exception of the 100-Mev values in Fig. 2, where only the estimated 10 percent uncertainty in the *relative* values at various angles is shown. The absolute value of the 100-Mev cross-section values is subject to an uncertainty of 20 percent.

* This work was supported by the AEC.

[1] O. Chamberlain and C. Wiegand, Phys. Rev. 79, 81 (1950).
[2] R. Jastrow, Phys. Rev. 79, 389 (1950); detailed account in Phys. Rev. 81, 165 (1951).
[3] Chamberlain, Segrè, and Wiegand, Phys. Rev. 81, 284 (1951).
[4] R. Birge, Phys. Rev. 80, 490 (1950).
[5] W. K. H. Panofsky and F. L. Fillmore, Phys. Rev. 79, 57 (1950).

Growth of Germanium Single Crystals Containing p-n Junctions

G. K. Teal, M. Sparks, and E. Buehler
Bell Telephone Laboratories, Murray Hill, New Jersey
December 21, 1950

THE growth in the number of ideas of possible conduction mechanisms of practical value that might be realized in germanium has emphasized the importance of developing specific methods of producing germanium single crystals in which the relevant properties of the material are controlled. Germanium single crystals of a variety of shapes, sizes, and electrical properties have been produced by means of a pulling technique distinguished from that of Czochralski and others in improvements necessary to produce controlled semiconducting properties.[1] Solidifying germanium is very sensitive to a variety of environmental factors such as physical strain (which give rise to twinning), thermal treatment, and minute impurities. Pulling the germanium single crystal progressively from the melt at such a rate as to have the interface between the solid and liquid substantially at the liquid surface is very well suited to this material, since it avoids the constraints inherent in solidifying the expanding germanium within inflexible walls and provides an approximately planar thermal gradient in the neighborhood of the interface, thereby minimizing thermally induced strains. Single crystal rods showing a high degree of crystalline perfection, as long as 8 inches, and as great as 1¼ inches in diameter have been grown. Measurements in these Laboratories have shown the bulk lifetimes of injected carriers in some of these materials to be greater than 600 μsec.

One type of such "long lifetime" crystals that is of special interest, which has been produced by the above means, is a single crystal in which the magnitude and type of conductivity in the direction of crystal growth is controlled by addition of a significant impurity such as gallium (acceptor) or antimony (donor) to the melt from which the crystal is being grown. Thus, p-n junctions have been formed in germanium single crystals which are exceptional in their agreement with theory[2] and in their electrical properties as discussed in an accompanying letter.[3]

We wish to acknowledge our indebtedness to many of our associates at Bell Telephone Laboratories for assistance and advice and especially to J. B. Little, who collaborated in the initial single-crystal program.

[1] G. K. Teal and J. B. Little, Phys. Rev. **78**, 647 (1950).
[2] W. Shockley, Bell System Tech. J. **28**, 435 (1949).
[3] Goucher, Pearson, Sparks, Teal, and Shockley, Phys. Rev. **81**, 637 (1951).

Theory and Experiment for a Germanium p-n Junction

F. S. Goucher, G. L. Pearson, M. Sparks, G. K. Teal, and W. Shockley
Bell Telephone Laboratories, Murray Hill, New Jersey
December 21, 1950

RECTIFYING p-n junctions in germanium have been produced in which the approach to the idealized conditions is so close that most of the expected theoretical features can be quantitatively verified experimentally, thus putting these junctions in a unique position in the field of solid rectifiers. The junctions discussed in this letter were produced in high back voltage n-type germanium by the addition of gallium so that one portion of the single crystal[1] was p-type. The unit reported here was 0.65×0.6 cm in cross section.

According to theory[2] the rectification curve for such a junction should be of Wagner[2] form $I=I_s[\exp(eV/kT)-1]$. Figure 1 shows a comparison between theory and experiment, the theoretical value 39 volt^{-1} being used for e/kT. The voltage values were measured between zero current probes near to the junction on each side and employed to eliminate ohmic series resistance.

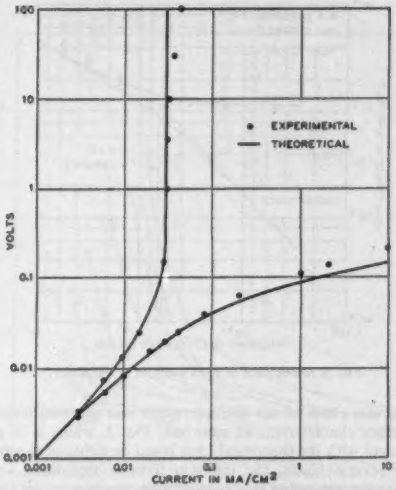

FIG. 1. Rectification characteristics of a p-n junction.

The conductance of the junction at low voltages, eI_s/kT, is due to hole flow in the n-region in parallel with electron flow in the p-region. It can be calculated in terms of the intrinsic conductivity σ_i taken as 0.0165 ohm^{-1} cm^{-1}, the conductivities of the two regions σ_p and σ_n, the lifetimes of injected carriers τ_p for holes and τ_n for electrons, and the diffusion constants D_p and D_n, and their ratio $b=D_p/D_n$. The lifetimes were measured by scanning with a slit of light of wavelength 1.85 microns, which penetrated deeply into the specimen. The abnormal carriers so produced should diffuse[4] a distance x to the junction with decay factors of $\exp(-x/L)$, where $L=(D\tau)^{\frac{1}{2}}$ is the diffusion length, a prediction which is in agreement with Fig. 2. Except for the decay due to

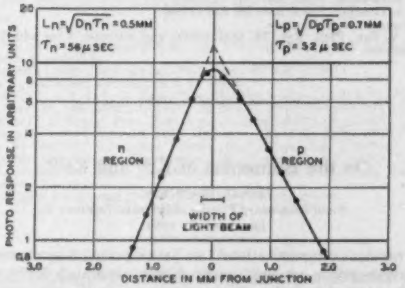

FIG. 2. Photo-response vs distance from junction.

finite τ, it was determined that each photon absorbed resulted in a transfer of one electron across the junction, in agreement with the previous finding of unit quantum efficiency.[5] This treatment of light as a voltage-independent current generator is in agreement with the findings of Pietenpol[6] and differs in emphasizing diffusion and photo-current rather than photo-voltage which is usually discussed.[7]

From the lifetimes of Fig. 2 and values of $\sigma_p=2.5$ and $\sigma_n=0.188$ determined by probe measurements, a value of 0.007 for eI_s/kT was found, compared with a dc low voltage value of 0.011 ohm^{-1} cm^{-2}.

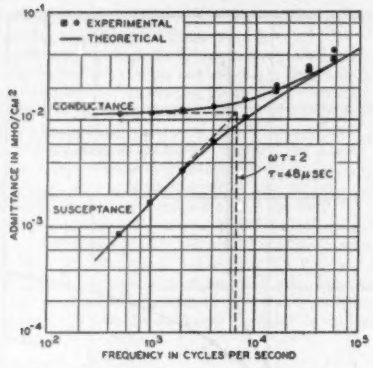

FIG. 3. Admittance of $p-n$ junction vs frequency.

A further check of the lifetime results was obtained from the impedance characteristic at zero bias, Fig. 3, which is in good agreement with the theoretical form based on diffusion theory.[2]

For reverse biases, the diffusion term is suppressed and a capacity corresponding to a concentration gradient in the transition region was found. From Eq. (2.46) of reference 2 a value of 10^{18} cm^{-4} was obtained.

The dependence of admittance on bias for intermediate biases has also been found to be in agreement with theory as has the effect of temperature. The dependence of the photo-response on wavelength has been used for the study of surface recombination, which is more important at the short wavelengths which do not penetrate deeply.

We are indebted to W. L. Bond and H. R. Moore for aid with the experimental techniques, and to J. A. Morton for encouragement in connection with the germanium single-crystal program.

[1] G. K. Teal and J. B. Little, Phys. Rev. **78**, 647 (1950).
[2] W. Shockley, Bell System Tech. J. **28**, 435–489 (1949). W. Shockley, *Electrons and Holes in Semiconductors* (D. Van Nostrand Company, New York, 1950).
[3] C. Wagner, Physik. Z. **32**, 641 (1931).
[4] F. S. Goucher, Phys. Rev. **81**, 475 (1951).
[5] F. S. Goucher, Phys. Rev. **78**, 816 (1950).
[6] Personal communication.
[7] H. Y. Fan, Phys. Rev. **75**, 1631 (1949) and reference 3 for additional publications.

On the Isomerism of Kr^{83} and Xe^{133}

INGMAR BERGSTRÖM
Nobel Institute of Physics, Stockholm, Sweden
December 28, 1950

IN previous communications[1,2] we have reported β-spectrometer investigations on electromagnetically separated Kr^{83m} and Xe^{133m} obtained in fission. By improvements in the experimental technique used we have obtained some new results which will be reported here.

Kr^{83m}.—Previously we had found[1] that only one γ-ray of energy 32.7 kev is associated with the isomeric transition in Kr^{83}. By the use of a thinner G-M window in the β-spectrometer (cutoff ~5.0 kev) four additional electron lines of energies 7.3, 9.0, 10.5, and 12.1 kev were found (Fig. 1). All six electron lines have the same half-life ~114 min. The first two lines are interpreted as the L and M lines of a γ-ray of energy 9.3 kev. The 10.5- and 12.2-kev lines have energies in agreement with the Auger lines K–$2L$ and K–L–M of Kr.

The $K2$ and $L2+M2$ lines of energies 17.7 and 30.5 kev are hardly absorbed in the G-M window. After making the window

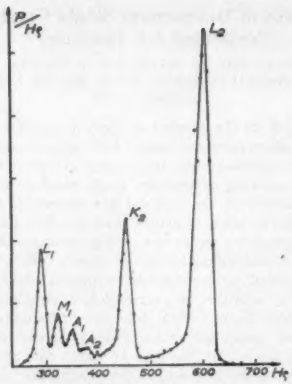

FIG. 1. β-spectrum of electromagnetically separated Kr^{83m} obtained in fission. Resolving power of the β-spectrometer ~5 percent.

absorption correction, we obtain the following intensity relations:

$$N_{L1}/N_{M1} \sim 3, \quad (1)$$

$$N_{K2}/(N_{L2}+N_{M2}) = 0.35, \quad (2)$$

$$(N_{L1}+N_{M1})/(N_{K2}+N_{L2}+N_{M2}) \sim 0.8. \quad (3)$$

From Eqs. (1) and (2) it must be concluded that the 32.2-kev (new energy value) γ-ray is responsible for the isomeric transition. Siegbahn and Thulin[3] have found a γ-ray of energy 27 kev in a separated Kr^{83} sample for which $N_K/(N_L+N_M) \sim 8$. This γ-ray, however, is not associated with an isomeric transition.

Because of the low energy both γ-rays should be almost completely converted. The intensity relation[3] is then in accordance with the assumption that the two soft γ-rays in Kr^{83m} are emitted in cascade.

The half-life 114±2 min (measured with the $L2+M2$ lines in the β-spectrometer) and the energy are consistent with the multipole order 4. The spin of the ground state of Kr^{83} is 9/2. It seems hard to explain the experiments without associating the lowest excited level in Kr^{83} with the spin 7/2 and the isomeric state with the spin $\frac{1}{2}$. Both the multipole order $l=4$ and the spin 7/2 are, however, in contradiction to the spin-orbit coupling nuclear theory. Because of the soft γ-energy 9.3 kev, the first excited state in Kr^{83} is most probably delayed. Delayed coincidence measurements

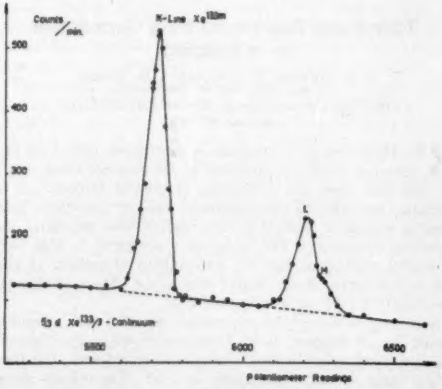

FIG. 2. Conversion lines of Xe^{133m} produced by neutron irradiation. Resolving power of the β-spectrometer ~1 percent.

must be performed before it is possible to assign spins and parities unambiguously to the levels in Kr^{83}.

Xe^{129m}.—We have given previously[3] a tentative decay scheme of Xe^{129m} based on the fact that the half-life of the β-spectrum was of the same order as that of the conversion lines of a γ-ray of energy 232 kev associated with the isomeric transition. Recently, however, Ketelle, *et al.*,[4] have shown that the half-life of the conversion lines of the 232-kev γ-ray is about 2 days, which partly contradicts our decay scheme.

When Xe was irradiated in the Harwell pile, the intensity of Xe^{135m} was so strong even after electromagnetic separation that it was possible to investigate the sample with a resolving power of 1 percent in the double-focusing β-spectrometer.[5] In this way it was possible to obtain a rather accurate value of the half-life of Xe^{135m}, which was not possible in our previous investigation. The ratio of the intensities of Xe^{135m} and Xe^{133} was also larger in this irradiation than was the case in the fission sample. The half-life of Xe^{135m} was found to be 2.30±0.08 days. Figure 2 shows the conversion lines of Xe^{135m}. The γ-energy of the isomeric transition is 232.8±0.4 kev. Because of larger intensity and higher resolving power we can now give a more accurate value of N_K/N_L, which was found to be 2.90±0.20.

On basis of the results of Ketelle, *et al.*, and of those obtained by us, it can be concluded that the β-spectrum of I^{133} is complex. I^{133} decays partly to the ground state of Xe^{133}, which decays with a half-life of 5.3 days to an 81-kev excited level in Cs^{133}. A smaller fraction of I^{133} decays to the 2.3-day isomeric state in Xe^{133}. With slow neutrons both the ground state and the isomeric state of Xe^{133} are produced.

The Xe sample was flown from England and was electromagnetically separated 14 hours after the pile irradiations were stopped. We wish to express our thanks to the Isotope Division at Harwell for their excellent service, which made the measurements on Xe^{135m} possible.

[1] Bergström, Thulin, and Andersson, Phys. Rev. **77**, 851 (1950).
[2] I. Bergström and S. Thulin, Phys. Rev. **79**, 538 (1950).
[3] K. Siegbahn and S. Thulin, Ark. Fysik. **2**, No. 22, 212 (1950).
[4] Ketelle, Brosi, and Zeldes, Phys. Rev. **80**, 485 (1950).
[5] Hedgran, Siegbahn and Svartholm, Proc. Roy. Soc. (London) **63**, 960 (1950).

Window Correction Curves and the Shape of Beta-Spectra*

D. Saxon
University of Wisconsin, Madison, Wisconsin
December 11, 1950

In a recent letter on the beta-spectrum of Th^{233}, Bunker, Langer, and Moffat[1] conclude that their observed deficiency of low energy electrons cannot be due to source or counter window effects. The possibility of low energy defocusing in the spectrometer is suggested instead. However, it is the present writer's strong opinion that most, if not all, of the observed deficiency is due to the counter window alone. The argument follows.

The counter window used was 3.6 mg/cm² mica. This weight corresponds in total range to an energy[2] of only about 40 kev, yet as a half-thickness this same weight would correspond to about 200 kev. Further, for a window effect of only 10 percent the corresponding energy could be as high as 500 kev. All these conditions are compatible with the observed results.

To show the argument more quantitatively, we can assume that the entire deficiency below a linear Fermi plot is due to the counter window. From the observed Fermi plot, the window correction for the momentum distribution can then be estimated. This is shown by the broken curve in Fig. 1. The twelve solid curves have been taken both from the literature and from the author's unpublished work.[3] In general, the curves were determined by adding additional absorbers to some initial thickness of counter window; however, a few of the points for the thinner windows have been determined from observed deficiencies of low

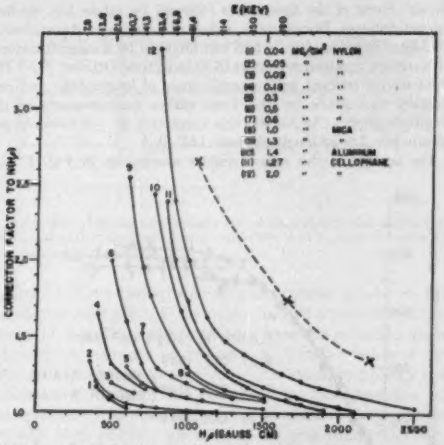

FIG. 1. The correction factors to $N(H\rho)$, the momentum plot, for various counter windows as indicated in the twelve solid curves. These results do not apply to corrections for effective source thicknesses, the scattering-in effects of the source having no analog in the counter window geometry.

energy electrons such as concern the present discussion. In view of the possibility of widely differing geometries for the various curves, they form a fairly consistent family.

Returning to the point in question, the broken line for the 3.6-mg/cm² mica window falls about where it should, relative to the thinner windows and the known range-energy relationships. There seems to be a lack of upward curvature at the low energy end. This can be interpreted as meaning that the assumption of a linear Fermi spectrum at low energies is incorrect; that, in fact, the spectrum of Th^{233} as measured, has an excess of low energy electrons instead of a deficiency. This conclusion is expected from the source thicknesses used, 16 and 0.6 mg/cm².

For more recent work on thin window corrections one can consult the work of Sturcken, Heller, and Weber,[4] and Cook and Chang.[5]

* This work was supported by the AEC and the Wisconsin Alumni Research Foundation.
[1] Bunker, Langer, and Moffat, Phys. Rev. **80**, 468 (1950).
[2] L. E. Glendenin, Nucleonics **2**, 12 (1948).
[3] Curves 1, 3, 4, 6, 7: D. Saxon (unpublished work). Curve 2: D. Saxon, Phys. Rev. **74**, 849 (1948). Curve 5: D. Saxon, Phys. Rev. **73**, 811 (1948). Curve 8: G. J. Neary, Proc. Roy. Soc. (London) **A175**, 71 (1940). T. H. Martin and A. A. Townsend, Proc. Roy. Soc. (London) **A170**, 190 (1939). Curve 9: Feather, Kyles, and Pringle, Proc. Phys. Soc. (London) **A61**, 466 (1948). Curve 10: A. Flammersfeld, Z. Physik **112**, 727 (1939). Curve 11: E. Haggstrom, Phys. Rev. **62**, 144 (1942). Curve 12: V. A. Nedzel (unpublished work).
[4] Sturcken, Heller, and Weber, Phys. Rev. **78**, 327 (1950).
[5] C. S. Cook and C. Chang, Phys. Rev. **79**, 244 (1950).

The Change of Cosmic-Ray Neutron Intensity Following Solar Disturbances†*

J. A. Simpson, Jr.
Institute for Nuclear Studies, University of Chicago, Chicago, Illinois
December 18, 1950

Measurements of the changes of fast neutron intensity at 30,000 feet pressure altitude (312 g-cm^{-2} air) as a function of latitude have been obtained following the occurrence of solar disturbances. Though the results are preliminary, they may be significant. The neutron detectors were BF_3 proportional counters surrounded by paraffin and were transported by B-29 aircraft over the range of magnetic latitudes 40°N to 65°N. Flares were reported of importance 1, 2, and 3 during the period 25 to 31 October.[1] None of the flares occurred when the aircraft was in

the air. Some of the flares were followed by minor but distinct magnetic storms. For example, a flare of importance 2 occurred at 0002 local time October 26 and was followed by a magnetic storm with sudden commencement at 0430 local time October 27.[1,2] The flight course covered only a small range of longitudes, and corrections were made for this from earlier measurements of the longitude effect. (At $\lambda=40°$ this correction is -8.3 counts per minute per degree longitude near 112° W.)

The results of the measurements are shown in Fig. 1 with

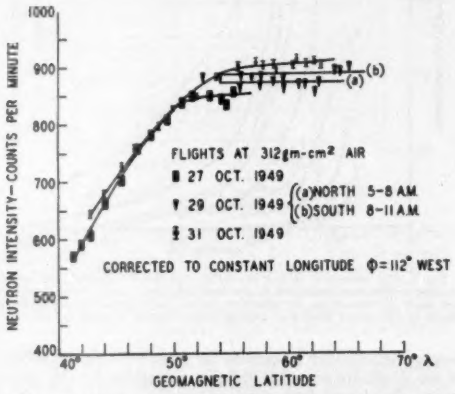

FIG. 1. The change of fast neutron intensity with geomagnetic latitude during solar activity and a magnetic storm. The maximum intensity on a quiet day is 660 events per minute. Counting rates for both quiet and disturbed day values were normalized at the geomagnetic equator.

standard deviations indicated for each point. These fast neutron intensity curves have five characteristics which are of interest in relation to the solar activity:

(1) The measured intensities above $\lambda=53°$ are all approximately 30 percent above the intensity of 660 events per minute observed on undisturbed days.[2] Also, the intensity increases with time during the period of the flights. Thus, the observations represent a continuing increase above normal quiet day intensity and not the recovery of the cosmic-ray intensity to normal which commonly occurs during a magnetic storm.

(2) If the "knee" of the latitude curve is arbitrarily defined as the intersection of the tangents to the approximately straight line portions of the latitude curve, it is seen that a northward shift of the knee takes place between October 27 and 31. This shift is 3° and lies outside the experimental errors. On undisturbed days this knee[3] is located at ~50°.

(3) Below $\lambda=51°$ there is no change or, at most, only a negligible change of intensity during the time interval 27 to 31 October. Due to the nature of the longitude corrections, the difference of intensity shown in the region of 42° may not be real.

(4) Above $\lambda=51°$ the intensity curves still appear to have positive slopes.

(5) Any assumed diurnal effect at 30,000 feet during the four day period was negligible, since in Fig. 1, (a) represents measurements in the local time interval 0500 to 0730 and (b) represents measurements from 0900 to 1130 local time.

The use of the neutron component as a sensitive indicator of changes in primary particle intensity and a comparison of neutron and charged particle intensity measurements will be published later.

The measurements in Fig. 1 show that beginning on October 27, additional primary particles with momenta lower than permitted by the apparent quiet day cut-off value at $\lambda\approx 50°$ arrive at the top of the atmosphere and that by October 31, particles, if singly charged, arrive with momenta as low as ~1 Bev/c corresponding to a cut off at $\lambda=56°$.

Either: (*I*) These low energy primaries are normally part of the cosmic radiation spectrum and a geo- or heliomagnetic field decreased during the period following solar activity to admit these particles, or (*II*) the low energy particles are added to the normal cosmic-ray flux during the disturbed period and are produced in the solar system.

The present measurements do not distinguish between these extreme alternatives. However, the absence of a pronounced shift in neutron intensity observed for $\lambda<50°$ N with time and the recent evidence against a strong helio dipole field make it difficult to support alternative (I). On the other hand, the approximate 30 percent increase of intensity above normal and the shift of the knee of the latitude curve northward are evidence for alternative (II).

The absence of a significant diurnal effect at 30,000 feet and the observed latitude dependence for the low energy primary particles arriving between $\lambda=51°$ and $\lambda=56°$ indicate that these low energy particles may be approximately isotropically distributed in space and are mostly charged particles.

The writer wishes to thank E. Hungerford for recording the data and to thank Major W. Gustafson, the officers, and crew of the Air Forces B-29 for their cooperation and skill in flying the aircraft.

† Reported at meeting Am. Phys. Soc. June, 1950, Phys. Rev. **80**, 135 (1950).

* Assisted by the joint program of the ONR and AEC.

[1] Data kindly compiled and supplied by A. H. Shapley of the Central Radio Propagation Laboratory, National Bureau of Standards.

[2] J. Geophys. Research **55**, 94 (1950).

[3] J. A. Simpson, Jr., Proc. of the Echo Lake Conference on Cosmic Rays, 1949.

The High Energy Beta-Spectrum of Sc^{46}

FRED T. PORTER AND C. SHARP COOK
Physics Department, Washington University, St. Louis, Missouri*
December 26, 1950

IN a recent study[1] of the disintegration of Ti^{45} a small amount of Sc^{46} was found as an impurity. A cloud-chamber histogram of the beta-particle radiations from this impurity clearly showed the lower energy group but failed to identify the higher energy group previously reported by Peacock and Wilkinson.[2] This has led to the further investigation of the disintegration of Sc^{46} herein described.

For this study three beta-ray spectrometer sources were prepared from an Oak Ridge sample of Sc^{46}. One was prepared as received with no further chemical separation. The second was separated chemically in accordance with the procedures outlined by Noyes and Bray[3] with special precautions being made to remove the scandium from any possible phosphorus or strontium

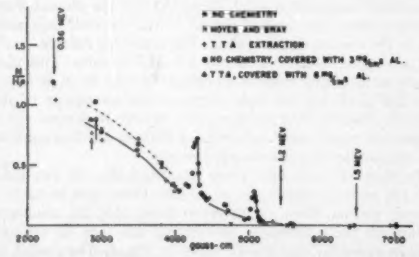

FIG. 1. Momentum spectrum of electrons, from sources of Sc^{46}, whose energies lie in the region higher than the high intensity, low energy beta-ray group. The solid line represents the best fit for the bare sources. Dashed line represents best fit when sources are covered with an aluminum foil whose surface density (in mg/cm²) is approximately equal to that of the source. The significance of this experiment is discussed in the text. The two peaks are the internal conversion lines for the 0.89- and the 1.12-Mev gamma-rays.

impurities. The third source was prepared by means of a thenoyl trifluoracetone (TTA) extraction[4] of scandium. Sources were deposited upon a cellophane foil 0.001 inch thick.

The results of the spectrometer studies are given by the momentum spectrum in Fig. 1. Since only the high energy spectrum is of interest, the low energy group of Sc^{46} is not shown. However, normalization of the three sources was made by comparing counting rates across the peak of this low energy, high intensity group. Statistical errors are no larger than the size of the marker which indicates the position of the experimental point. The arrows indicate experimental data taken 72 days and 112 days after initiation of the study with appropriate normalization by means of the peak counting rate of the lower energy beta-spectrum. This indicates that the higher energy group decays with the same half-life as does the lower energy group, this being 84 days, in good agreement with the accepted value for Sc^{46}. Since there is little difference in the shapes of the spectra obtained from all three sources and since the half-life is the same as that associated with Sc^{46}, it would appear that the recorded electrons are not produced by an impurity.

The results are not in agreement with those previously reported by Peacock and Wilkinson.[3] The maximum energy appears here to be about 1.2±0.1 Mev. Nothing above background counting could be observed at energies higher than 1.2 Mev. A Fermi-Kurie plot of the data shows a convexity toward the energy axis. This was expected since a thick source (3–6 mg/cm²) was necessary in order to obtain an appreciable counting rate over background for the higher energy group. Since it is conceivable that the radiation observed could be caused by Compton electrons ejected as secondary electrons from the source by the 0.89- and 1.12-Mev gamma-rays, it was decided to cover the source with an aluminum foil having a thickness approximately equal to that of the source. If the higher energy electrons were purely secondary Compton electrons one would expect an increase in counting rate over the higher energy group of approximately fifty percent. Although the spectrum in Fig. 1 does show a definite increase in counting rate when the source is covered, it amounts only to about 15 percent. It would therefore appear that, although part of the electron radiation is caused by secondary electrons ejected from the source by the Compton process, at least a part really belong to a high energy beta-group. This real group of higher energy beta-particles appears not to exceed 0.5 percent of the total number of such particles from Sc^{46}.

The authors wish to thank Mr. J. Hudis who performed the necessary chemical separations.

* Assisted by the joint program of the ONR and AEC.

[1] Ter-Pogossian, Cook, Porter, Morganstern, and Hudis, Phys. Rev. 80, 360 (1950).
[2] C. L. Peacock and R. G. Wilkinson, Phys. Rev. 74, 297 (1948).
[3] Noyes and Bray, *A System of Qualitative Analysis for the Rare Elements* (The Macmillan Company, New York, 1927), pp. 207–208, 221.
[4] A. Broido, AECD-2616 (1949); W. W. Meinke, AECD-2738 (1949), p. 28, unpublished.

Q-Values for (α, p) Reactions on Aluminum and Boron by Means of Photographic Emulsions

HILDING SLÄTIS, ELIS HJALMAR, AND RUNE CARLSSON
Nobel Institute of Physics, Stockholm, Sweden
December 18, 1950

IN the earlier experiments with natural α-particle sources the results of different authors were often inconsistent, partly because of the spread of the energy of the particles and partly because of the poor geometry. So far, photographic emulsions have been used in connection with (α, p) reactions mainly for recording the number of protons and measuring the energy of these protons. We have used the emulsions also for determining the directions of the different protons and from that the directions of the corresponding α-particles, thus improving the geometry.

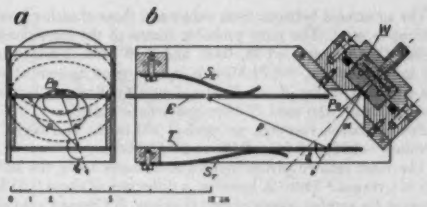

FIG. 1. Experimental arrangement for investigating proton tracks from different targets T, bombarded with α-particles from a polonium source Po. E is the photographic plate.

Figure 1 shows two sections of the apparatus employed. E is the photographic plate, T the target, and Po a polonium sample (about 12 mc). No direct α-particles from the polonium source can reach the emulsion on the plate E. A mica window of 0.67 mg/cm² thickness was placed before the source to prevent contamination of the walls and surfaces in the chamber when this was evacuated. The most frequent energy value of the α-particles was 4.80 Mev, and the half-width of the distribution 0.40 Mev. The positions of p and α in Fig. 1 were computed from the direction of the track in the emulsion. The proton energy was determined from the length of the track and the Q-values computed from the well-known formula. Figure 2 shows the Q-values found for the Al(α, p)Si-reaction. The figure gives the result for 100 tracks. Each Q-value is represented by a vertical line. If each Q-value is represented by a triangle of the shape marked to the right on the figure (the half-width of the triangle is the same as for the energy distribution of the α-particles), and the triangles integrated, we get the curves in the figure. The Q-values found belong to the groups −1.24, 0.14, and 2.30 Mev.

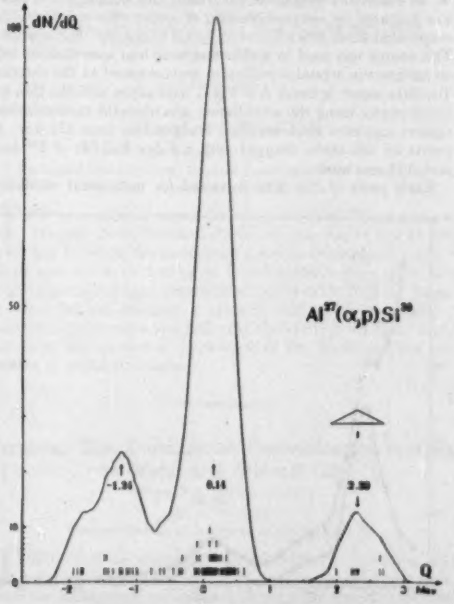

FIG. 2. The most probable Q-values for the Al(α, p)Si reaction, computed from the Q-values obtained from 100 proton tracks.

The agreement between these values and those of earlier investigations is good. The most probable means of the corresponding earlier Q-values are -1.28, 0.00, and 2.30 Mev. Furthermore, the lowest Q-value, -1.24 Mev, is in very good agreement with the highest Q-value of -1.27 Mev found by Brolley, Sampson, and Mitchell,[1] who used 22-Mev cyclotron α-particles.

For the boron reaction, we studied 200 tracks and found the Q-values -1.75, -0.55, -0.00, and 0.63 Mev.

The most reliable earlier investigation seems to be the second one of Creagan.[2] There is, however, a difference of about 0.63 Mev between his and our corresponding Q-values. If Creagan's Q-values are diminished by 0.21 Mev, we get the values shown in Fig. 3.

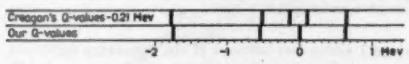

FIG. 3. Comparison between our Q-values for the B(α, p)C reaction and the corresponding Creagan values, reduced by 0.21 Mev.

Our 0.00-Mev group seems to be the unresolved mean of two of Creagan's groups. Apart from this, the agreement between the groups is good.

A further description of our investigations and a possible explanation of the discrepancy noted above will appear in *Arkiv för Fysik*.

[1] Brolley, Sampson, and Mitchell, Phys. Rev. 76, 624 (1949).
[2] R. J. Creagan, Phys. Rev. 76, 1769 (1949).

Low Intensity Radiations in I^{131} Decay*

H. ZELDES, A. R. BROSI, AND B. H. KETELLE
Chemistry Division, Oak Ridge National Laboratory, Oak Ridge, Tennessee
December 18, 1950

IN a search for previously unobserved transitions in I^{131} decay an essentially weightless, electrically conducting, 10-mc source was prepared by electrodeposition of iodine onto a 0.02-mg/cm² evaporated silver film supported by a 0.02-mg/cm² Formvar film. This source was used in a thin magnetic lens spectrometer with an anthracene crystal scintillation spectrometer[1] as the detector. The data shown in curve A of Fig. 1 were taken with the thin lens spectrometer using the scintillation spectrometer to discriminate against scattered electrons with energies less than 350 kev. All points on this curve decayed with a 8-day half-life of I^{131} for a period of two weeks.

Kurie plots of the data corrected for instrument resolution[2] are shown in Fig. 2. The K-conversion line of the 364-kev gamma-ray was used as an internal standard for energy calibration. In addition to the main beta-group with a maximum energy of 606±4 kev this analysis indicates a low intensity beta-group with a maximum energy of 810±5 kev. This beta-group has been postulated[3,4] as a transition from the ground state in I^{131} to the 12-day metastable level in Xe^{131}. Since only a small region of the 810-kev beta-energy distribution could be measured, the relative intensity and the shape are uncertain. Assuming either an allowed or a first-forbidden shape, the 810-kev beta-transition occurs in somewhat less than 1 percent of the I^{131} disintegrations. This is in reasonable agreement with the fraction[5] of I^{131} atoms decaying to the 12-day metastable level of Xe^{131}, indicating that most of the transitions to this level are through the 810-kev beta-group.

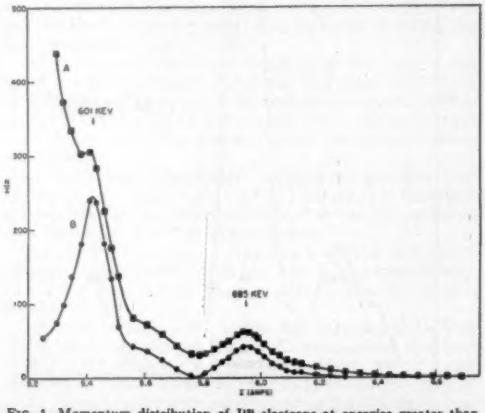

FIG. 1. Momentum distribution of I^{131} electrons at energies greater than 364-kev. (A) Original data. (B) After subtraction of beta-distributions.

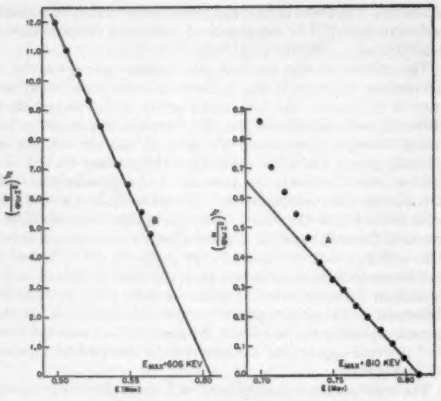

FIG. 2. Kurie plots of two I^{131} beta-groups.

Curve B in Fig. 1 shows the electron momentum distribution after subtraction of the two beta-groups. This curve shows the presence of conversion lines of 635±6-kev and 720±4-kev gamma-rays. The intensity of the 720-kev gamma-K conversion peak was found to be ½ that of the 635-kev gamma-K conversion peak. The intensity of the 635-kev gamma-K conversion peak was 4×10^{-4} times the intensity of the 606-kev beta-group. A very rough measurement of the relative intensities of the unconverted gamma-rays with a Tl activated NaI scintillation spectrometer indicated that the K-conversion coefficients of the 635-kev and 720-kev gamma-rays were equal within a factor of two.

The 720-kev gamma-ray is probably a transition to the ground state from the 717-kev level[6] in Xe^{131}. The presence of this gamma-ray lends support to the value[7] of 250 kev for the end point of the low energy beta-group of I^{131}.

* This document is based on work performed for the Atomic Energy Commission at Oak Ridge National Laboratory.
[1] W. H. Jordan and P. R. Bell, Nucleonics 5, 30 (1949).
[2] G. E. Owen and H. Primakoff, Phys. Rev. 74, 1406 (1948).
[3] Way, Fano, Scott, and Thew, Nat. Bur. Standards (U. S.) Circ. No. 499 (1950).
[4] I. Bergström, Phys. Rev. 80, 114 (1950).
[5] Brosi, DeWitt, and Zeldes 75, 1615 (1949).
[6] A. C. G. Mitchell, Revs. Modern Phys. 22, 36 (1950).
[7] Kern, Mitchell, and Zaffarano, Phys. Rev. 76, 94 (1949).

The High Energy Gamma Radiation† from Ta^{181}

J. M. CORK, W. J. CHILDS, C. E. BRANYAN, W. C. RUTLEDGE, AND A. E. STODDARD
University of Michigan, Ann Arbor, Michigan
December 14, 1950

SINCE our earlier report[1] on the low energy gamma-emission of Ta^{181}, several investigations have been made of its high energy gamma-spectrum. These measurements have been made

with spectrometers using G-M tubes, and the results are not in close agreement. To check the reported values, both conversion and photoelectrons for each gamma-ray have been observed in magnetic photographic spectrometers. The K electron lines are clearly resolved, being separated by several millimeters with the resolving power used. The relative intensities of the three K lines appear to be approximately 10, 5, and 7, for the 1.121, 1.189, and 1.219 Mev gamma-rays, respectively. The various results are summarized in Table I, with the initials of the authors at the top of the vertical column that contains their respective data. It is believed that the uncertainty in the presently reported values is not greater than 2 kev for each of the three gamma-energies.

TABLE I. Gamma-rays from Ta^{182}.

R. W.[a]	B. P. W.[b]	G. C.[c]	Present
1.13 Mev	1.133 Mev	1.12 Mev	1.121 Mev
...	1.219	1.19	1.189
1.22	1.237	1.23	1.219

[a] W. Rall and R. Wilkinson, Phys. Rev. 71, 321 (1947).
[b] Beach, Peacock, and Wilkinson, Phys. Rev. 75, 211 (1949).
[c] C. Goddard and C. Cook, Phys. Rev. 76, 1419 (1949).

† This project was supported jointly by the AEC and ONR.
[1] J. Cork, Phys. Rev. 72, 581 (1947). Cork, Keller, Rutledge, and Stoddard, Phys. Rev. 78, 95 (1950).

Calculations on the Number of Neutrons in the Atmosphere

S. LATTIMORE
Department of Physics, Imperial College, London, England
December 26, 1950

THERE have been many experiments over the last few years designed to measure the rate of production of neutrons by cosmic rays. In all cases, the number of thermal neutrons was measured. The experiments are of two types: (a) measurements made in the free atmosphere, and (b) measurements made inside a large bulk of solid material.

Now it is interesting to note that the experiments of the first type appear to give results which are very much lower than those of the second type. We would like to point out that this probably arises from errors in the calculations. Bethe[1] has shown that the number, n, of counts in a BF_3 counter of volume, V, and pressure, p, is related to the rate of production, q (per gram), by the formula

$$q=(n/V)(\sigma_A/\sigma_D)(780/p), \qquad (1)$$

where σ_A is the capture cross section per molecule of the surrounding material and σ_D is the capture cross section per molecule of the BF_3 detector.

Since air (nitrogen) is diatomic, σ_A is double the more usually defined atomic cross section. Several investigators[2,3] have omitted to use the molecular cross section, and their results should therefore be multiplied by two. It should be noted that formula (1) applies only when the neutrons are produced and slowed down in air; i.e., only to experiments of type (a).

Furthermore, there would appear to be some doubt as to the value of the ratio, σ_A/σ_D. Korff and Hamermesh use a value of 0.0027. (σ_D refers to natural BF_3, not to enriched $B^{10}F_3$ in this case.) For 100 percent $B^{10}F_3$, Davis uses a value of 0.00048, which is equivalent to the value 0.0024 for normal BF_3. However, Adair[4] gives $\sigma_D=116E^{-\frac{1}{2}}$ per molecule, and Melkonian[5] gives $\sigma_A=0.34E^{-\frac{1}{2}}$ per atom. This gives a true ratio of $(0.0029\times 2)=0.0058$, which should be used in formula (1). Therefore the results of Korff and Hamermesh should be multiplied by 2.15 and those of Davis by 2.4.

These corrected results are plotted in Fig. 1, together with the results of Montgomery and Tobey[6] and of Lattimore[7] who used method (b). As can be seen, the corrected values give considerably better agreement than do the old-ones. Yuan[8] has also given results on the number of thermal neutrons in the atmosphere, but he merely states that the counters used were calibrated. Whether the results depend on formula (1) is therefore not clear, although this formula is quoted on the figure given in his letter. However, since his results agree with those of Korff and Hamermesh before correction, it does seem possible that they should be increased also by a factor of 2.15, and these corrected results are shown in Fig. 1.

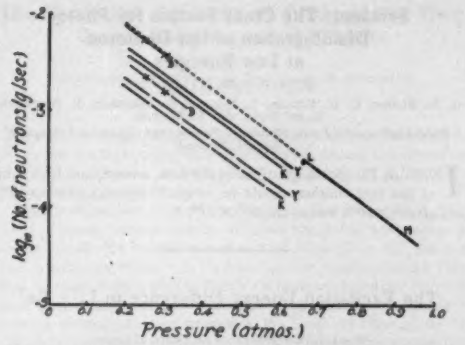

FIG. 1. The dashed and the full lines represent the uncorrected and the corrected results, respectively. The dotted line is an extrapolation of that found by Montgomery and Tobey. (K) Korff and Hamermesh (1946). (Y) Yuan (1946). (D) Davis (1950). (M) Montgomery and Tobey (1949). (L) Lattimore (1950).

In conclusion, it would appear that the various neutron experiments are in much better agreement, and give much more reasonable results, than has been thought hitherto.

[1] Bethe, Korff, and Placzek, Phys. Rev. 57, 573 (1940).
[2] S. A. Korff and B. Hamermesh, Phys. Rev. 69, 155 (1946).
[3] W. D. Davis, Phys. Rev. 80, 150 (1950).
[4] R. K. Adair, Revs. Modern Phys. 22, 249 (1950).
[5] E. Melkonian, Phys. Rev. 76, 1750 (1940).
[6] C. G. Montgomery and A. R. Tobey, Phys. Rev. 76, 1478 (1949).
[7] S. Lattimore, Phil. Mag. (in press).
[8] L. C. L. Yuan, Phys. Rev. 74, 804 (1948).

The Half-Life of I^{131}

JULES H. SEEB
Nucleonics Division, Naval Research Laboratory, Washington, D. C.
December 26, 1950

THE consensus of values for the half-life of I^{131}, as given in Nuclear Data, National Bureau of Standards Circular 499, is 8.0 and 8.1 days. We have made a precise determination of I^{131} decay and arrive at a value of 8.1409 ± 0.0062 days. This falls within the range of some unpublished results of Dr. F. N. D. Kurie, in which he has obtained a value of 8.16 ± 0.04 days using a Lauritsen electroscope and following the activity for about eight half-lives. We appreciate the interest of Dr. Kurie and the permission to quote his results.

Erratum: The Diamagnetic Correction for Protons in Water and Mineral Oil

[Phys. Rev. 80, 901 (1950)]

H. A. THOMAS
National Bureau of Standards, Washington, D. C.

THROUGH an oversight, the diamagnetic correction was applied to the value of e/m as well as to the value of γ. Since the diamagnetic correction does not affect the value of e/m, the previously reported[1] value of e/m should remain unchanged.

[1] Thomas, Driscoll, and Hipple, Phys. Rev. 78, 787 (1950).

Erratum: The Cross Section for Photo-Disintegration of the Deuteron at Low Energies

[Phys. Rev. 80, 211 (1950)]

G. R. Bishop, C. H. Collie, H. Halban, A. Hedgran, K. Siegbahn, S. du Toit, and R. Wilson
Nobel Institutet för Fysik, Stockholm, Sweden; and Clarendon Laboratory, Oxford, England

IN Table IX the designations in the first, second, and fifth rows of the first column should be, respectively, $\sigma_{2.75\mathrm{I}}(\mathrm{cm}^2)\times 10^{28}$, $\sigma_{2.61\mathrm{II}}(\mathrm{cm}^2)\times 10^{28}$, and $\sigma_{2.50\mathrm{I}}(\mathrm{cm}^2)\times 10^{28}$.

The Excitation Energy Difference in Li^7-Be^7

E. Feenberg
Washington University, St. Louis, Missouri*
December 15, 1950

IT has been observed that the Be^7-Li^7 Coulomb energy difference falls below the smooth empirical curve determined by the other $4n+3$ mirror systems.[1] The discrepancy is just about 10 percent. A related discrepancy occurs in the location of the low excited states. In Li^7 the excitation energy is 0.478 Mev; in Be^7 the recently discovered excited state occurs at 0.429 Mev, again smaller by about 10 percent.[2-5] These large differences can be correlated in a consistent manner with the small binding energy of Be^7 relative to He^4 and He^3 components. Denoting energies relative to the three and four particle components by script symbols and using subscripts g and e to distinguish ground and excited states and the subscript c for Coulomb energies, one may write

$$\mathcal{E}_g(\mathrm{Be}^7)=M(\mathrm{Be}^7)-M(\mathrm{He}^4)-M(\mathrm{He}^3)=-1.62\ \mathrm{Mev},$$
$$\mathcal{E}_g(\mathrm{Li}^7)=M(\mathrm{Li}^7)-M(\mathrm{He}^4)-M(\mathrm{H}^3)=-2.51\ \mathrm{Mev}; \tag{1}$$

$$\mathcal{E}_c(\mathrm{Be}^7)=E_c(\mathrm{Be}^7)-E_c(\mathrm{He}^4)-E_c(\mathrm{He}^3)\sim 2.08\ \mathrm{Mev},$$
$$\mathcal{E}_c(\mathrm{Li}^7)=E_c(\mathrm{Li}^7)-E_c(\mathrm{He}^4)\sim 1.04\ \mathrm{Mev}. \tag{2}$$

The estimated Coulomb energies appearing in Eq. (2) are not the actual values in the seven particle systems, but are rather the values which would obtain if these systems were not expanded by the Coulomb repulsion of the three and four particle systems.

The formula

$$\mathcal{E}_g(\lambda)=\lambda^2K-U(\lambda)+\lambda\mathcal{E}_c$$
$$=\mathcal{E}_{g0}(\lambda)+\lambda\mathcal{E}_c \tag{3}$$

expresses the energy as a function of a scale parameter λ, the kinetic and Coulomb terms depending on λ in the manner shown because the corresponding operators are homogeneous functions of degree -2 and -1, respectively, in the space coordinates. Nothing is required of the potential energy $U(\lambda)$ beyond the possibility of an expansion in powers of $\lambda-1$. In the absence of the Coulomb repulsion between the three and four particle components, minimum energy, associated with $\lambda=1$, requires $2K=U'(1)$. Including the Coulomb repulsion, minimum energy occurs at

$$\lambda_g=1-\mathcal{E}_c/\mathcal{E}_{g0}''(1) \tag{4}$$

and has the value

$$\mathcal{E}_g(\lambda_g)=\mathcal{E}_{g0}(1)+\mathcal{E}_c-\mathcal{E}_c^2/2\mathcal{E}_{g0}''(1). \tag{5}$$

Low excited states may be characterized by a reduction in the magnitude of the potential energy:

$$\mathcal{E}_e(\lambda)=\lambda^2K-(1-\delta)U(\lambda)+\lambda\mathcal{E}_e. \tag{6}$$

Then minimum energy occurs at

$$\lambda_e=1-(\mathcal{E}_e+2K\delta)/[\mathcal{E}_{g0}''(1)+U''(1)] \tag{7}$$

and has the value

$$\mathcal{E}_e(\lambda_e)=\mathcal{E}_{g0}(1)+U(1)\delta+\mathcal{E}_e$$
$$-(\mathcal{E}_e+2K\delta)^2/2[\mathcal{E}_{g0}''(1)+U''(1)\delta]. \tag{8}$$

Introducing numbers, it is found that the 10 percent discrepancy in Coulomb energy requires $\mathcal{E}_{g0}''(1)\sim 11$ Mev. The radius of Be^7 is approximately 10 percent greater than that of Li^7. The parameter δ is determined as a function of K/U by the condition $\mathcal{E}_e(\mathrm{Li}^7)-\mathcal{E}_g(\mathrm{Li}^7)=0.478$ Mev. In the range $0.2\leq K/U\leq 0.8$, δ varies between 0.139 and 0.034, and the difference in the excitation energies of Li^7 and Be^7 varies linearly with K/U from 24 kev (50 percent of the experimental difference) at the lower end to 79 kev (161 percent of the experimental difference) at the upper end of the range. Agreement with the experimental energy difference is found at $K/U\sim 0.4$.

* Assisted by the joint program of the ONR and AEC.
[1] E. Feenberg and G. Goertzel, Phys. Rev. 80, 850 (1950).
[2] J. C. Grosskreutz and K. B. Mather, Phys. Rev. 77, 580 (1950).
[3] Brown, Chao, Fowler, and Lauritsen, Phys. Rev. 78, 88 (1950).
[4] T. Lauritsen and R. G. Thomas, Phys. Rev. 78, 88 (1950).
[5] Johnson, Laubenstein, and Richards, Phys. Rev. 77, 413 (1950).

Experimental Search for the Beta-Decay of the π^+ Meson*

Helen L. Friedman and James Rainwater
Department of Physics, Columbia University, New York, New York
December 21, 1950

THE possibility that nuclear beta-decay is associated with the beta-decay of the meson, formed during an intermediate step, has long been of interest in the development of meson theories. The μ-meson does decay into an electron, but its coupling with nucleons is too weak for this purpose. To explain nuclear beta-decay, the beta-decay rate for the π-meson should be comparable to its μ-decay rate. We report the results of an investigation to detect other than $(\pi-\mu)$ events for π^+ mesons which stop in Ilford G-5 (beta-sensitive) 400- and 600-micron emulsions. The result to date is zero $(\pi-e)$ events compared to 829 $(\pi-\mu)$ events for mesons satisfying certain criteria discussed below.

A collimating exposure chamber was used in the fringing magnetic field inside the vacuum chamber of the Columbia 164-in. cyclotron. The mesons were produced by 385-Mev protons on copper. Plots of the expected meson orbits led to an expected total energy spread for any point X along the plate of about 0.5 Mev.

The meson energy distribution, calculated from the observed ranges, shows that 90 percent of the mesons were within 1 Mev of the mean energy for each X, which varied from 11 to 14 Mev. A comparison with the variation of the ranges of the (supposedly monoenergetic) μ-mesons from the $(\pi-\mu)$ decays suggests that a sizable fraction of the observed spread for the π-mesons is due to straggling rather than a true energy spread.

We consider only meson tracks entering the top surface of the emulsion which stop in the emulsion. Let A represent those associated with a $(\pi-\mu)$ event, B those with no $(\pi-\mu)$ event but with a meson-electron event, and C those with no $(\pi-\mu)$ event or observable meson-electron event. We investigate the ratio of events B and C to A. The following two factors are most apt to lead to false results for the $(\pi-e)$ occurrence rate. (a) Since the $(\pi-\mu)$ event is particularly striking, there is danger that mesons will tend to be recognized mainly because of the $(\pi-\mu)$ event. Thus, in the scanning there is greater relative probability of overlooking events B or C than A. (b) There will be some energetic μ-mesons entering the emulsion due to $(\pi-\mu)$ decays in flight. These will give meson-electron events which might be misinterpreted as π-electron events. We feel that both of these problems have been successfully solved in these studies.

Several scanning procedures were tried to test for, and avoid, effect (a). Techniques were gradually evolved by which mesons were always identified without reference to the $(\pi-\mu)$ event. The present method is to scan just the top surface of the plate. All

tracks entering the emulsion in the field of view at about the proper angle are recorded, followed, and identified. Mesons are always identified well before their endings. In the 600μ plates, about 40 percent of the entering tracks are mesons, of which about 40 percent stop in the emulsion.

Factor (b) is met by the collimating system which defines conditions such that 90 percent of the stopped mesons have their entrance directions and ranges well defined for each X. Mesons falling outside these limits are not counted. A few μ-mesons, formed in flight, gave tracks of type B and C, but, as expected, had considerably different ranges than the π-mesons. These investigations are being continued.

* This work is jointly supported by the ONR and AEC.

Paramagnetic Resonance at Very Low Fields

MARTIN A. GARSTENS
Electricity Division, Naval Research Laboratory, Washington, D. C.
December 18, 1950

WE have observed a very strong and narrow paramagnetic resonance absorption line at fields from 7.0 to 10.3 gauss (i.e., at frequencies of about 19.5 to 29.5 Mc) in a one-gram sample of the free radical α, α-diphenyl β-picryl hydrazyl, $(C_6H_5)_2N-NC_6H_3(NO_2)_2$, using a Bloembergen-Purcell-Pound type of apparatus designed for nuclear magnetic resonance experiments.[1] The modulation frequency used was 30 cycles/sec. The signal was sufficiently strong to be very easily observable on an oscilloscope, although the line width was obtained by means of slope measurements using a one-cycle wide amplifier. A solenoid operating from storage batteries supplied a steady field of sufficient homogeneity.

To our knowledge this is the lowest field strength at which paramagnetic resonance has been observed. Indications are that the line can be detected readily at even lower fields, thus providing a means of extending the range of precision magnetic field measurements provided by the nuclear resonance technique down to such fields. The nuclear resonance signal becomes too weak at low fields to be easily detectable. By inserting a paramagnetic material in place of one involving the use of nuclear magnetism, an enormous increase of signal to noise is obtained.

The observed line width at 29.5 Mc, as measured by the separation between the points of extreme slope of the absorption signal, was 1.4 ± 0.1 gauss. This is not necessarily the same as the width measured at the half-maximum absorption points, since the strong exchange narrowing occurring in the material tends to raise the extreme slope points above the half-maximum points. At microwave frequencies using the latter points a line width roughly double this has been reported.[2,3]

We wish to express our gratitude to Dr. H. A. Tanner and Mr. U. E. Hanninen of the Chemistry Division of the Naval Research Laboratory for the preparation of the hydrazyl used in this experiment.

[1] Bloembergen, Purcell, and Pound, Phys. Rev. 73, 679 (1948).
[2] Holden, Kittel, Merritt, and Yager, Phys. Rev. 77, 147 (1950).
[3] Townes and Turkevich, Phys. Rev. 77, 148 (1950).

The Qualitative Similarity of Origin of the Main Cosmic Radiation and of Showers

J. CLAY
Natuurkundig Laboratorium der Universiteit van Amsterdam, Amsterdam, Netherlands
December 18, 1950

IN a recent communication Cocconi[1] raises the question whether or not the total continuous cosmic radiation and the extensive atmospheric showers occurring in it are produced by entirely equivalent processes.

This problem has occupied our attention for many years, and, from different measurements, we have concluded that when a meson comes down there is a chance of from 40 to 100 percent that a coherent meson will be found in the neighborhood.[2] This was found by measuring the coincidences of a penetrating particle passing through a surface of size 6×6 cm, with another particle passing through another surface of 6×6 cm at three different distances from the first, of 9, 14, and 21 cm. From the exponential decrease in the coincidence rate with distance, we were able to find the total flux of soft and of penetrating particles around the direction of the primary particles. The ratio of the soft (which we take to be decay electrons) to the penetrating particles was found to lie between 0.09 and 0.12. In two independent sets of measurements the occurrence of coherent penetrating particles was found to be 40 to 100 percent, respectively, so that we concluded that generally at least one coherent meson, or an electron resulting from the decay of one, comes down with every meson.

In another experiment we took two sets of 3 counter boxes, with a sensitive surface of 140 cm² per set. The number of coherent particles registered at three distances enabled us to conclude that the distribution of the particles around each of the sets decreased exponentially with the distance to that set. We were able to compute the total number of particles coming down simultaneously with the particle in the first set. This was 202 per minute, while the number of particles counted in the first set was 260, so that we found that in 80 percent of the cases there must have been a coherent meson in the neighborhood.[3]

We must realize that in most cases the energy of the incident proton is not very large, so that the multiplicity of production is small. Moreover, since this production occurs at high altitudes, the number of coherent mesons which can be found in the lower parts of the atmosphere will be small, in general, and the number of secondaries accompanying the penetrating meson will be small also in the very extensive showers. But if two conditions are realized, (1) that the proton producing the mesons (which in their turn produce secondaries) has a high energy, and (2) that the position of the primary collision happens to lie in the lower atmosphere, the mesons and their secondaries will then be observed as a high concentration of particles, that is, as a shower. That the large showers are produced at low levels is confirmed by the fact that the barometric coefficient[4] is about 14 percent per cm Hg. Qualitatively, the original process will be the same in the case of the continuous radiation and of the showers.

[1] G. Cocconi, Phys. Rev. 79, 1006 (1950).
[2] J. Clay, Physica 13, 433 (1947).
[3] J. Clay, Physica 16, 278 (1949).

Proceedings of the American Physical Society

Minutes of the Meeting in Los Angeles, California, December 28, 29, and 30, 1950

THE 302nd meeting of the American Physical Society was held at the University of California, Los Angeles, on Thursday, Friday, and Saturday, December 28, 29, and 30, 1950. Two hundred and twenty members of the Society signed the registration book, and approximately three hundred attended the various sessions during the meetings. A noteworthy feature of the program was the increased participation in the program by physicists from several of the universities in the Rocky Mountain region. Invited papers were given by the heads of departments in several of these, and as a result the important advances in research and graduate teaching in these institutions were brought to the attention of the Society.

On Friday night there was a dinner and dance at the Deauville Club, which was attended by one hundred members and their wives and friends. The only serious part of this session was the informal talk by Dr. Lee DuBridge on "Science and the National Emergency." This was an excellent account of some of the problems that scientists must solve in a national emergency, and the talk included an up-to-date report on some of the actions already taken and plans to solve these problems. The dinner was organized by Dr. Byron T. Wright of the University of California, Los Angeles.

The Division of Fluid Dynamics met on Friday, December 29 under the general chairmanship of Dr. J. G. Kirkwood. The two sessions were presided over by Dr. Kirkwood and Dr. J. M. Burgers.

The text of the Bulletin, apart from preliminary pages, is republished intact in the following pages. Errata submitted by authors follow.

J. Kaplan, Local Secretary
for the Pacific Coast
University of California
Los Angeles 24, California

Errata Pertaining to Paper H8

H8, by F. H. Wright. Two misprints occur in line 18: . . . "ra*d*io S_T/S_L" . . . should read . . . "ra*t*io S_T/S_L." . . . "dimensionless parameter v'/U" . . . should read . . . "dimensionless parameter $(v'/U)(U/S_L)$". In line 22 there are also two misprints: . . . "*s*o significant effect of si*d*e of burner" . . . should read . . . "*n*o significant effect of si*s*e of burner."

PROGRAMME

THURSDAY MORNING AT 10:00

Room 19, Chemistry Building

(CARL D. ANDERSON presiding)

Contributed Papers

A1. Stopped Mesons in Pb and C Observed in a Cloud Chamber at Sea Level Triggered by Neutron Coincidences.* EDWARD J. ALTHAUS,† *Washington University.*—A large square cloud chamber containing six plates of Pb (5.9 g/cm²) and five of C (3.1 g/cm²) arranged alternately was triggered by an overhead fourfold crossed G-M tube telescope in long-gated coincidence with B^{10} neutron detectors. These were embedded in a C-shaped block of paraffin surrounding the chamber. Stopped μ-mesons were identified by ion density at least 2½ times the minimum in the first compartment above the plate and absence of an accompanying event in order to eliminate locally produced π-mesons. In 1215 neutron coincidence sets of pictures, 16 definite cases were observed in Pb and one in C. No decay electrons were evident. Of 1286 sets with G-M control alone, roughly equal numbers were observed in each material with some decay electrons. These findings agree with the results of other experiments[1] showing neutron emission from stopped mesons in Pb, and are consistent with the low capture probability for μ^- in C, but the results do not show whether or not capture in C leads to neutron emission.

* Research assisted by the joint program of the ONR and AEC.
† Now at University of Southern California.
[1] Sard, Conforto, and Crouch, Phys. Rev. 76, 1134 (1949). Fowler, Sard, Fowler, and Street, Phys. Rev. 78, 323 (1950).

A2. Energy Spectrum at 18° of Mesons Produced in Proton-Proton Collisions. VINCENT PETERSON,* EDWIN ILOFF, AND DORA SHERMAN, *University of California, Berkeley.*—Using a liquid hydrogen "point" source and photographic plate method of detection described earlier,[1] the energy spectrum of positive mesons produced from 340-Mev proton bombardment has been measured at a laboratory angle of 18°±0.85°. Improvements in the energy and angular resolution of the detector geometry have resulted in narrowing the half-width of the sharp peak at the upper end of the spectrum to ±1.8 Mev, most (if not all) of which is due to the energy spread of the primary proton beam. Present uncertainties in the meson mass and absolute accuracy of the proton range-energy relationship prevent the use of energetics in determining the existence of $p+p \rightarrow d+\pi^+$; however, if independent experiment confirms that the peak corresponds to this reaction, then the mean energy is a sensitive measure of meson mass. The integrated cross sections at 18° and 30° are, respectively, 0.163 and 0.058 mb/ster (+15 percent, −5 percent). The ratio $18°/30° = 2.8$ favors a $\cos^2\theta$ angular distribution in the center-of-mass system.

* Now at California Institute of Technology.
[1] Post-deadline paper by V. Peterson at 1950 Washington, D. C., meeting; Phys. Rev. 80, 136 (1950).

A3. An Automatic Ionization Chamber.* H. V. NEHER, *California Institute of Technology.*—For studying fluctuations of cosmic rays at balloon altitudes an automatic ionization chamber has been designed. A small, gold-coated quartz fiber is mounted at one end of, and at right angles to, an insulated collecting rod. When the potential of the collector drops to about ½ of its initial potential, the gold-coated fiber touches and recharges the collector. The electrical pulse so obtained is amplified and results in a transmitted pulse, which is picked up by a receiver on the ground. Barometric and temperature data are also transmitted. The calibration of the ion chamber thus should remain constant with time, provided the following do not change: (1) the quartz fiber, (2) the geometry of the system, and (3) the pressure of the enclosed argon. The ion chamber has a diameter of 25 cm and gives an accuracy of ±0.3 percent for each discharge for β-particles. The whole equipment weighs 2 kg.

* Supported in part by the joint program of the ONR and AEC.

A4. Large Ionization Bursts at High Altitude.* R. F. CHRISTY, A. T. BIEHL, E. INONU, AND H. V. NEHER, *California Institute of Technology.*—Extended airplane flights at 30,000 feet in recent years by two of the authors have shown a significant number of bursts of more than 400 fast particles as recorded by a 10-atmosphere argon-filled ionization chamber shielded by 10 cm Pb. In addition, similar data had been obtained previously with the same equipment at 14,500 feet and at sea level. The sea level data are consistent with those obtained by other investigators with similar equipment and are accounted for by the bremsstrahlung of μ-mesons in the lead shield. The two high altitude points, on the other hand, show a large increase with altitude consistent with an exponential length of ~130 gm of air and demand a different explanation. As Rossi has pointed out, they can be understood in terms of the production in the Pb shield, by the primaries, of neutral mesons which lead to cascade bursts by their decay γ-rays. The primary energies associated with these events are $\sim 10^{11}$ ev. Preliminary calculations show that it is possible to correlate numerically the number of such primaries with the number of bursts. More detailed calculations are in progress to reveal more about the number and spectrum of these primaries.

* This work was assisted by the joint program of the ONR and AEC.

Invited Papers

A5. Unstable Particles in Penetrating Cosmic Ray Showers. E. W. COWAN, *California Institute of Technology.* (30 min.)

A6. The Nature of the π-Meson. ROBERT SERBER, *University of California, Berkeley.* (30 min.)

THURSDAY MORNING AT 10:00

Room 45, Chemistry Building

(A. BAÑOS, JR., presiding)

Contributed Papers

B1. Corona in H_2 with Coaxial Cylinders. EUGENE J. LAUER, *University of California, Berkeley.*—Corona in pure H_2 and in H_2 with a small amount of N_2 or O_2 has been studied with the same system as used by C. G. Miller.[1] Positive wire corona in pure H_2 started with burst corona. Weissler observed no bursts in point-to-plane corona in pure H_2. This difference can be explained by the longer high field region along the wire allowing photoionization. Negative wire corona started at lower potential than the positive. There was a marked overshoot in onset which decreased in relative amount with decreasing pressure. The negative corona started as an invisible self-supporting discharge with a current several powers of ten smaller than that of the visible corona of microamperes current. In time, or upon small increase of potential, the small current changed suddenly to the large (microamperes) current discharge at conditioned spots on the wire. The addition of 0.1 percent of N_2 or O_2 to the H_2 resulted in pre-onset streamers from the positive wire. O_2 lowered the positive wire onset and raised the negative wire onset. N_2 had no marked effect on the onsets.

[1] Charles G. Miller, Phys. Rev. **75**, 1460 (1949).

B2. Corona from Ice Points. H. W. BANDEL,* *University of California, Berkeley.*—In connection with questions on atmospheric electricity some work has been done with corona from ice points using point-to-plane geometry. One- and two-mm diameter ice points were used with an 8-cm gap at −78°C and −10°C and compared with platinum points under the same conditions. With 1-mm points currents rose with voltage from low values of around 10^{-13} amp up to values, at well above onset voltage, of 10^{-11} amp with distilled water ice and 10^{-9} to 10^{-8} amp with tap water ice compared to 10^{-6} amp with platinum points. These relative magnitudes are in line with measured resistances of 10^{11} to 10^{13} ohms for tap water and 10^{14} ohms for distilled water ice points. Corona onsets occurred at roughly the same voltages as for metal points; but the burst pulses, streamers, and Trichel pulses characteristic of positive and negative metal point corona were not observed, although the oscilloscope showed random, low amplitude pulses with time duration of milliseconds for both polarities. Thus far it seems doubtful that ice crystals can lead to premature spark breakdown or to lightning discharge at lower potentials in air owing to the low currents passed.

* Supported by ONR funds.

B3. Principle of Similitude. L. B. LOEB AND E. E. DODD,* *University of California, Berkeley.*—In this country investigators of gaseous discharges have generally ignored the principle of simultude of Holm[1] and Steenbeck.[2] This is apparently due either to lack of familiarity with the principle, since it has not been presented completely in English, or to lack of confidence in it. For this reason the complete principle is presented and discussed. It is concluded that its best use today is as a check for theories of individual discharge mechanisms.

* Supported by ONR funds.
[1] Holm, Physik. Z. **25**, 504 (1924).
[2] Steenbeck, Wiss. Veröffenbl. Siemens-Konzern **11**, No. 2, 36 (1932).

B4. Spray Electrification of Liquid Drops. E. E. DODD,* *University of California, Berkeley.*—The simultaneous size and charge of many individual drops of various liquid sprays are being determined by the Hopper and Laby method. This data will be useful in resolving the present uncertainties concerning the effects of the various possible spray electrification mechanisms.[1] The apparatus built and described by Kunkel and Hansen[2] is being used with low vapor pressure liquids having varying physical properties. Drop diameters in a range of about 2 to 30 microns and with charge to diameter ratios up to about 500 electrons per micron can be measured. Observations made of more than 6000 drops produced by atomization indicate that the numbers of positively and negatively charged drops of poorly conducting liquids are roughly equal, as are their average charges, while drops of conducting liquids are predominately positively charged. Sample data are presented to illustrate the rather broad distribution in charge for a particular drop size and the variation of average charge per drop with drop size and physical properties of the liquid.

* Supported by ONR funds.
[1] Loeb, Science **102**, 573 (1945).
[2] W. B. Kunkel and J. W. Hansen, Rev. Sci. Inst. **21**, 308 (1950).

THURSDAY AFTERNOON AT 2:00

Room 19, Chemistry Building

(E. L. KINSEY presiding)

Contributed Papers

C1. Stars in Photographic Emulsions Initiated by Protons.* LAWRENCE S. GERMAIN, *University of California, Berkeley.*—A study has been made of stars in photographic emulsions initiated by protons from the 184-inch Berkeley cyclotron. Ilford G-5 electron sensitive plates were exposed to the proton beam with the emulsion parallel to the beam. A workable exposure, about 20 proton tracks per 100-micron field of view, was obtained by dropping the plates through the deflected proton beam of the cyclotron. Energies as low as 95 Mev were obtained by placing Al absorbers in front of the plates. The plates were scanned for all stars initiated by the protons, and the total length of proton track was found by examining sample areas. The average number of prongs per star and the cross section for production of stars of two or more prongs was calculated for various energies between 95 Mev and 340 Mev. Both of these quantities increased with increasing energy up

to the highest energy used. At 340 Mev the cross section was found to be 0.29 barn, while the average number of prongs per star was 3.9.

* This work was done under the auspices of the AEC. Work done at Reed College was assisted by a Research Corporation grant.

C2. Delayed Emission of Neutrons from Light Elements.* WILLIAM GARDNER, N. KNABLE, AND B. J. MOYER, *University of California, Berkeley.*—In addition to the delayed neutrons appearing with a 4.17-sec half-life from the decay of N^{17} previously identified at Berkeley, a 0.165-sec emission has been discovered. It has been obtained, at the time of this writing, by 190-Mev deuteron bombardment of Be_3N_2 and elemental boron. Observations are made by rapidly moving film exposures of an oscilloscope screen displaying a scaled output of BF_3 chamber pulses. The target under bombardment is surrounded by the chamber. The results of attempts to identify the neutron emitter and the parent β-decay will be presented.

* This work was performed under the auspices of the AEC.

C3. Photo Production of Neutral Mesons from Hydrogen.* J. S. STELLER AND W. K. H. PANOFSKY, *University of California, Berkeley.*—The work of Steinberger, *et al.*,[1] on the production of neutral mesons by photons from the Berkeley synchrotron has been extended using liquid hydrogen as target. Liquid scintillators (0.5 percent terphenyl in xylene) in sealed glass containers arranged as described in reference 1, were used to detect the decay gamma-rays. The experimental set-up permits measurement of both meson production angle and correlation angle between the decay gamma-rays. The correlation angle is a calculable function of the π^0-energy; therefore, the measured distribution limits the choice of π^0-energy distribution to a considerable extent. Here, the recoil nucleus is known to be a proton, so that one can calculate the incident photon energy and hence deduce the energy dependence of the production cross section. This is definitely a more rapidly rising function than the excitation function of photo production of charged mesons.[2] A value for the total cross section of 1×10^{-28} cm^2 per effective quantum is observed, in good agreement with the previously reported value from carbon-paraffin difference. Photo production cross section for charged and neutral mesons in hydrogen for 320-Mev bremsstrahlung are thus essentially equal. Work is continuing on the angular distribution of the π^0's.

* This work was performed under the auspices of the AEC.
[1] J. Steinberger, W. Panofsky, and J. Steller, Phys. Rev. **78**, 802 (1950).
[2] J. Steinberger and A. Bishop, Phys. Rev. **78**, 493 (1950).

C4. Grain Density Measurements in Nuclear Emulsions.* J. KENT BOWKER, JOHN R. GREEN,† AND WALTER H. BARKAS, *University of California, Berkeley.*—The validity of the relation $dN/dR=f(dE/dR)$ has been studied for high energy charged particles. N is the number of grains in a residual range R, and E is the kinetic energy of the moving particle. From grain counts of mesons, protons, and alpha particles it is found that the grain density does not depend explicitly on the charge of the moving particle, but to good approximation just on its rate of energy loss. It is found also that when dN/dR is small, it becomes proportional to dE/dR. A saturation effect exists because only a finite density of potentially developable grains are threaded by the moving particle, so dN/dR cannot rise in proportion to dE/dR as the particle slows down. By measuring the gap density, $g(R)$, in clogged tracks, one may determine the probability of grains *not* being rendered developable. A relation $G/M=F(R/M)$ holds for particles of the same charge, where $G(R)=\int_0^R g(R)dR$. Measurements on the "integrated emptiness" of tracks demonstrate that in the region where grain counting fails because of clogging, gap measurements provide reliable mass ratios.

* This work was performed under the auspices of the AEC.
† Now at the University of New Mexico, Albuquerque, New Mexico.

C5. Protons Scattered out of Nuclei at High Energies.* J. B. CLADIS, J. W. HADLEY, AND B. J. MOYER, *University of California, Berkeley.*—Proton energy spectra are obtained by deflecting scattered protons by a magnetic field into channels defined by proportional counters and a bank of 35 Geiger counters. With incident protons of 340 Mev, the scattered protons from light elements viewed at 22° have spectra resembling free particle scattering: the peaks fall at nearly the same energy, the deuterium yield is about twice the hydrogen yield, and the carbon points multiplied by 16/12 give a curve which is indistinguishable from that of oxygen. With incident neutrons of 270 Mev on deuterium, scattered proton yields in the forward direction are suppressed relative to corresponding yields from hydrogen. This is in keeping with predictions based on exclusion principle requirements pertaining to the two neutrons which now possess a small relative momentum.

* This work was sponsored by the AEC.

C6. Angular Distribution of Gammas in Showers.* JACK W. ROSE, *University of California, Berkeley.* A study has been made of the angular distribution of gammas in showers initiated in lead and copper by the 335-Mev bremsstrahlung of the Berkeley synchrotron. The x-ray beam, collimated to ¼ inch, passed normally through a thin monitor foil and then through plates of lead or copper. The shower gammas emerging from the far side of the plates were detected by means of the radioactivity of copper foils, by means of the reaction $Cu^{63}(\gamma, n)Cu^{62}$. The activities induced in the foils at various angles with the beam were compared to that in the monitor foil by means of G-M counters. Since the (γ, n) reaction utilized is believed to have a narrow excitation curve peaked at about 20 Mev,[1] the angular distribution curves obtained should be essentially those for 20-Mev gamma-rays. The preliminary results agree reasonably well with calculations of the lateral structure of showers to be published by L. Eyges and S. Fernbach.

* This work was sponsored by the AEC.
[1] G. C. Baldwin and G. S. Klaiber, Phys. Rev. **73**, 1156 (1948).

C7. Large Angle Scattering and Stars Produced by π^- Mesons in Flight.* HUGH BRADNER AND BAYARD RANKIN, *University of California, Berkeley.*—An investigation is being made of the scattering of energetic π^- mesons in photographic emulsion. Mesons of approximately 38 Mev are obtained by a channel inside the Berkeley cyclotron. These mesons traverse G-5 emulsion. Four-hundred- and 600-micron thick emulsions are placed with their surfaces parallel to the meson beam, so that individual meson tracks can be followed. Mesons are differentiated from protons by their grain density and small angle Coulomb scattering in the first 500 microns of observed track. μ-meson background is determined by observing tracks in a second set of emulsions placed beyond the range of the π^- mesons. Scatters between 5° and 25° are in agreement with single Coulomb scattering. 26 scatters of total angle greater than 30° and 11 stars have been observed in a total length of 902 cm of π^- track. Five mesons were seen to disappear in flight. The latter events may be attributed to the reaction π^-+p, π^0+n, or to "stars" with only neutrons emitted. The mean free paths for large angle scatters, stars, and total nuclear interactions are, respectively: 34.7 ± 4.6, 82.0 ± 16.7, 21.5 ± 2.2. Nuclear area of the elements of the emulsion corresponds to approximately 23-cm mean free path. Hence, it appears that the total cross section for nuclear interaction of 30–40-Mev π^- mesons in emulsion is equal to nuclear area.

* This work was performed under the auspices of the AEC.

C8. Proton-Proton Scattering at 75 Mev and 100 Mev.* ROBERT W. BIRGE† AND ULRICH E. KRUSE, *Harvard University.* The angular distribution of the proton-proton differential scattering cross section has been measured using the

Harvard 95-inch cyclotron.[1] The internal beam was intercepted by a ten-mil polyethylene foil. Protons scattered in the vertical plane were counted by scintillation crystals placed above and below the median plane. The C^{11} activity induced in the target was counted at the end of each five-minute run to serve as a monitor for the beam current and to give a rough value for the absolute scattering cross section. To obtain the 75-Mev incident protons, the target was moved inward radially from 40 inches to 35 inches and the counting probes lengthened accordingly. Complete results of the 100-Mev experiment and preliminary results of the 75-Mev experiment will be presented.

* Assisted by the joint program of the ONR and AEC.
† Now at the University of California Radiation Laboratory.
[1] R. W. Birge, Phys. Rev., to be published.

C9. Fast Protons from π^- Meson Absorptions in Photographic Emulsions.* F. L. ADELMAN, *University of California Berkeley.*—The spectrum of fast protons from 1631 π^- meson absorptions in Ilford G-5 and C-2 emulsions has been studied. Protons of energy >30 Mev were found to accompany (9.5±1.3) percent of all π^- absorptions, in agreement with other workers.[1,2] The proton energies were estimated by grain-counting in comparison with π^- mesons of known residual range. Allowance was made for variation of grain density with position and depth in the emulsion. The energy spectrum is fairly flat from 30–70 Mev, but only three events were found above 70 Mev. Examination of stars from which the fast protons were emitted shows more prongs ejected opposite to the direction of the fast proton than are accounted for by evaporation from a recoiling nucleus. The evidence suggests that the meson is captured by a proton, and that the resultant neutron recoils against a small, variable number of nucleons; the low energy star prongs apparently result from knock-on collisions of these nucleons with other nucleons inside the nucleus. Comparison is made between other theories and the experimental results.

* This work was sponsored by the AEC.
[1] W. Cheston and L. Goldfarb, Phys. Rev. 78, 683 (1950).
[2] M. Menon, H. Muirhead, and O. Rochet, Phil. Mag. 41, 583 (1950).

Invited Papers

C10. Current Research in Physics at the University of Utah. L. B. LINFORD, *University of Utah.* (30 min.)

C11. Nitrogen Absorption Coefficients in the Vacuum Ultraviolet, and Related Problems. G. L. WEISSLER, *University of Southern California.* (30 min.)

THURSDAY AFTERNOON AT 2:00

Room 45, Chemistry Building

(J. W. ELLIS presiding)

D1. Static and Dynamic Current-Voltage Characteristics of Glow Discharges. DAVID L. FAYMAN AND CHARLES G. MILLER, *University of California, Santa Barbara.*—The current-voltage characteristics of various electrode shapes and gases have been investigated, and a report is made of the voltage-regulating action and of some dynamic characteristics of glow discharges. In the case of positive-wire, concentric cylinder geometry, the use of diatomic, non-electron-attaching gases (H_2 and N_2), provide stable, high voltage voltage-regulator tubes. Certain electron-attaching polyatomic gases may also be used in particular geometries. In the case of negative wire systems, highly purified N_2 enables very high voltage voltage-regulator tubes to be realized. The role of the electron attaching impurities evolved from the electrodes is discussed. The dynamic characteristics of glow discharges are described in the range 60 cps to 30 kc/s for rare gases, for N_2 and for H_2. A hysteresis effect and a negative resistance region are found for the gases studied, and the manner in which these affect circuit designs are discussed.

D2. Positive and Negative Corona in Oxygen, in Freon, and in Mixtures. CHARLES G. MILLER AND DAVID L. FAYMAN, *University of California, Santa Barbara.*—Dc corona studies have been carried out in oxygen, in freon, and in mixtures using concentric cylindrical geometry, affording a comparison with the work of Weissler and Mohr[1] who used point-to-plane geometry and freon-air mixtures. In the present experiments using positive corona, the discharge in pure oxygen gives streamers at high pressures, burst pulses at low pressures. The addition of freon allows streamers at all pressures. In the case of the negative corona, in oxygen and in freon small patches of the cathode are cleaned by the action of the positive ions bombardment; and the current is then limited by the action of Trichel pulses.[2] The discharge in oxygen begins as a *general* glow, which disappears when the Trichel pulses and the Trichel pulse spots appear, while the current jump at onset is only slight for atmospheric pressure oxygen. As the pressure is lowered, the overshoot in voltage is more pronounced since a cleaned spot can be more easily maintained.

[1] G. L. Weissler and E. I. Mohr, Phys. Rev. 72, 289, 294 (1947).
[2] Loeb, Kip, Hudson, and Bennett, Phys. Rev. 60, 714 (1941).

D3. Pulse-Annealing for the Study of Relaxation Processes in Solids.* W. E. PARKINS AND G. J. DIENES, *North American Aviation, Inc.*—A "pulse-annealing" method has been developed for heating small samples of electrically conducting solids to chosen elevated temperatures for short periods. After each annealing pulse a physical property determination is made on the sample at a fixed reference temperature. From this record of the physical property changes resulting from successive annealing pulses, much can be learned of the nature of relaxation processes occurring within the solid. Types of lattice processes which can be studied include impurity diffusion, recrystallization, chemical reaction, and various types of phase changes. Activation energies for individual states can be accurately determined without any knowledge of the dependence of the physical property on the amount of lattice relaxation. In order to establish the rate constant and reaction order associated with the relaxation kinetics this property dependence must be known. For the pulse-annealing schedule it is sometimes advisable to obtain isothermal annealing results by repeated pulsing to some given temperature. In other cases annealing pulses are made to successively higher temperatures thereby simulating tempering treatment. Apparatus will be

described which has been used to measure electric resistivity changes in graphite and in metal samples. Typical experimental results will be given.

* This paper is based on work performed under Contract No. AT-11-1-GEN-8 for the AEC.

D4. Kinetics of Ordering in the Alloy AuCu.* G. J. DIENES, *North American Aviation, Inc.* (introduced by M. M. Mills).—The kinetics of ordering in AuCu has been studied using electrical resistivity as the index of order. A purely phenomenological analysis of isothermal resistivity-time curves showed that ordering in this alloy is a process characterized by a single constant activation energy of 29 Kcal. For further kinetic analysis it is necessary to transform the raw data into isothermal order parameter-time curves. This was accomplished via a semi-theoretical relation between resistivity and the average degree of short range order (σ) and substantiated by agreement with available experimental information. A consistent kinetic picture was obtained in terms of σ with the ordering process accurately described by a simple third-order rate equation with all the kinetic constants fully evaluated. The usual ln (rate constant) *vs.* $1/T$ plot gave an activation energy of 28.5 Kcal, in excellent agreement with the phenomenological activation energy. Further experiments showed that the proposed kinetics predicts correctly the response to complex time-temperature sequences. Some of the uncertainties arising in the analysis are pointed out. Future work, designed to elucidate the disordering kinetics, and thereby the equilibrium degree of order-temperature relation, will be briefly discussed.

* This paper is based on work performed under Contract No. AT-11-1-GEN-8 for the AEC.

D5. Singlet-Triplet Absorption Bands in Some Organic Molecules.* D. S. MCCLURE, N. BLAKE, AND P. HANST, *University of California, Berkeley.*—Singlet-triplet bands have been observed for several organic compounds in solution at room temperature and at 77°K. The absorption spectra at 77° are the first observations of absorption to the triplet state under the same conditions of temperature and medium at which the emission spectra have been observed. The low temperature work, using a meter path length, makes possible the resolution of S−T transitions which are not resolved at room temperature, and further allows the location of triplet levels for those molecules which have little or no T−S emission.

* Sponsored, in part, by the ONR.

D6. The Quantum Yields of Fluorescence and Phosphorescence of Some Organic Compounds. E. H. GILMORE* AND D. S. MCCLURE, *University of California, Berkeley.*—The quantum yields of phosphorescence and fluorescence have been determined for several organic compounds maintained in a rigid glass medium at 77°K. This work was undertaken as a supplement to the work of D. S. McClure,[1] who determined the emission decay lifetimes of the phosphorescence (triplet) levels of these compounds, and who further postulated a theory to explain these lifetimes. An accurate check of the the theory requires true electronic transition probabilities for the phosphorescence to ground level transition. These are obtained in the relation $\frac{\nu}{TG} = Q_P/\tau_0(1-Q_F)$, where $\frac{\nu}{TG}$ is the phosphorescence to ground level electronic transition probability, Q_P is the phosphorescence quantum yield, Q_F is the fluorescence quantum yield, and τ_0 is the emission decay lifetime (mean life). Quantum yield measurements were undertaken for nine compounds. Six had total quantum yields in excess of ten percent, and the remaining three were five percent or less. An indication of the explanation of the marked difference in aliphatic and aromatic ketone phosphorescence lifetimes is found in the quantum yield results. The aromatic hydrocarbons examined have very nearly the same transition probability value. Should this be true for aromatic hydrocarbons in general, it would appear that an identical mechanism is responsible for the transition in the entire class of compounds.

* Present address: U. S. Naval Ordnance Test Station.
[1] D. S. McClure, J. Chem. Phys. 17, 905–13 (1949).

D7. Aging of $BaTiO_3$ Ceramics. W. R. EUBANK AND L. E. SCHILBERG, *U. S. Naval Ordnance Test Station* (introduced by H. W. HUNTER).—For the purpose of exploring the aging of $BaTiO_3$ ceramics in great detail, with special reference to dielectric properties, approximately twenty-five specimens have been made (by various techniques) and studied during thermal cycling (50°C–140°C). The curves for dielectric constant *versus* temperature for specimens made of spectrographic grade materials were of the shape customarily reported in the literature, while those for specimens of reagent grade were much more rounded and had somewhat lower peak values. In general, both types of specimens showed progressive aging corresponding to a lowering dielectric constant, the effect being much more pronounced in those of spectrographic materials than in those of reagent grade. Although sufficient data are not yet available to allow correlations with known factors (as of methods of preparation), it is felt that the aging in $BaTiO_3$ ceramics may be so violent in some cases as to warrant this report in emphasis of the phenomenon.

D8. Effects of Thin Films of Silver and of Gas at the Surface of the (100) Face of a Silver Crystal.* H. E. FARNSWORTH AND EDWARD N. CLARKE,† *Brown University.*—Observations on a silver crystal in a single photoelectric and low speed electron diffraction tube, combined with observations previously obtained, indicate the following for silver: (1) Intensities of low energy diffraction beams (below 50 ev) are influenced primarily by the surface monolayer of atoms, while the surface photoelectric work function, φ, is determined by a volume layer more than one atom thick. This makes it possible to distinguish between true surface effects and those of thin layers just beneath the surface. (2) φ for silver increases as gas in the volume layer decreases. (3) Rapid deposition of doubly-distilled silver in high vacuum can form a clean surface as determined by electron diffraction. This deposited layer can cover a gas contaminated surface, at least for a limited time. (4) The silver film forms as a single crystal on the surface of a silver crystal and causes a decrease in φ. This decrease depends on (a) value of φ before deposit, (b) temperature of the crystal during deposition. It does not depend on (a) rate of deposition, (b) amount of silver deposited (within limits), (c) residual gas pressure in the range 10^{-6} to 10^{-9} mm Hg. (5) Low temperature heating (less than 75°C) of the silver film on bulk silver causes φ to increase. Significance of the above observations will be discussed.

* Assisted by the ONR and Research Corporation of New York.
† Socony Vacuum predoctoral fellow.

D9. Activation of a Solid Nickel Catalyst for the Hydrogenation of Ethylene by Heat Treatment in a High Vacuum.* R. K. SHERBURNE† AND H. E. FARNSWORTH, *Brown University.*—These results are preliminary to an investigation of the catalytic activities of individual faces of metal single crystals. A Nier-type mass spectrometer is used to analyze the products of the reaction. The nickel specimen, in the form of a sheet 15 mm diameter by 0.25 mm thickness, was cleaned, and electrolytically polished to produce a smooth surface free of points. It was outgassed in an evacuated reaction chamber by high frequency induction, with the residual air pressure successively at 10^{-4}, 10^{-6}, 2×10^{-7} mm Hg. After each outgassing equal volumes of hydrogen and ethylene were admitted to the reaction chamber, maintained at 135°C, at total pressures between 6 and 16 mm Hg. Subsequently,

samples of the resulting gas were analyzed in the mass spectrometer after various time intervals. The activity increased with decrease in residual air pressure during outgassing, and with increase of time of outgassing at dull red heat temperatures. Many hours of heat treatment at 400°C produced only a negligible amount of activity. Exposure of the active specimen to low residual air pressures for several hours reduced its activity, thus indicating that small amounts of adsorbed gas are sufficient to poison the active surface for the reaction in question.

* Assisted by the ONR and Research Corporation of New York.
† Now at New Mexico College of Agriculture and Mechanic Arts.

FRIDAY MORNING AT 9:00

Room 19, Chemistry Building

(R. T. BIRGE presiding)

Contributed Papers

E1. Decay Scheme of Mo^{99}. H. MEDICUS,* D. MAEDER, AND H. SCHNEIDER,† *Swiss Federal Institute of Technology, Zürich.*—β-decay of Mo^{99} proceeds in practically all cases by way of excited levels in Tc^{99}. About 87 percent of the transitions[1] ($\beta_{max}=1.225\pm0.015$ Mev) lead to the well-known isomeric level of Tc with 6 hours half-life[1] which lies 143 kev above the ground state. This will be reached by a cascade consisting of a highly converted 1.8 ± 0.3-kev transition (to which the isomeric behavior is to be attributed) and of a γ-ray of 141.2 ± 0.5-kev energy of low multipole order (conversion coefficient $\alpha=0.095\pm0.020$, $\alpha_K:\alpha_L:\alpha_{M+N}=(7.9\pm0.5):1:(0.30\pm0.03)$). About 13 percent of the transitions of Mo^{99} lead to an excited Tc level of 969 kev. Thence the 141.2-kev level is reached directly by emission of a 728 ± 8-kev γ-ray, whereupon transition to the ground state follows. Very weak γ-rays were also found with energies of 182 ± 3 and 360 ± 6 kev. The expected β-transition from isomeric Tc^{99} to the ground state of Ru^{99} could not be observed. Its probability must therefore be smaller than that of the isomeric transition by a factor of 3.10^{-4}.

* Present address: Radiation Laboratory, University of California, Berkeley.
† This work was performed under the auspices of the AEC.
[1] G. T. Seaborg and E. Segrè, Phys. Rev. 55, 808 (1939).

E2. Relative Photo-Neutron Yields from the 330-Mev Bremsstrahlung.* W. N. JARMIE, L. W. JONES, AND K. M. TERWILLIGER, *University of California, Berkeley.*—Relative photo-neutron yields were determined for 50 elements bombarded by the 330-Mev x-ray bremsstrahlung of the Berkeley synchrotron. The determinations were made at 90° to the beam axis with a BF_3 proportional counter surrounded by a paraffin moderator. Paraffin-cadmium shielding reduced the neutron background to less than 30 percent of the target yield for all but five targets, and to 4 percent for the heaviest elements. Statistical counting errors were kept below 3 percent. Absolute yields per unit beam energy were determined using calibrated Ra—Be and Po—Be sources and the beam energy measurements of Blocker and Kenney. Relative yields for high Z elements lie on a smooth curve and are in approximate agreement with Kerst. Deviations from a smooth curve for yields from low Z elements will be discussed. Angular distributions of photo-neutrons were briefly investigated, and a Pb transition curve for photo-neutrons was run.

* This work was performed under the auspices of the AEC.

E3. Angular Distribution of Neutrons from 20-Mev Deuterons. L. SCHECTER,* *University of California, Berkeley.*—The spatial distribution of neutrons produced by the impact of deuterons of maximum energy 20 Mev on various thick targets has been investigated, using the 60-inch cyclotron at the Crocker Laboratory. The neutrons in the energy regions above 20 Mev, 11 Mev, and 5 Mev were detected by the resulting β-activities induced in C, Cu, and Be, Al, Cu, Sn, Pb, and U. The distributions vary in a nonregular way from element to element, the characteristic features being the width at half-maximum, and the angular position of the maximum. Among the elements investigated, Be and Cu yield neutrons, which, above 20 Mev, have their spatial maximum displaced from the direction of the incident deuteron beam. At lower energies, this apparent "double peak" is washed out, indicating that the distributions result from the superpositions of several different nuclear processes of comparable importance. This is to be compared to the distributions resulting from 190-Mev deuteron impacts, which agree quantitatively with the single process of stripping.

* This work was performed under the auspices of the AEC.

E4. Multiple Traversals of High Energy Particles in a Cyclotron Beam through Thin Targets. W. J. KNOX,* *University of California, Berkeley.*—An experimental determination has been made of the average numbers of times that 340-Mev protons traverse various targets in the Berkeley 184-inch cyclotron. The numbers range from slightly above 1 for a 1-inch thick copper target to about 15 for an aluminum target 0.0015 inch thick. The results are compared with calculated values based on multiple scattering in the target and oscillations of the particles in the cyclotron. It is believed that the results can be adapted to apply to various particles of different energies in the cyclotron. Calculations are made on the energy distribution of beam particles which cause reactions in a target and distributions are shown for several targets. The selection of targets for the production of high energy neutron beams is discussed. Histograms are presented showing the depth of radial penetration of the 340-Mev proton beam into various targets.

* This work was performed under the auspices of the AEC.

E5. The Production of π^+ Mesons by Protons on Protons in the Direction of the Beam.* W. F. CARTWRIGHT, C. RICHMAN, M. H. WHITEHEAD, AND H. A. WILCOX, *University of California, Berkeley.*—The first measurements of the cross sections for π^+ meson production by proton-proton collisions showed a large peak in the energy spectrum near the maximum energy of the mesons.[1,2] To determine more accurately the spectrum in the region of the peak for mesons produced at zero degrees we have modified our original detection arrangement. By using a new magnet with a larger gap and bending the meson trajectories further away from the proton beam, we have decreased the background due to other particles and obtained better statistics. The proton beam energy fluctuations are minimized. With these improvements the peak has been in-

vestigated in detail. Two reactions may occur: (1) $p+p \rightarrow \pi^+ + d$ and (2) $p+p \rightarrow \pi^+ + n + p$. Mesons produced in (1) in the laboratory system have an energy four Mev higher than the maximum energy of those produced in (2). The measured values of the maximum meson energy and the proton beam energy indicate that if the meson mass is 276 electron masses, deuteron formation does take place. The peak in the spectrum is centered at 70 Mev and has a half-width of about 4 Mev.

* This work was performed under the auspices of the AEC.
[1] Cartwright, Richman, Whitehead, Wilcox, Phys. Rev. **78**, 823 (1950).
[2] Peterson, Phys. Rev. **79**, 407 (1950).

E6. Covariant Description of a Bound State. D. L. DRUKEY*† AND J. W. WEINBERG, *University of Minnesota.*—The description of a bound state is formulated in interaction representation using plane wave normal modes. For this, an invariant counting technique is devised. Approximate forms of the "interaction Hamiltonian" and the resulting energy-momentum four-vector operators are obtained from a particular coupling model by application of perturbation theory and the correspondence limit. The "Schrödinger equation" takes the form of an eigenvalue equation, $P_\mu \Psi = p_\mu \Psi$, where P_μ and p_μ are, respectively, operator and eigenvalue, and Ψ is the state functional. In order that the P_μ commute, it proves necessary that the space-like surfaces over which Ψ is defined be hyperplanes. This restriction does not destroy the covariance of the formalism, however. Solution of the Schrödinger equation may be effected by reducing from second to primary quantized form. This yields a set of integral equations with the energy and momentum of the compound system as eigenvalues. Equations for the deuteron will be presented.

* Now at the Radiation Laboratory, University of California, Berkeley, California.
† Part of this work was performed under an AEC Fellowship.

E7. Large Angle Focusing of π^+ and π^- Mesons.* R. SAGANE AND PETER C. GILES, *University of California, Berkeley.*—A test has been carried out to focus mesons with the use of the Spiral Orbit Spectrometer principle[1] (2π angular focusing of charged particles originated from the axis with the use of an axial symmetric heterogeneous magnetic field). Meson density of more than 10/sec/cm² of nearly homogeneous energy mesons has been obtained so far with 10^{-13} amp of protons at 345 Mev. Nuclear emulsion has been used to detect these focused mesons. Both thick and thin targets made of several different elements were used with and without an axial symmetric Cu tubular absorber. A study of the π^+/π^- ratio of a low (10-Mev) and a high (40-Mev) energy region of mesons from Al, Cu, Ag, Sn, and Pb is now going on. Focusing conditions are quite symmetric for mesons of both signs. Positive and negative mesons coming from opposite directions are stopped in the same portion of a stripped emulsion by using wedge absorbers on each side of the emulsion. An attempt to count the positrons from the decay of μ^+ mesons stopping in the target is being made with the same focusing arrangement.

* This work was performed under the auspices of the AEC.
[1] G. Miyamoto, Proc. Phys.-Math. Soc. Japan **17**, 587 (1943); M. Sakai, J. Phys. Soc. Japan **5**, 178–187 (1950).

Invited Papers

E8. The Inter-University High Altitude Laboratory and Atmospheric Research. B. E. COHN, *University of Denver.* (30 min.)
E9. High Altitude Solar Studies. W. B. PIETENPOL, *University of Colorado.* (30 min.)

FRIDAY MORNING AT 9:00

Room 45, Chemistry Building

(R. E. HOLZER presiding)

Contributed Papers

F1. Instrumentation for High Altitude Infrared Solar Measurements.* ROMUALD ANTHONY, *U. S. Naval Ordnance Test Station* (introduced by E. V. Ashburn).—In order to obtain solar infrared spectra in the 1 to 25 micron region at high altitudes, a potassium bromide double monochromator ordinarily used in the laboratory was installed in a B-29 aircraft. The behavior of the aircraft in flight and the delicate nature of the monochromator determined the design of the accessory apparatus. The monochromator was suspended in a cradle. The cradle was a portable structure containing all the reflecting optics necessary to direct the solar radiation received from the heliostat and focus it on the entrance slit of the monochromator. Approximately 25 minutes was required to scan the spectrum; therefore, a simple photo-cell heliostat was constructed to compensate for roll, yaw, and pitch of the aircraft as well as the motion of the sun in the sky. The heliostat, which could be operated manually, was an "off-on" dc system that controlled the direction of the incoming solar radiation by responding to the displacement of a solar image relative to four photo-cells. It performed the task of maintaining the solar image on the slit to ±2 mils during flight. Considerable variation in temperature was expected with change in altitude; therefore, an electric blanket was built to cover the monochromator and keep it at constant temperature. The total temperature change during flight did not exceed 2°F.

* Program supported by the ONR and in collaboration with Johns Hopkins University.

F2. The Density of the Upper Atmosphere and the Intensity of the Zenith Sky Light during Twilight.* EDWARD V. ASHBURN, *U. S. Naval Ordnance Test Station.*—An improved numerical treatment of the application of the Rayleigh scattering law to the atmosphere during twilight has been developed. This new treatment, combined with new measurements of the intensity and polarization of the zenith sky light has led to a determination of the density of the atmosphere to a height of 120 km. The results are in agreement with the U. S. Tentative Standard Atmosphere of the N.A.C.A.

* This work supported by the ONR.

F3. Aerosol Particle Size Studies using Natural Radioactivity as a Tracer. M. H. WILKENING, *New Mexico School of Mines, Socorro, New Mexico.*—Apparatus has been built

which (1) ionizes aerosol particles in an incoming air stream, (2) separates the resulting ions according to their mobilities, and (3) deposits them on a collecting surface. One can then study this distribution by means of the natural radon disintegration products which are present in an aerosol particle collection. The collection is on the outer electrode of a cylindrical condenser carrying an axial air stream, the ion-bearing air being introduced in a layer around the inner electrode. The distribution of radioactivity along the outer electrode is determined by a grid-type proportional counter. Knowing the air flow, the electric field and the geometry of the condenser, a value can be computed for the mobility of the ions deposited on any section of the electrode. The mobility is correlated with particle size by use of Stokes' Law with the Cunningham correction. Preliminary results indicate that most of the natural radioactivity in the atmosphere resides on particles in the size range 0.001 to 0.03 micron and that particles in this size range are far more abundant than larger ones.

F4. Boundary-Value Problems of Transverse Waves. WALTER M. ELSASSER,* *University of Utah.*—In textbooks of electrodynamics there are described transverse (nondivergent) solutions of the vector wave equation. The components of each such wave are expressions containing one corresponding solution of the scalar wave equation and its derivatives. We have studied the boundary conditions for which these transverse waves form a complete orthogonal set over a suitable finite domain. We find such sets to exist for only two types: Plane waves with cyclic boundary conditions in Cartesians, and spherical waves with some simple linear boundary conditions at a spherical surface. Even for a cylinder of finite cross section and either infinite or finite length, orthogonality of the "natural" set of cylindrical transverse waves cannot be achieved solely by the application of linear boundary conditions. Thus, it seems that the Sturm-Liouville scheme, so successful for scalar waves, is really of little avail for transverse waves, and new mathematical methods ought to be developed to deal with them and their physical applications.

* Supported by Contract N-7-ONR-388 with the Institute for Advanced Study in Princeton.

F5. A Magnetic Suspension for Vertical Seismometers. C. R. HOLMES AND E. J. WORKMAN, *New Mexico School of Mines.*—In any seismological problem where it is desirable to record low frequency oscillations with a displacement meter, the main difficulty is to obtain reliable spring suspensions having a sufficiently long period. The nonlinear properties that result from the conventional use of springs are discussed. The authors have devised an electromagnetic suspension which eliminates many of these disadvantages. A cylindrical coil which is constrained to move along its vertical axis intercepts a radial magnetic field in such a way that the mass is supported with a "spring" stiffness factor which can be made small enough so that the sprung mass is in effect a free inertia mass. The net forces acting upon the mass thus supported may be adjusted by a variety of methods in order to give the desired characteristics of oscillation. The pick up may be a second coil acting on the same magnetic field, or a second magnetic field, or a number of displacement or velocity measuring devices, some of which are discussed. This type of a suspension makes it possible to control the zero position automatically without introducing restoring forces that would give rise to undesirable oscillations.

FRIDAY AFTERNOON AT 2:00

Room 19, Chemistry Building

(R. F. BACHER presiding)

Contributed Papers

G1. The Elastic Scattering of Protons by Oxygen.* R. A. LAUBENSTEIN,† M. J. W. LAUBENSTEIN, R. C. MOBLEY, AND L. J. KOESTER,‡ *University of Wisconsin.*—The yield of elastically scattered protons from oxygen has been measured using a magnetic analyzer which detected protons scattered through laboratory angles of 159° to 169°. The proton energy range from 0.6 to 4.5 Mev was covered in 4.4-kev steps using protons from the Wisconsin electrostatic generator. Targets of BaO on 1000A nickel foil and on diamonds were used. At 2.66-Mev proton energy a resonance was observed with a width of 20 kev and at 3.47 Mev a resonance was observed with a width less than 3 kev. Near 4.0 Mev a broad maximum in the scattering cross section was obtained and a broad resonance appears to give another maximum slightly over 4.5 Mev. The resonance at 2.66 Mev was obtained as a nearly symmetrical dip in the scattering cross section. An analysis of part of the data in terms of potential scattering theory has been made.

* Work supported by the AEC and the Wisconsin Alumni Research Foundation.
† Now at North American Aviation, Inc.
‡ AEC Predoctoral Fellow.

G2. Capture of Protons by Oxygen.* M. J. W. LAUBENSTEIN, R. A. LAUBENSTEIN,† L. J. KOESTER,‡ AND R. C. MOBLEY, *University of Wisconsin.*—The capture cross section of oxygen for protons has been measured for incident proton energies from 1.4 to 4.1 Mev by counting the positrons from the decay of the F^{17} built up under the bombardment of oxidized tantalum targets. A method for compensating for fluctuating beam current was used and aluminum absorbers were used to prevent the counting of positrons from F^{18}. The cross section increases almost linearly with proton energy up to a maximum at 4 Mev except for a sharp resonance at 3.47 Mev. The effect of the level at 2.66 Mev was not detectable within the experimental error. The half-life of F^{17} was measured as 66.3±1 sec. An estimate of the beta-ray end point obtained from absorption measurements gave 1.75±0.2 Mev. The correspondence of the levels in F^{17} and its mirror nucleus O^{17} will be shown.

* Supported by the AEC and the Wisconsin Alumni Research Foundation.
† Now at North American Aviation, Inc.
‡ AEC Predoctoral Fellow.

G3. Some Pair-Theoretic Applications of the Dispersion Relation. JOHN TOLL AND JOHN A. WHEELER, *Los Alamos Scientific Laboratory and Princeton University.*—Analyzing different formulations of conditions for validity of the dispersion formula relating absorption and refraction of light, especially the condition that no wave be scattered before arrival of the primary wave (Kronig) we conclude: it is reasonable to apply the dispersion formula for arbitrarily high fre-

quencies. (1) From the Breit-Wheeler formula for pair *production* by two photons, the dispersion relation yields for all frequencies the cross section for forward *scattering* of light by light, and agrees with high and low frequency limits of Achieser, and Euler and Kockel, respectively. (2) We calculated the linear *absorption* coefficients for light in vacuum polarized by a uniform and static electromagnetic field. The dispersion relation then yields for all frequencies the *refractive index* of a polarized vacuum. (3) From the field Lagrangian of Heisenberg and Euler, we compute the refractive index of low frequency light in vacuum polarized by sinusoidally varying or constant background field. Results agree with (1) and (2). Reversing the reasoning gives the fourth-order terms in the Lagrangian without employing difficult fourth-order subtraction-theoretic calculations used by Heisenberg and Euler.

G4. Bases for an Estimate of Coherent Gamma-Ray Scattering. JOHN A. WHEELER AND JOHN TOLL, *Los Alamos Scientific Laboratory and Princeton University.*—Employing the dispersion formula (preceding paper), one can estimate coherent gamma-ray scattering. (a) The equivalent oscillator strength in each elementary frequency interval is found from known or estimated absorption at that frequency. (b) The amplitude of the elementary wave scattered in the forward direction is accurately given by the dispersion formula. (c) Elementary waves decrease at other angles according to a form factor which is suitably estimated: (i) for photoelectric and Compton processes from known atomic wave functions; (ii) for nucleonic processes from available information on relative strengths of dipole and quadrupole transitions; (iii) for mesonic absorption, assuming dipole transitions and adopting for individual nucleons two extreme pictures of a region of absorption of negligible extent and of extent of the mesonic wavelength, and combining contributions of the nucleons in accordance with a nuclear-radius-dependent form factor; (iv) for pair production, from Williams-Weizsäcker picture of space localization of pair creation processes. One thus finds approximate dependence of coherent scattering upon atomic number, gamma-ray energy, and scattering angle. One cannot exclude the possibility that new absorption processes enter at still higher frequencies which contribute to gamma-ray scattering even in the Mev region. Hence measurements of the coherent scattering would be most interesting.

G5. Cross Sections of Thermonuclear Reactions. W. A. FOWLER, *Kellogg Radiation Laboratory, California Institute of Technology.*—An analysis of the experimental data on the cross sections at low energies of the thermonuclear stellar reactions has been made. The results yield the empirical constant, a, in an expression for the cross section of the form $\sigma=(a/E_1)\exp(-0.989\ Z_0Z_1M_1^{\frac{1}{2}}E_1^{-\frac{1}{2}})$ where E_1 is the energy of the incident particle in Mev and M_1 is its mass in amu. In the direct proton-proton cycle it is believed that the cycle is most probably completed by the reaction $He^3(He^3, 2p)He^4$ and a value for a for this reaction is estimated using $\Gamma_p\sim 0.1$ Mev. This would suggest an abundance ratio of $He^3/He^4\sim 10^{-4}$ for conditions at the center of the sun. The values for a in Mev-barns are as follows: $C^{12}(p,\gamma)$, 2.0×10^{-3}; $C^{13}(p,\gamma)$, $\geq 10^{-4}$; $N^{14}(p,\gamma)$, 2.5×10^{-4}; $N^{15}(p,\alpha)$, 110; $N^{15}(p,\gamma)$, 10^{-2}; $H^1(p,\beta^+)$,[1] 2.6×10^{-23}; $D^2(p,\gamma)$, $3.1(1+40E_1)\times10^{-7}$; $He^3(He^3, 2p)$, ~ 2. This work was assisted by the joint program of the ONR and AEC.

[1] E. E. Salpeter, private communication.

G6. Performance of a High Energy Linear Electron Accelerator.* R. F. POST AND N. S. SHIREN, *Stanford University.*—The operating characteristics of the Stanford "Mark II" accelerator will be described. This accelerator, the second linear accelerator to be constructed at Stanford, was designed to be a prototype of the sections of the Bev machine now under construction. The Mark II accelerator tube is 12 feet in length and is designed to deliver a 1-microsecond pulse of 50-Mev electrons at the design power input. Performance to date is in good agreement with theory.[1] Energy spectra have been observed with about the expected shape and with peak energies in close agreement with the calculated values. With the available power (limited by power supply overloading) electrons up to almost 35 Mev have been observed, corresponding to an acceleration of 4.5 Mev per foot at the input end of the accelerator. Changes in peak energy with variations in power, frequency, and wave-guide temperature distribution will be discussed. This accelerator is in use for experiments in electron physics. Some of the problems arising in the use of this machine will be mentioned.

* The work reported herein was performed under a contract between Stanford University and the ONR.

[1] Ginzton, Hansen, and Kennedy, Rev. Sci. Instr. 19, 89 (1948).

G7. Theory of Errors in a Linear Electron Accelerator.* L. I. SCHIFF AND R. F. POST, *Stanford University.*—The effect of random constructional errors in the individual cavities of a linear electron accelerator is calculated and, where possible, the theory is compared with experiment. The particular case of traveling wave accelerators (such as those at Stanford) is considered in detail. Assuming the statistical independence of errors in the several unit cells of the accelerator wave guides it is shown that for single-feed operation, the expected minimized fractional energy loss is given by the expression

$$\frac{\delta W}{W}=\frac{1}{30}M\sigma^2,$$

where M is the number of unit cells and σ is the root-mean-square phase error increment per cell, measured in radians. The effects due to frequency variations and temperature gradients in the guide are calculated. It is shown that the traveling wave design exhibits marked insensitivity to errors and to such changes in operating conditions, in comparison with a separate resonator, standing wave type of acclerator.

* The work reported herein was performed under a contract between Stanford University and the ONR.

G8. Approximate Quantization of Nonlinear Bose Field. R. FINKELSTEIN, *University of California at Los Angeles* AND M. RUDERMAN, *California Institute of Technology.*—The addition of an invariant $-g\varphi^*\varphi\varphi^*\varphi$ to the usual Lagrangian for scalar bose fields yields a nonlinear differential equation. Viewed as a classical field equation, a discrete set of particle-like solutions can be found corresponding to positive, negative, or zero charge. This same state of affairs can be described quantum-mechanically in the configuration space formalism of Fock and Tomonaga. The state of the field is represented as a superposition of states with various numbers of plane wave bosons. Estimates can be made of the average number of bosons in the field and quantum fluctuations from this number. Finite quantum corrections to the classical mass spectrum can only be calculated by modifying the usual commutation rules.

G9. Nonlinear Spinor Fields. R. FINKELSTEIN AND R. LELEVIER, *University of California at Los Angeles* AND M. RUDERMAN, *California Institute of Technology.*—In view of the possibly fundamental role of spinor fields in the theory of matter (symmetric coupling between nucleons, muons, and leptons, and possibility of representing boson fields in terms of spinors) one may ask whether all the elementary particles may be described in terms of a single nonlinear spinor field. Lagrangian densities of the following type have been investigated: $L=aI_0+I_1+Q(I_0,\ I_1,\ J)$, where $I_0=i\varphi^+\varphi$, $I_1=(i/2)(\varphi^+\gamma_\alpha\partial_\alpha\varphi-\partial_\alpha\varphi^+\gamma_\alpha\varphi)$, Q is a simple nonlinear function, and J signifies other invariants constructed from the

sponor field. $Q=0$ corresponds to the usual Dirac Lagrangian. Typical cases studied are $Q=\epsilon I_0^2$ and $Q=\epsilon \sum_1^4 (\varphi^+\gamma_\alpha\varphi)^2$, the latter form corresponding to Rosenfeld-Møller meson theory. Classical solutions of the field equations, having simple angular and temporal dependence, and depending on only two radial functions, the usual large (F) and small (G) components, were obtained subject to the boundary conditions that the fields be regular and that all observable integrals be finite. These b.c. lead to a nonlinear eigenvalue problem, best described in the $F-G$ plane; in this plane a complete qualitative discussion of the nature of the solutions can be given. Numerical solutions were obtained with a differential analyzer. If the charge, spin, and mass are defined in terms of $\int s_4 d\mathbf{x}$, $\int M_{\alpha\alpha} d\mathbf{x}$, and $\int T_{44} d\mathbf{x}$, respectively, then the number of masses corresponding to the same charge turns out to be small in all cases investigated. In one case there are three masses, all having the same spin and charge, but these do not correspond to electron, muon, and nucleon. A noteworthy feature of results is that in certain cases the nonlinearity leads to solutions having positive mass *only*; in that case the formalism of hole theory would be unnecessary.

G10. A Device to Assist Injection into Betatrons. LEVERETT DAVIS, JR., *California Institute of Technology*.—An electron in a betatron or synchrotron oscillates about the steady-state orbit; i.e., the orbit that closes in one revolution. This orbit is rarely precisely a circle. In order that the electrons not be removed from the beam by striking the injector within the first few revolutions, it is necessary either that the oscillations be damped or that the steady-state orbit be shifted away from the injector during injection by some significant change in the situation. A variety of suitable changes have been proposed at various times. It is here proposed that a possible procedure would be a transient bending on the steady-state orbit in the neighborhood of the injector. Transient magnetic or electric fields, established before the start of injection and removed during injection, could sweep the steady-state orbit and the circulating electrons from a displaced path close to the injector at the start of injection to the normal position farther away at the end of injection. The amount of difficulty required to produce properly adjusted auxiliary fields has not been investigated carefully. However, this procedure should facilitate the use of doughnuts of minimum cross section except for a short enlargement near the injector.

G11. Scattering of Magnetic Poles by Atomic Nuclei. KENNETH FORD AND JOHN A. WHEELER, *Los Alamos Scientific Laboratory and Princeton University*.—The nucleus is assumed very heavy compared to the pole. The pole is treated relativistically by the Klein-Gordon equation. The interaction problem is comparable with that of Rutherford scattering in symmetry and elegance. These features drew our attention to the problem more than any belief in the existence of poles. The differential cross section times the square of the momentum is independent of the mass of the pole and of its velocity and varies at small angles much as the Rutherford cross section. At larger angles we find from a classical calculation certain characteristic singularities in the cross section at the "rainbow angles" 140.1°, 156.7°, 163.5°, . . ., independent of the integer n = (nuclear charge in units e)×(pole strength in units $137e/2$). The solution of the quantum-mechanical problem has been given as a formal series by Banderet. We have evaluated the series for $n=1, 2, 3$, where we find no trace of the classical singularities, and at $n=20$, where the angular distribution shows well-defined peaks near the first few rainbow angles. Generalizing, we conclude that scattering by heavy nuclei at certain universal angles is one characteristic of that quite possibly mythological entity, the magnetic pole.

G12. Zero-Zero Transition. S. D. DRELL, *Stanford University*.*—In the decay of a nucleus from an excited level of zero spin to a lower lying state of zero spin with no parity change, an orbital electron will be ejected from its path about the nucleus or, if the one excited level of the nucleus is higher than 2 mc^2 above the other level, an electron-positron pair may be created as well. Selection rules strictly forbid single gamma-emission. It is a unique property of these zero-zero transitions that the perturbing fields which induce the internal conversion or pair formation vanish identically outside of the nuclear radius.[1] Hence it is of particular interest to consider the effect of finite nuclear radius on the calculated rates of such processes. Presented here is a study of this effect. The K- to L-shell conversion ratio is independent of nuclear matrix elements. It is found to agree, within 10 percent, with the ratio as calculated for electrons in a point Coulomb field. Experimental data are employed to yield an approximate and reasonable value of $\frac{1}{4}(1.4\times10^{-13})^3 A^{\frac{1}{3}}$ cm^3 for the nuclear matrix elements for the zero-zero transitions in RaC′, O^{18}, and Ge^{73}.

* Work performed at Oak Ridge National Laboratories under the auspices of the AEC.

[1] R. H. Fowler, Proc. Roy. Soc. A129, 1 (1930). H. Yukawa and S. Sakata, Proc. Phys.-Math. Soc., Japan 17, 397 (1935).

G13. Scattering and Absorption of Gamma-Rays. S. T. COHEN, *Rand Corporation*, AND M. S. PLESSET, *California Institute of Technology*.—A formulation is presented of the scattering and absorption of gamma-rays which is suitable for radiological and shielding problems. For distances from a source small compared with the mean free path, only the unscattered and singly scattered beam need be considered. In this case, the results for the number of gamma-rays and the energy transmitted, as well as for the ionization produced, may be presented in useful and compact form. These calculations are compared with some experimental observations made on the transmission through air of gamma-rays of energy 3 mc^2. The transmission of gamma-rays through large thicknesses of materials is also discussed, and results for this case are presented for some light materials and for lead. These latter results are expressed in terms of a B-factor which is the ratio of total transmitted energy to the energy transmitted in the unscattered beam.

G14. Processing and Exposure of Electron-Sensitive Emulsion to High Energy Electrons and Positrons. CHARLES E. VIOLET, F. C. GILBERT, AND WALTER H. BARKAS, *University of California, Berkeley*.—In order to use sensitive emulsions for the study of electron interactions, it is necessary to erase the old tracks which interfere with the analysis. We have adopted a method suggested by J. Spence* for this purpose. The plates are kept at a temperature of 95°F in saturated water vapor for 60 hours just prior to use. This treatment eradicates virtually all the old electron tracks. After exposure the plates are developed using a modification of a procedure devised by Occhialini. With this development high energy electron tracks have a grain density of 40 grains/100 microns in G-5 emulsion. Tracks to be used in measuring mean free paths in emulsion for various electron and positron processes were produced by exposing G-5 plates in a magnetic pair spectrometer situated in the x-ray beam of the synchrotron. Separated electrons and positrons of 200, 100, 70, 40, and 20 Mev were recorded. This work was performed under the auspices of the AEC.

* Kodak Research Laboratory, Eastman Kodak Company.

G15. High Energy Electron Processes in Nuclear Emulsion. F. C. GILBERT, CHARLES E. VIOLET, AND WALTER H. BARKAS, *University of California, Berkeley*.—The existence of electron sensitive emulsions and a technique for eradicating accumulated background has made possible the study of high energy

electron and positron processes taking place within the nuclear emulsion. Tracks of magnetically separated electrons and positrons of 200-Mev energy produced by the synchrotron have been studied. The length of track scanned is recorded, and each measurable event is analyzed. The following processes have been observed: 1. Pair production by electrons and positrons, 2. electron-electron scattering, 3. positron-electron scattering, 4. nuclear scattering of electrons and positrons. The absolute cross sections for these processes are being determined. The results will be reported and photographs of events shown. This work was performed under the auspices of the AEC.

FRIDAY AFTERNOON AT 2:00

Room 45, Chemistry Building

(V. O. KNUDSEN presiding)

Contributed Papers

H1. Silver-Bearing Phosphate Glasses as Dosimeters. R. S. ALGER AND R. A. LEVY, *U. S. Naval Radiological Defense Laboratory* (introduced by R. I. Condit).—The fluorescence of certain silver-bearing phosphate glasses, which can be activated by exposure to x-rays, has been suggested as a basis of x-ray detection.[1] The x-rays reduce the silver ions to form impurity centers which make the glasses sensitive to ultraviolet excitation. The fluorescent yield has been measured as a function of x-ray dose for glasses containing up to 16 percent silver.[2] A piece of glass the size of a dime containing 8 percent or more silver will detect doses ranging from 25 to 2500 *r* at an effective x-ray energy of 100 kev. The fluorescent yield continues to increase after the x-ray exposure is terminated until a value is reached which is stable under moderate room illumination; however, direct exposure to sunlight, heat, or intense light reduces the fluorescent yield over a period of hours. Below 200 kev the fluorescent yield depends strongly on the effective energy of the x-rays. The maximum yield occurs at about 50 kev effective where the height of the peak is 15 times the value at 1 Mev.

[1] Wayle, Schulman, Gunther, and Evans, J. Electrochem. Soc. **95**, No. 2, 70 (1949).
[2] The glasses were furnished by Dr. J. Schulman of the Naval Research Laboratory, Washington, D. C.

H2. The Response of Geiger-Mueller Survey Instruments to Beta-Rays. E. TOCHILIN, A. B. WILLOUGHBY, AND P. R. HOWLAND, *U. S. Naval Radiological Defense Laboratory.*—G-M survey instruments have been investigated for their ability to measure correctly beta-rep doses over a range of beta-ray energies. Widespread laboratory employment of these instruments to assess tolerance doses of beta-radiation prompted this investigation. Theoretical considerations are presented which show that the number of counts recorded by a G-M tube for a given dose in rep units is proportional to: $E_{\beta_0}^{-1} \exp(-5.1g/E_{\beta_0}^{4/3})$ where g is the wall thickness of the tube in g/cm² and E_{β_0} is the average beta-ray energy. For a counter having negligible wall thickness the value of the exponent approaches unity and the number of counts per rep becomes proportional to the one third power of the average beta-ray energy. G-M instruments employing a cylindrical counter with a wall thickness of 30 mg/cm² and instruments employing an end-window counter with window thickness approximating 0 mg/cm² were investigated experimentally using beta-ray isotopes with maximum energies from 0.5 to 3.0 Mev. Absolute dose rates from the isotopes were obtained by extrapolation chamber measurements. Theoretical and experimental curves are presented for the two types of G-M instruments. In general, the rep response of both types of instruments agrees with predicted values.

H3. Current Carriers in Metals Exhibiting Positive Effects. SHELDON BROWN AND S. J. BARNETT, *California Institute of Technology and University of California, Los Angeles.*—Earlier direct measurements of e/m for the carriers in metals at normal temperatures have been made only on Cu, Ag, and Al, which have negative Hall coefficients, as predicted on the simple theories of conduction by (negative) electrons. A method suggested by Maxwell, but modified and first used with success by one of us[1] on copper, has now been further modified and extended to molybdenum and zinc, which have *positive* Hall coefficients. The existence of positive *carriers*, however, which would account simply for such coefficients, is apparently ruled out by the results of these experiments: Current and momentum of carriers are found to be oppositely directed even in metals having positive Hall coefficients. For both molybdenum and zinc the sign of e/m was found to be negative and the magnitude approximately identical with that for free electrons in slow motion. In experiments closely related to our own, but on *lead* (which also has a positive Hall coefficient at ordinary temperatures) Kikoin and Goobar[2] have shown that this material when in the *supraconducting* state gives the same value of e/m.

[1] S. J. Barnett, Phil. Mag. **12**, 349 (1931).
[2] Kikoin and Goobar, J. Phys. U.S.S.R. **3**, 333 (1940).

H4. The Attenuation of Ultrasonic Waves in Electrolytic Solutions.* O. B. WILSON, JR., *University of California, Los Angeles.*—The absorption coefficient for sound waves in several bivalent metal sulfates has been measured by a reverberation technique[1] over the frequency range 50–500 kc. In all cases studied, the measured absorption is larger than that which could be attributed to an increase in the shear viscosity coefficient. The absorption in $MgSO_4$ solutions is largest and is representable as a relaxation-type absorption in which the relaxation frequency lies within the range of these measurements. Graphs depicting the dependence of the absorption and relaxation frequency in $MgSO_4$ solutions upon the salt concentration and the temperature will be presented. Following Liebermann,[2] a possible explanation for these results will be discussed briefly in terms of a chemical equilibrium in the ionic solution which is perturbed by the passage of the sound wave.

* Research supported by Contract with the ONR, Contract N6 onr 27507.
[1] R. W. Leonard, Tech. Report No. 1, Project NR014-302, University of California, Los Angeles.
[2] L. N. Liebermann, Phys. Rev. **76**, 1520 (1949).

H5. Measurement of the Grazing Incidence Sound Field over an Absorbing Boundary. ROBERT B. LAWHEAD, *University of California, Los Angeles.*—Plane wave reflection theory has long been recognized as inadequate to explain grazing incidence propagation of electromagnetic or acoustic waves. The solution for the electromagnetic radiation from a vertically polarized dipole at the surface of a plane earth is now well known, and has received a great deal of attention

both theoretically and experimentally since the first work of Sommerfeld[1] in 1909. It was not until recently that the analysis used for the electromagnetic case was applied to the acoustic problem and a similar solution obtained.[2] This paper reports the results of measurements made in the frequency range 1–4 kc, using Fiberglas of three different densities as the acoustic boundary. With the sound source located at the boundary, the values of pressure amplitude and phase lag as a function of both receiver distance and height above the boundary show good agreement with theory.

[1] A. Sommerfeld, Ann. Physik **28**, 665 (1909).
[2] I. Rudnick, J. Acoust. Soc. Am. **19**, 348 (1947).

H6. The Absorption of Sound in Foggy Air at Low Audible Frequencies. YUNG TSIOH WEI, *University of California, Los Angeles* (introduced by L. P. Delsasso).—The anomalous sound absorption in water fog at low audible frequencies observed by Knudsen, Wilson, and Anderson has been further investigated by the method of standing waves. The theory on this effect given by Oswatitsch is critically examined and certain modifications proposed. Measurements were made in the frequency range of 25–250 cps for artificial fogs of several different concentrations and average droplet sizes. Artificial fogs produced by a water sprayer were introduced into the measuring tube and both droplet size and concentration measurements were made simultaneously with the acoustic measurements. The observed attenuation coefficients of the fog were computed from the ratios of the first pressure minimum to first maximum of the standing wave pattern with and without the fog. The maximum attenuation coefficients varied from 8.8 db/sec to 20.8 db/sec. The positions of maximum absorption were found to vary in the frequency range 35 to 50 cps. The calculated values based on both Oswatitsch's and the modified theory are compared with the experimental values. The experimentally obtained attenuation coefficients due to evaporation and condensation processes are found to be higher than those computed by both theories throughout the lower frequency range but in better agreement with the modified theory than with that of Oswatitsch.

H7. The Propagation of Sound in Carbon Dioxide Near the Critical Point. NEAL S. ANDERSON, *University of California, Los Angeles.*—The expression for the normal velocity of sound in a fluid becomes indeterminate at the critical point since the coefficient of elasticity tends to zero and the specific heat at constant pressure approaches infinity. An expression was obtained for the isentropic slope which does not become indeterminate at the critical point. A Pierce-type variable path acoustic interferometer was constructed to be placed completely inside a pressure tank with provisions for external control. The isothermal variation of velocity and absorption was measured as a function of pressure at 572 kc in carbon dioxide. The velocity variations agree with previously published results. The attenuation decreases steadily with increasing pressure and does show an abrupt rise as the critical point is reached which would be expected from critical fluctuation scattering. Using isotherm data the velocity at the critical point was calculated to be 198 meters per second. The experimental value obtained was significantly lower, being closer to the value of 148 meters per second which is obtained if van der Waals' equation of state is assumed.

H8. Measurements of Flame Speeds and Turbulence in a Mache-type Burner. F. H. WRIGHT, *Jet Propulsion Laboratory, California Institute of Technology.*—Combustion in a flowing system is known to be influenced by turbulence in the stream. How the turbulence exerts its influence is not known. Even the magnitude of the effect is uncertain because there are virtually no relevant experimental data. The measurements reported here do provide such data for one experimental configuration. The measurements were carried out in Mache-type burners (burner port dimension: 1×12, 2×12, 3×12, and 2×2 cm). Turbulence of variable intensity was produced by grids inserted upstream from the burner port. The turbulence in the stream with no combustion was measured with a hot wire anemometer. Flame speeds were measured both visually and photographically. The flame speeds were found to increase as the turbulence was increased. In fact, an approximately linear relationship was found to exist between the radio S_T/S_L and the dimensionless parameter v'/U. U is the mean speed of the stream, v' is the rms velocity of the cross component of the turbulence, S_T is the flame speed with turbulence v', S_L is the flame speed without turbulence. Within the accuracy of the measurements, so significant effect of side of burner or scale of turbulence was found.

H9. Growth of Critical Vapor Nuclei in Superheated Liquids. M. S. PLESSET AND S. A. ZWICK, *California Institute of Technology.**—A critical vapor nucleus is a vapor bubble for which the surface tension and the external pressure balance the vapor pressure at the given temperature so that any temperature rise of the liquid in which the vapor nucleus is situated causes the nucleus to grow. This growth is controlled by two factors: the inertia of the liquid, and the heat inflow requirements of evaporation to maintain the vapor pressure. The heat flow problem is of special interest since it represents a diffusion across a moving boundary. An approximate analytic solution for this diffusion problem has been found, and it is shown that the approximation is a good one. An analytic solution for the radius of the vapor bubble as a function of time has been derived which is valid for sufficiently large radius. This asymptotic solution covers the range of physical interest since the radius at which it becomes valid is near the lower limit of experimental observation.

* This study was supported by the ONR.

H10. A New Method for Measuring Transient Gas Densities. A. B. C. ANDERSON, *U. S. Naval Ordnance Test Station* (introduced by F. T. Rogers, Jr.).—A theoretical analysis of the dielectric properties of nonpolar gases (air, N_2, O_2, H_2, CO_2, Cl_4, CH_4, etc.) and an examination of available experimental data indicates, as pointed out elsewhere, that for such gases the dielectric constant is a linear function of the gas density alone. Over very wide ranges, the dielectric constant is independent of the particular values of temperature and pressure which determine the gas density. Thus, the capacitance of a capacitor with a gaseous dielectric is a linear measure of the density of the gas. The capacitance is independent of the gas pressure and temperature except as these are related to density by the gas law. Several capacitor pick-up arrangements are discussed for use as density pickups, and experimental data are presented for one of these, showing this type of instrument to be feasible. On the other hand, theoretical analysis of the dielectric properties of polar gases (H_2O, NH_3, HCl, H_2S, SO_2, etc.) shows that their dielectric constant depends on both density and temperature at ordinary capacitor excitation frequencies. It appears that the dielectric constant for all gases should be a linear function of the density alone.

H11. Factors Affecting Burning Rates of Solids. G. B. SHOOK, *U. S. Naval Ordnance Test Station.*—A differential equation for the burning of a solid is deduced from the thermal processes occurring within the solid, a general knowledge of the chemical processes, and the geometry. It is, for one-dimensional burning, $U_i = k^2 U_{xx} + A + B$, where $A = (\alpha I_0/c\rho) \times \exp(-\alpha x)$ and $B = (Hs/c)\exp(-E/RU)$ are heat sources within the solid due respectively to radiation absorption and the exothermic chemical reaction. Solutions of the above equation for $B = 0$ are obtained in closed form for boundary conditions pertinent to the ignition (i.e., incipient burning) and the burning periods. For the case $B \neq 0$, numerical methods

must be used. The effect of pressure, temperature, chemical reaction, and diffusion are discussed with respect to the parameters appearing in the mathematical model. In particular the absorption coefficient α, the radiant flux I_0 and the temperature of the burning surface U_1 are related to the gas density, temperature and geometry of the solid's environment, and it is shown that in some cases these factors may affect the predicted burning rate significantly.

H12. A Type of Fracture Produced in Steel by Explosive Attack. JOHN S. RINEHART, *U. S. Naval Ordnance Test Station, Inyokern.*—The phenomena of fracture are complicated and obscure. For this reason, Bridgman, among others, has encouraged workers in the field to acquire the broadest possible knowledge of the phenomena, particularly under extreme physical conditions. His studies, for example, on the effects of hydrostatic pressure on fracturing are well known. An equally fertile field for studies of fracture is that in which fracturing results from the application of the extremely high transient pressures that are produced by explosive charges. Among the more unexpected fractures, which occur in such cases, are those that can be attributed to the sudden release of the applied pressure. Several cases of this type of fracture have been observed in steel and are described. A quantitative treatment of the fractures in terms of known stress or strain distributions is not yet possible. Certain qualitative aspects of the stress distributions that probably exist during and immediately following application of the pressure are discussed and related to observe fracturing. Phenomenologically, the fractures seem to result from highly inhomogeneous stresses set up during application of the pressure, a volumetric expansion on load release, or a combination of both.

H13. Deceleration and Ionizing Efficiency of Meteors. D. W. R. MCKINLEY, *National Research Council, Ottawa,* (by title).—An improved technique for recording radar echoes from meteors has made it possible to determine the meteor deceleration in a few special cases. Three illustrative examples are described, with measured mean decelerations -0.48, -1.1, and -1.5 km sec^{-2}. Velocity data from a continuous-wave system were available for comparison with the radar observations. Using the present standard density values for the atmosphere at heights between 70 and 110 km, and adopting Lovell's scattering formula, it is computed that the ionizing efficiency, or the fraction of kinetic energy of the meteor converted to ionization, is 10^{-4} for a 60 km/sec meteor and 10^{-3} for a 20 km/sec meteor. With lower values of the air density the efficiency figures are increased, and the gap is narrowed between the rates of electron production deduced from loss of mass considerations and the rates calculated from the radar information. New data on the ionizing properties of 1000-ev atoms, and more radar observations are required before definite conclusions can be drawn regarding the upper air density and temperature.

H14. Optimum Source Size for the Mach-Zehnder Interferometer. F. D. BENNETT, *Ballistic Research Laboratories, Aberdeen Proving Ground, Maryland,* (by title).—A vector analytic treatment is given of the formation of undisturbed fringes by an ideal Mach-Zehnder interferometer with an extended source. The path difference of two interfering rays at an arbitrary point in the field is found to depend in a simple way upon the source point from which the rays originate, the field point examined, and a dyadic which is a function of the unit normals to the last mirror and divider plate of the interferometer. The fringe clarity condition that all pairs of interfering rays reaching the field point have path differences within a specified range is developed in the form of an inequality. Analysis of this fundamental inequality shows that all admissible area sources must be areas enclosed between two conics in the source plane. For fringes normal to the plane of centers of the interferometer elements, the optimum source is a circle with radius inversely proportional to the square root of the number of clear fringes desired. This result holds for all interferometers of parallelogram planform. For fringes parallel to the plane of centers, each interferometer orientation presents a special case. The optimum source area is obtained for two of these, *viz.*, the 45° and 30° interferometers.

SATURDAY MORNING AT 9:00

Room 147, Business Administration and Economics

(C. C. LAURITSEN presiding)

Invited Papers

I1. Ozone in the Earth's Atmosphere. VICTOR H. REGENER, *University of New Mexico.* (30 min.)

I2. Some Observations Bearing on the Physical Basis for Cloud Seeding. E. J. WORKMAN, *New Mexico School of Mines.* (45 min.)

I3. Nuclear Models and Nuclear Fission. JOHN A. WHEELER, *Los Alamos Scientific Laboratory and Princeton University.* (45 min.)

SATURDAY AFTERNOON AT 2:00

Room 19, Chemistry Building

(E. H. PLESSET presiding)

Contributed Papers

J1. Radiations from Chlorine 34 (33 Min.). LAWRENCE RUBY AND J. REGINALD RICHARDSON, *University of California, Los Angeles.*—The spectrum of Cl^{34} has been studied in a large magnetic lens beta-ray spectrometer calibrated with the 661.4-kev internally converted gamma-ray of Ba^{137}. Zah-Wei Ho,[1] using a cloud chamber, obtained a gamma-ray of 3.4 Mev

and two groups of positrons with end points at 5.1 and 2.4 Mev. The activity was produced in the UCLA cyclotron by $S^{34}(p, n)Cl^{34}$ and by $Cl^{35}(p, pn)Cl^{34}$. The shape of the positron distribution and the fact that the Kurie plot could not be resolved into two components indicated the existence of three groups of beta-particles. Internal conversion electrons corresponding to a gamma-ray of 145±3 kev have been found. The decay of this line has been followed in the spectrometer for three half-lives to verify its origin in Cl^{34}. In addition, the *L* photo-electron spectrum has been observed. From Compton electrons produced in a Cu converter, two further gamma-rays have been identified. A tentative decay scheme which associates one gamma-ray with each group of beta-particles is summarized below. The maximum beta-energies have been determined from a Kurie plot.

Maximum beta-energy in Mev	Gamma-energy in Mev	Total
4.45±0.11	0.145±0.003	4.60±0.11
2.58±0.26	2.13 ±0.12	4.71±0.38
1.3 ±0.2	3.30 ±0.14	4.6 ±0.3

This research was supported in part by the joint program of the ONR and AEC.

[1] Zah-Wei Ho, Phys. Rev. **70**, 782 (1946).

J2. The Absolute Energy Loss of 18-Mev Protons in Various Materials. DONALD C. SACHS AND J. REGINALD RICHARDSON, *University of California, Los Angeles.*—It has been possible by use of a thorium scatterer and magnetic analysis in the magnetic field of the UCLA cyclotron to produce a small beam of 18-Mev protons monoenergetic to 0.15 percent. This is accomplished by 180° focusing and momentum selection. At the 180° point, the beam may be made to pass through a thin metallic foil, and then it is focused through an additional 180° to a movable slit above but near the original thorium scatterer. The displacement of the 360° focus caused by the presence of the metallic foil is a measure of the absolute energy loss in the foil. The experimental results show that the absolute energy loss in 0.006 in. of aluminum, for example, is determined to better than ±1 percent. This allows the determination of the "mean" ionization energy *I* to ±5 percent. This research was supported in part by the joint program of the ONR and AEC.

J3. Maximum β^+ Energy From Na^{21}. GLEN E. SCHRANK AND J. REGINALD RICHARDSON, *University of California, Los Angeles.*—A 180° β-ray spectrometer was used to measure the maximum energy of the 23-sec positron activity in Na^{21}, a member of the mirror nucleii series. The sample was prepared from the reaction $Mg^{24}(p, x)Na^{21}$ by bombarding a foil of pure Mg with 18.5-Mev protons. At this proton energy, the (p, n) reaction produces two activities, Al^{28} and Al^{24}, but since these both have half-lives of about 7 sec, a waiting period of 60 sec was sufficient to allow these activities to disappear. After this interval only the 23-sec activity could be detected. The intensity was sufficient to allow the determination of decay curves for two values of momentum for each sample. In this way a series of bombardments was made and combined in order to give an extrapolated Kurie plot upper limit of E max-2.53 ± 0.02 Mev. This is to be compared with the value 2.56 Mev calculated from the difference in the Coulomb repulsion terms of the mirror nuclei, using $R=1.42\times10^{-13}A/$cm.[1] This research was supported in part by the joint program of the ONR and AEC.

[1] Rosenfeld, *Nuclear Forces*, p. 383.

J4. An Experimental Determination of the Range of 18-Mev Protons in Aluminum. E. L. HUBBARD AND K. R. MACKENZIE, *University of California, Los Angeles.*—The circulating proton beam in the 41-in. FM cyclotron was scattered upward by a 14-mil strip of thorium placed inside the dee. The energy was defined by the Th strip, a 0.25-in. slit at 139°, and a 20-mil slit at 170°. The magnetic field along the path was plotted with a nuclear magnetic resonance probe and the energy determined by graphical methods. Part of the 10^{-11} amp beam current that passed through the slits was collected by a 452.94 mg/cm² Al plate and part by a cup behind it. The current was measured with an electrometer tube. Fine adjustments of the effective thickness of the Al plate were made by placing thin Al foils in front of it. The mean range is the thickness for which the currents collected by the plate and the cup are equal. A preliminary result gives a range of 476.5±5.0 mg/cm² for an energy of 18.00±0.10 Mev. It is expected that the limits of error will be reduced by a factor of 5. This research was supported in part by the joint program of the ONR and AEC.

J5. Isomers in Cr and Mn. DAVID O. CALDWELL* AND HUGH F. STODDART, *Los Alamos Scientific Laboratory.*—Two activities ascribable to isomeric states in 29-neutron nuclei, have been found, one of which might serve as a test among nuclear shell structure theories. The activity in Cr variously described [1–3] as having a half-life of 1.3 to 2.3 hr has recently been shown[4, 5] not to be due to Cr^{55}. This disputed activity has been produced by activating normal and enriched (in Cr^{52}) Cr, both by 10-Mev deuterons and by thermal neutrons. The activity being stronger in the enriched targets indicated that the negatrons being counted were conversion electrons from an excited state in Cr^{52}. The second activity is a 2.1-min negatron, ascribed to an excited state in Mn^{54}, because of the ratio of activities in normal and enriched (in Fe^{54}) Fe after bombardments by 14-Mev neutrons and 10-Mev deuterons.

* Now at UCLA.
[1] Dickson, McDaniel, and Konopinski, Phys. Rev. **57**, 351 (1940).
[2] Amaki, Iimori, and Sugimoto, Phys. Rev. **57**, 751 (1940).
[3] Seren, Friedlander, and Turkel, Phys. Rev. **72**, 888 (1947).
[4] M. E. Nelson and M. L. Pool, Phys. Rev. **77**, 682 (1950).
[5] D. R. Miller, Phys. Rev. **78**, 808 (1950).

J6. Deuteron-Proton Scattering at 190 Mev. A. L. BLOOM AND M. O. STERN, *University of California, Berkeley.*—The differential cross section for elastic scattering of 190-Mev deuterons on protons has been measured at several angles, using the external deuteron beam of the 184-in. Berkeley cyclotron. A coincidence counting method was used, in which two stilbene scintillation counters were placed so as to count the scattered protons and deuterons simultaneously. The deuteron counter was large enough to count the deuteron corresponding to any proton that entered the proton counter. The target was polyethylene, alternating with a carbon target to measure background. The results show maxima in the backward and forward directions, corresponding to exchange effects and the pick-up process, in agreement with the theoretical predictions of Chew.[1] This work is sponsored by the AEC.

[1] G. F. Chew, Phys. Rev. **74**, 809 (1948).

J7. Cross Sections for $S^{32}(\gamma, n'p)P^{30}$ and $Rb^{87}(\gamma, \alpha)Br^{83}$ Reactions. E. L. HARRINGTON, L. KATZ, R. N. H. HASLAM, AND H. E. JOHNS, *University of Saskatchewan.*—Cross-section curves for the gamma-deuteron reaction in S^{32} and the gamma-alpha-reaction in Rb^{87} have been determined by analysis[1] of the activation curves of the resulting nuclides. The observed threshold for the (γ, d) reaction which leads to a pure 2.55-min P^{30} activity is 19.15±0.20 Mev, in good agreement with the value calculated from known reaction energies.[2] The cross-section curve may be interpreted as a superposition of curves for a (γ, d) and a (γ, np) reaction. The half-width of the combined cross section is about 3 Mev, with peaks at 24 and 26 Mev. The integrated cross section is 4.1×10^{-3} Mev-barn. In the case of $Rb^{87}(\gamma, \alpha)Br^{83}$ a chemical separation is necessary to isolate the weak 140-min bromine activity. Measurable activities were first observed at 16 Mev. The cross-section

curve has a maximum at 22.5 Mev, half-width of 6.6 Mev, and the integrated cross section is 4×10^{-4} Mev-barn. Arguments in support of the reaction $Rb^{87}(\gamma, \alpha)$ rather than $Rb^{85}(\gamma, 2p)$ are advanced.

[1] Katz, Johns, Douglas, and Haslam, Phys. Rev. **80**, 131 (1950).
[2] A. S. Penfold, Phys. Rev. **80**, 216 (1950).

J8. Proton-Proton Scattering in the Energy Range 120 to 345 Mev. O. CHAMBERLAIN, E. SEGRÈ, AND C. WIEGAND, *University of California, Berkeley.*—Previously reported[1] measurements on the differential scattering cross section in proton-proton collisions have been refined with the use of stilbene scintillation counters and coincidence circuits with short (2×10^{-8} sec) resolving time. Some measurements have been made at energies lower than 345 Mev by placing lithium absorbers in the proton beam of the 184-in. Berkeley cyclotron. The most remarkable feature of the results is that in all cases the differential scattering cross section in the center-of-mass system is between 3.6×10^{-27} and 4×10^{-27} cm^2 sterad^{-1}. The energies studied and the range of angles included are as follows: 345 Mev (36° to 90°); 249 Mev (48° to 90°); 164 Mev (60° to 90°); 119 Mev (63° to 90°). In all cases the energies are those of the laboratory coordinate system, while the angles (and differential cross section) are those of the center-of-mass system.

[1] O. Chamberlain and C. Wiegand, Phys. Rev. **79**, 81 (1950).

J9. Elastic Scattering Survey Experiment. J. W. BURKIG AND BYRON T. WRIGHT, *University of California, Los Angeles.*—With equipment similar to that of Fulbright,[1] the elastic scattering cross section for 18.4-Mev protons at 79° of eleven elements was measured relative to W. The resulting values for Al, Fe, Ni, Cu, Pd, Ag, Sn, Ta, W, Pt, Au, and Pb were 0.53, 0.15, 0.17, 0.30, 0.53, 0.49, 0.38, 1.0, 0.92, 1.2, 1.3, 1.5 respectively. The probable error in these ratios varies from six percent to nine percent. For Al, Ni, Pd, and W relative angular distributions with points every 15° from 26° to 106° were obtained. For W the distribution decreases monotonically and a plot of $\log\sigma$ *versus* $\log\theta$ approximates a straight line whose slope is $b=-4.7$ as compared to a slope $b=-3.5$ for Rutherford scattering, using the expression $\log\sigma=a+b\log\theta$. Thus the observed angular dependence decreases faster than the Rutherford dependence. Pd has local variations as large as ±50 percent around Rutherford dependence. For $\theta>50°$ Ni and Al distributions decrease slower than the Rutherford curve and have variations up to ±50 percent about their average angular dependence. This research was supported in part by the joint program of the ONR and AEC.

[1] H. W. Fulbright and R. R. Bush, Phys. Rev. **74**, 1323 (1948).

J10. Alpha-Spectrum of $Li^8(\beta)2\alpha$ and $B^{11}(p, \alpha)2\alpha$ Reactions. C. W. LI AND WARD WHALING, *Kellogg Radiation Laboratory, California Institute of Technology.*—There is evidence for the formation of a broad state in Be^8 of about 3-Mev excitation in at least 6 different nuclear reactions. The poor agreement between the excitation energy and width of this level observed in different reactions suggests the possibility of some structure. We have measured the energy spectrum of the alpha-particles from the two reactions (1) $Li^8(\beta)2\alpha$ and (2) $B^{11}(p, \alpha)2\alpha$ with a high resolution magnetic spectrograph and find no evidence of any structure in either reaction. The Li^8 was produced by deuteron bombardment of thin Li targets on thin Be foils, total thickness 0.7 mm air equivalent. After correcting the observed spectrum for the energy loss in the target, the peak in the alpha-spectrum is at $E_\alpha=1.52\pm0.02$ Mev and the width at half-maximum is 0.8 Mev. For reaction (2) thin targets of B_2O_3 on Cu were used. At a proton bombarding energy of 1.00 Mev and an angle of observation of 89.3 degrees, the peak in the alpha-spectrum is at $E_\alpha=4.37\pm0.02$ Mev and the width at half-maximum is 0.75 Mev. The experimental data must also be corrected for the motion of the center of mass and barrier penetration; however a preliminary analysis would indicate that possibly two different levels in Be^8 are involved in the two reactions. In reaction (2) a narrow alpha-line was observed corresponding to the formation of Be^8 in its ground state. The intensity of this weak group is 1/35 the intensity of the group corresponding to the formation of Be^8 in the 3-Mev excited state. This work was assisted by the joint program of the ONR and AEC.

J11. Interation of *S*-Wave Neutrons and Protons with C^{13}. R. G. THOMAS,* *Kellogg Radiation Laboratory, California Institute of Technology.*—In determining the reduced width of the *s*-wave $C^{13}(p, \gamma)N^{14}$ resonance at 0.456 Mev it is necessary to take into account the variation of the level shift with respect to energy. When this is done a value $\gamma^2\approx\hbar^2/Ma$ is obtained. This value is about equal to the reduced width expected for a simple one-body type of interaction. The reduced width of the low energy neutron *s*-wave scattering by C^{13} is also equally large. This width is determined by fitting a one-level dispersion curve, including potential scattering, to the neutron scattering data up to 2 Mev. In view of the large reduced widths of these interactions it is appropriate to analyze the data by means of the effective range theory. By taking the 3.10-Mev level in C^{13} as the bound state associated with the low energy neutron scattering, a scattering length of $6.1\cdot10^{-13}$ cm and an effective range of $3.0\cdot10^{-13}$ cm are obtained; with these parameters a good fit to the scattering data is obtained. The range and scattering length for the proton interaction, as determined from the gamma-ray and elastic scattering[1] experiments, are compared with the neutron interaction parameters. There is agreement within the uncertainties. The main difficulty in making a quantitative comparison is the lack of accurate knowledge of the Coulomb interaction for the proton within the nucleus.

* AEC Pre-doctoral Fellow.
[1] Goldhaber, Williamson, Jackson, and Laubenstein (to be published).

J12. *Q*-Values of the $Li^7(p, \alpha)\alpha$ and $Be^9(d, \alpha)Li^7$ Reactions. WARD WHALING AND C. W. LI, *Kellogg Radiation Laboratory, California Institute of Technology.*—The energy of the α-particles from the (1) $Li^7(p, \alpha)\alpha$ and (2) $Be^9(d, \alpha)Li^7$ reactions has been measured with a double-focusing 180° magnetic spectrograph. Both thick and thin metallic targets were used. Results have been corrected for the energy loss of incident and emitted particles in surface layers of C and O that appear on the target during bombardment. The spectrograph was calibrated against natural α-particles of energy close to the energy of the emitted particles, ThC′ for reaction (1), Po for reaction (2). Using exact masses and making appropriate relativistic corrections, $Q_1=17.338\pm0.011$ Mev, $Q_2=7.151\pm0.010$ Mev, where the probable error is calculated from various experimental uncertainties, principally in the angle of observation $89.3\pm0.2°$. Combined with the *Q*-values for the $Be^9(d, p)Be^8$ and $Be^9(\alpha)\alpha$ reactions, which have recently been measured with a magnetic spectrograph,[1] these *Q*-values give the α-particle mass in terms of the deuteron mass. Using 2.014723 ± 0.000004 for the mass of deuterium, we find for the mass of He^4 4.003840 ± 0.000018. This value, 0.060 mmu lower than the previously accepted value, is in excellent agreement with Ewald's[2] recent mass spectroscopic determination. This work was assisted by the joint program of the ONR and AEC.

[1] Tollestrup, Fowler, and Lauritsen, Phys. Rev. **78**, 372 (1950).
[2] H. Ewald, Z. Naturforschung **5A**, No. 1, 5 (1950).

J13. Excitation of the Reaction $C^{13}(p, \gamma)N^{14}$.* J. D. SEAGRAVE, R. B. DAY, AND J. E. PERRY, JR., *California Institute of Technology.*—An electrostatic accelerator has been used to obtain excitation functions between 400 and 2700 kev for the reaction $C^{13}(p, \gamma)N^{14}$. A thick target was made of C^{13}

enriched lampblack, and 1 to 20 kev thin targets were prepared by "cracking" enriched methyl iodide vapor on tantalum strips. Four previously unreported resonances have been located at $E_p = 1.16$, 1.3, 1.76, and 2.1 Mev. The resonance at 1.76 Mev exhibits a thick target yield 2.4 times that due to the well-known resonance at 0.554 Mev. Preliminary estimates are $\Gamma \leq 2$ kev and $\sigma \geq 3.5 \times 10^{-26}$ cm² at 1.76 Mev. The resonance centered at 1.3 Mev has a width of 600 kev and a thick target yield 1.6 times that due to the 0.554-Mev resonance. Coincidence counter measurements of the range of secondary electrons have been made at each resonance, and indicate that the transition to the ground state does not predominate at 1.16 and 2.1 Mev, as it does at 0.55 and 1.76 Mev. Assignment of these resonances to $C^{13}(p, \gamma)N^{14}$ has been confirmed by comparison with the yield of a thin target of normal carbon (1.1 percent C^{13}). This work was assisted by the joint program of the ONR and AEC.

J14. Angular Distributions of the γ-Rays from C(pγ). R. B. DAY AND J. E. PERRY, JR., *Kellogg Radiation Laboratory, California Institute of Technology.*—The angular distributions of the γ-rays from $C^{13}(p\gamma)$ at the 1694-kev resonance ($\Gamma = 70$ kev) and from $C^{13}(p\gamma)$ at the 1754-kev resonance ($\Gamma \leq 2$ kev) have been investigated. The detecting apparatus consisted of G-M counters in coincidence mounted on a frame that could be rotated about an axis through the target. The angular distributions have the form $1 + a\cos^2\theta$, where a is as follows:

	$C^{13}(p\gamma)$ (60-kev target)			$C^{13}(p\gamma)$ (100-kev target)
E_p	1670 kev	1724 kev	1749 kev	1770 kev
a	-0.394 ± 0.056	-0.474 ± 0.019	-0.516 ± 0.018	-0.399 ± 0.013

No convincing evidence has been found for the existence of terms in $\cos\theta$ or powers of $\cos\theta$ greater than 2. The first three values were obtained with 0.030 in. of aluminum absorber between the counters. The last was with 0.250 in. of aluminum absorber so that the measured distribution is essentially that of the 9.2-Mev transition to the ground state. Correction for the resolution of the detector will increase the magnitude of the observed coefficients by about 10–15 percent. The exact correction to be applied is being investigated.

SATURDAY AFTERNOON AT 2:00

Room 45, Chemistry Building

(J. KAPLAN presiding)

Contributed Papers

K1. X-Ray Absorption Structure in the *K*-Edges of Gaseous Cl_2 and HCl. S. T. STEPHENSON, R. KROGSTAD, AND W. NELSON, *The State College of Washington.**—Previous measurements in this and other laboratories indicate lack of agreement between theory and experiment for the fine structure to be found on the short wavelength side of the *K* absorption edges of various molecular gases. Since the phase shifts for chlorine have been computed in detail, and since Cl_2 is a simple diatomic molecule it would appear that the theory of the structure to be expected for Cl_2 should be very good and should offer the best chance for agreement with experiment. A detailed study of the Cl_2 edge is being made using a vacuum x-ray spectrometer first as a single crystal instrument and later as a double crystal instrument. The single crystal results will be described. There are significant discrepancies between the theoretical predictions and the structure observed both with respect to position and intensity. Measurements on HCl will also be described.

* Supported in part by the ONR.

K2. Intrinsic Curvature of Anastigmatic Fields. W. WALLIN, *U. S. Naval Ordnance Test Station* (introduced by F. T. Rogers, Jr.).—An anastigmatic lens system has a natural, or intrinsic, amount of field curvature associated with its focal length. It is shown that in the absence of internal foci, radical departures from the intrinsic curvature are not feasible. The development deals with a lens system comprising an indefinite number of elements.

K3. Ray Tracing Using the IBM Card Programmed Electronic Calculator. WILLIAM A. ALLEN, *U. S. Naval Ordnance Test Station.*—The IBM Card Programmed Electronic Calculator has been applied to the problem of lens design. Optical design is an inverse process consisting of a provisional choice of optical parameters, an exhaustive mathematical study of such a tentative prescription, and subsequent refinement of the lens system. The standard ray tracing equations can be adapted easily for machine use. The mathematical treatment is algebraic rather than trigonometric. Examples of meridional and skew ray tracing are given. A satisfactory lens has been calculated and tested entirely by machine methods. For at least one complicated optical system including decentered elements, refracting and reflecting prisms, and a multiplicity of interfaces, the standard equations required generalization. A further generalization has been the coding of the machine to trace a skew ray through an aspheric surface of revolution. The machine is expected to be of value in the refining of optical systems, in the determination of optical shop tolerances, and in the investigation of existing prescriptions.

K4. First-Order Focusing of the Spherical Electrostatic Analyzer for Particles at Relativistic Speeds. F. T. ROGERS, JR., *U. S. Naval Ordnance Test Station.*—Earlier calculations[1] of the focusing properties of the electrostatic analyzer for particles of relativistic speeds have been extended to the case of the $1/r$-potential focusing field. These reveal a marked "chromatic" dependence of focusing power upon $\beta = v/c$, known previously[2]; but, as in reference 1, there is no indication of anomaly or divergence as $\beta \to 1$. The equations describing focusing take on the usual standard forms and allow estimates readily to be made concerning regions of least confusion; effects of geometrical aperture and of the band width in energy for transmitted particles can likewise be estimated.

[1] C. W. Horton and F. T. Rogers, Jr., Rev. Sci. Instr. 14, 216 (1943).
[2] E. M. Purcell, Phys. Rev. 54, 818 (1938).

K5. Equilibrium in Rotating White Dwarf Stars. B. A. JACOBSOHN, *University of Washington.*—After having used up its hydrogen, a normal star contracts to a white dwarf with conservation of angular momentum. At a small enough radius, the centrifugal force becomes comparable to the gravitational force. There thus exists a mechanism through which a star which exceeds Chandrasekhar's critical mass will not collapse to a point. The equation of equilibrium for rotating degenerate

matter is solved for the case of large rotation by the use of a variational principle, employing simple trial functions for the density. In this way, approximate curves for the effective radius as a function of mass and angular momentum are plotted. The radius of Sirius *B*, which is two times larger than that predicted by Chandrasekhar's theory,[1] is examined from the point of view of these considerations.

[1] R. E. Marshak, Astrophys. J. 92, 321 (1940).

K6. Precision Measurement of the Hall and Magneto-Resistivity Coefficients with some Results for Graphite.* W. P. EATHERLY AND J. J. DONOGHUE, *Atomic Energy Research Department, North American Aviation, Inc.*—A circuit capable of measuring alternating current potentials up to 1000 microvolts with a precision of 0.01 microvolt has been devised and applied to the measurement of the Hall and magneto-resistivity coefficients. The circuit is essentially an alternating current potentiometer whose out-of-balance signal is supplied to a peaked amplifier tuned by a parallel-*T* feedback network. The null of the amplifier output indicates the potentiometer balance. The circuit arrangement is particularly advantageous for the evaluation of the galvano-magnetic coefficients, since the circuit then becomes a voltage divider which is insensitive to current fluctuations. As an example, a set of data on the graphitization of gas-baked carbon is given. For this material marked changes in the electrical resistivity, the Hall effect, and the magneto-resistivity occur for graphitizing temperatures in the range 1700 to 2500°C. These are correlated with crystallite growth and the evaporation of impurities, and maybe qualitatively explained on the basis of the band structure and scattering of the conduction electrons. The precision computed from this set of data is representative and amounts to 0.4 percent and 0.1 percent, respectively, of the terminal values for the Hall and magneto-resistivity coefficients.

* This paper is based on work performed under Contract No. AT-11-1-GEN-8 for the AEC.

K7. A New Apparatus for Determining the Magnetic Susceptibility of Very Small Samples.* J. J. DONOGHUE, *Atomic Energy Research Department, North American Aviation, Inc.*—An apparatus has been constructed for the precise determination of the magnetic susceptibility of very small samples by the Faraday, or non-uniform field method. Pole faces of a new design have eliminated the effect of errors in positioning the sample, by producing a uniform vertical force field within the gap. While the sample may be of arbitrary geometry, provision is made for accommodating an elongated shape. This is done by means of pole faces whose surfaces are parallel transcendental cylinders. The required equipotential surfaces were found by straightforward application of two-dimensional potential theory. Exploration of the gap with a small specimen indicated that a uniform force field existed over a large fraction of the volume within the gap. Measurable deviations from uniformity appeared only when edge or saturation effects became evident. An electrodynamic balance similar to that described by McGuire and Lane[1] has been used to measure the force on the sample. The detectable change in $m\chi$ of 1×10^{-10} g-cgs units is at present limited by tremors in the balance transmitted from the foundation.

* This paper is based on work performed under Contract No. AT-11-1-GEN-8 for the AEC.
[1] T. R. McGuire and C. T. Lane, Rev. Sci. Instr. 20, 489 (1949).

K8. Graphical Location of Approximate Roots of a Polynomical and More Accurate Values of a Particular Root with a Mechanical Harmonic Synthesizer. S. LEROY BROWN, *University of Texas.*—It has been shown that the real roots of a polynomial of degree as high as fifteen may be determined with the aid of a mechanical harmonic synthesizer.[1] By a change of variable to a trigonometric function, and after expansion of the powers of the trigonometric function into functions of multiple frequencies, the roots of the polynomial are determined from a graph that is traced by the mechanical harmonic synthesizer. If the variable in the polynomical is changed to $\cos\theta$, approximate values of all roots having values between -1 and $+1$ are determined from a graph as θ is varied (by the synthesizer) from zero to 180°; and if the variable is changed to $1/\cos\theta$, approximate values of all roots are determined except those between -1 and $+1$. Once the approximate value of a root is determined, a more accurate value may be found from a graph (traced by the synthesizer) after the variable has been changed to a trigonometric function that changes only slightly from the approximate value.

[1] S. Leroy Brown and Lisle L. Wheeler, J. Frank. Inst. 231 (March, 1941).

K9. A High Speed Camera with Electronic Controls. R. B. BOWERSOX, *Jet Propulsion Laboratory, California Institute of Technology.*—A new high speed motion picture camera has been constructed to take pictures at a maximum rate of 50,000 frames/sec. It features independent control of the framing rate and the duration of each exposure as well as electronic Kerr cell shutters which permit easy synchronization with transient phenomena. The camera takes 620 frames on a 4-ft strip of 70-mm film with exposures of 1 microsecond or longer. The film strip is mounted on the inside of a drum 15 in. in diameter which may be rotated by an electric motor at speeds up to 5000 rpm. The frames, each 0.3-in. square, are arranged in four parallel rows in order to make room for more pictures in one revolution of the camera drum. Four small camera lenses with a Kerr cell in front of each are mounted in a vertical line inside the drum near the film. The lens aperture of f/2.5 combines with the transmission of the Kerr cell gives an effective aperture of f/5.0. One or more #22 flash bulbs have been found to give sufficient illumination for most subjects.

K10. Diffraction of a Plane Electromagnetic Wave by a Circular Aperture. M. J. EHRLICH, *Hughes Aircraft Company.*—Measurements have been made, both in phase and amplitude, of the electric and magnetic field components of the near zone diffraction region. The components were measured for a series of apertures ranging from one-half to fifteen wavelengths in diameter. The scattered field components were also measured for the complementary obstacles. The range of obstacle diameters was that of the circular apertures. Normal components of magnetic field are present in the near zone of the aperture and normal electric components in the near zone region of the complementary obstacle. The tangential electric field displays considerable variation, both in phase and amplitude, across the plane of the aperture while the tangential magnetic field remains constant. The axial distribution of the tangential magnetic field has a Freshnel type behavior but unlike the electric field has no amplitude variation in the aperture as the aperture changes in diameter. Verification of the electromagnetic Babinets principle was obtained from the vector sum of the complementary fields. The research was supported by Bureau of Ships contract at the Antenna Laboratory, University of California, Berkeley, California.

K11. Cyclotron Methods for Producing Irradiation Effects in Materials. H. P. YOCKEY, M. R. JEPPSON, AND C. D'A. HUNT, *North American Aviation, Inc.*—Experimental methods of maintaining a desired temperature in solid material during irradiation with 35-Mev alphas, 19-Mev deuterons, and 8-Mev protons from the Berkeley 60-in. cyclotron will be described. Low temperatures are maintained by means of refrigerated helium recirculated in a closed system. The present system allows a 10°C rise per microampere. The base temperature at the sample is 100°K so that samples run at about 125°K during irradiation. A new refrigeration system includes a

pumped liquid nitrogen trap which will allow ½°C rise per μamp and will have a base temperature of about 70°K. A target box has been built in which samples are mounted on a turret and are rotated into the beam in succession without breaking the cooling system. Samples can be irradiated at controlled temperatures from 300°C to 2000°C. Because of beam current instability it is necessary to utilize a servo system which can correct for a temperature fall of 50°C per sec. The beam intensity and distribution is measured by a current integrator and by activation of bismuth foil. The specimen irradiation is made uniform by oscillating the specimen with a cam.

K12. The Effect of Cyclotron Bombardment of the Physical Properties of Metals.* A. B. MARTIN, S. B. AUSTERMAN, R. R. EGGLESTON, J. F. MCGEE, AND M. TARPINIAN, *North American Aviation, Inc.*—Samples of aluminum, copper, and the order-disorder alloys, AuCu and $AuCu_3$, have been irradiated with the alpha-particle beam of the Berkeley 60-in. cyclotron and the effects of such irradiations on several physical properties have been investigated. Measurements made during the irradiations while the sample temperature was held at −150°C, revealed large changes in the electric resistivity of all of these materials. Preliminary annealing studies indicated that these irradiation-induced resistivity changes began to anneal out at temperatures as low as −80°C. Room temperature measurements were made before and after each bombardment on the electric resistivity, temperature coefficient of resistivity, hardness, dimensions, and lattice parameters. Aluminum showed no appreciable change in any of these properties. Copper retained an appreciable increase in hardness at room temperature, but showed no other significant effects as a result of irradiation. Ordered samples of both AuCu and $AuCu_3$ retained large changes in electric resistivity, temperature coefficient of resistivity, and lattice parameters, similar to the changes that are observed in an order-disorder transformation. Disordered samples of these alloys showed only small changes in these properties after irradiation. An increase in hardness was observed in both the ordered and the disordered materials.

* This paper is based on work performed for the AEC.

MEETING OF THE DIVISION OF FLUID DYNAMICS

FRIDAY MORNING AT 9:00

Room 147, Business Administration and Economics

(J. G. KIRKWOOD presiding)

Forty-five minutes will be allowed for presentation and fifteen minutes for the discussion of each paper.

Turbulence, Theory and Experiment

L1. On Correlation Problems in a Model of Turbulence. J. M. BURGERS, Delft, Holland.

L2. On Recent Developments in the Statistical Theory of Turbulence. C. C. LIN, *Massachusetts Institute of Technology.*

L3. Experimental Investigations of Turbulent Flow. H. LIEPMANN, *California Institute of Technology.*

FRIDAY AFTERNOON AT 2:00

Room 147, Business Administration and Economics

(H. LEIPMANN presiding)

Hydrodynamics of Rarefied Gases

M1. Solution of the Boltzmann Equation in the Theory of Non-Uniform Gases. H. GRAD, *New York University.*

M2. Recent Results on Fluid Flow and Heat Transfer in Rarefied Gases. E. D. KANE, *University of California, Berkeley.*

M3. A Comparison of Theory and Experiment for High Speed Free Molecule Flow. JACKSON R. STALDER, GLEN GOODWIN, AND MARDUS O. CREAGER, *Ames Aeronautical Laboratory NACA.*

Author Index to Papers Presented at the Los Angeles Meeting

Adelman, F. L.—C9
Alger, R. S. and R. A. Levy—H1
Allen, William A.—K3
Althaus, Edward J.—A1
Anderson, A. B. C.—H10
Anderson, Neal S.—H7
Anthony, Romuald—F1
Ashburn, Edward V.—F2
Bandel, H. W.—B2
Bennett, F. D.—H14
Birge, Robert W. and Ulrich E. Kruse—C8
Bloom, A. L. and M. O. Stern—J6
Bowersox, R. B.—K9
Bowker, J. Kent, John R. Green, and Walter H. Barkas—C4
Bradner, Hugh and Bayard Rankin—C7
Brown, S. Leroy—K8
Brown, Sheldon, and S. J. Barnett—H3
Burgers, J. M.—L1
Burkig, J. W. and Byron T. Wright—J9
Caldwell, David O. and Hugh F. Stoddard—J5
Cartwright, W. F., C. Richman, M. H. Whitehead, and H. A. Wilcox—E5
Chamberlain, O., E. Segrè, and C. Wiegand—J8
Christy, R. F., A. T. Biehl, E. Inonu, and H. V. Neher—A4
Cladis, J. B., J. W. Hadley, and B. J. Moyer—C5
Cohen, S. T. and M. S. Plesset—G13
Cohn, B. E.—E8
Cowan, E. W.—A5
Davis, Leverett, Jr.—G10
Day, R. B. and J. E. Perry, Jr.—J14
Dienes, G. J.—D4
Dodd, E. E.—B4
Donoghue, J. J.—K7
Drell, S. D.—G12
Drukey, D. L. and J. W. Weinberg—E6
Eatherly, W. P. and J. J. Donoghue—K6
Ehrlich, M. J.—K10
Elsasser, Walter M.—F4
Eubank, W. R. and L. E. Schilberg—D7
Farnsworth, H. E. and Edward N. Clarke—D8
Fayman, David L. and Charles G. Miller—D1
Finkelstein, R. and M. Ruderman—G8
Finkelstein, R., R. LeLevier, and M. Ruderman—G9
Ford, Kenneth and John A. Wheeler—G11
Fowler, W. A.—G5
Gardner, William, N. Knable, and B. J. Moyer—C2
Germain, Lawrence S.—C1
Gilmore, E. H. and D. S. McClure—D6
Gilbert, F. C., Charles E. Violet, and Walter H. Barkas—G15
Grad, H.—M1
Harrington, E. L., L. Katz, R. N. H. Haslam, and H. E. Johns—J7
Holmes, C. R. and E. J. Workman—F5
Hubbard, E. L. and K. R. MacKenzie—J4
Jacobsohn, B. A.—K5
Jarmie, W. N., L. W. Jones, and K. M. Terwilliger—E2
Kane, E. D.—M2
Knox, W. J.—E4
Laubenstein, M. J. W., R. A. Laubenstein, L. J. Koester, and R. C. Mobley—G2
Laubenstein, R. A., M. J. W. Laubenstein, R. C. Mobley, and L. J. Koester—G1
Lauer, Eugene J.—B1
Lawhead, Robert B.—H5
Li, C. W. and Ward Whaling—J10
Liepmann, H.—L3
Lin, C. C.—L2
Linford, L. B.—C10
Loeb, L. B. and E. E. Dodd—B3
McClure, D. S., N. Blake, and P. Hanst—D5
McKinley, D. W. R.—H13
Martin, A. B., S. B. Austerman, R. R. Eggleston, J. F. McGee, and M. Tarpinian—K12
Medicus, H., D. Maeder, and H. Schneider—E1
Miller, Charles G. and David L. Fayman—D2
Neher, H. V.—A3
Parkins, W. E. and G. J. Dienes—D3
Peterson, Vincent, Edwin Iloff, and Dora Sherman—A2
Pietenpol, W. B.—E9
Plesset, M. S. and S. A. Zwick—H9
Post, R. F. and N. S. Shiren—G6
Regener, Victor H.—I1
Rinehart, John S.—H12
Rogers, F. T., Jr.—K4
Rose, Jack W.—C6
Ruby, Lawrence and J. Reginald Richardson—J1
Sachs, Donald C. and J. Reginald Richardson—J2
Sagane, R. and Peter C. Giles—E7
Schecter, L.—E3
Schiff, L. I. and R. F. Post—G7
Schrank, Glen E. and J. Reginald Richardson—J3
Seagrave, J. D., R. B. Day, and J. E. Perry, Jr.—J13
Serber, Robert—A6
Sherburne, R. K. and H. E. Farnsworth—D9
Shook, G. B.—H11
Stalder, Jackson R., Glen Goodwin, and Marcus O. Creager—M3
Steller, J. S. and W. K. H. Panofsky—C3
Stephenson, S. T., R. Krogstad, and W. Nelson—K1
Thomas, R. G.—J11
Tochilin, E., A. B. Willoughby, and P. R. Howland—H2
Toll, John and John A. Wheeler—G3
Violet, Charles E., F. C. Gilbert, and Walter H. Barkas—G14
Wallin, W.—K2
Wei, Yung Tsioh—H6
Weissler, G. L.—C11
Whaling, Ward and C. W. Li—J12
Wheeler, John A.—I3
Wheeler, John A. and John Toll—G4
Wilkening, M. H.—F3
Wilson, O. B., Jr.—H4
Workman, E. J.—I2
Wright, F. H.—H8
Yockey, H. P., M. R. Jeppson, and C. d'A. Hunt—K11